

QUANTITATIVE MAPPING OF LIGNIN

Gijs van Erven

2020

QUANTITATIVE MAPPING OF LIGNIN

COMPREHENSIVE INSIGHT INTO
FUNGAL DELIGNIFICATION
OF PLANT BIOMASS

Gijs van Erven

PROPOSITIONS

1. All lignin macromolecules are unequal, but some are more unequal than others.
based on George Orwell's Animal Farm (1945)
(this thesis)
2. Fungal ligninolysis follows pathways of deconstruction that allow their reconstruction.
(this thesis)
3. The invisibility of citations in supporting information sections of scientific publications is jeopardizing the evaluation of impact.
4. Science without conscience is con-science.
5. Current medicine resembles ancient mythology by pointing at stress to explain the unexplainable.
6. Summer solstice will unite people of a whole hemisphere when celebrated as public holiday.

Propositions belonging to the thesis, entitled

Quantitative mapping of lignin

Comprehensive insight into fungal delignification of plant biomass

Gijs van Erven

Wageningen, 8 May 2020

Quantitative mapping of lignin

**Comprehensive insight into
fungal delignification of plant biomass**

Gijs van Erven

Thesis Committee

Promotor

Prof. Dr W.J.H. van Berkel
Personal Chair at the Laboratory of Food Chemistry
Wageningen University & Research

Co-promotor

Dr M.A. Kabel
Associate Professor, Laboratory of Food Chemistry
Wageningen University & Research

Other members

Prof. Dr R.N.J. Comans, Wageningen University & Research
Prof. Dr P.C.A. Bruijninx, Utrecht University
Prof. Dr J.C. del Río, IRNAS-CSIC, Seville, Spain
Dr J.J.P. Baars, Wageningen University & Research

This research was conducted under the auspices of the Graduate School VLAG (Advanced studies in Food Technology, Agrobiotechnology, Nutrition and Health Sciences)

Quantitative mapping of lignin

Comprehensive insight into fungal delignification of plant biomass

Gijs van Erven

Thesis

submitted in fulfilment of the requirements for the degree of doctor
at Wageningen University
by the authority of the Rector Magnificus,
Prof. Dr A.P.J. Mol,
in the presence of the
Thesis Committee appointed by the Academic Board
to be defended in public
on Friday 8 May 2020
at 1:30 p.m. in the Aula.

Gijs van Erven

Quantitative mapping of lignin

Comprehensive insight into fungal delignification of plant biomass

259 pages.

PhD thesis, Wageningen University, Wageningen, The Netherlands (2020)

With references, with summary in English

ISBN: 978-94-6395-365-8

DOI: <https://doi.org/10.18174/518519>

ABSTRACT

Plant biomass delignification is crucial for terrestrial carbon cycling and is essential for incentives aiming at the valorization of lignocellulose. For understanding this central process in nature and biorefinery, we need to elucidate and comprehend the mechanisms that govern recalcitrance and conversion at the molecular level. This insight can only be obtained by accurate analysis of the molecules involved, both contentwise and structurewise. This research, therefore, aimed to advance the quantitative mapping of lignin and employ the developed analytical toolkit to unravel the underlying mechanisms of a process that has largely remained elusive to date: the fungal delignification of plant biomass.

We demonstrate through careful method validation that py-GC-MS analysis can be used for the concurrent quantification and structural characterization of grass, hardwood and softwood lignin, when employing uniformly ^{13}C labeled lignin internal standards and relative response factors for the individual pyrolysis products.

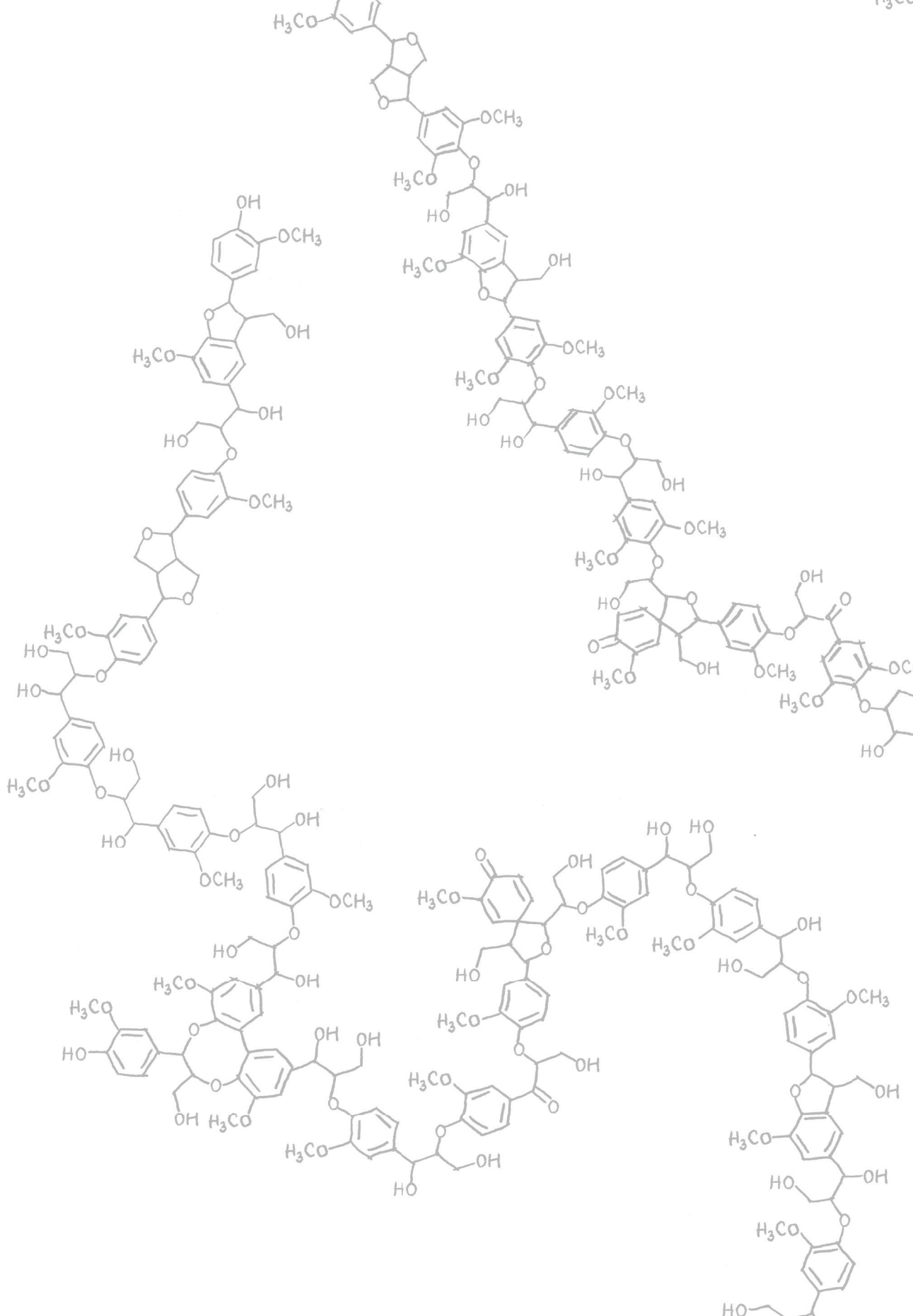
The developed method was used to assess three white-rot fungal species in terms of delignification effectivity and selectivity. In both important traits, *Ceriporiopsis subvermispora* outperformed *Lentinula edodes* and *Pleurotus eryngii*.

Comprehensive structural analyses of the residual lignin after growth of *C. subvermispora* allowed us to reconstruct various degradation routes of lignin's most abundant β -O-4' ethers and determine the relative susceptibility of various β -O-4' substructures. Our results imply that one-electron oxidation initiates *in situ* ligninolysis, which then cascades into the cleavage of C_α - C_β , C_β -O and O-4'-aryl bonds. Ligninolysis was shown to depend on the electron density of the 4'-O-subunit, diastereochemistry and γ -acylation.

In addition to white-rot basidiomycete fungi, we studied the ligninolytic capacity of the ascomycete fungus *P. anserina*. Substrate characterization unambiguously confirmed lignin degradation and secretome analysis suggested that laccases and H_2O_2 producing enzymes were likely involved in the observed ligninolysis.

TABLE OF CONTENTS

CHAPTER 1	General introduction	1
CHAPTER 2	Quantification of lignin and its structural features in plant biomass using ^{13}C lignin as internal standard for pyrolysis-GC-SIM-MS	29
CHAPTER 3	Uniformly ^{13}C labelled lignin internal standards for quantitative pyrolysis-GC-MS analysis of grass and wood	61
CHAPTER 4	Mechanistic insight into the selective delignification of wheat straw by three white-rot fungal species through quantitative ^{13}C -IS py-GC-MS and whole cell wall HSQC NMR	81
CHAPTER 5	Elucidation of <i>in situ</i> ligninolysis mechanisms of the selective white-rot fungus <i>Ceriporiopsis subvermispora</i>	115
CHAPTER 6	Structural motifs of wheat straw lignin differ in susceptibility to degradation by the white-rot fungus <i>Ceriporiopsis subvermispora</i>	155
CHAPTER 7	Evidence for ligninolytic activity of the ascomycete fungus <i>Podospora anserina</i>	187
CHAPTER 8	General discussion	209
SUMMARY		245
ACKNOWLEDGEMENTS		249
ABOUT THE AUTHOR		255



CHAPTER 1

General Introduction

Relevance of this research: Lignin research to enable lignocellulose biorefinery

The Circular Economy Package launched in 2017 by the Directorate General Environment of the European Commission promotes a transition from burning plant biomass for energy towards integrated biorefineries, in which non-food competing agricultural and forest side-streams are valorized as source of green specialty and platform chemicals, fuels, animal feed and biobased materials.¹⁻⁵ The crux of biorefinery is that, in essence, this process can be carbon-neutral: emitted CO₂ is assimilated again to new plant biomass, yielding a closed cycle.⁶

However, non-edible plant biomass is highly resistant against conversion, especially due to the presence of lignin, an extremely complex aromatic polymer.⁷ Currently, biorefinery processes consume extensive amounts of chemicals and/or energy to overcome lignin's recalcitrance and, therefore, do not conform to the circular premise. This has created a momentum towards plant breeding and genetic engineering to reduce the recalcitrance of the lignin component and got us engaged into a quest for more sustainable pretreatment alternatives. In nature, the conversion of lignin is essential to terrestrial carbon cycling and nature, therefore, has evolved ingenious mechanisms largely built upon fungi to degrade this heterogeneous macromolecule, without being accompanied by substantial environmental impact.⁸ As such, these nature-inspired strategies might help to meet the envisaged targets.

For exploiting plant biomass to its fullest and evaluate the above outlined incentives, we need to understand the mechanisms that control recalcitrance and conversion at the molecular level. This insight can only be obtained by accurate analysis of the molecules involved, both in terms of content and structure. The aim of this thesis, therefore, can be divided into two main facets. The first is to enable the quantitative analysis of lignin and the second is to apply the developed analyses to gain mechanistic insight into the fungal degradation of lignin.

Lignocellulosic biomass

Composition and architecture of the plant cell wall

In this thesis, three main plant biomass sources are distinguished: grasses (e.g. wheat straw), hardwoods (e.g. oak wood) and softwoods (e.g. spruce wood). The dry matter of these agricultural and forest side-streams, also referred to as lignocellulosic biomass, mostly consists of cell wall material. The plant cell wall is assembled into three main layers, the middle lamella, the primary cell wall and the secondary cell wall (Figure 1).⁹ The last mentioned layer makes up the largest part of the dry matter of cell walls and, hence, is most relevant for biorefinery. The secondary cell wall is mainly comprised of cellulose, hemicellulose and lignin, of which the former two are polysaccharides and the latter is a heterogeneous aromatic polymer.¹⁰ These macromolecules form a three-dimensional network on the basis of non-covalent and covalent interactions (Figure 1), and lignin in

particular provides the plant with mechanical strength and protection against environmental and pathogenic attack.¹¹⁻¹² Lignin is highly recalcitrant and beyond its physiological function in the plant, its presence limits the enzymatic and chemical conversion of the plant's polysaccharides in biorefinery approaches.⁷

In general, grasses consist of 30-40% (w/w) of cellulose with hemicellulose and lignin accounting for another 20-40% (w/w) and 15-30% (w/w), respectively.¹³⁻¹⁴ Woods generally contain more cellulose and lignin than grasses, approximating to 50% (w/w) and 25-35% (w/w), respectively.¹⁵ The exact composition, three-dimensional organization and molecular structure of these macromolecules is, amongst others, dependent on the family, species, part, age, and origin of the plant and is, furthermore, dependent on the methods used to establish them.¹⁶⁻¹⁸

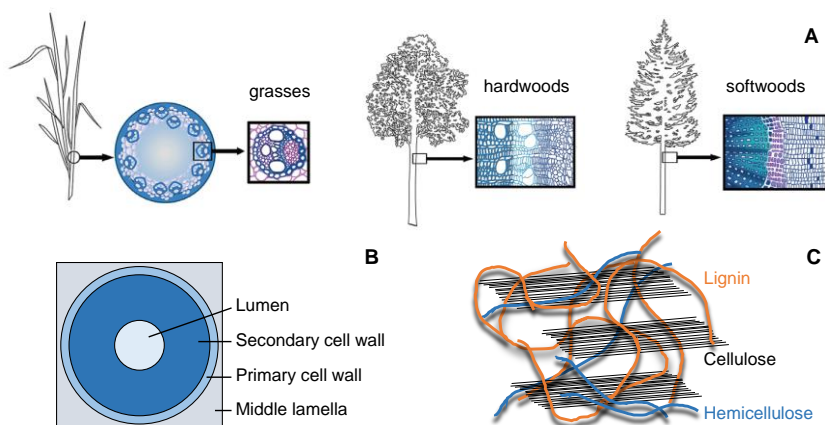


Figure 1. Schematic representation of cells (A), the cell wall (B) and secondary cell wall polymer organization (C). Panel A is adapted from Meents et al. (2018).¹⁹

Cellulose

Cellulose is a homogeneous linear polymer of β -(1 \rightarrow 4)-linked glucosyl units (Figure 2). Each glucosyl unit rotates 180° along the axis of the glucosidic bond and the chains can polymerize to a degree of polymerization (DP) of over 10⁴. These glucan chains interact via hydrogen bonds and van der Waals interactions to microfibrils with both crystalline and amorphous regions.²⁰

Hemicellulose

In contrast to cellulose, hemicellulose is much more heterogeneous, and its structure is highly varied across plant species.^{17, 21-22} The major part of hemicellulose in grasses is composed of glucuronoarabinoxylan (GAX) (Figure 2). GAX consists of a backbone of β -(1 \rightarrow 4)-linked xylopyranosyl units that is substituted by α -L-arabinofuranosyl units at the O-3 or O-3 and O-2 position (disubstitution), by (4-O-methyl)glucuronosyl units at the O-2 position and by acetyl groups at the O-2 or O-3 position, with the degree and pattern of substitution depending on the plant species.²²

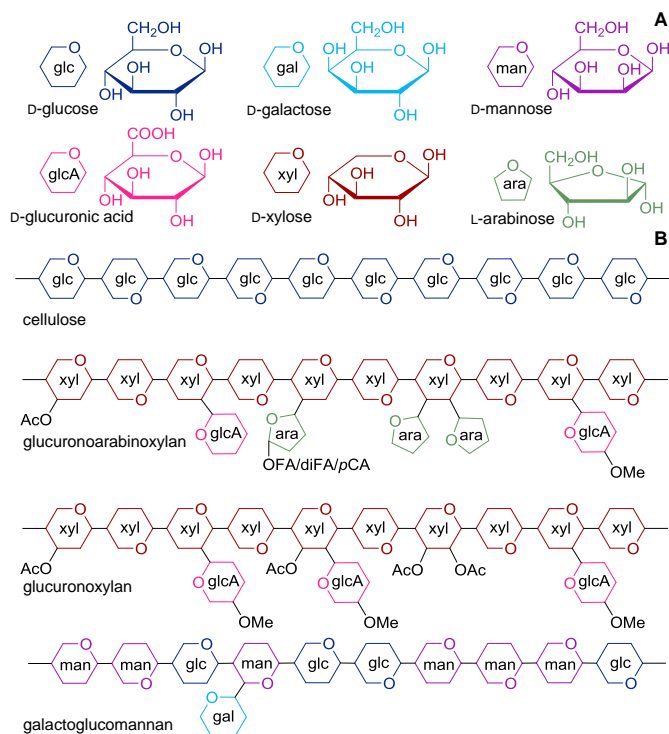


Figure 2. Structural representation of constituent monosaccharides (A) and polysaccharides (B) of the secondary plant cell wall. Me = methyl, Ac = acetate, FA = ferulate, diFA = diferulate, pCA = *p*-coumarate.

The arabinosyl units can be esterified at their *O*-5 position to ferulic or diferulic acid and, although in much lesser extents, to *p*-coumaric acid.²³ The ferulate substructures are involved in intramolecular crosslinking as well as crosslinking to lignin, as will be elaborated in the section 'lignin-carbohydrate complexes'. In hardwoods the main hemicellulosic component consists of glucuronoxylan (GX) (Figure 2). GX contains a β -(1 \rightarrow 4)-linked xylopyranosyl backbone, *O*-2 substituted by 4-*O*-methyl- α -D-glucuronosyl units and is generally much richer in acetyl substituents than GAX.¹⁷ In addition to GAX and GX, grass and hardwoods contain minor amounts of mannans and glucomannans, consisting of a β -(1 \rightarrow 4)-linked mannosyl and β -(1 \rightarrow 4)-linked mixed mannosyl-glucosyl backbone, with *O*-2 and/or *O*-3 acetylation.¹⁷ Vice versa, (galacto)glucomannans comprise the major hemicellulosic polysaccharide in softwood secondary cell walls, consisting of the same mannosyl-glucosyl backbone, *O*-6 substituted with α -D-galactosyl units (Figure 2). Like grasses, softwoods contain GAX, though it structurally differs in terms of substitution degree and pattern. Softwood GAX is generally richer in α -L-arabinosyl and 4-*O*-methyl- α -D-glucuronosyl substituents with low amounts of acetyl groups.^{17, 22}

Lignin

Lignin is an aromatic heterogeneous plant cell wall polymer that is mainly built up from the radical coupling of 4-hydroxyphenylpropanoids.²⁴ The precursors or 'monolignols' that take part in these combinatorial coupling reactions are *p*-coumaryl, coniferyl and sinapyl alcohol, which respectively result in *p*-hydroxyphenyl (H), guaiacyl (G) and syringyl (S) units when incorporated into the polymer (Figure 3).

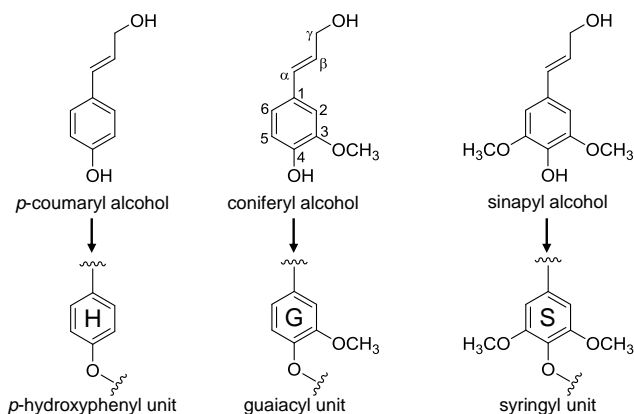


Figure 3. Precursors of and corresponding subunits when incorporated into lignin. Wavy lines indicate main positions of further coupling. Note that in H and G units, respectively, 3 and 5 and 5 positions are available for further coupling (see Figure 5).

The relative and absolute levels of incorporation mainly depend on the taxon, but are known to vary with species, cell type, cell wall layer, developmental phase and even environmental conditions are reported to influence the subunit composition.²⁵⁻²⁶ In general, softwood lignin comprises G-units only, whereas hardwood lignin is mainly composed of G- and S-units, with traces of H-units. Grass lignin contains the same subunits as hardwood, but is generally richer in H-units.¹⁸ Upon synthesis from phenylalanine, the precursors are transported to the cell wall periphery and transformed into their free radical forms by laccases and/or peroxidases.^{19, 24} The underlying biosynthetic pathways have been extensively discussed elsewhere and are considered to be out of the scope of this thesis.^{18, 27} Subsequent lignification is majorly initiated by the 'end-wise' coupling of two free radicals, i.e. the coupling of monomers to a growing oligomer or polymer with dehydrodimerization reactions being a minor event.²⁸ Via combinatorial radical mechanisms various aryl-ether and carbon-carbon interunit linkages are formed, with the β -O-4' aryl ether as most abundant interunit linkage (Figure 4).

In the first step of β -O-4' aryl ether formation, a phenolic and β -carbon-centered radical resonance form react to a quinone methide intermediate creating a new chiral center on the β -carbon. In the second step, water nucleophilically attacks the α -carbon due to which the structure rearomatizes to the final β -O-4' aryl ether linkage under formation of an additional chiral center on the α -carbon.²⁸ The

resulting racemic mixture, therefore, consists of two diastereomeric pairs of enantiomers, with *RR/SS* and *RS/SR* being referred to as *threo* and *erythro*, respectively (Figure 3).²⁸ The face of the planar quinone methide intermediate that water is added to is largely determined by the degree of methoxylation of the subunits of the interunit linkage. The formation of *erythro*-diastereomers is favored for S-units, while G-units tend to link without a clear diastereomeric preference.²⁹

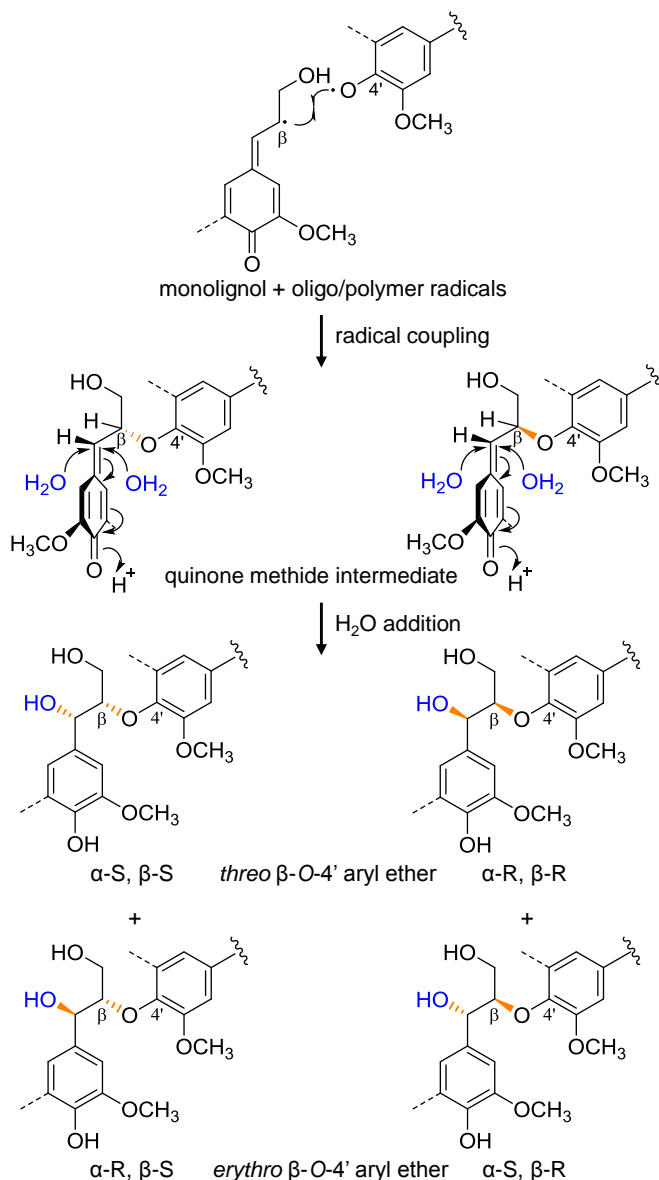


Figure 4. Combinatorial β -O-4' aryl ether radical coupling mechanism. Dashed lines indicate optional methoxyl groups, wavy lines indicates main position of further coupling.

β -O-4' aryl ethers generally account for 80% of all interunit linkages, with resinols (β - β'), phenylcoumarans (β -5'), dibenzodioxocins (4-O- β /5-5') and spirodienones (β -1'/ α -O- α') making up for the other interunit substructures (Figure 5).²⁸ Obviously, the degree of methoxylation also influences the formation of condensed carbon-carbon bonded linkages, which requires a free 5'-carbon position for coupling. As a consequence, softwood lignins generally contain larger amounts of such condensed phenylcoumaran (β -5') and dibenzodioxocin (4-O- β /5-5') substructures.³⁰ The latter dibenzodioxocin linkage, together with 5-5' and 4-O-5' linkages, have long been assumed a 'branching point' of lignins.³¹ However, these linkages have to date only been detected in their free-phenolic form and consequently, lignin might be more linear than generally considered.^{30, 32}

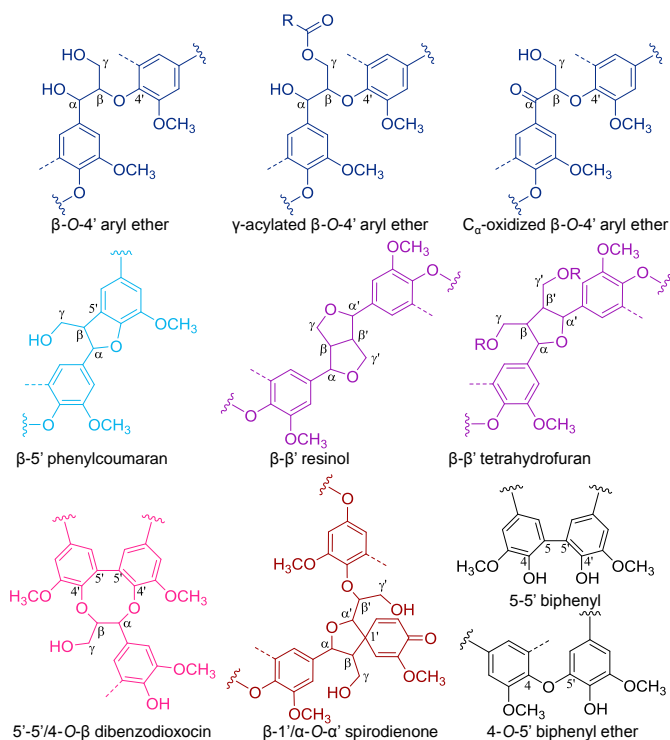


Figure 5. Lignin's interunit linkages. Dashed lines indicate optional methoxyl groups, wavy lines indicates main confirmed positions of further coupling. R in γ -acylated β -O-4' aryl ethers and β - β' tetrahydrofuran can represent acetate, *p*-coumarate and *p*-hydroxybenzoate.

In addition to the 'traditional' subunits, grass and hardwood lignins incorporate monolignols that are esterified at the γ -position with, respectively, acetate/*p*-coumarate and *p*-hydroxybenzoate (Figure 6).³³⁻³⁴ It is important to note that these substructures are present during lignification reactions and are not added later as 'decorations' and should, therefore, be considered an integral part of the lignin macromolecule.³⁴ The presence of these monolignol conjugates during lignification

results in the formation of 'new' interunit linkages in some grass species that are high in such γ -acylated moieties. Due to the blocked or 'occupied' γ -position, resinol linkages cannot be formed anymore and tetrahydrofuran substructures are formed instead (Figure 5).³⁵⁻³⁶ Yet, the β -O-4' aryl ether linkage is still most abundantly formed, and γ -acylation is therefore mostly found in these substructures. A rather surprising feature of the γ -conjugates is that they seem to only occur as 'free' or pendant phenolic moieties, i.e. their 4-OH group does not take part in radical coupling reactions.³⁴ The current theory to explain this phenomenon is by a 'radical transfer mechanism', in which phenolic γ -conjugates are oxidized to radicals, but these radicals then transfer quickly to the subunit they are attached to, facilitating their participation in coupling reactions as discussed above and leaving the γ -esters unchanged.³⁷

More recently, it was discovered that substructures outside the canonical monolignol pathway can participate in the same lignification reactions. Examples of such 'exotic' monomers include hydroxystilbenes in palm fruit endocarps and spruce bark, diferuloylputrescine in corn cobs and perhaps the most striking example is the flavonoid tricin in grasses (Figure 6).^{13, 38-41}

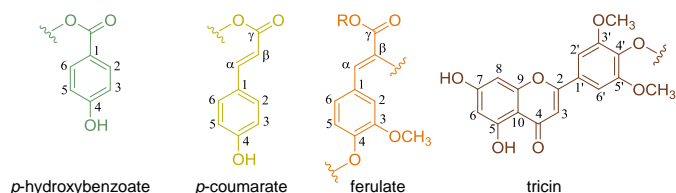


Figure 6. Structural moieties beyond the traditional monomers incorporated into the lignin macromolecule. Wavy lines indicate main confirmed positions of further coupling. R in ferulate is an arabinosyl unit when present as lignin-carbohydrate complex.

The incorporation of tricin has severe implications for the process of lignification in grasses and is now considered as an initiation point of the growing lignin polymer.⁴²⁻⁴³ The latter function was previously only considered for ferulates attached to glucuronoarabinoxylan, which results in the formation of so-called lignin-carbohydrate complexes, as will be elaborated in the next section.⁴⁴ Not only do these examples provide implications for the lignification process, they also portray the potentially unlimited variability that can be encountered within lignins.²⁸

Taking all the above-mentioned structural parameters into account, this clearly demonstrates the wealth of physically distinct polymers a lignin chemist is confronted with. As such, we contend that all lignin macromolecules are unequal, but some are more unequal than others (based on George Orwell's *Animal Farm*). Overall, the timing of monolignol deposition governs the plant control, albeit indirect, over lignin structure and might enable the plant to 'tune' lignin to its purpose.⁴⁵ Though lignin structure might be considered random or at least without apparent order, this certainly does not equal uncontrolled.

Lignin-carbohydrate complexes

Covalent linkages between lignin and hemicellulose, so-called lignin-carbohydrate complexes (LCCs), have long been suggested and debated.⁴⁶ In woods, five main LCC linkage types have been proposed to occur, namely α -ether, α -ester, γ -ester, phenyl glycoside and acetal linkages, but only very recently the first unambiguous evidence of one of such linkages was presented.⁴⁷⁻⁵¹ In Japanese red pine, the direct linkage between a mannosyl unit in glucomannan and the benzylic carbon of a β -O-4' aryl ether via an α -ether bond was elucidated via multidimensional NMR analyses.⁵² The formation of this bond can be explained on the basis of the reactivity of the primary hydroxyl group (C6) of the saccharide that can fulfill the same role as water, i.e. nucleophilic attack, in the second step of interunit linkage formation (see section 'lignin').

In grasses, it is generally accepted that the main LCCs are formed indirectly via ferulate and diferulate 'bridges' between GAX and lignin.⁵³⁻⁵⁵ Esterified at the O-5 position of arabinosyl units, the (di)ferulates can participate in similar combinatorial coupling reactions as described for the monolignols and monolignol conjugates.^{34, 44, 56} Alternatively, these ferulates may also be 'passively' incorporated into the lignins if their phenolic hydroxyl groups participate in nucleophilic addition to the quinone methide intermediates (see section 'lignin') to yield ferulate α -ethers.^{44, 57} The various diferulate structures known to exist add to the already vastly complex structure of grass lignins.^{34, 58}

Delignification of plant biomass to enable carbohydrate utilization

The presence of lignin and lignin-carbohydrate complexes hinders the (enzymatic) conversion of the polysaccharides contained within plant biomass.^{3-4, 7} Besides physical entrapment and covalent interactions, also the adsorption of enzymes to lignin negatively impacts the conversion.⁵⁹ The degradation of lignin, therefore, is crucial for terrestrial carbon recycling in Nature and is a principal goal for the industrial utilization of lignocellulose for the production of animal feed, biochemicals and biofuels.⁶⁰⁻⁶² Here, we focus mainly on processes to valorize the cell wall carbohydrates and, ergo, at pretreatments primarily aiming to degrade and/or remove lignin. However, the chemical nature and structural heterogeneity of lignin make the macromolecule highly recalcitrant against decomposition.

Industrial lignocellulose pretreatment

Several strategies are currently in operation for the pretreatment of plant biomass at industrial scale. They can be roughly categorized, based on the nature by which they disrupt the secondary cell wall matrix, into physical, thermochemical and solvent fractionation (ionic-liquids) pretreatments or combinations thereof.⁶³⁻⁶⁵ The common denominator of these processes is that they all consume extensive amounts of energy and/or chemicals to overcome lignin's recalcitrance.⁶⁶ Therefore, they cannot be considered sustainable or truly 'green'.

Biological lignocellulose pretreatment

Alternatively, Nature heavily relies on the action of bacteria and fungi for lignin degradation, with white-rot fungi being the key players.⁶⁷ These fungi are named after the color of the residual biomass after their growth, which is generally lighter in color due to the degradation of lignin, especially when it exceeds the degradation of cellulose and hemicellulose.⁶⁸⁻⁶⁹ Brown rot fungi, in sheer contrast, preferentially target carbohydrates and leave the remaining lignin largely intact, hence the brown color of the residue.⁷⁰⁻⁷¹ Due to their lignin degrading capacity, white-rot fungi are biotechnologically most relevant.⁷² Since the fungal delignification process is non-energy intensive and unaccompanied by the production of inhibitors for downstream processes commonly produced through thermochemical pretreatments, this biological pretreatment strategy is increasingly receiving attention.⁷³⁻⁷⁴ However, extensive fungal delignification requires long residence times, generally up to two months, and (some) carbohydrate consumption is inherent to fungal growth.⁷⁵⁻⁷⁸ Notably, both the extent and selectivity of delignification depend on the used methodology to establish them (Table 1 and Table 2). Methodological details are discussed in the section 'the analysis of lignin'.

Table 1. Efficiency and selectivity of wheat straw delignification by selected white-rot fungi as determined by Klason lignin and constituent monosaccharide analyses. Treatment time 3 weeks, except reference 77 (4 weeks).

Fungus	Degradation (% w/w) ^a			Selectivity ^b		Reference
	Lignin	Hemicellulose	Cellulose	L/C	L/HC	
<i>Ceriporiopsis subvermispota</i>	30	36	13	2.3	0.8	76
<i>Pleurotus eryngii</i>	17	8	0	-	2.1	76
<i>Phanerochaete chrysosporium</i>	17	36	40	0.4	0.5	77
<i>Pleurotus ostreatus</i>	27	52	22	1.2	0.5	76
<i>Trametes versicolor</i>	46	21	23	2.0	2.2	77
<i>Irpex lacteus</i>	34	26	17	2.0	1.3	77

^a lignin based on sum of acid-insoluble and acid-soluble lignin, ash correction not specifically reported; hemicellulose based on anhydroxylose; cellulose based on anhydroglucose.

^b L/C based on lignin versus cellulose degradation; L/HC based on lignin versus hemicellulose degradation

Table 2. Efficiency and selectivity of wheat straw delignification by selected white-rot fungi as determined by Van Soest compositional analysis. Treatment time 7 weeks.

Fungus	Degradation (% w/w) ^a			Selectivity ^b		Reference
	Lignin	Hemicellulose	Cellulose	L/C	L/HC	
<i>Ceriporiopsis subvermispota</i>	63	57	3	21	1.1	78
<i>Pleurotus eryngii</i>	32	28	6	5.3	1.1	78
<i>Phanerochaete chrysosporium</i>	41	38	35	1.2	1.1	78
<i>Pleurotus ostreatus</i>	39	38	21	1.9	1.0	78
<i>Trametes versicolor</i>	62	45	45	1.4	1.4	78
<i>Lentinula edodes</i>	59	53	9	6.6	1.1	78

^a lignin based on acid detergent lignin (ADL); hemicellulose based on difference between neutral detergent fiber (NDF) and acid detergent fiber (ADF); cellulose based on difference between ADF and ADL.

^b L/C based on lignin versus cellulose degradation; L/HC based on lignin versus hemicellulose degradation

Both the time-efficiency and selectivity of the fungal delignification process require optimization before (most) industrial scale applications can be realized.^{62, 79} Screening of the most effective and selective species combined with an improved understanding of the underlying delignification mechanisms at the molecular level are expected to contribute to achieving this aim. These incentives highlight the need for accurate analyses of both lignin content and structure.

Enzymes involved in fungal lignin degradation

For lignin degradation, white-rot fungi rely on an intricate extracellular oxidoreductase machinery based on several peroxidases, laccases and accessory H_2O_2 producing enzymes, although the relative dependencies widely vary among species.⁸⁰⁻⁸² Lignin peroxidases (LiPs) were the initial enzymes held responsible for fungal ligninolysis, hence also coined ligninases, and found in the extensively studied white-rot fungus *Phanerochaete chrysosporium* (see also Table 1+2).⁸³⁻⁸⁴ Due to a high redox potential, LiPs can directly oxidize lignin related molecules after initial oxidation of the enzyme by H_2O_2 . A solvent-exposed tryptophan residue was shown to be involved in the oxidative action of LiP, which allows the enzyme to act on polymeric lignin.⁸⁵⁻⁸⁶ However, fungal lignin degradation occurs before cell wall porosity would allow enzymes to penetrate.⁸⁷⁻⁸⁸ Therefore, the enzymes have often been associated to work in concert with veratryl alcohol, that should act as diffusible oxidant or electron shuttle, also called mediator. Though, a recent study largely debunked this widely accepted mediator function as it was shown that LiP-generated veratryl alcohol cation radicals were unable to oxidize the interior of specifically designed beads with a normalized porosity.⁸⁹

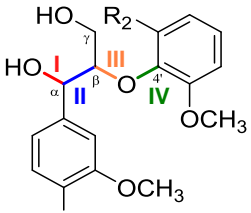
Certain white-rot species, such as *Ceriporiopsis subvermispora* (see also Table 1+2), can degrade lignin effectively in the absence of LiP. Instead, these fungi depend on manganese peroxidases (MnPs), enzymes that are omnipresent amongst white-rot fungi.⁹⁰ MnPs oxidize Mn^{2+} to Mn^{3+} , again after 'activation' of the enzyme by H_2O_2 . The resulting Mn^{3+} , stabilized by chelation to oxalic acid, mediates lignin degradation but, is, however, only able to oxidize phenolic subunits. The enzymes have been shown to be able to degrade non-phenolic subunits as well, when they act concerted with other mediators, presumably lipids, although controversy on the exact nature and role of these mediators remains.⁹¹⁻⁹³ The third main peroxidase type are the versatile peroxidases (VP), enzymes that combine the catalytic properties and characteristics of LiPs and MnPs.⁹⁴

In contrast to these peroxidases, laccases do not require the presence of H_2O_2 for activity and catalyze the one-electron oxidation of aromatic substrates using molecular oxygen as electron acceptor.⁹⁵ Laccases can only directly oxidize phenolic subunits and require mediators, operating via different oxidation mechanisms, to oxidize non-phenolic subunits.⁹⁶ For the same steric hindrance reasons described above, it can be doubted that laccases work directly on polymeric lignin.

The H_2O_2 required by peroxidases is largely provided by accessory enzymes grouped into the flavin-dependent glucose-methanol-choline (GMC) oxidoreductase family, including aryl-alcohol oxidases (AAO).^{69, 97} The latter enzymes catalyze the oxidation of lignin-derived low molecular weight aromatics or aromatic fungal metabolites under the reduction of molecular oxygen to hydrogen peroxide. A cyclic redox reaction is ensured by the enzymatic reduction of aromatic products resulting from AAO oxidation.⁹⁷

Mechanisms underlying fungal delignification

As a result of lignin's structural complexity, model compounds are often used to study the mechanisms underlying chemical and biological lignin conversion.⁹⁸⁻¹⁰³ Through these lignin mimics, it has been established that the enzymes responsible for fungal ligninolysis degrade lignin oxidatively via reactions that are initiated by hydrogen atom and/or single electron transfer.^{83, 93, 103-104} These reactions result in various products that can be mainly ascribed to four pathways: I C_α -oxidation; II C_α - C_β cleavage; III C_β -O cleavage and IV O-4' cleavage (Figure 7), though aryl-alkyl and aromatic-ring cleavage have been described as well. Clearly, the reactions that take place depend on the ligninolytic system, but importantly, the structure of the model compound also largely influences the reaction outcome (Figure 7).^{83, 93, 101, 104-106}



System	R ₁ , R ₂	I	II	III	IV	Reference
LiP + H ₂ O ₂	CH ₃ , H	+	++	-	++	83
	C ₂ H ₅ , OCH ₃	-	+	-	++	105
Laccase + HBT	CH ₃ , H	++	-	++	-	101
	C ₂ H ₅ , OCH ₃	++	+	++	+	104
MnP + H ₂ O ₂ + FA	CH ₃ , H	++	+	-	-	106
	C ₂ H ₅ , OCH ₃	++	+	++	++	93

I C_α -oxidation II C_α - C_β cleavage
 III C_β -O cleavage IV O-4' cleavage

Figure 7. Reaction outcomes for mechanistic studies on fungal ligninolysis by using lignin model dimers. Cleavage reaction not observed (-); cleavage reaction observed (+); major cleavage reaction (++). LiP lignin peroxidase; HBT hydroxybenzotriazole; MnP manganese peroxidase; FA fatty acid.

Though these lignin model compound studies have formed the basis of our understanding of fungal delignification mechanisms, it can be doubted whether the results obtained on these simplified systems can be extrapolated directly to *in situ* fungal delignification. Not only do the lignin mimics oversimplify lignin structure and exclude the effect of the secondary cell wall matrix lignin is naturally contained in, these studies employed individual enzymes while *in situ* a complex enzyme collective is responsible for ligninolysis, as outlined in the section 'enzymes involved in fungal lignin degradation'.

When fungi are used directly rather than (purified) enzyme extracts to investigate the degradation mechanisms of lignin model compounds, it cannot be excluded that these compounds are transported intracellularly and converted via mechanisms irrelevant to the conversion of polymeric lignin, unable to cross the fungal cell membrane.^{103, 107-108} Ideally, mechanistic insight is, therefore, obtained through characterization of the residual lignin structures after fungal growth on actual lignocellulosic biomass and reconstructing reaction pathways on the basis of the elucidated reaction products and/or intermediates. Obtaining *in situ* mechanistic insight has thus far found to be troublesome, particularly because of lignin's structural complexity and the concomitant analytical difficulties. The advancement of lignin's analytical toolbox is expected to contribute to the understanding of *in situ* fungal delignification mechanisms.

The analysis of lignin

In general, the analysis of lignin is complicated due to its insoluble nature in most common solvents, structural heterogeneity and resistance against controlled depolymerization. Over the past decades several qualitative and quantitative analyses for the characterization of lignin have been developed. Yet, only more recent advancements have begun to shed light on the polymer that had always been considered a black box.¹⁰⁹⁻¹¹¹ In the next sections, the most relevant analyses of lignin content and lignin structure will be discussed.

Lignin content

Despite the developments in the lignin field, lignin content analyses still heavily rely on traditional, unspecific gravimetric and spectrophotometric tools.¹¹²⁻¹¹³ The gravimetric approaches mainly aim to hydrolyze carbohydrates and quantify lignin as the insoluble residue. Acid-insoluble lignin (AIL), commonly referred to as Klason lignin, is obtained after a two-step sulfuric acid hydrolysis comprising incubation with concentrated acid at moderate temperature (~30 °C) followed by boiling after dilution.¹¹⁴ Alternatively, acid-detergent lignin (ADL) is obtained when the order of the two steps is reversed and a detergent is present during hydrolysis.¹¹⁵ Logically, any non-lignin acid-insoluble material remaining after hydrolysis interferes with the analysis. Such interferences can vary and might, amongst others, comprise of ash and protein in native plant biomass, chitin in fungal treated material and humic substances in soil samples. Due to the severe hydrolysis conditions a fraction of the lignin is solubilized. This acid-soluble lignin (ASL) is truly formed during the procedure, rather than being a distinct fraction initially present in the samples and its formation is expected to depend on the initial lignin structure.¹¹⁶ Heavily degraded lignins are likely more prone to acid solubilization. In the Klason methodology, ASL is determined spectrophotometrically, which outcome strongly depends on the wavelength and corresponding extinction coefficient used for quantification.¹¹³⁻¹¹⁴ The ADL procedure generally

results in more ASL and the fact that it is not quantified largely explains why this methodology underestimates lignin content by a factor 2 to 5.¹¹⁷⁻¹¹⁸

Contrarily, the acetylbromide method is based on complete solubilization of lignin through derivatization prior to spectrophotometric analysis and is, besides residual insoluble lignin, skewed by any nonlignin compounds with absorbance in the 280 nm region.¹¹⁹⁻¹²⁰ These interfering compounds are also formed during the experiment itself.¹¹⁹

Given the above, one can question the delignification data presented in Tables 1 and 2. This advertises for the need of an alternative method for the determination of lignin content, especially in fungal treated samples.

Lignin structure

This section is limited to techniques used for the analyses of polymeric lignin and techniques employed in this thesis are emphasized. LC-MS, GC-MS, and MALDI-TOF-MS analyses mainly find application for the analysis of low(er) molecular weight lignin-derived molecules and, thus, will not be dealt with.^{93, 121-122} In most cases, the analytical tools used for the structural characterization of polymeric lignin reveal information on specific features only (Table 3). Therefore, multiple techniques are required to obtain comprehensive insight into lignin's structure and despite major advancements some serious drawbacks of the current methods still remain.

As can be observed in Table 3, ¹H-¹³C HSQC NMR proves most versatile with regard to the structural information that can be obtained in a single analysis. In principle, any compound with specific chemical shifts for C-H pairs can be detected, though the technique is mostly applied for the analysis of lignin's interunit linkages.¹²⁴ However, the technique suffers from serious limitations in terms of quantification, particularly caused by relaxation dependencies on the molecular weight and 'pendant' versus 'core-lignin' units, and, consequently, is currently still semiquantitative at best.^{125, 141-143} For a more quantitative analysis of β -O-4' aryl ethers, derivatization followed by reductive cleavage (DFRC) has proven very useful and recent advancements now also allow the accurate detection of γ -acylated substructures.¹³⁸⁻¹⁴⁰ In addition to the quantification challenges, HSQC NMR analysis requires lignin isolation for detailed structural characterization.¹²⁴

Lignin isolations are always a tradeoff between yield, structural integrity and purity. Innumerable efforts have thus far aimed to determine the optimal lignin isolation procedure and find the perfect balance between the latter three parameters.¹⁴⁴⁻¹⁴⁵ Most commonly, however, lignin is still isolated via the classical protocol developed by Björkman or modifications thereof. In these procedures plant biomass is always planetary ball-milled and extracted by aqueous dioxane and optionally includes enzymatic carbohydrate degradation prior to dioxane extraction to improve yields.¹⁴⁶⁻¹⁴⁷ Although care must be taken to avoid excessive structural modification during ball-milling and yields are generally low, these lignin

preparations are still considered fairly representative of the total lignin structure present.¹⁴⁸⁻¹⁴⁹

Table 3. Common analytical methods used for the structural assessment of lignin.

	HSQC NMR ^a	³¹ P NMR ^a	SEC ^a	Py-GC-MS ^a	FTIR ^a	DFRC ^a
Structural features	Subunit composition	✓		✓	✓	✓ ^b
	Interunit linkages	✓				✓ ^b
	Molecular weight		✓			
	γ-conjugates	✓		✓ ^c		✓ ^d
	C _α oxidized moieties	✓	✓ ^e	✓	✓	
	Phenolic hydroxyl		✓	✓ ^c	✓	
	LCCs	✓				
	Diastereomer ratio ^f	✓				
Specification	State	dissolved/gel	dissolved	dissolved	solid	solid
	Isolation required	no	yes	yes	no	no
	Sample amount	20-100 mg	20-100 mg	2-10 mg	<100 μg	<5 mg
	Analysis time	<2 h	<1 h	<1 h	<1 h	<10 min
	Sample preparation	ball-milling + dissolution	derivatization	dissolution or derivatization	milling + weighing	milling + tableting
	Quantitativeness	Relative	Absolute ^g	Absolute ^h	Relative	Relative
References	123-125	126-128	129-131	132-134	135-137	138-140

^a Heteronuclear Single Quantum Coherence Nuclear Magnetic Resonance; ³¹P Nuclear Magnetic Resonance; Size-Exclusion Chromatography; Pyrolysis combined with Gas Chromatography and Mass Spectrometric detection; Fourier Transform Infrared spectroscopy; Derivatization Followed by Reductive Cleavage

^b only β-O-4' aryl ether linkages

^c only distinguished in presence of tetramethylammonium hydroxide (TMAH), excluding acetyl groups and tricin

^d only γ-acylating conjugates of β-O-4' aryl ether linkages

^e only carboxylic OH

^f only β-O-4' aryl ether linkages (*erythro* vs *threo*)

^g relative to internal standard

^h often established through system calibration with polystyrene sulfonate standards that poorly resemble lignin structure

Likewise, ³¹P NMR and SEC can only be applied on lignin isolates as both procedures require complete solubility of the sample, for phosphitylating derivatization and chromatographic separation, respectively.^{128, 130} The latter chromatography is, therefore, often performed by using strong alkaline conditions.¹²⁹ These conditions cleave alkali-labile ester structures present in the lignins, e.g. γ-acyl groups, and hence, are expected to influence the molecular weights observed. To avoid such cleavage reactions, derivatization (often acetylation) of the isolated lignins has been applied to allow solubility in organic solvents like tetrahydrofuran.¹²⁹ A major drawback of such derivatization, however, is that the number of derivatized groups is not known, which logically is detrimental to the accuracy of the molecular weight determination.¹⁵⁰ Without the need for derivatization, DMSO containing lithium bromide was found to be able to dissolve a wide range of structurally different lignins and therefore was considered a more-or-less universal lignin solvent and eluent for SEC analyses.¹³¹ All SEC variants, however, suffer from a dependency

on polystyrene sulfonate standards for system calibration, which generally tend to poorly resemble lignin structure. Recent advancements with multi-angle light scattering (MALS) detection now circumvent this calibration problem and enable the more accurate assessment of lignin's molecular weight.¹⁵¹

To overcome the problems associated with lignin isolation, mainly in terms of low recovery and chemical modifications, techniques that allow *in situ* lignin analysis are seriously gaining popularity. Even though cryogenically cooled probes and high-field (600 Hz and up) NMR analyses greatly improve resolution and start to become general practice, these still not provide sufficient resolution to completely resolve lignin and carbohydrate related peaks in the aliphatic region and some lignin- and protein derived peaks in the aromatic region. Furthermore, such measurements in the gel state still require planetary ball-milling of the samples.^{125, 152}

Lignin analysis by py-GC-MS

Alternatively, pyrolysis combined with gas chromatography and mass spectrometric detection (py-GC-MS) can be used for the direct characterization of lignin contained within lignocellulose, i.e. without lignin isolation. The term "pyrolysis" suggests the involvement of some sort of "pyro", for fire, and "lysis", for separation or cleavage. Yet, only such lysis indeed occurs as the process is defined as the decomposition of a material at elevated temperatures (for lignin generally at 500 °C and above) in the absence of oxygen. Lignocellulose pyrolysis yields low molecular weight, unspecific, gaseous products such as CO₂ and methane and a solid residue called char, but importantly also results in the formation of lignin-specific products.¹⁵³ These lignin-derived pyrolysis products can principally be distinguished as phenolic monomers, retaining their methoxyl substituents and containing various side-chains (e.g. methyl, aldehyde, propenyl).^{132, 154} Lignin's thermal decomposition is severely affected by the pyrolysis conditions, with temperature, heating rate and residence time of the released products as major parameters, and the process thus depends on the system and setup used.¹⁵⁵ A temperature of 500 °C is often used for the analytical pyrolysis of lignin. This temperature gives an optimal balance between pyrolysis efficiency, yield of monomeric products and their structural integrity, i.e. ring cleavage and demethoxylation reactions are kept to a minimum.¹⁵⁶ Combined with sufficiently short residence times to minimize secondary (and up) reactions, this ensures that the measured products are representative of the lignin they derive from.¹⁵⁵ The advancement of micro-furnace pyrolysis systems enables robust and reproducible analyses and especially the development of the auto-sampler setup now allows the employment of the technique in a more routine and higher throughput fashion (Figure 8).^{155, 157} Nonetheless, py-GC-MS analyses itself have principally remained the same since the early efforts of Faix et al.¹⁵⁴ and Ralph & Hatfield¹³², and mostly have been used to give qualitative insight into the relative

distributions of the released pyrolysis products, thereby providing a 'fingerprint' of the lignin structure.¹³⁴

Upon pyrolysis, the hydroxycinnamic acids *p*-coumarate and ferulate decarboxylate respectively to 4-vinylphenol and 4-vinylguaiacol, products that also arise from the pyrolysis of 'core lignin' itself.¹³² Particularly relevant for the pyrolysis of grass lignocellulose, therefore, tetramethylammonium hydroxide (TMAH) is often added to the samples before pyrolysis to methylate phenolic and carboxylic hydroxyl groups and be able to deduce the origin of such vinylproducts.^{36, 158-159}

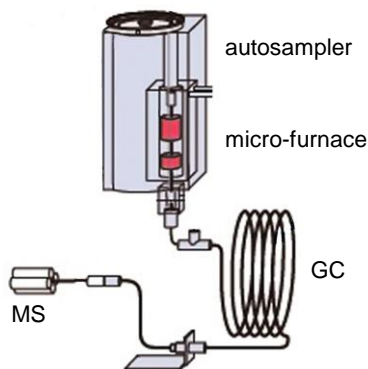


Figure 8. Schematic representation of a micro-furnace py-GC-MS setup equipped with an autosampler.

Some studies have also attempted to apply py-GC-MS analysis for the quantification of lignin content, which has, thus far, resulted in insufficient accuracy. This inaccuracy followed from two main analytical approaches. The first approach relates to the use of relative peak areas for the quantification of lignin, i.e. peak area of lignin-derived products versus total peak area was used as a quantitative measure.¹⁶⁰⁻¹⁶² Differences in pyrolysis efficiencies of the constituents of lignocellulose, the absence of (relative) response factors of the released products and matrix-effects yield unreliable lignin contents when following this approach.¹³² Second, monomeric internal standards were used for the absolute quantification of the released pyrolysis products.¹⁶³⁻¹⁶⁴ Although some studies attempted to include (relative) response factors, this approach always neglects the formation of unspecific pyrolysis products from lignin and, consequentially, greatly underestimates lignin content.¹⁵⁵ In addition, matrix-effects exerted on polymeric lignin are unlikely to similarly affect monomeric internal standards, further contributing to the inaccuracy.¹⁶⁵

In spite of the analytical challenges outlined above, we do not think that the quantitative potential of py-GC-MS analysis has been fully exploited. Furthermore, the unique low sample investments for py-GC-MS analysis call for a broader employment of this analytical tool for the quantitative analysis of lignin, which, therefore, is one of the central aims of this thesis.

Project Aim

The aim of this project is two-faceted. The first relates to enabling the quantitative mapping of lignin both in terms of content and structure and sets to achieve this aim by employing py-GC-MS analysis. Secondly, the project aims to use the developed py-GC-MS method in parallel with various other analytical tools to obtain comprehensive insight into fungal delignification in terms of efficiency and selectivity, underlying mechanisms and susceptibility of specific structural motifs towards degradation.

Outline of this thesis

In **Chapter 1** the relevance of this project and current state of knowledge on lignin, lignin analysis and fungal delignification are succinctly outlined.

In **Chapter 2** we demonstrate how uniformly ^{13}C labeled wheat straw lignin can be employed as internal standard for py-GC-MS analyses and enables the quantification of lignin and its structural features.

Chapter 3 describes our efforts to further advance the ^{13}C internal standard py-GC-MS method by employing high-resolution mass spectrometric detection and extending the method to hardwoods and softwoods by using uniformly ^{13}C labeled willow and douglas fir lignin, respectively.

In **Chapter 4** three white-rot fungal species are compared in terms of their efficiency and selectivity of lignin removal and underlying delignification mechanisms by quantitative py-GC-MS and whole-cell wall NMR analyses. We show that *Ceriporiopsis subvermispota* is particularly effective and selective and achieves so via fundamentally different delignification mechanisms.

Chapter 5 describes our work to further understand the delignification mechanisms of *C. subvermispota*. Herein, we elucidate *in situ* delignification reaction pathways through selectively extracted and comprehensively characterized diagnostic substructures.

In **Chapter 6** the relative susceptibilities of various structural motifs of wheat straw lignin to degradation by *C. subvermispota* are delineated and we discuss our findings in light of the underlying delignification mechanisms.

In **Chapter 7** we unambiguously confirm that the ascomycete *Podospora anserina* possesses ligninolytic capacity through comprehensive structural analyses of lignin after fungal growth and analysis of the fungus' secretome.

Finally, in **Chapter 8**, we discuss the (combined) results obtained in the preceding chapters alongside some unpublished findings and present future perspectives for the application of the novel analytical methods and fungi to valorize lignocellulose.

References

1. Rogelj, J.; Den Elzen, M.; Höhne, N.; Fransen, T.; Fekete, H.; Winkler, H.; Schaeffer, R.; Sha, F.; Riahi, K.; Meinshausen, M., Paris Agreement climate proposals need a boost to keep warming well below 2 °C. *Nature* **2016**, *534*, 631-639.
2. Lund, H., Renewable energy strategies for sustainable development. *Energy* **2007**, *32*, 912-919.
3. Ragauskas, A. J.; Williams, C. K.; Davison, B. H.; Britovsek, G.; Cairney, J.; Eckert, C. A.; Frederick, W. J.; Hallett, J. P.; Leak, D. J.; Liotta, C. L., The path forward for biofuels and biomaterials. *Science* **2006**, *311*, 484-489.
4. Ragauskas, A. J.; Beckham, G. T.; Bidy, M. J.; Chandra, R.; Chen, F.; Davis, M. F.; Davison, B. H.; Dixon, R. A.; Gilna, P.; Keller, M., Lignin valorization: improving lignin processing in the biorefinery. *Science* **2014**, *344*, 1246843.
5. Hassan, S. S.; Williams, G. A.; Jaiswal, A. K., Lignocellulosic biorefineries in Europe: Current state and prospects. *Trends Biotechnol* **2019**, *37*, 231-234.
6. Vanholme, B.; Desmet, T.; Ronsse, F.; Rabaey, K.; Van Breusegem, F.; De Mey, M.; Soetaert, W.; Boerjan, W., Towards a carbon-negative sustainable bio-based economy. *Front Plant Sci* **2013**, *4*, 174.
7. Himmel, M. E.; Ding, S.-Y.; Johnson, D. K.; Adney, W. S.; Nimlos, M. R.; Brady, J. W.; Foust, T. D., Biomass recalcitrance: engineering plants and enzymes for biofuels production. *Science* **2007**, *315*, 804-807.
8. Floudas, D.; Binder, M.; Riley, R.; Barry, K.; Blanchette, R. A.; Henrissat, B.; Martínez, A. T.; Otilar, R.; Spatafora, J. W.; Yadav, J. S., The Paleozoic origin of enzymatic lignin decomposition reconstructed from 31 fungal genomes. *Science* **2012**, *336*, 1715-1719.
9. Carpita, N., The cell wall. In *Biochemistry and Molecular Biology of Plants*, 2nd Edition, Buchanan, B. B.; Gruissem, W.; Jones, R. L., Eds. American Society of Plant Physiologists: Rockville, MD, USA, 2000; pp 52-108.
10. Pauly, M.; Keegstra, K., Cell-wall carbohydrates and their modification as a resource for biofuels. *Plant J* **2008**, *54*, 559-568.
11. Achyuthan, K. E.; Achyuthan, A. M.; Adams, P. D.; Dirk, S. M.; Harper, J. C.; Simmons, B. A.; Singh, A. K., Supramolecular self-assembled chaos: polyphenolic lignin's barrier to cost-effective lignocellulosic biofuels. *Molecules* **2010**, *15*, 8641-8688.
12. Moura, J. C. M. S.; Bonine, C. A. V.; de Oliveira Fernandes Viana, J.; Dornelas, M. C.; Mazzafera, P., Abiotic and biotic stresses and changes in the lignin content and composition in plants. *J Integr Plant Biol* **2010**, *52*, 360-376.
13. Del Río, J. C.; Rencoret, J.; Prinsen, P.; Martínez, A. T.; Ralph, J.; Gutiérrez, A., Structural characterization of wheat straw lignin as revealed by analytical pyrolysis, 2D-NMR, and reductive cleavage methods. *J Agric Food Chem* **2012**, *60*, 5922-5935.
14. Martínez, P. M.; Bakker, R.; Harmsen, P.; Gruppen, H.; Kabel, M. A., Importance of acid or alkali concentration on the removal of xylan and lignin for enzymatic cellulose hydrolysis. *Ind Crops Prod* **2015**, *64*, 88-96.
15. Sun, Y.; Cheng, J., Hydrolysis of lignocellulosic materials for ethanol production: a review. *Bioresour Technol* **2002**, *83*, 1-11.
16. Cosgrove, D. J., Growth of the plant cell wall. *Nat Rev Mol Cell Biol* **2005**, *6*, 850-861.
17. Ebringerová, A.; Hromádková, Z.; Heinze, T., Hemicellulose. In *Polysaccharides I: Structure, Characterization and Use*, Heinze, T., Ed. Springer: Berlin, Heidelberg, Germany, 2005; pp 1-67.
18. Boerjan, W.; Ralph, J.; Baucher, M., Lignin biosynthesis. *Annu Rev Plant Biol* **2003**, *54*, 519-546.
19. Meents, M. J.; Watanabe, Y.; Samuels, A. L., The cell biology of secondary cell wall biosynthesis. *Ann Bot* **2018**, *121*, 1107-1125.
20. Jarvis, M., Chemistry: cellulose stacks up. *Nature* **2003**, *426*, 611-612.

21. Scheller, H. V.; Ulvskov, P., Hemicelluloses. *Annu Rev Plant Biol* **2010**, *61*, 263-289.
22. Gírio, F. M.; Fonseca, C.; Carvalheiro, F.; Duarte, L. C.; Marques, S.; Bogel-Łukasik, R., Hemicelluloses for fuel ethanol: a review. *Bioresour Technol* **2010**, *101*, 4775-4800.
23. Lapierre, C.; Voxeur, A.; Karlen, S. D.; Helm, R. F.; Ralph, J., Evaluation of feruloylated and *p*-coumaroylated arabinosyl units in grass arabinoxylans by acidolysis in dioxane/methanol. *J Agric Food Chem* **2018**, *66*, 5418-5424.
24. Ralph, J.; Lundquist, K.; Brunow, G.; Lu, F.; Kim, H.; Schatz, P. F.; Marita, J. M.; Hatfield, R. D.; Ralph, S. A.; Christensen, J. H., Lignins: natural polymers from oxidative coupling of 4-hydroxyphenyl-propanoids. *Phytochem Rev* **2004**, *3*, 29-60.
25. Campbell, M. M.; Sederoff, R. R., Variation in lignin content and composition (mechanisms of control and implications for the genetic improvement of plants). *Plant Physiol* **1996**, *110*, 3-13.
26. Rencoret, J.; Gutiérrez, A.; Nieto, L.; Jiménez-Barbero, J.; Faulds, C. B.; Kim, H.; Ralph, J.; Martínez, Á. T.; del Río, J. C., Lignin composition and structure in young versus adult *Eucalyptus globulus* plants. *Plant Physiol* **2011**, *155*, 667-682.
27. Vanholme, R.; Demedts, B.; Morreel, K.; Ralph, J.; Boerjan, W., Lignin biosynthesis and structure. *Plant Physiol* **2010**, *153*, 895-905.
28. Ralph, J.; Brunow, G.; Harris, P. J.; Dixon, R. A.; Schatz, P. F.; Boerjan, W., Lignification: are lignins biosynthesized via simple combinatorial chemistry or via proteinaceous control and template replication? In *Recent Advances in Polyphenol Research*, Lattanzio, V.; Daayf, F., Eds. Wiley-Blackwell: Oxford, 2009; Vol. 1, pp 36-66.
29. Akiyama, T.; Goto, H.; Nawawi, D. S.; Syafii, W.; Matsumoto, Y.; Meshitsuka, G., Erythro/threo ratio of β -O-4 structures as an important structural characteristic of lignin. Part 4: Variation in the erythro/threo ratio in softwood and hardwood lignins and its relation to syringyl/guaiacyl ratio. *Holzforschung* **2005**, *59*, 276-281.
30. Ralph, J.; Lapierre, C.; Boerjan, W., Lignin structure and its engineering. *Curr Opin Biotechnol* **2019**, *56*, 240-249.
31. Crestini, C.; Melone, F.; Sette, M.; Saladino, R., Milled wood lignin: a linear oligomer. *Biomacromolecules* **2011**, *12*, 3928-3935.
32. Yue, F.; Lu, F.; Ralph, S.; Ralph, J., Identification of 4-O-5-units in softwood lignins via definitive lignin models and NMR. *Biomacromolecules* **2016**, *17*, 1909-1920.
33. Del Río, J. C.; Rencoret, J.; Marques, G.; Gutiérrez, A.; Ibarra, D.; Santos, J. I.; Jiménez-Barbero, J.; Zhang, L.; Martínez, A. T., Highly acylated (acetylated and/or *p*-coumaroylated) native lignins from diverse herbaceous plants. *J Agric Food Chem* **2008**, *56*, 9525-9534.
34. Ralph, J., Hydroxycinnamates in lignification. *Phytochem Rev* **2010**, *9*, 65-83.
35. Lu, F.; Ralph, J., Novel tetrahydrofuran structures derived from β - β -coupling reactions involving sinapyl acetate in Kenaf lignins. *Org Biomol Chem* **2008**, *6*, 3681-3694.
36. Del Río, J. C.; Lino, A. G.; Colodette, J. L.; Lima, C. F.; Gutiérrez, A.; Martínez, Á. T.; Lu, F.; Ralph, J.; Rencoret, J., Differences in the chemical structure of the lignins from sugarcane bagasse and straw. *Biomass Bioenergy* **2015**, *81*, 322-338.
37. Hatfield, R.; Ralph, J.; Grabber, J. H., A potential role for sinapyl *p*-coumarate as a radical transfer mechanism in grass lignin formation. *Planta* **2008**, *228*, 919.
38. Del Río, J. C.; Rencoret, J.; Gutiérrez, A.; Kim, H.; Ralph, J., Hydroxystilbenes are monomers in palm fruit endocarp lignins. *Plant Physiol* **2017**, *174*, 2072-2082.

39. Rencoret, J.; Neiva, D.; Marques, G.; Gutiérrez, A.; Kim, H.; Gominho, J.; Pereira, H.; Ralph, J.; del Río, J. C., Hydroxystilbene glucosides are incorporated into Norway spruce bark lignin. *Plant Physiol* **2019**, *180*, 1310-1321.
40. Del Río, J. C.; Rencoret, J.; Gutiérrez, A.; Kim, H.; Ralph, J., Structural characterization of lignin from maize (*Zea mays* L.) fibers: evidence for diferuloylputrescine incorporated into the lignin polymer in maize kernels. *J Agric Food Chem* **2018**, *66*, 4402-4413.
41. Lan, W.; Rencoret, J.; Lu, F.; Karlen, S. D.; Smith, B. G.; Harris, P. J.; Río, J. C.; Ralph, J., Tricin-lignins: occurrence and quantitation of tricin in relation to phylogeny. *Plant J* **2016**, *88*, 1046-1057.
42. Lan, W.; Lu, F.; Regner, M.; Zhu, Y.; Rencoret, J.; Ralph, S. A.; Zakai, U. I.; Morreel, K.; Boerjan, W.; Ralph, J., Tricin, a flavonoid monomer in monocot lignification. *Plant Physiol* **2015**, *167*, 1284-1295.
43. Lan, W.; Morreel, K.; Lu, F.; Rencoret, J.; del Río, J. C.; Voorend, W.; Vermerris, W.; Boerjan, W.; Ralph, J., Maize tricin-oligolignol metabolites and their implications for monocot lignification. *Plant Physiol* **2016**, *171*, 810-820.
44. Ralph, J.; Grabber, J. H.; Hatfield, R. D., Lignin-ferulate cross-links in grasses: active incorporation of ferulate polysaccharide esters into ryegrass lignins. *Carbohydr Res* **1995**, *275*, 167-178.
45. Tobimatsu, Y.; Schuetz, M., Lignin polymerization: how do plants manage the chemistry so well? *Curr Opin Biotechnol* **2019**, *56*, 75-81.
46. Giummarella, N.; Pu, Y.; Ragauskas, A. J.; Lawoko, M., A critical review on the analysis of lignin carbohydrate bonds. *Green Chem* **2019**, *21*, 1573-1595.
47. Takahashi, N.; Koshijima, T., Ester linkages between lignin and glucuronoxylan in a lignin-carbohydrate complex from beech (*Fagus crenata*) wood. *Wood Sci Technol* **1988**, *22*, 231-241.
48. Balakshin, M. Y.; Capanema, E. A.; Chang, H.-m., MWL fraction with a high concentration of lignin-carbohydrate linkages: Isolation and 2D NMR spectroscopic analysis. *Holzforschung* **2007**, *61*, 1-7.
49. Balakshin, M.; Capanema, E.; Berlin, A., Isolation and analysis of lignin-carbohydrate complexes preparations with traditional and advanced methods: a review. In *Studies in Natural Products Chemistry*, Atta-ur-Rahman, Ed. Elsevier: Amsterdam, The Netherlands, 2014; Vol. 42, pp 83-115.
50. Yuan, T.-Q.; Sun, S.-N.; Xu, F.; Sun, R.-C., Characterization of lignin structures and lignin-carbohydrate complex (LCC) linkages by quantitative ¹³C and 2D HSQC NMR spectroscopy. *J Agric Food Chem* **2011**, *59*, 10604-10614.
51. Xie, Y.; Yasuda, S.; Wu, H.; Liu, H., Analysis of the structure of lignin-carbohydrate complexes by the specific ¹³C tracer method. *J Wood Sci* **2000**, *46*, 130-136.
52. Nishimura, H.; Kamiya, A.; Nagata, T.; Katahira, M.; Watanabe, T., Direct evidence for a ether linkage between lignin and carbohydrates in wood cell walls. *Sci Rep* **2018**, *8*, 6538.
53. Iiyama, K.; Lam, T. B.-T.; Stone, B. A., Covalent cross-links in the cell wall. *Plant Physiol* **1994**, *104*, 315.
54. Ishii, T., Structure and functions of feruloylated polysaccharides. *Plant Sci* **1997**, *127*, 111-127.
55. Ralph, J.; Bunzel, M.; Marita, J. M.; Hatfield, R. D.; Lu, F.; Kim, H.; Schatz, P. F.; Grabber, J. H.; Steinhart, H., Peroxidase-dependent cross-linking reactions of *p*-hydroxycinnamates in plant cell walls. *Phytochem Rev* **2004**, *3*, 79-96.
56. Ralph, J.; Helm, R. F.; Quideau, S.; Hatfield, R. D., Lignin-feruloyl ester cross-links in grasses. Part 1. Incorporation of feruloyl esters into coniferyl alcohol dehydrogenation polymers. *J Chem Soc Perkin Trans 1* **1992**, 2961-2969.
57. Lam, T.; Kadoya, K.; Iiyama, K., Bonding of hydroxycinnamic acids to lignin: ferulic and *p*-coumaric acids are predominantly linked at the benzyl position of lignin, not the β -position, in grass cell walls. *Phytochemistry* **2001**, *57*, 987-992.
58. Vismeh, R.; Lu, F.; Chundawat, S. P.; Humpala, J. F.; Azarpira, A.; Balan, V.; Dale, B. E.; Ralph, J.; Jones, A. D., Profiling of diferulates (plant cell wall cross-

- linkers) using ultrahigh-performance liquid chromatography-tandem mass spectrometry. *Analyst* **2013**, *138*, 6683-6692.
59. Vermaas, J. V.; Petridis, L.; Qi, X.; Schulz, R.; Lindner, B.; Smith, J. C., Mechanism of lignin inhibition of enzymatic biomass deconstruction. *Biotechnol Biofuels* **2015**, *8*, 217.
 60. Behera, S.; Arora, R.; Nandhagopal, N.; Kumar, S., Importance of chemical pretreatment for bioconversion of lignocellulosic biomass. *Renewable and Sustainable Energy Rev* **2014**, *36*, 91-106.
 61. Isikgor, F. H.; Becer, C. R., Lignocellulosic biomass: a sustainable platform for the production of bio-based chemicals and polymers. *Polym Chem* **2015**, *6*, 4497-4559.
 62. Van Kuijk, S. J. A.; Sonnenberg, A. S. M.; Baars, J. J. P.; Hendriks, W. H.; Cone, J. W., Fungal treated lignocellulosic biomass as ruminant feed ingredient: a review. *Biotechnol Adv* **2015**, *33*, 191-202.
 63. Harmsen, P.; Huijgen, W.; Bermudez, L.; Bakker, R. *Literature review of physical and chemical pretreatment processes for lignocellulosic biomass*; 9085857570; Wageningen UR-Food & Biobased Research: 2010.
 64. Hendriks, A.; Zeeman, G., Pretreatments to enhance the digestibility of lignocellulosic biomass. *Bioresour Technol* **2009**, *100*, 10-18.
 65. Mosier, N.; Wyman, C.; Dale, B.; Elander, R.; Lee, Y.; Holtzapple, M.; Ladisch, M., Features of promising technologies for pretreatment of lignocellulosic biomass. *Bioresour Technol* **2005**, *96*, 673-686.
 66. Da Costa Sousa, L.; Chundawat, S. P.; Balan, V.; Dale, B. E., 'Cradle-to-grave' assessment of existing lignocellulose pretreatment technologies. *Curr Opin Biotechnol* **2009**, *20*, 339-347.
 67. Bugg, T. D.; Ahmad, M.; Hardiman, E. M.; Rahmanpour, R., Pathways for degradation of lignin in bacteria and fungi. *Nat Prod Rep* **2011**, *28*, 1883-1896.
 68. Hammel, K. E., Fungal degradation of lignin. In *Driven by nature: plant litter quality and decomposition*, Cadish, G.; Giller, K. E., Eds. CAB-International: Wallingford, 1997; pp 33-47.
 69. Martínez, A. T.; Speranza, M.; Ruiz-Dueñas, F. J.; Ferreira, P.; Camarero, S.; Guillén, F.; Martínez, M. J.; Gutiérrez, A.; del Río, J. C., Biodegradation of lignocellulosics: microbial, chemical, and enzymatic aspects of the fungal attack of lignin. *Int Microbiol* **2005**, *8*, 195-204.
 70. Martínez, A. T.; Rencoret, J.; Nieto, L.; Jiménez-Barbero, J.; Gutiérrez, A.; del Río, J. C., Selective lignin and polysaccharide removal in natural fungal decay of wood as evidenced by *in situ* structural analyses. *Environ Microbiol* **2011**, *13*, 96-107.
 71. Yelle, D. J.; Wei, D.; Ralph, J.; Hammel, K. E., Multidimensional NMR analysis reveals truncated lignin structures in wood decayed by the brown rot basidiomycete *Postia placenta*. *Environ Microbiol* **2011**, *13*, 1091-1100.
 72. Martínez, A. T.; Ruiz-Dueñas, F. J.; Martínez, M. J.; del Río, J. C.; Gutiérrez, A., Enzymatic delignification of plant cell wall: from nature to mill. *Curr Opin Biotechnol* **2009**, *20*, 348-357.
 73. Tian, X. f.; Fang, Z.; Guo, F., Impact and prospective of fungal pre-treatment of lignocellulosic biomass for enzymatic hydrolysis. *Biofuels Bioprod Biorefin* **2012**, *6*, 335-350.
 74. Sindhu, R.; Binod, P.; Pandey, A., Biological pretreatment of lignocellulosic biomass—An overview. *Bioresour Technol* **2016**, *199*, 76-82.
 75. Otjen, L.; Blanchette, R.; Effland, M.; Leatham, G., Assessment of 30 white rot basidiomycetes for selective lignin degradation. *Holzforschung* **1987**, *41*, 343-349.
 76. Salvachúa, D.; Prieto, A.; López-Abelairas, M.; Lu-Chau, T.; Martínez, Á. T.; Martínez, M. J., Fungal pretreatment: an alternative in second-generation ethanolol from wheat straw. *Bioresour Technol* **2011**, *102*, 7500-7506.

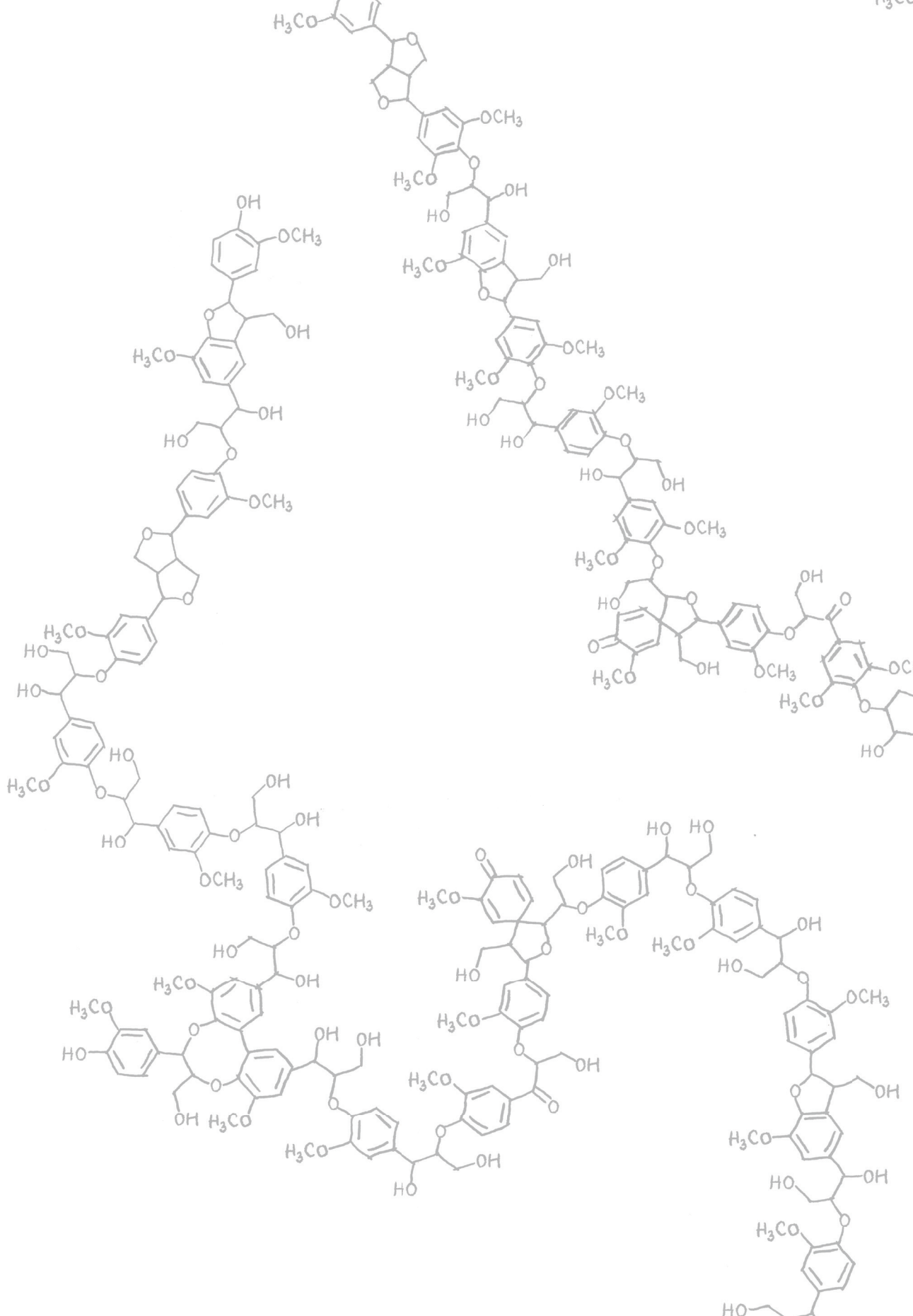
77. Zeng, J.; Singh, D.; Gao, D.; Chen, S., Effects of lignin modification on wheat straw cell wall deconstruction by *Phanerochaete chrysosporium*. *Biotechnol Biofuels* **2014**, *7*, 161.
78. Tuyen, V.; Cone, J.; Baars, J.; Sonnenberg, A.; Hendriks, W., Fungal strain and incubation period affect chemical composition and nutrient availability of wheat straw for rumen fermentation. *Bioresour Technol* **2012**, *111*, 336-342.
79. Wan, C.; Li, Y., Fungal pretreatment of lignocellulosic biomass. *Biotechnol Adv* **2012**, *30*, 1447-1457.
80. Hatakka, A., Lignin-modifying enzymes from selected white-rot fungi: production and role in lignin degradation. *FEMS Microbiol Rev* **1994**, *13*, 125-135.
81. Martinez, D.; Larrondo, L. F.; Putnam, N.; Gelpke, M. D. S.; Huang, K.; Chapman, J.; Helfenbein, K. G.; Ramaiya, P.; Detter, J. C.; Larimer, F., Genome sequence of the lignocellulose degrading fungus *Phanerochaete chrysosporium* strain RP78. *Nat Biotechnol* **2004**, *22*, 695-700.
82. Fernández-Fueyo, E.; Ruiz-Dueñas, F. J.; Ferreira, P.; Floudas, D.; Hibbett, D. S.; Canessa, P.; Larrondo, L. F.; James, T. Y.; Seelenfreund, D.; Lobos, S.; Polanco, R.; Tello, M.; Honda, Y.; Watanabe, T.; Watanabe, T.; Ryu, J. S.; Kubicek, C. P.; Schmoll, M.; Gaskell, J.; Hammel, K. E.; St. John, F. J.; Vanden Wymelenberg, A.; Sabat, G.; Splinter Bondurant, S.; Khajamohiddin, S.; Jagit, Y. S.; Doppapaneni, H.; Subramanian, V.; José, L. L.; Oguiza, J. A.; Perez, G.; Pisabarro, A. G.; Ramirez, L.; Santoyo, F.; Master, E.; Coutinho, P. M.; Henrissat, B.; Lombard, V.; Magnuson, J. K.; Kues, U.; Hori, C.; Igarashi, K.; Samejima, M.; Held, B. W.; Barry, K. W.; Labutti, K. M.; Lapidus, A.; Lindquist, E. A.; Lucas, S. M.; Riley, R.; Salamov, A. A.; Hoffmeister, D.; Schwenk, D.; Hadar, Y.; Yarden, O.; de Vries, R. P.; Wiebenga, A.; Stenlid, J.; Eastwood, D.; Grigoriev, I. V.; Berka, R. M.; Blanchette, R. A.; Kersten, P.; Martínez, A. T.; Vicuna, R.; Cullen, D., Comparative genomics of *Ceriporiopsis subvermispora* and *Phanerochaete chrysosporium* provide insight into selective ligninolysis. *Proc Natl Acad Sci* **2012**, *109*, 5458-5463.
83. Kirk, T. K.; Tien, M.; Kersten, P. J.; Mozuch, M. D.; Kalyanaraman, B., Ligninase of *Phanerochaete chrysosporium*. Mechanism of its degradation of the non-phenolic arylglycerol β -aryl ether substructure of lignin. *Biochem J* **1986**, *236*, 279-287.
84. Hammel, K. E.; Cullen, D., Role of fungal peroxidases in biological ligninolysis. *Curr Opin Plant Biol* **2008**, *11*, 349-355.
85. Sáez-Jiménez, V.; Rencoret, J.; Rodríguez-Carvajal, M. A.; Gutiérrez, A.; Ruiz-Dueñas, F. J.; Martínez, A. T., Role of surface tryptophan for peroxidase oxidation of nonphenolic lignin. *Biotechnol Biofuels* **2016**, *9*, 198.
86. Mester, T.; Ambert-Balay, K.; Ciofi-Baffoni, S.; Banci, L.; Jones, A. D.; Tien, M., Oxidation of a tetrameric nonphenolic lignin model compound by lignin peroxidase. *J Biol Chem* **2001**, *276*, 22985-22990.
87. Srebotnik, E.; Messner, K.; Foisner, R., Penetrability of white rot-degraded pine wood by the lignin peroxidase of *Phanerochaete chrysosporium*. *Appl Environ Microbiol* **1988**, *54*, 2608-2614.
88. Blanchette, R. A.; Krueger, E. W.; Haight, J. E.; Akhtar, M.; Akin, D. E., Cell wall alterations in loblolly pine wood decayed by the white-rot fungus *Ceriporiopsis subvermispora*. *J Biotechnol* **1997**, *53*, 203-213.
89. Houtman, C. J.; Maligaspe, E.; Hunt, C. G.; Fernández-Fueyo, E.; Martínez, A. T.; Hammel, K. E., Fungal lignin peroxidase does not produce the veratryl alcohol cation radical as a diffusible ligninolytic oxidant. *J Biol Chem* **2018**, *293*, 4702-4712.
90. Hofrichter, M., Review: lignin conversion by manganese peroxidase (MnP). *Enzyme Microb Technol* **2002**, *30*, 454-466.
91. Kapich, A. N.; Jensen, K. A.; Hammel, K. E., Peroxyl radicals are potential agents of lignin biodegradation. *FEBS Lett* **1999**, *461*, 115-119.
92. Kapich, A. N.; Korneichik, T. V.; Hatakka, A.; Hammel, K. E., Oxidizability of unsaturated fatty acids and of a non-phenolic lignin structure in the manganese

- peroxidase-dependent lipid peroxidation system. *Enzyme Microb Technol* **2010**, *46*, 136-140.
93. Nishimura, H.; Sasaki, M.; Seike, H.; Nakamura, M.; Watanabe, T., Alkadienyl and alkenyl itaconic acids (ceriporic acids G and H) from the selective white-rot fungus *Ceriporiopsis subvermispora*: a new class of metabolites initiating ligninolytic lipid peroxidation. *Org Biomol Chem* **2012**, *10*, 6432-6442.
94. Perez-Boada, M.; Ruiz-Duenas, F. J.; Pogni, R.; Basosi, R.; Choinowski, T.; Martínez, M. J.; Piontek, K.; Martínez, A. T., Versatile peroxidase oxidation of high redox potential aromatic compounds: site-directed mutagenesis, spectroscopic and crystallographic investigation of three long-range electron transfer pathways. *J Mol Biol* **2005**, *354*, 385-402.
95. Munk, L.; Sitarz, A. K.; Kalyani, D. C.; Mikkelsen, J. D.; Meyer, A. S., Can laccases catalyze bond cleavage in lignin? *Biotechnol Adv* **2015**, *33*, 13-24.
96. Couto, S. R.; Herrera, J. L. T., Industrial and biotechnological applications of laccases: a review. *Biotechnol Adv* **2006**, *24*, 500-513.
97. Hernández-Ortega, A.; Ferreira, P.; Martínez, A. T., Fungal aryl-alcohol oxidase: a peroxide-producing flavoenzyme involved in lignin degradation. *Appl Microbiol Biotech* **2012**, *93*, 1395-1410.
98. Li, Y.; Demir, B.; Ramos, L. M. V.; Chen, M.; Dumesic, J. A.; Ralph, J., Kinetic and mechanistic insights into hydrogenolysis of lignin to monomers in a continuous flow reactor. *Green Chem* **2019**, *21*, 3561-3572.
99. Lahive, C. W.; Deuss, P. J.; Lancefield, C. S.; Sun, Z.; Cordes, D. B.; Young, C. M.; Tran, F.; Slawin, A. M.; de Vries, J. G.; Kamer, P. C., Advanced model compounds for understanding acid-catalyzed lignin depolymerization: identification of renewable aromatics and a lignin-derived solvent. *J Am Chem Soc* **2016**, *138*, 8900-8911.
100. Hilgers, R.; Vincken, J.-P.; Gruppen, H.; Kabel, M. A., Laccase/mediator systems: their reactivity toward phenolic lignin structures. *ACS Sustainable Chem Eng* **2018**, *6*, 2037-2046.
101. Hilgers, R.; Twentyman-Jones, M.; Van Dam, A.; Gruppen, H.; Zuilhof, H.; Kabel, M. A.; Vincken, J.-P., The impact of lignin sulfonation on its reactivity with laccase and laccase/HBT. *Catal Sci Technol* **2019**, *9*, 1535-1542.
102. Baiocco, P.; Barreca, A. M.; Fabbrini, M.; Galli, C.; Gentili, P., Promoting laccase activity towards non-phenolic substrates: a mechanistic investigation with some laccase-mediator systems. *Org Biomol Chem* **2003**, *1*, 191-197.
103. Srebotnik, E.; Jensen, K.; Kawai, S.; Hammel, K. E., Evidence that *Ceriporiopsis subvermispora* degrades nonphenolic lignin structures by a one-electron-oxidation mechanism. *Appl Environ Microbiol* **1997**, *63*, 4435-4440.
104. Kawai, S.; Nakagawa, M.; Ohashi, H., Degradation mechanisms of a nonphenolic β -O-4 lignin model dimer by *Trametes versicolor* laccase in the presence of 1-hydroxybenzotriazole. *Enzyme Microb Technol* **2002**, *30*, 482-489.
105. Umezawa, T.; Higuchi, T., Aromatic ring cleavage of β -O-4 lignin model dimers without prior demeth(ox)ylation by lignin peroxidase. *FEBS Lett* **1986**, *205*, 293-298.
106. Kapich, A. N.; Steffen, K. T.; Hofrichter, M.; Hatakka, A., Involvement of lipid peroxidation in the degradation of a non-phenolic lignin model compound by manganese peroxidase of the litter-decomposing fungus *Stropharia coronilla*. *Biochem Biophys Res Commun* **2005**, *330*, 371-377.
107. Jensen, K. A.; Bao, W.; Kawai, S.; Srebotnik, E.; Hammel, K. E., Manganese-dependent cleavage of nonphenolic lignin structures by *Ceriporiopsis subvermispora* in the absence of lignin peroxidase. *Appl Environ Microbiol* **1996**, *62*, 3679-3686.
108. Mäkelä, M. R.; Marinović, M.; Nousiainen, P.; Liwanag, A. J.; Benoit, I.; Sipilä, J.; Hatakka, A.; de Vries, R. P.; Hildén, K. S., Aromatic metabolism of filamentous fungi in relation to the presence of aromatic compounds in plant biomass. In *Advances in applied microbiology*, Elsevier: 2015; Vol. 91, pp 63-137.

109. Lin, S. Y.; Dence, C. W., *Methods in lignin chemistry*. Springer: Berlin, Heidelberg, Germany, 2012.
110. Brunow, G., Methods to reveal the structure of lignin. *Biopolymers Online* **2005**.
111. Lupoi, J. S.; Singh, S.; Parthasarathi, R.; Simmons, B. A.; Henry, R. J., Recent innovations in analytical methods for the qualitative and quantitative assessment of lignin. *Renewable and Sustainable Energy Rev* **2015**, *49*, 871-906.
112. Hatfield, R.; Fukushima, R. S., Can lignin be accurately measured? *Crop Sci* **2005**, *45*, 832-839.
113. Sluiter, J. B.; Ruiz, R. O.; Scarlata, C. J.; Sluiter, A. D.; Templeton, D. W., Compositional analysis of lignocellulosic feedstocks. 1. Review and description of methods. *J Agric Food Chem* **2010**, *58*, 9043-9053.
114. Dence, C. W., The determination of lignin. In *Methods in lignin chemistry*, Lin, S. Y.; Dence, C. W., Eds. Springer: Berlin, Heidelberg, Germany, 1992; pp 33-61.
115. Van Soest, P. v.; Robertson, J.; Lewis, B., Methods for dietary fiber, neutral detergent fiber, and nonstarch polysaccharides in relation to animal nutrition. *J Dairy Sci* **1991**, *74*, 3583-3597.
116. Kaar, W. E.; Brink, D. L., Simplified analysis of acid soluble lignin. *J Wood Chem Technol* **1991**, *11*, 465-477.
117. Hatfield, R. D.; Jung, H. J. G.; Ralph, J.; Buxton, D. R.; Weimer, P. J., A comparison of the insoluble residues produced by the Klason lignin and acid detergent lignin procedures. *J Sci Food Agric* **1994**, *65*, 51-58.
118. Jung, H.-J. G.; Varel, V. H.; Weimer, P. J.; Ralph, J., Accuracy of Klason lignin and acid detergent lignin methods as assessed by bomb calorimetry. *J Agric Food Chem* **1999**, *47*, 2005-2008.
119. Hatfield, R.; Grabber, J.; Ralph, J.; Brei, K., Using the acetyl bromide assay to determine lignin concentrations in herbaceous plants: some cautionary notes. *J Agric Food Chem* **1999**, *47*, 628-632.
120. Moreira-Vilar, F. C.; de Cássia Siqueira-Soares, R.; Finger-Teixeira, A.; de Oliveira, D. M.; Ferro, A. P.; da Rocha, G. J.; Maria de Lourdes, L. F.; dos Santos, W. D.; Ferrarese-Filho, O., The acetyl bromide method is faster, simpler and presents best recovery of lignin in different herbaceous tissues than Klason and thioglycolic acid methods. *PloS one* **2014**, *9*, e110000.
121. Morreel, K.; Kim, H.; Lu, F.; Dima, O.; Akiyama, T.; Vanholme, R.; Niculaes, C.; Goeminne, G.; Inze, D.; Messens, E., Mass spectrometry-based fragmentation as an identification tool in lignomics. *Anal Chem* **2010**, *82*, 8095-8105.
122. Bowman, A. S.; Asare, S. O.; Lynn, B. C., Matrix-assisted laser desorption/ionization time-of-flight mass spectrometry analysis for characterization of lignin oligomers using cationization techniques and 2,5-dihydroxyacetophenone (DHAP) matrix. *Rapid Commun Mass Spectrom* **2019**, *33*, 811-819.
123. Kim, H.; Ralph, J.; Akiyama, T., Solution-state 2D NMR of ball-milled plant cell wall gels in DMSO- d_6 . *BioEnergy Res* **2008**, *1*, 56-66.
124. Ralph, J.; Landucci, L. L., NMR of Lignins. In *Lignin and Lignans: Advances in Chemistry*, Heithner, C.; Dimmel, D.; Schmidt, J. A., Eds. CRC Pres, Taylor & Francis: Boca Raton, FL, USA, 2010; pp 137-244.
125. Mansfield, S. D.; Kim, H.; Lu, F.; Ralph, J., Whole plant cell wall characterization using solution-state 2D NMR. *Nat Protoc* **2012**, *7*, 1579-1589.
126. Crestini, C.; Argyropoulos, D. S., Structural analysis of wheat straw lignin by quantitative ^{31}P and 2D NMR spectroscopy. The occurrence of ester bonds and α -O-4 substructures. *J Agric Food Chem* **1997**, *45*, 1212-1219.
127. Gosselink, R. J. A.; van Dam, J. E. G.; de Jong, E.; Scott, E. L.; Sanders, J. P. M.; Li, J.; Gellerstedt, G., Fractionation, analysis, and PCA modeling of properties of four technical lignins for prediction of their application potential in binders. *Holzforschung* **2010**, *64*, 193-200.
128. Meng, X.; Crestini, C.; Ben, H.; Hao, N.; Pu, Y.; Ragauskas, A. J.; Argyropoulos, D. S., Determination of hydroxyl groups in biorefinery resources via quantitative ^{31}P NMR spectroscopy. *Nat Protoc* **2019**, *14*, 2627-2647.

129. Constant, S.; Wienk, H. L. J.; Frissen, A. E.; de Peinder, P.; Boelens, R.; Van Es, D. S.; Grisel, R. J. H.; Weckhuysen, B. M.; Huijgen, W. J. J.; Gosselink, R. J. A., New insights into the structure and composition of technical lignins: a comparative characterisation study. *Green Chem* **2016**, *18*, 2651-2665.
130. Tolbert, A.; Akinoshio, H.; Khunsupat, R.; Naskar, A. K.; Ragauskas, A. J., Characterization and analysis of the molecular weight of lignin for biorefining studies. *Biofuels Bioprod Biorefin* **2014**, *8*, 836-856.
131. Sulaeva, I.; Zinovyev, G.; Plankeele, J. M.; Sumerskii, I.; Rosenau, T.; Potthast, A., Fast track to molar-mass distributions of technical lignins. *ChemSusChem* **2017**, *10*, 629-635.
132. Ralph, J.; Hatfield, R. D., Pyrolysis-GC-MS characterization of forage materials. *J Agric Food Chem* **1991**, *39*, 1426-1437.
133. Camarero, S.; Galletti, G. C.; Martinez, A. T., Preferential degradation of phenolic lignin units by two white rot fungi. *Appl Environ Microbiol* **1994**, *60*, 4509-4516.
134. Rencoret, J.; del Río, J. C.; Nierop, K. G.; Gutiérrez, A.; Ralph, J., Rapid Py-GC/MS assessment of the structural alterations of lignins in genetically modified plants. *J Anal Appl Pyrolysis* **2016**, *121*, 155-164.
135. Faix, O.; Bremer, J.; Schmidt, O.; Tatjana, S. J., Monitoring of chemical changes in white-rot degraded beech wood by pyrolysis-gas chromatography and Fourier-transform infrared spectroscopy. *J Anal Appl Pyrolysis* **1991**, *21*, 147-162.
136. Faix, O., Classification of lignins from different botanical origins by FT-IR spectroscopy. *Holzforschung* **1991**, *45*, 21-28.
137. Boeriu, C. G.; Bravo, D.; Gosselink, R. J. A.; van Dam, J. E. G., Characterisation of structure-dependent functional properties of lignin with infrared spectroscopy. *Ind Crops Prod* **2004**, *20*, 205-218.
138. Lu, F.; Ralph, J., Derivatization followed by reductive cleavage (DFRC method), a new method for lignin analysis: protocol for analysis of DFRC monomers. *J Agric Food Chem* **1997**, *45*, 2590-2592.
139. Karlen, S. D.; Smith, R. A.; Kim, H.; Padmakshan, D.; Bartuce, A.; Mobley, J. K.; Free, H. C.; Smith, B. G.; Harris, P. J.; Ralph, J., Highly decorated lignins in leaf tissues of the Canary Island date palm *Phoenix canariensis*. *Plant Physiol* **2017**, *175*, 1058-1067.
140. Regner, M.; Bartuce, A.; Padmakshan, D.; Ralph, J.; Karlen, S. D., Reductive cleavage method for quantitation of monolignols and low-abundance monolignol conjugates. *ChemSusChem* **2018**, *11*, 1600-1605.
141. Hu, K.; Westler, W. M.; Markley, J. L., Simultaneous quantification and identification of individual chemicals in metabolite mixtures by two-dimensional extrapolated time-zero ^1H - ^{13}C HSQC (HSQC₀). *J Am Chem Soc* **2011**, *133*, 1662-1665.
142. Okamura, H.; Nishimura, H.; Nagata, T.; Kigawa, T.; Watanabe, T.; Katahira, M., Accurate and molecular-size-tolerant NMR quantitation of diverse components in solution. *Sci Rep* **2016**, *6*, 21742.
143. Lancefield, C. S.; Wienk, H. L.; Boelens, R.; Weckhuysen, B. M.; Bruijninx, P. C., Identification of a diagnostic structural motif reveals a new reaction intermediate and condensation pathway in kraft lignin formation. *Chem Sci* **2018**, *9*, 6348-6360.
144. Capanema, E.; Balakshin, M.; Katahira, R.; Chang, H.-M.; Jameel, H., How well do MWL and CEL preparations represent the whole hardwood lignin? *J Wood Chem Technol* **2015**, *35*, 17-26.
145. Guerra, A.; Filpponen, I.; Lucia, L. A.; Saquing, C.; Baumberger, S.; Argyropoulos, D. S., Toward a better understanding of the lignin isolation process from wood. *J Agric Food Chem* **2006**, *54*, 5939-5947.
146. Björkman, A., Studies on finely divided wood. Part 1. Extraction of lignin with neutral solvents. *Sven Papperstidn* **1956**, *59*, 477-485.
147. Chang, H.-M.; Cowling, E. B.; Brown, W., Comparative studies on cellulolytic enzyme lignin and milled wood lignin of sweetgum and spruce. *Holzforschung* **1975**, *29*, 153-159.

148. Fujimoto, A.; Matsumoto, Y.; Chang, H.-M.; Meshitsuka, G., Quantitative evaluation of milling effects on lignin structure during the isolation process of milled wood lignin. *J Wood Sci* **2005**, *51*, 89-91.
149. Zinovyev, G.; Sumerskii, I.; Rosenau, T.; Balakshin, M.; Potthast, A., Ball milling's effect on pine milled wood lignin's structure and molar mass. *Molecules* **2018**, *23*, 2223.
150. Lange, H.; Rulli, F.; Crestini, C., Gel permeation chromatography in determining molecular weights of lignins: critical aspects revisited for improved utility in the development of novel materials. *ACS Sustainable Chem Eng* **2016**, *4*, 5167-5180.
151. Zinovyev, G.; Sulaeva, I.; Podzimek, S.; Rössner, D.; Kilpeläinen, I.; Sumerskii, I.; Rosenau, T.; Potthast, A., Getting closer to absolute molar masses of technical lignins. *ChemSusChem* **2018**, *11*, 3259-3268.
152. Kim, H.; Padmakshan, D.; Li, Y.; Rencoret, J.; Hatfield, R. D.; Ralph, J., Characterization and elimination of undesirable protein residues in plant cell wall materials for enhancing lignin analysis by solution-state nuclear magnetic resonance spectroscopy. *Biomacromolecules* **2017**, *18*, 4184-4195.
153. Bridgwater, A.; Peacocke, G., Fast pyrolysis processes for biomass. *Renewable and Sustainable Energy Rev* **2000**, *4*, 1-73.
154. Faix, O.; Meier, D.; Grobe, I., Studies on isolated lignins and lignins in woody materials by pyrolysis-gas chromatography-mass spectrometry and off-line pyrolysis-gas chromatography with flame ionization detection. *J Anal Appl Pyrolysis* **1987**, *11*, 403-416.
155. Patwardhan, P. R.; Brown, R. C.; Shanks, B. H., Understanding the fast pyrolysis of lignin. *ChemSusChem* **2011**, *4*, 1629-1636.
156. Hu, J.; Shen, D.; Xiao, R.; Wu, S.; Zhang, H., Free-radical analysis on thermochemical transformation of lignin to phenolic compounds. *Energy Fuels* **2012**, *27*, 285-293.
157. Jurak, E.; Punt, A. M.; Arts, W.; Kabel, M. A.; Gruppen, H., Fate of carbohydrates and lignin during composting and mycelium growth of *Agaricus bisporus* on wheat straw based compost. *PLoS One* **2015**, *10*, e0138909.
158. Del Río, J.; Martín, F.; Gonzalez-Vila, F., Thermally assisted hydrolysis and alkylation as a novel pyrolytic approach for the structural characterization of natural biopolymers and geomacromolecules. *TrAC Trends Anal Chem* **1996**, *15*, 70-79.
159. Del Río, J. C.; Gutiérrez, A.; Rodríguez, I. M.; Ibarra, D.; Martínez, A. T., Composition of non-woody plant lignins and cinnamic acids by Py-GC/MS, Py/TMAH and FT-IR. *J Anal Appl Pyrolysis* **2007**, *79*, 39-46.
160. Alves, A.; Schwanninger, M.; Pereira, H.; Rodrigues, J., Analytical pyrolysis as a direct method to determine the lignin content in wood: Part 1: Comparison of pyrolysis lignin with Klason lignin. *J Anal Appl Pyrolysis* **2006**, *76*, 209-213.
161. Alves, A.; Rodrigues, J.; Wimmer, R.; Schwanninger, M., Analytical pyrolysis as a direct method to determine the lignin content in wood: Part 2: Evaluation of the common model and the influence of compression wood. *J Anal Appl Pyrolysis* **2008**, *81*, 167-172.
162. Lourenço, A.; Gominho, J.; Marques, A. V.; Pereira, H., Comparison of Py-GC/FID and wet chemistry analysis for lignin determination in wood and pulps from *Eucalyptus globulus*. *BioResources* **2013**, *8*, 2967-2980.
163. Bocchini, P.; Galletti, G.; Camarero, S.; Martinez, A., Absolute quantitation of lignin pyrolysis products using an internal standard. *J Chromatogr A* **1997**, *773*, 227-232.
164. Torri, C.; Adamiano, A.; Fabbri, D.; Lindfors, C.; Monti, A.; Oasmaa, A., Comparative analysis of pyrolysate from herbaceous and woody energy crops by Py-GC with atomic emission and mass spectrometric detection. *J Anal Appl Pyrolysis* **2010**, *88*, 175-180.
165. Groenewold, G. S.; Johnson, K. M.; Fox, S. C.; Rae, C.; Zarzana, C. A.; Kersten, B. R.; Rowe, S. M.; Westover, T. L.; Gresham, G. L.; Emerson, R. M., Pyrolysis two-dimensional GC-MS of *Miscanthus* biomass: Quantitative measurement using an internal standard method. *Energy Fuels* **2017**, *31*, 1620-1630.



The background of the slide is filled with various chemical structures of lignin, which are complex polymers of aromatic units linked by oxygen-containing bonds. These structures are rendered in a light gray color, providing a scientific context for the chapter title.

CHAPTER 2

Quantification of lignin and its structural features in plant biomass using ^{13}C lignin as internal standard for pyrolysis-GC-SIM-MS

Gijs van Erven, Ries de Visser, Donny W. H. Merkx,

Willem Strolenberg, Peter de Gijssel

Harry Gruppen, Mirjam A. Kabel

Based on: Analytical Chemistry, 2017, 89, 10907-10916

Abstract

Understanding mechanisms underlying plant biomass recalcitrance at molecular level can only be achieved by accurate analyses of both content and structural features of the molecules involved. Current quantification of lignin is, however, majorly based on unspecific gravimetric analysis after sulfuric acid hydrolysis. Hence, our research aimed at specific lignin quantification with concurrent characterization of its structural features. Hereto, for the first time, a polymeric ^{13}C lignin was used as internal standard (IS) for lignin quantification via analytical pyrolysis coupled to gas chromatography with mass-spectrometric detection in selected ion monitoring mode (py-GC-SIM-MS). In addition, relative response factors (RRFs) for the various pyrolysis products obtained were determined and applied. First, ^{12}C and ^{13}C lignin were isolated from nonlabeled and uniformly ^{13}C labeled wheat straw, respectively, and characterized by heteronuclear single quantum coherence (HSQC) nuclear magnetic resonance (NMR) and py-GC-MS. The two lignin isolates were found to have identical structures. Second, ^{13}C -IS based lignin quantification by py-GC-SIM-MS was validated in reconstituted biomass model systems with known contents of the ^{12}C lignin analogue and was shown to be extremely accurate ($>99.9\%$, $R^2>0.999$) and precise ($\text{RSD} < 1.5\%$). Third, ^{13}C -IS based lignin quantification was applied to four common poaceous biomass sources (wheat straw, barley straw, corn stover and sugarcane bagasse) and lignin contents were in good agreement with the total gravimetrically determined lignin contents. Our robust method proves to be a promising alternative for the high-throughput quantification of lignin in milled biomass samples directly and simultaneously provides a direct insight into the structural features of lignin.

Introduction

Understanding and improving the conversion of plant biomass heavily depends on the characterization and quantification of its constituents. The major constituents of poaceous plant biomasses are cellulose (30-50% (w/w)), hemicellulose (mainly xylan, 20-40% (w/w)) and lignin (5-25% (w/w)).¹ Cellulose and xylan are polysaccharides and lignin is a cross-linked phenolic macromolecule, which is composed of *p*-hydroxyphenyl (H), guaiacyl (G) and syringyl (S) subunits. These subunits are linked through multiple carbon-carbon and aryl-ether linkages, resulting in a complex structure.² While characterization and quantification of the plant carbohydrates are considered routine analyses, the quantification of lignin and its subunit composition is not well established.³⁻⁵

Common quantification of lignin, still, mainly relies on gravimetric analysis after sulphuric acid hydrolysis known as Klason-lignin analysis or a variant hereof.⁶⁻⁷ The outcome of such gravimetric analysis is highly disturbed by the presence of non-lignin acid-insoluble material, e.g. proteins and chitin of fungal origin. In addition, this analysis does not distinguish different lignin structures.⁶ Therefore, one of the main challenges for biomass analysis, is the development of an analytical tool for the specific quantification of lignin in absolute amounts that is able to simultaneously characterize lignins structural features in a robust and high-throughput manner.

Solving this analytical challenge has been attempted with vibrational spectroscopy and nuclear magnetic resonance (NMR), both proven powerful techniques for the structural elucidation of lignin.^{5, 8-11} For quantification of lignin, however, serious drawbacks remained: both techniques suffered from poor accuracy, dependency on structurally similar calibration standards and/or minimal structural information that was obtained.⁸⁻¹¹ Additionally, for NMR throughput was low.¹²

As alternative, our research aimed at the development of a rapid and specific lignin quantification method via analytical pyrolysis coupled to gas chromatography with mass-spectrometric detection (py-GC-MS). This technique requires minimal sample amounts (10-100 µg) and only milling of the sample is needed prior to analysis. Furthermore, py-GC-MS has been shown to enable distinguishing lignins' subunits, i.e. H, G and S substructures.¹³⁻¹⁵ In contrast, thus far, py-GC-MS has been found inaccurate for the absolute quantification of lignin in plant biomass.¹⁶⁻²⁰ That inaccuracy has been proposed to relate to two main aspects. The first relates to the need for a proper internal standard (IS), that during pyrolysis behaves like (native) lignin in biomass, together with the large number of pyrolysis products formed.^{13, 21} Secondly, different ratios of pyrolysis products ask for the determination and use of (relative) response factors.^{16, 21-22}

Previously, absolute lignin quantification by py-GC-MS and py-GC-FID (Flame Ionization Detection) was attempted by relating the relative peak area of lignin-derived compounds, so-called 'py-lignin', to lignin content as determined by gravimetric methods. The models that were obtained showed low and/or unstable

accuracy.¹⁷⁻²⁰ Partially, this was a consequence of the absence of response factors for the obtained pyrolysis products. Furthermore, the extents to which CO₂ and other low molecular weight gasses and char were formed from both lignin and non-lignin components of the cell-wall upon pyrolysis was not accounted for. Matrix-effects during pyrolysis may have further influenced the outcomes.²²⁻²⁴ Alternatively, Bocchini et al.¹⁶ approached lignin quantification by the measurement of lignin-derived pyrolysis products via monomeric internal standards and the application of response factors, which resulted in severe underestimation. Again, the formation of non-monomeric pyrolysis products was excluded and matrix-effects were expected to affect the monomeric internal standard differently than lignin macromolecules in biomass.

To specifically correct for the formation of non-monomeric pyrolysis products from lignin and monitor matrix-effects properly, the use of polymeric lignin as internal standard can be hypothesized for lignin quantification by py-GC-MS, a currently unexplored field of research.

Thereeto, this research aimed to apply the 'ideal' standard, a ¹³C-labeled polymeric lignin isolate, for the absolute lignin quantification by py-GC-MS. Relative response factors for lignin-derived products were determined and applied to allow quantification, via the ¹³C-lignin as internal standard, of structurally diverse lignins in four poaceous biomasses.

Experimental Section

Materials. All chemicals were obtained from commercial suppliers and used without further purification. Water used in all experiments was purified via a Milli-Q water system (Millipore, Billerica, MA, USA). For lignin content determination experiments, wheat straw (WS) and corn stover (CS) were kindly provided by CNC (Milsbeek, The Netherlands). Sugar cane bagasse (SCB) and barley straw (BS) were supplied by Sime Darby (Kuala Lumpur, Malaysia) and Unifarm Wageningen (Wageningen, The Netherlands), respectively. Compositional analysis was performed as described in Supporting Information.

Preparation of nonlabeled and ¹³C-labeled wheat straw. Nonlabeled ("¹²C", 98.9 atom % ¹²C) and uniformly ¹³C-labeled ("¹³C", 97.7 atom % ¹³C) spring wheat plants (*Triticum aestivum* L. cv. 'Baldus') were produced under identical growth conditions in modified, custom designed, air-tight, high-irradiance labeling chambers of the facility ESPAS (Experimental Soil Plant Atmosphere System, IsoLife, Wageningen, The Netherlands).²⁵ Details of wheat straw preparation are provided in Supporting Information.

Isolation of lignin from ¹²C and ¹³C wheat straw. The isolation of lignin was performed according to a modified method reported by Björkman.²⁶ Freeze-dried straw (3 g), either ¹²C or ¹³C, was cut to a size of 1-3 mm and acetone-extracted for 3 hours at 30 °C under magnetic stirring (750 rpm) to remove extractives.

Insoluble material was removed by filtration, dried under a stream of nitrogen and ball-milled in a PM100 planetary ball mill (Retsch, Haan, Germany) in a 50 mL zirconium dioxide jar containing 17 ϕ 10 mm zirconium dioxide balls at a frequency of 600 rpm with a net milling time of 4 h. After every 15 min of milling a pause of 10 min was set to prevent overheating. Ball-milled material was subsequently water-extracted in a concentration of 5% (w/w) at 50 °C for 15 hours under magnetic stirring (750 rpm). Insoluble material (water unextractable solids, WUS) was removed by centrifugation (60,000 $\times g$, 10 min, 20 °C) and washed 3 times with 30 mL water. The wet residue was suspended in dioxane and adjusted to 80% aqueous dioxane (v/v) at a material loading of 5% (w/w) and extracted twice (2 \times 24 h) at room temperature with magnetic stirring (500 rpm) under nitrogen atmosphere. Supernatants were recovered by centrifugation (30,000 $\times g$, 5 min, 20 °C), combined and freeze-dried to obtain crude lignin isolates (ISOcrude). The obtained crude isolates were purified by enzymatic carbohydrate removal. ISOcrude was thereto suspended in 50 mM sodium acetate buffer at pH 4.8 at 5% (w/w) material loading, charged with 0.075% (w/w) ViscoStar 150L (Dyadic, Jupiter, FL, USA) (protein content²⁷: 40 mg mL⁻¹) and incubated under rotary shaking (20 rpm) at 50 °C for 4 h. Insoluble material was removed by centrifugation (8,000 $\times g$, 5 min, 20 °C) and washed 3 times with water before freeze-drying to obtain pure lignin isolates (LIGpure).

Compositional analysis of total biomass and lignin isolates. Carbohydrate content and composition, protein content, ash content and lignin content were determined by modifications of previously published procedures.^{3, 15, 28} Detailed procedures are provided in Supporting Information.

Characterization total biomass and lignin isolates

NMR Spectroscopy. NMR of the pure lignin isolates (¹²C-LIGpure and ¹³C-LIGpure) was performed according to del Río et al.²⁹ For NMR experiments around 12 mg ¹²C-LIGpure was dissolved in 450 μ L DMSO-*d*₆, while for ¹³C-LIGpure around 1.3 mg was used. The heteronuclear single quantum coherence (HSQC) NMR-experiments were recorded with a hsqcetgpsisp2.2 pulse sequence on a Bruker AVANCE III 600 MHz NMR spectrometer (Bruker BioSpin, Rheinstetten, Germany) equipped with a 5 mm cryoprobe. The internal temperature of the probe was set at 298 K. The spectral widths were 6000 Hz (10-0 ppm) for the ¹H-dimension and 25000 Hz (165-0 ppm) for the ¹³C-dimension. The number of complex points was 2048 in the ¹H-dimension, 32 scans were collected with a relaxation time of 1.5 s. In the ¹³C-dimension, 256 time increments were recorded. The ¹J_{CH} was set at 145 Hz. For the Fourier transformation in the ¹H-dimension, Gaussian apodization was used. For the ¹³C-dimension, zero-filling up to 1024 was applied prior to Fourier transformation with a squared cosine window function. Zero-order phase correction was performed manually. The DMSO solvent-peak was set as internal reference at δ_c 39.5; δ_H 2.49 ppm. HSQC correlation peaks were assigned by comparison with

literature.²⁹⁻³¹ Semiquantitative analysis of the volume integrals was performed according to del Río et al.²⁹, by using Bruker TopSpin 3.2 software.

Py-GC-MS. Pyrolysis was performed with an EGA/PY-3030D Multi-shot pyrolyzer (Frontier Laboratories, New Ulm, MN, USA) equipped with an AS-1020E Autoshot auto-sampler. The pyrolyzer was coupled to GC-MS by using a Trace GC equipped with a DB-1701 fused-silica capillary column (30 m x 0.25 mm i.d. 0.25 μ m film thickness) coupled to a DSQ-II mass spectrometer (both Thermo Scientific, Waltham, MA, USA). Pyrolysis, GC and MS settings were similar as previously described.¹⁵ Samples were weighed by using an XP6 excellence-plus microbalance (Mettler Toledo, Columbus, OH, USA). Pyrolysis of total biomass (80-90 μ g) and lignin isolates (20-30 μ g) was performed at 500 °C for 1 min with an interface temperature of 300 °C. Pyrolysis products were injected on the column via split/splitless injection (at 250 °C) with a splitratio of 1:133 and helium was used as carrier gas with constant flow at 1.5 mL min⁻¹. The GC oven was programmed from 70 °C (2 min) to 270 °C at 5 °C min⁻¹ and held at 270 °C for 15 min. MS detection was used with EI at 70 eV, a source temperature of 250 °C, a scan range of *m/z* 50-550 and a scan rate of 4.0 scans s⁻¹. Compounds were identified by comparing retention time and mass spectrum with standards, the NIST library and data published by Ralph and Hatfield.¹³ Results were combined in a (¹²C) target library. A unique ¹³C target library was built on the basis of retention time and expected fragmentation from ¹²C mass spectra and carbon number.

For qualitative identification, pyrograms were processed by AMDIS software (version 2.71, NIST, USA). For identification and deconvolution the following software settings were used: minimum match factor at 60 with multiple identifications per compound, component width at 20, adjacent peak subtraction at two, resolution at high, sensitivity at very high and shape requirements at low. Compounds identified on the basis of reference standards were annotated by evaluation of retention time (\pm 0.1 min), reverse search (\geq 80) and simple search (\geq 45). Peak molar area was calculated as defined by del Río et al.³² All samples were analyzed in triplicate.

Absolute lignin quantification using py-GC-MS

Relative response factor determination of pyrolysis products. Relative response factors of 21 (of a total of 46) lignin-derived pyrolysis products, indicated in Table 1 with an asterisk, were determined by injecting an equimolar mixture of authentic standards and 9-fluorenone as internal standard into the py-GC-MS system.²¹ Standards and 9-fluorenone were dissolved in 50:50 (v/v) ethanol (EtOH):chloroform (CHCl₃) in a concentration of 10 mM, taking the declared purity of the standard into account, and mixed to give an equimolar solution of 0.45 mM. All solutions were kept in amber vials with minimal exposure to air and kept at -20 °C. Five microliter of the equimolar mixture was injected into a pyrolysis cup and directly measured by py-GC-MS as described in section 'Characterization total

biomass and lignin isolates – py-GC-MS' in triplicate. Different injection volumes were tested and showed similar relative response factors, confirming linearity of the response over the used concentration range.

Table 1. Pyrolysis products and their signature fragments used for py-GC-SIM-MS analyses. Of compounds marked with an asterisk (*) the relative response factors (RRFs) were measured.

#	Compound	CAS	Retention time (min)	Structural feature	RRF (-)	M _w ¹² C (g mol ⁻¹)	Fragments ¹² C ^a (g mol ⁻¹)	M _w ¹³ C (g mol ⁻¹)	Fragments ¹³ C ^a (g mol ⁻¹)	Segment (min)
1	phenol*	108952	9.98	H, unsub.	0.54	94	94, 66	100	100, 71	9.7-10.3
2	guaiacol*	90051	10.12	G, unsub.	0.67	124	124, 109	131	131, 115	
3	2-methylphenol*	95487	11.10	H, methyl	0.81	108	108, 107	115	114, 115	10.3-13.0
4	4-methylphenol*	106445	12.14	H, methyl	0.76	108	107, 108	115	114, 115	
5	4-methylguaiacol*	93516	12.77	G, methyl	0.70	138	138, 123	146	146, 130	
6	2,4-dimethylphenol	105679	13.26	H, methyl	0.79 ^g	122	107, 122	130	114, 130	13.0-15.4
7	4-ethylphenol*	123079	14.32	H, ethyl	1.00	122	107, 122	130	114, 130	
8	4-ethylguaiacol*	2785899	14.91	G, ethyl	0.95	152	137, 152	161	145, 161	
9	4-vinylguaiacol*	7786610	16.39	G, vinyl	0.22	150	150, 135	159	159, 143	15.4-16.8
10	4-vinylphenol*	2628173	16.57	H, vinyl	0.33	120	120, 91	128	128, 98	
11	eugenol*	97530	16.98	G, misc. ^b	0.40	164	164, 149	174	174, 158	16.8-17.3
12	4-propylguaiacol	2785877	17.05	G, misc.	0.37 ^h	166	137, 166	175	145, 175	
13	syringol*	91101	17.73	S, unsub.	0.48	154	154, 139	162	162, 146	17.3-18.5
14	cis-isoeugenol*	97541	18.33	G, misc.	0.34	164	164, 149	174	174, 158	
15	3-methoxy-5-methylphenol ⁱ	3209130	18.92	G, methyl	-	138	138, 109	146	146, 116	18.5-19.45
16	4-propenylphenol	539128	19.31	H, misc.	0.27 ⁱ	134	134, 133	143	143, 142	
17	trans-isoeugenol*	97541	19.60	G, misc.	0.34	164	164, 149	174	174, 158	19.45-19.8
18	4-methylsyringol*	6638057	19.95	S, methyl	0.55	168	168, 153	177	177, 161	19.8-20.2
19	vanillin*	121335	20.08	G, C _α -O ^c	0.66	152	151, 152	160	159, 160	
20	4-propyleneguaiacol	-	20.33	G, misc.	0.40 ^j	162	162, 147	172	172, 156	20.2-21.0
21	4-alleneguaiacol	-	20.59	G, misc.	0.40 ^j	162	162, 147	172	172, 156	
22	hydroquinone ^f	123319	20.61	H, misc.	-	110	110, 81	116	116, 85	
23	homovanillin	5603242	21.53	G, C _β -O ^d	0.59 ^k	166	137, 166	175	145, 175	21.0-21.85
24	4-ethylsyringol	14059928	21.69	S, ethyl	0.98 ^l	182	167, 182	192	176, 192	
25	acetovanillone*	498022	22.00	G, C _α -O	0.51	166	151, 166	175	159, 175	21.85-22.9
26	4-hydroxybenzaldehyde	123080	22.81	H, C _α -O	0.53 ^m	122	122, 121	129	129, 128	
27	4-vinylsyringol	28343228	23.01	S, vinyl	0.28	180	180, 165	190	190, 174	22.9-23.3
28	guaiacylacetone*	2503460	23.19	G, C _β -O	0.53	180	137, 180	190	145, 190	
29	4-allylsyringol*	6627889	23.41	S, misc.	0.27	194	194, 167	205	205, 176	23.3-24.4
30	guaiacyl vinyl ketone	-	24.16	G, C _α -O	0.53 ⁿ	178	151, 178	188	188, 159	
31	cis-4-propenylsyringol	26624135	24.55	S, misc.	0.27 ^o	194	194, 179	205	205, 189	24.4-26.1
32	4-propynesyringol	-	25.19	S, misc.	0.27 ^o	192	192, 131	203	203, 140	
33	4-allenesyringol	-	25.39	S, misc.	0.27 ^o	192	192, 131	203	203, 140	
34	trans-4-propenylsyringol	26624135	25.84	S, misc.	0.27 ^o	194	194, 179	205	205, 189	
35	syringaldehyde*	134963	26.45	S, C _α -O	0.30	182	182, 181	191	191, 190	26.1-27.2
36	cis-coniferyl-alcohol	458355	26.53	G, C _γ -O ^e	0.097 ^p	180	137, 180	190	145, 190	
37	homosyringaldehyde	-	27.42	S, C _β -O	0.30 ^q	196	167, 196	206	176, 206	27.2-28.05
38	acetosyringone*	2478388	27.88	S, C _α -O	0.44	196	181, 196	206	190, 206	
39	trans-coniferyl alcohol	458355	28.23	G, C _γ -O	0.097 ^p	180	137, 180	190	145, 190	28.05-28.7
40	trans-coniferldehyde*	458366	28.60	G, C _γ -O	0.097	178	178, 135	188	143, 188	
41	syringylacetone	19037582	28.79	S, C _β -O	0.30 ^q	210	167, 210	221	176, 221	28.7-29.85
42	syringyl vinyl ketone	-	29.67	S, C _α -O	0.30 ^q	208	208, 181	219	219, 190	
43	coniferylacetate ^f	-	29.88	S, C _γ -O	-	222	131, 222	234	140, 234	29.85-32.6
44	cis-sinapyl-alcohol	537337	31.74	S, C _γ -O	0.068 ^r	210	167, 210	221	176, 221	
45	trans-sinapyl alcohol	537337	33.45	S, C _γ -O	0.068 ^r	210	210, 167	221	176, 221	32.6-34.0
46	trans-sinapaldehyde*	4206580	33.65	S, C _γ -O	0.068	208	208, 165	219	219, 174	

^amost abundant fragment first; ^bmiscellaneous; ^cC_α-oxygen; ^dC_β-oxygen; ^eC_γ-oxygen; ^fnot included in quantitative analyses due to background interference; ^gaverage #3, #4; ^haverage #11, #17; ⁱ#17/#2 x #1; ^j#11; ^kaverage #19, #25; ^laverage #7, #8; ^m#7/#2 x #1; ⁿ#28; ^o#29; ^p#40; ^q#35; ^r#46

Stability of compounds during pyrolysis, i.e. the formation of a single compound peak only, was confirmed by injecting all compounds individually at 0.4 mM mixed with 9-fluorenone at the same concentration. Xcalibur 2.2 was used for data analysis. The two most abundant fragments per compound were used for quantification (Table 1). Peak areas (A_i) were manually integrated to avoid erroneous integration by method settings and normalized for molarity (M_i). Areas for *cis*-isoeugenol and *trans*-isoeugenol were summed as they were present as a mixture. Relative response factors (RRFs) were calculated versus the highest peak area (4-ethylphenol, A_{4EP}) normalized for molarity (M_{4EP}) according to equation 1.

$$RRF_i = \frac{A_i/M_i}{A_{4EP}/M_{4EP}} \quad (1)$$

where i refers to compound number (Table 1). *Cis*- and *trans*-isomers were assumed to have similar RRFs, where RRFs for pyrolysis products for which no commercial standard was available were estimated from structurally closest molecules (Table 1). In addition, RRFs of *cis/trans*-coniferyl alcohol and *cis/trans*-sinapyl alcohol, were estimated from their aldehyde analogues as they were shown to be insufficiently stable to analyze via 'liquid injection'. Molar RRFs (^{12}C) were assumed to be similar for ^{13}C analogues.

^{13}C lignin internal standard based lignin quantification in reconstituted biomass model systems. ^{12}C -LIGpure was dissolved in 50:50 (v/v) EtOH:CHCl₃ in a concentration of 1.0 mg mL⁻¹. 10-35 μL of this solution was added to 40-65 μg cellulose to obtain 75 μg 'reconstituted' biomass (m_{sample}) with six different lignin contents (12-43% (w/w)) and dried at 30 °C for 1 h. ^{13}C -LIGpure (=internal standard, IS) was dissolved in a similar manner. Ten microliter IS solution of 1.0 mg mL⁻¹ (m_{IS}) was added to the reconstituted biomass and dried overnight at room temperature before analysis. All samples were prepared and analyzed by py-GC-MS in triplicate.

Py-GC-MS settings and data processing for quantitative analyses. The pyrolysis and GC setup used was similar to the qualitative analysis. MS detection was applied in selected ion monitoring (SIM) mode. The two most abundant fragments per compound were monitored, with a maximum of 8 fragments (4 ^{12}C + 4 ^{13}C) per segment (Table 1). Dwell time was set at 25 ms to ensure at least 25 data points per peak. Data was processed by using Xcalibur 2.2. Peaks were integrated by using ICIS peak integration with peak smoothing set at 5, area noise factor set at 5, peak noise factor set at 10 and baseline window optimized per compound (range 12-55). A manual correction was only applied when irregular peak shapes led to erroneous peak integration with method settings. Peak areas were normalized by dividing by RRFs and summed. To correct for the higher molecular weight and concomitant lower response per weight of ^{13}C pyrolysis products, a correction factor for detected ^{13}C total area was included. This

correction factor was determined by calculating total molar area of ^{13}C -LIGpure on the basis of ^{12}C and ^{13}C pyrolysis product molecular weights (Table 1) as described del Río et al.³² in >25 samples. The calculated correction factor was equal to 1.057 with a standard deviation below 0.05%. Lignin content was quantified following equation 2.

$$\text{Lignin content \%}(w/w) = \frac{\sum_{i=1}^{46} \frac{A_i^{12\text{C}}}{\text{RRF}_i} m_{\text{IS}} \cdot P_{\text{IS}}}{\sum_{i=1}^{46} \frac{A_i^{13\text{C}}}{\text{RRF}_i} m_{\text{sample}} \cdot 1.057} \cdot 100 \quad (2)$$

where i refers to compound number (Table 1), A is area, RRF is relative response factor (Table 1), m_{IS} is the amount of IS (μg ; ^{13}C -LIGpure), m_{sample} is the amount of sample (μg) and P_{IS} is a correction factor for the purity of the IS (0.895). In compounds 15, 22 and 23 were not included.

Application of ^{13}C lignin IS method for lignin quantification. Lignin in water-unextractable solids (WUS) of WS, CS, BS and SCB, obtained as described in Supporting Information, was quantified by using the novel method as described in the section 'Py-GC-MS settings and data processing for quantitative analysis'. Approximately 75 μg of material was mixed with 10 μL ^{13}C -IS solution (1.0 mg mL^{-1}) and dried at 30 $^{\circ}\text{C}$ for 3 h. All samples were prepared and analyzed by py-GC-MS in triplicate and compared to Klason lignin content (AIL corrected for ash and protein + ASL).

Results & Discussion

The quantification potential of our new approach could best be evaluated using reconstituted biomass model systems, on the basis of structurally similar ^{12}C and ^{13}C lignins to which cellulose was added, to mimic a plant biomass matrix. This allowed us to evaluate the performance of the novel method on samples with a known, 'true' lignin content, without relying on inaccurate and unselective procedures. Thereto, first lignin was isolated from nonlabeled (^{12}C) and uniformly ^{13}C -labeled (^{13}C) wheat straw that was produced under identical growth conditions.

Compositional analysis of lignin isolates

The abundance of the main constituents of the lignin isolates is indicated in Table 2. Lignin content was calculated as the remaining content of dry matter after subtraction of carbohydrates, protein and ash, since acetone and water extractives were removed prior to dioxane extraction. High purity ($\sim 90\%$) isolates were obtained, with carbohydrates as the most abundant impurity ($\sim 7\%$). Carbohydrate contents of the isolates were approximately two times lower than previously reported for unpurified dioxane/milled wood lignins, achieved by water extraction prior to and enzymatic carbohydrate removal after dioxane extraction.³³ Enzymatic purification is considered a milder and less laborious alternative compared to the

commonly used chemical work-up procedure, maintaining efficiency.^{26, 34} The significant amount of protein (nitrogen) found in the isolates was likely the result of protein adsorption, although co-extraction has been reported as well.³⁵⁻³⁶ Estimated lignin contents of ¹²C and ¹³C wheat straw (total biomass) were $20.6 \pm 0.8\%$ (w/w) and $19.3 \pm 1.3\%$ (w/w), respectively, and used for calculation of isolation yields.¹⁵ Final lignin isolation yields of approximately 20% were achieved for both isolates, which is in line with literature on lignin isolates obtained from wheat straw with similar a extraction procedure.²⁹

Table 2. Composition and yield of ¹²C and ¹³C lignin isolates % (w/w) determined in duplicate.

	¹² C-WS	¹³ C-WS	¹² C-LIGpure	¹³ C-LIGpure
carbohydrate	68.5 ± 0.5	67.3 ± 0.3	6.8 ± 0.2	7.1 ± 0.1
protein	0.9 ± 0.04	0.7 ± 0.1	4.3 ± 0.1	3.0 ± 0.1
ash	1.5 ± 0.2	1.4 ± 0.1	0.8 ± 0.4	0.4 ± 0.1
lignin	20.6 ± 0.8 ^a	19.3 ± 1.3 ^a	88.1 ± 0.5 ^b	89.5 ± 0.2 ^b
isolation yield (%)	-	-	19.0 ± 0.7	21.5 ± 1.4

^aestimated according to Jurak et al.¹⁵

^bremaining content of dry matter after subtraction of carbohydrates, protein and ash

Characterization of lignin isolates

The lignin isolates were characterized by 2D-NMR to provide information on the interunit linkages present within the lignins. Chemical shifts assignments were based on previous studies.²⁹⁻³¹ The aliphatic (δ_C/δ_H 50-90/2.5-6.0) and aromatic/unsaturated (δ_C/δ_H 90-160/6.0-8.0) regions of the recorded HSQC spectra along with the structures of the assigned correlation peaks are shown in Supporting Information Figure S1 and S2. Clear lignin signals could be observed in the aromatic region ($S_{2,6}$, G_2 , $H_{2,6}$ and several tricin, *p*-coumarate and ferulate related signals). The aliphatic region was dominated by methoxyl group- and β -O-4' substructure (A, A' and A_{ox}) related correlation peaks. Other interunit linkages like phenylcoumaran (B) and resinol (C), and to lesser extent spirodienone (F) and dibenzodioxocins (D) substructures were also observed in the HSQC spectra. α,β -diaryl ethers (E) substructures, the presence of which was confirmed by del Río et al.,²⁹ albeit in minor amounts, could not be detected in the isolated lignins. A summary of relative abundance of the aromatic units and interunit linkages of the ¹²C and ¹³C lignin isolates, determined by semiquantitative analysis, is presented in Table 3.

Besides lignin, multiple carbohydrate-related signals (δ_C/δ_H 65-80/2.8-3.6 ppm) were readily detectable in both isolates, despite their relatively low abundance (Table 2), which could provide additional information on structural features of carbohydrates and lignin involved in lignin-carbohydrate complexes (LCC). This is, however, not further discussed in this paper.

The distribution of aromatic units and lignin interunit linkages closely matched with earlier reports on HSQC NMR analyses of wheat straw lignin.^{29, 31, 33} Hence, it was concluded that the isolated lignins were representative of lignin in wheat straw. In addition, a highly similar relative abundance of lignin interunit linkages and

aromatic units was found for both isolates. This good similarity of the ^{12}C and ^{13}C lignins was further used for py-GC-MS analysis to identify and annotate for the first time pyrolysis products formed from ^{13}C lignin.

Table 3. Relative abundance of lignin interunit linkages and aromatic units of $^{12}\text{C}/^{13}\text{C}$ lignin isolates by semiquantitative HSQC NMR analysis.

	^{12}C -LIGpure	^{13}C -LIGpure
Lignin interunit linkages (%)^a		
β -O-4' aryl ethers (A/A')	80	81
C α -oxidized β -O-4' aryl ethers (A $_{ox}$)	3	3
β -5' phenylcoumarans (B)	8	8
β - β' resinols (C)	5	4
5-5/4-O- β dibenzodioxocins (D)	1	1
β -1' spirodienones (F)	4	4
α,β -diaryl ether (E)	n.d.	n.d.
total	100	100
Lignin aromatic units^b		
H (%)	6 (14)	3 (13)
G (%)	58 (54)	60 (56)
S (%)	36 (30)	37 (31)
S/G	0.62 (0.56)	0.62 (0.56)

^apercentage of total lignin interunit linkage (A-F; see Supporting Information for details).

^bMolar percentages (H + G + S = 100) excluding or including *p*-coumaric acid (H) and ferulic acid (G) (in parentheses); n.d.: not detected

Pyrograms for of the two lignin isolates can be found in Supporting Information Figure S3. Due to the lack of authentic ^{13}C standards, ^{13}C pyrolysis products were identified on the basis of expected retention time ($R_{t,12\text{C}} = R_{t,13\text{C}}$) and molecular ion ($M^{+ \cdot 13\text{C}} = M^{+ \cdot 12\text{C}} + \text{carbon number}$) and fragmentation spectra of their ^{12}C counterparts. The ^{12}C and ^{13}C MS fragmentation spectra of two abundant lignin-related pyrolysis products are shown in Figure 1. Identical fragmentation behavior was observed for ^{12}C and ^{13}C analogues. MS fragmentation spectra of all other identified ^{13}C lignin-related pyrolysis products are presented in Supporting Information Figure S4.

Like NMR, py-GC-MS analysis revealed that the chemical composition of the isolated ^{12}C and ^{13}C lignins was highly similar. Furthermore, all lignin-related pyrolysis products found for the isolates were also present in 'native' lignin in total biomass, although their relative distribution differed (Table 4). Note that in Table 4 the data were not corrected for relative response factors (see text below) to allow comparison with literature. Most profound were the lower relative amounts of unsubstituted and vinyl substituted compounds in the isolates and higher amounts of methyl substituted and C $_v$ -oxygen containing products, which is in line with findings by del Río et al.²⁹ The lower amount of vinyl substituted products in the isolates can be explained by the fact that a significant part of the detected vinyl compounds arise from (di)ferulic structures that are linked to arabinoxylan and could, therefore, have remained in the residue after dioxane extraction.³⁷

Furthermore, changes in the relative distribution of structural features might be the result of modification and/or selective extraction of a specific lignin population.

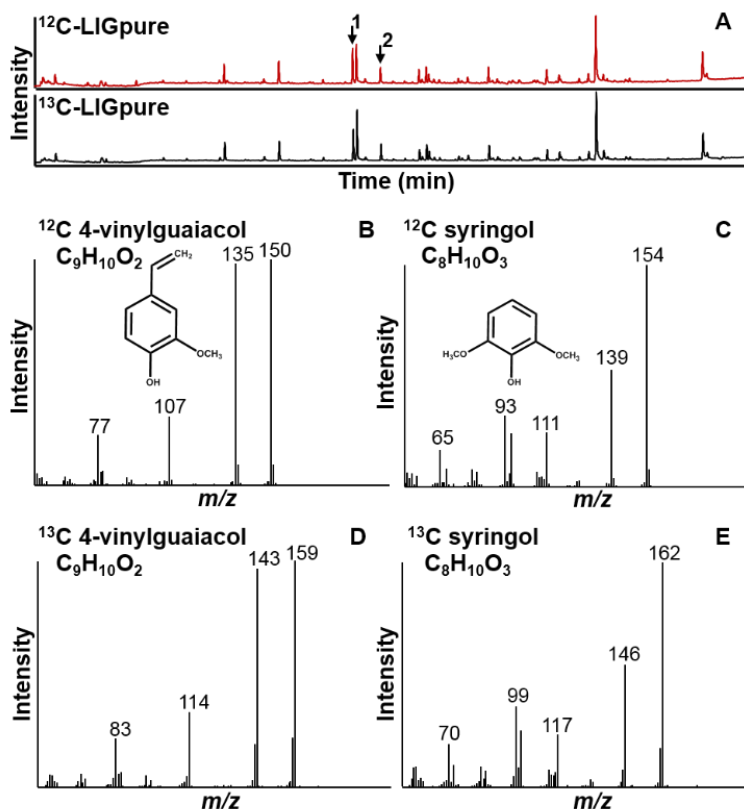


Figure 1. Pyrograms (A) of ^{12}C -LIGpure and ^{13}C -LIGpure where 4-vinylguaiacol (1) and syringol are indicated (2) and EI-MS (70 eV) spectra of ^{12}C 4-vinylguaiacol (B), ^{12}C syringol (C), ^{13}C 4-vinylguaiacol (D), and ^{13}C syringol (E). Most abundant fragments are indicated. Full size pyrograms with peak annotation can be found in Supporting Information Figure S3.

It should be noted that in py-GC-MS lignin interunit linkages as well as *p*-coumarate (*p*CA) and ferulate (FA) led to the formation of the same pyrolysis products, namely 4-vinylphenol and 4-vinylguaiacol, respectively, and can therefore not be independently quantified.³⁸⁻³⁹ Interestingly, our findings showed that when relative response factors for pyrolysis products, discussed in the next section, were taken into account, the relative distribution of aromatic units by py-GC-MS (H:G:S = 15:58:26) and NMR (including *p*CA and FA) (H:G:S = 13:56:31) were in good agreement. This showed that the commonly found discrepancy between py-GC-MS and NMR partially originates from the analytical approach, and heavily depends on the used definition of lignin.³⁷

Table 4. Py-GC-MS relative abundance of structural features within $^{12}\text{C}/^{13}\text{C}$ wheat straw (WS) and $^{12}\text{C}/^{13}\text{C}$ lignin isolates (LIGpure) on the basis of molar peak area. Structural classification is shown in Table 1. Average and standard deviation of triplicates. Not corrected for relative response factors.

	^{12}C -WS	^{13}C -WS	^{12}C -LIGpure	^{13}C -LIGpure
Lignin subunits (%)				
H	36.3±2.0	41.1±1.7	22.4±2.1	25.5±3.3
G	47.9±2.1	45.1±1.5	52.4±1.5	49.7±3.6
S	15.7±0.7	13.9±0.4	25.2±0.7	24.8±0.9
S/G	0.3	0.3	0.5	0.5
Structural moieties (%)				
unsub.	21.6±1.6	18.5±0.5	13.9±0.5	13.5±0.6
methlyl	4.1±0.2	3.8±0.2	13.3±1.0	11.9±0.4
ethyl	2.0±0.2	1.6±0.1	2.7±0.2	2.5±0.3
vinyl	49.1±2.4	52.4±2.0	28.1±2.1	30.2±3.4
C α -O ^a	4.4±0.2	5.0±0.5	9.5±0.2	10.4±0.3
C β -O ^b	2.9±0.3	2.2±0.1	4.6±0.1	4.7±0.3
C γ -O ^c	9.9±0.5	10.9±0.3	20.3±1.2	19.8±3.6
misc. ^d	6.0±0.2	5.5±0.4	8.9±0.4	8.0±0.3

^aC α -oxygen, ^bC β -oxygen, ^cC γ -oxygen, ^dmiscellaneous

Lignin quantification in reconstituted biomass model systems

After establishing a complete pyrolysis product library for ^{12}C and ^{13}C products, as explained in the previous section, a py-GC-SIM-MS method was set up for quantification purposes. By applying ^{13}C lignin as internal standard, the necessity of monitoring the formation of nonmonomeric pyrolysis products from lignin, such as CO_2 or char, is bypassed. Furthermore, matrix-effects during pyrolysis and system performance are corrected for properly via the use of polymeric ^{13}C lignin as internal standard. In our opinion, this can be seen as huge improvement compared to previous lignin quantification attempts by py-GC-MS.^{16-20, 22}

Selected ion monitoring (SIM) was used for detection as this MS-mode benefits from a significant reduction of background noise and therefore lowers the limit of quantification. Previously it was shown that the lignin-derived pyrolysis products of various grasses, soft- and hardwoods are similar, although their distribution is different.^{17, 20, 29, 32} Monitoring all identified lignin-derived pyrolysis products (43, Table 1) thereto ensured unbiased and complete quantification, also when the method is ultimately applied on samples with different product ratios.

Quantification with ^{13}C lignin as internal standard (IS) requires the simultaneous measurement of ^{12}C -sample derived and ^{13}C -IS derived products. Therefore, the number of quantified products was equal to 86. Pyrograms were thereto divided in segments to ensure sufficient data points per peak.

To prove the principle of ^{13}C lignin internal standard based quantification via py-GC-MS, the developed method was applied on ^{12}C lignin with close to identical structure (Tables 3 and 4) in reconstituted biomass systems with known lignin content. The pyrolysis products derived from cellulose in these mixtures were

similar as previously reported, of which levoglucosan was the most abundant, and did not interfere with lignin analysis.^{13, 23}

In the latter setup similar (molar based) relative abundances of lignin-derived pyrolysis products in the used ^{12}C lignin and ^{13}C lignin internal standard circumvented the need for response factor corrections and allowed the use of total peak area for quantification directly. However, as a consequence of weight-based quantification, a correction factor was required to compensate for the molecular weight differences between ^{12}C and ^{13}C pyrolysis products. This correction factor was calculated from the difference in ^{12}C and ^{13}C molecular weight based total molar peak area calculated for the same IS sample. As a result, it was found that ^{13}C total areas should be multiplied with a correction factor of 1.057. Resulting correlations for ^{12}C lignin input and ^{13}C lignin IS-based quantified ^{12}C lignin amount are shown in Figure 2.

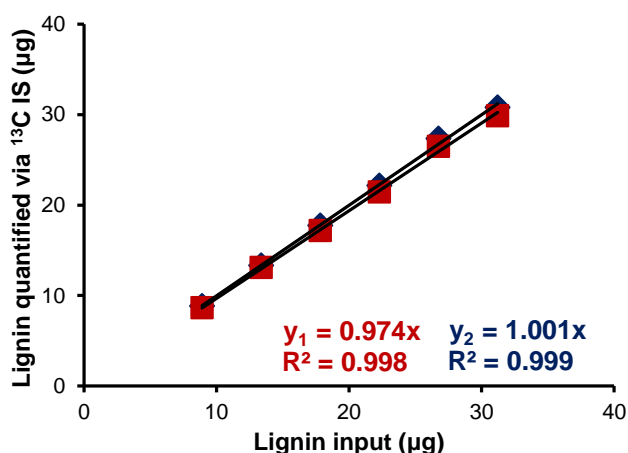


Figure 2. Lignin input and quantified ^{13}C -IS based (total area SIM-MS) output in a reconstituted biomass model system. Square, y_1 : uncorrected, Diamond, y_2 : corrected for RRF. Average and standard deviation on the basis of triplicates (RSD<1.5%).

It can be observed from the slope of the equation (0.974) and excellent linearity ($R^2>0.998$) that ^{12}C lignin can be correctly quantified on the basis of the ^{13}C lignin internal standard in the applied lignin content range. The high reproducibility (RSD < 2%) was achieved by solubilizing the lignin isolates in 50:50 (v/v) EtOH: CHCl_3 and pipetting specified volumes, opposed to the use of a microbalance. Besides improving reproducibility, this approach facilitated high-throughput sample preparation.

To allow the ultimate use of the internal standard for the quantification of lignins with dissimilar relative distribution of pyrolysis products as well, relative molar response factors (RRFs) were determined and applied. RRFs are of utmost importance since they include compound stability during pyrolysis at 500 °C, transfer efficiency through injector and column and sensitivity of the detector as a

result of ionization efficiency and ion coverage by the monitored fragments in SIM. An overview of the relative response factors of all lignin-derived pyrolysis products can be found in Table 1. The relative response factors that were obtained were different from RRFs calculated from calibration curves published by Groenewold et al.²¹ Underlying might be different ion coverages as a result of a different number of fragments that were followed per compound. Furthermore, the lability of compounds during pyrolysis at 500 °C was taken into account in our approach, while Groenewold et al. determined RRFs directly with MS without pyrolysis.²¹ By applying the RRFs, correcting for small differences in the relative composition of the pyrolysis products between the ¹²C and ¹³C isolates (Table 4), the obtained slope was similar to the theoretical slope of 1 (1.001) and resulted in excellent accuracy (>99.9%) across the measured lignin content range (Figure 2). Surprisingly, highly similar outcomes were obtained when RRFs of Groenewold et al. were applied (data not shown).²¹

Considerations regarding the selectivity of ¹³C-IS lignin quantification

In grasses, relatively high amounts of *p*-coumaric acid and ferulic acid are present, that form similar products as 'core lignin' upon pyrolysis, and can thus not be distinguished.¹³ Both coumarylation and feruloylation of arabinoxylan and lignin have been described in literature and potentially could be a source of error when quantifying lignin on the basis of the formed pyrolysis products. Nevertheless, the major part of the hydroxycinnamic acids found in grasses is thought to be attached to lignin, and is considered an integral part of it, rather than being present as 'free decorations' of arabinoxylan.^{37, 40} Hence, all vinylic pyrolysis products were assumed to be fully lignin-derived.

Traces of selected masses for ¹²C pyrolysis products at given retention times were detected in the ¹³C lignin isolate, and vice-versa, but did not form a significant interference (<1% of total peak area) and were therefore neglected. Further, the pyrolysis products phenol, 2-methylphenol, 4-methylphenol can originate from both lignin and non-lignin components of the cell wall (like aromatic amino acids in protein) (data not shown). These products were fully included in our lignin quantification as they comprised only a minor part (<1% of total peak area) of lignin-derived products. Nevertheless, to avoid significant interference in samples that are high in protein and low in lignin it is suggested to monitor the formation of indole as protein marker pyrolysis product (*R*_t 17.81 min, *m/z* 117) and correct detected areas for phenol, 2-methylphenol and 4-methylphenol accordingly.⁴¹

Extensive changes in relative distribution of pyrolysis products over the applied full range (10 to 35 µg) were not observed, indicating that besides content, valuable information about the lignin structure can be obtained concurrently. To further explore the potential of the novel quantitative method, ¹³C-IS based lignin quantification was applied on four different common poaceous biomass sources and compared to the classical Klason method. Compositional data of these four grasses is presented in Supporting Information Table S1 and S2.

Lignin quantification in poaceous biomass

In Figure 3, a comparison is shown between lignin content as quantified by the classical Klason lignin method and the novel ^{13}C -IS based py-GC-SIM-MS method. The results of Klason lignin analysis are presented as acid-insoluble lignin (AIL) corrected for ash and protein and acid-soluble lignin (ASL). AIL determined by this method is often not corrected or contaminated with chitin from fungal origin that cannot be corrected for.^{15, 17, 20} The importance of ash correction was clearly demonstrated as ash contents of hydrolysis residues (AI ash) up to 25% (w/w) were found. Even though the amount of acid insoluble protein was rather limited (~4% of hydrolysis residue), it might be important to be taken into account for more protein-rich samples. The spectrophotometric analysis of ASL depends highly on the used wavelength and corresponding extinction coefficients. As a result of different lignin compositions per biomass, extinction coefficients vary per biomass. Since the determination of this extinction coefficient is laborious, all types of biomass were analyzed at the same wavelength (205 nm) with an averaged extinction coefficient ($110 \text{ g L}^{-1} \text{ cm}^{-1}$), based on literature.^{7, 42-43} For that reason the ASL-content based on the common Klason protocol does not result in an accurate lignin content. Lignin contents determined according to Klason (AIL and ASL) agreed well with previous studies on these biomasses and were therefore considered valid for the evaluation of the performance of the novel method.^{29, 44-45}

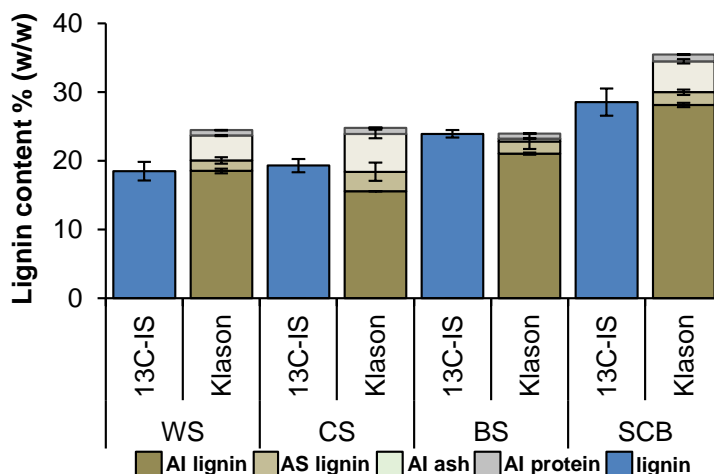


Figure 3. Lignin content determination via ^{13}C -IS based py-GC-SIM-MS (triplicate) and Klason (duplicate). WS: wheat straw, CS: corn stover, BS: barley straw, SCB: sugar cane bagasse, AI: acid-insoluble, AS: acid-soluble.

Lignin contents of the four biomasses quantified via the ^{13}C -IS py-GC-MS approach were in good accordance with the classical Klason method (AIL + ASL) with an insignificant relative deviation in the order of 5%. High reproducibility was obtained for the lignin content of all biomasses (RSD < 7%). Compared to previous py-GC-MS attempts on lignin quantification, our novel method thus showed greatly

enhanced accuracy and reproducibility, with acceptable costs and time-investments.^{16-20, 22} The latter is concluded from the fact that from 1 gram of ¹³C labeled wheat straw 45 mg of 90% pure ¹³C lignin internal standard can be isolated in one week, which is sufficient to perform 45.000 pyrolysis runs. Compared to external ¹²C lignin based quantification significant enhancements in terms of accuracy were achieved by applying ¹³C lignin as internal standard (Supporting Information Figure S5), indicating the importance of matrix-effects during pyrolysis.

The use of extractive-free biomasses ensured compounds potentially interfering with lignin-analysis by py-GC-MS analysis to be removed. Furthermore, the presence of ash and/or chitin (in fungal treated biomass) does not interfere with py-GC-MS analysis as potential matrix-effects are corrected for by the internal standard approach and all chitin-derived pyrolysis products can be distinguished from lignin-derived products. Thereto, the sum of the lignin derived pyrolysis products was a reliable representation of lignin content and lignin content could thus be similarly determined as shown for reconstituted biomass samples. Due to the fact that the internal standard was added as a liquid and subsequently dried, the internal standard was well dispersed throughout the sample. The use of a microfurnace pyrolyzer combined with low standardized particle size (<250 µm) and standardized low sample amount (~75 µg) furthermore ensured rapid pyrolysis with heating rates expected to be >2000 °C s⁻¹.²³⁻²⁴ The mechanisms underlying pyrolysis were thereto expected not to differ between sample lignin and internal standard lignin.

The application of relative response factors (Table 1) enabled us to accurately determine the content of lignins that were structurally distinct and dissimilar to the structure of the internal standard as well (Table 5 and Figure S5). This flexibility is a clear benefit compared to existing alternatives for the quantification of lignin content in plant biomass, that depend on structurally similar calibration standards.⁸⁻¹¹ Future analysis of a larger variety of biomasses, including softwoods, hardwoods and chemically and/or enzymatically modified ones, will further improve understanding of the performance of our ¹³C-IS based novel method for lignin quantification.

As previously discussed in the section '*Characterization of lignin isolates*' (this chapter), the relative composition of the lignin subunits as found by py-GC-MS when RRFs were applied was comparable to 2D-NMR. Besides content, valuable information on the subunit composition of the biomasses could thus be obtained concurrently. A more accurate view on the composition of the pyrolysates was obtained and demonstrated the importance of oxygen-containing pyrolysis products (C_α-O, C_β-O and C_γ-O) for describing lignins structural features.

Table 5. Py-GC-SIM-MS relative abundance of structural features within biomasses and ^{13}C internal standard (^{13}C -IS) on the basis of RRF corrected molar peak area. Structural classification is shown in Table 1. Average and standard deviation of triplicates. WS: wheat straw, CS: corn stover, BS: barley straw, SCB: sugarcane bagasse.

	WS	CS	BS	SCB	^{13}C -IS ^a
Lignin % (w/w)^b	18.5±1.3	19.3±1.0	23.9±0.6	28.5±2.0	-
Lignin subunits (%)					
H	16.3±0.8	42.8±0.8	15.4±0.7	49.0±4.2	17.1±5.0
G	66.2±1.4	47.7±1.1	59.9±1.4	35.8±1.8	60.2±3.9
S	17.5±0.4	9.5±0.2	24.7±0.7	15.3±0.7	22.7±1.2
S/G	0.3	0.2	0.4	0.4	0.4
Structural moieties (%)					
unsub.	6.2±0.2	5.1±0.1	5.4±0.05	6.8±0.4	4.5±0.3
methyl	2.8±0.1	3.0±0.1	2.5±0.1	4.6±0.5	2.1±0.5
ethyl	0.3±0.01	0.3±0.1	0.2±0.01	0.4±0.05	0.2±0.04
vinyl	40.8±0.9	68.3±1.3	34.8±1.3	59.5±4.2	25.3±5.1
C $_{\alpha}$ -O ^c	3.1±0.1	4.0±0.1	3.5±0.06	4.1±0.2	4.3±0.3
C $_{\beta}$ -O ^d	1.2±0.03	0.8±0.05	1.4±0.05	1.5±0.1	1.4±0.2
C $_{\gamma}$ -O ^e	42.9±1.4	15.9±0.3	49.4±1.2	17.7±1.7	58.8±3.0
misc. ^f	2.7±0.04	2.6±0.08	2.7±0.06	5.1±0.2	3.3±0.4

^aaverage and standard deviation of ^{13}C -IS added to all biomasses in triplicate

^bdetermined by ^{13}C lignin IS based py-GC-SIM-MS

^cC $_{\alpha}$ -oxygen, ^dC $_{\beta}$ -oxygen, ^eC $_{\gamma}$ -oxygen, ^fmiscellaneous

Conclusions

Here, we describe a novel method for the concurrent quantification of absolute lignin content and subunit composition in plant biomass. By employing a ^{13}C -labeled polymeric lignin isolate as internal standard (IS) for the first time and correcting for relative response factors of the formed lignin-derived pyrolysis products, py-GC-MS could be applied for this purpose. Our ^{13}C lignin IS based approach was validated in biomass model system containing a structurally similar ^{12}C lignin analogue with known lignin contents. Structurally distinct lignins in four common poaceous biomass sources were quantified with an insignificant relative deviation in the order of 5% compared to classic gravimetric analysis. The simultaneous acquirement of structural information with high reproducibility in a more high-throughput fashion makes our method a huge improvement compared to current alternative methods for lignin quantification. We reckon that our new lignin quantification method opens up possibilities for more accurate analysis of lignin content and subunit composition in various research fields dealing with lignin containing plant biomass.

References

1. Buranov, A. U.; Mazza, G., Lignin in straw of herbaceous crops. *Ind Crops Prod* **2008**, *28*, 237-259.
2. Vanholme, R.; Demedts, B.; Morreel, K.; Ralph, J.; Boerjan, W., Lignin biosynthesis and structure. *Plant Physiol* **2010**, *153*, 895-905.
3. Englyst, H. N.; Cummings, J. H., Simplified method for the measurement of total non-starch polysaccharides by gas-liquid chromatography of constituent sugars as alditol acetates. *Analyst* **1984**, *109*, 937-942.
4. Ruiz, R.; Date, T. E. In *Determination of carbohydrates in biomass by high performance liquid chromatography*, Laboratory Analytical Procedure No. 002, National Renewable Research Laboratory, 1996.
5. Lupoi, J. S.; Singh, S.; Parthasarathi, R.; Simmons, B. A.; Henry, R. J., Recent innovations in analytical methods for the qualitative and quantitative assessment of lignin. *Renewable Sustainable Energy Rev* **2015**, *49*, 871-906.
6. Hatfield, R.; Fukushima, R. S., Can lignin be accurately measured? *Crop Sci.* **2005**, *45*, 832-839.
7. Sluiter, J. B.; Ruiz, R. O.; Scarlata, C. J.; Sluiter, A. D.; Templeton, D. W., Compositional analysis of lignocellulosic feedstocks. 1. Review and description of methods. *J Agric Food Chem* **2010**, *58*, 9043-9053.
8. Rodrigues, J.; Faix, O.; Pereira, H., Determination of lignin content of *Eucalyptus globulus* wood using FTIR spectroscopy. *Holzforschung* **1998**, *52*, 46-50.
9. Wolfrum, E. J.; Sluiter, A. D., Improved multivariate calibration models for corn stover feedstock and dilute-acid pretreated corn stover. *Cellulose* **2009**, *16*, 567-576.
10. Jiang, N.; Pu, Y.; Ragauskas, A. J., Rapid determination of lignin content via direct dissolution and ^1H NMR analysis of plant cell walls. *ChemSusChem* **2010**, *3*, 1285-1289.
11. Fu, L.; McCallum, S. A.; Miao, J.; Hart, C.; Tudryn, G. J.; Zhang, F.; Linhardt, R. J., Rapid and accurate determination of the lignin content of lignocellulosic biomass by solid-state NMR. *Fuel* **2015**, *141*, 39-45.
12. Gao, X.; Laskar, D. D.; Zeng, J.; Helms, G. L.; Chen, S., A ^{13}C CP/MAS-based nondegradative method for lignin content analysis. *ACS Sustainable Chem Eng* **2014**, *3*, 153-162.
13. Ralph, J.; Hatfield, R. D., Pyrolysis-GC-MS characterization of forage materials. *J Agric Food Chem* **1991**, *39*, 1426-1437.
14. Murciano Martínez, P.; Punt, A. M.; Kabel, M. A.; Gruppen, H., Deconstruction of lignin linked *p*-coumarates, ferulates and xylan by NaOH enhances the enzymatic conversion of glucan. *Bioresour Technol* **2016**, *216*, 44-51.
15. Jurak, E.; Punt, A. M.; Arts, W.; Kabel, M. A.; Gruppen, H., Fate of carbohydrates and lignin during composting and mycelium growth of *Agaricus bisporus* on wheat straw based compost. *PLoS ONE* **2015**, *10*, e0138909.
16. Bocchini, P.; Galletti, G.; Camarero, S.; Martinez, A., Absolute quantitation of lignin pyrolysis products using an internal standard. *J Chromatogr A* **1997**, *773*, 227-232.
17. Alves, A.; Schwanninger, M.; Pereira, H.; Rodrigues, J., Analytical pyrolysis as a direct method to determine the lignin content in wood: Part 1: Comparison of pyrolysis lignin with Klason lignin. *J Anal Appl Pyrolysis* **2006**, *76*, 209-213.
18. Alves, A.; Rodrigues, J.; Wimmer, R.; Schwanninger, M., Analytical pyrolysis as a direct method to determine the lignin content in wood: Part 2: Evaluation of the common model and the influence of compression wood. *J Anal Appl Pyrolysis* **2008**, *81*, 167-172.
19. Ross, K.; Mazza, G., Comparative analysis of pyrolysis products from a variety of herbaceous Canadian crop residues. *World J of Agric Sci* **2011**, *7*, 763-776.
20. Lourenço, A.; Gominho, J.; Marques, A. V.; Pereira, H., Comparison of Py-GC/FID and wet chemistry analysis for lignin determination in wood and pulps from *Eucalyptus globulus*. *BioResources* **2013**, *8*, 2967-2980.

21. Groenewold, G. S.; Johnson, K. M.; Fox, S. C.; Rae, C.; Zarzana, C. A.; Kersten, B. R.; Rowe, S. M.; Westover, T. L.; Gresham, G. L.; Emerson, R. M., Pyrolysis two-dimensional GC-MS of miscanthus biomass: quantitative measurement using an internal standard method. *Energy Fuels* **2017**.
22. Torri, C.; Adamiano, A.; Fabbri, D.; Lindfors, C.; Monti, A.; Oasmaa, A., Comparative analysis of pyrolysate from herbaceous and woody energy crops by Py-GC with atomic emission and mass spectrometric detection. *J Anal Appl Pyrolysis* **2010**, *88*, 175-180.
23. Patwardhan, P. R.; Satrio, J. A.; Brown, R. C.; Shanks, B. H., Influence of inorganic salts on the primary pyrolysis products of cellulose. *Bioresour Technol* **2010**, *101*, 4646-4655.
24. Patwardhan, P. R.; Brown, R. C.; Shanks, B. H., Understanding the fast pyrolysis of lignin. *ChemSusChem* **2011**, *4*, 1629-1636.
25. Gorissen, A.; Kraut, N. U.; de Visser, R.; de Vries, M.; Roelofsen, H.; Vonk, R. J., No *de novo* sulforaphane biosynthesis in broccoli seedlings. *Food Chem* **2011**, *127*, 192-196.
26. Björkman, A., Studies on finely divided wood. Part 1. Extraction of lignin with neutral solvents. *Sven. Papperstidn.* **1956**, *59*, 477-485.
27. Kabel, M. A.; Van der Maarel, M. J.; Klip, G.; Voragen, A. G.; Schols, H. A., Standard assays do not predict the efficiency of commercial cellulase preparations towards plant materials. *Biotechnol Bioeng* **2006**, *93*, 56-63.
28. Jones, D. B., Factors for converting percentages of nitrogen in foods and feeds into percentages of proteins. *US Agric Circ* **1931**, 1-16.
29. Del Río, J. C.; Rencoret, J.; Prinsen, P.; Martínez, Á. T.; Ralph, J.; Gutiérrez, A., Structural characterization of wheat straw lignin as revealed by analytical pyrolysis, 2D-NMR, and reductive cleavage methods. *J Agric Food Chem* **2012**, *60*, 5922-5935.
30. Rencoret, J.; Marques, G.; Gutiérrez, A.; Nieto, L.; Santos, J. I.; Jiménez-Barbero, J.; Martínez, A. T.; del Río, J. C., HSQC-NMR analysis of lignin in woody (*Eucalyptus globulus* and *Picea abies*) and non-woody (*Agave sisalana*) ball-milled plant materials at the gel state 10th EWLP, Stockholm, Sweden, August 25-28, 2008. *Holzforschung* **2009**, *63*, 691-698.
31. Zeng, J.; Helms, G. L.; Gao, X.; Chen, S., Quantification of wheat straw lignin structure by comprehensive NMR analysis. *J Agric Food Chem* **2013**, *61*, 10848-10857.
32. Del Río, J. C.; Gutiérrez, A.; Rodríguez, I. M.; Ibarra, D.; Martínez, Á. T., Composition of non-woody plant lignins and cinnamic acids by Py-GC/MS, Py/TMAH and FT-IR. *J Anal Appl Pyrolysis* **2007**, *79*, 39-46.
33. Zikeli, F.; Ters, T.; Fackler, K.; Srebotnik, E.; Li, J., Successive and quantitative fractionation and extensive structural characterization of lignin from wheat straw. *Ind Crops Prod* **2014**, *61*, 249-257.
34. Chang, H.-m.; Cowling, E. B.; Brown, W., Comparative studies on cellulolytic enzyme lignin and milled wood lignin of sweetgum and spruce. *Holzforschung* **1975**, *29*, 153-159.
35. Rencoret, J.; Prinsen, P.; Gutiérrez, A.; Martínez, Á. T.; del Río, J. C., Isolation and structural characterization of the milled wood lignin, dioxane lignin, and cellulolytic lignin preparations from brewer's spent grain. *J Agric Food Chem* **2015**, *63*, 603-613.
36. Zeng, J.; Singh, D.; Gao, D.; Chen, S., Effects of lignin modification on wheat straw cell wall deconstruction by *Phanerochaete chrysosporium*. *Biotechnol Biofuels* **2014**, *7*, 161.
37. Ralph, J., Hydroxycinnamates in lignification. *Phytochem Rev* **2010**, *9*, 65-83.
38. Akazawa, M.; Kojima, Y.; Kato, Y., Effect of pyrolysis temperature on the pyrolytic degradation mechanism of β -aryl ether linkages. *J Anal Appl Pyrolysis* **2016**, *118*, 164-174.

39. Akazawa, M.; Kato, Y.; Kojima, Y., Application of two resinols as lignin dimer models to characterize reaction mechanisms during pyrolysis. *J Anal Appl Pyrolysis* **2016**, *122*, 355-364.
40. Koshijima, T.; Watanabe, T., *Association between lignin and carbohydrates in wood and other plant tissues*. Springer-Verlag: Berlin, 2003.
41. Biller, P.; Ross, A., Pyrolysis GC-MS as a novel analysis technique to determine the biochemical composition of microalgae. *Algal Res* **2014**, *6*, 91-97.
42. Nicholson, D.; Aaron, T.; Francis, R. C., A three-stage Klason method for more accurate determinations of hardwood lignin content. *Cellul Chem Technol.* **2013**, *48*, 53-59.
43. Dence, C. W., The Determination of Lignin. In *Methods in Lignin Chemistry*, Lin, S. Y.; Dence, C. W., Eds. Springer Berlin Heidelberg: Berlin, Heidelberg, 1992; pp 33-61.
44. Murciano Martínez, P.; Bakker, R.; Harmsen, P.; Gruppen, H.; Kabel, M. A., Importance of acid or alkali concentration on the removal of xylan and lignin for enzymatic cellulose hydrolysis. *Ind Crops Prod* **2015**, *64*, 88-96.
45. Kim, T. H.; Kim, J. S.; Sunwoo, C.; Lee, Y., Pretreatment of corn stover by aqueous ammonia. *Bioresour Technol* **2003**, *90*, 39-47.

Supporting Information

Preparation of nonlabeled and ^{13}C -labeled wheat straw Nonlabeled (^{12}C) and uniformly ^{13}C -labeled (97 atom % ^{13}C , " ^{13}C ") spring wheat plants (*Triticum aestivum* L. cv. "Baldus") (WS) were produced under identical growth conditions in the custom designed, air-tight, high-irradiance labeling chambers of the facility ESPAS (Experimental Soil Plant Atmosphere System, IsoLife, Wageningen, The Netherlands).¹ The environmental and atmospheric conditions were fully controlled. Plants were grown hydroponically at a photosynthetic photon flux density (PPFD) of 900 $\mu\text{mol m}^{-2} \text{s}^{-1}$ (top of plants) at a 16 h day length, a day/night temperature of 24/16 °C and RH of 75 %, in a closed atmosphere containing either regular CO_2 (1.1 atom % ^{13}C ; " ^{12}C ") or 98 atom % $^{13}\text{CO}_2$ (CO_2 labeled with the stable isotope ^{13}C ; from pressurized cylinders, Sigma-Aldrich, St Louis, USA; " $\text{U-}^{13}\text{C}$ ") from the seedling stage until fully mature and ripened (Haun, Feeke's and Zadoks scales 16.0, 11.4 and 92, respectively).²⁻⁴ The ^{13}C abundance of the CO_2 in the chamber was continuously monitored by analysis both $^{12}\text{CO}_2$ and $^{13}\text{CO}_2$ using Non-Dispersive Infrared (NDIR) throughout the culturing time (IsoLife). Minerals were supplied as Hoagland-type nutrient solutions with micro-nutrients and iron, maintaining pH between 5 and 6.⁵⁻⁶ After 14 weeks of culture, plants were harvested. Immediately after removing the plants from the labeling facility, plants were dissected and stems cut to 3-6 cm pieces, weighed, packaged in food-grade PE pouches and stored at -30 °C till freeze-drying (lyophilization at 0.6 mbar). The final dried material was stored in a dry place in the dark till analysis. After freeze-drying, subsamples were prepared for analysis of atom % ^{13}C by high-abundance Isotope-ratio Mass Spectrometry (IRMS) (Sigma-Aldrich, St Louis, USA and Stable Isotope Facility, UC-Davis, CA, USA) and were equal to 1.1 at% ^{13}C and 97.6 at% ^{13}C for ^{12}C and ^{13}C WS, respectively. Two spring wheat plants were used with a total of approximately 80 stalks for the nonlabeled as well as ^{13}C labeled straw. From the total material a randomly selected sample of 3 grams (approx. 4% of total material) was taken for the isolation of the lignins.

Compositional analysis of total biomass and lignin isolates

Carbohydrate content and composition. was determined in duplicate as constituent monosaccharides after acid hydrolysis by a modified method reported by Englyst & Cummings.⁷ Samples were treated with 72% (w/w) H₂SO₄ for 2 h at 30 °C followed by 1 M H₂SO₄ for 4 h at 100 °C and diluted (20x) before analysis. Degradation of monosaccharides during hydrolysis was corrected for by including monosaccharide standard mixtures in hydrolysis. Analysis was performed on a High Performance Anion Exchange Chromatography (HPAEC) Dionex ICS-5000 system (Thermo Scientific, Synnyvale, CA, USA). The system was equipped with a CarboPac PA-1 column (250 mm x 2 mm ID) in combination with a CarboPac guard column (50 mm x 2 mm ID) with pulsed amperometric detection (PAD) (all Dionex). 10 µL of sample was injected and eluted at a flow rate of 0.4 mL min⁻¹ using a combination of three mobile phases: A) 0.1 M NaOH, B) 1 M NaOAc in 0.1 M NaOH and C) H₂O. The elution profile used was as follows: 0-35 min isocratic on 100% C; 35-50 min linearly from 100% A to 40% B; 50-55 min isocratic on 100% B; 55-63 min isocratic on 100%A; 63-78 min isocratic on 100% C. Post-column addition of 0.5 M NaOH at 0.1 mL min⁻¹ was performed between 0-35 min and 63-78 min.

Protein content. Nitrogen content was analyzed in duplicate using the combustion method (DUMAS) on a Flash EA 1112 Nitrogen Analyzer (Thermo Scientific, Synnyvale, CA, USA). Methionine (Acros Organics, Geel, Belgium) was used as calibration standard. A nitrogen to protein conversion factor of 6.25 was used.⁸

Ash content. Ash content of oven dried samples (40 °C, 8 h) was determined gravimetrically after burning samples at 550 °C for 16 h. Analyses were performed in triplicate.

Lignin content. Acetone-extractive-free wheat straw (WS) and corn stover (CS) and unextracted barley straw (BS) and sugarcane bagasse (SCB) were milled in a Mixer Mill MM 400 (Retsch, Haan, Germany) and passed through a 0.25 mm sieve. Water unextractable solids (WUS) were obtained by extracting as explained in the section 'Isolation of lignin from ¹²C and ¹³C wheat straw'. Final residues were freeze-dried. Acid insoluble (Klason) lignin corrected for ash and protein and acid soluble lignin contents of biomass WUS samples were determined in duplicate according to Jurak et al.⁹ Protein content of acid insoluble residues was determined as described above.

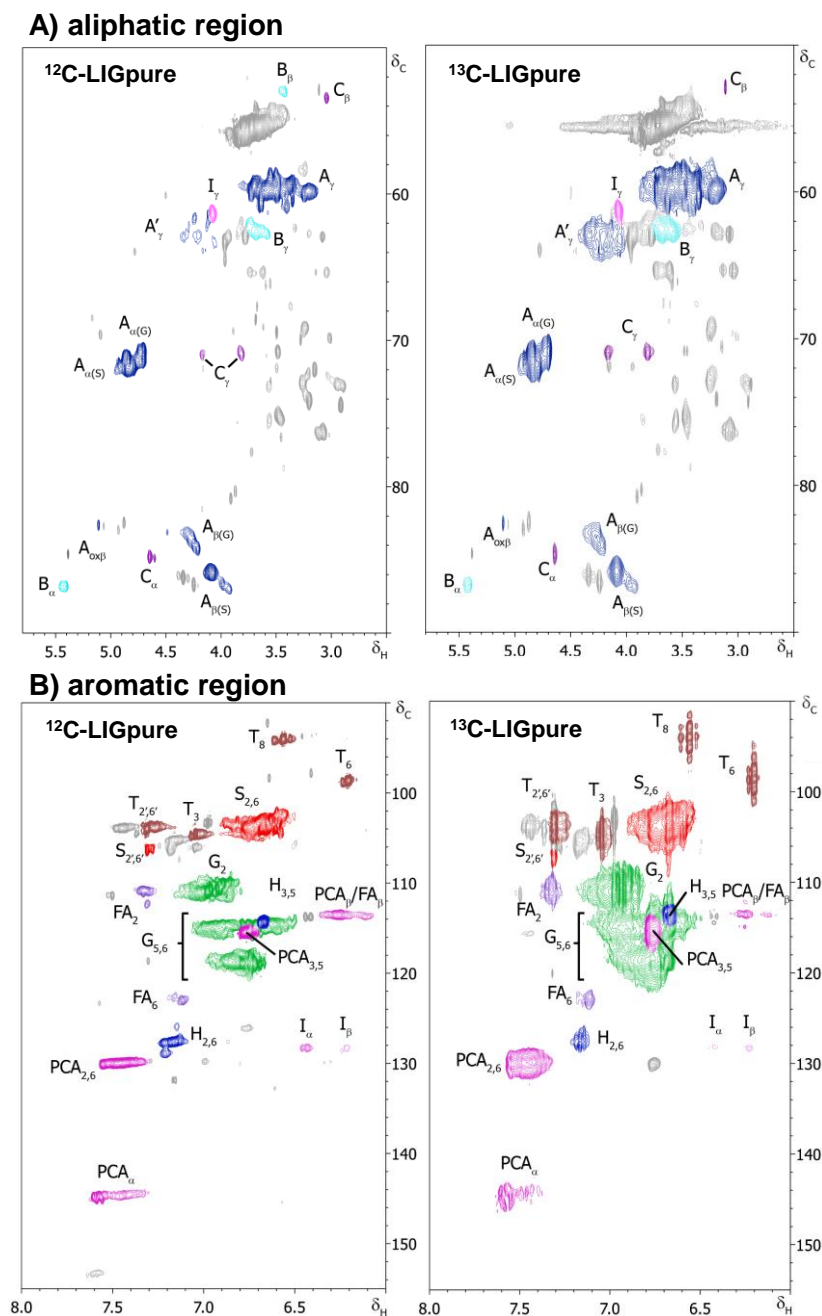


Figure S1. Representative HSQC-NMR spectra of ^{12}C -LIGpure and ^{13}C -LIGpure. Structures of annotated correlation peaks are presented in Figure S2. Annotated structures D and F are not visible at this zoom level. Note that in the aromatic region of the ^{13}C spectrum (D) significant ^{13}C - ^{13}C coupling is observed.

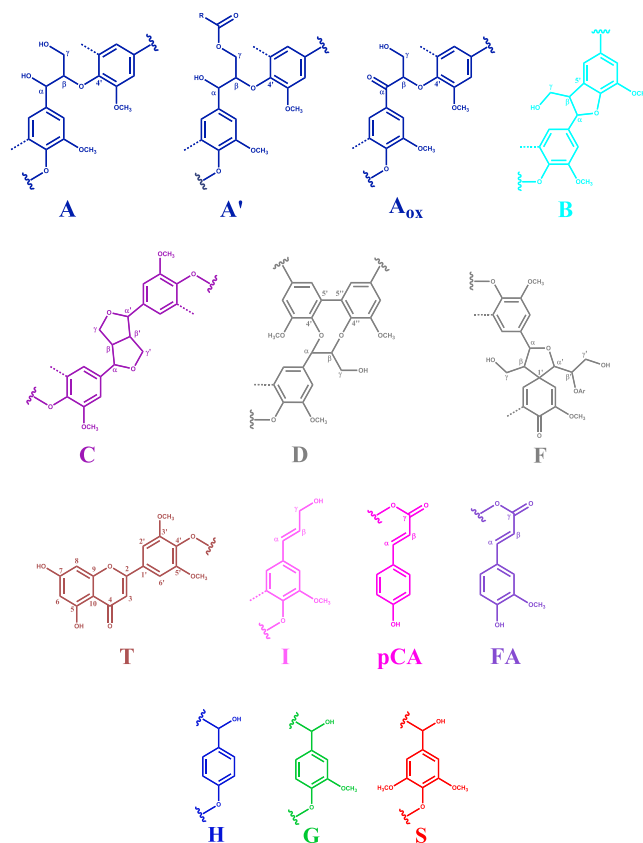


Figure S2. Structures annotated by HSQC-NMR. A: β -O-4' aryl ether; A': β -O-4' aryl ether γ -acetylated; A_{ox}: C α -oxidized β -O-4' aryl ether; B: phenylcoumaran; C: resinol; D: dibenzodioxocins; F: spirodienone; I: cinnamyl alcohol end-group; pCA: *p*-coumarate; FA: ferulate; T: triclin; H: *p*-hydroxyphenyl unit; G: guaiacyl unit; S: syringyl unit. Dotted line represents -H or -OCH₃. α,β -diarylether, and cinnamaldehyde end group structures were not detected.

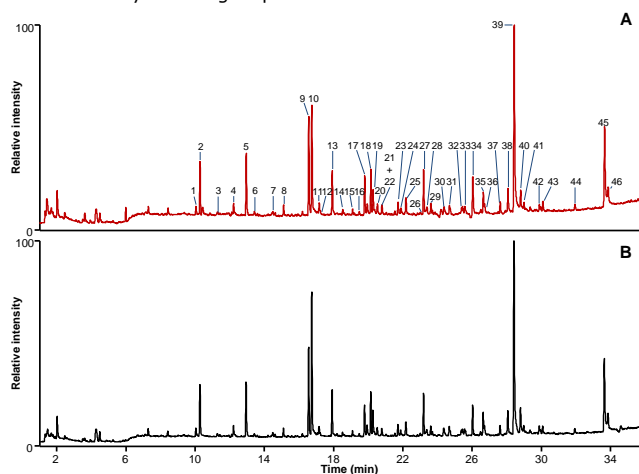


Figure S3. Representative py-GC-MS pyrograms (TIC) of ¹²C-LIGpure (A) and ¹³C-LIGpure (B). Peak annotation according to Table 1.

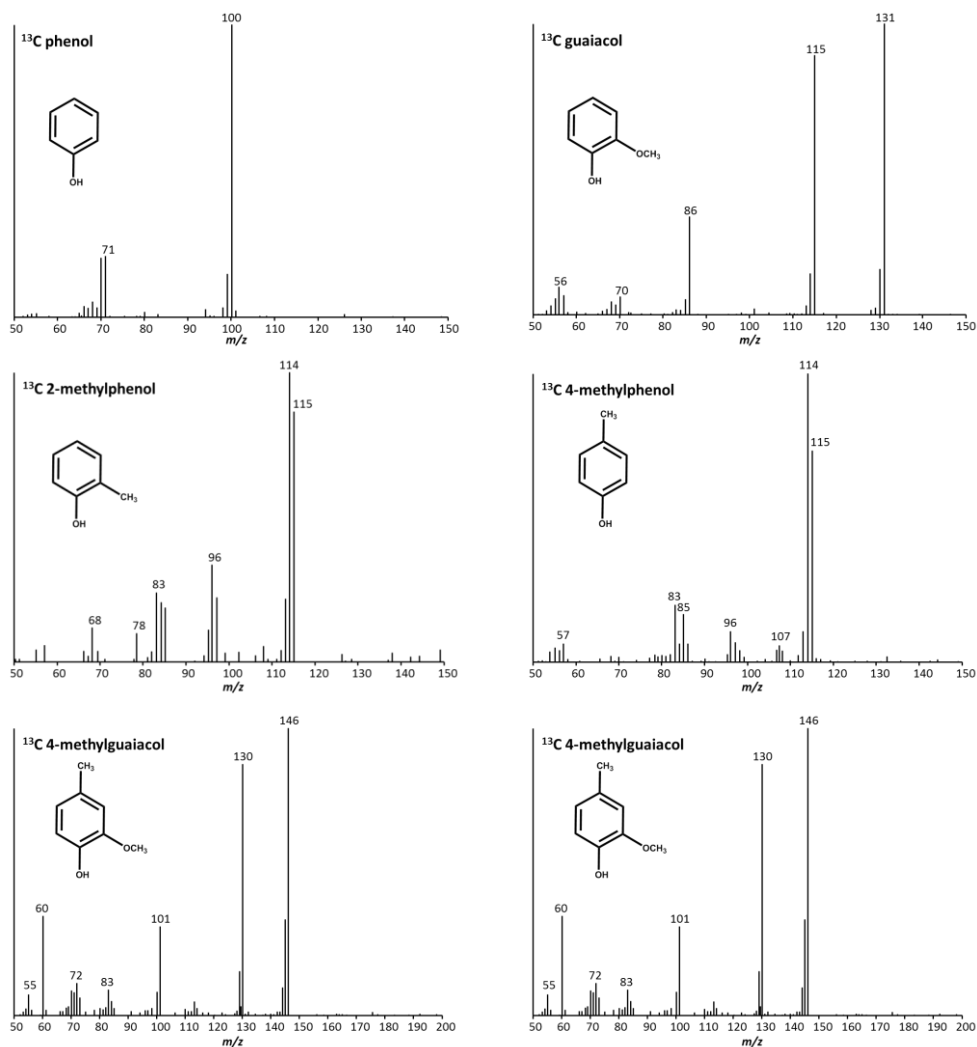


Figure S4. EI-MS (70 eV) spectra of ¹³C-labeled lignin-derived pyrolysis products. Compounds were identified on the basis of retention time, fragmentation spectra and carbon number of ¹²C analogues. Average mass spectrum across the chromatographic peak with noise subtraction at two sides. Indicated masses are >10% relative abundance, where the highest fragment is put at 100%. CAS numbers of corresponding ¹²C compounds are specified in Table 1.

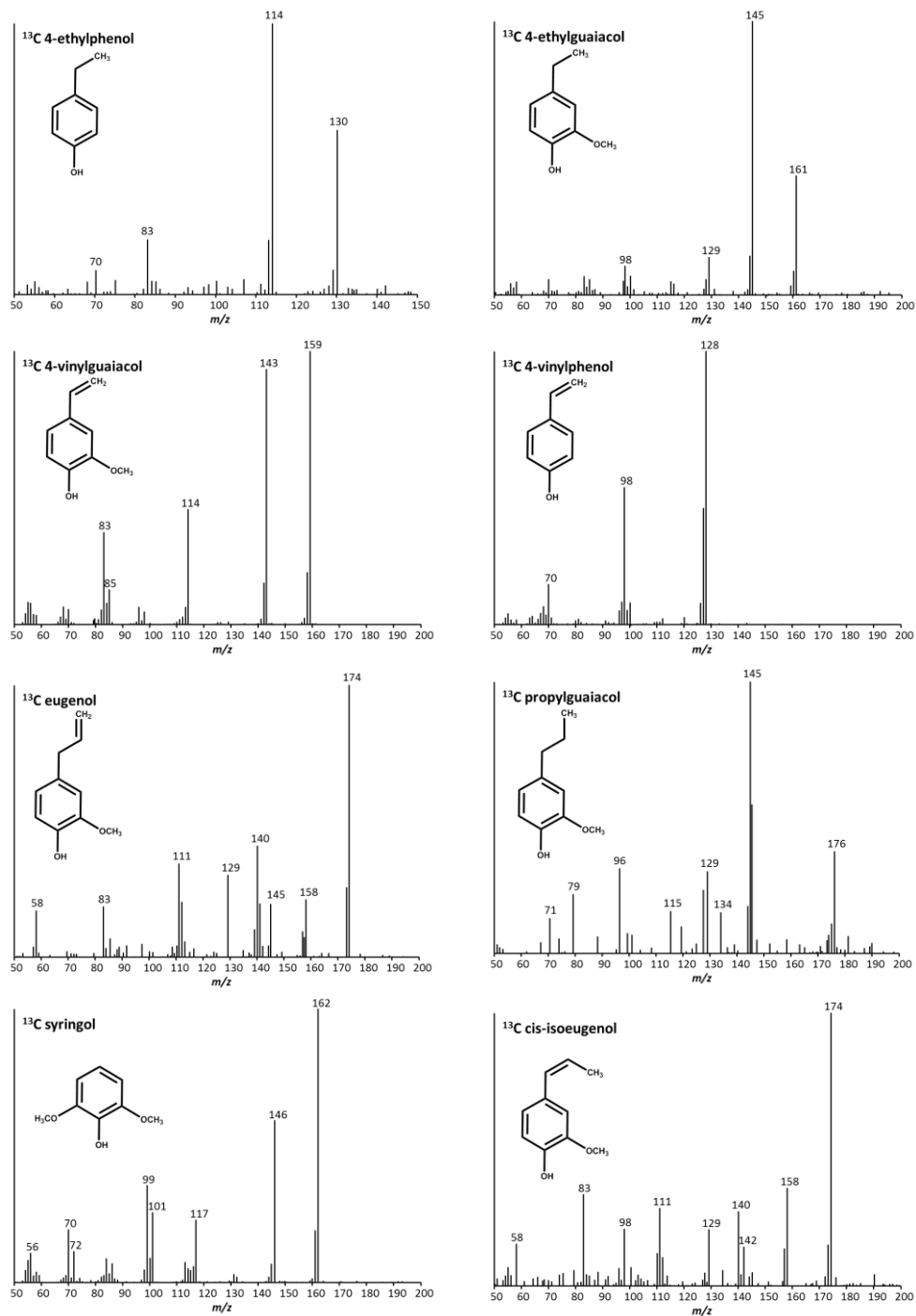


Figure S4. Continuation.

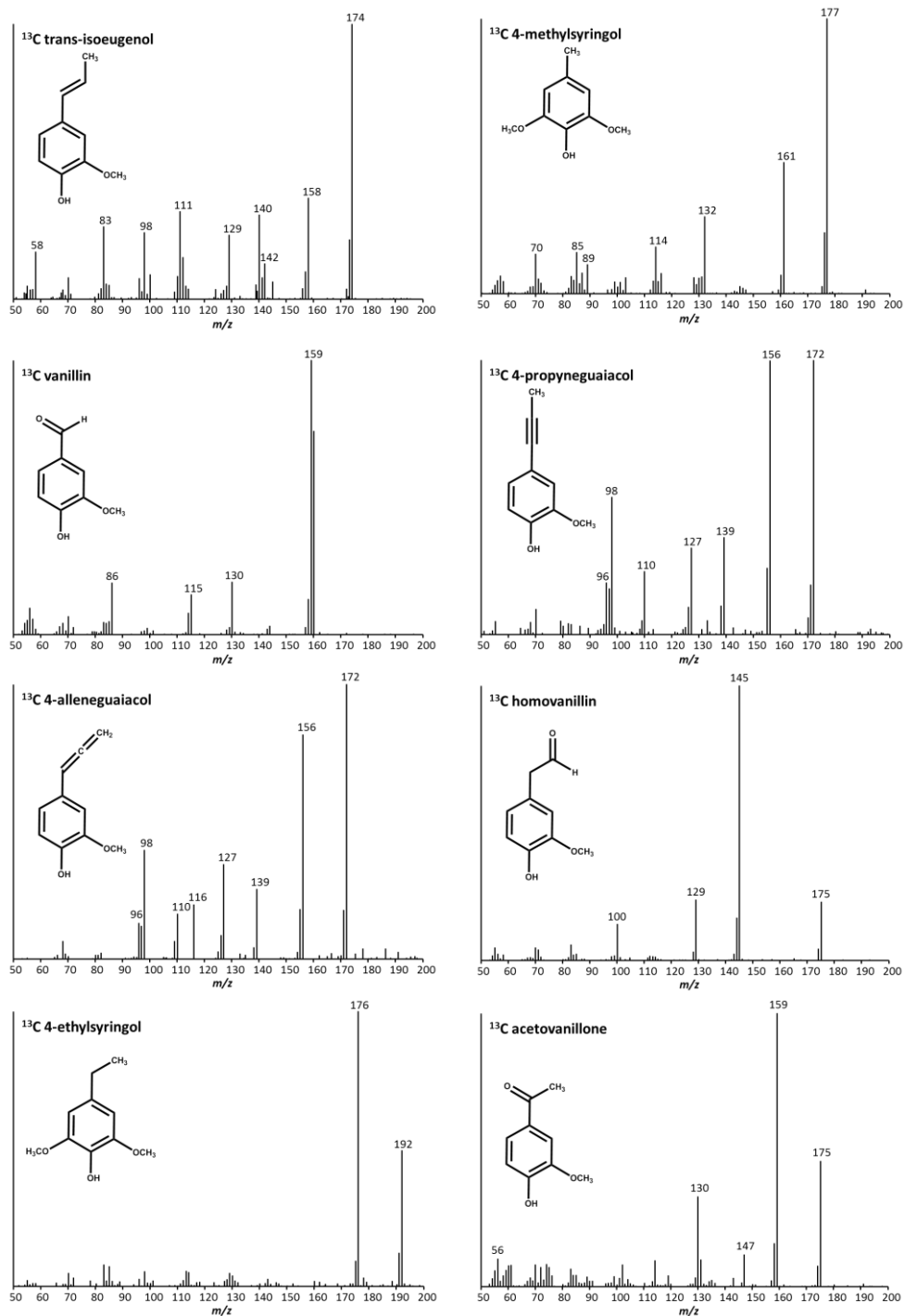


Figure S4. Continuation.

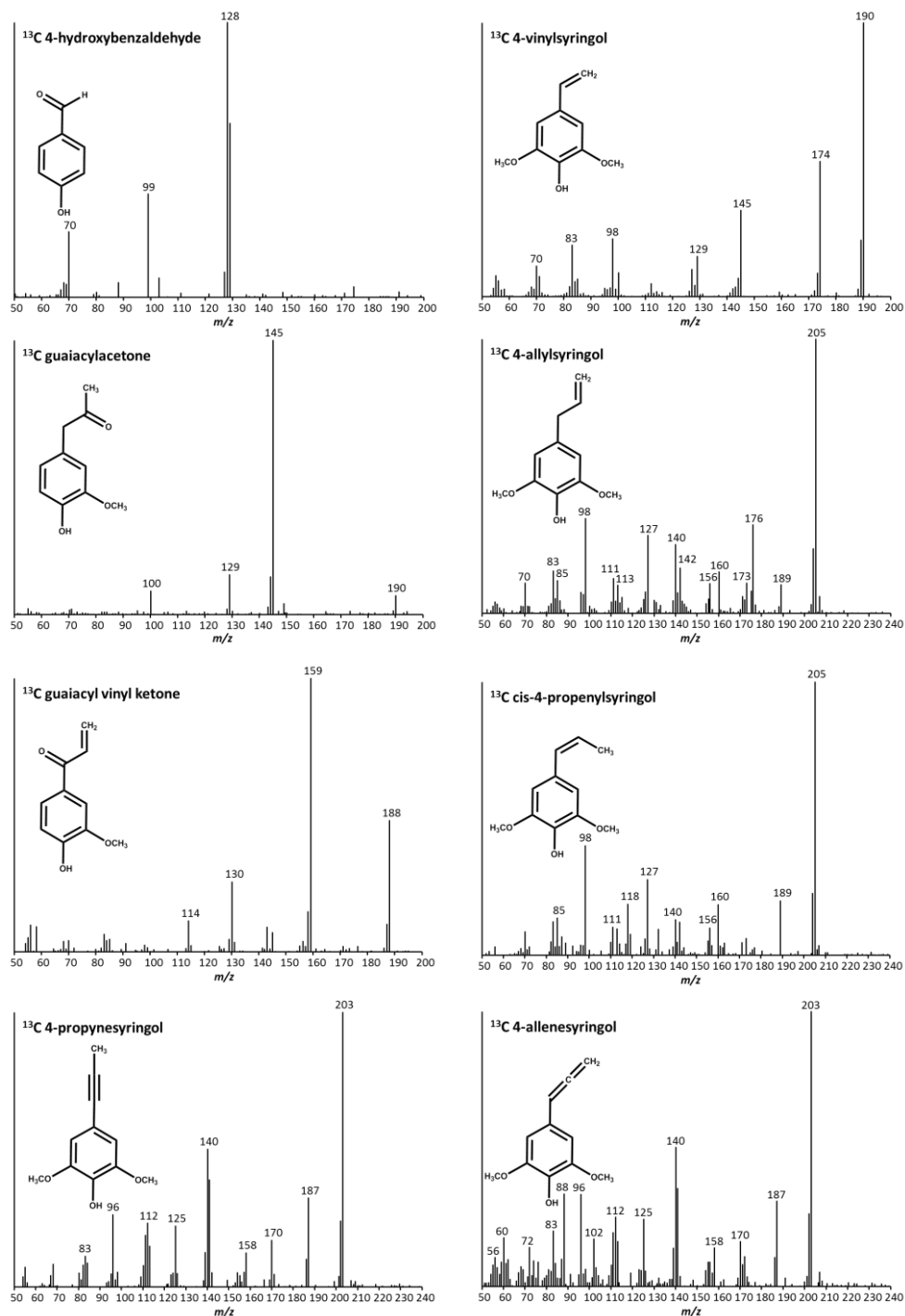


Figure S4. Continuation.

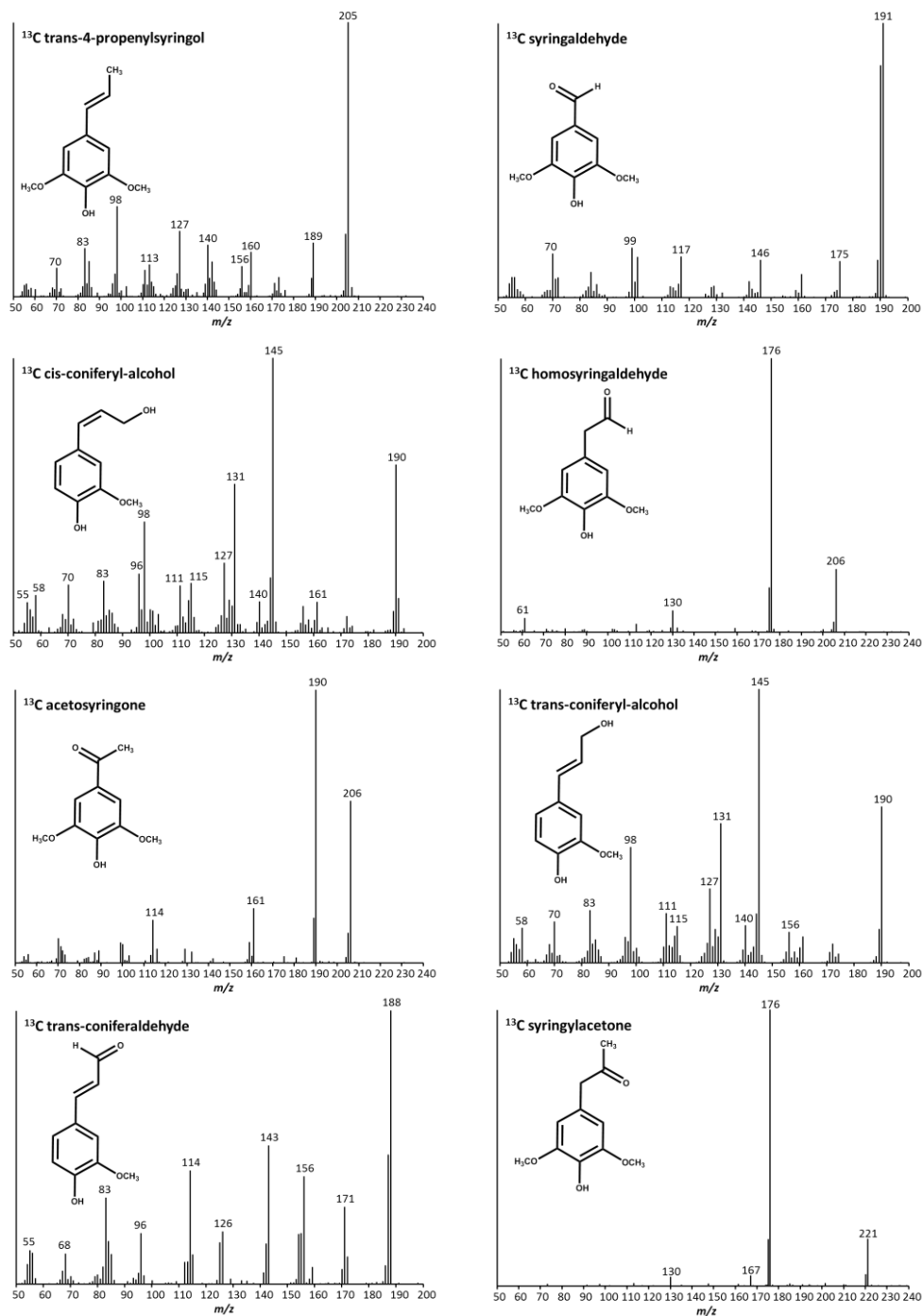


Figure S4. Continuation.

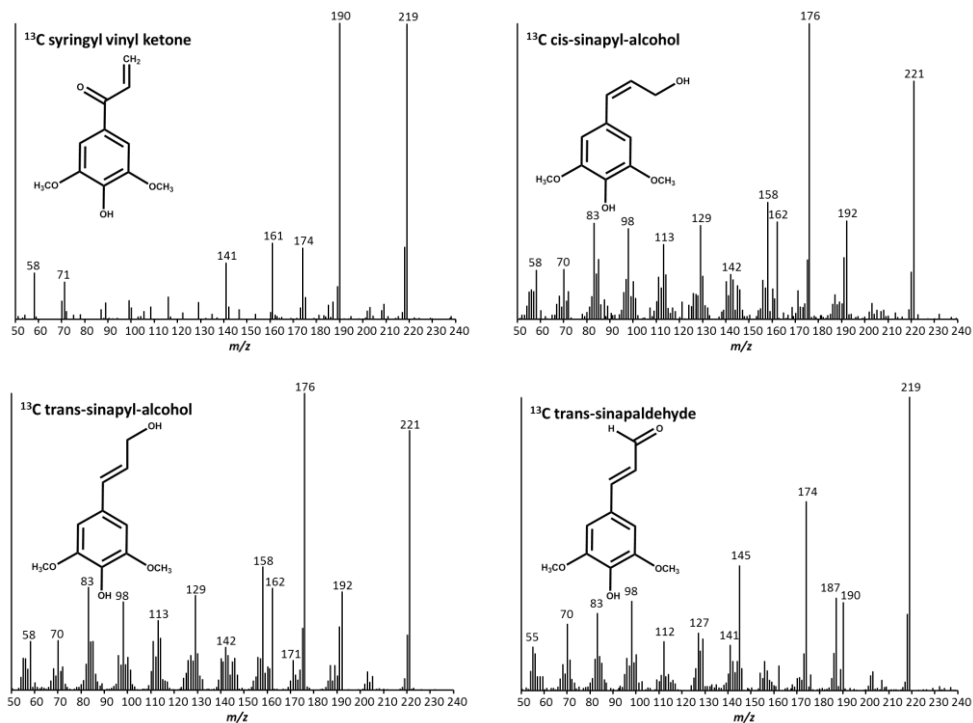


Figure S4. Continuation.

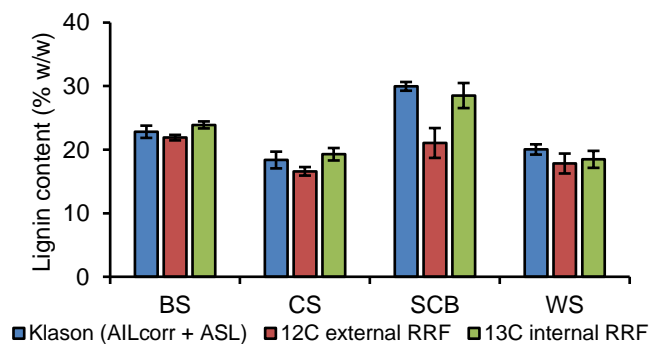


Figure S5. Lignin content determination via Klason (duplicate) (Acid-insoluble lignin corrected for ash and protein (AIL_{corr}) + Acid-soluble lignin (ASL)), ¹²C external standard with RRF correction via py-GC-SIM-MS (triplicate) and ¹³C internal standard with RRF correction via py-GC-SIM-MS (triplicate). WS: wheat straw, CS: corn stover, BS: barley straw, SCB: sugar cane bagasse.

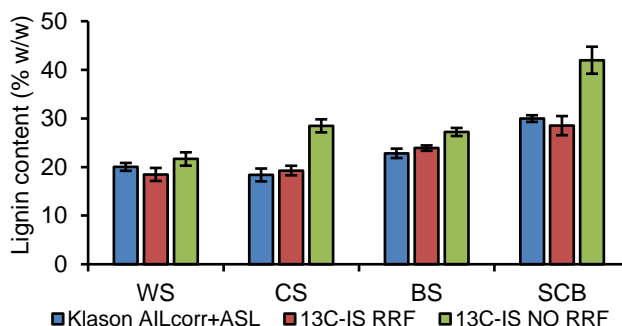


Figure S6. Lignin content determination via Klason (duplicate) (Acid-insoluble lignin corrected for ash and protein (AIL_{corr}) + Acid-soluble lignin (ASL)) and ¹³C-IS based py-GC-SIM-MS (triplicate) with and without application of relative response factors (RRF) for lignin-derived pyrolysis products. WS: wheat straw, CS: corn stover, BS: barley straw, SCB: sugar cane bagasse, AIL: acid-insoluble, AS: acid-soluble.

Table S1. Composition of poaceous biomasses (% dry weight) determined in duplicate, except for ash in triplicate. WS: wheat straw, CS: corn stover, BS: barley straw, SCB: sugarcane bagasse, AI: acid-insoluble, AS: acid soluble.

	carbohydrate ^a	protein	ash	AI lignin ^b	AS lignin
WS	64.72±2.26	1.70±0.01	4.45±0.21	18.5±0.2	1.5±0.3
CS	63.53±1.20	2.20±0.01	8.01±0.11	15.6±0.01	2.8±0.9
BS	68.60±1.33	1.49±0.02	0.97±0.09	21.0±0.1	1.8±0.8
SCB	60.71±0.40	1.26±0.02	4.99±0.68	28.1±0.2	1.9±0.3

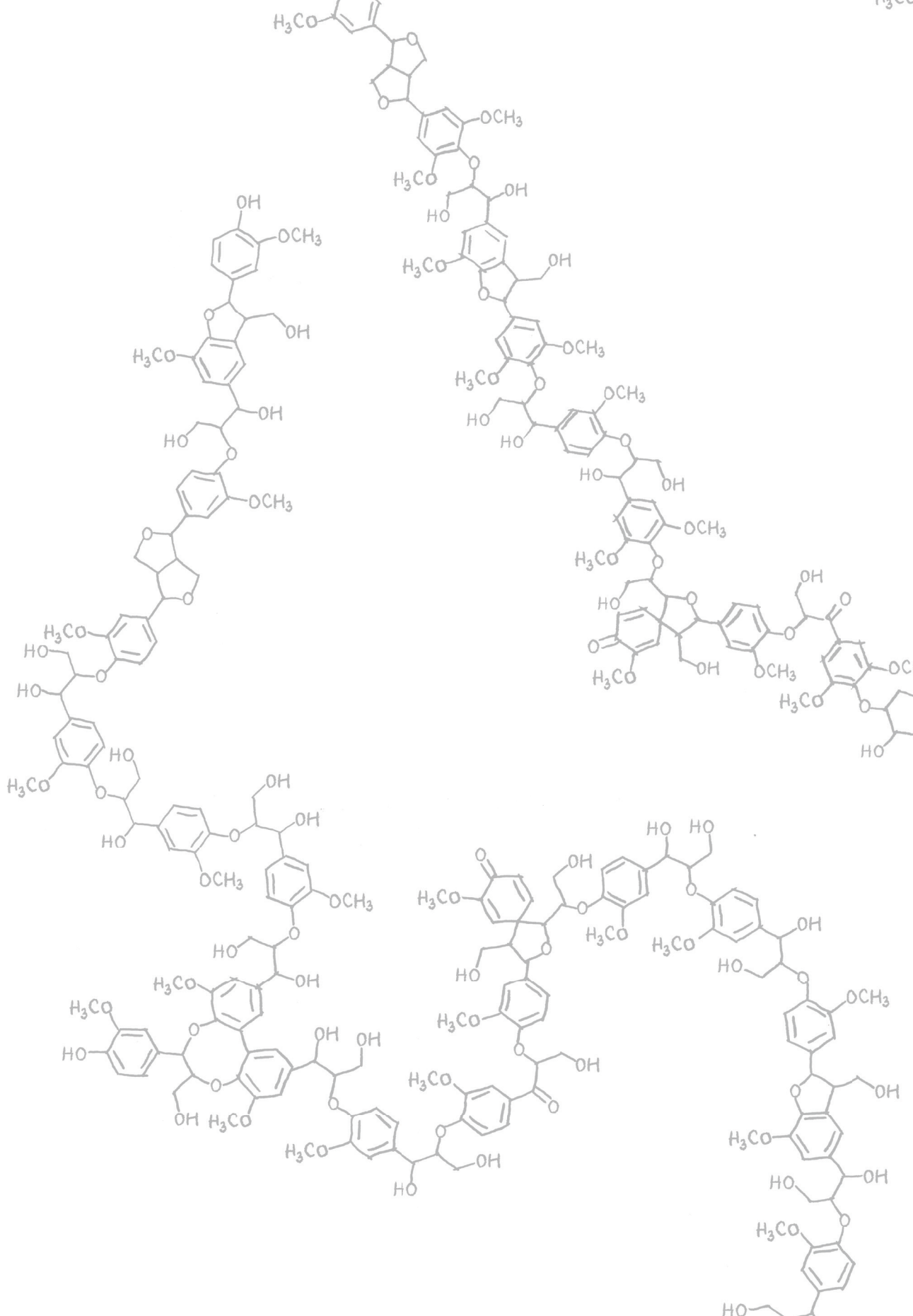
^apresented as anhydrosugars, ^bcorrected for ash and protein

Table S2. Molar composition of carbohydrates of poaceous biomasses (% mol) determined in duplicate. BS: barley straw, WS: wheat straw, CS: corn stover, BS: barley straw, SCB: sugarcane bagasse.

	arabinose	galactose	glucose	xylose	uronic acid
WS	3.84±0.00	0.97±0.01	53.24±0.26	37.37±0.05	4.22±0.19
CS	4.90±0.19	1.49±0.04	49.33±0.56	40.00±0.42	4.28±0.10
BS	3.39±0.04	0.84±0.00	56.49±0.17	35.24±0.25	4.04±0.04
SCB	0.78±0.01	0.24±0.01	66.80±0.39	29.12±0.41	3.06±0.01

Supporting Information References

- Gorissen, A.; Kraut, N. U.; de Visser, R.; de Vries, M.; Roelofsen, H.; Vonk, R. J., No *de novo* sulforaphane biosynthesis in broccoli seedlings. *Food Chem* **2011**, *127*, 192-196.
- Haun, J., Visual quantification of wheat development. *Agron J* **1973**, *65*, 116-119.
- Large, E. C., Growth stages in cereals illustration of the Feekes scale. *Plant Pathol* **1954**, *3*, 128-129.
- Zadoks, J. C.; Chang, T. T.; Konzak, C. F., A decimal code for the growth stages of cereals. *Weed Res* **1974**, *14*, 415-421.
- Smakman, G., Energy metabolism of *Plantago lanceolata*, as affected by change in root temperature. *Physiol Plant* **1982**, *56*, 33-37.
- Visser, R. D.; Vianden, H.; Schnyder, H., Kinetics and relative significance of remobilized and current C and N incorporation in leaf and root growth zones of *Lolium perenne* after defoliation: assessment by ¹³C and ¹⁵N steady-state labelling. *Plant Cell Environ* **1997**, *20*, 37-46.
- Englyst, H. N.; Cummings, J. H., Simplified method for the measurement of total non-starch polysaccharides by gas-liquid chromatography of constituent sugars as alditol acetates. *Analyst* **1984**, *109*, 937-942.
- Jones, D. B., Factors for converting percentages of nitrogen in foods and feeds into percentages of proteins. *US Agric Circ* **1931**, 1-16.
- Jurak, E.; Punt, A. M.; Arts, W.; Kabel, M. A.; Gruppen, H., Fate of carbohydrates and lignin during Composting and mycelium growth of *Agaricus bisporus* on wheat straw based compost. *PLoS ONE* **2015**, *10*, e0138909.



The background of the slide is filled with various chemical structures of lignin, which are complex polymers of aromatic rings connected by ether and carbon-carbon bonds. Some structures show methoxy groups (H3CO) and hydroxyl groups (OH).

CHAPTER 3

Uniformly ^{13}C labeled lignin internal standards for quantitative pyrolysis-GC-MS analysis of grass and wood

Gijs van Erven, Ries de Visser, Pieter de Waard,
Willem J. H. van Berkel, Mirjam A. Kabel

Based on: ACS Sustainable Chemistry & Engineering, 2019, 7, 20070-20076

Abstract

With the ever-advancing lignocellulose valorization strategies, lignin analyses need to advance as well. However, lignin quantification still heavily relies on unspecific, time- and sample consuming gravimetric and spectrophotometric analyses. Here, we demonstrate that lignin isolates from uniformly ^{13}C labeled wheat straw, willow and douglas fir, serve as 'ideal' internal standards for py-GC-HR-MS analyses of plant biomass, allowing the accurate and precise quantification and structural characterization of lignin in grasses, hardwoods and softwoods. The ^{13}C lignin internal standards were comprehensively structurally characterized by HSQC NMR and py-GC-HR-MS analyses and their application for lignin quantification was validated in biomass model systems and in actual plant biomass. For all botanical origins and species, lignin content was determined within 5% relative deviation of the Klason benchmark. These results establish the capability of the developed analytical platform to selectively quantify and structurally characterize lignin simultaneously and demonstrate a valuable addition to the lignin analysis toolbox.

Introduction

As major constituent and main recalcitrant factor in plant biomass, lignin plays a crucial role in terrestrial carbon recycling and the valorization of lignocellulose.¹⁻³ Continuous efforts, therefore, aim to understand the mechanisms underlying lignin formation and conversion, depending strongly on analyses of lignin content and structure.⁴ Though structural characterization of lignin has greatly advanced in recent years, mainly through developments in NMR spectroscopy, lignin content determination has not followed suit.⁵⁻⁶ This is largely due to lignin's complex and heterogeneous structure, which impedes its accurate and efficient quantification.

Lignin consists of *p*-hydroxyphenyl (H), guaiacyl (G) and syringyl (S) subunits, with the composition primarily differing among taxa, that are linked through various aryl-ether and carbon-carbon linkages.⁷ Lignin of softwoods is composed solely of G-units, whereas hardwood lignin is mainly composed of G- and S-units with traces of H-units. Grass lignin consists of the same subunits as hardwood lignin, but generally contains larger numbers of H-units.⁷ Independent of the botanical origin, the β -O-4' aryl ether is the most abundant interunit linkage. Softwood lignins are generally richer in condensed phenylcoumaran and dibenzodioxocin linkages.⁸⁻⁹ Besides the 'traditional' lignin monomers, hardwoods and grasses also incorporate *p*-hydroxybenzoic acid and acetate/*p*-coumaric acid, respectively, as γ -esters. In addition, grass lignins contain triclin and ferulate moieties.⁹⁻¹⁰

As a result of this structural complexity, lignin quantification, still, heavily relies on unspecific gravimetric and spectrophotometric methods.¹¹⁻¹² Not only is there a general demand for enhanced specificity and accuracy, advances in the genetic engineering of lignin and lignin-active organisms and enzymes call for reduced sample and time investments for lignin assessment.¹³⁻¹⁶

In this context, py-GC-MS offers substantial advantages over other efforts aiming at lignin quantification by FTIR, NIR and NMR spectroscopy as analyses are relatively fast and sensitive, require minimal sample preparation (milling only) and strikingly low amounts of material (~ 10 -100 μ g).¹⁷⁻²⁴ Furthermore, different structural features can be distinguished, which enables the 'fingerprinting' of the lignin structure.²³⁻²⁴

Recently, we developed a quantitative py-GC-MS method that meets the above outlined criteria by employing polymeric uniformly ¹³C labeled wheat straw lignin as internal standard (¹³C-WS-IS) combined with the use of relative response factors for the pyrolysis products.²⁵ The developed method was validated on model systems with known amounts of nonlabeled (¹²C) grass lignin and actual grass biomass with different lignin structures, showing excellent accuracy and precision. The method presented a major advancement of py-GC-MS analysis, that had previously always resulted in insufficient accuracy when employed for absolute lignin quantification,²⁶⁻³⁰ as discussed in detail in our recent work.²⁵ Furthermore, the method facilitated the mapping of fungal delignification of wheat straw by

providing insight into delignification efficiencies through accurate and specific quantification of lignin content as well as understanding of the underlying mechanisms through accurate quantification of specific pyrolysis markers for degraded substructures.³¹⁻³³

Despite its proven usefulness, the quantitative ^{13}C -IS py-GC-MS method has, thus far, only been applied to grass lignin samples and achieved limited flexibility because of the selected ion monitoring mode that was used for MS detection, requiring pre-defined target compounds within particular retention time windows.²⁵ In this work, we extend the analytical platform to hardwoods and softwoods by employing comprehensively characterized isolated lignin from uniformly ^{13}C labeled willow and uniformly ^{13}C labeled douglas fir as respective internal standards. In addition, we demonstrate an improved robustness and sensitivity of the method by using high-resolution mass spectrometry (HR-MS) full MS detection. The ^{13}C -IS py-GC-HR-MS method achieved excellent accuracy and precision in biomass model systems and actual plant biomass for grasses, hardwoods and softwoods, while simultaneously providing valuable structural insight.

Experimental Section

Materials. All chemicals and enzyme preparations were obtained from commercial suppliers and used without further purification. Wheat straw was kindly provided by CNC (Milsbeek, The Netherlands). Sugar cane bagasse and barley straw were supplied by Sime Darby (Kuala Lumpur, Malaysia) and Unifarm Wageningen (Wageningen, The Netherlands), respectively. Spruce (*Picea abies*), red cedar (*Thuja plicata*), scots pine (*Pinus sylvestris*), eucalyptus (*Eucalyptus grandis*), oak (*Quercus alba*) and beech (*Fagus sylvatica*) samples were kindly provided by SHR B.V. (Wageningen, The Netherlands). Willow wood, described previously,³⁴ was a gift from Food & Biobased Research (Wageningen University, Wageningen, The Netherlands). All biomass samples were milled to <250 μm and sequentially extracted by acetone and water before further analyses. Water used in all experiments was purified via a Milli-Q water system (Millipore, Billerica, MA, USA).

Preparation of ^{13}C labeled plant biomass. Nonlabeled (^{12}C , 98.9 atom % ^{12}C) and uniformly ^{13}C -labeled (^{13}C , 97.7 atom % ^{13}C) spring wheat plants (*Triticum aestivum* L. cv. "Baldus"; plant age 14 weeks), uniformly ^{13}C -labeled (^{13}C , 96 atom % ^{13}C) willow (*Salix alba*; plant age 15 weeks) and uniformly ^{13}C -labeled (^{13}C , 97 atom % ^{13}C) douglas fir (*Pseudotsuga menziesii*; plant age 50 weeks) were produced in modified, custom designed, airtight, high-irradiance labeling chambers of the facility ESPAS (Experimental Soil Plant Atmosphere System, IsoLife, Wageningen, The Netherlands),³⁵ with nutrients and climate conditions as described elsewhere,²⁵ except for the douglas fir nutrient solution which contained 25% of nitrogen as ammonium at a pH maintained between 4 and 5.

Isolation of lignin from nonlabeled wood biomass. Lignin was isolated from nonlabeled willow and spruce according to a modified method reported by Björkman, previously described in detail.^{25, 36} Briefly, extractives were removed by consecutive extractions with acetone and water after which the extractive-free residue was planetary ball-milled. Ball-milled material was subsequently water-extracted and freeze-dried prior to aqueous dioxane extraction (80% v/v) for 2 x 24 h at room temperature under nitrogen atmosphere. The soluble fractions were obtained by centrifugation, combined and freeze-dried and used without further purification. Note that planetary ball-milling can induce structural changes of lignin and, therefore, should be carefully optimized to balance yield, purity and structural integrity of the isolated lignins.³⁷

Isolation of lignin from ¹³C-labeled biomass. ¹³C labeled wheat straw lignin was isolated as described previously.²⁵ The isolation protocol described for nonlabeled wood biomass did not yield sufficient isolated material from ¹³C-labeled woods to allow all further analyses. Therefore, the insoluble material obtained after dioxane extraction was treated with commercial enzyme cocktails for carbohydrate removal prior to another dioxane extraction cycle. To homogenize the freeze-dried insoluble residue, the material (200 mg) was planetary ball-milled in a 12 mL stainless steel milling jar containing 40 Ø5 mm stainless steel balls for 15 min at 600 rpm (Retsch PM100, Haan, Germany). The ball-milled material was subsequently suspended in 6 mL 50 mM sodium acetate pH 5 to which 12.5 µL ViscoStar 150 L (Dyadic, Jupiter, FL, USA) and 500 µL of a 1 mg mL⁻¹ solution of Rovabio Advance (Adisseo, Antony, France) were added. For douglas fir, 5 µL of Gamanase 1.5 L (Novozymes, Bagsværd, Denmark), an enzyme cocktail aiming at mannan degradation, was additionally included. The suspensions were incubated for 18 h at 50 °C under rotary shaking, followed by centrifugation and freeze-drying of the insoluble residue. This cycle was performed twice. The resulting lignin-enriched residues were dioxane extracted as described above to afford ¹³C wood lignin isolates.

Carbohydrate content and composition of lignin isolates. Carbohydrate content and composition was determined in duplicate as constituent monosaccharides after acid hydrolysis by a modified method reported by Englyst & Cummings (see Supporting Information for details).³⁸

Purity of lignin isolates. The purity of the nonlabeled lignin isolates was set to equal the remaining dry matter content after subtraction of carbohydrates and other nonlignin impurities (estimated at 5% w/w for wood lignin isolates).²⁵ The nonlabeled wood isolates were used to determine the purity of the uniformly labeled ¹³C wood lignin isolates spectrophotometrically. Lignin isolates were weighed on an XP6 excellence-plus microbalance (Mettler Toledo, Columbus, OH, USA) and dissolved in 80% v/v aqueous dioxane. Absorbance at 280 nm was

quantified by using a Shimadzu UV-1800 spectrophotometer (Kyoto, Japan). Nonlabeled lignin isolates of the respective botanical origins were used to construct calibration curves for the determination of extinction coefficients. Structural resemblance of nonlabeled and uniformly ^{13}C labeled isolates validate the use of the same extinction coefficient.

Characterization of lignin isolates by NMR spectroscopy. Around 1 mg of ^{13}C labeled lignin isolate was dissolved in 0.6 mL DMSO- d_6 and transferred to a NMR tube. NMR spectra were recorded at 25 °C with Bruker's standard pulse sequences on a Bruker AVANCE III 600 MHz NMR spectrometer (Bruker BioSpin, Rheinstetten, Germany) equipped with a 5 mm cryoprobe located at MAGNEFY (MAGNETic resonance research FacilityY, Wageningen, The Netherlands) by using the adiabatic "hsqcetgpsisp2.2" pulse sequence. Detailed acquisition and processing settings have been reported previously.³³

Quantitative py-GC-MS with ^{13}C lignin as internal standard. Samples were weighed by using an XP6 excellence-plus microbalance. Pyrolysis was performed with an EGA/PY-3030D Multi-shot pyrolyzer (Frontier Laboratories, New Ulm, MN, USA) equipped with an AS-1020E Autoshot auto-sampler as previously described.^{25, 31} The pyrolyzer was coupled to a Trace 1300 GC equipped with a Restek DB-1701 fused-silica capillary column (30 m \times 0.25 mm i.d. 0.25 μm film thickness) coupled to an Exactive Orbitrap Mass Spectrometer (both Thermo Scientific). Pyrolysis products were applied to the column via split/splitless injection (at 280 °C) with a split ratio of 1:133 and helium was used as carrier gas with constant flow at 1.5 mL min⁻¹. The GC oven was programmed from 70 °C (2 min) to 270 °C at 5 °C min⁻¹ and held at 270 °C for 15 min. The MS was always operated in full MS mode, with EI at 70 eV, a source temperature of 275 °C, a resolution of 60.000, AGC target at 10⁶, maximum IT at 'auto' and a scan range of m/z 35-550. Relative response factors for lignin-derived pyrolysis products on the py-GC-HR-MS system were determined as previously described, taking relative ion abundancies into account.²⁵

TraceFinder 4.0 software was used for data processing. The most abundant ion per compound was used for quantification and peaks were automatically integrated by using ICIS peak integration with optimized settings per compound. A manual correction was only applied when irregular peak shapes led to erroneous peak integration with method settings. Lignin contents (equation 1) and relative abundances of lignin-derived pyrolysis products were calculated as described previously, including a correction for 4-vinylphenol to cover for decarboxylation that precedes its formation from *p*-coumarate moieties.^{31, 33}

$$\text{Lignin content \%}(w/w) = \frac{\sum_{i=1}^{51} \frac{A_i^{12C} \cdot M_{w12C}}{RRF_{run,i}} m_{IS}}{\sum_{i=1}^{51} \frac{A_i^{13C} \cdot M_{w13C}}{RRF_{run,i}} m_{sample}} \cdot 100 \quad (1)$$

where i refers to compound number,³³ A is area, M_w is the molecular weight, RRF_{run} is the updated relative response factor,³¹ m_{IS} is the amount of IS (corrected for purity, μg) and m_{sample} is the amount of sample (μg).

Method validation in model systems. Validation of the py-GC-HR-MS method (full MS mode) was performed as described previously.²⁵ Briefly, nonlabeled ^{12}C lignin isolate (from wheat straw, willow or spruce) was dissolved in 50:50 (v/v) ethanol:chloroform in a concentration of 1.0 mg mL^{-1} and added to cellulose to give biomass model systems with four different lignin contents, always adding up to $80 \mu\text{g}$ of dry matter. Uniformly ^{13}C labeled lignin isolate (from wheat straw, willow or douglas fir) was dissolved in a similar manner and $10 \mu\text{L}$ of this solution was added to the biomass model system samples and dried. Samples were prepared and analyzed in triplicate.

Method validation in actual biomass. To approximately $80 \mu\text{g}$ of biomass, $10 \mu\text{L}$ of a 1.0 mg mL^{-1} solution of the appropriate ^{13}C lignin IS was added. Samples were prepared and analyzed in triplicate. Lignin contents determined by py-GC-HR-MS (full MS mode) were compared to Klason lignin contents that were determined by a previously described procedure.^{11, 25} Total lignin contents consisting of acid insoluble lignin corrected for ash and protein combined with acid soluble lignin were used for comparison.

Results & Discussion

Having established the accurate quantification and characterization of grass lignin, we attempted to quantify hardwood and softwood lignin by the recently developed ^{13}C -wheat straw IS py-GC-MS method.^{25, 31} The performance of the method was evaluated by comparing the determined lignin contents with traditional gravimetrical analyses (Figure S1). Though this resulted in quite decent lignin contents and relative comparisons between lignin samples would likely be possible, we were not satisfied with the 15-30% discrepancy to the Klason benchmark. The latter presumably related to the substantially different structural characteristics of grass, i.e. the ^{13}C wheat straw lignin IS, and wood lignin as described above. To achieve accurate lignin contents in absolute terms, we, therefore, aimed to employ uniformly ^{13}C labeled lignin internal standards being specific for each botanical source.

In addition, we attempted to advance the method further by making use of high-resolution mass-spectrometry (HR-MS) detection. By using an Orbitrap system, we observed a significant reduction in background noise, allowing the quantification of low-abundance pyrolysis products with greater accuracy (Figure 1).

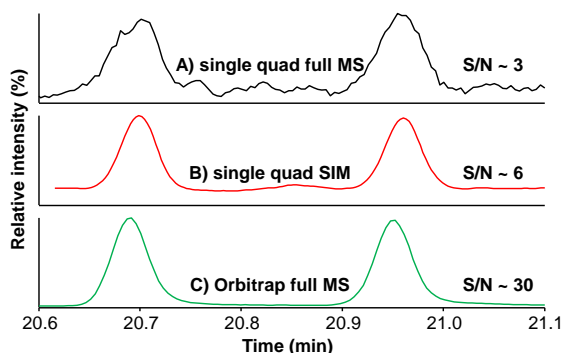


Figure 1. Pyrograms of the low relative abundance (<0.1%) pyrolysis products 4-propyneguaiaicol (20.70 min) and 4-allenegaiaicol (20.95 min) of wheat straw with single quad full MS detection, EIC m/z 162 with 1 amu mass accuracy (A), single quad SIM detection m/z 147+162 with 1 amu mass accuracy (B), Orbitrap full MS detection, EIC m/z 162.06753 (M-e) with 5 ppm mass accuracy (C).

The enhanced sensitivity and higher scan rate of the Orbitrap system enabled us to run the analyses in full MS mode, rather than selective ion monitoring (SIM) mode that was used on the single quad system. Not only did this greatly improve the robustness of the method as detection was no longer dependent on fixed retention time windows, it also led to greater flexibility as, theoretically, an infinite number of products can be monitored, instead of a pre-defined compound list.²⁵ This more robust py-GC-HR-MS method was used to set up the lignin quantification in wood biomass.

Lignin isolation from wood biomass. Lignin isolation following the classical protocols resulted in expected yields (~10%) and purities (>85%) for nonlabeled (^{12}C) willow and spruce (Table S1).^{36, 39} In contrast, similarly extracted uniformly ^{13}C labeled woods did not yield sufficient isolated material. Lignin contents of the ^{13}C labeled woods were expected to be rather low as relatively young plants were used, which likely affected the isolated amounts. To obtain sufficient ^{13}C labeled wood lignin isolate, the initially obtained dioxane insoluble residue was enzymatically treated to remove carbohydrates and re-extracted with dioxane. Though yields were still lower than expected for regular wood samples, the total isolated amounts allowed all required analyses. Furthermore, the ^{13}C willow lignin isolate showed a high purity (~91%). The ^{13}C douglas fir lignin isolate, however, was of lower purity (~45%) than anticipated on the basis of carbohydrate content analysis (Table S1) and relatively low abundance of carbohydrate-derived pyrolysis products (data not shown). The latter was consistent with NMR and py-GC-MS analyses that both showed approximately half of the lignin-specific area per weight of isolate in comparison to the other ^{13}C and ^{12}C lignin isolates. We did not attempt to further specify the impurities or (chemically) purify the ^{13}C labeled douglas fir isolate as a limited amount of this isolate was available. Most importantly, the ^{13}C labeled lignin isolates showed representative structural features of the respective botanical classes, as will be elaborated in the next section.

Structural characterization of lignin isolates. Py-GC-HR-MS analyses of the ^{13}C lignin isolates showed typical structural characteristics of their respective botanical origins (Figure 2, Table S2). Related to the presence of *p*-coumarate moieties, the ^{13}C labeled wheat straw lignin isolate showed substantial amounts of 4-vinylphenol.²³ The high abundance of pyrolysis products with an intact α,β,γ -side chain suggested that lignins were obtained with a high amount of intact interunit linkages, as can be expected from the mild isolation procedure (Table S2).³¹

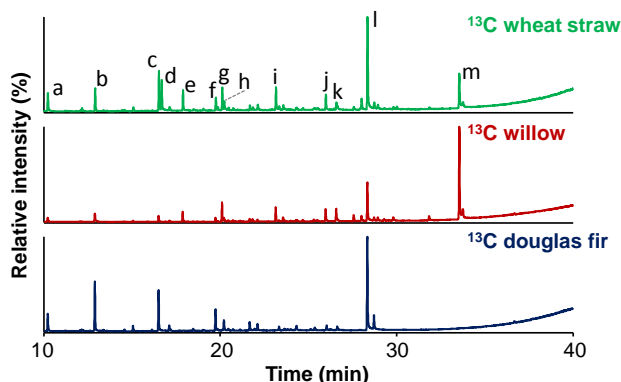


Figure 2. Py-GC-HR-MS pyrograms (TIC, full MS) of uniformly ^{13}C labeled lignin isolates. Letters refer to major lignin-derived compounds: a guaiacol; b 4-methylguaiacol; c 4-vinylguaiacol; d 4-vinylphenol; e syringol; f *trans*-isoeugenol; g 4-methylsyringol; h vanillin; i 4-vinylsyringol; j *trans*-propenylsyringol; k syringaldehyde; l *trans*-coniferyl alcohol; m *trans*-sinapyl alcohol.

HSQC NMR analyses showed typical spectra for grass, hardwood and softwood for the isolated lignins from the respective uniformly ^{13}C labeled plants (Figure 3). As we have reported previously, the ^{13}C wheat straw lignin showed typical signals for acylated β -O-4' aryl ethers and β -O-4' aryl ethers linked to triclin in the aliphatic region.²⁵ In the aromatic region, signals for the three aromatic subunits (H, G and S) and triclin, *p*-coumarate and ferulate could be observed. The wood lignins were characterized by the absence of any additional moieties besides the 'regular' subunits (willow G and S, douglas fir G) in the aromatic region. In the aliphatic region, the uniformly ^{13}C labeled willow lignin showed a clear signal for spirodienone interunit linkage substructures, whereas dibenzodioxocin substructures were evidently present in the uniformly ^{13}C labeled douglas fir lignin in addition to the β -O-4' aryl ether, β -5' phenylcoumaran and β - β' resinols substructures common to all three botanical sources of lignin. The structural features of the lignin isolates are summarized in Table S3 on the basis of semiquantitative analyses of the volume integrals. The distribution of the aromatic units and interunit linkages is in accordance with previous reports on HSQC NMR analyses on nonlabeled wheat straw, willow and douglas fir.⁴¹⁻⁴³ Hence, it was concluded that the isolated lignins were representative of lignin of the respective biomasses.⁹ The fact that these lignins were obtained from relatively young plants could suggest a limited influence of age on lignin composition.⁴⁴ Interestingly, the

found subunit distribution matched reasonably well with py-GC-HR-MS analyses (Table S3). Note that for comparative purposes *p*-CA and FA were included in the subunit composition determinations by NMR, as regular py-GC-MS analyses without methylating agents such as tetramethylammonium hydroxide (TMAH) cannot distinguish vinyl products originating from hydroxycinnamic acids and 'core lignin'.⁴⁵ Similar structural characteristics were found for the three lignin isolates obtained from nonlabeled plant biomass (Table S3).

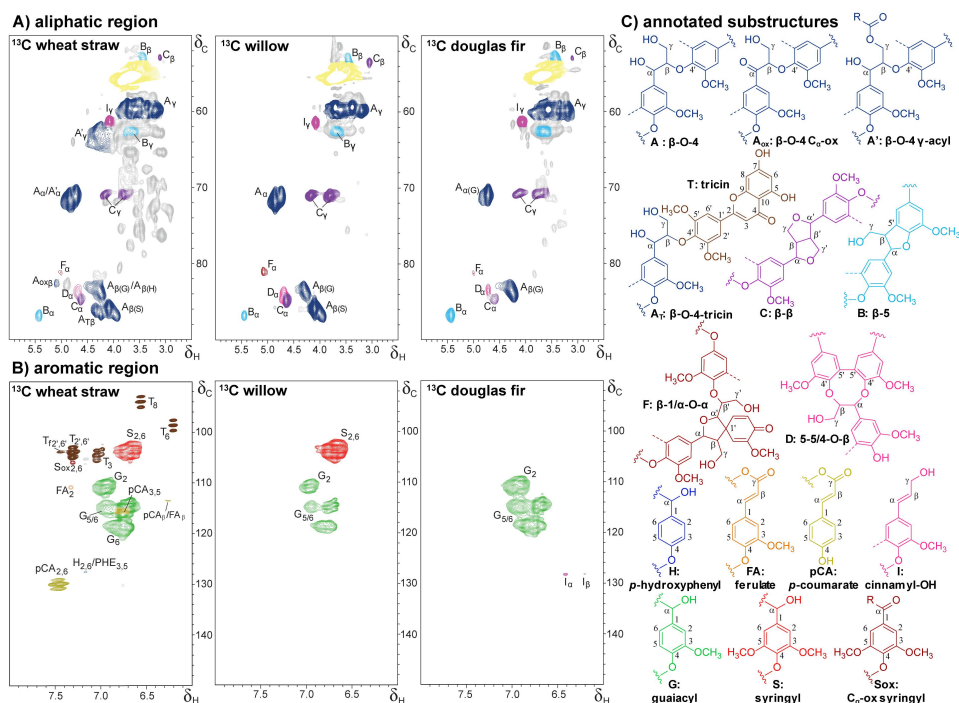


Figure 3. Aliphatic (A) and aromatic (B) regions of ^1H - ^{13}C HSQC NMR spectra of lignin isolates from uniformly ^{13}C labeled biomass and annotated substructures (C). Dotted lines represent $-\text{H}$ or $-\text{OCH}_3$. Wavy lines indicate main positions for further coupling. Note that through uniform ^{13}C labeling a signal enhancement of at least a factor 100 is achieved and possibly up to 140% through additional signal gain by neighboring ^{13}C atoms, though this is accompanied by abundant ^{13}C - ^{13}C cross-coupling, especially in the aromatic region of the spectra.⁴⁰

Lignin quantification in biomass model systems. We have previously established that biomass model systems, consisting of known amounts of pure nonlabeled ^{12}C lignin (lignin input) mixed with cellulose, are an effective tool for the validation and proof-of-concept demonstration of lignin quantification by ^{13}C -IS py-GC-MS.²⁵ Accordingly, our first step in validating the extension of the method to wood biomass was to apply the ^{13}C wood lignin internal standards in these model systems (Figure 4).

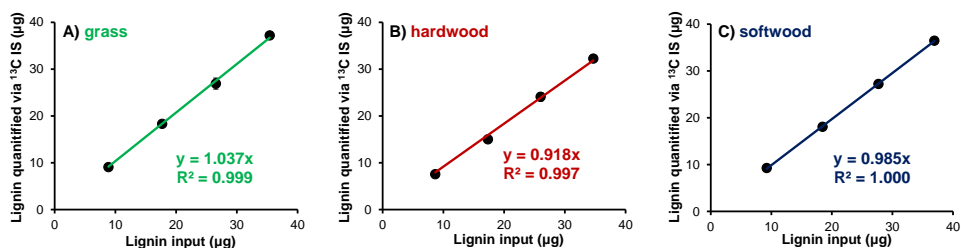


Figure 4. ^{13}C -IS py-GC-HR-MS lignin quantification in biomass model systems. Grass (A): ^{12}C wheat straw (lignin input) and ^{13}C wheat straw IS; hardwood (B): ^{12}C willow (lignin input) and ^{13}C willow IS; softwood (C): ^{12}C spruce (lignin input) and ^{13}C douglas fir IS. The MS was operated in full MS mode. Average and standard deviation on the basis of triplicates.

Excellent correlations were achieved between lignin input and lignin quantified via the ^{13}C internal standard for the respective botanical sources, in terms of accuracy (slope), linearity ($R^2 > 0.99$) and precision ($\text{RSD} < 5\%$). Grass and softwood lignins were quantified with excellent accuracy as 3.7% and 1.5% deviations from the theoretical slope of 1 were obtained, respectively. Hardwood lignin was quantified with decent accuracy, showing an average deviation across the lignin content range of 8.2%. Presumably, the somewhat higher deviation was caused by slight differences in the structural features, such as the subunit composition, of the respective nonlabeled ($\text{S/G} = 1.6$) and ^{13}C labeled lignin isolates ($\text{S/G} = 2.1$) (Table S3). Constant relative distributions of the nonlabeled pyrolysis products were obtained across the content range, showing that, besides content, structural insight can simultaneously be obtained with great accuracy as well (Table S4). The observed structural features of the nonlabeled lignins included in these biomass model systems matched reasonably well with semiquantitative HSQC NMR analyses (Table S3).

Lignin quantification in actual lignocellulosic biomass. In actual plant biomass samples the ^{13}C -IS py-GC-HR-MS method performed with excellent accuracy and precision (Figure 5). Minor deviations were found when comparing the novel method with carefully executed gravimetric lignin content analyses for three grasses, hardwoods and softwoods. A comparison of all botanical origins in a single plot showed an outstanding correlation of the two methods, with an average relative deviation of approximately 1%, although a somewhat lower linearity ($R^2 = 0.963$) was obtained than in the model systems (Figure 5D). Hence, we conclude that lignin content can be accurately determined by py-GC-HR-MS when employing ^{13}C lignin of the respective botanical origin as internal standard. Conversely, Klason lignin contents poorly correlated with total peak areas of sample-derived (nonlabeled) pyrolysis products, even when relative response factors were included (Figure S2). This demonstrated that substantial matrix-effects occurred during pyrolysis, affecting the amount and composition of the pyrolysate.⁴⁶

In previous attempts to quantify lignin by py-GC-MS such matrix-effects and variations in system performance were not properly accounted for, which certainly has contributed to the inaccuracies found.²⁶⁻³⁰ As a consequence of these matrix and system effects, external standard quantification would not be adequate for the determination of lignin contents by py-GC-MS. Hence, the ^{13}C lignin internal standard is absolutely required for accurate quantification. For clarification, each analysis requires only 10 μg of internal standard from which it follows that a gram of labeled biomass would allow the isolation of sufficient lignin for thousands of analyses.

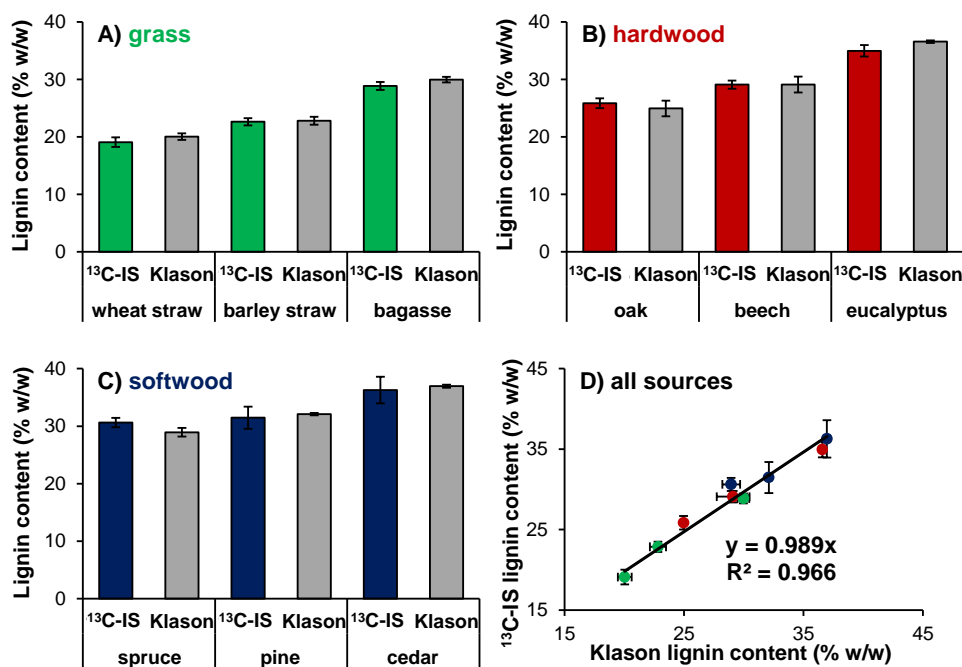


Figure 5. ^{13}C -IS py-GC-MS lignin quantification in biomass model systems. Grass (A): ^{12}C wheat straw (lignin input) and ^{13}C wheat straw IS; hardwood (B): ^{12}C willow (lignin input) and ^{13}C willow IS; softwood (C): ^{12}C spruce (lignin input) and ^{13}C douglas fir IS. The MS was operated in full MS mode. Average and standard deviation on the basis of triplicates.

The fact that the incorporation of the ^{13}C lignin internal standard ensures accuracy further corroborates the assumption that matrix-effects exerted on sample and polymeric internal standard lignin are comparable. The latter is ensured by adding the internal standard in liquid form, i.e. dissolved in a quickly evaporating organic solvent, which results in proper mixing with the sample. Besides facilitating dispersion of the internal standard throughout the sample, this approach also improved precision and throughput.

Structural characterization of lignin in actual biomass by quantitative py-GC-HR-MS. Simultaneously with accurate lignin content, valuable insight into lignin's structural features was obtained (Table S5). This confirmed that as long as the internal standard is from the same botanical source or taxon, structurally dissimilar lignins can be properly quantified. The tested grasses were structurally more diverse than the woods and mainly differed in terms of the abundance of 4-vinylphenol derived from γ -acylating *p*-coumaroyl units. Future analyses will expand to structurally diverse lignins to further develop our method. The reasonable consistency between py-GC-MS and HSQC NMR analyses in terms of subunit composition (Table S3 and S4) is promising for future evaluations of both techniques for structurally different biomass samples. Initial comparisons of both techniques suggested that information on other structural features beyond the classical subunit composition, like oxidized functionalities and amount of intact interunit linkages can be 'predicted' rather well by quantitative py-GC-MS analyses.^{31, 33, 47} Similar to what has recently been achieved with an FTIR-chemometrics approach, we envision such a predictive role of our novel method, significantly reducing the investments in terms of equipment and time.⁴⁸

Conclusions

In this work, we establish that the quantitative nature of py-GC-MS analysis of lignin primarily lays in the use of proper internal standards. Through careful validation we demonstrate that employing uniformly ^{13}C labeled lignin internal standards specific to the botanical source in combination with high-resolution mass-spectrometric detection, enable accurate and precise lignin quantification and structural characterization in grasses, hardwoods and softwoods. We anticipate that the ^{13}C -IS method will allow specific lignin analysis of lignocellulosic samples that previously could not be measured, either due to limited amounts of sample available, e.g. of transgenic plants, or due to the presence of interfering compounds, e.g. fungal-grown samples and, therefore, will find broad application.

Acknowledgements

The authors acknowledge René Klaassen (Stichting Hout Research, Wageningen, The Netherlands) for providing wood samples.

References

1. Ragauskas, A. J.; Williams, C. K.; Davison, B. H.; Britovsek, G.; Cairney, J.; Eckert, C. A.; Frederick, W. J.; Hallett, J. P.; Leak, D. J.; Liotta, C. L.; Mielenz, J.; Murphy, R.; Templer, R.; Tschaplinski, T., The path forward for biofuels and biomaterials. *Science* **2006**, *311*, 484-489.
2. Behera, S.; Arora, R.; Nandhagopal, N.; Kumar, S., Importance of chemical pretreatment for bioconversion of lignocellulosic biomass. *Renewable and Sustainable Energy Rev* **2014**, *36*, 91-106.
3. Hammel, K. E., Fungal degradation of lignin. In *Driven by nature: plant litter quality and decomposition*, Cadish, G.; Giller, K. E., Eds. CAB-International: Wallingford, 1997; pp 33-47.
4. Rinaldi, R.; Jastrzebski, R.; Clough, M. T.; Ralph, J.; Kennema, M.; Bruijninx, P. C.; Weckhuysen, B. M., Paving the way for lignin valorisation: recent advances in bioengineering, biorefining and catalysis. *Angew Chem Int Ed* **2016**, *55*, 8164-8215.
5. Lupoi, J. S.; Singh, S.; Parthasarathi, R.; Simmons, B. A.; Henry, R. J., Recent innovations in analytical methods for the qualitative and quantitative assessment of lignin. *Renewable and Sustainable Energy Rev* **2015**, *49*, 871-906.
6. Ralph, J.; Landucci, L. L., NMR of Lignins. In *Lignin and Lignans: Advances in Chemistry*, Heithner, C.; Dimmel, D.; Schmidt, J. A., Eds. CRC Pres, Taylor & Francis: Boca Raton, FL, USA, 2010; pp 137-244.
7. Vanholme, R.; Demedts, B.; Morreel, K.; Ralph, J.; Boerjan, W., Lignin biosynthesis and structure. *Plant Physiol* **2010**, *153*, 895-905.
8. Ralph, J.; Brunow, G.; Harris, P. J.; Dixon, R. A.; Schatz, P. F.; Boerjan, W., Lignification: are lignins biosynthesized via simple combinatorial chemistry or via proteinaceous control and template replication? In *Recent Advances in Polyphenol Research*, Lattanzio, V.; Daayf, F., Eds. Wiley-Blackwell: Oxford, 2009; Vol. 1, pp 36-66.
9. Ralph, J.; Lapierre, C.; Boerjan, W., Lignin structure and its engineering. *Curr Opin Biotechnol* **2019**, *56*, 240-249.
10. Ralph, J., Hydroxycinnamates in lignification. *Phytochem Rev* **2010**, *9*, 65-83.
11. Sluiter, J. B.; Ruiz, R. O.; Scarlata, C. J.; Sluiter, A. D.; Templeton, D. W., Compositional analysis of lignocellulosic feedstocks. 1. Review and description of methods. *J Agric Food Chem* **2010**, *58*, 9043-9053.
12. Hatfield, R.; Fukushima, R. S., Can lignin be accurately measured? *Crop Sci* **2005**, *45*, 832-839.
13. Baucher, M.; Halpin, C.; Petit-Conil, M.; Boerjan, W., Lignin: genetic engineering and impact on pulping. *Crit Rev Biochem Mol Biol* **2003**, *38*, 305-350.
14. Vanholme, R.; Morreel, K.; Darrah, C.; Oyarce, P.; Grabber, J. H.; Ralph, J.; Boerjan, W., Metabolic engineering of novel lignin in biomass crops. *New Phytol* **2012**, *196*, 978-1000.
15. Fernández-Fueyo, E.; Ruiz-Dueñas, F. J.; Martínez, A. T., Engineering a fungal peroxidase that degrades lignin at very acidic pH. *Biotechnol Biofuels* **2014**, *7*, 114.
16. Su, Y.; Yu, X.; Sun, Y.; Wang, G.; Chen, H.; Chen, G., Evaluation of screened lignin-degrading fungi for the biological pretreatment of corn stover. *Sci Rep* **2018**, *8*, 5385.
17. Rodrigues, J.; Faix, O.; Pereira, H., Determination of lignin content of *Eucalyptus globulus* wood using FTIR spectroscopy. *Holzforschung* **1998**, *52*, 46-50.
18. Wolfrum, E. J.; Lorenz, A. J.; DeLeon, N., Correlating detergent fiber analysis and dietary fiber analysis data for corn stover collected by NIRS. *Cellulose* **2009**, *16*, 577-585.
19. Yeh, T.-F.; Chang, H.-M.; Kadla, J. F., Rapid prediction of solid wood lignin content using transmittance near-infrared spectroscopy. *J Agric Food Chem* **2004**, *52*, 1435-1439.

20. Jiang, N.; Pu, Y.; Ragauskas, A. J., Rapid determination of lignin content via direct dissolution and ^1H NMR analysis of plant cell walls. *ChemSusChem* **2010**, *3*, 1285-1289.
21. Fu, L.; McCallum, S. A.; Miao, J.; Hart, C.; Tudryn, G. J.; Zhang, F.; Linhardt, R. J., Rapid and accurate determination of the lignin content of lignocellulosic biomass by solid-state NMR. *Fuel* **2015**, *141*, 39-45.
22. Gao, X.; Laskar, D. D.; Zeng, J.; Helms, G. L.; Chen, S., A ^{13}C CP/MAS-based nondegradative method for lignin content analysis. *ACS Sustainable Chem Eng* **2014**, *3*, 153-162.
23. Ralph, J.; Hatfield, R. D., Pyrolysis-GC-MS characterization of forage materials. *J Agric Food Chem* **1991**, *39*, 1426-1437.
24. Rencoret, J.; del Río, J. C.; Nierop, K. G.; Gutiérrez, A.; Ralph, J., Rapid Py-GC/MS assessment of the structural alterations of lignins in genetically modified plants. *J Anal Appl Pyrolysis* **2016**, *121*, 155-164.
25. Van Erven, G.; de Visser, R.; Merckx, D. W.; Strolenberg, W.; de Gijssel, P.; Gruppen, H.; Kabel, M. A., Quantification of lignin and its structural features in plant biomass using ^{13}C lignin as internal standard for pyrolysis-GC-SIM-MS. *Anal Chem* **2017**, *89*, 10907-10916.
26. Alves, A.; Schwanninger, M.; Pereira, H.; Rodrigues, J., Analytical pyrolysis as a direct method to determine the lignin content in wood: Part 1: Comparison of pyrolysis lignin with Klason lignin. *J Anal Appl Pyrolysis* **2006**, *76*, 209-213.
27. Alves, A.; Rodrigues, J.; Wimmer, R.; Schwanninger, M., Analytical pyrolysis as a direct method to determine the lignin content in wood: Part 2: Evaluation of the common model and the influence of compression wood. *J Anal Appl Pyrolysis* **2008**, *81*, 167-172.
28. Lourenço, A.; Gominho, J.; Marques, A. V.; Pereira, H., Comparison of Py-GC/FID and wet chemistry analysis for lignin determination in wood and pulps from *Eucalyptus globulus*. *BioResources* **2013**, *8*, 2967-2980.
29. Bocchini, P.; Galletti, G.; Camarero, S.; Martinez, A., Absolute quantitation of lignin pyrolysis products using an internal standard. *J Chromatogr A* **1997**, *773*, 227-232.
30. Torri, C.; Adamiano, A.; Fabbri, D.; Lindfors, C.; Monti, A.; Oasmaa, A., Comparative analysis of pyrolysate from herbaceous and woody energy crops by Py-GC with atomic emission and mass spectrometric detection. *J Anal Appl Pyrolysis* **2010**, *88*, 175-180.
31. Van Erven, G.; Nayan, N.; Sonnenberg, A. S.; Hendriks, W. H.; Cone, J. W.; Kabel, M. A., Mechanistic insight in the selective delignification of wheat straw by three white-rot fungal species through quantitative ^{13}C -IS py-GC-MS and whole cell wall HSQC NMR. *Biotechnol Biofuels* **2018**, *11*, 262.
32. Nayan, N.; van Erven, G.; Kabel, M. A.; Sonnenberg, A. S.; Hendriks, W. H.; Cone, J. W., Improving ruminal digestibility of various wheat straw types by white-rot fungi. *J Sci Food Agric* **2019**, *99*, 957-965.
33. Van Erven, G.; Hilgers, R.; de Waard, P.; Gladbeek, E.-J.; van Berkel, W. J. H.; Kabel, M. A., Elucidation of *in situ* ligninolysis mechanisms of the selective white-rot fungus *Ceriporiopsis subvermispora*. *ACS Sustainable Chem Eng* **2019**, *7*, 16757-16764.
34. Huijgen, W. J.; Smit, A. T.; Reith, J. H.; Uil, H. d., Catalytic organosolv fractionation of willow wood and wheat straw as pretreatment for enzymatic cellulose hydrolysis. *J Chem Technol Biotechnol* **2011**, *86*, 1428-1438.
35. Gorissen, A.; Kraut, N. U.; de Visser, R.; de Vries, M.; Roelofs, H.; Vonk, R. J., No *de novo* sulfuraphane biosynthesis in broccoli seedlings. *Food Chem* **2011**, *127*, 192-196.
36. Björkman, A., Studies on finely divided wood. Part 1. Extraction of lignin with neutral solvents. *Sven Papperstidn* **1956**, *59*, 477-485.
37. Zinovyev, G.; Sumerskii, I.; Rosenau, T.; Balakshin, M.; Potthast, A., Ball milling's effect on pine milled wood lignin's structure and molar mass. *Molecules* **2018**, *23*, 2223.

38. Englyst, H. N.; Cummings, J. H., Simplified method for the measurement of total non-starch polysaccharides by gas-liquid chromatography of constituent sugars as alditol acetates. *Analyst* **1984**, *109*, 937-942.
39. Chang, H.-M.; Cowling, E. B.; Brown, W., Comparative studies on cellulolytic enzyme lignin and milled wood lignin of sweetgum and spruce. *Holzforschung* **1975**, *29*, 153-159.
40. Rosenau, T.; Potthast, A.; Hofinger, A.; Bacher, M.; Yoneda, Y.; Mereiter, K.; Nakatsubo, F.; Jäger, C.; French, A. D.; Kajiwara, K., Toward a Better Understanding of Cellulose Swelling, Dissolution, and Regeneration on the Molecular Level. In *Cellulose Science and Technology: Chemistry, Analysis, and Applications*, Rosenau, T.; Potthast, A.; Hell, J., Eds. John Wiley & Sons: Hoboken, NJ, USA, 2018; pp 99-125.
41. Del Río, J. C.; Rencoret, J.; Prinsen, P.; Martínez, A. T.; Ralph, J.; Gutiérrez, A., Structural characterization of wheat straw lignin as revealed by analytical pyrolysis, 2D-NMR, and reductive cleavage methods. *J Agric Food Chem* **2012**, *60*, 5922-5935.
42. Dou, J.; Kim, H.; Li, Y.; Padmakshan, D.; Yue, F.; Ralph, J.; Vuorinen, T., Structural characterization of lignins from willow bark and wood. *J Agric Food Chem* **2018**, *66*, 7294-7300.
43. Yoo, C. G.; Pu, Y.; Li, M.; Ragauskas, A. J., Elucidating structural characteristics of biomass using solution-state 2D NMR with a mixture of deuterated dimethylsulfoxide and hexamethylphosphoramide. *ChemSusChem* **2016**, *9*, 1090-1095.
44. Rencoret, J.; Gutiérrez, A.; Nieto, L.; Jiménez-Barbero, J.; Faulds, C. B.; Kim, H.; Ralph, J.; Martínez, A. T.; del Río, J. C., Lignin composition and structure in young versus adult *Eucalyptus globulus* plants. *Plant Physiol* **2011**, *155*, 667-682.
45. Del Río, J. C.; Gutiérrez, A.; Rodríguez, I. M.; Ibarra, D.; Martínez, A. T., Composition of non-woody plant lignins and cinnamic acids by Py-GC/MS, Py/TMAH and FT-IR. *J Anal Appl Pyrolysis* **2007**, *79*, 39-46.
46. Patwardhan, P. R.; Brown, R. C.; Shanks, B. H., Understanding the fast pyrolysis of lignin. *ChemSusChem* **2011**, *4*, 1629-1636.
47. Van Erven, G.; Wang, J.; Sun, P.; de Waard, P.; van der Putten, J.; Frissen, G. E.; Gosselink, R. J. A.; Zinovyev, G.; Potthast, A.; van Berkel, W. J. H.; Kabel, M. A., Structural motifs of wheat straw lignin differ in susceptibility to degradation by the white-rot fungus *Ceriporiopsis subvermispora*. *ACS Sustainable Chem Eng* **2019**, *7*, 20032-20042.
48. Lancefield, C. S.; Constant, S.; de Peinder, P.; Bruijninx, P. C., Linkage abundance and molecular weight characteristics of technical lignins by attenuated total reflection-FTIR spectroscopy combined with multivariate analysis. *ChemSusChem* **2019**, *12*, 1139-1146.

Supporting Information

Experimental details carbohydrate content and composition

Carbohydrate content and composition of lignin isolates was determined in duplicate as constituent monosaccharides after acid hydrolysis by a modified method reported by Englyst & Cummings.¹ Samples were treated with 72% (w/w) H₂SO₄ for 1 h at 30 °C followed by 1 M H₂SO₄ for 3 h at 100 °C after which samples were centrifuged (9,000xg, 5 min, 20 °C) and supernatants were analyzed after appropriate dilution. Monosaccharide degradation during hydrolysis was corrected for by including monosaccharide standards in hydrolysis. Analysis was performed on a High Performance Anion Exchange Chromatography (HPAEC) Dionex ICS-5000 system (Thermo Scientific, Synnyvale, CA, USA). The system was equipped with a CarboPac PA-1 column (250 mm x 2 mm ID) in combination with a CarboPac guard column (50 mm x 2 mm ID) with pulsed amperometric detection (PAD) (all Dionex). 10 µL of sample

was injected and eluted at a flow rate of 0.4 mL min⁻¹ by using a combination of three mobile phases: A) 0.1 M NaOH, B) 1 M NaOAc in 0.1 M NaOH and C) H₂O. The elution profile used was as follows: 0-35 min isocratic on 100% C; 35-50 min linearly from 100% A to 40% B; 50-55 min isocratic on 100% B; 55-63 min isocratic on 100% A; 63-78 min isocratic on 100% C. Post-column addition of 0.5 M NaOH at 0.1 mL min⁻¹ was performed between 0-35 min and 63-78 min. Data was processed by using Chromeleon 7 (Thermo Scientific). Uronic acids released after acid hydrolysis were determined in duplicate as anhydrouronic acids by an automated meta-hydroxydiphenyl assay with addition of sodium tetraborate by using an auto-analyzer (Skalar Analytical BV, Breda, The Netherlands).² Glucuronic acid (Fluka AG, Busch, Switzerland) was used as a reference (0 – 100 µg mL⁻¹). Total carbohydrate content was calculated as the sum of neutral anhydrocarbohydrates and anhydrouronic acids.

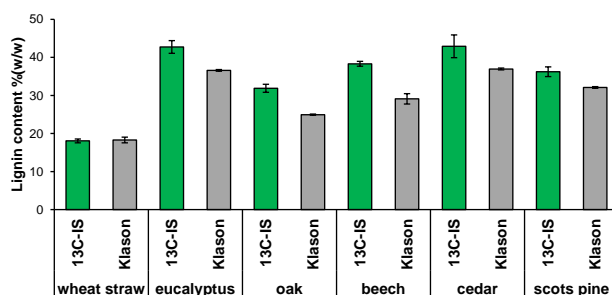


Figure S1. Lignin quantification in hardwoods and softwoods by ¹³C-IS py-GC-MS (triplicate) employing ¹³C wheat straw lignin as internal standard and by Klason methodology (duplicate). Mass spectrometric detection with a single quad DSQ-II system.³ Total Klason lignin represents acid-insoluble lignin corrected for ash and protein plus acid-soluble lignin.⁴

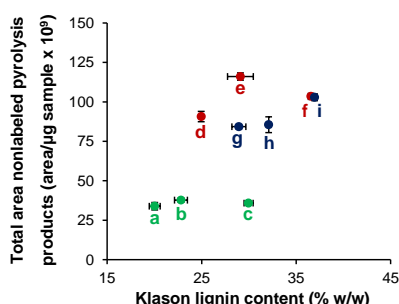


Figure S2. Py-GC-HR-MS total area of lignin-derived pyrolysis products from nonlabeled biomass samples (triplicate) versus Klason lignin content (duplicate). Areas corrected for relative response factor. Grasses in green (a wheat straw; b barley straw; c sugarcane bagasse), hardwoods in red (d oak; e beech; f eucalyptus), softwoods in blue (g spruce; h pine; i cedar). Klason lignin is presented as acid-insoluble lignin corrected for ash and protein combined with acid-soluble lignin.⁴

Table S1. Composition and yield of ¹²C and ¹³C lignin isolates.

	¹² C wheat straw ^a	¹³ C wheat straw ^a	¹² C willow	¹³ C willow	¹² C spruce	¹³ C douglas fir
carbohydrate (% w/w)	6.8 ± 0.2	7.1 ± 0.1	9.4 ± 0.0	4.0 ± 0.2	6.3 ± 0.1	6.9 ± 0.5
lignin (% w/w)	88.1	89.5	85.6 ^b	91.2 ^c	88.7 ^b	44.7 ^c
isolation yield (%)	19.0	21.5	10.4 ^d	n.d. ^e	9.4 ^d	n.d. ^e

^apreviously published in van Erven et al. 2017⁴

^bremaining content after subtracting carbohydrates and other nonlignin impurities from total dry matter

^cdetermined spectrophotometrically

^dyield versus Klason lignin content of whole biomass sample.

^elignin content was not determined for whole uniformly ¹³C labeled woods, hence no yields could be determined.

Table S2. Py-GC-HR-MS relative abundance of lignin compounds in uniformly ^{13}C labeled lignin isolates. Corrected for relative response factors. Sum on the bases of structural classification according to van Erven et al.^{3, 5} Average and standard deviation of analytical duplicates.

	^{13}C wheat straw	^{13}C willow	^{13}C douglas fir
Lignin subunits (%)			
H	12.2 ± 0.5	0.6 ± 0.0	2.5 ± 0.1
G	56.5 ± 0.2	27.9 ± 0.1	96.5 ± 0.0
S	31.3 ± 0.2	71.6 ± 0.1	1.0 ± 0.1
S/G	0.6 ± 0.0	2.6 ± 0.0	0.0 ± 0.0
Structural moieties (%)			
Unsubstituted	7.2 ± 0.6	3.5 ± 0.0	7.0 ± 0.4
Methyl	5.9 ± 0.7	4.0 ± 0.0	11.5 ± 0.1
Vinyl	27.2 ± 1.5	6.9 ± 0.1	19.8 ± 0.1
4-VP ^a	9.7 ± 0.3	0.0 ± 0.0	0.2 ± 0.0
4-VG ^b	13.2 ± 0.9	3.1 ± 0.0	19.5 ± 0.1
C α -ox	4.3 ± 0.2	6.6 ± 0.1	4.0 ± 0.1
C β -ox ^c	2.9 ± 0.2	5.0 ± 0.4	3.7 ± 0.1
C γ -ox	46.9 ± 3.9	69.7 ± 0.5	48.1 ± 0.3
Miscellaneous	5.4 ± 0.6	4.3 ± 0.0	5.9 ± 0.1
PhC γ ^d	53.7 ± 3.2	76.0 ± 0.4	54.8 ± 0.4

^a 4-vinylphenol. ^b 4-vinylguaiacol. ^c excluding diketones. ^d phenols with intact α, β, γ carbon side chain.

Table S3. Py-GC-HR-MS relative abundance of lignin compounds in uniformly ^{13}C labeled lignin isolates. Corrected for relative response factors. Sum on the bases of structural classification according to van Erven et al.^{3, 5} Average and standard deviation of analytical duplicates.

	^{13}C wheat straw	^{12}C wheat straw	^{13}C willow	^{12}C willow	^{13}C douglas fir	^{12}C spruce
Lignin subunits (%)^a						
H	1 (11)	4 (14)	0	1	0	0
G	59 (53)	57 (52)	32	39	100	98
G _{ox}	0 (0)	0 (0)	0	1	0	2
S (S _{ox})	39 (34)	38 (33)	68	56	0	0
S _{ox}	2 (1)	1 (1)	0	4	0	0
S/G	0.7 (0.7)	0.7 (0.7)	2.1	1.6	0.0	0.0
Hydroxycinnamates (%)^b						
<i>p</i> -benzoate	0	0	0	1	0	0
<i>p</i> -coumarate	12	12	0	0	0	0
ferulate	2	3	0	0	0	0
Flavonolignin (%)^b						
tricin	15	20	0	0	0	0
Lignin interunit linkages (%)^c						
β -O-4' G+H	32	29	23	20	66	65
β -O-4' S	35	41	61	63	0	0
β -O-4' C α -ox	3	<1	0	0	0	0
β -O-4' triclin	18	19	0	0	0	0
total β -O-4' aryl ethers	88	90	84	82	66	65
β -5' phenylcoumarans	6	8	4	6	23	26
β - β' resinols	4	3	8	11	5	4
5-5'/4-O- β' dibenzodioxocin	0 ^d	0	0 ^d	0	5	5
β -1' spirodienone	2	0	4	0	2	0
total	100	100	100	100	100	100
Side-chain γ-acylation (%)^a	22	16	0	0	0	0

^a relative distribution of lignin subunits (H+G+G_{ox}+S+S_{ox} = 100). Values in parentheses include *p*-CA (as H-unit) and FA (as G-unit) for comparative purposes to py-GC-MS analyses (H+*p*-CA+G+FA+G_{ox}+S+S_{ox} = 100).

^b relative volume integral of substructure versus volume integral of total lignin subunits

^c relative distribution of total interunit linkages

^d not quantified due to overlap with resinol substructures

^e percentage of β -O-4' aryl ethers

Table S4. Py-GC-HR-MS relative abundance of lignin compounds in nonlabeled lignin isolates across the measured content range (10-40 µg lignin/80 µg sample) in biomass model systems. Corrected for relative response factors and relative abundance of ^{13}C analogues. Sum on the bases of structural classification according to van Erven et al.^{3, 5} Average and standard deviation of analytical triplicates.

	grass 10	grass 40	hardwood 10	hardwood 40	softwood 10	softwood 40
Lignin subunits (%)						
H	6.3 ± 0.0	5.6 ± 0.0	1.4 ± 0.0	1.0 ± 0.0	1.5 ± 0.0	1.3 ± 0.2
G	62.7 ± 0.1	63.0 ± 0.2	39.9 ± 0.4	39.8 ± 0.4	98.3 ± 0.0	98.6 ± 0.2
S	31.1 ± 0.1	31.3 ± 0.2	58.7 ± 0.4	59.2 ± 0.4	0.2 ± 0.0	0.2 ± 0.0
S/G	0.5 ± 0.0	0.5 ± 0.0	1.5 ± 0.0	1.5 ± 0.0	0.0 ± 0.0	0.0 ± 0.0
Structural moieties (%)						
Unsubstituted	4.5 ± 0.0	3.9 ± 0.0	4.1 ± 0.0	3.1 ± 0.0	5.2 ± 0.1	5.0 ± 0.1
Methyl	3.4 ± 0.0	3.2 ± 0.0	3.4 ± 0.1	2.9 ± 0.1	6.7 ± 0.2	6.8 ± 0.1
Vinyl	19.7 ± 0.1	19.3 ± 0.1	13.2 ± 0.3	11.0 ± 0.3	12.4 ± 0.1	13.8 ± 0.1
4-VP ^a	4.2 ± 0.0	4.0 ± 0.0	0.1 ± 0.0	0.1 ± 0.0	0.1 ± 0.0	0.1 ± 0.0
4-VG ^b	12.5 ± 0.2	12.3 ± 0.1	8.2 ± 0.2	6.9 ± 0.2	12.3 ± 0.1	13.7 ± 0.0
C _α -ox	5.7 ± 0.1	5.5 ± 0.0	6.0 ± 0.1	6.0 ± 0.1	6.7 ± 0.1	6.7 ± 0.2
C _β -ox ^c	1.4 ± 0.0	1.3 ± 0.0	1.8 ± 0.0	1.6 ± 0.0	2.5 ± 0.0	2.5 ± 0.1
C _γ -ox	61.5 ± 0.1	63.0 ± 0.1	67.5 ± 0.5	72.0 ± 0.5	61.6 ± 0.3	60.1 ± 0.3
Miscellaneous	3.7 ± 0.0	3.8 ± 0.0	4.1 ± 0.0	3.5 ± 0.0	5.0 ± 0.0	5.2 ± 0.1
PhC _γ ^d	66.5 ± 0.0	68.0 ± 0.1	73.5 ± 0.4	77.2 ± 0.4	67.9 ± 0.3	66.6 ± 0.2

^a 4-vinylphenol. ^b 4-vinylguaiacol. ^c excluding diketones. ^d phenols with intact α,β,γ carbon side chain.

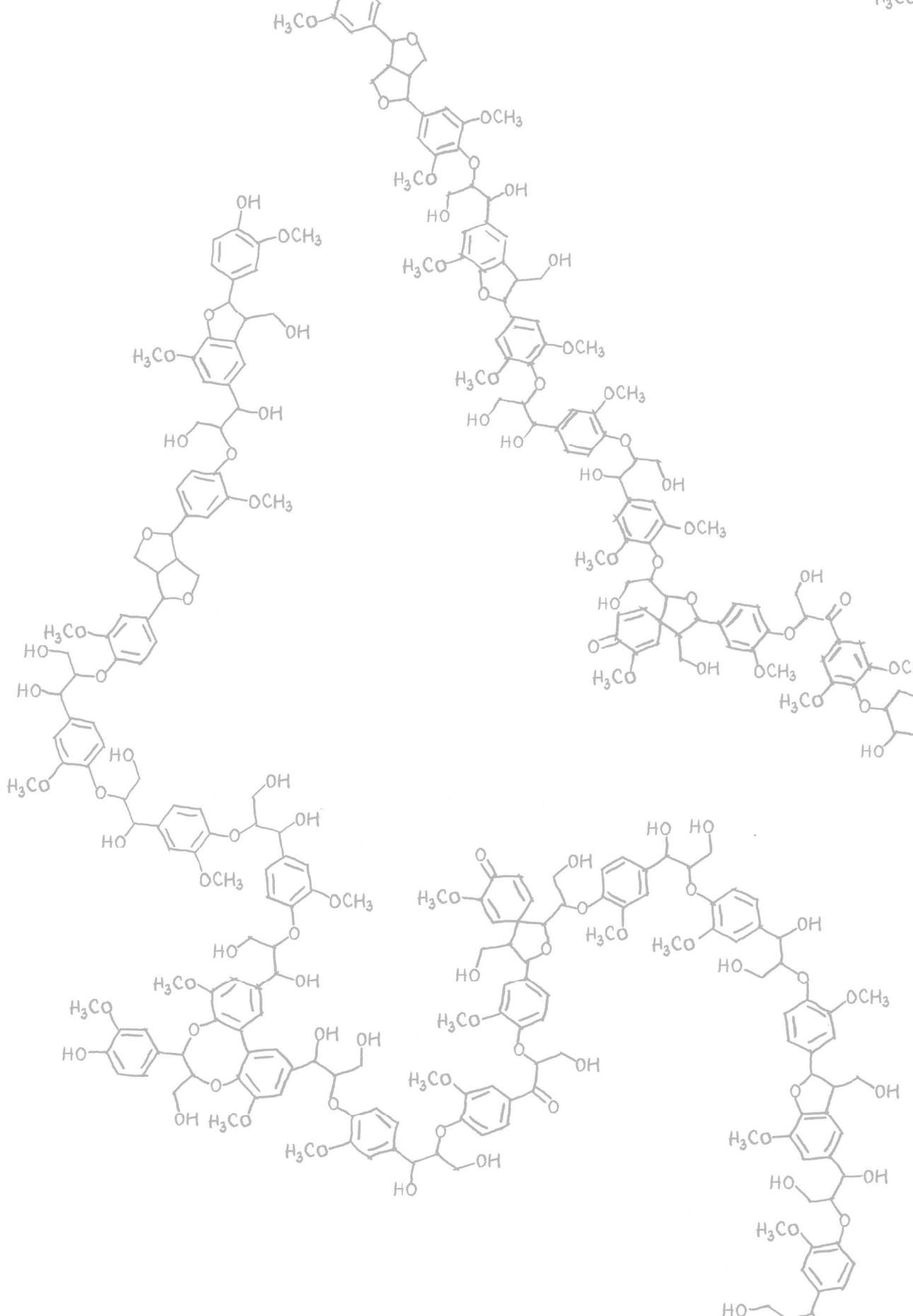
Table S5. Py-GC-HR-MS relative abundance of lignin compounds in grass, hardwood and softwood biomass. Corrected for relative response factors and relative abundance of ^{13}C analogues. Sum on the bases of structural classification according to van Erven et al.^{3, 5} Average and standard deviation of analytical triplicates.

	grass			hardwood			softwood		
	wheat straw	barley straw	bagasse	oak	beech	eucalyptus	spruce	pine	cedar
Lignin content (% w/w)	19.1 ± 0.9	22.9 ± 0.6	28.7 ± 0.6	25.8 ± 0.8	29.1 ± 0.7	34.9 ± 1.0	30.6 ± 0.8	31.5 ± 1.9	36.3 ± 2.3
Lignin subunits (%)									
H	11.4 ± 0.1	14.0 ± 0.5	45.7 ± 1.3	0.7 ± 0.0	0.8 ± 0.0	0.8 ± 0.0	1.1 ± 0.0	2.9 ± 0.1	0.9 ± 0.0
G	64.0 ± 0.6	56.7 ± 0.6	35.7 ± 1.4	32.8 ± 0.4	32.5 ± 0.5	33.6 ± 0.1	98.8 ± 0.0	97.0 ± 0.1	99.0 ± 0.0
S	24.6 ± 0.7	29.3 ± 0.4	18.6 ± 0.1	66.6 ± 0.4	66.7 ± 0.5	65.7 ± 0.1	0.2 ± 0.1	0.2 ± 0.0	0.2 ± 0.0
S/G	0.4 ± 0.0	0.5 ± 0.0	0.5 ± 0.0	2.0 ± 0.0	2.1 ± 0.0	2.0 ± 0.0	0.0 ± 0.0	0.0 ± 0.0	0.0 ± 0.0
Structural moieties (%)									
Unsubstituted	6.5 ± 0.2	6.1 ± 0.1	8.2 ± 0.3	5.2 ± 0.1	4.9 ± 0.1	5.8 ± 0.0	3.7 ± 0.0	4.4 ± 0.0	4.0 ± 0.0
Methyl	3.0 ± 0.1	2.5 ± 0.0	3.3 ± 0.1	5.0 ± 0.1	5.9 ± 0.2	6.2 ± 0.0	8.6 ± 0.1	9.2 ± 0.2	9.0 ± 0.1
Vinyl	42.0 ± 0.2	40.4 ± 0.4	61.1 ± 0.6	17.8 ± 0.2	18.4 ± 0.0	19.2 ± 0.1	11.5 ± 0.0	11.8 ± 0.2	11.7 ± 0.0
4-VP ^a	9.3 ± 0.1	12.0 ± 0.5	40.9 ± 1.4	0.0 ± 0.0	0.0 ± 0.0	0.1 ± 0.0	0.0 ± 0.0	0.2 ± 0.0	0.0 ± 0.0
4-VG ^b	29.1 ± 0.3	24.2 ± 0.4	16.3 ± 0.9	6.2 ± 0.1	6.1 ± 0.1	6.9 ± 0.0	11.5 ± 0.0	11.7 ± 0.2	11.7 ± 0.0
C _α -ox	4.0 ± 0.1	3.9 ± 0.0	4.8 ± 0.2	3.9 ± 0.0	4.5 ± 0.1	4.5 ± 0.1	5.7 ± 0.0	5.7 ± 0.0	5.2 ± 0.1
C _β -ox ^c	1.0 ± 0.0	1.1 ± 0.0	1.2 ± 0.1	2.9 ± 0.0	2.9 ± 0.0	3.2 ± 0.0	2.7 ± 0.0	2.8 ± 0.0	3.2 ± 0.0
C _γ -ox	39.9 ± 0.4	42.8 ± 0.3	17.2 ± 0.2	55.9 ± 0.4	53.7 ± 0.6	51.5 ± 0.1	58.0 ± 0.3	55.9 ± 0.5	58.0 ± 0.2
Miscellaneous	3.5 ± 0.1	3.3 ± 0.0	4.3 ± 0.1	9.2 ± 0.1	9.7 ± 0.2	9.6 ± 0.1	9.8 ± 0.2	10.2 ± 0.1	8.8 ± 0.1
PhC _γ ^d	44.3 ± 0.3	47.0 ± 0.4	22.8 ± 0.2	67.7 ± 0.3	65.9 ± 0.3	63.9 ± 0.0	69.0 ± 0.0	67.4 ± 0.4	68.7 ± 0.2

^a 4-vinylphenol. ^b 4-vinylguaiacol. ^c excluding diketones. ^d phenols with intact α,β,γ carbon side chain.

Supporting Information References

- Englyst, H. N.; Cummings, J. H., Simplified method for the measurement of total non-starch polysaccharides by gas-liquid chromatography of constituent sugars as alditol acetates. *Analyst* **1984**, *109*, 937-942.
- Blumenkrantz, N.; Asboe-Hansen, G., New method for quantitative determination of uronic acids. *Anal Biochem* **1973**, *54*, 484-489.
- Van Erven, G.; Hilgers, R.; de Waard, P.; Gladbeek, E.-J.; van Berkel, W. J. H.; Kabel, M. A., Elucidation of *in situ* ligninolysis mechanisms of the selective white-rot fungus *Ceriporiopsis subvermispora*. *ACS Sustainable Chem Eng* **2019**, *7*, 16757-16764.
- Van Erven, G.; de Visser, R.; Merckx, D. W.; Strolenberg, W.; de Gijssel, P.; Gruppen, H.; Kabel, M. A., Quantification of lignin and its structural features in plant biomass using ^{13}C lignin as internal standard for pyrolysis-GC-SIM-MS. *Anal Chem* **2017**, *89*, 10907-10916.
- Van Erven, G.; Nayan, N.; Sonnenberg, A. S.; Hendriks, W. H.; Cone, J. W.; Kabel, M. A., Mechanistic insight in the selective delignification of wheat straw by three white-rot fungal species through quantitative ^{13}C -IS py-GC-MS and whole cell wall HSQC NMR. *Biotechnol Biofuels* **2018**, *11*, 262.





CHAPTER 4

Mechanistic insight into the selective delignification of wheat straw by three white-rot fungal species through quantitative ^{13}C -IS py-GC-MS and whole cell wall HSQC NMR

Gijs van Erven, Nazri Nayan, Anton S. M. Sonnenberg,
Wouter H. Hendriks, John W. Cone, Mirjam A. Kabel

Based on: *Biotechnology for Biofuels*, 2018, 11, 262

Abstract

The white-rot fungi *Ceriporiopsis subvermispora* (Cs), *Pleurotus eryngii* (Pe) and *Lentinula edodes* (Le) have been shown to be high-potential species for selective delignification of plant biomass. This delignification improves polysaccharide degradability, which currently limits the efficient lignocellulose conversion into biochemicals, biofuels and animal feed. Since selectivity and time-efficiency of fungal delignification still needs optimization, detailed understanding of the underlying mechanisms at molecular level is required. The recently developed methodologies for lignin quantification and characterization now allow for the in-depth mapping of fungal modification and degradation of lignin and, thereby, enable resolving underlying mechanisms.

Wheat straw treated by two strains of Cs (Cs1 and Cs12), Pe (Pe3 and Pe6) and Le (Le8 and Le10) was characterized by using semiquantitative py-GC-MS during fungal growth (1, 3 and 7 weeks). The remaining lignin after 7 weeks was quantified and characterized by using ^{13}C lignin internal standard based py-GC-MS and whole cell wall HSQC NMR. Strains of the same species showed similar patterns of lignin removal and degradation. Cs and Le outperformed Pe in terms of extent and selectivity of delignification ($\text{Cs} \geq \text{Le} \gg \text{Pe}$). The highest lignin removal (66% (w/w); Cs1) was obtained after 7 weeks, without extensive carbohydrate degradation (factor 3 increased carbohydrate to lignin ratio). Further, though after treatment with Cs and Le comparable amounts of lignin remained, the structure of the residual lignin vastly differed. For example, C_α -oxidized substructures accumulated in Cs-treated lignin up to 24% of the total aromatic lignin, a factor two higher than in Le-treated lignin. Contrarily, ferulic acid substructures were preferentially targeted by Le (and Pe). Interestingly, Pe-spent lignin was specifically depleted of tricin (40% reduction). The overall subunit composition (H:G:S) was not affected by fungal treatment.

Cs and Le are both able to effectively and selectively delignify wheat straw, though the underlying mechanisms are fundamentally different. We are the first to identify that Cs degrades the major β -O-4' ether linkage in grass lignin mainly via C_β -O-aryl cleavage, while C_α - C_β cleavage of interunit linkages predominated for Le. Our research provides new insight into how fungi degrade lignin, which contributes to further optimizing the biological upgrading of lignocellulose.

Introduction

Lignocellulosic biomass, such as wheat straw, is a highly abundant, valuable source of polysaccharides for the production of animal feed or biofuels and biochemicals.¹⁻⁴ The presence of lignin, however, hinders the conversion of these polysaccharides and, therefore, necessitates the use of pretreatments aimed at lignin removal or degradation. These physical and/or chemical hydrothermal pretreatments require extensive amounts of energy and chemicals.⁵ A sustainable alternative is the use of white-rot fungi as a biological pretreatment and is increasingly receiving attention.^{2, 6-9} Among these fungi, the species *Ceriporiopsis subvermispora* (Cs), *Pleurotus eryngii* (Pe) and *Lentinula edodes* (Le) were shown to be particularly promising as they extensively and selectively removed lignin over cell wall polysaccharides, in comparison to other more commonly studied white-rot fungi like *P. chrysosporium*.¹⁰ Such fungal delignification results in a greatly enhanced enzymatic degradability of polysaccharides in further downstream processes.¹¹⁻¹³ To optimize the pretreatment with these fungi, mainly in terms of selectivity and time-efficiency, it is important to understand delignification and the underlying mechanisms at a molecular level. Such mechanistic insight facilitates the pinpointing of potential bottlenecks in the (enzymatic) process and might provide means to circumvent them, e.g. via supplementation of co-factors for the respective enzymes. Besides enabling control of the pretreatment process, mechanistic insight expands our understanding of how fungi function in nature and how they contribute to terrestrial carbon-recycling.

Lignin is a heterogeneous phenolic polymer that, in grasses, is composed of *p*-hydroxyphenyl (H), guaiacyl (G) and syringyl (S) subunits, which are linked through a variety of carbon-carbon and aryl-ether linkages, with the β -O-4' ether as most abundant interunit linkage (~80%).¹⁴⁻¹⁶ Structural complexity of grass-type lignin is further enhanced by the incorporation of *p*-coumaric acid, ferulic acid and triclin in the macromolecule.¹⁷⁻¹⁹ A schematic structure of wheat straw lignin is presented in Figure 1.

Lignin degradation by white-rot fungi in general relies on a complex enzymatic machinery which is, depending on the species, mainly based on lignin peroxidases (LiP), manganese peroxidases (MnP), laccases (Lac) and the H₂O₂ generating aryl-alcohol oxidases (AAO). Collectively, the catalytic performance of these enzymes results in the generation of radicals, i.e. aromatic or hydroxyl radicals, which can lead to various reactions such as C α -C β cleavage, breakdown of the β -O-4' ether, aromatic ring cleavage and demethoxylation, but also to polymerization.²⁰⁻²⁴

Although *C. subvermispora*, *P. eryngii* and *L. edodes* all produce MnP, Lac and AAO, they were shown to differ in the number of genes encoding for these enzymes, which suggests different dependencies on the particular enzymes.²⁵⁻²⁹ Interestingly, none of these fungi possess genes encoding LiP. Instead, versatile peroxidases were detected in *Pe*, whereas Cs was shown to produce two enzymes with lignin peroxidase and versatile peroxidase like activity.²⁹⁻³⁰ It is clear from

this variation in ligninolytic enzyme encoding genes that these fungi employ different strategies for delignification. However, whether these different strategies emerge into different underlying mechanisms remains unknown. Furthermore, it is poorly understood whether certain structural motifs of lignin are preferentially degraded or modified by the respective enzymatic machineries and, thus, lead to different residual lignin structures.^{20, 22}

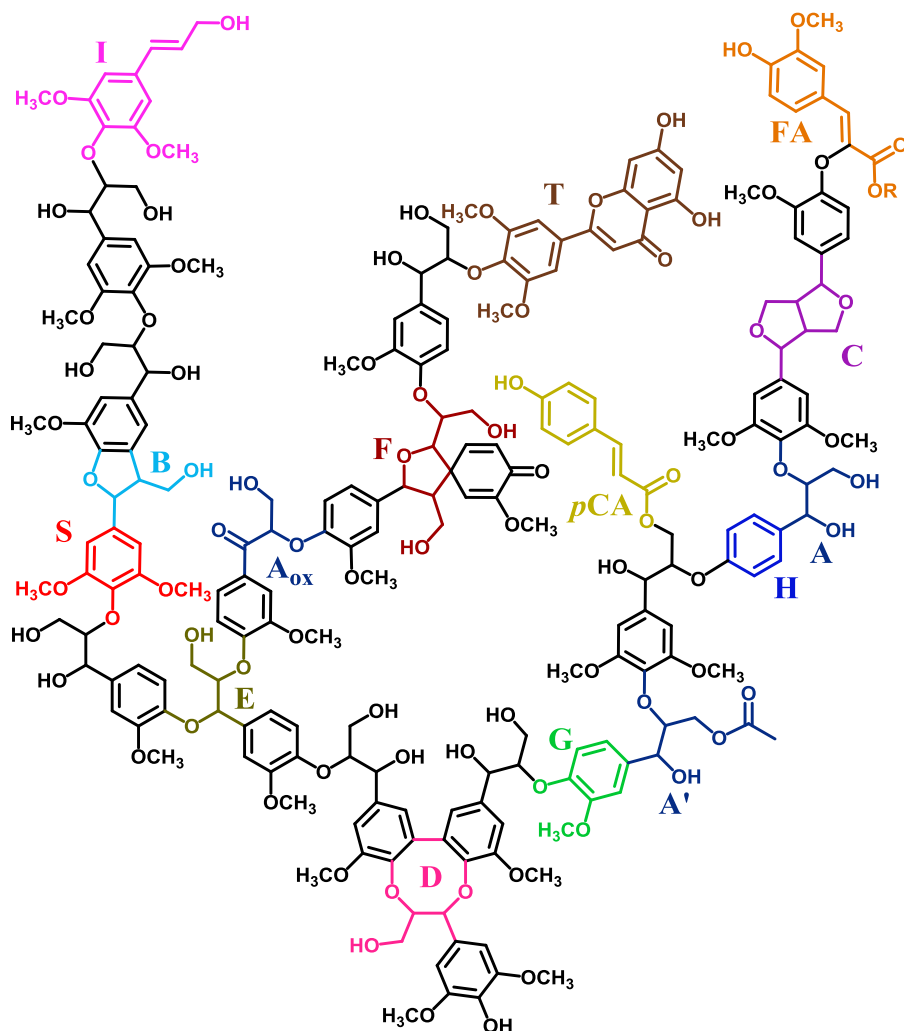


Figure 1. Wheat straw lignin model. The most abundant substructures are included, attempting to fairly represent the relative abundances of each moiety, based on literature.¹⁴⁻¹⁹ H: *p*-hydroxyphenyl unit; G: guaiacyl unit; S: syringyl unit; A: β -O-4' aryl ether; A': β -O-4' aryl ether γ -acylated; Aox: C α -oxidized β -O-4' aryl ether; B: phenylcoumaran; C: resinol; D: dibenzodioxocin; E: α,β -diarylether; F: spirodienone; I: cinnamyl alcohol (or aldehyde); T: triclin; pCA: *p*-coumarate; FA: ferulate (R = H or arabinose). Note that γ -acylation here is only shown on β -O-4' linkages, while in fact any free γ -OH can be acylated. For simplicity only monomeric 8-O-4' linked FA is shown, though many other ferulate and diferulate linkages are known to exist. For more detailed structures see Figure 5.

To the best of our knowledge, research on the conversion of grass lignin is limited,³¹⁻³³ and studies where the fungi were compared under the same experimental conditions are scarce.^{11-12, 34} Furthermore, lignin degradation was, contentwise, only determined by using unspecific gravimetric analysis, which is thought to be particularly inaccurate for fungal-grown samples due to the presence of residual chitin and this methodology includes (acid) recalcitrant lignin only.^{20, 35} Moreover, the scarce studies aimed at elucidating structural features of fungal-treated lignin *in situ* focused on using qualitative pyrolysis gas chromatography mass spectrometry (py-GC-MS). Though considerable structural changes in fungal-treated wheat straw lignin could be revealed, mainly in terms of preference for phenolic lignin substructures and accumulation of C_α-oxidized substructures, underlying mechanisms could not be elucidated.^{11-12, 31} More accurate and in-depth analysis of both lignin content as well as lignin structural features in fungal-treated biomass is expected to further resolve the underlying lignin degrading mechanisms.

The recent development of a highly accurate pyrolysis gas chromatography mass spectrometry (py-GC-MS) method that uses ¹³C lignin as internal standard (¹³C-IS) offers a great opportunity to specifically quantify residual lignin content *in situ*, while simultaneously providing structural insight.³⁶ In addition, developments in the use of heteronuclear single quantum coherence (HSQC) nuclear magnetic resonance (NMR) allow the analysis of whole cell wall samples *in situ*, without prior isolation or derivatisation of lignin.³⁷⁻³⁸ *In situ* analysis avoids the need for laborious lignin isolation procedures that may lead to partial extraction and polymer modification, especially for fungal-treated lignin.³⁹⁻⁴¹

In this research, the combination of quantitative ¹³C-IS py-GC-MS and whole cell wall HSQC NMR was applied to fungal-treated wheat straw after growth of two strains of *C. subvermispora*, *P. eryngii* and *L. edodes* to obtain a better understanding of their delignification mechanisms. We found that both *Cs* and *Le* outperform *Pe* in terms of delignification effectivity and selectivity and, furthermore, vastly differed in residual lignin structures. We were able to identify that these lignin structures originated from fundamentally different delignification mechanisms.

Experimental Section

Materials. All chemicals were obtained from commercial suppliers and used without further purification. Water used in all experiments was purified via a Milli-Q water system (Millipore, Billerica, MA, USA).

Preparation of the fungal-treated wheat straw. Samples used in the present study were collected from a main experiment on selecting the best performing fungal strains based on their capability to improve the *in vitro* ruminal degradability of the treated straw.¹³ Two high potential strains from three different fungal species were selected: *Cs*1 (CBS 347.63) and *Cs*12 (ME-485) strains for

Ceriporiopsis subvermispora, Pe3 (Mycelia2600) and Pe6 (AL04) for *Pleurotus eryngii* and Le8 (sh 03/08) and Le10 (LE75) for *Lentinula edodes*. Procedures for fungal strain preparation and pretreatment of the wheat straw has been previously described in detail.⁴² Briefly, all strains were maintained on malt extract agar before a piece of that agar (1.5 × 2.0 cm) was used to prepare the spawn for each fungus. The spawn was prepared using sterilized sorghum grains and was incubated at 24 °C for up to 5 weeks. Organic wheat straw (*Triticum aestivum* L.) was purchased from a local farmer in the Netherlands (batch size 300 kg) and chopped into pieces of approximately 3 cm. Approximately 5 kg of the chopped wheat straw was soaked in water for 3 days at room temperature and excess water was drained for 5 h, resulting in a dry matter loss of 9.3% (w/w). Each container (185×185×78 mm, Combiness, Nevele, Belgium) was adjusted to contain 90.2 ± 0.3 g of dry matter with a moisture content of ~74% (w/w). After autoclaving at 121 °C for 1 h, the straw was inoculated with the prepared spawn at 10% of the dry weight, thereby introducing negligible amounts of sorghum lignin.⁴³⁻⁴⁴ The wheat straw (treated and untreated with fungi) was incubated in triplicate under solid state fermentation at 24 °C in a climate-controlled chamber (relative humidity = 75%) for 1, 3 and 7 weeks. After weighing and thorough mixing, ~5g of fresh sample was taken for pH measurements. The remaining sample material was freeze-dried and ground over a 1 mm sieve using a cross beater mill (100AN, Peppink, Olst, the Netherlands). Since biological triplicates showed ~5% RSD in conventional compositional feed analysis, they were thoroughly mixed in equal dry matter amounts (1 g each) to one replicate and ball-milled in a MM200 mixer mill (Retsch, Haan, Germany) for further analyses.¹³ We previously showed that untreated straws were stable during incubation and showed minimal variation.⁴² Therefore, the untreated wheat straw without incubation was used as control sample in this study.

Carbohydrate content and composition. Carbohydrate content and composition was determined in triplicate by a modified method reported by Englyst & Cummings (1984), using inositol as internal standard.⁴⁵ Ten mg of each sample was treated with 72% (w/w) H₂SO₄ for 1 h at 30 °C followed by 1 M H₂SO₄ for 3 h at 100 °C. The constituent monosaccharides released were analyzed as their alditol-acetate derivatives by using gas chromatography (Thermo Scientific, Synnyvale, CA, USA) and represented as anhydromonosaccharides. The uronic acids released after the acid hydrolysis step were determined in duplicate as anhydrouronic acid content by an automated meta-hydroxydiphenyl assay with addition of sodium tetraborate using an auto-analyzer (Skalar Analytical BV, Breda, The Netherlands).⁴⁶ Glucuronic acid (Fluka AG, Busch, Switzerland) was used as a reference (0 – 100 µg mL⁻¹). Total carbohydrate content was calculated as the sum of neutral anhydrocarbohydrates and anhydrouronic acids.

Semiquantitative py-GC-MS. Pyrolysis was performed with an EGA/PY-3030D Multi-shot pyrolyzer (Frontier Laboratories, New Ulm, MN, USA) equipped with an AS-1020E Autoshot auto-sampler as previously described.³⁵⁻³⁶ The pyrolyzer was coupled to a GC-MS using a Trace GC equipped with a DB-1701 fused-silica capillary column (30 m × 0.25 mm i.d. 0.25 µm film thickness) coupled to a DSQ-II mass spectrometer (both Thermo Scientific, Waltham, MA, USA). Samples were weighed using an XP6 excellence-plus microbalance (Mettler Toledo, Columbus, OH, USA). Pyrolysis of total biomass (~80 µg) was performed at 500 °C for 1 min with an interface temperature of 300 °C. Pyrolysis products were injected on the column via split/splitless injection (at 250 °C) with a splitratio of 1:133 and helium was used as carrier gas with constant flow at 1.5 mL min⁻¹. The GC oven was programmed from 70 °C (2 min) to 270 °C at 5 °C min⁻¹ and held at 270 °C for 15 min. MS detection was used with EI at 70 eV, a source temperature of 250 °C, a scan range of *m/z* 50-550 and a scan rate of 4.0 scans/sec. Compounds were identified by comparing retention time and mass spectrum with standards, the NIST library and data published by Ralph and Hatfield.⁴⁷

For semiquantitative analysis, pyrograms were processed by Xcalibur 2.2 software. The two most abundant fragments per compounds were automatically integrated using ICIS peak integration with optimized settings per compound. A manual correction was only applied when irregular peak shapes led to erroneous peak integration with method settings. Areas were normalized by dividing by corresponding relative response factors (RRF), as previously published, multiplied with the molecular weight of the respective compound and summed.³⁶ Lignin content was estimated on the basis of total area of lignin-derived pyrolysis products and compared to a wheat straw reference sample with known Klason lignin content (acid-insoluble lignin + acid-soluble lignin = 20.5% (w/w)), as described by Jurak et al.³⁵ Relative abundances of lignin-derived pyrolysis products were based on areas without molecular weight correction as previously described by del Río et al.,¹⁵ as relative response factor (RRF) values are mole-based. Compounds were classified according to their structural feature (Supporting Information Table S1) and summed. All samples were prepared and analyzed in triplicate.

Quantitative py-GC-MS with ¹³C lignin as internal standard. Pyrolysis was carried out as previously described in detail and in the section semiquantitative py-GC-MS.³⁶ Briefly, 10 µL of a ¹³C lignin internal standard (IS) solution (1 mg mL⁻¹ ethanol/chloroform 50:50 v/v) was mixed with ~80 µg of sample and dried before analysis. Lignin-derived compounds of which fungal action increased the content above detection limits were identified by qualitative Py-GC-MS using full-MS detection and added to the existing SIM method. Lignin-derived pyrolysis products were monitored in selected ion monitoring (SIM) mode on the two most abundant fragments per compound (both ¹²C and ¹³C). The compound vanilloyl acetaldehyde (VAL) was not properly detected in SIM due to a shifted segment and

therefore was estimated from full MS analysis. The relative area of VAL versus vanillin as measured by full MS was thereto multiplied by the area of vanillin as measured by SIM. For correction of matrix-effects similar behavior as syringoyl acetaldehyde (SAL) was assumed. Areas for each compound were normalized by dividing by the respective RRF. Relative response factor values were updated to system performance by recalculation to obtain an identical relative abundance of lignin-derived pyrolysis products of the ^{13}C -IS added to a wheat straw reference sample (Supporting Information eq 1). Lignin content (% (w/w)) was determined from the sum of lignin-derived pyrolysis products, where RRF corrected areas for each compound were multiplied with the molecular weight of the respective compound and summed instead of the application of the published correction factor of 1.057 (Supporting Information eq 2).³⁶ Areas were not corrected for molecular weight before relative abundance determination as previously described by del Río et al.¹⁵ to allow direct comparison with data obtained by 2D-NMR analysis. Relative abundances of lignin-derived pyrolysis products were normalized for the ^{13}C analogues from the IS present in the same sample to distinguish matrix and treatment effects (Supporting Information eq 3-5). Compounds were classified according to their structural feature (Supporting Information Table S1) and summed. All samples were prepared and analyzed in triplicate. Extractive-free samples were identical to total biomass samples for Cs1 and, therefore, not measured for the other fungi.

Whole cell wall 2D HSQC NMR spectroscopy. For NMR analysis of the whole cell wall material, ground wheat straw (1 mm, 2 g) was successively extracted with acetone until the solvent became clear; followed by hot water treatment (100 °C) for 3 h to remove low molecular weight compounds that would interfere with the analysis.³⁸ The extractive-free residues were then freeze-dried before mixing biological replicates (1 g each) and fine milling in a PM100 planetary ball mill (Retsch, Haan, Germany). Though lignin became increasingly extractable as fungal action proceeded, the structural features of the remaining lignin were highly comparable to that of the total unextracted sample, allowing comparison of NMR and ^{13}C -IS py-GC-MS analyses. Two g of sample was milled in a 50 mL ZrO_2 beaker using 17 Φ 10 mm balls of the same material at a frequency of 600 rpm with a net milling time of 4 h. After every 15 min of milling, a pause of 10 min was set to avoid overheating of the sample. Around 100 mg of ball-milled sample was swollen in 0.75 mL $\text{DMSO}-d_6$. 2D heteronuclear single quantum coherence (HSQC) NMR was performed according to previously described methods.^{15, 37-38} The spectra were recorded at 25 °C with Bruker's standard pulse sequence "hsqcetgpsisp2.2" on a Bruker AVANCE III 600 MHz NMR spectrometer (Bruker BioSpin, Rheinstetten, Germany) equipped with a 5 mm cryoprobe located at MAGNEFY (MAGNEtic resonance facility, Wageningen, The Netherlands). The spectral widths were 7,200 and 30,000 Hz for the ^1H and ^{13}C dimensions, respectively. The number of collected complex points was 2018 in the ^1H dimension with a relaxation time of 1 s. The

number of collected scans was 16 and 400 increments of time were recorded in the ^{13}C dimension. The $^1\text{J}_{\text{CH}}$ used was 145 Hz. The data were processed with Bruker TopSpin 3.5 software. Processing used Gaussian apodization in ^1H and a squared cosine function in the ^{13}C dimension. For ^{13}C , data were zero filled up to 1024 points prior to Fourier transformation. The solvent peak ($\text{DMSO-}d_6$) was used as an internal reference (δ_{C} 39.5 ppm; δ_{H} 2.49 ppm). HSQC correlation peaks were assigned by comparison with literature.^{15, 48-54} Semiquantitative analysis of the volume integrals was performed according to del Río et al.¹⁵ Alternatively, in the aliphatic oxygenated region $\beta\text{-O-4'}$ substructures were estimated from their $\text{C}_{\beta}\text{-H}_{\beta}$ correlations, since they were shown to be interfered to a lesser extent by the presence of carbohydrates.³⁸ For phenylcoumaran and resinol substructures, their respective $\text{C}_{\alpha}\text{-H}_{\alpha}$ correlations were used. Volume integrals for resinol substructures were logically halved. $\text{S}_{2,6}$, G_2 and $\text{H}_{2,6}$ signals were used for S, G and H units, respectively, where S and H integrals were halved as well. Oxidized analogues were estimated in a similar manner. Tricin, *p*CA and FA were similarly estimated from their respective $\text{T}_{2',6'}$, $\text{pCA}_{2,6}$ and FA_2 signals. $\text{H}_{2,6}$ integrals were corrected for the overlapping phenylalanine cross-peak ($\text{PHE}_{3,5}$) by subtraction of the isolated $\text{PHE}_{2,6}$ cross-peak.⁵⁵ Volume integration was performed at equal contour levels. Amounts were calculated both as a percentage of total lignin ($\text{H} + \text{G} + \text{G}_{\text{ox}} + \text{G}_{\text{mod}} + \text{S} + \text{S}_{\text{ox}} + \text{S}_{\text{mod}}$) and total lignin including *p*CA, FA and T.⁵⁶⁻⁵⁷

Statistical analysis. In earlier work, we showed that the biological variation in the delignification of wheat straw by the strains used in this study was low (pooled standard deviation of biological and analytical triplicates $\sim 5\%$ RSD)¹³. For the purpose of this study, biological triplicates were thoroughly mixed (in equal dry matter amounts) and ball-milled (as explained in the section 'preparation of the fungal-treated straw'), thereby ensuring homogeneous samples for analyses. Albeit low, biological variation was, therefore, not included in the outcomes of this study. Results are presented as average \pm standard deviation on the basis of analytical triplicates (when replicates were included). Student's *t* test ($\alpha = 0.05$) was used to evaluate significant differences between strains in terms of lignin and carbohydrate removal.

Results & Discussion

Wheat straw delignification during fungal growth. The extent of wheat straw delignification during growth of the different fungal strains was monitored by semiquantitative py-GC-MS (Figure 2). This technique does not experience interference from fungal cell wall material and the entire lignin population is measured.^{20, 35} In comparison to conventional gravimetric analysis, semiquantitative py-GC-MS, therefore, is considered to provide a more accurate insight into the delignification characteristics of the studied fungi. Clear lignin removal was observed from the first week of growth and all strains extensively delignified the wheat straw within 7 weeks. *Cs* and *Le* were the most effective

species, which is in line with the initial evaluation of these fungi by conventional compositional feed analysis.¹³ Not only were *Cs* and *Le* more effective, compared to *Pe*, they also showed a distinct pattern of lignin removal in time. For *Cs* and *Le*, the major part (>70%) of the final lignin removal occurred within the first 3 weeks, whereas both *Pe* strains showed a more gradual lignin removal in time, reaching less than 50% of the final lignin removal within 3 weeks. No significant differences ($P>0.05$) were found in the extents of lignin removal after 7 weeks of growth between strains of the same species. Though the fungal species (and strains) varied considerably in growth pattern, as recently shown by Nayan et al.,¹³ the extent of growth (amount of ergosterol formed) was not directly correlated to the extent of lignin degradation.

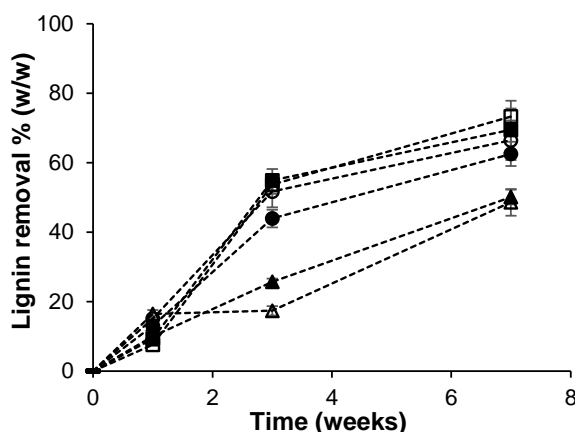


Figure 2. Semiquantitative py-GC-MS determination of lignin removal from wheat straw after 1, 3 and 7 weeks of fungal growth. *Cs* *Ceriporiopsis subvermispora*, *Pe* *Pleurotus eryngii*, *Le* *Lentinula edodes*. □ *Cs*1, ■ *Cs*12, △ *Pe*3, ▲ *Pe*6, ○ *Le*8, ● *Le*10. Average and standard deviation of analytical triplicates on pooled biological triplicates.

Though semiquantitative py-GC-MS clearly proved useful for the comparison of the delignification efficiency of the different fungi, we strived for more accurate and precise quantification and characterization of the residual lignin. At the end-point of the treatment (7 weeks), the wheat straw was most affected by fungal growth and, for that reason, considered the most informative to further investigate the underlying delignification mechanisms.^{12, 58} Therefore, lignin in fungal-treated wheat straw after 7 weeks of growth was quantified by the recently developed quantitative ¹³C-IS py-GC-MS method.³⁶ In this method, a ¹³C lignin internal standard is mixed with the sample to correct for matrix-effects and system performance, which was previously shown to improve the accuracy of lignin quantification in sound biomass samples.³⁶ From the total dry matter recovered and lignin contents in the treated material, the amount of lignin removed was calculated (Figure 3).

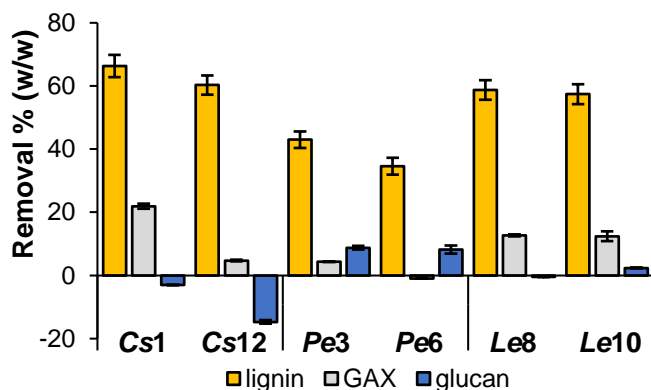


Figure 3. Lignin, glucuronoarabinoxylan (GAX) and glucan (cellulose) removal after 7 weeks of fungal growth. *Cs* *Ceriporiopsis subvermispota*, *Pe* *Pleurotus eryngii*, *Le* *Lentinula edodes*. Compositional analysis by using quantitative ^{13}C -IS py-GC-MS (lignin) and constituent monosaccharide analysis after H_2SO_4 hydrolysis (carbohydrates). Average and standard deviation of analytical triplicates on pooled biological triplicates. It is important to take some limitations of the methods used for carbohydrate quantification into consideration. Firstly, the hydrolysis of polysaccharides to constituent monosaccharides does not allow cellulose and fungal β -glucan to be distinguished. Cellulose determination was, however, not expected to be largely affected, since fungal biomass was present in minor amounts only, as estimated from ergosterol content.¹³ Secondly, fungal treated cellulose and glucuronoarabinoxylan (GAX) were expected to be more completely acid-hydrolyzed than untreated material, thereby resulting in underestimation of the amount of degraded carbohydrates.

Although semiquantitative py-GC-MS gave fair estimates of lignin removal (Figure 2), the method overestimated lignin removal in all samples by approximately 15%, mainly due to overestimation of the lignin content of the starting material (Supporting Information Table S2). The results of quantitative py-GC-MS confirmed the effectiveness of *Cs*, *Le* and *Pe* in degrading lignin, where in the case of *Cs* and *Le* more than 60% (w/w) of lignin was removed from the wheat straw within 7 weeks of treatment. *Cs1* outperformed both *Le* and *Pe* strains whereas it was not significantly different from *Cs12* in terms of lignin removal. *Pe3* removed significantly more lignin than *Pe6*, while both *Le* strains were not significantly different.

The three fungal species, furthermore, were capable of removing lignin highly selectively over cell wall carbohydrates (Figure 3, Supporting Information Figure S1). After 7 weeks of growth *Pe* strains were found to have degraded considerable amounts of glucan (8% (w/w) of initial glucan), whereas *Cs* and *Le* less affected glucan. Instead, these species degraded glucuronoarabinoxylan (GAX), but to a lesser extent than lignin. *Cs1* showed a remarkably higher degradation of GAX than *Cs12* (21 vs 5% (w/w) of initial GAX), while both *Le* strains degraded approximately 12% (w/w) of initial GAX. The selective removal of lignin over carbohydrates has been described in previous studies for the three fungi used. Though, more extensive hemicellulose degradation has been reported.^{12-13, 42} This is due to the gravimetric method that was used in these previous studies, in which solubilization and removal cannot be discriminated.

Based on the removal of lignin, glucan and GAX after 7 weeks of fungal growth (Figure 3), it was concluded that *Pe* removed considerably more carbohydrates versus lignin than *Cs* and *Le*. In addition to the effectiveness of lignin removal, the latter fungi, thus, also seem to outperform *Pe* in terms of selectivity.

Structural features of fungal treated lignin. Besides accurate lignin content, quantitative ^{13}C -IS py-GC-MS simultaneously provided accurate insight into the structural features of the remaining lignin.³⁶ By correcting for any changes in the structural features of the ^{13}C -IS lignin, it was ensured that the observed changes in residual lignin were indeed fungal-induced. The same samples were also subjected to 2D-HSQC NMR analysis allowing comparison with the ^{13}C -IS py-GC-MS data, which is discussed further on. Table 1 shows the relative abundances of the structural features of lignin of untreated and treated wheat straw (^{13}C -IS py-GC-MS data). The bases of structural classification and relative abundances of individual lignin-derived pyrolysis products can be found in Supporting Information Table S1. The structural features of the untreated straw matched well with that of wheat straw that was previously analyzed in a similar manner, which confirmed that a representative wheat straw sample was used.³⁶

Unexpectedly, fungal treatment was found to have a minimal effect on the overall composition of lignin subunits, with the largest effect observed for *Le*8 (H:G:S = 11:64:25) compared to control (H:G:S = 10:62:28), which indicates that all lignin units were targeted in the process of lignin degradation. Although minimal, all fungi except *Cs*12, showed a preference towards the removal of S units (over H- and G-units) as demonstrated by slightly lowered S/G (e.g. 0.45 to 0.38 by *Le*8; Table 1). This preference was less pronounced compared to a previous study, where a factor 2 decrease in S/G was found within 8 weeks of treatment by both *Cs* and *Le*.^{12, 58} The main difference is the higher S/G of the wheat straw used in the previous study (S/G = 0.7) compared to our wheat straw (S/G = 0.45). Hence, the most likely explanation of the lower S/G preference in our study was the difference in wheat straw used, which differed not only in the overall subunit composition, but might also have differed in the way these subunits were linked.

Preferential degradation of (sub-)structures with a higher degree of methoxylation has been related to the corresponding lower redox potential and reduced frequency of carbon-carbon ('condensed') substructures.^{12, 33, 58-59} Still, as mentioned above, *Cs*, *Pe* and *Le* did not show a clear preference for degrading the more methoxylated S-units over G- and H-units in our research. Demethoxylation, due to which S units 'transform' into G units, and likewise G units into H units, is known to occur due to fungal action, and might, hence, potentially have masked the preferential removal of certain subunits.^{20, 24}

When categorized according to structural moiety, the residual lignin structures pointed out clear effects related to fungal growth (Table 1).

Table 1. ^{13}C -IS py-GC-MS relative abundance of residual lignin compounds of control and fungal-treated wheat straw after 7 weeks of growth. *Cs Ceriporiopsis subvermispora*, *Pe Pleurotus eryngii*, *Le Lentinula edodes*. Corrected for RRF and relative abundance of ^{13}C analogues. Sum on the bases of structural classification according Supporting Information Table S1. Average and standard deviation of analytical triplicates on pooled biological triplicates.

	Control	Cs1	Cs12	Pe3	Pe6	Le8	Le10
Lignin subunits (%)							
H	9.6 ± 0.4	12.0 ± 0.7	12.1 ± 0.3	10.0 ± 0.7	10.1 ± 0.8	11.1 ± 0.5	11.3 ± 0.5
G	62.2 ± 0.7	62.1 ± 0.5	59.3 ± 0.3	62.8 ± 1.4	63.3 ± 0.3	64.2 ± 0.2	63.0 ± 0.6
S	28.2 ± 0.5	26.0 ± 0.4	28.6 ± 0.1	27.2 ± 0.8	26.7 ± 0.9	24.7 ± 0.4	25.6 ± 0.1
S/G	0.45 ± 0.0	0.42 ± 0.0	0.48 ± 0.0	0.43 ± 0.0	0.42 ± 0.0	0.38 ± 0.0	0.41 ± 0.0
Structural moieties (%)							
Unsubstituted	4.2 ± 0.2	9.4 ± 0.5	9.4 ± 0.4	6.1 ± 0.4	5.8 ± 0.02	7.1 ± 0.4	7.7 ± 0.4
Methyl	2.0 ± 0.0	3.2 ± 0.3	3.4 ± 0.2	2.6 ± 0.1	2.5 ± 0.2	2.9 ± 0.1	2.9 ± 0.1
Vinyl	30.6 ± 1.0	30.1 ± 1.7	30.3 ± 0.3	29.6 ± 0.1	31.6 ± 1.2	31.7 ± 0.6	31.3 ± 0.7
4-VP ^a	7.8 ± 0.4	7.7 ± 0.5	7.8 ± 0.3	7.3 ± 0.4	7.8 ± 0.6	7.8 ± 0.3	7.9 ± 0.4
4-VG ^b	20.3 ± 0.7	20.4 ± 1.1	20.3 ± 0.0	19.9 ± 0.6	21.4 ± 0.6	21.7 ± 0.4	21.0 ± 0.7
C _α -ox	3.7 ± 0.1	13.6 ± 0.6	14.7 ± 0.7	6.0 ± 0.3	5.2 ± 0.3	6.6 ± 0.1	6.9 ± 0.3
C _α -ox G	2.0 ± 0.1	8.0 ± 0.3	8.1 ± 0.4	3.2 ± 0.2	2.7 ± 0.2	3.9 ± 0.1	4.0 ± 0.2
C _α -ox S	1.6 ± 0.0	5.6 ± 0.3	6.6 ± 0.3	2.7 ± 0.2	2.5 ± 0.1	2.7 ± 0.03	3.0 ± 0.1
Acetaldehyde	0.4 ± 0.0	7.7 ± 0.4	7.9 ± 0.5	1.9 ± 0.2	1.9 ± 0.2	2.7 ± 0.1	2.9 ± 0.2
C _β -ox	1.4 ± 0.0	2.5 ± 0.1	2.7 ± 0.1	1.7 ± 0.1	1.6 ± 0.0	1.8 ± 0.0	1.8 ± 0.0
C _γ -ox	54.8 ± 0.9	45.3 ± 2.3	43.9 ± 1.4	52.1 ± 0.6	51.4 ± 1.4	48.8 ± 0.6	48.6 ± 0.6
Miscellaneous	3.3 ± 0.1	3.5 ± 0.1	3.5 ± 0.1	3.9 ± 0.1	3.5 ± 0.5	3.8 ± 0.1	3.8 ± 0.2
PhC _γ ^c	58.5 ± 1.0	50.0 ± 2.3	48.7 ± 0.8	56.6 ± 0.6	55.4 ± 1.6	53.3 ± 0.6	53.0 ± 0.5
PhC _γ -acetaldehyde ^d	58.1 ± 0.9	42.4 ± 2.3	40.8 ± 1.3	54.7 ± 0.8	53.9 ± 1.7	50.6 ± 0.7	50.2 ± 0.3

^a 4-vinylphenol. ^b 4-vinylguaiacol. ^c phenols with intact α,β,γ carbon side chain. ^d phenols with intact α,β,γ carbon side chain, excluding acetaldehydes. No statistical analysis was applied.

Most pronounced was the increase of unsubstituted and C_α-oxidized pyrolysis products at the expense of products with three carbons in the side-chain (PhC_γ) in fungal-treated straw. The relative abundances of these moieties greatly varied across species, with the Cs strains showing the highest increases in unsubstituted (two-fold) and C_α-oxidized (five-fold) substructures compared to untreated wheat straw. Again, minimal differences were found between strains of the same species. These observations are in line with previous py-GC-MS studies on fungal-treated biomass and have been suggested to indicate degradation of interunit linkages within the lignin macromolecule.^{12, 58-60} To add to the latter, we hypothesize that in particular the relative abundance of PhC_γ is a measure for the amount of intact interunit linkages present, which is substantiated by the NMR data shown below. To explain, it is well known that upon pyrolysis of lignin, the intact (β-O-4') interunit linkages, consisting of C_α-C_β-C_γ aliphatic chains, decompose into products with various structures and chain-lengths (unsubstituted, C_α, C_β and C_γ side-chains).⁴⁷ At the pyrolysis conditions applied in our study, secondary reactions are absent. Therefore, lignin pyrolysis mainly yields monomeric products that are a direct result of bond-cleavage.⁶¹ Hence, the maximum chain length of the pyrolysis products equals the chain length of the substructures they originate from. PhC_γ

products can, thus, only form from structures in which the three carbon side-chain was initially present, being mainly intact interunit linkages. Furthermore, since the content of pendant cinnamyl alcohol and cinnamyl aldehyde end-groups in wheat straw was found to be rather low,^{15, 62} their contribution to PhC_γ products is considered marginal.

Interestingly, for both Cs strains, the increase in C_α-oxidized pyrolysis products was for more than half determined by the two compounds vanilloyl acetaldehyde (VAL) and syringoyl acetaldehyde (SAL). These compounds are respectively G and S-unit derivatives with three carbons in the side-chain and a ketone at the C_α position (Supporting Information Table S1 and Figure S2). Analogous to the explanation given above for PhC_γ products, we hypothesize that VAL and SAL solely formed from oxidized β-O-4' linkages and/or their cleavage products of which the three carbon (α, β and γ) side chain remained intact. To challenge this hypothesis, it can be postulated that pyrolysis of triclin (Figure 5) can result in SAL from the cleavage of the A-ring and rearrangement of the double bond. However, since we observed no SAL in the pyrograms of triclin-enriched extracts, triclin can be ruled out as potential (interfering) source of acetaldehyde products. If indeed acetaldehyde products originated from cleavage products of the interunit linkages, rather than intact oxidized β-O-4' linkages, they should be subtracted from the PhC_γ products for a more fair representation of the intact interunit linkages (PhC_γ-acetaldehyde in Table 1). Our results, thus, indicate that fungal-treated lignin was considerably reduced in intact interunit linkages, in particular for Cs strains (~30% compared to control). As C_α-oxidized products greatly accumulated, this reduction in intact interunit linkages was likely caused by oxidative cleavage.

Semiquantitative py-GC-MS confirmed that the observed structures were a direct effect of lignin degradation, i.e. that they accumulated during fungal growth as lignin degradation proceeded (Supporting Information Figure S3). Intriguingly, though Cs and Le followed a highly similar pattern of lignin degradation in time (Figure 2), they vastly differed in the remaining lignin structures after their growth. To further substantiate these findings, we also assessed the residual lignin structures by whole cell wall 2D-NMR.

Sample preparation for *in situ* whole cell wall gel state 2D-NMR requires finely divided, planetary ball-milled samples. Planetary ball-milling is associated with structural changes in lignin, mainly with regards to the cleavage of β-O-4 interunit linkages.⁶³ ¹³C-IS py-GC-MS analysis of the ball-milled samples showed that the milling did not induce structural changes in the lignin present and that the interunit linkages remained unaffected (PhC_γ constant). Thus, 2D-NMR could be appropriately used.

The aliphatic (δ_C/δ_H 50-90/2.5-6.0) and aromatic/unsaturated (δ_C/δ_H 90-160/6.0-8.0) regions of the recorded HSQC spectra of untreated and Cs1 treated wheat straw are presented in Figure 4, with structures of the assigned correlation peaks shown in Figure 5, of which chemical shift assignments were based on literature and shown in Supporting Information Table S3.^{15, 48-54}

Aliphatic and aromatic/unsaturated regions of the HSQC spectra of the wheat straw treated by the other fungi are shown in Supporting Information Figure S4. The aliphatic regions were dominated by polysaccharide signals, mainly derived from xylan and acetylated xylan moieties, which (partially) overlapped with β -O-4' substructures. This overlap was more severe for fungal-treated samples, from which lignin was selectively removed. Despite this overlap, phenylcoumaran (β -5') and resinol (β - β') substructures were readily observed, whereas C α -oxidized (α -keto) β -O-4', dibenzodioxocins (5-5'/4-O- β'), spirodienones (β -1'/ α - α') and α , β -diaryl ether linkages were only observed at higher zoom levels. At these zoom levels other contours were not resolved anymore, which would result in a lower accuracy of volume integration.

In the aromatic region, clear lignin signals, typical for wheat straw, were observed (S_{2,6}, G₂, H_{2,6} and several tricin (T), *p*CA and FA related signals).^{15, 62} Interestingly, in the fungal-treated samples, C α -oxidized aromatic units became more apparent, especially after treatment with Cs and is discussed in detail below. Although C α -oxidized S-units (δ_C/δ_H 106.6/7.2) are commonly found in NMR studies on (native) lignin, C α -oxidized G-units (δ_C/δ_H 111.2/7.5) are less often described and have, hitherto, never been observed at the levels shown here.^{48, 51, 64} Notably, two different C α -oxidized G-units substructures could be distinguished, although their exact structures remained unidentified (GoxI₂ δ_C/δ_H 111.2/7.5, GoxII₂ δ_C/δ_H 112.4/7.4). Another structural aspect resulting from fungal action is the increased intensity of derivatives of both S (S_{mod}, δ_C/δ_H 103.4/6.96) and G units (G_{mod}, δ_C/δ_H 112.8/6.76). Though the NMR database of lignin and cell wall model compounds could confirm that these signals originated from either S or G units, their exact structures could not be elucidated.⁴⁹ To identify both the unidentified oxidized G-units and S and G-derivatives, future extensive NMR-research is needed, not being the aim of the current research. A summary of the semiquantitative analysis of the volume integrals of aromatic units and interunit linkages (see materials and methods for details) is given in Table 2. Main trends were observed by comparing species, though slight variations between strains of the same species could be recognized.

Similar to ¹³C-IS py-GC-MS (Table 1), 2D-NMR showed minor changes in H:G:S composition after fungal treatment (Table 2). For instance, the H:G:S composition changed from 2:54:44 in control to 3:61:38 in Cs1-treated straw. Again a (slight) preferential removal of S-units was observed, thereby confirming our previous findings by py-GC-MS. However, for a fair comparison of the H:G:S composition found by the two techniques, it should be considered that whereas the hydroxycinnamic acids (*p*-CA and FA) and tricin (T) can be distinguished from 'core-lignin' substructures in 2D-NMR, in py-GC-MS they result in similar pyrolysis products. Upon pyrolysis both *p*-CA and FA as well as interunit linkages result in the formation of 4-vinylphenol and 4-vinylguaiacol, respectively. Analogous, tricin is expected to result in S-unit derivatives upon pyrolysis.

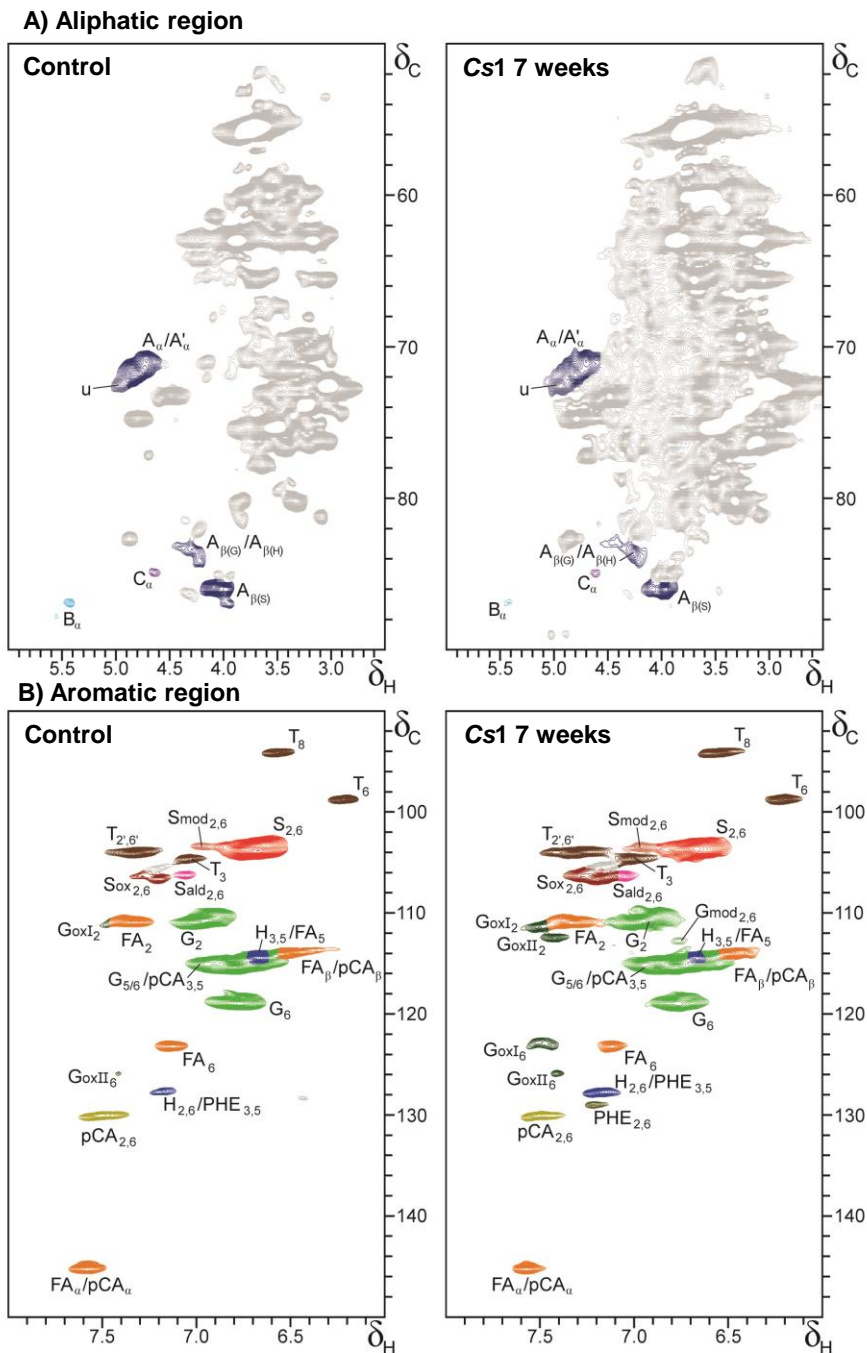


Figure 4. HSQC NMR spectra of control and 7 weeks Cs1-treated wheat straw. Structures of annotated correlation peaks are presented in Figure 5. GoxII₂ and GoxII₆ are tentatively assigned. G_{mod} and S_{mod}, being unknown derivatives of G and S units, respectively, are presented in a lighter color of the original subunit. Carbohydrate and unassigned signals are presented in gray. u: unassigned signal overlapping A_α/A'_α.

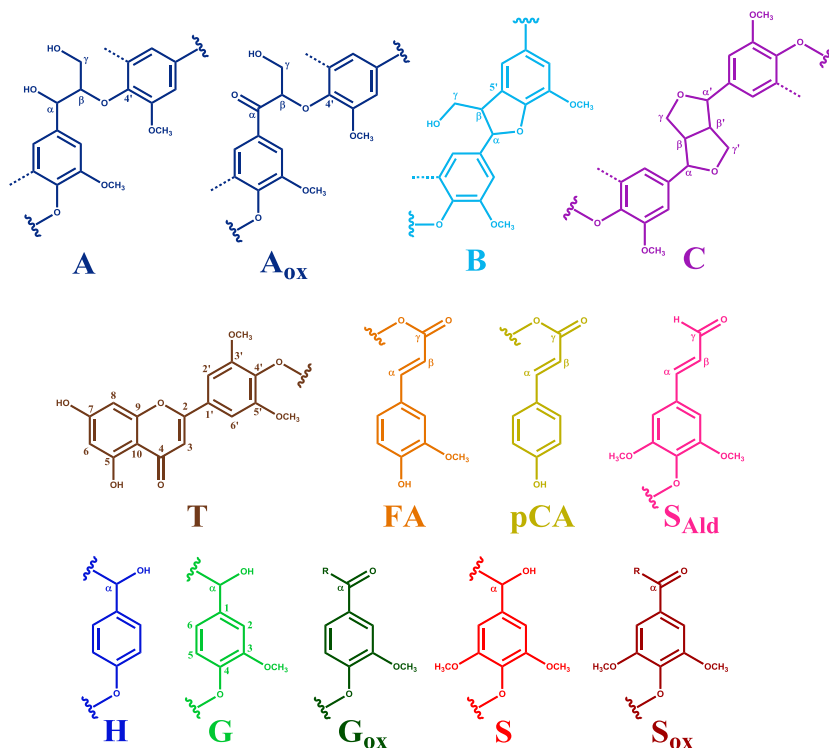


Figure 5. Structures annotated by HSQC NMR. A: β -O-4' aryl ether (A': γ -acylated β -O-4' aryl ether); A_{ox}: C_α-oxidized β -O-4' aryl ether; B: β -5' phenylcoumaran; C: β - β' resinol; T: tricetin; pCA: *p*-coumarate; FA: ferulate; G: guaiacyl unit; G_{ox}: C_α-oxidized guaiacyl unit; S: syringyl unit; S: C_α-oxidized syringyl unit; H: *p*-hydroxyphenyl unit; S_{ald}: syringaldehyde; Dotted line represents -H or -OCH₃. R in G_{ox} and S_{ox} can be a side chain in ketones or hydroxyl in carboxylic acids. Wavy lines indicate main positions of further coupling. Colors match the assigned contours in Figure 4.

To enable a comparison of both techniques in terms of H:G:S composition (mole based), *p*-CA (H), FA (G) and T (S) were included in the determination of the subunit composition by NMR (Table 2, numbers in parentheses). Besides analytical comparability, the obtained subunit composition is, in our opinion, more representative of 'true lignin' as these substructures were shown to be an integral part of lignin.^{17, 65} Upon inclusion of these substructures the obtained subunit compositions found by both techniques matched better, though they remained different (Cs1 H:G:S (NMR) = 5:59:35, H:G:S (py-GC-MS) = 12:62:26). It cannot be expected that both techniques result in identical values, as different entities are measured.³⁸ Still, because similar trends were observed, complementary structural information can be obtained by comparing both techniques. One of the explanations for the observed difference is that the semi-quantitative nature of the NMR technique results in over-estimation of end-units as a result of differences in relaxation behavior compared to 'core-lignin'.³⁸ Another explanation is that hydroxycinnamic acids are pyrolyzed more efficiently compared to 'core-lignin', which results in overestimation of their abundances and contributions to lignin.¹⁵

Table 2. Semiquantitative HSQC NMR structural characterization of residual lignin in control and fungal-treated wheat straw after 7 weeks of growth. *Cs* *Ceriporiopsis subvermispora*, *Pe* *Pleurotus eryngii*, *Le* *Lentinula edodes*. Volume integration of cross peaks in the aliphatic region likely suffered from overlap with carbohydrates, especially after extensive delignification.

	Control	Cs1	Cs12	Pe3	Pe6	Le8	Le10
Lignin subunits (%)^a							
H	2 (6)	3 (5)	3 (6)	3 (6)	2 (6)	2 (5)	3 (5)
G	52 (53)	47 (49)	42 (46)	57 (57)	53 (53)	53 (54)	57 (56)
G _{ox}	2 (1)	11 (8)	12 (9)	2 (2)	3 (3)	6 (5)	4 (3)
G _{mod}	0 (0)	3 (2)	4 (3)	0 (0)	1 (1)	0 (0)	0 (0)
S	37 (34)	25 (26)	25 (26)	31 (30)	32 (31)	30 (29)	29 (30)
S _{ox}	5 (4)	10 (7)	12 (9)	6 (5)	6 (5)	6 (5)	5 (4)
S _{mod}	2 (1)	3 (2)	2 (2)	1 (1)	1 (1)	2 (2)	1 (1)
S/G	0.8 (0.7)	0.6 (0.6)	0.7 (0.6)	0.6 (0.6)	0.7 (0.6)	0.6 (0.6)	0.6 (0.6)
Hydroxycinnamates (%)^b							
p-coumarate	6 (5)	5 (3)	5 (3)	5 (4)	5 (4)	5 (3)	4 (3)
ferulate	21 (15)	19 (14)	18 (13)	15 (12)	15 (12)	16 (13)	17 (13)
Flavonolignin (%)^b							
tricin	10 (7)	11 (8)	9 (7)	6 (5)	7 (5)	8 (6)	10 (8)
Lignin interunit linkages (%)^c							
β-O-4' aryl ethers	43 (90)	37 (93)	32 (97)	39 (90)	39 (85)	40 (86)	40 (88)
β-5' phenylcoumarans	3 (6)	2 (4)	1 (2)	3 (7)	5 (11)	4 (10)	3 (7)
β-β' resinols	1 (3)	1 (3)	0 (1)	1 (3)	2 (4)	2 (4)	2 (4)
total	48 (100)	40 (100)	33 (100)	43 (100)	46 (100)	46 (100)	45 (100)

^apercentage of subunits (H+G+G_{ox}+G_{mod}+S+S_{ox}+S_{mod}=100), in parentheses (subunits+pCA(H)+FA(G)+T(S)=100).

^bpercentage versus aromatic units and subunits + pCA+FA+T (see subscript a).

^cpercentage of interunit linkages versus total subunits and in parenthesis as percentage of total interunit linkages.

The most pronounced change observed by NMR was the increase in C_α-oxidized aromatic units in fungal-treated samples, with a three-fold accumulation in Cs-treated lignin (up to 19-24% of total aromatic units; Table 2). This increase coincides with the increase in C_α-oxidized products in py-GC-MS and these compounds, hence, were mostly derived from C_α-oxidized units initially present in the polymer. Even relative abundances (% mol) of C_α-oxidized substructures obtained by both techniques were in fairly good accordance (Cs1 C_α-ox (NMR) = 15%, C_α-ox (py-GC-MS) = 14%). It can be assumed that the C_α-oxidized substructures accumulated in fungal-treated lignin due to the fact that, once oxidized, these units cannot be further oxidized (by the respective fungal oxidases present) and are, therefore, resistant to further degradation and further metabolization. C_α-oxidized S-units appeared more prone to accumulate than their C_α-oxidized G-unit counterparts (S_{ox}/S > G_{ox}/G) for all fungi. This might on the one hand be explained by their ease of formation, as discussed in the previous section. On the other hand, S-units might be more difficult to be consumed and fully metabolized.

Interestingly, while the C_α-oxidized aromatic units clearly increased, no apparent increase in C_α-oxidized (α-keto) β-O-4' substructures could be observed. The latter observation shows that the C_α-oxidized signals mainly originated from cleaved

linkages, and simultaneously highlights the importance of corresponding VAL and SAL compounds in the py-GC-MS analysis. The suggestion that cleaved linkages accumulated in the residual lignin is further substantiated by the reduced amounts of intact interunit linkages in fungal-treated lignin. Intact interunit linkages were severely reduced by *Cs* treatment (*Cs*1 -20%, *Cs*12 -34%; Table 2), which was also observed by py-GC-MS. The abundance of the pyrolysis PhC_v products excluding acetaldehydes, thus, seems to be a highly valuable parameter for the investigation of intact β -O-4' linkages in the lignin structure by py-GC-MS.

Previous studies also reported on the reduction of interunit linkages in *Cs*-treated lignin.^{60, 66} However, these studies were conducted on wood, of which the lignin is of a different structure. Still, in these biomasses the β -O-4' interunit linkage is most abundant and, therefore, can be used to compare fungal action. Guerra et al.⁶⁶ found that *Cs*-treated pine was preferentially reduced in β -O-4' linkages, while carbon-carbon linked units were more resistant against fungal degradation. Our results, indicated that all interunit linkages in wheat straw lignin were comparable in their susceptibility towards fungal degradation as their relative composition was rather stable (<10% different from control; Table 2).

Another clear result from the 2D-NMR analysis was the reduction in FA moieties after fungal treatment, particularly by the *Pe* strains (around 30% reduction; Table 2). Possibly, the lignin-carbohydrate linkages in which FA participates were targeted in a more preferential manner.^{17, 67} Though, the specific removal of glucuronoarabinoxylan (GAX) linked ferulates and crosslinked diferulates cannot be excluded. Such structures could be cleaved by feruloyl esterases, which have been shown to occur extracellularly for *Pe* and *Le*.⁶⁸

The specific targeting of FA moieties is in line with the concurrent lignin and GAX degradation during fungal growth. The magnitudes of FA and GAX removal were, however, not directly linked (Figure 3, Supporting Information Figure S1). In contrast to FA, *p*-CA moieties were not preferentially removed.

Tricin was surprisingly shown to be specifically targeted during fungal growth, in particular by *Pe* strains (-40% vs total lignin; Table 2). Tricin has recently been suggested to play an important role in the biosynthesis of lignin in poaceous crops by functioning as a nucleation site for lignin formation.^{15, 18-19, 65} The preferential removal of triclin suggests that, besides lignin formation, triclin may play a crucial role in the fungal degradation of lignin as well.

Mechanistic insight into fungal delignification by combining results of ¹³C-IS py-GC-MS and 2D-NMR

The combination of 2D-NMR and ¹³C-IS py-GC-MS analysis provided more insight into the reaction mechanisms underlying delignification by the studied fungi, in particular for the *Cs* strains. The absence of C_o-oxidized (α -keto) β -O-4' substructures in 2D-NMR combined with decreased amounts of intact interunit linkages (both techniques) confirmed that the C_o-oxidized substructures were present in the fungal-treated lignin macromolecule as cleavage products of the

interunit linkages. Upon pyrolysis, these cleavage products resulted in the formation of the acetaldehydes VAL and SAL. Since these pyrolysis products contain an intact α,β,γ carbon side chain, the structures they originate from should contain this three-carbon side chain as well. Hence, we postulate that acetaldehyde pyrolysis products originated from remaining structures after C_β -O cleavage of the β -O-4' ether.

C_α -oxidized pyrolysis products with an α -carbon side-chain, like vanillin and syringaldehyde, were likewise, but not specifically, formed from cleavage products and thus are suggested to be the result of C_α - C_β cleavage.

The high proportion of acetaldehyde pyrolysis products formed from *Cs*-treated lignin suggests that C_β -O-aryl cleavage was the main underlying mechanism of lignin degradation, while for *Pe* and *Le* C_α - C_β cleavage predominated (Figure 6).

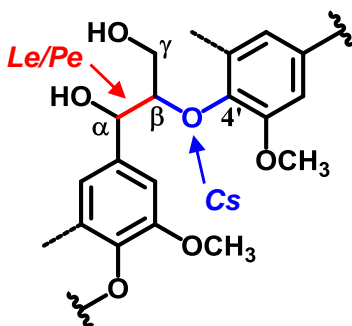


Figure 6. Proposed predominant linkages targeted by fungal action. For simplicity only the most abundant β -O-4' aryl ether linkage is shown where dotted lines represent -H or -OCH₃ and wavy lines indicate main positions of further coupling. *Cs* *Ceriporiopsis subvermispora*, *Pe* *Pleurotus eryngii*, *Le* *Lentinula edodes*. *Cs* C_β -O-aryl cleavage, *Le/Pe* C_α - C_β cleavage.

The latter two species, however, showed less accumulation of C_α -oxidized substructures in treated lignin, at the respective levels of lignin removal. This might indicate that other cleavage reactions not yielding C_α -oxidation might be more dominant than previously thought.⁶⁹ On the other hand, if C_β -O-aryl cleavage did occur, but the resulting intermediate products were further degraded in follow-up reactions, we cannot pick this up in residual lignin structures after 7 weeks of fungal growth. Collectively, the enzymes produced by *Le* and *Pe* might thus be able to degrade each lignin subunit further, without resulting in increased, content-wise, lignin degradation. Our results clearly put forward that the delignification mechanism of *Cs* is fundamentally different from *Le* and *Pe*. The explanation of the underlying delignification mechanisms likely lays in the type of enzymes involved. It is expected from genome sequencing of strains of *Cs*, *Le* and *Pe* that all rely on manganese peroxidases (MnPs) and laccases (Lacs), though their dependency on the particular enzymes might vary.²⁵⁻³⁰ *In vitro*, MnPs were shown to degrade lignin model compounds in the presence of unsaturated fatty acids via lipid peroxidation into products that, upon pyrolysis, could yield the acetaldehyde products we observed, in particular after *Cs* action.⁷⁰⁻⁷¹

Interestingly, a similar MnP-peroxidation reaction was suggested to involve alkylitaconic acids, secondary metabolites that are abundantly produced by *Cs* but not by *Le* and *Pe*.^{12, 72-74} It can be postulated that the presence of alkylitaconic acids underlies the observed predominance of the C_β-O-aryl cleavage reaction of the β-O-4' ether by *Cs*. However, laccases and the recently identified enzymes with a LiP/VP like activity could have resulted in similar products, due to which unambiguity regarding the underlying enzyme system remains.⁷⁵⁻⁷⁸ For further validation and interpretation of our observations, genomes of the particular strains should be sequenced next to the application of proteomic and transcriptomic approaches.

Conclusions

Ceriporiopsis subvermispura (*Cs*) and *Lentinula edodes* (*Le*) are more effective and selective wheat straw lignin degrading fungi than *Pleurotus eryngii* (*Pe*). They degraded more than 60 % (w/w) of lignin without extensive carbohydrate degradation within 7 weeks of treatment. Though *Cs* and *Le* followed a similar pattern of lignin degradation in time, the structural-features of residual lignin as determined by quantitative ¹³C-IS py-GC-MS and *in situ* HSQC NMR were vastly different. Both techniques revealed that *Cs*-treated lignin was exceptionally high in C_α-oxidized substructures (up to 24% of aromatic units) and a factor two higher than *Le*-treated lignin. *Le* and *Pe*, on the other hand, more specifically targeted ferulic acid substructures, while *Pe* preferentially removed tricin up to 40% more than other substructures. Furthermore, *Cs* delignification mainly proceeded via C_β-O-aryl and C_α-C_β cleavage of the lignin interunit linkages, while interunit degradation by *Le* and *Pe* seemed dominated by C_α-C_β cleavage with C_β-O-aryl cleavage occurring to lesser extents. We, therefore, suggest that the underlying delignification mechanisms of these fungi are fundamentally different.

Besides assisting the further optimization of fungal pretreatment of plant biomass, we highlight that the choice of fungus impacts the structure of residual lignin and results in lignin with remarkable structure. Thus, fungal pretreatment not only enhances the degradability of plant cell wall polysaccharides, but also results in an interesting lignin fraction that can be exploited to further increase the sustainability of the process.

Acknowledgements

The authors gratefully acknowledge the financial support from the University Fund Wageningen (UFW) as part of the project "More Meat and Milk from Straw" which is sponsored by DEKA, ForFarmers and the Victam Foundation. The authors acknowledge the scholarship provided by the Ministry of Higher Education of Malaysia and the Universiti Putra Malaysia. All funding bodies had no involvement in planning and conduct of the research. Maud Pfeiffer is acknowledged for formatting NMR spectra.

References

1. Buranov, A. U.; Mazza, G., Lignin in straw of herbaceous crops. *Ind Crops Prod* **2008**, *28*, 237-259.
2. Isroi; Millati, R.; Syamsiah, S.; Niklasson, C.; Cahyanto, M. N.; Ludquist, K.; Taherzadeh, M. J., Biological pretreatment of lignocelluloses with white-rot fungi and its applications: a review. *BioResources* **2011**, *6*, 5224-5259.
3. Isikgor, F. H.; Becer, C. R., Lignocellulosic biomass: a sustainable platform for the production of bio-based chemicals and polymers. *Polym Chem* **2015**, *6*, 4497-4559.
4. Čilerdžić, J.; Galić, M.; Vukojević, J.; Brčeski, I.; Stajić, M., Potential of selected fungal species to degrade wheat straw, the most abundant plant raw material in Europe. *BMC Plant Biol* **2017**, *17*, 249.
5. Behera, S.; Arora, R.; Nandhagopal, N.; Kumar, S., Importance of chemical pretreatment for bioconversion of lignocellulosic biomass. *Renewable and Sustainable Energy Rev* **2014**, *36*, 91-106.
6. Tian, X. f.; Fang, Z.; Guo, F., Impact and prospective of fungal pre-treatment of lignocellulosic biomass for enzymatic hydrolysis. *Biofuels Bioprod Biorefin* **2012**, *6*, 335-350.
7. Sindhu, R.; Binod, P.; Pandey, A., Biological pretreatment of lignocellulosic biomass—An overview. *Bioresour Technol* **2016**, *199*, 76-82.
8. Keller, F. A.; Hamilton, J. E.; Nguyen, Q. A., Microbial pretreatment of biomass. *Appl Biochem Biotechnol* **2003**, *105*, 27-41.
9. Van Kuijk, S. J. A.; Sonnenberg, A. S. M.; Baars, J. J. P.; Hendriks, W. H.; Cone, J. W., Fungal treated lignocellulosic biomass as ruminant feed ingredient: a review. *Biotechnol Adv* **2015**, *33*, 191-202.
10. Tuyen, V.; Cone, J.; Baars, J.; Sonnenberg, A.; Hendriks, W., Fungal strain and incubation period affect chemical composition and nutrient availability of wheat straw for rumen fermentation. *Bioresour Technol* **2012**, *111*, 336-342.
11. Van Kuijk, S. J. A.; Sonnenberg, A. S. M.; Baars, J. J. P.; Hendriks, W. H.; Cone, J. W., Fungal treatment of lignocellulosic biomass: Importance of fungal species, colonization and time on chemical composition and in vitro rumen degradability. *Anim Feed Sci and Technol* **2015**, *209*, 40-50.
12. Van Kuijk, S. J. A.; Sonnenberg, A. S. M.; Baars, J. J. P.; Hendriks, W. H.; del Río, J. C.; Rencoret, J.; Gutiérrez, A.; de Ruijter, N. C. A.; Cone, J. W., Chemical changes and increased degradability of wheat straw and oak wood chips treated with the white rot fungi *Ceriporiopsis subvermispora* and *Lentinula edodes*. *Biomass Bioenergy* **2017**, *105*, 381-391.
13. Nayan, N.; Sonnenberg, A. S.; Hendriks, W. H.; Cone, J. W., Screening of white-rot fungi for bioprocessing of wheat straw into ruminant feed. *J Appl Microbiol* **2018**, *125*, 468-479.
14. Vanholme, R.; Demedts, B.; Morreel, K.; Ralph, J.; Boerjan, W., Lignin biosynthesis and structure. *Plant Physiol* **2010**, *153*, 895-905.
15. Del Río, J. C.; Rencoret, J.; Prinsen, P.; Martínez, A. T.; Ralph, J.; Gutiérrez, A., Structural characterization of wheat straw lignin as revealed by analytical pyrolysis, 2D-NMR, and reductive cleavage methods. *J Agric Food Chem* **2012**, *60*, 5922-5935.
16. Ralph, J.; Brunow, G.; Harris, P. J.; Dixon, R. A.; Schatz, P. F.; Boerjan, W., Lignification: are lignins biosynthesized via simple combinatorial chemistry or via proteinaceous control and template replication? In *Recent Advances in Polyphenol Research*, Lattanzio, V.; Daayf, F., Eds. Wiley-Blackwell: Oxford, 2009; Vol. 1, pp 36-66.
17. Ralph, J., Hydroxycinnamates in lignification. *Phytochem Rev* **2010**, *9*, 65-83.
18. Lan, W.; Lu, F.; Regner, M.; Zhu, Y.; Rencoret, J.; Ralph, S. A.; Zakai, U. I.; Morreel, K.; Boerjan, W.; Ralph, J., Tricin, a flavonoid monomer in monocot lignification. *Plant Physiol* **2015**, *167*, 1284-1295.

19. Li, M.; Pu, Y.; Yoo, C. G.; Ragauskas, A. J., The occurrence of tricin and its derivatives in plants. *Green Chem* **2016**, *18*, 1439-1454.
20. Martínez, A. T.; Speranza, M.; Ruiz-Dueñas, F. J.; Ferreira, P.; Camarero, S.; Guillén, F.; Martínez, M. J.; Gutiérrez, A.; del Río, J. C., Biodegradation of lignocellulosics: microbial, chemical, and enzymatic aspects of the fungal attack of lignin. *Int Microbiol* **2005**, *8*, 195-204.
21. Ten Have, R.; Teunissen, P. J., Oxidative mechanisms involved in lignin degradation by white-rot fungi. *Chem Rev* **2001**, *101*, 3397-3414.
22. Hatakka, A.; Hammel, K. E., Fungal biodegradation of lignocelluloses. In *Industrial Applications. The Mycota*, Hofrichter, M., Ed. Springer-Verlag: Berlin, 2011; Vol. 10, pp 319-340.
23. Hernández-Ortega, A.; Ferreira, P.; Martínez, A. T., Fungal aryl-alcohol oxidase: a peroxide-producing flavoenzyme involved in lignin degradation. *Appl Microbiol Biotech* **2012**, *93*, 1395-1410.
24. Camarero, S.; Martínez, M. J.; Martínez, A. T., Understanding lignin biodegradation for the improved utilization of plant biomass in modern biorefineries. *Biofuels, Bioprod Biorefin* **2014**, *8*, 615-625.
25. Fernández-Fueyo, E.; Ruiz-Dueñas, F. J.; Ferreira, P.; Floudas, D.; Hibbett, D. S.; Canessa, P.; Larrondo, L. F.; James, T. Y.; Seelenfreund, D.; Lobos, S.; Polanco, R.; Tello, M.; Honda, Y.; Watanabe, T.; Watanabe, T.; Ryu, J. S.; Kubicek, C. P.; Schmoll, M.; Gaskell, J.; Hammel, K. E.; St. John, F. J.; Vanden Wymelenberg, A.; Sabat, G.; Splinter Bondurant, S.; Khajamohiddin, S.; Jagit, Y. S.; Doppapaneni, H.; Subramanian, V.; José, L. L.; Oguiza, J. A.; Perez, G.; Pisabarro, A. G.; Ramirez, L.; Santoyo, F.; Master, E.; Coutinho, P. M.; Henrissat, B.; Lombard, V.; Magnuson, J. K.; Kües, U.; Hori, C.; Igarashi, K.; Samejima, M.; Held, B. W.; Barry, K. W.; Labutti, K. M.; Lapidus, A.; Lindquist, E. A.; Lucas, S. M.; Riley, R.; Salamov, A. A.; Hoffmeister, D.; Schwenk, D.; Hadar, Y.; Yarden, O.; de Vries, R. P.; Wiebenga, A.; Stenlid, J.; Eastwood, D.; Grigoriev, I. V.; Berka, R. M.; Blanchette, R. A.; Kersten, P.; Martínez, A. T.; Vicuna, R.; Cullen, D., Comparative genomics of *Ceriporiopsis subvermispora* and *Phanerochaete chrysosporium* provide insight into selective ligninolysis. *Proc Natl Acad Sci* **2012**, *109*, 5458-5463.
26. Nagai, M.; Sakamoto, Y.; Nakade, K.; Sato, T., Isolation and characterization of the gene encoding a manganese peroxidase from *Lentinula edodes*. *Mycoscience* **2007**, *48*, 125-130.
27. Sakamoto, Y.; Nakade, K.; Sato, S.; Yoshida, K.; Miyazaki, K.; Natsume, S.; Konno, N., *Lentinula edodes* genome survey and postharvest transcriptome analysis. *Appl Environ Microbiol* **2017**, *83*, e02990-3016.
28. Park, S.-G.; il Yoo, S.; Ryu, D. S.; Lee, H.; Ahn, Y. J.; Ryu, H.; Ko, J.; Hong, C. P., Long-read transcriptome data for improved gene prediction in *Lentinula edodes*. *Data in brief* **2017**, *15*, 454-458.
29. Yang, R.-H.; Li, Y.; Wang, Y.; Wan, J.-N.; Zhou, C.-L.; Wang, Y.; Gao, Y.-N.; Mao, W.-J.; Tang, L.-H.; Gong, M., The genome of *Pleurotus eryngii* provides insights into the mechanisms of wood decay. *J Biotechnol* **2016**, *239*, 65-67.
30. Fernández-Fueyo, E.; Ruiz-Dueñas, F. J.; Miki, Y.; Martínez, M. J.; Hammel, K. E.; Martínez, A. T., Lignin-degrading peroxidases from genome of selective ligninolytic fungus *Ceriporiopsis subvermispora*. *J Biol Chem* **2012**, *287*, 16903-16916.
31. Camarero, S.; Galletti, G. C.; Martinez, A. T., Preferential degradation of phenolic lignin units by two white rot fungi. *Appl Environ Microbiol* **1994**, *60*, 4509-4516.
32. Crestini, C.; Sermanni, G. G.; Argyropoulos, D. S., Structural modifications induced during biodegradation of wheat lignin by *Lentinula edodes*. *Bioorg Med Chem* **1998**, *6*, 967-973.
33. Martínez, A.; Camarero, S.; Gutiérrez, A.; Bocchini, P.; Galletti, G., Studies on wheat lignin degradation by *Pleurotus* species using analytical pyrolysis. *J Anal Appl Pyrolysis* **2001**, *58*, 401-411.

34. Dorado, J.; Almendros, G.; Camarero, S.; Martínez, A. T.; Vares, T.; Hatakka, A., Transformation of wheat straw in the course of solid-state fermentation by four ligninolytic basidiomycetes. *Enzyme Microb Technol* **1999**, *25*, 605-612.
35. Jurak, E.; Punt, A. M.; Arts, W.; Kabel, M. A.; Gruppen, H., Fate of carbohydrates and lignin during composting and mycelium growth of *Agaricus bisporus* on wheat straw based compost. *PLoS One* **2015**, *10*, e0138909.
36. Van Erven, G.; de Visser, R.; Merks, D. W.; Strolenberg, W.; de Gijssel, P.; Gruppen, H.; Kabel, M. A., Quantification of lignin and its structural features in plant biomass using ^{13}C lignin as internal standard for pyrolysis-GC-SIM-MS. *Anal Chem* **2017**, *89*, 10907-10916.
37. Kim, H.; Ralph, J.; Akiyama, T., Solution-state 2D NMR of ball-milled plant cell wall gels in DMSO- d_6 . *BioEnergy Res* **2008**, *1*, 56-66.
38. Mansfield, S. D.; Kim, H.; Lu, F.; Ralph, J., Whole plant cell wall characterization using solution-state 2D NMR. *Nat Protoc* **2012**, *7*, 1579-1589.
39. Björkman, A., Studies on finely divided wood. Part 1. Extraction of lignin with neutral solvents. *Sven Papperstidn* **1956**, *59*, 477-485.
40. Chang, H.-M.; Cowling, E. B.; Brown, W., Comparative studies on cellulolytic enzyme lignin and milled wood lignin of sweetgum and spruce. *Holzforschung* **1975**, *29*, 153-159.
41. Kirk, T. K.; Chang, H.-M., Decomposition of lignin by white-rot fungi. I. Isolation of heavily degraded lignins from decayed spruce. *Holzforschung* **1974**, *28*, 217-222.
42. Nayan, N.; Sonnenberg, A. S. M.; Hendriks, W. H.; Cone, J. W., Differences between two strains of *Ceriporiopsis subvermispota* on improving the nutritive value of wheat straw for ruminants. *J Appl Microbiol* **2017**, *123*, 352-361.
43. Knudsen, K. E. B., Fiber and nonstarch polysaccharide content and variation in common crops used in broiler diets. *Poult Sci* **2014**, *93*, 2380-2393.
44. Van Kuijk, S. J.; Sonnenberg, A. S.; Baars, J. J.; Hendriks, W. H.; Cone, J. W., The effect of particle size and amount of inoculum on fungal treatment of wheat straw and wood chips. *J Anim Sci Biotechnol* **2016**, *7*, 39.
45. Englyst, H. N.; Cummings, J. H., Simplified method for the measurement of total non-starch polysaccharides by gas-liquid chromatography of constituent sugars as alditol acetates. *Analyst* **1984**, *109*, 937-942.
46. Blumenkrantz, N.; Asboe-Hansen, G., New method for quantitative determination of uronic acids. *Anal Biochem* **1973**, *54*, 484-489.
47. Ralph, J.; Hatfield, R. D., Pyrolysis-GC-MS characterization of forage materials. *J Agric Food Chem* **1991**, *39*, 1426-1437.
48. Yuan, T.-Q.; Sun, S.-N.; Xu, F.; Sun, R.-C., Characterization of lignin structures and lignin-carbohydrate complex (LCC) linkages by quantitative ^{13}C and 2D HSQC NMR spectroscopy. *J Agric Food Chem* **2011**, *59*, 10604-10614.
49. Ralph, S. A.; Ralph, J.; Landucci, L., NMR database of lignin and cell wall model compounds. **2009**, Available at URL www.glbric.org/databases_and_software/nmrdatabase/.
50. Rencoret, J.; Gutiérrez, A.; Nieto, L.; Jiménez-Barbero, J.; Faulds, C. B.; Kim, H.; Ralph, J.; Martínez, Á. T.; del Río, J. C., Lignin composition and structure in young versus adult *Eucalyptus globulus* plants. *Plant Physiol* **2011**, *155*, 667-682.
51. Rencoret, J.; Pereira, A.; del Río, J. C.; Martínez, Á. T.; Gutiérrez, A., Delignification and saccharification enhancement of sugarcane byproducts by a laccase-based pretreatment. *ACS Sustainable Chem Eng* **2017**, *5*, 7145-7154.
52. Del Río, J. C.; Lino, A. G.; Colodette, J. L.; Lima, C. F.; Gutiérrez, A.; Martínez, Á. T.; Lu, F.; Ralph, J.; Rencoret, J., Differences in the chemical structure of the lignins from sugarcane bagasse and straw. *Biomass Bioenergy* **2015**, *81*, 322-338.
53. Villaverde, J. J.; Li, J.; Ek, M.; Ligerio, P.; de Vega, A., Native lignin structure of *Miscanthus x giganteus* and its changes during acetic and formic acid fractionation. *J Agric Food Chem* **2009**, *57*, 6262-6270.

54. Das, A.; Rahimi, A.; Ulbrich, A.; Alherech, M.; Motagamwala, A. H.; Bhalla, A.; da Costa Sousa, L.; Balan, V.; Dumesic, J. A.; Hegg, E. L.; Dale, B. E.; Ralph, J.; Coon, J. J.; Stahl, S. S., Lignin conversion to low-molecular-weight aromatics via an aerobic oxidation-hydrolysis sequence: comparison of different lignin sources. *ACS Sustainable Chem Eng* **2018**, *6*, 3367-3374.
55. Kim, H.; Padmakshan, D.; Li, Y.; Rencoret, J.; Hatfield, R. D.; Ralph, J., Characterization and elimination of undesirable protein residues in plant cell wall materials for enhancing lignin analysis by solution-state nuclear magnetic resonance spectroscopy. *Biomacromolecules* **2017**, *18*, 4184-4195.
56. Sette, M.; Wechselberger, R.; Crestini, C., Elucidation of lignin structure by quantitative 2D NMR. *Chem - Eur J* **2011**, *17*, 9529-9535.
57. Wen, J.-L.; Sun, S.-L.; Xue, B.-L.; Sun, R.-C., Recent advances in characterization of lignin polymer by solution-state nuclear magnetic resonance (NMR) methodology. *Materials* **2013**, *6*, 359-391.
58. Van Kuijk, S. J.; del Río, J. C.; Rencoret, J.; Gutiérrez, A.; Sonnenberg, A. S.; Baars, J. J.; Hendriks, W. H.; Cone, J. W., Selective ligninolysis of wheat straw and wood chips by the white-rot fungus *Lentinula edodes* and its influence on in vitro rumen degradability. *J Anim Sci Biotechnol* **2016**, *7*, 55.
59. Del Río, J. C.; Speranza, M.; Gutiérrez, A.; Martínez, M.; Martínez, A. T., Lignin attack during eucalypt wood decay by selected basidiomycetes: a Py-GC/MS study. *J Anal Appl Pyrolysis* **2002**, *64*, 421-431.
60. Choi, J.; Choi, D.; Ahn, S.; Lee, S.; Kim, M.; Meier, D.; Faix, O.; Scott, G. M., Characterization of trembling aspen wood (*Populus tremuloides* L.) degraded with the white rot fungus *Ceriporiopsis subvermispora* and MWLs isolated thereof. *Holz Roh Werkst* **2006**, *64*, 415-422.
61. Patwardhan, P. R.; Brown, R. C.; Shanks, B. H., Understanding the fast pyrolysis of lignin. *ChemSusChem* **2011**, *4*, 1629-1636.
62. Zeng, J.; Helms, G. L.; Gao, X.; Chen, S., Quantification of wheat straw lignin structure by comprehensive NMR analysis. *J Agric Food Chem* **2013**, *61*, 10848-10857.
63. Fujimoto, A.; Matsumoto, Y.; Chang, H.-M.; Meshitsuka, G., Quantitative evaluation of milling effects on lignin structure during the isolation process of milled wood lignin. *J Wood Sci* **2005**, *51*, 89-91.
64. Rencoret, J.; Pereira, A.; del Río, J. C.; Martínez, A. T.; Gutiérrez, A., Laccase-mediator pretreatment of wheat straw degrades lignin and improves saccharification. *BioEnergy Res* **2016**, *9*, 917-930.
65. Lan, W.; Rencoret, J.; Lu, F.; Karlen, S. D.; Smith, B. G.; Harris, P. J.; Río, J. C.; Ralph, J., Tricin-lignins: occurrence and quantitation of tricin in relation to phylogeny. *Plant J* **2016**, *88*, 1046-1057.
66. Guerra, A.; Mendonça, R.; Ferraz, A.; Lu, F.; Ralph, J., Structural characterization of lignin during *Pinus taeda* wood treatment with *Ceriporiopsis subvermispora*. *Appl Environ Microbiol* **2004**, *70*, 4073-4078.
67. Hatfield, R. D.; Rancour, D. M.; Marita, J. M., Grass cell walls: a story of cross-linking. *Front Plant Sci* **2017**, *7*, 2056.
68. Haase-Aschoff, P.; Linke, D.; Berger, R. G., Detection of feruloyl- and cinnamoyl esterases from basidiomycetes in the presence of interfering laccase. *Bioresour Technol* **2013**, *130*, 231-238.
69. Crestini, C.; Jurasek, L.; Argyropoulos, D. S., On the mechanism of the laccase-mediator system in the oxidation of lignin. *Chem - Eur J* **2003**, *9*, 5371-5378.
70. Jensen, K. A.; Bao, W.; Kawai, S.; Srebotnik, E.; Hammel, K. E., Manganese-dependent cleavage of nonphenolic lignin structures by *Ceriporiopsis subvermispora* in the absence of lignin peroxidase. *Appl Environ Microbiol* **1996**, *62*, 3679-3686.
71. Bao, W.; Fukushima, Y.; Jensen Jr, K. A.; Moen, M. A.; Hammel, K. E., Oxidative degradation of non-phenolic lignin during lipid peroxidation by fungal manganese peroxidase. *FEBS Lett* **1994**, *354*, 297-300.

72. Gutiérrez, A.; del Río, J. C.; Martínez-Íñigo, M. J.; Martínez, M. J.; Martínez, Á. T., Production of new unsaturated lipids during wood decay by ligninolytic basidiomycetes. *Appl Environ Microbiol* **2002**, *68*, 1344-1350.
73. Martínez, M. J.; Barrasa, J. M.; Gutiérrez, A.; del Río, J. C.; Martínez, A. T., Fungal screening for biological removal of extractives from *Eucalyptus globulus* wood. *Can J Bot* **2000**, *77*, 1513-1522.
74. Nishimura, H.; Sasaki, M.; Seike, H.; Nakamura, M.; Watanabe, T., Alkadienyl and alkenyl itaconic acids (ceriporic acids G and H) from the selective white-rot fungus *Ceriporiopsis subvermispota*: a new class of metabolites initiating ligninolytic lipid peroxidation. *Org Biomol Chem* **2012**, *10*, 6432-6442.
75. Srebotnik, E.; Jensen, K.; Kawai, S.; Hammel, K. E., Evidence that *Ceriporiopsis subvermispota* degrades nonphenolic lignin structures by a one-electron-oxidation mechanism. *Appl Environ Microbiol* **1997**, *63*, 4435-4440.
76. Yelle, D. J.; Kapich, A. N.; Houtman, C. J.; Lu, F.; Timokhin, V. I.; Fort, R. C.; Ralph, J.; Hammel, K. E., A highly diastereoselective oxidant contributes to ligninolysis by the white rot basidiomycete *Ceriporiopsis subvermispota*. *Appl Environ Microbiol* **2014**, *80*, 7536-7544.
77. Kawai, S.; Nakagawa, M.; Ohashi, H., Degradation mechanisms of a nonphenolic β -O-4 lignin model dimer by *Trametes versicolor* laccase in the presence of 1-hydroxybenzotriazole. *Enzyme Microb Technol* **2002**, *30*, 482-489.
78. Cantarella, G.; Galli, C.; Gentili, P., Free radical versus electron-transfer routes of oxidation of hydrocarbons by laccase/mediator systems: Catalytic or stoichiometric procedures. *J Mol Catal B: Enzym* **2003**, *22*, 135-144.

Supporting Information

Formulae for calculation of lignin content and relative abundance by ^{13}C -IS py-GC-MS

$$RRF_{run,i} = RRF_{start,i} \cdot \frac{A_{i,start}^{WS ref}}{A_{i,run}^{WS ref}} \cdot \frac{\sum_{i=1}^{43} RRF_{start,i}^{WS ref}}{\sum_{i=1}^{43} RRF_{run,i}^{WS ref}} \quad (1)$$

where i refers to compound number (Table S1) (only initially monitored products included (van Erven et al.¹), A is peak area of reference wheat straw at system performance relative response factors (RRF) were determined ('start') and in each run performed ('run'). M_w is the molecular weight. Run refers to one sequence of measurements.

$$\text{Lignin content \% (w/w)} = \frac{\sum_{i=1}^{49} \frac{A_i^{12C} \cdot M_{w12C}}{RRF_{run,i}} \cdot m_{IS}}{\sum_{i=1}^{49} \frac{A_i^{13C} \cdot M_{w13C}}{RRF_{run,i}} \cdot m_{sample}} \cdot 100 \quad (2)$$

where i refers to compound number (Table S1), A is area, RRF_{run} is corrected relative response factor, m_{IS} is the amount of IS (corrected for purity) (μg ; ^{13}C -LIGpure), m_{sample} is the amount of sample (μg).

$$\text{Relative abundance (RA) (\%)} = \frac{\frac{A_i}{RRF_{run,i}}}{\sum_{i=1}^{49} \frac{A_i}{RRF_{run,i}}} \cdot 100 \quad (3)$$

where i refers to compound number (Table S1), A is area, RRF_{run} is corrected relative response factor.

$$\text{Relative abundance factor (RAF)}_i^{13C} = \frac{RA_i^{13C IS}}{RA_i^{13C WS ref}} \quad (4)$$

where i refers to compound number (Table S1), RA is relative abundance.

$$\text{Relative abundance}_{i,corrected} = \frac{RA_i}{RAF_i^{13C}} \cdot \left(\frac{100}{\sum_{i=1}^{49} \frac{RA_i}{RAF_i^{13C}}} \right) \quad (5)$$

where i refers to compound number (Table S1), RA is relative abundance, RAF is relative abundance factor (eq 4).

Table S1. Identity, structural classification and relative abundance of lignin-derived pyrolysis products by ^{13}C -IS py-GC-MS. Control and fungal-treated wheat straw samples after 7 weeks of treatment. *Cs Ceriporiopsis subvermisporea*, *Pe Pleurotus eryngii*, *Le Lentinula edodes*. Average of analytical triplicates on pooled biological triplicates.

#	Compound	CAS	Retention time (min)	Structural feature	Sidechain length	M _w ^{12}C (g mol ⁻¹)	Control	Cs1	Cs12	Pe3	Pe6	Le8	Le10
1	phenol	108952	10.03	H, unsub.	0	94	0.7	2.0	1.9	1.1	0.9	1.5	1.6
2	guaiacol	90051	10.31	G, unsub.	0	124	2.1	4.2	4.0	2.7	2.5	3.2	3.4
3	2-methylphenol	95487	11.29	H, methyl	C _α	108	0.2	0.4	0.4	0.2	0.2	0.3	0.3
4	4-methylphenol (+3-MP)	106445	12.23	H, methyl	C _α	108	0.5	1.1	1.2	0.8	0.7	0.9	1.0
5	4-methylguaiacol	93516	13.01	G, methyl	C _α	138	0.7	1.0	1.0	0.9	0.9	0.9	0.9
6	2,4-dimethylphenol	105679	13.46	H, methyl	C _α	122	0.1	0.2	0.2	0.1	0.1	0.1	0.2
7	4-ethylphenol	123079	14.52	H, misc.	C _β	122	0.1	0.1	0.1	0.1	0.1	0.1	0.1
8	4-ethylguaiacol	2785899	15.19	G, misc.	C _β	152	0.1	0.2	0.2	0.2	0.2	0.2	0.2
9	4-vinylguaiacol	7786610	16.64	G, vinyl	C _β	150	20.3	20.4	20.3	19.9	21.4	21.7	21.0
10	4-vinylphenol	2628173	16.77	H, vinyl	C _β	120	7.8	7.7	7.8	7.3	7.8	7.8	7.9
11	eugenol	97530	17.26	G, misc.	C _γ	164	0.2	0.2	0.2	0.2	0.2	0.2	0.2
12	4-propylguaiacol	2785877	17.34	G, misc.	C _γ	166	0.1	0.2	0.2	0.2	0.2	0.2	0.2
13	syringol	91101	18.00	S, unsub.	0	154	1.9	3.2	3.5	2.3	2.3	2.4	2.7
14	cis-isoeugenol	97541	18.63	G, misc.	C _γ	164	0.1	0.1	0.1	0.1	0.1	0.1	0.1
15	4-propenylphenol	539128	19.54	H, misc.	C _γ	134	0.1	0.1	0.1	0.1	0.1	0.1	0.1
16	trans-isoeugenol	97541	19.90	G, misc.	C _γ	164	0.8	1.0	0.9	1.1	1.1	1.1	1.1
17	4-methylsyringol	6638057	20.26	S, methyl	C _α	168	0.5	0.6	0.6	0.6	0.6	0.6	0.6
18	vanillin	121335	20.35	G, C _α -O	C _α	152	1.2	2.1	2.3	1.4	1.2	1.4	1.4
19	4-propynguaiacol	-	20.64	G, misc.	C _γ	162	0.1	0.1	0.1	0.1	0.1	0.1	0.1
20	4-alleneguaiacol	-	20.90	G, misc.	C _γ	162	0.1	0.1	0.1	0.1	0.1	0.1	0.1
21	homovanillin	5603242	21.81	G, C _β -O	C _β	166	0.5	0.7	0.8	0.5	0.5	0.5	0.5
22	4-ethylsyringol	14059928	22.00	S, misc.	C _β	182	0.0	0.0	0.1	0.1	0.0	0.0	0.0
23	acetovanillone	498022	22.27	G, C _α -O	C _β	166	0.3	1.1	1.2	0.6	0.5	0.6	0.7
24	4-hydroxybenzaldehyde	123080	23.01	H, C _α -O	C _α	122	0.2	0.3	0.3	0.2	0.1	0.2	0.2
25	4-vinylsyringol	28343228	23.32	S, vinyl	C _β	180	2.4	2.0	2.2	2.3	2.4	2.3	2.3
26	guaiacylacetone	2503460	23.50	G, C _β -O	C _γ	180	0.3	0.7	0.7	0.4	0.3	0.4	0.4
27	4-allylsyringol	6627889	23.75	S, misc.	C _γ	194	0.2	0.2	0.2	0.2	0.2	0.2	0.2
28	propiovanillone	1835149	24.18	S, C _α -O	C _γ	180	0.0	0.1	0.1	0.0	0.0	0.1	0.1
29	guaiacyl vinyl ketone	-	24.47	G, C _α -O	C _γ	178	0.1	0.2	0.2	0.1	0.1	0.1	0.1
30	vanilloyl acetaldehyde	-	24.69	G, C _α -O, C _γ -O	C _γ	194	0.2	4.3	3.9	0.9	0.6	1.5	1.5
31	cis-4-propenylsyringol	26624135	24.88	S, misc.	C _γ	194	0.1	0.1	0.1	0.1	0.1	0.1	0.1
32	4-propynesyringol	-	25.52	S, misc.	C _γ	192	0.1	0.1	0.1	0.1	0.2	0.1	0.1
33	4-allenesyringol	-	25.73	S, misc.	C _γ	192	0.1	0.1	0.1	0.1	0.1	0.1	0.1
34	trans-4-propenylsyringol	26624135	26.19	S, misc.	C _γ	194	0.9	0.8	0.9	1.0	0.6	0.9	0.9
35	dihydroconiferyl alcohol	2305137	26.22	S, C _γ -O	C _γ	182	0.1	0.1	0.1	0.1	0.1	0.1	0.1
36	syringaldehyde	134963	26.75	S, C _α -O	C _α	182	0.7	0.8	1.0	0.7	0.7	0.6	0.7
37	cis-coniferyl-alcohol	458355	26.82	G, C _γ -O	C _γ	180	1.3	1.1	1.0	1.4	1.3	1.3	1.3
38	homosyringaldehyde	-	27.75	S, C _β -O	C _γ	196	0.3	0.4	0.5	0.3	0.3	0.3	0.3
39	acetosyringone	2478388	28.20	S, C _α -O	C _β	196	0.6	1.2	1.4	0.9	0.8	0.8	0.8
40	trans-coniferyl alcohol	458355	28.55	G, C _γ -O	C _γ	180	31.6	22.4	20.0	30.0	29.8	28.3	27.7
41	trans-coniferldehyde	458366	28.92	G, C _γ -O	C _γ	178	1.8	2.0	1.8	2.1	1.9	2.0	1.9
42	syringylacetone	19037582	29.13	S, C _β -O	C _γ	210	0.3	0.7	0.8	0.4	0.4	0.5	0.5
43	propiosyringone	5650431	29.75	S, C _α -O	C _γ	210	0.0	0.1	0.1	0.1	0.1	0.0	0.1
44	syringoyl acetaldehyde	-	29.90	S, C _α -O, C _γ -O	C _γ	224	0.2	3.4	4.0	1.0	0.9	1.1	1.4
45	syringyl vinyl ketone	-	30.03	S, C _α -O	C _γ	208	0.0	0.1	0.1	0.1	0.1	0.0	0.0
46	dihydrosinapyl alcohol	20736258	30.22	G, C _γ -O	C _γ	212	0.0	0.0	0.0	0.0	0.0	0.0	0.0
47	cis-sinapyl alcohol	537337	32.07	S, C _γ -O	C _γ	210	0.9	0.6	0.6	0.8	0.8	0.7	0.7
48	trans-sinapyl alcohol	537337	33.79	S, C _γ -O	C _γ	210	16.6	9.3	10.0	13.6	13.7	11.6	11.9
49	trans-sinapaldehyde	4206580	34.00	S, C _γ -O	C _γ	208	2.0	2.3	2.4	2.4	2.3	2.1	2.0

Table S2. Lignin content and removal determined by semi-quantitative and quantitative ¹³C-IS py-GC-MS of control and fungal-treated wheat straw after 7 weeks of fungal growth. *Cs* *Ceriporiopsis subvermispora*, *Pe* *Pleurotus eryngii*, *Le* *Lentinula edodes*. Average and standard deviation of analytical triplicates on pooled biological triplicates.

	Control	Cs1	Cs12	Pe3	Pe6	Le8	Le10
Dry matter (g)	90.2 ± 0.3	84.4 ± 0.4	89.4 ± 0.2	87.3 ± 0.1	88.0 ± 0.2	83.7 ± 1.4	84.6 ± 3.0
Lignin content (% w/w)							
semiquan	30.5 ± 1.4	8.6 ± 0.4	9.3 ± 0.8	16.2 ± 1.2	15.6 ± 0.2	10.9 ± 0.9	12.2 ± 0.2
¹³ C-IS quan	23.2 ± 0.8	8.3 ± 0.3	9.3 ± 0.3	13.7 ± 0.7	15.6 ± 1.0	10.3 ± 0.4	10.5 ± 0.2
Lignin removal (% w/w)							
semiquan	-	73.7 ± 5.0	69.7 ± 6.5	48.6 ± 4.2	50.1 ± 2.4	66.8 ± 6.4	62.6 ± 3.8
¹³ C-IS quan	-	66.4 ± 3.5	60.3 ± 3.0	43.0 ± 2.6	34.6 ± 2.6	58.8 ± 3.1	57.4 ± 3.2

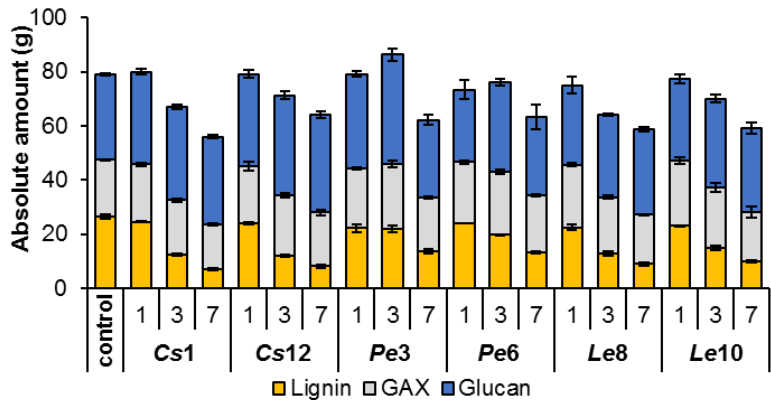


Figure S1. Residual lignin, glucuronoarabinoxylan (GAX) and glucan (cellulose) in fungal-treated wheat straw during growth (1, 3 and 7 weeks). *Cs* *Ceriporiopsis subvermispora*, *Pe* *Pleurotus eryngii*, *Le* *Lentinula edodes*. Average and standard deviation of analytical triplicates on pooled biological triplicates.

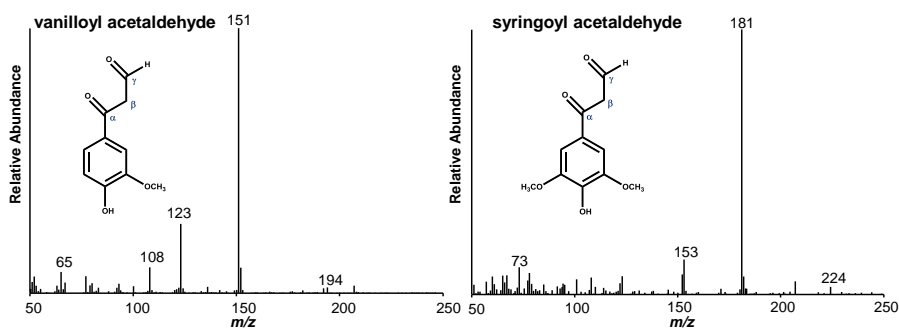


Figure S2. EI-MS (70 eV) spectra and structures of vanilloyl acetaldehyde (VAL) and syringoyl acetaldehyde (SAL) observed by py-GC-MS. Compounds were identified on the basis of fragmentation pattern and retention time. Average mass spectrum across the chromatographic peak with noise subtraction at two sides.

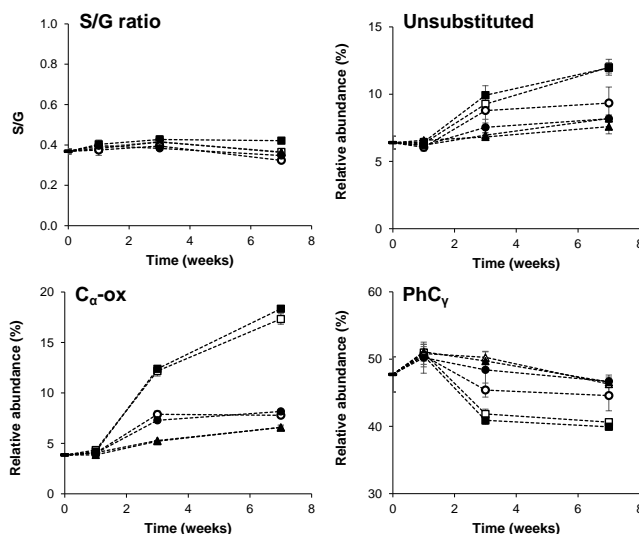


Figure S3. Structural changes of fungal-treated wheat straw lignin during fungal growth (1, 3 and 7 weeks) determined by semiquantitative py-GC-MS. *Cs Ceriporiopsis subvermisporea*, *Pe Pleurotus eryngii*, *Le Lentinula edodes*. Structural classification based on Table S1. □ Cs1, ■ Cs12, △ Pe3, ▲ Pe6, ● Le10. Average and standard deviation of analytical triplicates on pooled biological triplicates.

Table S3. Assignments of the lignin ¹³C-¹H correlation peaks in the HSQC spectra of control and fungal-treated wheat straw. (t) tentative assignment.

label	δ _C /δ _H (ppm)	Assignment ^a
A _α (G)	70.9/4.70	C _α -H _α in β-O-4' substructures linked to G-unit
A _α (S)	71.8/4.82	C _α -H _α in β-O-4' substructures linked to S-unit
A _β (G)	83.5/4.25	C _β -H _β in β-O-4' substructures linked to G-unit
A _β (S)	85.9/4.09	C _β -H _β in β-O-4' substructures linked to S-unit
C _α	84.9/4.64	C _α -H _α in resinol substructures
B _α	86.9/5.42	C _α -H _α in phenylcoumaran substructures
T ₈	94.1/6.56	C ₈ -H ₈ in tricin
T ₆	98.8/6.20	C ₆ -H ₆ in tricin
Smod _{2,6}	103.5/6.97	C ₂ -H ₂ and C ₆ -H ₆ in S-unit derivative (t)
S _{2,6}	103.6/6.68	C ₂ -H ₂ and C ₆ -H ₆ in S-unit
T _{2,6}	104.0/7.31	C ₂ -H ₂ and C ₆ -H ₆ in tricin
T ₃	104.6/6.99	C ₃ -H ₃ in tricin
Sox _{2,6}	106.4/7.32	C ₂ -H ₂ and C ₆ -H ₆ in C _α -oxidized (C _α =O) S-unit
Sox _{2,6}	106.5/7.18	C ₂ -H ₂ and C ₆ -H ₆ in C _α -oxidized (C _α OOH) S-unit
Sald _{2,6}	106.3/7.03	C ₂ -H ₂ and C ₆ -H ₆ in cinnamaldehyde end-group S-unit
G ₂	110.5/6.94	C ₂ -H ₂ in G-unit
FA ₂	110.9/7.32	C ₂ -H ₂ in ferulate
GoxI ₂	111.4/7.53	C ₂ -H ₂ in C _α -oxidized G-unit
GoxII ₂	112.4/7.42	C ₂ -H ₂ in C _α -oxidized G-unit (t)
Gmod ₂	112.7/6.76	C ₂ -H ₂ in G-unit derivative (t)
FA ₆ /pCA ₆	113.9/6.51	C ₆ -H ₆ in ferulate/p-coumarate
H _{3,5} /FA ₅	114.5/6.69	C ₃ -H ₃ and C ₅ -H ₅ in H-unit, C ₅ -H ₅ in FA
G ₅ /G ₆ /pCA _{3,5}	115.1/6.94 and 115.3/6.72	C ₅ -H ₅ and C ₆ -H ₆ in G-unit, C ₃ -H ₃ and C ₅ -H ₅ of pCA
G ₅	118.9/6.77	C ₅ -H ₅ in G-unit
GoxI ₆	122.8/7.49	C ₆ -H ₆ in C _α -oxidized G-unit
FA ₆	123.1/7.12	C ₆ -H ₆ in ferulate
GoxII ₆	125.8/7.40	C ₂ -H ₂ in C _α -oxidized G-unit (t)
H _{2,6} /PHE _{3,5}	127.7/7.17	C ₂ -H ₂ and C ₆ -H ₆ in H-unit, C ₃ -H ₃ and C ₅ -H ₅ in phenylalanine
PHE _{2,6}	129.0/7.20	C ₂ -H ₂ and C ₆ -H ₆ in phenylalanine
pCA _{2,6}	130.1/7.48	C ₂ -H ₂ and C ₆ -H ₆ in p-coumarate
FA _α /pCA _α	145.0/7.56	C _α -H _α in ferulate/p-coumarate

^a: assignment by comparison with literature.²⁻¹⁰

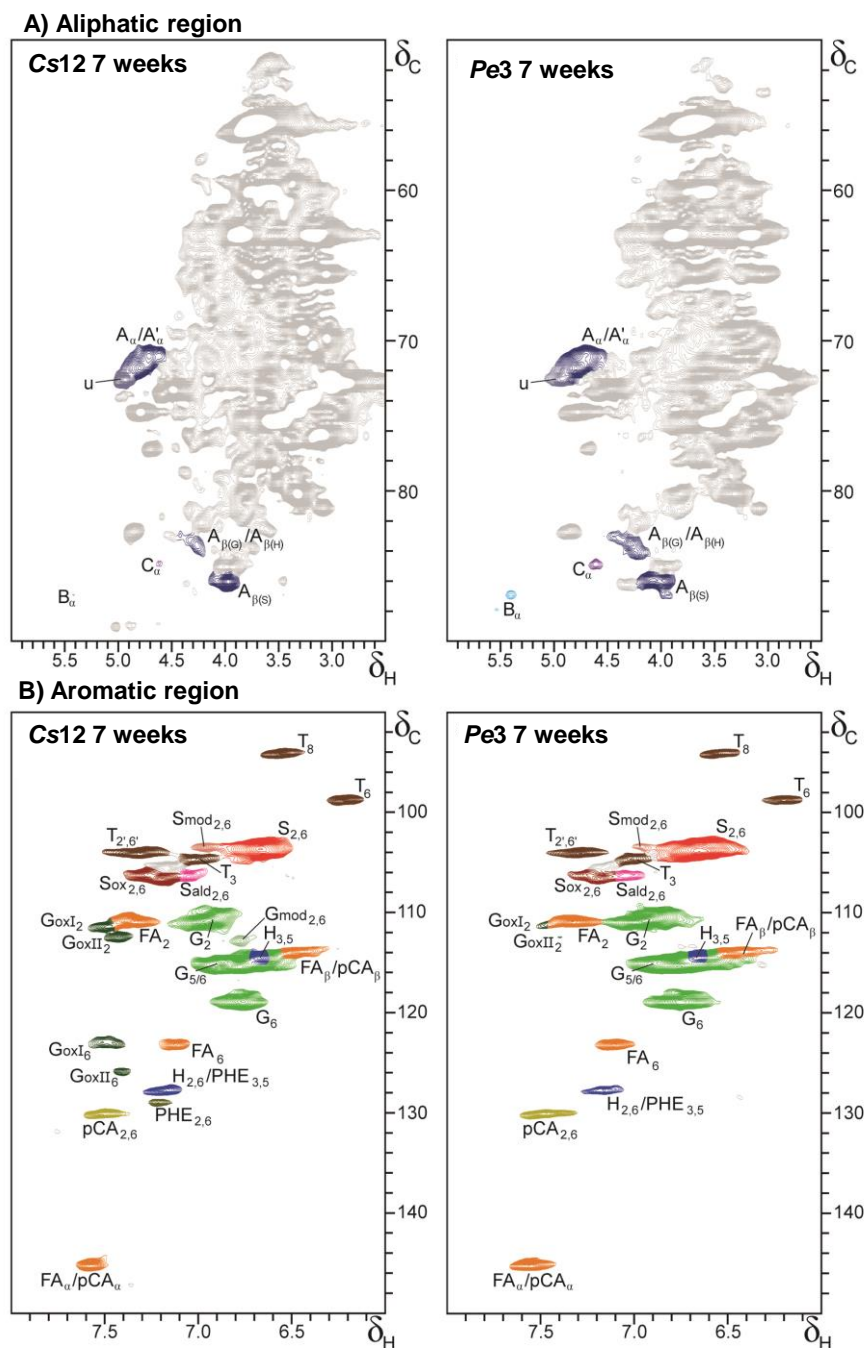


Figure S4. HSQC NMR spectra of fungal-treated wheat straw. Structures of annotated correlation peaks are presented in Figure 5. G_{mod} and S_{mod} are presented in a lighter colour of G and S, respectively. Carbohydrate and unassigned signals are presented in gray. u: unassigned signal overlapping A_α/A'_α.

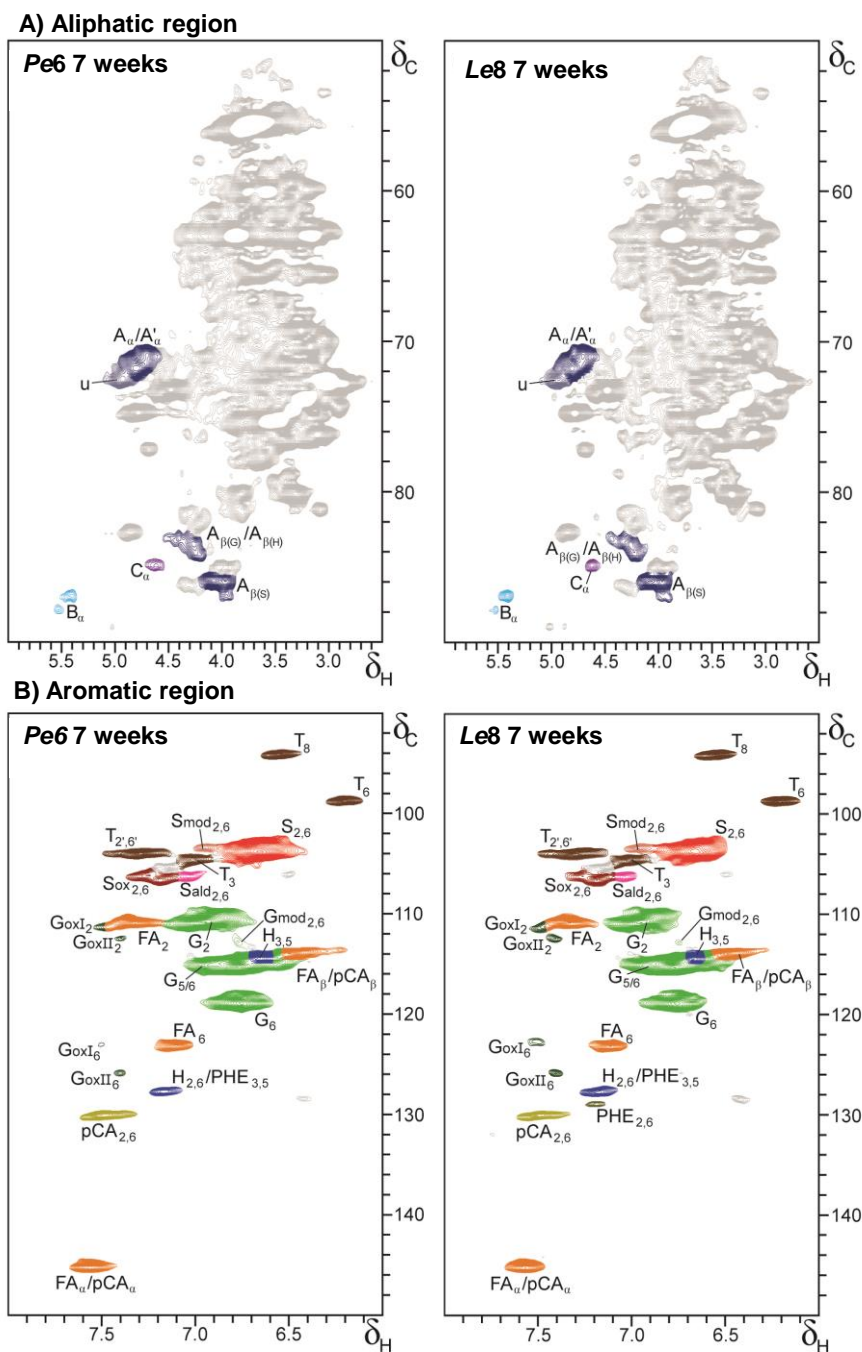
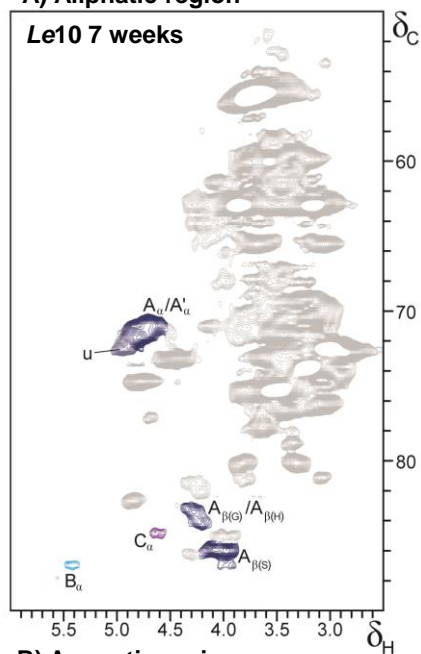
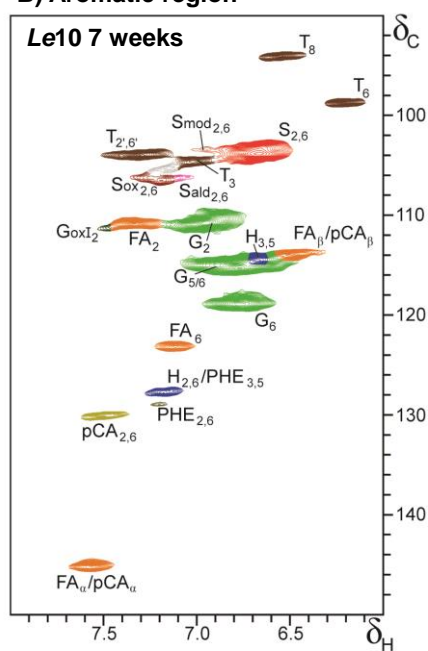
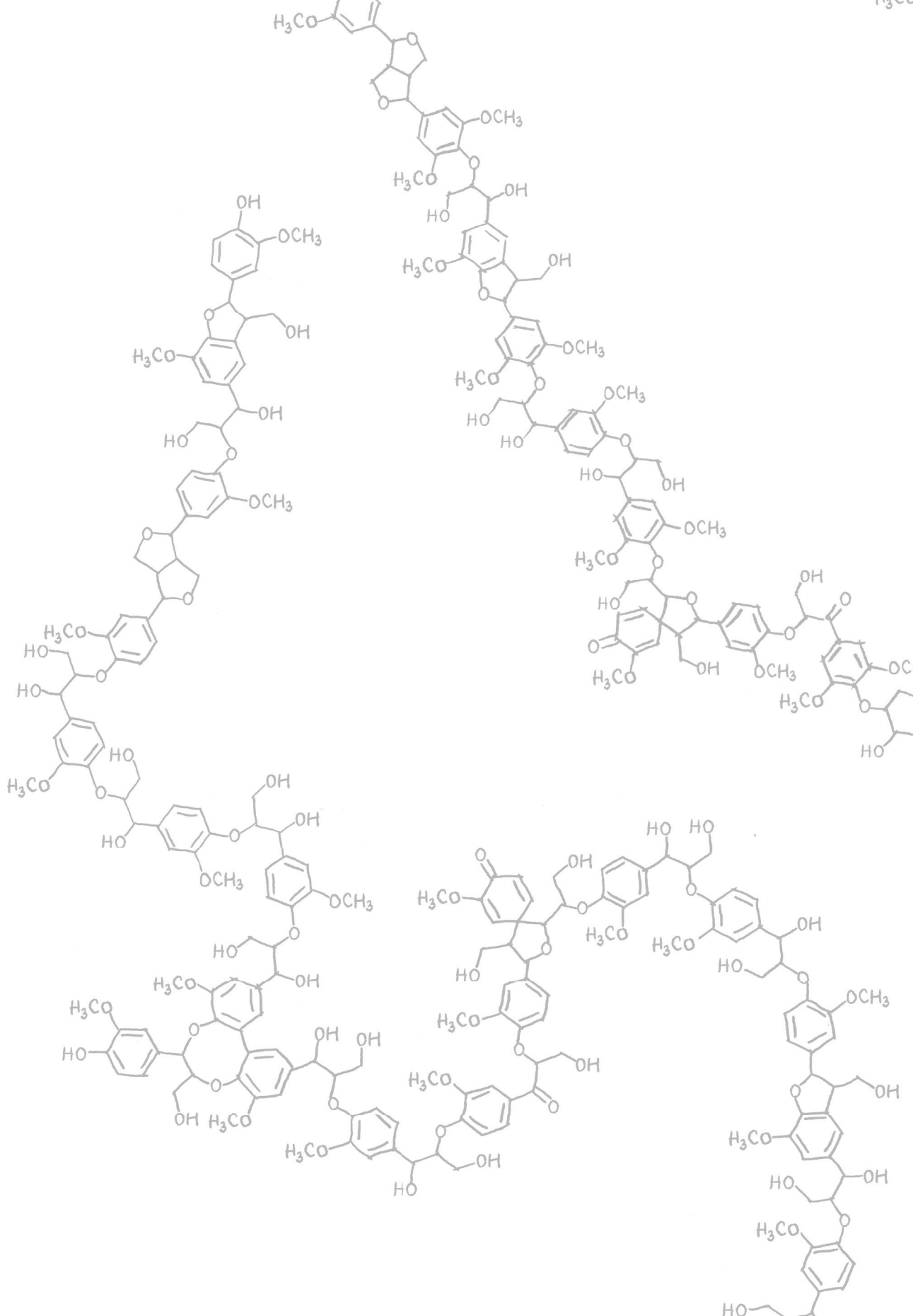


Figure S4. Continued.

A) Aliphatic region**B) Aromatic region****Figure S4.** Continued.

Supporting Information References

1. Van Erven, G.; de Visser, R.; Merckx, D. W. H.; Strolenberg, W.; de Gijss, P.; Gruppen, H.; Kabel, M. A., Quantification of lignin and its structural features in plant biomass using ^{13}C lignin as internal standard for pyrolysis-GC-SIM-MS. *Anal Chem* **2017**, *89*, 10907-10916.
2. Del Río, J. C.; Rencoret, J.; Prinsen, P.; Martínez, Á. T.; Ralph, J.; Gutiérrez, A., Structural characterization of wheat straw lignin as revealed by analytical pyrolysis, 2D-NMR, and reductive cleavage methods. *J Agric Food Chem* **2012**, *60*, 5922-5935.
3. Yuan, T.-Q.; Sun, S.-N.; Xu, F.; Sun, R.-C., Characterization of lignin structures and lignin-carbohydrate complex (LCC) linkages by quantitative ^{13}C and 2D HSQC NMR spectroscopy. *J Agric Food Chem* **2011**, *59*, 10604-10614.
4. Ralph, S. A.; Ralph, J.; Landucci, L., NMR database of lignin and cell wall model compounds. **2009**, Available at URL www.glbrc.org/databases_and_software/nmrdatabase/.
5. Rencoret, J.; Gutiérrez, A.; Nieto, L.; Jiménez-Barbero, J.; Faulds, C. B.; Kim, H.; Ralph, J.; Martínez, Á. T.; del Río, J. C., Lignin composition and structure in young versus adult *Eucalyptus globulus* plants. *Plant Physiol* **2011**, *155*, 667-682.
6. Rencoret, J.; Pereira, A.; del Río, J. C.; Martínez, Á. T.; Gutiérrez, A., Delignification and saccharification enhancement of sugarcane byproducts by a laccase-based pretreatment. *ACS Sustainable Chem Eng* **2017**, *5*, 7145-7154.
7. Del Río, J. C.; Lino, A. G.; Colodette, J. L.; Lima, C. F.; Gutiérrez, A.; Martínez, Á. T.; Lu, F.; Ralph, J.; Rencoret, J., Differences in the chemical structure of the lignins from sugarcane bagasse and straw. *Biomass Bioenergy* **2015**, *81*, 322-338.
8. Villaverde, J. J.; Li, J.; Ek, M.; Ligerio, P.; de Vega, A., Native lignin structure of *Miscanthus x giganteus* and its changes during acetic and formic acid fractionation. *J Agric Food Chem* **2009**, *57*, 6262-6270.
9. Das, A.; Rahimi, A.; Ulbrich, A.; Alherech, M.; Motagamwala, A. H.; Bhalla, A.; da Costa Sousa, L.; Balan, V.; Dumesic, J. A.; Hegg, E. L.; Dale, B. E.; Ralph, J.; Coon, J. J.; Stahl, S. S., Lignin conversion to low-molecular-weight aromatics via an aerobic oxidation-hydrolysis sequence: comparison of different lignin sources. *ACS Sustainable Chem Eng* **2018**, *6*, 3367-3374.
10. Kim, H.; Padmakshan, D.; Li, Y.; Rencoret, J.; Hatfield, R. D.; Ralph, J., Characterization and elimination of undesirable protein residues in plant cell wall materials for enhancing lignin analysis by solution-state nuclear magnetic resonance spectroscopy. *Biomacromolecules* **2017**, *18*, 4184-4195.



The background of the slide is filled with various chemical structures of lignin fragments. These structures are complex, featuring multiple aromatic rings (benzene and furan) connected by ether and carbon-carbon bonds. They are decorated with various functional groups, including hydroxyl (-OH), methoxy (-OCH3), and hydroxymethyl (-CH2OH) groups. The structures are drawn in a light gray, semi-transparent style, creating a textured effect behind the text.

CHAPTER 5

Elucidation of *in situ* ligninolysis mechanisms of the selective white-rot fungus *Ceriporiopsis subvermispora*

Gijs van Erven, Roelant Hilgers, Pieter de Waard,
Erik-Jan Gladbeek, Willem J. H. van Berkel,
Mirjam A. Kabel

Based on: ACS Sustainable Chemistry & Engineering, 2019, 7, 16757-16765

Abstract

Lignin degradation by white-rot fungi is an essential step in terrestrial carbon cycling and has great potential for biotechnological applications. Selective white-rot fungi have been recognized for their ability to effectively delignify lignocellulose, but the underlying mechanisms, particularly *in situ*, have largely remained elusive to date. In this work, we elucidate specific degradation routes of β -O-4 aryl ethers in actual lignocellulosic biomass for the industrially relevant selective white-rot fungus *Ceriporiopsis subvermispota*. Multidimensional NMR and py-GC-MS analyses together with enzymatically synthesized model compounds enabled, for the first time, the identification of various diagnostic lignin cleavage products in residual wheat straw. Our results support that *in situ* ligninolysis by *C. subvermispota* is initiated by single-electron transfer, which then cascades into the cleavage of C $_{\alpha}$ -C $_{\beta}$, C $_{\beta}$ -O and O-4-aryl bonds of β -O-4 aryl ethers. The high abundance of 1-(benzyl)-2,3-dihydroxypropan-1-ones indicated that β -O-4 cleavage is a more important pathway than previously considered. Our approach highlights key diagnostic substructures for providing mechanistic insight into fungal ligninolysis.

Introduction

Selective delignification of lignocellulose has been a long-standing primary objective for the valorization of plant biomass.¹⁻² In Nature, this process is crucial for terrestrial carbon recycling and relies heavily on the action of white-rot fungi.³ Unlike thermochemical industrial processes, some white-rot fungi can degrade lignin selectively while leaving the polysaccharides largely intact, without serious environmental impact.⁴⁻⁵ Selective white-rot fungi, therefore, increasingly spark interest for use in biotechnological applications such as biopulping⁶ and biofuel production.⁷

Ever since the early discovery of the fungal white-rot process, dimeric lignin model compounds have been used to understand the mechanisms underlying delignification as well to identify and characterize the enzymes involved.⁸⁻⁹ For lignin depolymerization, white-rot fungi rely on an intricate oxidoreductase machinery, consisting of various peroxidases, laccases and several accessory enzymes like H₂O₂-generating aryl alcohol oxidases, acting in concert with low molecular weight electron shuttles, also called mediators.¹⁰⁻¹¹

The action of these enzymes and enzyme-mediator systems on dimeric lignin model compounds has been demonstrated to result in a large variety of products, which were ascribed to multiple degradative pathways. Depolymerization of these lignin mimics is initiated by single-electron or hydrogen atom transfer and results in the formation of aryl cation and benzylic radical intermediates, respectively, and consequently undergo C_α-C_β cleavage, C_α-oxidation, β-ether cleavage, or aromatic ring cleavage reactions.¹²⁻¹⁵

The insights obtained on relatively simple β-O-4 dimers can, however, not be directly extrapolated to polymeric lignin as present *in situ*. In the latter case, lignin is embedded in the secondary cell wall matrix and occurs as an extremely complex macromolecule, consisting of *p*-hydroxyphenyl (H), guaiacyl (G) and syringyl (S) subunits, depending on the botanical origin, that are linked through various aryl-ether and carbon-carbon bonds. The β-O-4 aryl ether bond is the most abundant interunit linkage.¹⁶⁻¹⁷ Grass-type lignin is particularly complex as it is comprised of all three subunits and additionally contains acetate, *p*-coumarate, ferulate and tricin moieties.¹⁸

As a result of lignin's structural complexity, the elucidation of the degradation pathways of lignin in actual lignocellulosic biomass is challenging and is hindered by the fact that it requires the accumulation of partially degraded substructures in the residual material. Though a myriad of research has been dedicated to the action of white-rot fungi on lignocellulose, thus far, the only confirmed ligninolysis route is C_α-C_β cleavage, deduced from the presence of benzoic acid residues.¹⁹⁻²²

Recently, we suggested on the basis of whole-cell wall NMR and quantitative py-GC-MS analyses of wheat straw which was treated with a particularly selective and effective white-rot fungus, *Ceriporiopsis subvermispora*, that besides C_α-C_β cleavage, ether-cleavage is a major degradative route of the β-O-4 aryl ethers.²³

To unambiguously confirm these ether-cleavage routes, we selectively extracted and purified diagnostic substructures from fungal treated wheat straw. State-of-the art analytical techniques were used for comprehensive structure elucidation and quantification and provided novel insights into the *in situ* ligninolysis mechanisms of *C. subvermispora*.

Experimental Section

Materials. All chemicals were obtained from commercial suppliers and used without further purification. Water used in all experiments was purified via a Milli-Q water system (Millipore, Billerica, MA, USA). See Supporting Information Section 1 for details.

Preparation of fungal treated wheat straw. Procedures for fungal strain preparation and solid-state pretreatment of the wheat straw by *C. subvermispora* (CBS 347.63, Cs1) have been previously described in detail.²³⁻²⁵ Biological triplicates of wheat straw treated for 0, 1, 3 and 7 weeks were thoroughly mixed in equal dry matter amounts to one replicate for further experiments and analyses.

Extraction and purification of diagnostic substructures. Briefly, diagnostic substructures were selectively extracted from untreated and fungal treated wheat straw by sequential extraction with acetone and water (Figure S1). Acetone soluble substructures were purified by solvent extraction with hexane. Water extractable lignin substructures were purified by enzymatic carbohydrate degradation followed by solid phase extraction by using reversed phase (flash) chromatography. A description of the extraction and purification strategy is presented in the Supporting Information (Section 2 and 4).

Production and purification of guaiacyl diketone and syringyl diketone. Diketones were formed through acidolysis of klason lignin and subsequent liquid extraction by a method described by Govender et al.²⁶ Diketones were purified by using flash chromatography (see Supporting Information Section 2 for details).

Enzymatic synthesis and purification of veratryl model compounds. C_α-oxidized veratrylglycerol- β -guaiacyl ether (VerBG_{ox}), hydroxypropioveratrone (HPVer) and dihydroxypropioveratrone (DHPVer) were enzymatically synthesized by incubating veratrylglycerol- β -guaiacyl ether (VerBG) with laccase and 1-hydroxybenzotriazole (HBT), after which the reaction products were purified by using flash chromatography (see Supporting Information Section 2 for details).²⁷

Analytical methods. Extracted diagnostic substructures and synthesized model compounds were comprehensively analyzed by using quantitative py-GC-MS with ¹³C lignin as internal standard, NMR spectroscopy, and size-exclusion chromatography, based on previously reported procedures as described in detail in the Supporting Information (Section 3; Table S1).^{18, 23, 28-35}

Results & Discussion

We have recently described that fungal action on wheat straw resulted in extensive lignin degradation and removal up to 70% (w/w) after seven weeks of fungal growth and that degraded substructures accumulated in the residual material.²³ Here, we aimed to selectively extract these degraded substructures to gain further mechanistic insight into the fungal delignification process (for details see Supporting Information Section 4; Figure S1-3 and Table S2-6).

Py-GC-MS analysis indicated that after seven weeks of fungal growth, C_α-oxidized compounds comprised 38% of the abundance of pyrolysis products in the water extracts (Table S2 and S5). 42% of these C_α-oxidized products was comprised of benzyl diketones, compounds we, as others have, previously annotated as benzoyl acetaldehydes (Figure S4, Table S7).^{23, 36-37} Besides correct identification, we also ascertained their accurate quantification by the determination of relative response factors for py-GC-MS analyses. Being particularly rich in diagnostic substructures, the water extracts were used for detailed structural characterization.

The structural features of the untreated water-extractable lignin greatly resembled that of native wheat straw lignin as occurring *in situ*, albeit that the water-extractable lignin was remarkably low in tricin (Figure 1).^{18, 38} In contrast, after seven weeks of fungal growth, the extracts were fully devoid of initial intact interunit linkages and all regular structural features of wheat straw lignin were replaced by C_α-oxidized guaiacyl and syringyl substructures (Figure 1).

Although heavily degraded, the extracted lignin structures remained oligomeric, as confirmed by MALS-corrected SEC analyses (Figure S9).³⁴⁻³⁵ This might point towards the relative accumulation of interunit linkages not detected or resolved in HSQC NMR analyses and/or to the occurrence of repolymerization reactions. There was no spectral evidence, in both the HSQC and HMBC spectra, for the presence of repolymerized substructures in the extracts. However, it cannot be excluded that such reactions might have resulted in products that cannot be detected in these spectra.

The C_α-oxidized substructures were analyzed to consist of benzoic acids, aldehydes and ketones, as concluded from their respective signature δ_{13C} correlations at 167, 191 and 198 ppm in the HMBC spectrum (Figure 2). The structural assignments were validated by additional correlations between the ring carbons with unprecedented completeness for actual biomass-derived samples.³⁹⁻⁴¹

To further clarify the identity of the C_α-ketones, we performed a 3D TOCSY-HSQC NMR experiment (Figure 3), which confirmed the annotation of several new peaks that appeared in the aliphatic region of the HSQC spectrum of the treated sample (Figure 1A). In the resulting 3D spectra, the peaks presented clear correlations between C_β and C_γ protons. The presence of 1-(benzyl)-2,3-dihydroxypropan-1-one (Figure 3B) and 3-hydroxy-1-(benzyl)propan-1-one (Figure 3C) was further confirmed by NMR analyses of enzymatically synthesized model compounds, which

(Figure 4). Upon pyrolysis, all model compounds underwent dehydration reactions. In the case of the intact C_α -oxidized veratrylglycerol- β -guaiacyl ether (VerBGox), this resulted in acetoveratrone and extensive 'unproductive' pyrolysis yielding an intact dimer-H₂O, as previously observed.⁴²

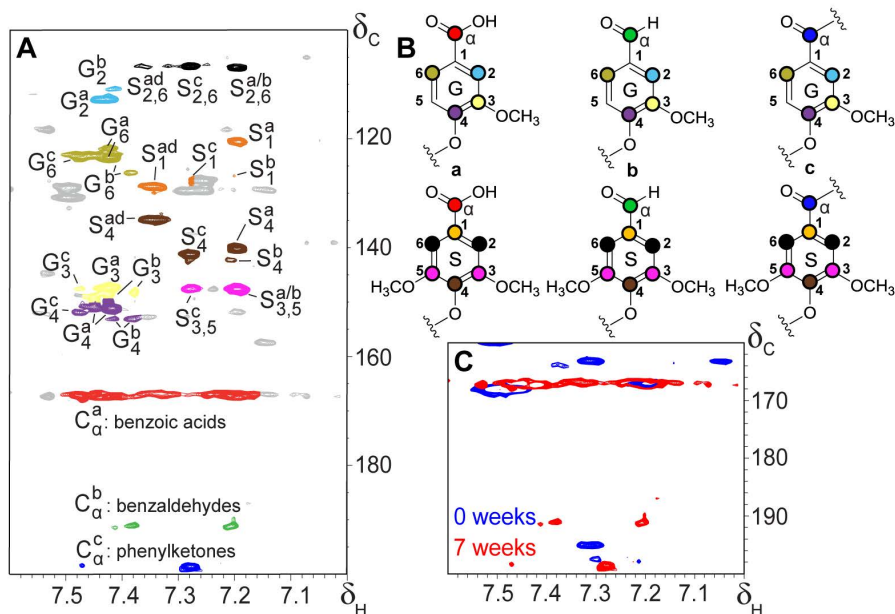


Figure 2. Aromatic region of ¹H-¹³C HMBC spectrum of purified water extract from seven weeks *C. subvermispota* treated wheat straw (A), annotated substructures (B) and overlaid sections of spectra of untreated and fungal treated extracts (C). Unassigned signals in grey. ad: benzoic acid derivative. Typical annotated signals clearly appeared upon treatment (B).

Pyrolysis of hydroxypropioveratrone (HPVer) resulted in the formation of acetoveratrone and the dehydration derivate veratryl vinylketone. In a similar fashion, veratryl propanedione was formed as single product from dihydroxypropioveratrone (DHPVer). The latter product was neither formed from VerBGox and HPVer. We, therefore, conclude that benzyl diketones are markers for the presence of 1-(benzyl)-2,3-dihydroxypropan-1-ones and that, consequently, they can be used as markers for *O*-4-cleavage of β -*O*-4 aryl ethers. The presence of both G- and S-diketones confirms that the cleavage reactions occurred on both guaiacyl and syringyl subunits (Table S4-S6).

Both py-GC-MS and semiquantitative analysis of the HSQC spectra established that the phenylketols DHPV and DHPS steadily accumulated during fungal growth at the expense of intact interunit linkages and reached 20% of the aromatic units after seven weeks of fungal growth (Table S8-S10). Given the fact that C_α - C_β cleavage is often considered only, the abundance of these products clearly indicates that we need to unravel the routes leading to their formation for a better understanding of *in situ* fungal ligninolysis mechanisms.

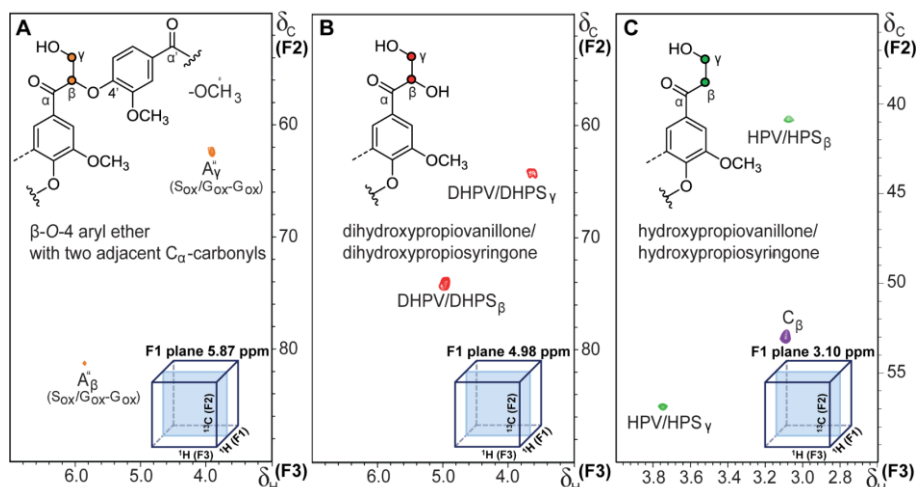


Figure 3. 3D ^1H - ^{13}C TOCSY-HSQC spectra of purified water extract from seven weeks *C. subvermisporea* treated wheat straw. Cross-peaks in $^1\text{H}_\beta$ planes A-C match closely with those reported previously.^{39, 43-45} Note that in panel C the chemical shift of the β -protons of HPV/HPS and resinol substructures (C_β) coincide.

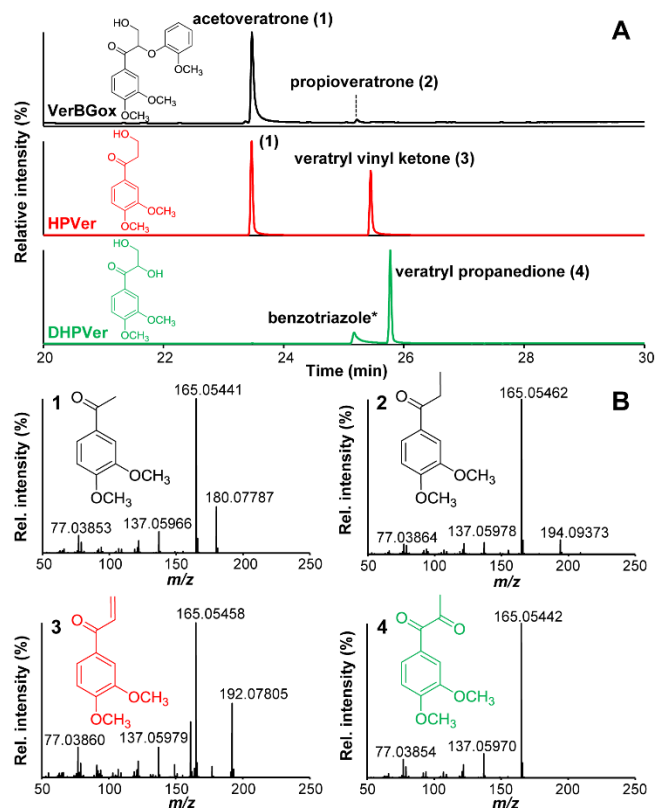


Figure 4 Pyrograms (TIC) (A) of VerBG_{ox}, HPVer and DHPVer and EI-HR-MS spectra of derived pyrolysis products (B). The benzotriazole (*) in the pyrogram of DHPVer remained as impurity after laccase-HBT incubations of VerBG.

Our observations allow a reconstruction of the *in situ* cleavage routes of β -O-4 aryl ethers through action of *C. subvermispora* at a level of detail previously only attained for lignin model dimers and sets the stage for *in situ* fungal delignification pathways in general.^{14-15, 46} Even though our analyses suggested that phenylcoumaran and resinol linkages were susceptible to degradation as well, we did not detect specific degradation products diagnostic for pathways underlying their cleavage. However, their degradation might have contributed, albeit slightly, to the same product pool attributed to β -O-4 aryl ether C_{α} - C_{β} cleavage reactions. To describe ligninolysis mechanisms of polymeric lignin, we here considered reaction pathways for the smallest β -O-4 aryl ether oligomer, a trimer, with the oxidation of the middle aromatic ring, ring B, as starting point (Figure 5). Dimeric structures do not suffice to exemplify that the effects of subunit oxidation can be exerted on linkages present at both the 1 as well as the 4 position, i.e. B-ring oxidation can initiate cleavage between ring A and B and between ring B and C. Four main pathways are proposed to follow one-electron oxidation of the B-ring: I C_{α} -oxidation, II C_{α} - C_{β} cleavage, III β -|O-4 cleavage and IV β -O-|4 cleavage. The presence of benzaldehydes and benzoic acids (Figure 2) confirmed that C_{α} - C_{β} cleavage was a major reaction underlying ligninolysis. Benzaldehydes are a direct result of spontaneous cleavage of the C_{α} - C_{β} bond after aryl cation formation, which due to their instability in oxidative environments likely react further to benzoic acids.^{8, 47} The C_{α} - C_{β} cleavage reaction results in an unstable hemiacetal structure bound to ring C, which decomposes to release hydroxyacetaldehyde and yields ring C as phenolic subunit.⁴⁸

B-ring oxidation can, upon elimination of the adjacent benzylic proton, also lead to the formation of 1-benzylpropene-1,3-diols, which through keto-enol tautomerization accumulate as 3-hydroxy-1-(benzyl)propan-1-ones (Figure 3C) (route III).¹³ If elimination of the benzylic proton is followed by reaction with molecular oxygen and subsequent release of a hydroperoxy radical, C_{α} -oxidized products are formed (route I).¹³ As routes I and III might involve benzyl radical intermediates they could, in theory, also be the result of initial hydrogen abstraction at the benzyl position and thus follow a hydrogen atom transfer (HAT) mechanism instead.⁴⁹ These routes are, however, far less prominent than routes II and IV and, therefore, are considered of lesser importance.

The substructures resulting from route III, HPV and HPS, have previously been described to result from a reductive reaction cascade involving β -etherases, intracellular enzymes recently also shown to occur in white-rot fungi.⁵⁰⁻⁵¹ We, however, do not expect that the latter enzymes were responsible for HPV/HPS formation in our samples as the substructures were observed in oligomeric fractions (> 2000 Da, i.e. approximately decameric, Figure S9), unable to be transported across the fungal cell-membrane.

Though we are the first to establish such a detailed overview of *in situ* cleavage reactions, we would like to emphasize route IV. We infer that the latter route is

seriously underrepresented in the literature, but clearly shown here to be a major reaction in *in situ* fungal ligninolysis.

Note that route IV has previously been suggested for wheat straw ligninolysis by a bacterial DyP-type peroxidase on the basis of LC-MS product analysis,⁵² though several isomers of the annotated product can be devised with similar mass spectrometric behavior, including those resulting from C_α-C_β cleavage.

Route IV is proposed to proceed via an initial reaction of the aryl cation radical with adjacent C_α-OH or C_γ-OH groups to produce cyclohexadienone ketals (tentatively assigned, Figure 1) or with H₂O, which induces β-O-4 cleavage and yields phenylglycerols as initial products.¹²⁻¹³ Phenylglycerols have previously been demonstrated in brown-rotted wood, but seemed absent in our samples.⁴⁰ Presumably, these structures directly reacted further upon formation and instead accumulated in the residue as 1-(benzyl)-2,3-dihydroxypropan-1-ones (Figure 3B). The latter structures can also be formed directly from C_α-oxidized β-O-4 aryl ethers.

Route IV might be especially prevalent on β-O-4 aryl ethers with two adjacent C_α-carbonyls (Figure 3A), as these α-ketones are expected to prevent pathways I-III from occurring. However, C_α-oxidation also decreases the redox potential of the aromatic ring(s) and thereby largely influences the reactivity towards oxidation by ligninolytic enzymes.¹²⁻¹³ Hence, only if an electron can still be withdrawn from these B-rings, subsequent cleavage would likely follow route IV. Whether the enzyme-mediator machinery of *C. subvermispora* holds such oxidative capacity remains to be elucidated.^{11, 53}

C. subvermispora is expected to mainly depend on manganese peroxidases (MnPs) for ligninolysis, based on the number of MnP-encoding genes (13) and secretome analysis.^{11, 53} Given the fact that chelated Mn³⁺ is only able to oxidize phenolic substructures, this would not allow the fungus to degrade lignin as extensively and effectively as observed (70% w/w lignin removal within seven weeks of fungal growth).⁵⁴ Instead, the fungus presumably depends on MnP-mediated lipid peroxidation reactions, which likely involve secondary metabolites of the fungus, alkylitaconic acids also referred to as 'ceriporic acids'.⁵⁵⁻⁵⁶

However, no consensus has been reached on the radical species that initiate this ligninolytic cascade nor on the initial reaction pathway.⁵⁷⁻⁵⁹ Ohashi et al. calculated that the bond-dissociation energy (BDE) of the benzylic C-H bond of the *erythro*-diastereomer of a lignin model compound is substantially lower than that of the *threo*-analogue. For that reason, if hydrogen abstraction (HAT) would be the sole underlying mechanism, a preference for the *erythro*-form can be expected. However, Nishimura et al. and Yelle et al. showed, for a non-phenolic dimer and actual spruce lignin, respectively, a clear preference for the *threo*-diastereomer.^{15, 22} The latter is consistent with other oxidants known to operate via single-electron transfer (SET).⁶⁰⁻⁶¹ Therefore, the currently available evidence favors mechanisms that are initiated by SET rather than HAT.^{14, 22, 46}

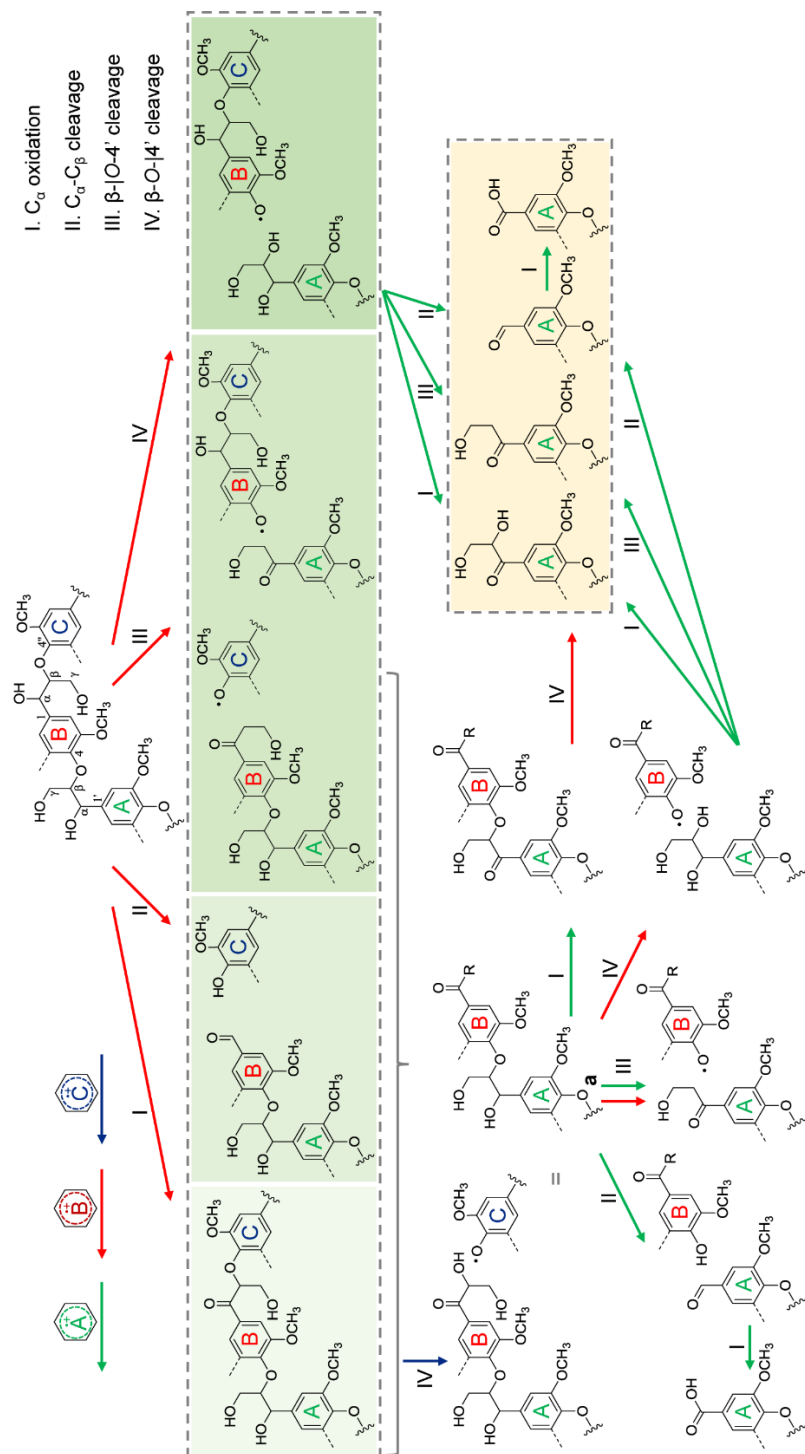


Figure 5. Reconstruction of *in situ* cleavage routes of β-O-4 aryl ethers initiated by single-electron transfer through action of *C. subvermispora*. Identification of diagnostic substructures in Figure 2 and 3. Primary reaction products and final diagnostic structures are indicated in dashed boxes. Primary reaction products after route I, II and III and secondary products after route I-IV are represented by structure (a) for follow-up reactions. Colored arrows indicate which ring is oxidized by single-electron transfer to an aryl cation intermediate.

However, we would like to stress that HAT and SET do not, per se, exclude one another and might occur concurrently in the delignification by *C. subvermispora*. The high abundance of the β -O-|4 cleavage reaction in comparison with previous studies conducted on wood might relate to the initial lignin structure as present in wheat straw.²² Lignin in grass differs fundamentally from wood, and particularly from softwood lignin, which consists solely of guaiacyl units.¹⁶ For lignin model compounds, it was previously shown that the pattern and degree of methoxylation of the aromatic rings not only influenced the oxidizability, but also impacted the prevalence of degradation routes.^{12, 14-15} The difference in electron-donating substituents of the aromatic rings of wheat straw and wood lignin might have resulted in substantially more β -O-|4 cleavage reactions for the former substrate.

Conclusions

In summary, we have provided mechanistic insight into *in situ* ligninolysis by the selective white-rot fungus *C. subvermispora*. Through key diagnostic structures, we obtained compelling evidence for the occurrence of multiple degradation routes initiated by single-electron oxidation, of which β -O-|4 cleavage was confirmed as major route in actual plant biomass for the first time. We reckon that these diagnostic structures now enable the comparison of fungi in terms of *in situ* delignification mechanisms. Our work contributes to understanding how selective white-rot fungi, and *C. subvermispora* in particular, function in Nature and how we can exploit their ligninolytic capacity for the valorization of lignocellulose.

Acknowledgements

The authors thank Nazri Nayan, John W. Cone and Anton S.M. Sonnenberg (Wageningen University & Research) for providing the *C. subvermispora* treated wheat straw. Richard Gosselink, Jacqueline Donkers and Jacintha van der Putten (Wageningen Food & Biobased Research) are acknowledged for performing alkaline SEC analyses. Antje Potthast and Grigory Zinovyev (BOKU, Vienna, Austria) are acknowledged for performing organic SEC analyses. Maud Pfeiffer is acknowledged for designing the graphical abstract.

References

1. Ragauskas, A. J.; Williams, C. K.; Davison, B. H.; Britovsek, G.; Cairney, J.; Eckert, C. A.; Frederick, W. J.; Hallett, J. P.; Leak, D. J.; Liotta, C. L., The path forward for biofuels and biomaterials. *Science* **2006**, *311*, 484-489.
2. Behera, S.; Arora, R.; Nandhagopal, N.; Kumar, S., Importance of chemical pretreatment for bioconversion of lignocellulosic biomass. *Renewable and Sustainable Energy Rev* **2014**, *36*, 91-106.
3. Hammel, K. E., Fungal degradation of lignin. In *Driven by nature: plant litter quality and decomposition*, Cadish, G.; Giller, K. E., Eds. CAB-International: Wallingford, 1997; pp 33-47.
4. Wan, C.; Li, Y., Fungal pretreatment of lignocellulosic biomass. *Biotechnol Adv* **2012**, *30*, 1447-1457.
5. Camarero, S.; Martínez, M. J.; Martínez, A. T., Understanding lignin biodegradation for the improved utilization of plant biomass in modern biorefineries. *Biofuels, Bioprod Biorefin* **2014**, *8*, 615-625.
6. Ferraz, A.; Guerra, A.; Mendonça, R.; Masarin, F.; Vicentim, M. P.; Aguiar, A.; Pavan, P. C., Technological advances and mechanistic basis for fungal biopulping. *Enzyme Microb Technol* **2008**, *43*, 178-185.
7. Wan, C.; Li, Y., Microbial pretreatment of corn stover with *Ceriporiopsis subvermispora* for enzymatic hydrolysis and ethanol production. *Bioresour Technol* **2010**, *101*, 6398-6403.
8. Hammel, K. E.; Cullen, D., Role of fungal peroxidases in biological ligninolysis. *Curr Opin Plant Biol* **2008**, *11*, 349-355.
9. Wong, D. W., Structure and action mechanism of ligninolytic enzymes. *Appl Biochem Biotechnol* **2009**, *157*, 174-209.
10. Martinez, D.; Larrondo, L. F.; Putnam, N.; Gelpke, M. D. S.; Huang, K.; Chapman, J.; Helfenbein, K. G.; Ramaiya, P.; Detter, J. C.; Larimer, F., Genome sequence of the lignocellulose degrading fungus *Phanerochaete chrysosporium* strain RP78. *Nat Biotechnol* **2004**, *22*, 695-700.
11. Fernández-Fueyo, E.; Ruiz-Dueñas, F. J.; Ferreira, P.; Floudas, D.; Hibbett, D. S.; Canessa, P.; Larrondo, L. F.; James, T. Y.; Seelenfreund, D.; Lobos, S.; Polanco, R.; Tello, M.; Honda, Y.; Watanabe, T.; Watanabe, T.; Ryu, J. S.; Kubicek, C. P.; Schmoll, M.; Gaskell, J.; Hammel, K. E.; St. John, F. J.; Vanden Wymelenberg, A.; Sabat, G.; Splinter Bondurant, S.; Khajamohiddin, S.; Jagit, Y. S.; Doppapaneni, H.; Subramanian, V.; José, L. L.; Oguiza, J. A.; Perez, G.; Pisabarro, A. G.; Ramirez, L.; Santoyo, F.; Master, E.; Coutinho, P. M.; Henrissat, B.; Lombard, V.; Magnuson, J. K.; Kues, U.; Hori, C.; Igarashi, K.; Samejima, M.; Held, B. W.; Barry, K. W.; Labutti, K. M.; Lapidus, A.; Lindquist, E. A.; Lucas, S. M.; Riley, R.; Salamov, A. A.; Hoffmeister, D.; Schwenk, D.; Hadar, Y.; Yarden, O.; de Vries, R. P.; Wiebenga, A.; Stenlid, J.; Eastwood, D.; Grigoriev, I. V.; Berka, R. M.; Blanchette, R. A.; Kersten, P.; Martínez, A. T.; Vicuna, R.; Cullen, D., Comparative genomics of *Ceriporiopsis subvermispora* and *Phanerochaete chrysosporium* provide insight into selective ligninolysis. *Proc Natl Acad Sci* **2012**, *109*, 5458-5463.
12. Kirk, T. K.; Tien, M.; Kersten, P. J.; Mozuch, M. D.; Kalyanaraman, B., Ligninase of *Phanerochaete chrysosporium*. Mechanism of its degradation of the non-phenolic arylglycerol β -aryl ether substructure of lignin. *Biochem J* **1986**, *236*, 279-287.
13. Kawai, S.; Nakagawa, M.; Ohashi, H., Degradation mechanisms of a nonphenolic β -O-4 lignin model dimer by *Trametes versicolor* laccase in the presence of 1-hydroxybenzotriazole. *Enzyme Microb Technol* **2002**, *30*, 482-489.
14. Srebotnik, E.; Jensen, K.; Kawai, S.; Hammel, K. E., Evidence that *Ceriporiopsis subvermispora* degrades nonphenolic lignin structures by a one-electron-oxidation mechanism. *Appl Environ Microbiol* **1997**, *63*, 4435-4440.
15. Nishimura, H.; Sasaki, M.; Seike, H.; Nakamura, M.; Watanabe, T., Alkadienyl and alkenyl itaconic acids (ceriporic acids G and H) from the selective white-rot

- fungus *Ceriporiopsis subvermispora*: a new class of metabolites initiating ligninolytic lipid peroxidation. *Org Biomol Chem* **2012**, *10*, 6432-6442.
16. Vanholme, R.; Demedts, B.; Morreel, K.; Ralph, J.; Boerjan, W., Lignin biosynthesis and structure. *Plant Physiol* **2010**, *153*, 895-905.
 17. Ralph, J.; Brunow, G.; Harris, P. J.; Dixon, R. A.; Schatz, P. F.; Boerjan, W., Lignification: are lignins biosynthesized via simple combinatorial chemistry or via proteinaceous control and template replication? In *Recent Advances in Polyphenol Research*, Lattanzio, V.; Daayf, F., Eds. Wiley-Blackwell: Oxford, 2009; Vol. 1, pp 36-66.
 18. Del Río, J. C.; Rencoret, J.; Prinsen, P.; Martínez, A. T.; Ralph, J.; Gutiérrez, A., Structural characterization of wheat straw lignin as revealed by analytical pyrolysis, 2D-NMR, and reductive cleavage methods. *J Agric Food Chem* **2012**, *60*, 5922-5935.
 19. Ralph, J.; Landucci, L. L., NMR of Lignins. In *Lignin and Lignans: Advances in Chemistry*, Heithner, C.; Dimmel, D.; Schmidt, J. A., Eds. CRC Press, Taylor & Francis: Boca Raton, FL, USA, 2010; pp 137-244.
 20. Daly, P.; López, S. C.; Peng, M.; Lancefield, C. S.; Purvine, S. O.; Kim, Y. M.; Zink, E. M.; Dohnalkova, A.; Singan, V. R.; Lipzen, A., *Dichomitus squalens* partially tailors its molecular responses to the composition of solid wood. *Environ Microbiol* **2018**, *20*, 4141-4156.
 21. Martínez, A. T.; Rencoret, J.; Nieto, L.; Jiménez-Barbero, J.; Gutiérrez, A.; del Río, J. C., Selective lignin and polysaccharide removal in natural fungal decay of wood as evidenced by *in situ* structural analyses. *Environ Microbiol* **2011**, *13*, 96-107.
 22. Yelle, D. J.; Kapich, A. N.; Houtman, C. J.; Lu, F.; Timokhin, V. I.; Fort, R. C.; Ralph, J.; Hammel, K. E., A highly diastereoselective oxidant contributes to ligninolysis by the white rot basidiomycete *Ceriporiopsis subvermispora*. *Appl Environ Microbiol* **2014**, *80*, 7536-7544.
 23. Van Erven, G.; Nayan, N.; Sonnenberg, A. S.; Hendriks, W. H.; Cone, J. W.; Kabel, M. A., Mechanistic insight in the selective delignification of wheat straw by three white-rot fungal species through quantitative ¹³C-IS py-GC-MS and whole cell wall HSQC NMR. *Biotechnol Biofuels* **2018**, *11*, 262.
 24. Nayan, N.; Sonnenberg, A. S.; Hendriks, W. H.; Cone, J. W., Screening of white-rot fungi for bioprocessing of wheat straw into ruminant feed. *J Appl Microbiol* **2018**, *125*, 468-479.
 25. Nayan, N.; Sonnenberg, A. S. M.; Hendriks, W. H.; Cone, J. W., Differences between two strains of *Ceriporiopsis subvermispora* on improving the nutritive value of wheat straw for ruminants. *J Appl Microbiol* **2017**, *123*, 352-361.
 26. Govender, M.; Bush, T.; Spark, A.; Bose, S. K.; Francis, R. C., An accurate and non-labor intensive method for the determination of syringyl to guaiacyl ratio in lignin. *Bioresour Technol* **2009**, *100*, 5834-5839.
 27. Hilgers, R.; Vincken, J.-P.; Gruppen, H.; Kabel, M. A., Laccase/mediator systems: their reactivity toward phenolic lignin structures. *ACS Sustainable Chem Eng* **2018**, *6*, 2037-2046.
 28. Van Erven, G.; de Visser, R.; Merckx, D. W.; Strolenberg, W.; de Gijssels, P.; Gruppen, H.; Kabel, M. A., Quantification of lignin and its structural features in plant biomass using ¹³C lignin as internal standard for pyrolysis-GC-SIM-MS. *Anal Chem* **2017**, *89*, 10907-10916.
 29. Mansfield, S. D.; Kim, H.; Lu, F.; Ralph, J., Whole plant cell wall characterization using solution-state 2D NMR. *Nat Protoc* **2012**, *7*, 1579-1589.
 30. Ralph, J.; Lu, F., Cryoprobe 3D NMR of acetylated ball-milled pine cell walls. *Org Biomol Chem* **2004**, *2*, 2714-2715.
 31. Ralph, J.; Akiyama, T.; Kim, H.; Lu, F.; Schatz, P. F.; Marita, J. M.; Ralph, S. A.; Reddy, M. S.; Chen, F.; Dixon, R. A., Effects of coumarate 3-hydroxylase down-regulation on lignin structure. *J Biol Chem* **2006**, *281*, 8843-8853.

32. Nishimura, H.; Kamiya, A.; Nagata, T.; Katahira, M.; Watanabe, T., Direct evidence for a ether linkage between lignin and carbohydrates in wood cell walls. *Sci Rep* **2018**, *8*, 6538.
33. Constant, S.; Wienk, H. L.; Frissen, A. E.; de Peinder, P.; Boelens, R.; van Es, D. S.; Grisel, R. J.; Weckhuysen, B. M.; Huijgen, W. J.; Gosselink, R. J., New insights into the structure and composition of technical lignins: a comparative characterisation study. *Green Chem* **2016**, *18*, 2651-2665.
34. Sulaeva, I.; Zinoviyev, G.; Plankeele, J. M.; Sumerskii, I.; Rosenau, T.; Potthast, A., Fast track to molar-mass distributions of technical lignins. *ChemSusChem* **2017**, *10*, 629-635.
35. Zinoviyev, G.; Sulaeva, I.; Podzimek, S.; Rössner, D.; Kilpeläinen, I.; Sumerskii, I.; Rosenau, T.; Potthast, A., Getting closer to absolute molar masses of technical lignins. *ChemSusChem* **2018**, *11*, 3259-3268.
36. Ralph, J.; Hatfield, R. D., Pyrolysis-GC-MS characterization of forage materials. *J Agric Food Chem* **1991**, *39*, 1426-1437.
37. Rencoret, J.; Gutiérrez, A.; Nieto, L.; Jiménez-Barbero, J.; Faulds, C. B.; Kim, H.; Ralph, J.; Martínez, Á. T.; José, C., Lignin composition and structure in young versus adult *Eucalyptus globulus* plants. *Plant Physiol* **2011**, *155*, 667-682.
38. Zeng, J.; Helms, G. L.; Gao, X.; Chen, S., Quantification of wheat straw lignin structure by comprehensive NMR analysis. *J Agric Food Chem* **2013**, *61*, 10848-10857.
39. Ralph, S. A.; Ralph, J.; Landucci, L., NMR database of lignin and cell wall model compounds. **2009**, Available at URL www.glbrc.org/databases_and_software/nmrdatabase/.
40. Yelle, D. J.; Wei, D.; Ralph, J.; Hammel, K. E., Multidimensional NMR analysis reveals truncated lignin structures in wood decayed by the brown rot basidiomycete *Postia placenta*. *Environ Microbiol* **2011**, *13*, 1091-1100.
41. Ibarra, D.; Chavez, M. I.; Rencoret, J.; del Río, J. C.; Gutiérrez, A.; Romero, J.; Camarero, S.; Martínez, M. J.; Jiménez-Barbero, J.; Martínez, A. T., Structural modification of eucalypt pulp lignin in a totally chlorine-free bleaching sequence including a laccase-mediator stage. *Holzforschung* **2007**, *61*, 634-646.
42. Choi, Y. S.; Singh, R.; Zhang, J.; Balasubramanian, G.; Sturgeon, M. R.; Katahira, R.; Chupka, G.; Beckham, G. T.; Shanks, B. H., Pyrolysis reaction networks for lignin model compounds: Unraveling thermal deconstruction of β -O-4 and α -O-4 compounds. *Green Chem* **2016**, *18*, 1762-1773.
43. Guo, H.; Miles-Barrett, D. M.; Neal, A. R.; Zhang, T.; Li, C.; Westwood, N. J., Unravelling the enigma of lignin OX: can the oxidation of lignin be controlled? *Chem Sci* **2018**, *9*, 702-711.
44. Gall, D. L.; Ralph, J.; Donohue, T. J.; Noguera, D. R., A group of sequence-related sphingomonad enzymes catalyzes cleavage of β -aryl ether linkages in lignin β -guaiacyl and β -syringyl ether dimers. *Environ Sci Technol* **2014**, *48*, 12454-12463.
45. Higuchi, Y.; Aoki, S.; Takenami, H.; Kamimura, N.; Takahashi, K.; Hishiyama, S.; Lancefield, C. S.; Ojo, O. S.; Katayama, Y.; Westwood, N. J., Bacterial catabolism of β -hydroxypropiovanillone and β -hydroxypropiosyringone produced in the reductive cleavage of arylglycerol- β -aryl ether in lignin. *Appl Environ Microbiol* **2018**, *84*, e02670-17.
46. Jensen, K. A.; Bao, W.; Kawai, S.; Srebotnik, E.; Hammel, K. E., Manganese-dependent cleavage of nonphenolic lignin structures by *Ceriporiopsis subvermispota* in the absence of lignin peroxidase. *Appl Environ Microbiol* **1996**, *62*, 3679-3686.
47. Sankar, M.; Nowicka, E.; Carter, E.; Murphy, D. M.; Knight, D. W.; Bethell, D.; Hutchings, G. J., The benzaldehyde oxidation paradox explained by the interception of peroxy radical by benzyl alcohol. *Nat Commun* **2014**, *5*, 3332.
48. Tien, M.; Kirk, T. K., Lignin-degrading enzyme from *Phanerochaete chrysosporium*: purification, characterization, and catalytic properties of a unique H₂O₂-requiring oxygenase. *Proc Natl Acad Sci* **1984**, *81*, 2280-2284.

49. Baiocco, P.; Barreca, A. M.; Fabbrini, M.; Galli, C.; Gentili, P., Promoting laccase activity towards non-phenolic substrates: a mechanistic investigation with some laccase–mediator systems. *Org Biomol Chem* **2003**, *1*, 191-197.
50. Gall, D. L.; Ralph, J.; Donohue, T. J.; Noguera, D. R., Biochemical transformation of lignin for deriving valued commodities from lignocellulose. *Curr Opin Biotechnol* **2017**, *45*, 120-126.
51. Marinović, M.; Nousiainen, P.; Dilokpimol, A.; Kontro, J.; Moore, R.; Sipila, J.; de Vries, R. P.; Mäkelä, M. R.; Hildén, K., Selective cleavage of lignin β -O-4 aryl ether bond by β -etherase of the white-rot fungus *Dichomitus squalens*. *ACS Sustainable Chemistry & Engineering* **2018**, *6*, 2878-2882.
52. Rahmanpour, R.; Bugg, T. D., Characterisation of Dyp-type peroxidases from *Pseudomonas fluorescens* Pf-5: oxidation of Mn (II) and polymeric lignin by Dyp1B. *Arch Biochem Biophys* **2015**, *574*, 93-98.
53. Hori, C.; Gaskell, J.; Igarashi, K.; Kersten, P.; Mozuch, M.; Samejima, M.; Cullen, D., Temporal alterations in secretome of selective ligninolytic fungi *Ceriporiopsis subvermispora* during growth on aspen wood reveal its strategy of degrading lignocellulose. *Appl Environ Microbiol* **2014**, *80*, 2062-2070.
54. Hofrichter, M., Review: lignin conversion by manganese peroxidase (MnP). *Enzyme Microb Technol* **2002**, *30*, 454-466.
55. Enoki, M.; Watanabe, T.; Nakagame, S.; Koller, K.; Messner, K.; Honda, Y.; Kuwahara, M., Extracellular lipid peroxidation of selective white-rot fungus, *Ceriporiopsis subvermispora*. *FEMS Microbiol Lett* **1999**, *180*, 205-211.
56. Gutiérrez, A.; del Río, J. C.; Martínez-Iñigo, M. J.; Martínez, M. J.; Martínez, Á. T., Production of new unsaturated lipids during wood decay by ligninolytic basidiomycetes. *Appl Environ Microbiol* **2002**, *68*, 1344-1350.
57. Kapich, A. N.; Jensen, K. A.; Hammel, K. E., Peroxyl radicals are potential agents of lignin biodegradation. *FEBS Lett* **1999**, *461*, 115-119.
58. Kapich, A. N.; Korneichik, T. V.; Hatakka, A.; Hammel, K. E., Oxidizability of unsaturated fatty acids and of a non-phenolic lignin structure in the manganese peroxidase-dependent lipid peroxidation system. *Enzyme Microb Technol* **2010**, *46*, 136-140.
59. Ohashi, Y.; Uno, Y.; Amirta, R.; Watanabe, T.; Honda, Y.; Watanabe, T., Alkoxy- and carbon-centered radicals as primary agents for degrading non-phenolic lignin-substructure model compounds. *Org Biomol Chem* **2011**, *9*, 2481-2491.
60. Bohlin, C.; Andersson, P.-O.; Lundquist, K.; Jönsson, L. J., Differences in stereo-preference in the oxidative degradation of diastereomers of the lignin model compound 1-(3, 4-dimethoxyphenyl)-2-(2-methoxyphenoxy)-1, 3-propanediol with enzymic and non-enzymic oxidants. *J Mol Catal B: Enzym* **2007**, *45*, 21-26.
61. Bohlin, C.; Lundquist, K.; Jönsson, L. J., Diastereomer selectivity in the degradation of a lignin model compound of the arylglycerol β -aryl ether type by white-rot fungi. *Enzyme Microb Technol* **2008**, *43*, 199-204.

Supporting Information

1. Chemicals and materials

All chemicals were obtained from commercial suppliers and used without further purification. Acetone, acetonitrile (ACN), chloroform, ethanol (EtOH), n-hexane, methanol (MeOH), petroleum ether 40-60 °C and toluene were all of HPLC grade and purchased from Biosolve BV (Valkenswaard, The Netherlands). Acetic acid (glacial, 100%), citric acid monohydrate (99%), dioxane (anhydrous, 99.8%), ethanol (99.5%), formic acid (98-100%), 1-hydroxybenzotriazole (HBT, wetted with 14% w/w water), laccase from *Trametes versicolor*, lithium bromide (LiBr, 99%) and sodium acetate (99%) were purchased from Sigma Aldrich (St. Louis, MO, USA). DMSO was purchased from Duchefa Biochemie BV (Haarlem, The Netherlands). Veratrylglycerol- β -guaiacyl ether (VerBG) was purchased from ABCR

(Karlsruhe, Germany). Hydrochloric acid (37%) and dimethyl sulfoxide- d_6 (99.8% atom D) were purchased from Merck (Darmstadt, Germany). Di-sodium hydrogen phosphate dihydrate was purchased from VWR (Radnor, PA, USA). Sodium hydroxide (50%) was purchased from Boom BV (Meppel, The Netherlands). The xylanase-enriched commercial enzyme cocktail Rovabio Advance was purchased from Adisseo (Antony, France). Water used in all experiments was purified via a Milli-Q water system (Millipore, Billerica, MA, USA).

2. Experimental methods

Lignin fractionation. Lignin in untreated and fungal-treated wheat straw was fractionated according to Figure S1. Ground wheat straw (~13 g) was soxhlet-extracted in triplicate with acetone in a B-811 system (BÜCHI, Flawil, Switzerland) in Whatman® cellulose extraction thimbles for 3 h. The residue was further extracted with 200 mL of acetone at 40 °C for 4.5 h and centrifuged (18,600 $\times g$, 10 min, 20 °C). The pellet was dried overnight under reduced pressure (30 °C, 0.2 bar) to obtain acetone insoluble material (R1). Triplicates of R1 were subsequently mixed and water-extracted in duplicate with 350 mL of water (dry matter loading 5% (w/w)) with rotary shaking (20 rpm) at 50 °C for 17 h. Insoluble material was removed by centrifugation (18,600 $\times g$, 10 min, 20 °C) and washed 3 times with 200 mL of water before the material was freeze-dried to obtain R2. Dried duplicates were then mixed and ball-milled by using a PM100 planetary ball mill (Retsch, Haan, Germany) in batches of 3 g per 50 mL zirconium dioxide (ZrO₂) grinding jar containing 17 ϕ 10 mm ZrO₂ balls. Milling was performed at 600 rpm with a net milling time of 4 h. After every 15 min of milling, a pause of 10 min was set to prevent the material from overheating. The fractionation was continued in duplicate with two portions of 12 g milled material (R3). R3 was water-extracted at 5% (w/w) dry matter loading under rotary shaking (20 rpm) at 50 °C for 18 h. Insoluble material was removed by centrifugation (38,400 $\times g$, 10 min, 20 °C) and washed twice with 130 mL of water before the material was freeze-dried to obtain R4. All soluble fractions were stored at -20 °C until further analyses.

Purification of acetone extractable lignin. Acetone soluble fractions (S1, 30 mL) were dried under a stream of nitrogen and extracted twice with hexane (10 mL) for 10 min under continuous sonication (Bransonic ultrasonic MH, Branson, Danbury CT, USA). The pellet was collected through centrifugation (4,700 $\times g$, 10 min, 20 °C) and dried under a stream of nitrogen. Residual hexane was removed from the insoluble material by the addition and subsequent evaporation of petroleum ether (40-60 °C) to obtain S1_{pure}.

Purification of water extractable lignin. Water extractable lignin fractions were treated with the xylanase-enriched commercial enzyme cocktail Rovabio Advance to degrade carbohydrates prior to solid phase extraction by using reversed phase chromatography. Hereto, 100 mL of S2 and 250 mL of S4 were concentrated by freeze-drying to approximately 30 mL and sonicated for 10 min, prior to the addition of 3 mL 550 mM sodium acetate buffer (pH 5.5). Enzyme powder was suspended at 12 mg mL⁻¹ in a 50 mM sodium acetate buffer pH 5.5 with rotary shaking (20 rpm, 20 min, 20 °C). The suspension was centrifuged (4700 $\times g$, 10 min, 20 °C) and 10 mL of the supernatant was added to each sample. Samples were subsequently incubated with rotary shaking (20 rpm) at 40 °C for 25 h. Any insoluble material was removed by centrifugation (4700 $\times g$, 10 min, 20 °C) before loading the material on the reversed phase chromatography system.

Enzyme treated water extracts S2 and S4 were purified on a Grace Reveleris Flash chromatography system (Grace, Columbia, MD, USA), equipped with an ELSD and UV detector (recording 280 nm and 310 nm). Samples (40 mL) were manually injected onto a Reveleris

C18 reversed phase cartridge (80 g, particle size 40 μm) (Büchi Labortechnik AG, Flawil, Switzerland). Water (A) and acetonitrile (B), both containing 1% (v/v) formic acid were used as eluents. After activation of the cartridge with eluent B and conditioning of the column with at least 5 column volumes eluent A, the sample was injected. The flow rate was 60 mL min⁻¹ at room temperature. The following gradient was used: 0-3 min, isocratic on 0% B; 3-13 min, linear gradient from 0-60% B; 13-17 min, linear gradient from 60-100% B; 17-25 min, isocratic on 100% B; 25-27 min linear gradient from 100-0% B, 27-31 min, isocratic on 0% B. For S2 of untreated straw (S2-0), the gradient was as follows: 0-3 min, isocratic on 0% B; 3-11 min, linear gradient from 0-48% B; 11-12 min, linear gradient from 48-100% B; 12-20 min, isocratic on 100% B; 20-21 min linear gradient from 100-0% B, 21-25 min, isocratic on 0% B. For S4 after 7 weeks of fungal growth (S4-7), the gradient was as follows: 0-3 min, isocratic on 0% B; 3-33 min, linear gradient from 0-60% B; 33-37 min, linear gradient from 60-100% B; 37-45 min, isocratic on 100% B; 45-47 min linear gradient from 100-0% B, 47-51 min, isocratic on 0% B. In all cases, 20 mL fractions were collected. Fractions between 28 and 60% B were pooled, except for S4-7, for which the fractions between 16.6 and 50% B were pooled. Pools were diluted with water to <20% (v/v) ACN, flash frozen in liquid nitrogen and freeze-dried to obtain S2_{pure} and S4_{pure}.

Saponification of purified water extract after fungal growth (S2-7). To 25 mg of S2-7 2.5 mL 0.2 M NaOH was added and kept at 4 °C for 2 h. Subsequently, 2.5 mL 0.2 M HCl was added to neutralize the sample, while keeping the sample on ice. The saponified lignin products were obtained by solid-phase extraction using a 2 g SEP-PAK C18 cartridge (Waters, Milford, MA, USA). The column was activated with methanol (12 mL), washed with water (60 mL), loaded with the sample (5 mL), washed with water (30 mL) and sequentially eluted by using 25% ACN (8 mL), 50% ACN (8 mL), 75% ACN (8 mL) and 100% ACN (8 mL). The eluates were pooled, diluted with water to <20% (v/v) ACN, flash frozen in liquid nitrogen and freeze-dried.

Production and purification of guaiacyl diketone and syringyl diketone. Diketones were formed through acidolysis of klason lignin and subsequent liquid extraction by a method described by Govender et al.¹ Klason lignin was obtained as previously described.² Mixed softwood klason lignin was used for the production of guaiacyl diketone, whereas for syringyl diketone mixed hardwood klason lignin was used. Klason lignin was dispersed in 0.2 M HCl in aqueous dioxane (90 % v/v dioxane) and incubated for 4 h at 100 °C with shaking every 30 min. After reaction, the samples were cooled to room temperature and partially neutralized by 0.4 M Na₂CO₃. The reaction products were extracted by toluene, dried under a stream of nitrogen, dispersed in 4% methanol and centrifuged to obtain a pre-purified diketone extract in the soluble phase. The extracts were further purified by using flash chromatography. Hereto, the centrifuged extracts were injected onto a Grace Reveleris Flash chromatography system, equipped with a 4 g Reveleris RP Flash cartridge, ELSD detector and UV detector. The eluents used were water (eluent A) and ACN (eluent B), both containing 1% (v/v) formic acid. After activation of the cartridge with eluent B, and washing with 5 column volumes of eluent A, the reaction mixtures were injected. The reaction products were separated by using the following gradient profile: 0-1 min at 3% B (isocratic), 1-12 min linear from 3 to 22% B, 12-14 min linear from 22 to 60% B, 14-14.5 min linear from 60 to 100% B, 14.5-15.7 min at 100% B (isocratic). The flow was set at 18 mL min⁻¹ and fractions of 7 mL were collected. The resulting fractions were analyzed by using RP-UHPLC-PDA-MS as previously described.³ Fractions that contained the reaction products and that were free of by-products were pooled, flash frozen in liquid nitrogen and freeze-dried.

Enzymatic synthesis and purification of veratryl model compounds. Co-oxidized Veratrylglycerol- β -guaiacyl ether (VerBG_{ox}), hydroxypropioveratrone (HPVer) and dihydroxypropioveratrone (DHPVer) were enzymatically synthesized by incubating veratrylglycerol- β -guaiacyl ether (VerBG) with laccase and 1-hydroxybenzotriazole (HBT), after which the reaction products were purified. Two batches of 50 mg VerBG and 125 mg HBT were incubated in 40 mL phosphate citrate buffers at pH 4 and pH 6 (prepared from 100 mM phosphate and 50 mM citrate stock solutions). Laccase was added to obtain a final activity of 10 U mL⁻¹.³ After 48 h, the reaction mixtures were centrifuged (5000 \times g, 20 °C, 10 min) and the soluble products were purified by using flash chromatography as described for the benzyl diketones, using a different gradient.

The reaction products and remaining VerBG were separated by using the following gradient profile: 0-5 min at 0% B (isocratic), 5-33 min from 0 to 32% B (linear gradient), 33-33.6 min from 32 to 100% B (linear gradient), 33.6-36 min at 100% B (isocratic). Fractions of 4 mL were collected.

The diketone 1-(3,4-dimethoxyphenyl)propane-1,2-dione was prepared by using VerBG_{ox} as a starting material (prepared as described above). VerBG_{ox} was then converted to the diketone based on the procedure reported by Rahimi et al.⁴ Hereto, 5 mg of VerBG_{ox} was dissolved in 1.5 mL of aqueous formic acid (90% v/v). The solution was incubated for 20 h at 110 °C, after which the solution was cooled down and formic acid was evaporated under a flow of nitrogen. The remaining sample was analyzed by using UHPLC-MS and contained the diketone, guaiacol and a VerBG_{ox}-formate ester (data not shown). The diketone was then purified using the same flash chromatography procedure as described above and lyophilized.

3. Analytical methods

Quantitative py-GC-MS with ¹³C lignin as internal standard. Pyrolysis was performed with an EGA/PY-3030D Multi-shot pyrolyzer (Frontier Laboratories, New Ulm, MN, USA) equipped with an AS-1020E Autoshot auto-sampler as previously described.⁵⁻⁶ Samples were weighed using an XP6 excellence-plus microbalance (Mettler Toledo, Columbus, OH, USA). Ten μ L of a ¹³C wheat straw lignin internal standard (IS) solution (1 mg mL⁻¹ ethanol/chloroform 50:50 v/v) was mixed with ~80 μ g of sample and dried before analysis. Pyrolysis was performed at 500 °C for 1 min with an interface temperature of 300 °C. For the analyses of unextractable residues (R1-R4), the pyrolyzer was coupled to a Trace GC equipped with a DB-1701 fused-silica capillary column (30 m \times 0.25 mm i.d. 0.25 μ m film thickness) coupled to a DSQ-II mass spectrometer (both Thermo Scientific, Waltham, MA, USA). Pyrolysis products were injected on the column via split/splitless injection (at 250 °C) with a splitratio of 1:133 and helium was used as carrier gas with constant flow at 1.5 mL min⁻¹. The GC oven was programmed from 70 °C (2 min) to 270 °C at 5 °C min⁻¹ and held at 270 °C for 15 min. MS detection was used with EI at 70 eV, a source temperature of 250 °C, a scan range of m/z 50-550 and a dwell time of 25 ms to ensure at least 25 data points per peak. Compounds were identified by comparing retention time and mass spectrum with standards, the NIST library and data published by Ralph and Hatfield (1991).⁷ Lignin-derived pyrolysis products were monitored in selected ion monitoring (SIM) mode on the two most abundant fragments per compound (both ¹²C and ¹³C).⁵ The compound guaiacyl diketone (GDK) was monitored on its m/z 194 fragment rather than its two most abundant fragments (m/z 153, 123) due to the fact that the closely eluting compounds in that region of the pyrogram did not allow further segmenting. The area of GDK was multiplied by 25 (relative intensity m/z 194/ m/z (153+123) = 25) to be comparable to the other compounds. For correction of matrix-effects similar behavior as syringyl diketone (SDK) was assumed.

For the analyses of (purified) extracts (~40 µg) and synthesized compounds (~5 µg, no ^{13}C -IS was added), the pyrolyzer was coupled to a Trace 1300 GC coupled to an Exactive Orbitrap Mass Spectrometer (both Thermo Scientific). The same column, injection and oven settings were used, with the only difference being the injection temperature at 280°C. The MS was operated in full MS mode, with EI at 70 eV, a source temperature of 275°C, a resolution of 60,000, AGC target at 10^6 , maximum IT at 'auto' and a scan range of m/z 35-550. Relative response factors (RRF) for lignin-derived pyrolysis products on the py-GC-HR-MS system were determined as previously described.⁵ RRFs for newly synthesized guaiacyl and syringyl diketones, were determined relative to vanillin and syringaldehyde, respectively. Data was processed as previously described.⁶ DSQ-II pyrograms were processed by Xcalibur 2.2 software. Orbitrap pyrograms were processed by TraceFinder 4.0 software. In both programs, the selected ions (two most abundant on DSQ-II, single most abundant on Orbitrap, Table S1) per compound were automatically integrated using ICIS peak integration with optimized settings per compound. A manual correction was only applied when irregular peak shapes led to erroneous peak integration with method settings. Lignin contents and relative abundances of lignin-derived pyrolysis products were calculated as described previously.⁶

NMR spectroscopy. NMR spectra were recorded at 25 °C with Bruker's standard pulse sequences on a Bruker AVANCE III 600 MHz NMR spectrometer (Bruker BioSpin, Rheinstetten, Germany) equipped with a 5 mm cryoprobe located at MAGNEFY (MAGNETic resonance research Facility, Wageningen, The Netherlands) and based on previously reported procedures.⁸⁻¹² Around 20 mg of purified extracts (see Figure S1) was dissolved in 0.6 mL DMSO- d_6 and transferred to an NMR tube. ^1H - ^{13}C HSQC NMR spectra were recorded by using the adiabatic "hsqcetgpsisp2.2" pulse sequence using the following parameters: spectral width of 7,200 Hz (12 ppm) in F1 (^1H) using 2018 increments for an acquisition time (AQ) of 0.14 s and interscan delay (D1) of 0.86 s and a spectral width of 33,000 Hz (220 ppm) in F2 (^{13}C) using 400 increments with an AQ of 6 ms with 16 scans per increment. The $^1J_{\text{CH}}$ used was 145 Hz. Processing used Gaussian apodization (GB = 0.001, LB = -0.2) in ^1H and a squared cosine function and one level of linear prediction (32 coefficients) in the ^{13}C dimension. Multiplicity edited ^1H - ^{13}C HSQC NMR spectra were recorded by using the "hsqcedetgpsisp2.2", with D21 set to $1/2^1J_{\text{CH}}$ to obtain spectra with opposite signals for -CH/-CH₃ groups and -CH₂ groups. D21 was set to $1/3^1J_{\text{CH}}$ to obtain spectra with opposite signals for -CH and -CH₃ groups.

^1H - ^{13}C HMBC NMR spectra were recorded by using the "hmbcgp1pndqf" pulse sequence using the following parameters: spectral width of 7,200 Hz (12 ppm) in F1 (^1H) using 8192 increments with an AQ of 0.57 s and D1 of 1.5 s and a spectral width of 39,200 Hz (260 ppm) in F2 (^{13}C) using 400 increments with an AQ of 10 ms with 64 scans per increment, using a 76 ms long-range coupling delay (D6). Processing used Gaussian apodization (GB = 0.8, LB = -5.0) in ^1H and a squared sine function and one level of linear prediction (32 coefficients) in the ^{13}C dimension.

The 3D ^1H - ^{13}C -TOCSY-HSQC spectrum was recorded by using the "mlevhsqcetgp3d" pulse sequence using the following parameters: spectral width of 7,200 Hz (12 ppm) in F3 (^1H) using 2018 increments with an AQ of 0.14 s and D1 of 0.86 s, a spectral width of 9000 Hz (35-95 ppm) in F2 (^{13}C) using 200 increments with an AQ of 11 ms, a spectral width of 7,200 Hz (12 ppm) in F1 (^1H) using 128 increments with an AQ of 8.9 ms, with 8 scans per increment, using a 100 ms TOCSY spin lock period (D9). Processing used Gaussian apodization (GB = 0.001, LB = -0.2) in F3 (^1H) and a squared cosine function and in the F2 (^{13}C) and F3 (^1H) dimension.

^1H - ^1H COSY NMR spectra were recorded for synthesized model compounds by using the "cosygppqf" pulse sequence using the following parameters: spectral width of 6,000 Hz (10 ppm) in F2 (^1H) using 8192 increments with an AQ of 0.68 s and D1 of 1 s and a spectral width of 6,000 Hz (10 ppm) in F1 (^1H) using 400 increments with an AQ of 66 ms with 2 scans per increment.

For all experiments, the solvent peak (DMSO- d_6) was used as an internal reference (δ_c 39.5 ppm; δ_H 2.49 ppm) and the data were processed with Bruker TopSpin 4.0.5 following manual phase correction and automatic baseline correction. Correlation peaks were assigned by comparison with literature.^{9, 13-17}

Semiquantitative analysis of the HSQC volume integrals was performed according to del Río et al. (2012).⁹ $S_{2,6}$, G_2 and $H_{2,6}$ signals were used for S, G and H units, respectively, where S and H integrals were logically halved. Oxidized analogues were estimated in a similar manner. Tricin, *p*CA and FA were similarly estimated from their respective $T_{2,6'}$, $pCA_{2,6}$ and FA_2 signals, respectively. $H_{2,6}$ integrals were corrected for the overlapping phenylalanine cross-peak (PHE_{3,5}) by subtraction of the isolated PHE_{2,6} cross-peak.¹⁴ Alternatively, in the aliphatic oxygenated region β -O-4 substructures were estimated from their C_β - H_β correlations, since they were shown to be interfered to a lesser extent by the presence of carbohydrates.^{6, 8} C_α -oxidized analogues of the β -O-4 substructures were estimated from their C_β - H_β correlations as well. For phenylcoumaran and resinol substructures, their respective C_α - H_α correlations were used. Volume integrals for resinol substructures were logically halved. DHPV/DHPS and HPV/HPS were estimated from their C_β - H_β correlations. Volume integration was performed at equal contour levels. Contour levels were normalized at equal size of the $-\text{OCH}_3$ integral. Amounts were calculated as a percentage of total lignin ($H + G + G_{ox} + S + S_{ox}$) (per 100 aromatic rings).

Size-exclusion chromatography. Alkaline size-exclusion chromatography (SEC) was performed as described by Constant et al. (Method D).¹⁸ Briefly, freeze-dried samples were dissolved (1 mg mL^{-1}) in 0.5 M NaOH and separated with the same solvent by using two TSKgel GMPWxl columns at 30 °C with a 1 mL min^{-1} flowrate. Absorption was monitored at 280 nm with an ultraviolet spectroscopy detector. Sodium polystyrene sulphonate (PSS) standards and phenol were used for calibration. Protobind™ 1000 lignin (GreenValue S.A, Switzerland) was used as reference. For organic SEC analyses, freeze-dried samples were dissolved (10 mg mL^{-1}) in DMSO containing 0.5% w/v LiBr, filtered through a $0.45 \mu\text{m}$ PTFE syringe filter and analyzed as previously described using PSS standards for system calibration and RI and UV (280 nm) for detection.¹⁹ Multi-angle light scattering (MALS) correction factors were applied to obtain a more accurate description of the absolute molar masses of the extracted lignin fractions as described by Zinovyev et al.²⁰

4. Extraction and purification of diagnostic substructures

As fungal action proceeded, lignin substructures became selectively extractable from the remaining wheat straw by acetone and water (Figure S1, Figure S2 and Table S2). Ball-milling of fungal treated wheat straw yielded additional water-extractable lignin and resulted in similar recoveries of lignin in the insoluble residue (R4) after sequential extraction for all time points of fungal growth ($\sim 70\%$ w/w) (Figure S2). This result became apparent by performing an additional water extraction, a step that is uncommon in classical lignin isolation procedures.²¹⁻²⁴ The water extractability could simply have originated from an increased surface contact between the straw particles and the solvent, while it might also point to lignin degradation during ball-milling.²⁵ Based on py-GC-MS analyses, it is suggested that ball-milling did not induce major structural changes (Table S3). The degradation of a few linkages

within the macromolecule might, however, have profound consequences for its molecular weight distribution, especially when lignin is more linear than generally considered.²⁶ Analytical tools that measure the abundance of occurring bonds cannot pick up these relatively subtle changes, and as such are not conclusive for evaluating ball-milling effects on lignins macromolecular structure.⁸ All determinations of lignins molecular weight distribution, however, require lignin to be soluble in a particular solvent system, and, therefore, require some extent of ball-milling.²⁷ In fact, the effects of ball-milling on the macromolecular lignin structure can, thus, not be properly evaluated. The origin of water extractable lignin, therefore, remains to be further elucidated.

For detailed structural characterization of lignin degradation products, the obtained extracts were purified (Figure S1). Acetone solubles were washed with hexane, primarily to remove ceriporic acids, which are known secondary metabolites produced by the fungus (Figure S3).²⁸ Water-soluble extracts were purified by enzymatic carbohydrate degradation and subsequent reversed phase chromatography. Decent recoveries were achieved for all extracts and, more importantly, the C_α-oxidized structures indicative of fungal action were fully preserved (Table S4-S6). Being particularly rich in diagnostic substructures, the purified water extract obtained before ball-milling from seven weeks treated straw was used for further extensive structural characterization.

5. Tentative annotation of cyclohexadienone ketals

Besides the phenylketols, a clear correlation peak at δ_C/δ_H 51.6/3.6 could be observed in the HSQC spectrum of the fungal treated straw extract (Figure 3B). Multiplicity edited HSQC analysis demonstrated that the signal originated from a methyl group and saponification of the extract showed that this group was part of a base-labile substructure (Figure S6, Figure S7 Table S11, Table S12). The correlation peak at δ_C/δ_H 51.6/3.6 might, therefore, partially originate from methyl esters, as judged from a characteristic HMBC cross-peak at 172 ppm, part of which might be benzoic acid methyl esters, although no correlation peak was visible in the aromatic region of the spectrum.¹³ Based on the reappearance of intact β -O-4 aryl ethers and non-oxidized guaiacyl and syringyl subunits upon saponification together with chemical shift predictions, we tentatively assigned the correlation peak to methoxyl groups of cyclohexadiene ketal substructures (Figure S8). These structures have previously been suggested to result from aryl cation radical formation in lignin model compounds.²⁹⁻³¹ However, further diagnostic peaks in HSQC, HMBC or 3D-TOCSY-HSQC spectra could not be observed. Further analyses are, therefore, required for confirming the presence of these substructures.

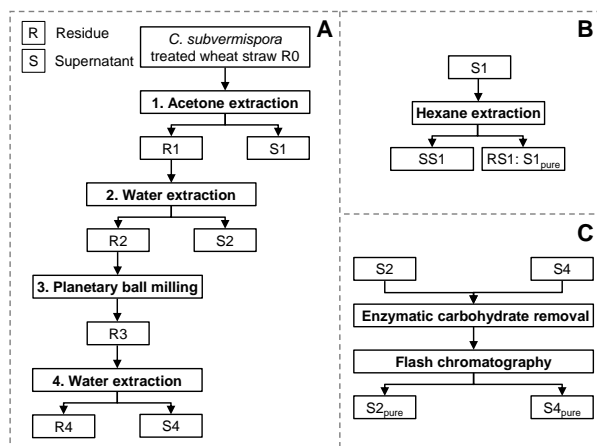


Figure S1. Fractionation scheme for untreated and fungal-treated wheat straw (A) and purification of acetone (B) and water extracts (C).

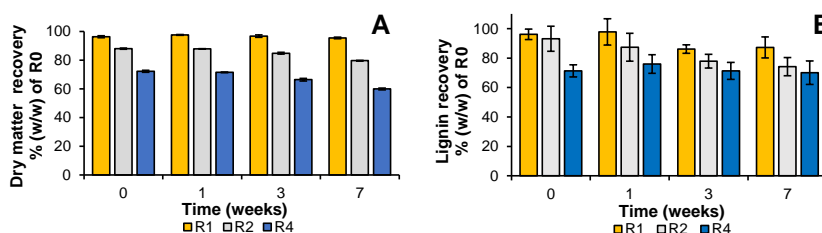


Figure S2. Dry matter and lignin recovery versus starting material during fractionation. Average and standard deviation of duplicates. Codes refer to Figure S1.

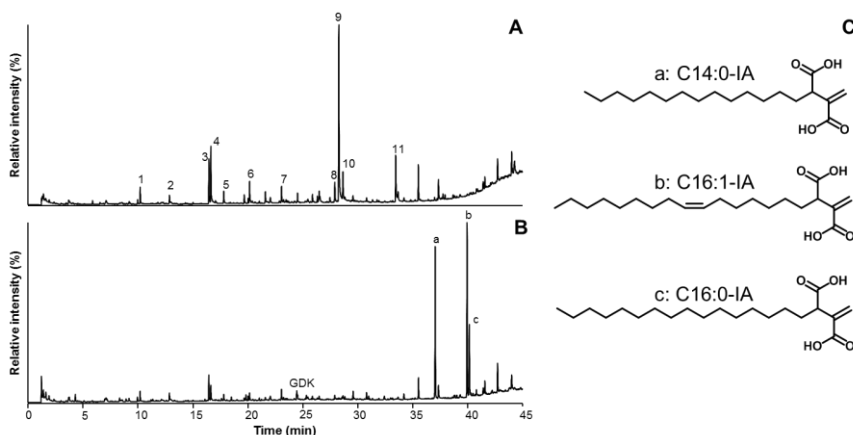


Figure S3. Pyrograms (TIC) of acetone extractives (Figure 1, S1) from untreated (A) and 7 weeks *C. subvermispora* treated (B) wheat straw and structures of annotated ceriporic acids (C). Numbers refer to major lignin-derived compounds: (1) guaiacol; (2) 4-methylguaiacol; (3) 4-vinylguaiacol; (4) 4-vinylphenol; (5) syringol; (6) vanillin; (7) acetovanillone; (8) acetosyringone; (9) *trans*-coniferyl alcohol; (10) *trans*-coniferaldehyde; (11) *trans*-sinapaldehyde. Letters refer to annotated ceriporic acids presented in (C).²⁸ GDK: guaiacyl diketone. Note that ¹³C-IS lignin was added to these samples, which is included in TIC of these pyrograms.

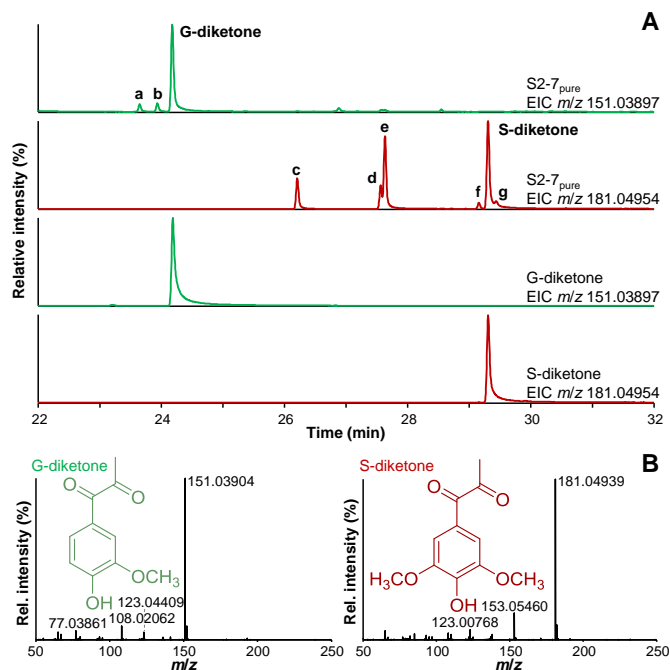


Figure S4. Extracted ion chromatograms (EIC) of purified water extract from seven weeks *C. subvermispora* treated wheat straw and synthesized standards (A) and corresponding EI-HR-MS spectra (B). Letters refer to the following compounds: a propiovanillone; b guaiacyl vinyl ketone; c syringaldehyde; d syringic acid methyl ester; e acetosyringone; f propiosyringone; g syringyl vinyl ketone. Note that benzyl diketones have previously been annotated as benzoyl acetaldehydes on the basis of MS spectra and retention times published by Ralph & Hatfield.⁶⁻⁷ The synthesized standards enabled us to unambiguously annotate these compounds as guaiacyl- and syringyl diketones. Furthermore, standards were obtained in sufficient amounts to determine their relative response factors which allowed for a more accurate quantification. See Table S12 for NMR characterization data of the synthesized benzyl diketones.

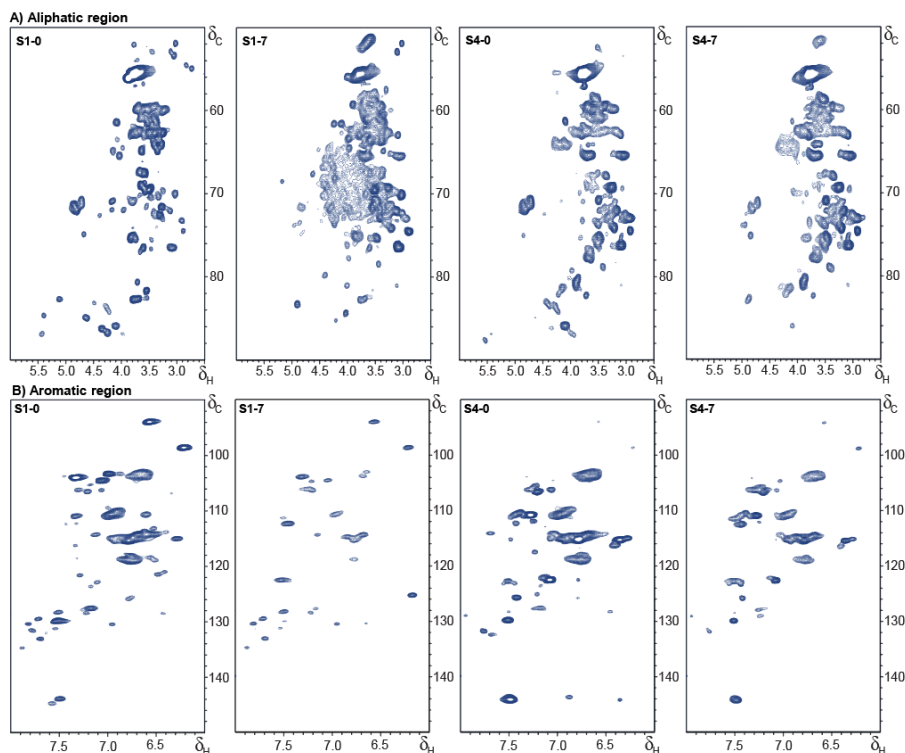


Figure S5. Aliphatic (A) and aromatic (B) regions of ^1H - ^{13}C HSQC NMR spectra of purified acetone (S1) and purified water-extracts after planetary ball-milling (S4) from untreated (0) and seven weeks *C. subvermispota* treated (7) wheat straw.

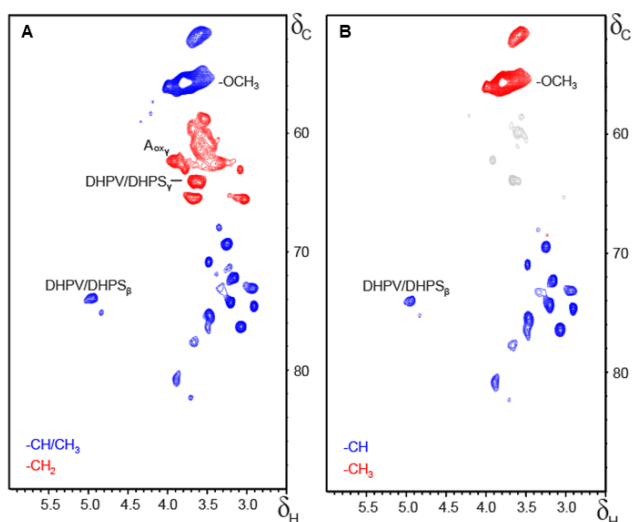


Figure S6. Aliphatic region ($\delta_{\text{C}}/\delta_{\text{H}}$ 50-90/2.5-6.0) of multiplicity edited ^1H - ^{13}C HSQC NMR spectra of purified water extract from seven weeks *C. subvermispota* treated wheat straw. A: D21 set to $1/2 J_{\text{CH}}$, B: D21 set to $1/3 J_{\text{CH}}$.

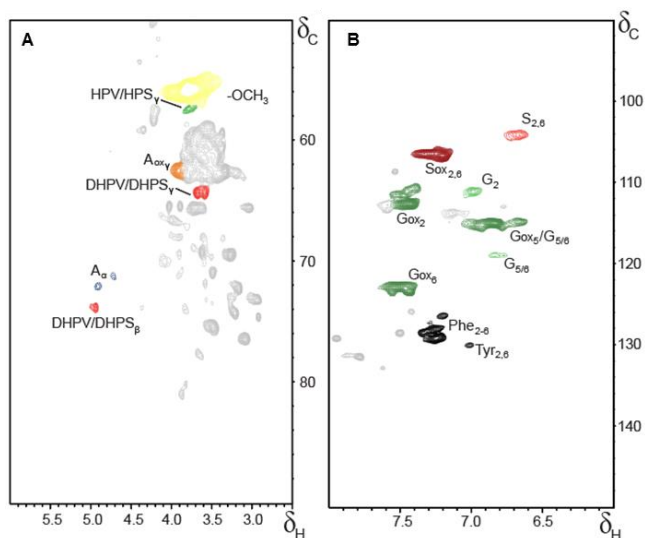


Figure S7. Aliphatic (A) (δ_C/δ_H 50-90/2.5-6.0) and aromatic (B) (δ_C/δ_H 90-150/6.0-8.0) region of ^1H - ^{13}C HSQC NMR spectra of saponified purified water extracts from seven weeks *C. subvermispora* treated wheat straw. See Figure 1 for comparison to sample before saponification and abbreviations for annotated signals.

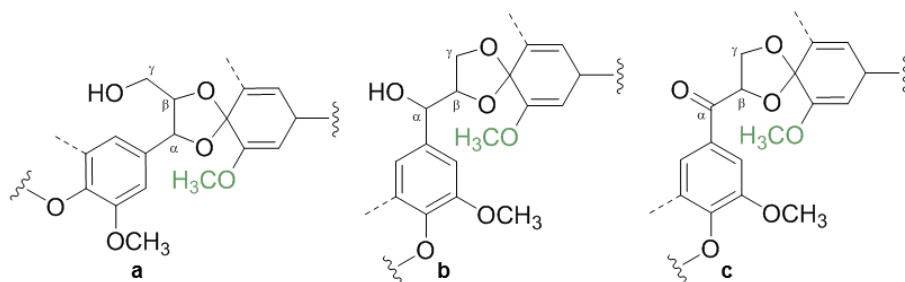


Figure S8. Tentatively assigned cyclohexadiene ketal substructures. Structure (a) and structure (b),(c) originate from cyclization with $\text{C}_\alpha\text{-OH}$ and $\text{C}_\gamma\text{-OH}$, respectively. Annotated $-\text{OCH}_3$ is presented in green.

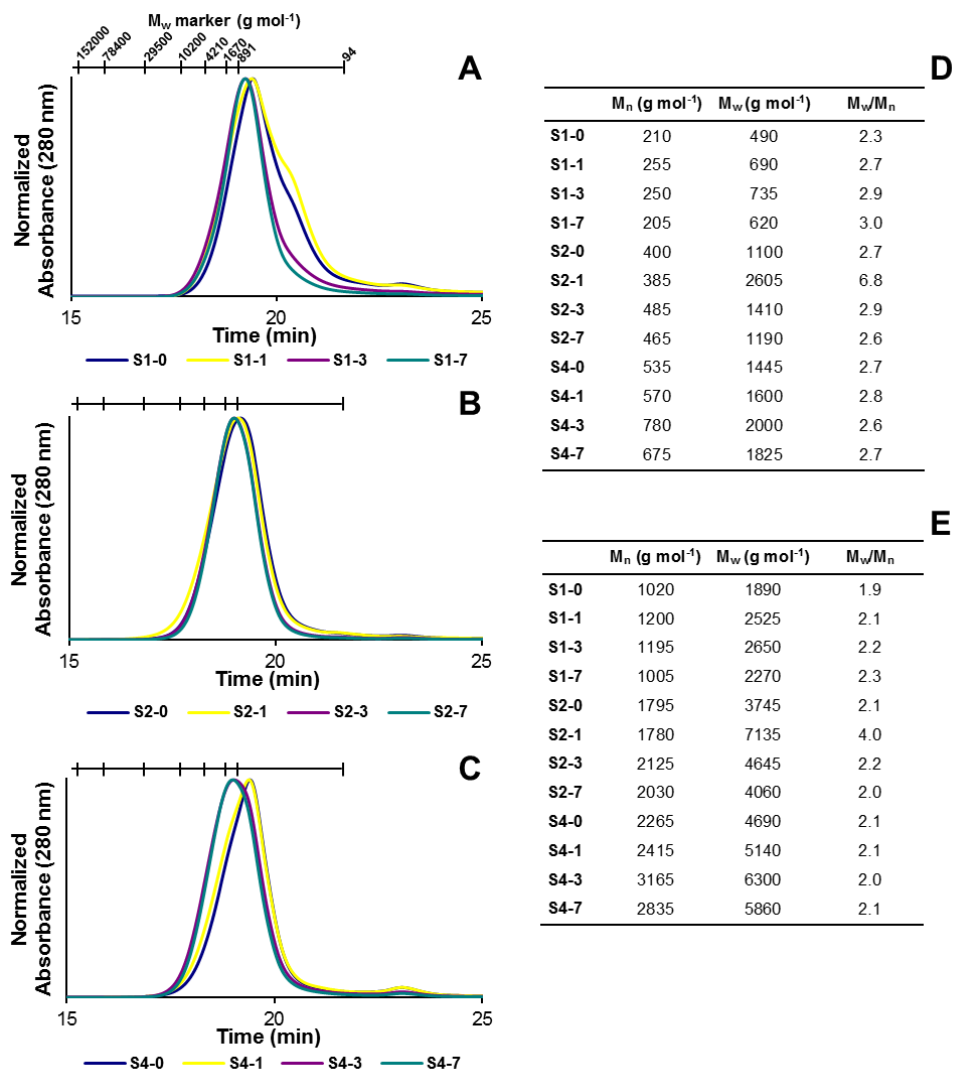


Figure S9. Normalized alkaline SEC chromatograms of S1 (A), S2 (B), S4 (C), organic SEC statistical moments of molar masses calculated based on PSS standards (D) and organic SEC statistical moments of molar masses calculated based on MALS-corrected standards (E).

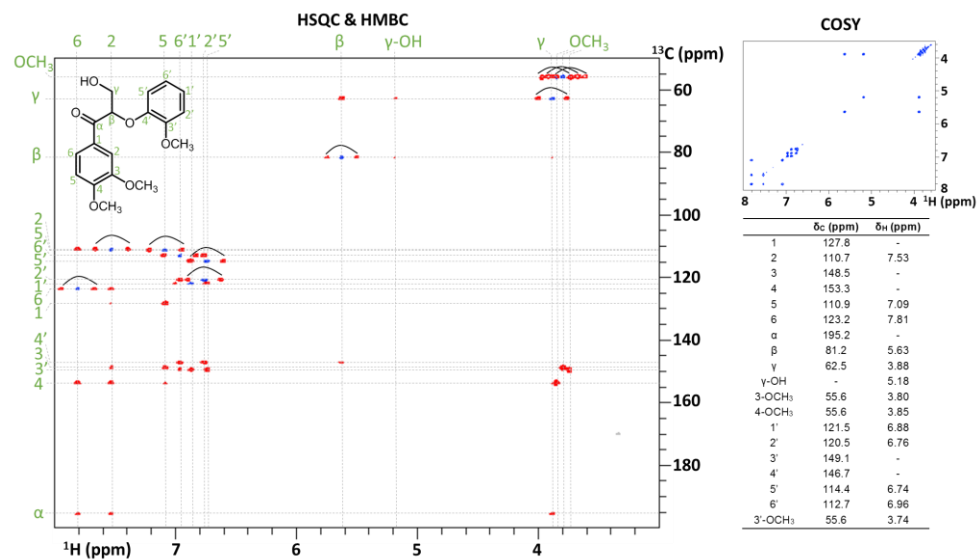


Figure S10. ^1H - ^{13}C HSQC (blue) and ^1H - ^{13}C HMBC (red) annotation of VerBGox.

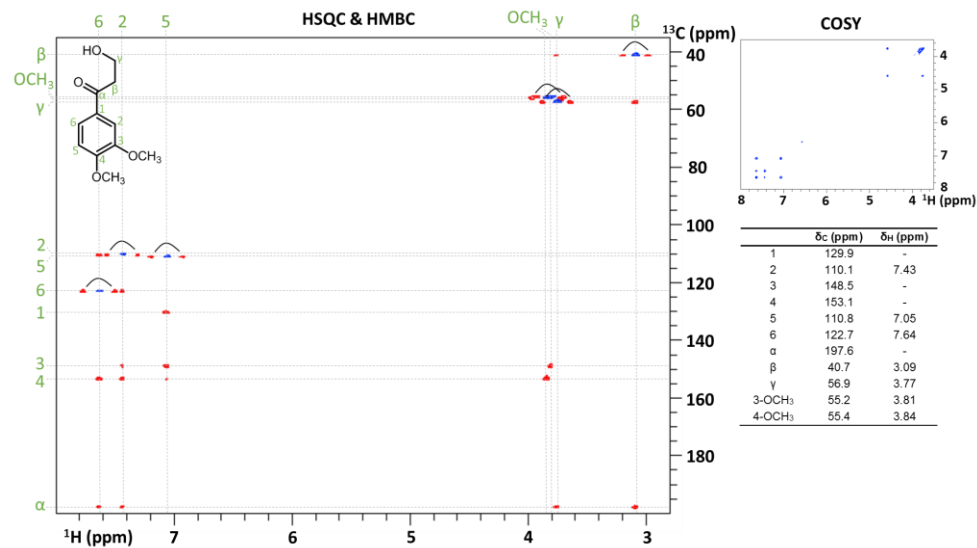


Figure S11. ^1H - ^{13}C HSQC (blue) and ^1H - ^{13}C HMBC (red) annotation of HPVer.

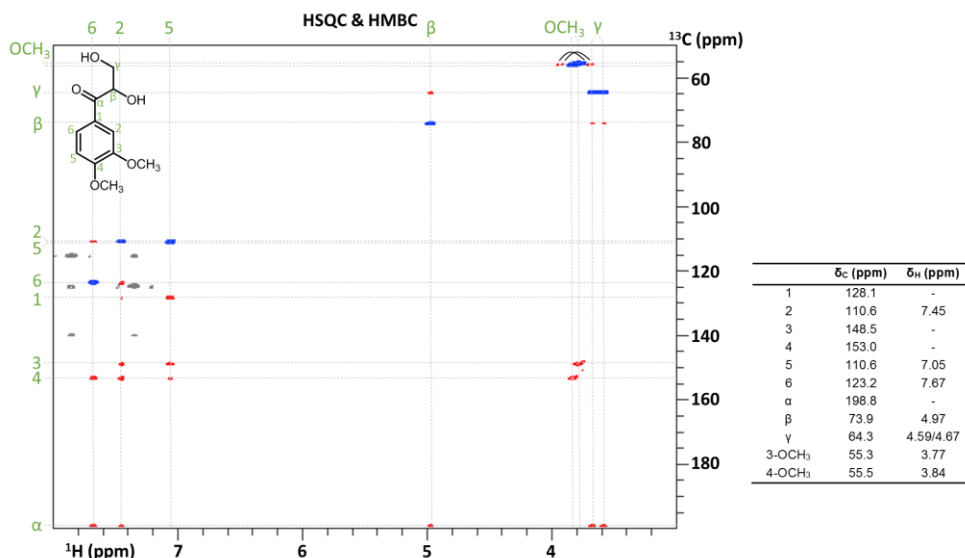


Figure S12. ^1H - ^{13}C HSQC (blue) and ^1H - ^{13}C HMBC (red) annotation of DHPVer.

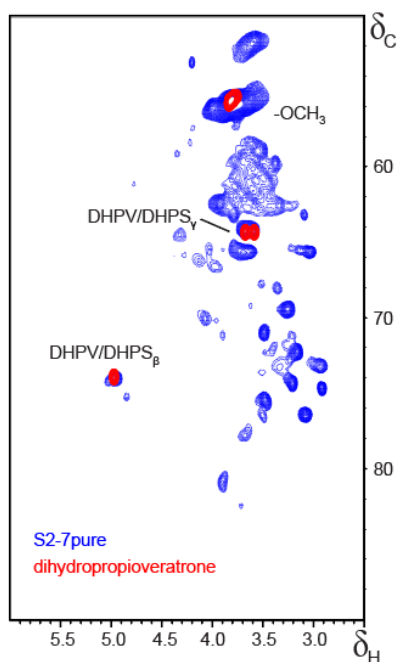


Figure S13. Overlaid aliphatic region (δ_C/δ_H 50-90/2.5-6.0) of ^1H - ^{13}C HSQC NMR spectra of purified water extracts from seven weeks *C. subvermispota* treated wheat straw (blue) and enzymatically synthesized dihydropropioveratrone (DHPVer, red).

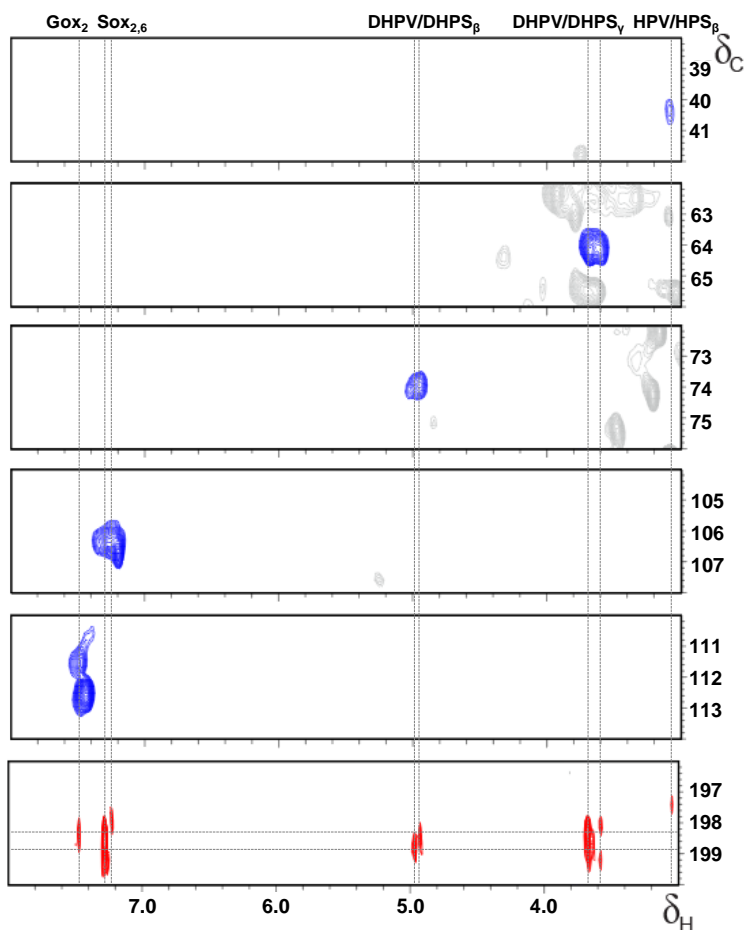


Figure S14. Sections of ^1H - ^{13}C HSQC (blue) and ^1H - ^{13}C HMBC (red) spectra of purified water extract from seven weeks *C. subvermispora* treated wheat straw showing the main correlations with the diagnostic carbonyl signals.

Table S1. Identity and structural classification of lignin-derived pyrolysis products by ^{13}C -IS py-GC-HR-MS.

#	Compound	CAS	Retention time (min)	Structural feature	Sidechain length	$M_w^{12}\text{C}$ (g mol $^{-1}$)	Quan ion ^{12}C [M-e]	$M_w^{13}\text{C}$ (g mol $^{-1}$)	Quan ion ^{13}C [M-e]
1	phenol	108952	9.79	H, unsub.	0	94	94.04132	100	100.06145
2	guaiacol	90051	10.03	G, unsub.	0	124	124.05188	131	115.04853
3	2-methylphenol	95487	11.03	H, methyl	C $_{\alpha}$	108	108.05698	115	115.08045
4	4-methylphenol (+3-MP)	106445	12.00	H, methyl	C $_{\alpha}$	108	107.04914	115	114.07263
5	4-methylguaiacol	93516	12.71	G, methyl	C $_{\alpha}$	138	138.06753	146	146.09437
6	2,4-dimethylphenol	105679	13.18	H, methyl	C $_{\alpha}$	122	107.04914	130	114.07263
7	4-ethylphenol	123079	14.25	H, misc.	C $_{\beta}$	122	107.04914	130	114.07263
8	4-ethylguaiacol	2785899	14.83	G, misc.	C $_{\beta}$	152	137.05971	161	145.08654
9	4-vinylguaiacol	7786610	16.29	G, vinyl	C $_{\beta}$	150	150.06753	159	159.09754
10	4-vinylphenol	2628173	16.46	H, vinyl	C $_{\beta}$	120	120.05697	128	128.08381
11	eugenol	97530	16.89	G, misc.	C $_{\gamma}$	164	164.08318	174	174.11673
12	4-propylguaiacol	2785877	16.99	G, misc.	C $_{\gamma}$	166	137.05971	175	145.08654
13	syringol	91101	17.64	S, unsub.	0	154	154.06245	162	162.08928
14	cis-isoeugenol	97541	18.25	G, misc.	C $_{\gamma}$	164	164.08318	174	174.11673
15	4-propenylphenol	539128	19.24	H, misc.	C $_{\gamma}$	134	133.06479	143	142.09498
16	trans-isoeugenol	97541	19.50	G, misc.	C $_{\gamma}$	164	164.08318	174	174.11673
17	4-methylsyringol	6638057	19.86	S, methyl	C $_{\alpha}$	168	168.07810	177	177.10829
18	vanillin	121335	19.99	G, C $_{\alpha}$ -O	C $_{\alpha}$	152	151.03897	160	159.06581
19	4-propylneguaiccol	-	20.23	G, misc.	C $_{\gamma}$	162	162.06753	172	172.10108
20	4-alleneguaiccol	-	20.49	G, misc.	C $_{\gamma}$	162	162.06753	172	172.10108
21	homovanillin	5603242	21.44	G, C $_{\beta}$ -O	C $_{\beta}$	166	137.05971	175	145.08654
22	4-ethylsyringol	14059928	21.58	S, misc.	C $_{\beta}$	182	167.07022	192	176.10046
23	vanillic acid methyl ester ^a	3943746	21.82	G, C $_{\alpha}$ -O	C $_{\alpha}$	182	182.05736	191	191.08766
24	acetovanillone	498022	21.89	G, C $_{\alpha}$ -O	C $_{\beta}$	166	151.03897	175	159.06581
25	4-hydroxybenzaldehyde	123080	22.76	H, C $_{\alpha}$ -O	C $_{\alpha}$	122	121.02848	129	128.05189
26	4-vinylsyringol	28343228	22.90	S, vinyl	C $_{\beta}$	180	180.07810	190	190.11164
27	guaiacylacetone	2503460	23.10	G, C $_{\beta}$ -O	C $_{\gamma}$	180	137.05971	190	145.08654
28	4-allylsyringol	6627889	23.31	S, misc.	C $_{\gamma}$	194	194.09373	205	205.13065
29	propiovanillone	1835149	23.79	S, C $_{\alpha}$ -O	C $_{\gamma}$	180	151.03897	190	159.06581
30	guaiacyl vinyl ketone	-	24.09	G, C $_{\alpha}$ -O	C $_{\gamma}$	178	151.03897	188	159.06581
31	guaiacyl diketone	2034608	24.32	G, C $_{\alpha}$ -O, C $_{\beta}$ -O	C $_{\gamma}$	194	151.03897	204	159.06581
32	cis-4-propenylsyringol	26624135	24.43	S, misc.	C $_{\gamma}$	194	194.09373	205	205.13065
33	4-propynylsyringol	-	25.06	S, misc.	C $_{\gamma}$	192	192.07810	203	203.11500
34	4-allenylsyringol	-	25.27	S, misc.	C $_{\gamma}$	192	192.07810	203	203.11500
35	trans-4-propenylsyringol	26624135	25.72	S, misc.	C $_{\gamma}$	194	194.09373	205	205.13065
36	dihydroconiferyl alcohol	2305137	25.81	S, C $_{\gamma}$ -O	C $_{\gamma}$	182	137.05971	192	145.08654
37	syringaldehyde	134963	26.34	S, C $_{\alpha}$ -O	C $_{\alpha}$	182	182.05736	191	191.08755
38	cis-coniferyl-alcohol	458355	26.42	G, C $_{\gamma}$ -O	C $_{\gamma}$	180	137.05971	190	145.08654
39	homosyringaldehyde	-	27.32	S, C $_{\beta}$ -O	C $_{\beta}$	196	167.07027	206	176.10046
40	syringic acid methyl ester ^a	884355	27.66	S, C $_{\alpha}$ -O	C $_{\alpha}$	212	212.06793	222	222.10147
41	acetosyringone	2478388	27.76	S, C $_{\alpha}$ -O	C $_{\beta}$	196	181.04954	206	190.07973
42	trans-coniferyl alcohol	458355	28.11	G, C $_{\gamma}$ -O	C $_{\gamma}$	180	137.05971	190	145.08654
43	trans-coniferinaldehyde	458366	28.50	G, C $_{\gamma}$ -O	C $_{\gamma}$	178	147.04406	188	156.07425
44	syringylacetone	19037582	28.68	S, C $_{\beta}$ -O	C $_{\gamma}$	210	167.07027	221	176.10046
45	propiosyringone	5650431	29.29	S, C $_{\alpha}$ -O	C $_{\gamma}$	210	181.04954	221	190.07973
46	syringyl diketone	6925651	29.43	S, C $_{\alpha}$ -O, C $_{\beta}$ -O	C $_{\gamma}$	224	181.04954	235	190.07973
47	syringyl vinyl ketone	-	29.57	S, C $_{\alpha}$ -O	C $_{\gamma}$	208	181.04954	219	190.07973
48	dihydrosinapyl alcohol	20736258	31.13	G, C $_{\gamma}$ -O	C $_{\gamma}$	212	168.07841	223	177.10829
49	cis-sinapyl alcohol	537337	31.63	S, C $_{\gamma}$ -O	C $_{\gamma}$	210	167.07027	221	176.10046
50	trans-sinapyl alcohol	537337	33.31	S, C $_{\gamma}$ -O	C $_{\gamma}$	210	167.07027	221	176.10046
51	trans-sinapaldehyde	4206580	33.54	S, C $_{\gamma}$ -O	C $_{\gamma}$	208	208.07301	219	219.10994

^a: not included in py-GC-MS analyses on DSQ-II system.

Table S2. ^{13}C -IS py-GC-MS relative abundance of lignin derived pyrolysis products in unpurified acetone and water extracts of untreated and *C. subvermispota* treated wheat straw. Corrected for RRF and relative abundance of ^{13}C analogues. Sum on the bases of structural classification (Table S1) according to van Erven et al. (2018).⁶ Average and standard deviation of analytical duplicates on pooled biological triplicates. Codes refer to Figure 1.

	S1 (weeks)		S2 (weeks)		S4 (weeks)	
	0	7	0	7	0	7
Lignin subunits (%)						
H	11.7 ± 0.2	7.9 ± 0.8	14.1 ± 0.0	14.8 ± 0.5	7.7 ± 0.2	10.2 ± 0.2
G	65.6 ± 0.0	61.7 ± 4.4	63.1 ± 0.1	54.2 ± 0.3	69.1 ± 0.3	61.8 ± 0.5
S	22.7 ± 0.2	30.4 ± 5.1	22.8 ± 0.0	31.1 ± 0.2	23.2 ± 0.4	28.0 ± 0.7
S/G	0.35 ± 0.0	0.50 ± 0.1	0.36 ± 0.0	0.57 ± 0.0	0.34 ± 0.0	0.45 ± 0.0
Structural moieties (%)						
Unsubstituted	4.7 ± 0.2	7.1 ± 0.6	13.8 ± 0.1	31.9 ± 0.4	5.1 ± 0.4	12.0 ± 0.6
Methyl	1.7 ± 0.1	1.7 ± 0.2	5.9 ± 0.0	4.0 ± 0.0	2.1 ± 0.2	2.8 ± 0.2
Vinyl	19.4 ± 0.2	10.2 ± 0.8	35.6 ± 0.2	6.7 ± 0.1	47.9 ± 1.5	35.2 ± 1.7
4-VP ^a	8.9 ± 0.2	3.1 ± 0.3	7.1 ± 0.0	1.7 ± 0.0	5.5 ± 0.2	5.7 ± 0.1
4-VG ^b	9.2 ± 0.0	5.7 ± 0.4	26.2 ± 0.2	4.1 ± 0.1	40.2 ± 1.2	27.3 ± 1.5
C _α -ox	8.0 ± 0.3	12.7 ± 1.1	6.0 ± 0.1	38.2 ± 0.0	9.8 ± 0.8	20.7 ± 0.8
G-diketone	0.5 ± 0.0	2.4 ± 0.0	0.3 ± 0.0	8.0 ± 0.1	0.4 ± 0.0	2.9 ± 0.2
S-diketone	0.3 ± 0.0	1.6 ± 0.1	0.8 ± 0.0	8.1 ± 0.1	0.3 ± 0.0	3.3 ± 0.0
vinylketone	0.2 ± 0.0	0.4 ± 0.0	0.2 ± 0.0	3.4 ± 0.1	0.5 ± 0.1	0.6 ± 0.0
C _β -ox ^c	5.5 ± 0.2	2.2 ± 0.1	2.9 ± 0.0	8.1 ± 0.3	3.5 ± 0.2	7.7 ± 0.0
C _γ -ox	58.6 ± 1.1	64.4 ± 3.0	32.8 ± 0.1	10.2 ± 0.8	29.3 ± 1.4	19.5 ± 1.8
Miscellaneous	2.1 ± 0.1	1.7 ± 0.2	2.9 ± 0.0	1.0 ± 0.0	2.3 ± 0.2	2.1 ± 0.1
PhC _γ ^d	62.2 ± 0.9	71.0 ± 2.6	37.0 ± 0.0	33.0 ± 0.6	33.2 ± 1.3	30.0 ± 1.9
PhC _γ -corrected ^e	61.1 ± 1.0	66.6 ± 2.7	35.8 ± 0.0	13.5 ± 0.7	32.0 ± 1.3	23.2 ± 1.7

^a 4-vinylphenol. ^b 4-vinylguaiaicol. ^c excluding diketones. ^d phenols with intact α,β,γ carbon side chain. ^e phenols with intact α,β,γ carbon side chain, excluding diketones and vinylketones.

Table S3. ^{13}C -IS py-GC-MS relative abundance of lignin compounds before (R2) and after (R3) planetary ball-milling of wheat straw treated with *C. subvermispota*. Corrected for RRF and relative abundance of ^{13}C analogues. Sum on the bases of structural classification (Table S1) according to van Erven et al. (2018).⁶ Average and standard deviation of analytical duplicates on pooled biological triplicates. Codes refer to Figure 1.

	Before ball-milling (weeks)				After ball-milling (weeks)			
	0	1	3	7	0	1	3	7
Lignin subunits (%)								
H	12.5 ± 1.4	12.5 ± 0.0	13.3 ± 1.0	17.7 ± 0.4	10.9 ± 0.5	12.4 ± 0.9	12.9 ± 0.4	14.6 ± 0.5
G	61.2 ± 3.1	60.1 ± 1.4	60.2 ± 0.6	57.5 ± 0.8	62.0 ± 0.6	59.5 ± 0.1	59.8 ± 0.1	61.6 ± 0.3
S	26.3 ± 1.7	27.4 ± 1.5	26.5 ± 0.4	24.8 ± 0.5	27.1 ± 0.1	28.1 ± 0.8	27.3 ± 0.4	23.8 ± 0.2
S/G	0.43 ± 0.0	0.46 ± 0.0	0.44 ± 0.0	0.43 ± 0.0	0.44 ± 0.0	0.47 ± 0.0	0.46 ± 0.0	0.39 ± 0.0
Structural moieties (%)								
Unsubstituted	4.0 ± 0.2	4.3 ± 0.2	7.0 ± 0.5	8.3 ± 0.0	4.1 ± 0.5	4.7 ± 0.0	6.8 ± 0.2	7.8 ± 0.0
Methyl	2.1 ± 0.2	2.2 ± 0.1	3.4 ± 0.1	3.3 ± 0.0	2.1 ± 0.0	2.2 ± 0.1	2.9 ± 0.3	3.3 ± 0.1
Vinyl	34.1 ± 0.1	32.8 ± 0.5	35.5 ± 0.8	37.4 ± 0.0	31.7 ± 1.2	33.4 ± 2.1	34.0 ± 1.4	36.5 ± 1.2
4-VP ^a	10.9 ± 1.4	10.9 ± 0.1	10.7 ± 0.7	14.0 ± 0.3	9.2 ± 0.4	10.6 ± 0.9	10.3 ± 0.3	11.1 ± 0.6
4-VG ^b	20.8 ± 1.6	19.4 ± 0.6	21.9 ± 0.3	20.9 ± 0.2	20.1 ± 0.7	20.3 ± 1.1	20.9 ± 1.0	22.7 ± 0.5
C _α -ox	3.1 ± 0.1	3.7 ± 0.2	7.8 ± 0.4	9.5 ± 0.1	4.4 ± 0.4	4.8 ± 0.0	8.6 ± 0.0	10.3 ± 0.1
G-diketone	0.0 ± 0.0	0.0 ± 0.0	0.4 ± 0.1	0.8 ± 0.1	0.1 ± 0.0	0.1 ± 0.0	0.3 ± 0.0	0.7 ± 0.0
S-diketone	0.1 ± 0.0	0.1 ± 0.0	1.1 ± 0.1	1.5 ± 0.0	0.1 ± 0.0	0.2 ± 0.0	1.0 ± 0.0	1.4 ± 0.0
vinylketone	0.2 ± 0.0	0.2 ± 0.0	0.3 ± 0.0	0.3 ± 0.0	0.2 ± 0.0	0.2 ± 0.0	0.3 ± 0.0	0.3 ± 0.0
C _β -ox ^c	1.3 ± 0.1	1.5 ± 0.0	2.6 ± 0.0	2.8 ± 0.1	1.4 ± 0.0	1.6 ± 0.0	2.6 ± 0.2	2.9 ± 0.0
C _γ -ox	52.1 ± 0.7	52.0 ± 0.8	39.6 ± 1.7	34.9 ± 0.5	52.9 ± 1.4	49.6 ± 2.4	41.0 ± 2.2	35.0 ± 1.2
Miscellaneous	3.3 ± 0.1	3.5 ± 0.1	4.2 ± 0.3	3.9 ± 0.1	3.5 ± 0.1	3.7 ± 0.2	4.1 ± 0.2	4.1 ± 0.0
PhC _γ ^d	56.7 ± 0.5	57.2 ± 0.6	48.4 ± 1.6	44.8 ± 0.2	58.1 ± 1.5	55.3 ± 2.2	49.6 ± 1.9	45.0 ± 1.1
PhC _γ -corrected ^e	56.5 ± 0.5	56.9 ± 0.7	46.6 ± 1.9	42.2 ± 0.3	57.7 ± 1.4	54.8 ± 2.2	48.0 ± 1.9	42.5 ± 1.2

^a 4-vinylphenol. ^b 4-vinylguaiaicol. ^c excluding diketones. ^d phenols with intact α,β,γ carbon side chain. ^e phenols with intact α,β,γ carbon side chain, excluding diketones and vinylketones.

Table S4. ^{13}C -IS py-GC-MS relative abundance of lignin derived pyrolysis products in purified acetone extracts of untreated and *C. subvermispota* treated wheat straw. Corrected for RRF and relative abundance of ^{13}C analogues. Sum on the bases of structural classification (Table S1) according to van Erven et al. (2018).⁶ Average and standard deviation of analytical duplicates on pooled biological triplicates. Codes refer to Figure 1. Recoveries could not be determined because lignin contents of unpurified samples were severely underestimated.

	S1 pure (weeks)			
	0	1	3	7
Lignin subunits (%)				
H	15.4 ± 0.1	11.7 ± 0.1	10.4 ± 0.1	11.3 ± 0.3
G	62.5 ± 0.0	64.7 ± 0.1	59.6 ± 0.0	61.5 ± 0.1
S	22.2 ± 0.1	23.6 ± 0.1	30.0 ± 0.1	27.2 ± 0.3
S/G	0.36 ± 0.0	0.37 ± 0.0	0.50 ± 0.0	0.44 ± 0.0
Structural moieties (%)				
Unsubstituted	6.1 ± 0.1	6.1 ± 0.1	10.3 ± 0.1	13.3 ± 1.6
Methyl	2.2 ± 0.0	2.4 ± 0.1	3.0 ± 0.0	3.1 ± 0.1
Vinyl	27.7 ± 0.2	22.8 ± 0.1	20.4 ± 0.7	18.1 ± 0.5
4-VP ^a	13.1 ± 0.1	9.5 ± 0.1	7.0 ± 0.1	6.3 ± 0.1
4-VG ^b	13.1 ± 0.1	11.5 ± 0.0	11.2 ± 0.5	9.8 ± 0.3
C _α -ox	6.5 ± 0.0	6.4 ± 0.1	13.8 ± 0.0	20.2 ± 0.4
G-diketone	0.2 ± 0.0	0.2 ± 0.0	1.8 ± 0.1	4.0 ± 0.2
S-diketone	0.5 ± 0.0	0.5 ± 0.0	4.8 ± 0.2	7.3 ± 0.3
vinylketone	0.2 ± 0.0	0.3 ± 0.0	0.5 ± 0.0	0.7 ± 0.0
C _β -ox ^c	2.8 ± 0.0	1.6 ± 0.0	2.5 ± 0.0	2.2 ± 0.1
C _γ -ox	52.3 ± 0.1	57.9 ± 0.0	47.3 ± 0.5	40.4 ± 2.6
Miscellaneous	2.4 ± 0.0	2.8 ± 0.0	2.9 ± 0.0	2.7 ± 0.0
PhC _γ ^d	55.8 ± 0.1	61.8 ± 0.0	56.1 ± 0.7	51.8 ± 2.3
PhC _γ -corrected ^e	54.9 ± 0.2	60.9 ± 0.0	49.0 ± 0.4	39.8 ± 2.8

^a 4-vinylphenol. ^b 4-vinylguaiaicol. ^c excluding diketones. ^d phenols with intact α,β,γ carbon side chain. ^e phenols with intact α,β,γ carbon side chain, corrected for acetaldehydes and vinylketones.

Table S5. ^{13}C -IS py-GC-MS relative abundance of lignin derived pyrolysis products in purified water extracts (before ball-milling) of untreated and *C. subvermispota* treated wheat straw. Corrected for RRF and relative abundance of ^{13}C analogues. Sum on the bases of structural classification (Table S1) according to van Erven et al. (2018).⁶ Average and standard deviation of analytical triplicates on pooled biological triplicates. Codes refer to Figure 1.

	S2 pure (weeks)			
	0	1	3	7
Recovery % (w/w)^a				
	44	33	39	48
Lignin subunits (%)				
H	9.7 ± 0.4	10.7 ± 0.2	11.7 ± 0.2	10.1 ± 0.1
G	63.2 ± 0.2	58.2 ± 0.1	50.6 ± 0.5	57.3 ± 0.8
S	27.2 ± 0.2	31.1 ± 0.3	37.7 ± 0.2	32.6 ± 0.8
S/G	0.43 ± 0.0	0.53 ± 0.0	0.74 ± 0.0	0.57 ± 0.0
Structural moieties (%)				
Unsubstituted	8.6 ± 0.1	11.1 ± 0.2	12.7 ± 0.4	14.0 ± 0.2
Methyl	2.6 ± 0.0	3.1 ± 0.2	2.7 ± 0.1	2.8 ± 0.1
Vinyl	30.1 ± 0.3	23.5 ± 0.2	10.8 ± 0.3	8.3 ± 0.4
4-VP ^b	5.4 ± 0.0	4.6 ± 0.1	2.7 ± 0.1	2.1 ± 0.1
4-VG ^c	22.1 ± 0.3	16.3 ± 0.3	6.4 ± 0.2	5.0 ± 0.2
C _α -ox	5.5 ± 0.2	9.3 ± 0.2	44.4 ± 0.3	45.2 ± 1.8
G-diketone	0.3 ± 0.0	0.6 ± 0.0	5.4 ± 0.1	8.1 ± 0.5
S-diketone	0.3 ± 0.0	1.1 ± 0.0	8.1 ± 0.3	6.9 ± 0.3
vinylketone	0.2 ± 0.0	0.3 ± 0.0	1.1 ± 0.0	1.2 ± 0.0
C _β -ox ^d	3.5 ± 0.0	4.1 ± 0.0	4.7 ± 0.1	4.2 ± 0.2
C _γ -ox	47.0 ± 0.3	46.3 ± 0.8	23.0 ± 1.2	23.9 ± 1.7
Miscellaneous	2.7 ± 0.4	2.6 ± 0.1	1.7 ± 0.1	1.7 ± 0.1
PhC _γ ^e	50.7 ± 0.3	51.5 ± 0.7	41.1 ± 0.8	43.8 ± 1.1
PhC _γ -corrected ^f	50.0 ± 0.3	49.5 ± 0.7	26.5 ± 1.1	27.6 ± 1.8

^a of lignin in unpurified extracts. ^b 4-vinylphenol. ^c 4-vinylguaiaicol. ^d excluding diketones. ^e phenols with intact α,β,γ carbon side chain. ^f phenols with intact α,β,γ carbon side chain, corrected for diketones and vinylketones.

Table S6. ^{13}C -IS py-GC-MS relative abundance of lignin derived pyrolysis products in purified water extracts (after ball-milling) of untreated and *C. subvermispora* treated wheat straw. Corrected for RRF and relative abundance of ^{13}C analogues. Sum on the bases of structural classification (Table S1) according to van Erven et al. (2018).⁶ Average and standard deviation of analytical triplicates on pooled biological triplicates. Codes refer to Figure 1.

	S4 pure (weeks)			
	0	1	3	7
Recovery % (w/w) ^a	37	50	65	52
Lignin subunits (%)				
H	7.4 ± 0.1	7.6 ± 0.0	8.3 ± 0.1	8.2 ± 0.1
G	67.8 ± 0.1	65.2 ± 0.4	58.9 ± 0.6	64.1 ± 0.4
S	24.8 ± 0.2	27.2 ± 0.4	32.8 ± 0.7	27.3 ± 0.4
S/G	0.37 ± 0.0	0.42 ± 0.0	0.56 ± 0.0	0.43 ± 0.0
Structural moieties (%)				
Unsubstituted	3.5 ± 0.1	3.9 ± 0.1	5.6 ± 0.0	12.2 ± 0.1
Methyl	1.3 ± 0.0	1.4 ± 0.1	1.9 ± 0.0	2.3 ± 0.1
Vinyl	44.7 ± 0.4	39.8 ± 0.5	31.8 ± 0.9	37.3 ± 0.5
4-VP ^b	5.6 ± 0.0	5.6 ± 0.0	5.3 ± 0.1	5.1 ± 0.0
4-VG ^c	37.3 ± 0.3	32.2 ± 0.6	23.9 ± 0.8	30.2 ± 0.5
C α -ox	12.6 ± 0.4	13.3 ± 0.2	23.2 ± 0.3	22.7 ± 0.2
G-diketone	0.3 ± 0.0	0.4 ± 0.0	1.4 ± 0.0	2.0 ± 0.1
S-diketone	0.3 ± 0.0	0.4 ± 0.0	2.1 ± 0.2	5.3 ± 0.2
vinylketone	0.4 ± 0.0	0.5 ± 0.0	0.7 ± 0.0	0.7 ± 0.0
C β -ox ^d	2.2 ± 0.0	2.5 ± 0.1	4.0 ± 0.0	3.2 ± 0.2
C γ -ox	33.9 ± 0.1	37.2 ± 0.3	31.3 ± 1.1	20.1 ± 0.6
Miscellaneous	1.8 ± 0.0	1.9 ± 0.1	2.2 ± 0.0	2.1 ± 0.1
PhC γ ^e	37.1 ± 0.1	40.8 ± 0.4	38.6 ± 1.2	29.4 ± 0.4
PhC γ -corrected ^f	36.0 ± 0.1	39.5 ± 0.4	34.5 ± 1.1	21.4 ± 0.7

^a of lignin in unpurified extracts. ^b4-vinylphenol. ^c4-vinylguaiacol. ^d excluding diketones ^e phenols with intact α,β,γ carbon side chain. ^f phenols with intact α,β,γ carbon side chain, corrected for diketones and vinylketones.

Table S7. ^1H - ^{13}C HSQC NMR and ^1H - ^{13}C HMBC NMR assignments of guaiacyl- and syringyl diketones in DMSO- d_6 . Assignments are in accordance with previously reported spectra by Rahimi et al.⁴

	GDK		SDK	
	δ_c (ppm)	δ_H (ppm)	δ_c (ppm)	δ_H (ppm)
1	-	-	-	-
2	111.1	7.34	107.7	7.15
3	-	-	-	-
4	148.6	-	148.0	-
5	115.4	6.75	-	-
6	126.7	7.36	107.7	7.15
α	190.2	-	190.3	-
β	202.6	-	202.3	-
γ	26.4	2.42	26.4	2.44
-OCH $_3$	55.1	3.77	55.9	3.78

Table S8. Semiquantitative ^1H - ^{13}C HSQC NMR structural characterization of purified acetone extracts of untreated and *C. subvermispota* treated wheat straw.

	S1-pure			
	0	1	3	7
Lignin subunits (%)^a				
H	4	6	1	1
G	62	59	43	30
G _{ox}	0	1	13	40
S	29	30	25	13
S _{ox}	4	4	18	17
S/G	0.5	0.6	0.8	0.4
Hydroxycinnamates (%)^b				
p-coumarate	13	10	4	2
ferulate	8	3	0	0
Flavonolignin (%)^b				
tricin	39	46	23	13
Lignin interunit linkages (%)^{b,c}				
β-O-4 G+H	8 (16)	8 (16)	6 (30)	0
β-O-4 S	10 (21)	12 (23)	7 (36)	3 (100)
β-O-4 C _α -ox	5 (10)	3 (5)	0 (0)	0
β-O-4 triclin	19 (39)	23 (44)	6 (28)	0
total β-O-4 aryl ethers	42 (86)	46 (87)	19 (94)	3 (100)
β-5 phenylcoumarans	3 (6)	3 (6)	0 (0)	0
β-β resinols	4 (8)	3 (6)	1 (6)	0
total	49 (100)	53 (100)	21 (100)	3 (100)
β-O-aryl cleavage products (%)^b				
HPV/HPS	1.4	0	0.8	10.9
DHPV/DHPS	0	0	3.3	10.5

^a relative distribution of lignin subunits (H+G+G_{ox}+S+S_{ox} = 100)^b relative volume integral of substructure versus volume integral of total lignin subunits^c relative distribution of total interunit linkages in parentheses**Table S9.** Semiquantitative ^1H - ^{13}C HSQC NMR structural characterization of purified water extracts (before ball-milling) of untreated and *C. subvermispota* treated wheat straw.

	S2-pure			
	0	1	3	7
Lignin subunits (%)^a				
H	0	0	0	0
G	59	53	9	0
G _{ox}	0	0	44	69
S	34	36	11	0
S _{ox}	6	10	35	31
S/G	0.7	0.9	0.9	0.4
Hydroxycinnamates (%)^b				
p-coumarate	4	3	0	0
ferulate	13	0	0	0
Flavonolignin (%)^b				
tricin	1	0	0	0
Lignin interunit linkages (%)^{b,c}				
β-O-4 G+H	17 (38)	12 (34)	0	0
β-O-4 S	18 (41)	20 (55)	0	0
β-O-4 C _α -ox	0 (0)	0 (0)	0	0 ^d
β-O-4 triclin	2 (5)	< 1 (< 1)	0	0
total β-O-4 aryl ethers	38 (85)	32 (89)	0	0
β-5 phenylcoumarans	4 (9)	2 (6)	0	0
β-β resinols	2 (5)	2 (5)	0	0
total	44 (100)	36 (100)	0	0
β-O-aryl cleavage products (%)^b				
HPV/HPS	0.4	3.2	3.2	2.1
DHPV/DHPS	0	0.4	16.4	18.1

^a relative distribution of lignin subunits (H+G+G_{ox}+S+S_{ox} = 100)^b relative volume integral of substructure versus volume integral of total lignin subunits^c relative distribution of total interunit linkages in parentheses^d Due to required zooming, β-O-4 aryl ethers with two adjacent C_α-carbonyls (A''_{ox}) were not included in semiquantitative analyses

Table S10. Semiquantitative ^1H - ^{13}C HSQC NMR structural characterization of purified water extracts of ball-milled untreated and *C. subvermispota* treated wheat straw.

	S4-pure			
	0	1	3	7
Lignin subunits (%)^a				
H	3	2	1	1
G	43	44	29	28
G _{ox}	16	15	23	32
S	29	29	28	20
S _{ox}	10	10	19	18
S/G	0.7	0.7	0.9	0.6
Hydroxycinnamates (%)^b				
p-coumarate	8	7	5	4
ferulate	45	37	27	20
Flavonolignin (%)^b				
tricin	<1	1	1	1
Lignin interunit linkages (%)^{b,c}				
β-O-4 G+H	14 (45)	15 (44)	7 (57)	0
β-O-4 S	14 (47)	14 (42)	5 (43)	3 (100)
β-O-4 C _α -ox	0 (0)	0 (0)	0	0
β-O-4 triclin	1 (5)	3 (9)	0	0
total β-O-4 aryl ethers	30 (97)	33 (95)	13 (100)	3 (100)
β-5 phenylcoumarans	1 (2)	1 (2)	0	0
β-β resinols	0 (0)	1 (2)	0	0
total	30 (100)	34 (100)	13 (100)	3 (100)
β-O-aryl cleavage products (%)^b				
HPV/HPS	2.4	2.9	1.9	3.9
DHPV/DHPS	0	0.5	3.3	6.3

^a relative distribution of lignin subunits (H+G+G_{ox}+S+S_{ox} =100)^b relative volume integral of substructure versus volume integral of total lignin subunits^c relative distribution of total interunit linkages in parentheses**Table S11.** ^{13}C -IS py-GC-MS relative abundance of lignin derived pyrolysis products in saponified purified water extract (before ball-milling) of seven weeks *C. subvermispota* treated wheat straw. Corrected for RRF and relative abundance of ^{13}C analogues. Sum on the bases of structural classification (Table S1) according to van Erven et al. (2018).⁶ Average and standard deviation of analytical triplicates on pooled biological triplicates. Codes refer to Figure 1.

	S2 pure (7 weeks)	
	without saponification	with saponification
Recovery % (w/w)^a	n.a.	71
Lignin subunits (%)		
H	10.1 ± 0.1	9.1 ± 0.2
G	57.3 ± 0.8	60.9 ± 0.7
S	32.6 ± 0.8	30.0 ± 0.7
S/G	0.57 ± 0.0	0.49 ± 0.0
Structural moieties (%)		
Unsubstituted	14.0 ± 0.2	30.3 ± 4.1
Methyl	2.8 ± 0.1	3.2 ± 0.1
Vinyl	8.3 ± 0.4	9.9 ± 0.6
4-VP ^b	2.1 ± 0.1	2.3 ± 0.1
4-VG ^c	5.0 ± 0.2	6.4 ± 0.4
C _α -ox	45.2 ± 1.8	35.3 ± 2.0
G-diketone	8.1 ± 0.5	2.8 ± 0.1
S-diketone	6.9 ± 0.3	5.7 ± 0.3
vinylketone	1.2 ± 0.0	1.3 ± 0.1
C _β -ox ^d	4.2 ± 0.2	3.6 ± 0.2
C _γ -ox	23.9 ± 1.7	16.5 ± 1.4
Miscellaneous	1.7 ± 0.1	1.3 ± 0.1
PhC _γ ^e	43.8 ± 1.1	26.2 ± 1.7
PhC _γ -corrected ^f	27.6 ± 1.8	16.4 ± 1.4

^a of lignin in purified extract. ^b4-vinylphenol. ^c4-vinylguaiacol. ^d excluding diketones. ^e phenols with intact α,β,γ carbon side chain. ^f phenols with intact α,β,γ carbon side chain, corrected for diketones and vinylketones.

Table S12. Semiquantitative ^1H - ^{13}C HSQC NMR structural characterization of saponified purified water extract (before ball-milling) of *C. subvermispura* treated wheat straw.

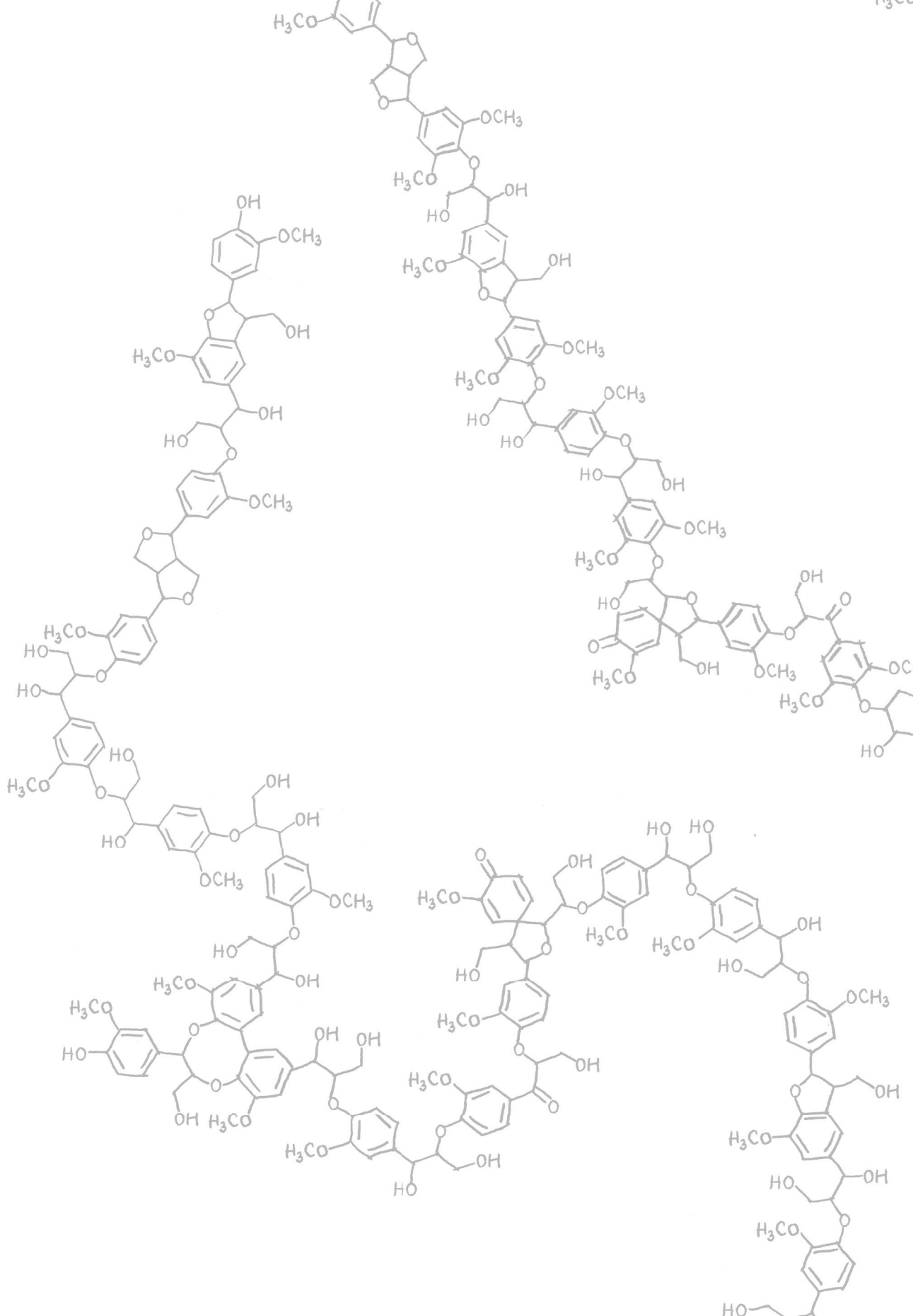
	S2-pure (7 weeks)	
	without saponification	with saponification
Lignin subunits (%)^a		
H	0	0
G	0	9
G _{ox}	69	58
S	0	6
S _{ox}	31	27
S/G	0.4	0.5
Hydroxycinnamates (%)^b		
p-coumarate	0	0
ferulate	0	0
Flavonolignin (%)^b		
tricin	0	0
Lignin Interunit linkages (%)^b		
β-O-4 G+H	0	4
β-O-4 S	0	2
β-O-4 C _α -ox	0	0
β-O-4 tricin	0	0
total β-O-4 aryl ethers	0	0
β-5 phenylcoumarans	0	0
β-β resinols	0	0
total	0	0
β-O-aryl cleavage products (%)^b		
HPV/HPS	2.1	1.0
DHPV/DHPS	18.1	4.7

^a relative distribution of lignin subunits (H+G+G_{ox}+S+S_{ox} = 100)^b relative volume integral of substructure versus volume integral of total lignin subunits

Supporting Information References

- Govender, M.; Bush, T.; Spark, A.; Bose, S. K.; Francis, R. C., An accurate and non-labor intensive method for the determination of syringyl to guaiacyl ratio in lignin. *Bioresour Technol* **2009**, *100*, 5834-5839.
- Sluiter, J. B.; Ruiz, R. O.; Scarlata, C. J.; Sluiter, A. D.; Templeton, D. W., Compositional analysis of lignocellulosic feedstocks. 1. Review and description of methods. *J Agric Food Chem* **2010**, *58*, 9043-9053.
- Hilgers, R.; Vincken, J.-P.; Gruppen, H.; Kabel, M. A., Laccase/mediator systems: their reactivity toward phenolic lignin structures. *ACS Sustainable Chem Eng* **2018**, *6*, 2037-2046.
- Rahimi, A.; Ulbrich, A.; Coon, J. J.; Stahl, S. S., Formic-acid-induced depolymerization of oxidized lignin to aromatics. *Nature* **2014**, *515*, 249-252.
- Van Erven, G.; de Visser, R.; Merx, D. W.; Strolenberg, W.; De Gijssel, P.; Gruppen, H.; Kabel, M. A., Quantification of lignin and its structural features in plant biomass using ^{13}C lignin as internal standard for pyrolysis-GC-SIM-MS. *Anal Chem* **2017**, *89*, 10907-10916.
- Van Erven, G.; Nayan, N.; Sonnenberg, A. S.; Hendriks, W. H.; Cone, J. W.; Kabel, M. A., Mechanistic insight in the selective delignification of wheat straw by three white-rot fungal species through quantitative ^{13}C -IS py-GC-MS and whole cell wall HSQC NMR. *Biotechnol Biofuels* **2018**, *11*, 262.
- Ralph, J.; Hatfield, R. D., Pyrolysis-GC-MS characterization of forage materials. *J Agric Food Chem* **1991**, *39*, 1426-1437.
- Mansfield, S. D.; Kim, H.; Lu, F.; Ralph, J., Whole plant cell wall characterization using solution-state 2D NMR. *Nat Protoc* **2012**, *7*, 1579-1589.
- Del Río, J. C.; Rencoret, J.; Prinsen, P.; Martínez, A. T.; Ralph, J.; Gutiérrez, A., Structural characterization of wheat straw lignin as revealed by analytical pyrolysis, 2D-NMR, and reductive cleavage methods. *J Agric Food Chem* **2012**, *60*, 5922-5935.
- Ralph, J.; Lu, F., Cryoprobe 3D NMR of acetylated ball-milled pine cell walls. *Org Biomol Chem* **2004**, *2*, 2714-2715.
- Ralph, J.; Akiyama, T.; Kim, H.; Lu, F.; Schatz, P. F.; Marita, J. M.; Ralph, S. A.; Reddy, M. S.; Chen, F.; Dixon, R. A., Effects of coumarate 3-hydroxylase down-regulation on lignin structure. *J Biol Chem* **2006**, *281*, 8843-8853.

12. Nishimura, H.; Kamiya, A.; Nagata, T.; Katahira, M.; Watanabe, T., Direct evidence for a ether linkage between lignin and carbohydrates in wood cell walls. *Sci Rep* **2018**, *8*, 6538.
13. Ralph, S. A.; Ralph, J.; Landucci, L., NMR database of lignin and cell wall model compounds. **2009**, Available at URL www.glbrc.org/databases_and_software/nmrdatabase/.
14. Kim, H.; Padmakshan, D.; Li, Y.; Rencoret, J.; Hatfield, R. D.; Ralph, J., Characterization and elimination of undesirable protein residues in plant cell wall materials for enhancing lignin analysis by solution-state nuclear magnetic resonance spectroscopy. *Biomacromolecules* **2017**, *18*, 4184-4195.
15. Guo, H.; Miles-Barrett, D. M.; Neal, A. R.; Zhang, T.; Li, C.; Westwood, N. J., Unravelling the enigma of lignin OX: can the oxidation of lignin be controlled? *Chem Sci* **2018**, *9*, 702-711.
16. Gall, D. L.; Ralph, J.; Donohue, T. J.; Noguera, D. R., A group of sequence-related sphingomonad enzymes catalyzes cleavage of β -aryl ether linkages in lignin β -guaiacyl and β -syringyl ether dimers. *Environ Sci Technol* **2014**, *48*, 12454-12463.
17. Higuchi, Y.; Aoki, S.; Takenami, H.; Kamimura, N.; Takahashi, K.; Hishiyama, S.; Lancefield, C. S.; Ojo, O. S.; Katayama, Y.; Westwood, N. J., Bacterial catabolism of β -hydroxypropiovanillone and β -hydroxypropiosyringone produced in the reductive cleavage of arylglycerol- β -aryl ether in lignin. *Appl Environ Microbiol* **2018**, *84*, e02670-17.
18. Constant, S.; Wienk, H. L.; Frissen, A. E.; de Peinder, P.; Boelens, R.; van Es, D. S.; Grisel, R. J.; Weckhuysen, B. M.; Huijgen, W. J.; Gosselink, R. J., New insights into the structure and composition of technical lignins: a comparative characterisation study. *Green Chem* **2016**, *18*, 2651-2665.
19. Sulaeva, I.; Zinoviyev, G.; Plankeel, J. M.; Sumerskii, I.; Rosenau, T.; Potthast, A., Fast Track to Molar-Mass Distributions of Technical Lignins. *ChemSusChem* **2017**, *10*, 629-635.
20. Zinoviyev, G.; Sulaeva, I.; Podzimek, S.; Rössner, D.; Kilpeläinen, I.; Sumerskii, I.; Rosenau, T.; Potthast, A., Getting closer to absolute molar masses of technical lignins. *ChemSusChem* **2018**, *11*, 3259-3268.
21. Björkman, A., Studies on finely divided wood. Part 1. Extraction of lignin with neutral solvents. *Sven Papperstidn* **1956**, *59*, 477-485.
22. Chang, H.-M.; Cowling, E. B.; Brown, W., Comparative studies on cellulolytic enzyme lignin and milled wood lignin of sweetgum and spruce. *Holzforschung* **1975**, *29*, 153-159.
23. Jiang, B.; Cao, T.; Gu, F.; Wu, W.; Jin, Y., Comparison of the structural characteristics of cellulolytic enzyme lignin preparations isolated from wheat straw stem and leaf. *ACS Sustainable Chem Eng* **2016**, *5*, 342-349.
24. Zikeli, F.; Ters, T.; Fackler, K.; Srebotnik, E.; Li, J., Successive and quantitative fractionation and extensive structural characterization of lignin from wheat straw. *Ind Crops Prod* **2014**, *61*, 249-257.
25. Fujimoto, A.; Matsumoto, Y.; Chang, H.-M.; Meshitsuka, G., Quantitative evaluation of milling effects on lignin structure during the isolation process of milled wood lignin. *J Wood Sci* **2005**, *51*, 89-91.
26. Crestini, C.; Melone, F.; Sette, M.; Saladino, R., Milled wood lignin: a linear oligomer. *Biomacromolecules* **2011**, *12*, 3928-3935.
27. Tolbert, A.; Akinoshio, H.; Khunsupat, R.; Naskar, A. K.; Ragauskas, A. J., Characterization and analysis of the molecular weight of lignin for biorefining studies. *Biofuels Bioprod Biorefin* **2014**, *8*, 836-856.
28. Gutiérrez, A.; del Río, J. C.; Martínez-Íñigo, M. J.; Martínez, M. J.; Martínez, Á. T., Production of new unsaturated lipids during wood decay by ligninolytic basidiomycetes. *Appl Environ Microbiol* **2002**, *68*, 1344-1350.
29. Kawai, S.; Umezawa, T.; Higuchi, T., *p*-Benzoquinone monoketals, novel degradation products of β -O-4 lignin model compounds by *Coriolus versicolor* and lignin peroxidase of *Phanerochaete chrysosporium*. *FEBS Lett* **1987**, *210*, 61-65.
30. Kawai, S.; Nakagawa, M.; Ohashi, H., Degradation mechanisms of a nonphenolic β -O-4 lignin model dimer by *Trametes versicolor* laccase in the presence of 1-hydroxybenzotriazole. *Enzyme Microb Technol* **2002**, *30*, 482-489.
31. Kirk, T. K.; Tien, M.; Kersten, P. J.; Mozuch, M. D.; Kalyanaraman, B., Ligninase of *Phanerochaete chrysosporium*. Mechanism of its degradation of the non-phenolic arylglycerol β -aryl ether substructure of lignin. *Biochem J* **1986**, *236*, 279-287.



The background of the slide is filled with various chemical structures of lignin, which are complex polymers of aromatic units linked by oxygen-containing bonds. These structures are rendered in a light gray, semi-transparent style, allowing the text to be the primary focus. They include various methoxy (H3CO) and hydroxyl (OH) groups attached to the aromatic rings.

CHAPTER 6

Structural motifs of wheat straw lignin differ in susceptibility to degradation by the white-rot fungus *Ceriporiopsis subvermispora*

Gijs van Erven, Jianli Wang, Peicheng Sun

Pieter de Waard, Jacinta van der Putten, Guus E. Frissen,

Richard J. A. Gosselink, Grigory Zinovyev, Antje Potthast,

Willem J. H. van Berkel, Mirjam A. Kabel

Based on: ACS Sustainable Chemistry & Engineering, 2019, 7, 20032-20042

Abstract

The white-rot fungus *Ceriporiopsis subvermispora* delignifies plant biomass extensively and selectively and, therefore, has great biotechnological potential. We previously demonstrated that after 7 weeks of fungal growth on wheat straw 70% w/w of lignin was removed and established the underlying degradation mechanisms via selectively extracted diagnostic substructures. In this work, we fractionated the residual (more intact) lignin and comprehensively characterized the obtained isolates to determine the susceptibilities of wheat straw lignin's structural motifs to fungal degradation. By using ^{13}C -IS py-GC-MS, HSQC NMR, ^{31}P NMR, and SEC analyses, it was shown that β -O-4' ethers and the more condensed phenylcoumarans and resinols were equally susceptible to fungal breakdown. Interestingly, for β -O-4' ether substructures marked cleavage preferences could be observed: β -O-4'-syringyl substructures were degraded more frequently than their β -O-4'-guaiacyl and β -O-4'-tricin analogues. Furthermore, diastereochemistry (*threo* > *erythro*) and γ -acylation (γ -OH > γ -acyl) influenced cleavage susceptibility. These results indicate that electron density of the 4'-O-coupled ring and local steric hindrance are important determinants of oxidative β -O-4' ether degradation. Our findings provide novel insight into the delignification mechanisms of *C. subvermispora* and contribute to improving the valorization of lignocellulosic biomass.

Introduction

Most of the terrestrial fixed carbon is contained in lignocellulosic biomass, consisting mainly of cellulose, hemicellulose and lignin. The aromatic lignin polymer plays a pivotal role in carbon recycling as it protects the polysaccharides within lignocellulose against (enzymatic) conversion. Degradation of lignin is a crucial step in nature and is a principal goal for the industrial upgrading of lignocellulosic biomass aiming at the efficient utilization of cellulose, hemicellulose and lignin to produce biomaterials, animal feed, biochemicals and biofuels.¹⁻⁴ Whereas nature's strategy to overcome lignin's recalcitrance is largely based on white-rot fungi, industry currently relies on severe thermochemical pretreatments that consume extensive amounts of energy and chemicals.⁵⁻⁷ Unaccompanied by such environmental impact, several white-rot fungal species degrade lignin selectively, without extensively modifying and/or degrading cellulose and hemicellulose.⁸⁻⁹ Biological pretreatment as a more sustainable alternative to the physical and/or chemical pretreatment processes that are currently applied in industry is, therefore, increasingly receiving attention.¹⁰⁻¹²

A particularly promising white-rot fungus is *Ceriporiopsis subvermispota*. The unique effectivity and selectivity of this fungus for plant biomass delignification greatly improves ruminal and enzymatic degradability of the remaining polysaccharides.¹³⁻¹⁷ Furthermore, this biological delignification is not resulting in inhibitory compounds for downstream processes commonly produced through chemical pre-treatment.¹⁸⁻¹⁹ The potential of this fungus has, therefore, been tested for a range of biotechnological applications, including biofuel production¹⁸ and biopulping.²⁰⁻²¹

An unsolved issue, impairing its industrial application thus far, is the low time-efficiency of fungal delignification processes, i.e. fungal growth for extensive delignification can take up to ten weeks.^{4, 22} Improving this time-efficiency might be achieved through increasing our understanding of the delignification mechanisms at the molecular level. This insight contributes to the identification of the rate-limiting step(s) in the (enzymatic) oxidative process and, furthermore, might enable the selection of substrates that are more fit-for-purpose. Yet, the underlying delignification mechanisms are far from completely understood.

Most of our understanding of the delignification strategies employed by *C. subvermispota* is deduced from lignin model compound studies combined with genomics and proteomics research, rather than through characterization of its action on native lignin as present in lignocellulosic biomass.²³⁻²⁸ As lignin model compounds usually comprise of simple dimeric structures, such structures can never fairly represent degradation reactions of polymeric lignin contained in lignocellulose.

Within plant biomass, lignin occurs as a heterogeneous cross-linked macromolecule that, in grasses, is composed of *p*-hydroxyphenyl (H), guaiacyl (G) and syringyl (S) subunits. These subunits are linked through a variety of aryl ether and carbon-

carbon interunit linkages, of which the β -O-4' aryl ether is the most abundant (~80%). The latter β -O-4' aryl ethers are present as two diastereomeric pairs of enantiomers, *threo* (RR/SS) and *erythro* (RS/SR), of which the ratio is largely determined by the subunits of the interunit linkage (Figure 1).²⁹⁻³²

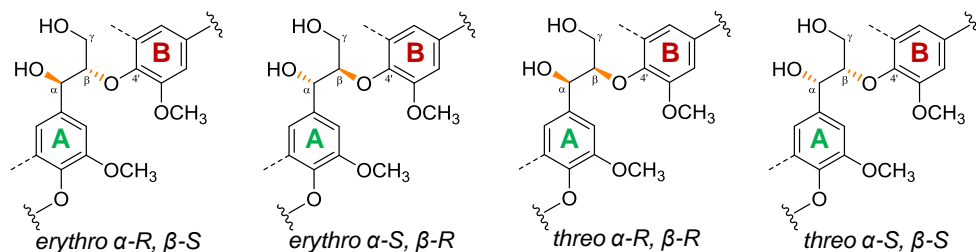


Figure 1. Diastereomers of β -O-4' aryl ethers. Dotted lines represent -H or -OCH₃ in guaiacyl and syringyl units, respectively. Wavy lines indicate main positions of further coupling within lignin.

To add to the structural complexity of lignin, in grasses, these interunit linkages are partially esterified at the γ -OH position with acetate and *p*-coumarate.^{30, 33} Additionally, a variety of ferulate and diferulate substructures is etherified to grass-type lignin, functioning as cross-linking agents between lignin and carbohydrate moieties, thereby resulting in so-called lignin-carbohydrate-complexes (LCCs).³⁴⁻³⁵ Recently, the view on grass-type lignins complexity was even further extended, as the flavonoid triclin was found to be an integral part of this macromolecule.^{30, 36-37} Although the structure of grass lignin is highly complex, *C. subvermispora* is able to effectively degrade this aromatic polymer.¹³ For this purpose, the fungus relies on an oxidative enzymatic machinery that mainly depends on manganese peroxidases (MnP) and H₂O₂ generating aryl alcohol oxidases (AAO) and to a lesser extent on laccases, while lignin peroxidases (LiP) and versatile peroxidases (VP), commonly found in other white-rot fungi, are absent.²³⁻²⁵ Instead, the fungal genome was found to encode two enzymes with LiP/VP-like activity, though secretome and transcriptome analyses failed to confirm their actual production during fungal growth on lignocellulose.²³⁻²⁵ The collective action of the oxidative enzymes likely concert with diffusible low-molecular weight mediators, as lignin degradation occurs before the secondary cell wall porosity would allow enzymes to penetrate.³⁸⁻⁴¹ The exact nature and role of these mediating oxidants as well as the reactions they catalyze, however, remain unresolved.^{39-40, 42-44}

So far, few studies have been dedicated to the structural modification of actual lignocellulosic biomass during degradation by *C. subvermispora*. The studies that were conducted focused on the biodegradation of wood, of which the lignin structurally strongly differs from grasses. Some studies demonstrated that β -O-4' aryl ethers were cleaved during fungal growth, but the underlying cleavage mechanisms and relative susceptibilities of the various substructures could not be elucidated.⁴⁵⁻⁴⁷ Yelle et al. found that spruce wood β -O-4' aryl ethers were majorly degraded through C_α-C_β cleavage and that this degradation proceeded

diastereoselectively for the *threo*-form.⁴⁸ Contrarily, by analyzing entire fungal-treated wheat straw samples *in situ*, we recently showed that grass lignin is degraded through a combination of C_α-C_β and C_β-O-aryl ether cleavages.¹³ The ligninolysis pathways were unambiguously confirmed through multidimensional NMR analyses of extracts containing diagnostic substructures.⁴⁹ Despite this unprecedented *in situ* mechanistic insight, detailed information on the susceptibility of specific structural motifs within the lignin macromolecule, particularly those exclusively occurring in grass lignins, is yet to be obtained. Understanding of such cleavage preferences might be derived from remaining intact substructures.

To shed further light on lignin deconstruction by *C. subvermispora*, this research aimed to comprehensively map the remaining intact lignin structures during the fungus' growth on wheat straw. Thereto, lignin in untreated and fungal-treated wheat straw after 1, 3 and 7 weeks of fungal growth was quantitatively fractionated and extensively characterized by using quantitative ¹³C-IS py-GC-MS, HSQC and ³¹P NMR, and size-exclusion chromatography (SEC). We show that *C. subvermispora* degraded wheat straw lignin with a marked preference for β-O-4'-S substructures over their β-O-4'-G and β-O-4'-tricin counterparts. These β-O-4' ethers were, furthermore, diastereoselectively removed with a clear *threo*-preference. Acylation of the γ-OH moieties was shown to yield substructures more resistant against fungal attack, and as a result these substructures accumulated in the fungal-treated residue.

Experimental Section

Materials. All chemicals were obtained from commercial suppliers and used without further purification. Water used in all experiments was purified via a Milli-Q water system (Millipore, Billerica, MA, USA).

Preparation of fungal-treated wheat straw. *Ceriporiopsis subvermispora* (CBS 347.63, Cs1) was used in this study.^{13, 15, 50} Procedures for fungal strain preparation and solid-state pretreatment of the wheat straw have been previously described in detail.^{13, 15, 50} Biological triplicates of wheat straw treated for 0, 1, 3 and 7 weeks showed minimal variation and, therefore, were thoroughly mixed in equal dry matter amounts to one replicate for further experiments and analyses.¹⁵

Lignin fractionation. Lignin in untreated and fungal-treated wheat straw was fractionated according to modified procedures of Björkman and Chang et al. as presented in Figure 2.⁵¹⁻⁵² Fractionation steps 1-4 have been described in our previous work, and therefore, will only be briefly described here.⁴⁹ Ground wheat straw (~13 g; untreated and fungal-treated) was soxhlet-extracted in triplicate with acetone and the residue was dried under reduced pressure to obtain R1. Triplicates of R1 were mixed to one replicate and extracted with water in duplicate. Residues obtained through centrifugation were freeze-dried to obtain R2. Dried

duplicates were combined and planetary ball-milled by using a PM100 planetary ball mill (Retsch, Haan, Germany) in batches of 3 g per 50 mL zirconium dioxide (ZrO_2) beaker containing 17 $\phi 10$ mm ZrO_2 balls, at 600 rpm with a net milling time of 4 h (excluding 10 min pauses after every 15 min of milling).

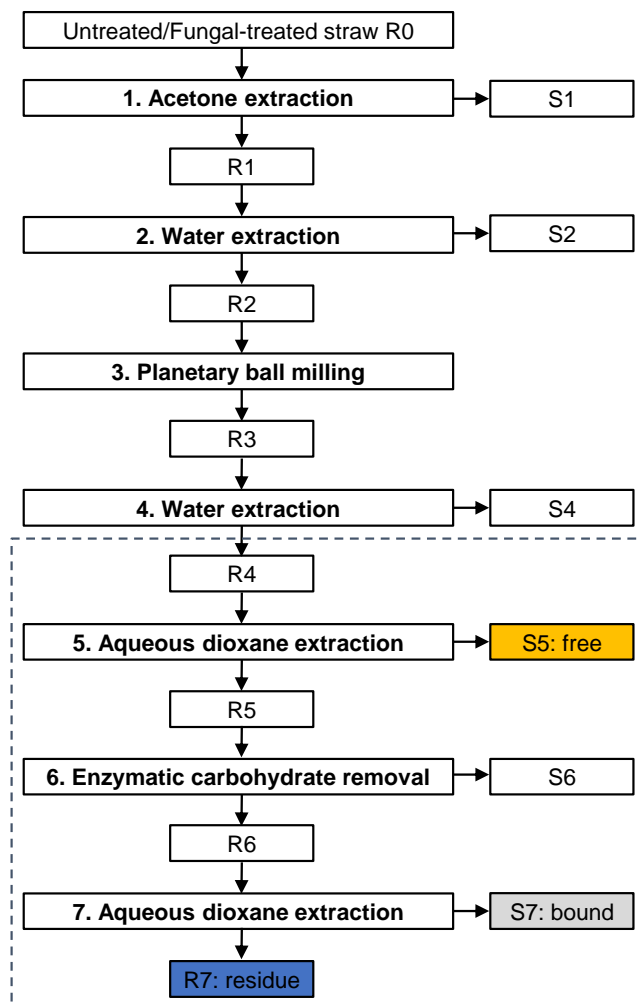


Figure 2. Fractionation scheme for untreated and *C. subvermispora* treated wheat straw. Fractionation steps 1-4 have been described in our previous work.⁴⁹ This work describes fractionation steps 4-7, indicated with a dashed box. R: insoluble residue, S: soluble fraction.

The fractionation was continued in duplicate with two portions of 12 g milled material (R3). The remainder of the fractionation procedure was continued using these duplicates, i.e. samples were never mixed after the respective steps. R3 was water-extracted at 5% (w/w) dry matter loading under rotary shaking (20 rpm) at 50 °C for 18 h. Insoluble material was removed by centrifugation (38,400 $\times g$, 10 min, 20 °C) and washed twice with 130 mL of water before the material was freeze-

dried to obtain R4. The dried residue (R4) was subsequently suspended in 80% (v/v) aqueous dioxane at 10% (w/w) dry matter loading and extracted twice (2 x 24 h) at room temperature with magnetic stirring (500 rpm) under nitrogen atmosphere. The supernatants were recovered by centrifugation (30,000xg, 5 min, 20 °C) and combined. The resulting combined supernatants and the residue were freeze-dried, washed with water to remove traces of dioxane, and freeze-dried again to obtain the dioxane soluble fraction S5, further referred to as 'free lignin', and the dioxane insoluble fraction R5. R5 was incubated at 5% (w/w) dry matter and 0.025% (w/w) ViscoStar 150L protein loading in 170 mL 50 mM sodium acetate at pH 4.8 with rotary shaking (20 rpm) at 50 °C for 16 h. Insoluble material was removed by centrifugation (30,000xg, 5 min, 20 °C) and washed twice with 170 mL of water before the material was freeze-dried to obtain R6. R6 was dioxane extracted in the same manner as described for R4, but without pooling the supernatants after both extraction cycles. The resulting dioxane soluble fractions (S7-1 and S7-2) and the insoluble fraction (R7) are further referred to as 'bound lignin' and 'residual lignin', respectively. After every fractionation step about 150 mg freeze-dried material was kept apart and stored at -20 °C for further analyses.

Quantitative py-GC-MS with ^{13}C lignin as internal standard. Analytical pyrolysis coupled to gas chromatography with mass spectrometric detection (DSQ-II, Thermo Scientific, Waltham, MA, USA) was performed as previously described.^{13, 49, 53} To each sample (~80 µg), 10 µL of a ^{13}C lignin internal standard (IS) solution (1 mg mL⁻¹ ethanol/chloroform 50:50 v/v) was added and dried prior to analysis. All samples were prepared and analyzed in triplicate. Lignin-derived pyrolysis products were monitored in selected ion monitoring (SIM) mode on the two most abundant fragments per compound (both ^{12}C and ^{13}C). Pyrograms were processed by Xcalibur 2.2 software. Lignin contents and relative abundances of lignin-derived pyrolysis products were calculated as described previously.^{13, 49}

2D HSQC NMR spectroscopy. Around 25 mg of lignin isolate was dissolved in 0.25 mL DMSO-*d*₆ containing 0.01 M chromium(III) acetylacetonate (Cr(acac)₃) and pipetted into a Shigemi microcell. 2D heteronuclear single quantum coherence (HSQC) NMR was performed according to previously described methods.^{30, 54-55} The spectra were recorded at 25 °C with Bruker's standard pulse sequence "hsqcetgpsisp2.2" on a Bruker AVANCE III 600 MHz NMR spectrometer (Bruker BioSpin, Rheinstetten, Germany) equipped with a 5 mm cryoprobe located at MAGNEFY (MAGNETic resonance research Facility, Wageningen, The Netherlands) using the same settings as described elsewhere.⁴⁹ HSQC correlation peaks were assigned by comparison with literature.^{30, 56-61} Semiquantitative analysis of the volume integrals was performed according to del Río et al. by using TopSpin 4.0.5 software (Bruker), with previously published modifications.^{13, 30, 49} Contours were colored by using Adobe Illustrator software.

³¹P NMR spectroscopy. ³¹P NMR was performed as previously described.⁶² Around 30 mg of lignin isolate was mixed with 100 μ L *N,N*-dimethylformamide (DMF)/pyridine (50:50 v/v) and 100 μ L pyridine containing 15 mg mL⁻¹ cyclohexanol as internal standard and 2.5 mg mL⁻¹ Cr(acac)₃ as relaxation agent and stirred overnight to dissolve. Derivatization of the dissolved lignins was performed by the addition of 2-chloro-4,4,5,5-tetramethyl-1,3,2-dioxaphospholane (100 μ L pre-mixed with 400 μ L of deuterated chloroform). The phosphitylated lignins were measured on a Varian 400 MHz spectrometer using a standard phosphorus pulse sequence with 30° pulse angle (zgig30), inverse gated proton decoupling, interscan delay of 5 s and 256 scans. Signals were assigned according to Granata and Agyropoulos (1995) and integrated by using MestReNova 10 software.⁶³

Size-exclusion chromatography (SEC). Alkaline SEC was performed as described by Constant et al. (Method D).⁶⁴ Briefly, lignin isolates were dissolved in 0.5 M NaOH (eluent) in a concentration of 1 mg mL⁻¹ and the separation was performed by using two TSKgel GMPWxl columns (7.8 x 300 mm, particle size 13 μ m) in series equipped with a TSKgel guardcolumn PWxl (6.0 x 40 mm, particle size 12 μ m). Absorption was monitored at 280 nm with an ultraviolet spectroscopy detector. Sodium polystyrene sulphonate (PSS) standards and phenol were used for calibration. Protobind™ 1000 lignin (GreenValue S.A, Switzerland) was used as reference.

Organic SEC analyses were performed as previously described.⁶⁵ Briefly, lignin isolates were dissolved in DMSO containing 0.5% (w/v) LiBr (eluent) in a concentration of 10 mg mL⁻¹ and filtered through a 0.45 μ m PTFE filter before injection. The separation was performed by using a Agilent PL gel guard column (7.5 x 50 mm) and three Agilent PolarGel M columns (7.5 x 300 mm, particle size 5 μ m) in series.⁶⁶ Protonated PSS standards were utilized for calibration of the columns and RI and UV (280 nm) for detection. In order to obtain a more accurate molar mass correction factors from multi-angle light scattering (MALS) were applied as previously described.⁶⁵

Carbohydrate content and composition. Carbohydrate content and composition was determined in duplicate as constituent monosaccharides after acid hydrolysis by a modified method reported by Englyst & Cummings (see Supporting Information for details).⁶⁷

Results & Discussion

Fungal delignification of wheat straw. We previously described that *C. subvermispora* is able to effectively and selectively delignify wheat straw during seven weeks of growth (70% (w/w) lignin removal, 90% (w/w) carbohydrate retention) and showed through *in situ* analyses that the residual lignin was extensively altered in structure (see Figure S1 and Table S1 for new data of

additional time-points).¹³ Though the use of these *in situ* analyses ensured that the entire sample was analyzed, the whole-cell wall NMR analyses suffered from overlapping carbohydrate signals in the interunit linkage region. To allow a more comprehensive and in-depth structural characterization of residual lignin in fungal treated straw, lignin was fractionated according to the scheme presented in Figure 2. In recent work, we showed that diagnostic truncated structures were selectively extracted in fractionation steps 1-4, which enabled us to elucidate multiple *in situ* delignification pathways.⁴⁹ In the current work, we focused on the intact structural motifs that remained after fungal action to determine their relative susceptibilities to degradation. To that end, we analyzed the lignin remaining in the ball-milled water insoluble residue (R4). Similar relative amounts of lignin (~70% w/w) were recovered in this fraction for all time-points, allowing a fair comparison.⁴⁹

Fractionation of untreated and fungal-treated wheat straw lignin. Lignin in the ball-milled water-insoluble residue (R4) was quantitatively fractionated into 'free', 'bound' and unextractable (residue) lignin, achieving > 90% recovery in these three fractions at all time-points (Figure 3).

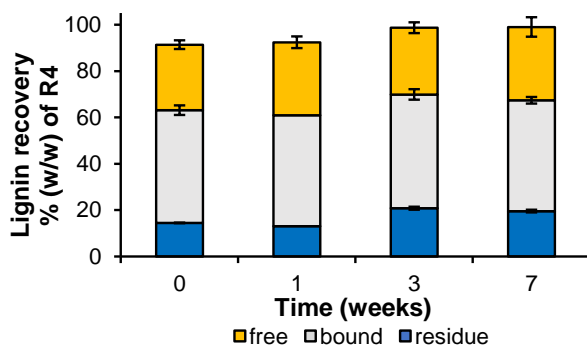


Figure 3. Recovery of lignin isolates. Recoveries were determined by using ¹³C-IS py-GC-MS. Average and standard deviation of analytical duplicates of fractionation duplicates. One fractionation replicate was obtained for bound and residue fractions of the week 1 sample. See Figure 2 and the experimental section for lignin fractionation details. 'Free' directly dioxane-extractable, 'bound' dioxane-extractable after enzymatic carbohydrate degradation, 'residue' dioxane unextractable.

A slight, but significant ($P < 0.05$) increase in unextractable lignin (res) was found after 3 and 7 weeks of fungal treatment, although at all time-points the combined extractable fractions (free + bound) summed up to ~80% of R4. Hence, the lignin fractions obtained were considered highly representative of the total lignin as present in the (residual) starting material. Yields for 'free' and 'bound' lignin were comparable to what has previously been reported for similar lignin isolations from untreated wheat straw.^{30, 68-69} In order to obtain a representative sample without unintentional degradation and further fractionation, the lignin isolates were not chemically purified.⁵¹⁻⁵² The purities of the crude isolates were comparable to what has previously been achieved with isolation schemes in which chemical workup was

omitted (Table S2).^{51-52, 69} In all isolates, carbohydrates were the major impurity and ranged from 14-26% (w/w). Other impurities most likely comprised fungal metabolites, especially in free lignin fractions.

Structural features of lignin isolates. Besides yield, also structure-wise the obtained isolates were highly representative of the lignin present in R4 (Table S3 and Table S4). Note that in regular py-GC-MS analyses, i.e. in the absence of methylating agents such as tetramethylammonium hydroxide (TMAH), the origin of vinyl products cannot be deduced.⁷⁰⁻⁷¹ Upon pyrolysis, these products arise from lignin's interunit linkages as well from decarboxylation reactions of hydroxycinnamic acids, in grasses mainly ferulate and *p*-coumarate, yielding 4-vinylguaiacol and 4-vinylphenol, respectively.^{30, 71} Compared to R4, the isolates showed very similar relative distributions of pyrolysis products, except for a decrease in such vinyl products. As ferulates and to lesser extents *p*-coumarates are attached to polysaccharides, they were more retained in the dioxane-insoluble residue R7 (Table S5). Furthermore, these substructures were partially solubilized, and hence removed, during enzymatic carbohydrate removal (data not shown). The fact that the fractions R4 and R7 showed close to identical relative distributions of pyrolysis products, further highlights that representative isolates were obtained. Additionally, this implied that R7, with low lignin contents (6-13% w/w), could be fairly excluded from detailed structural analyses without affecting the overall insights obtained.

SEC analyses of the isolates confirmed that polymeric lignins were obtained, also after fungal growth (Figure S2). Alkaline SEC of free lignin isolated from untreated straw showed a weight-average (M_w) molecular mass of 3535 g mol⁻¹ and a number-average (M_n) molecular mass of 1650 g mol⁻¹, resulting in a relatively narrow dispersity (M_w/M_n , \bar{D}) of 2.1, which is in agreement with previous lignin isolations from wheat straw.^{30, 69} Bound lignin of untreated straw showed considerably larger molar masses, with 5280 g mol⁻¹ and 2155 g mol⁻¹, for M_w and M_n , respectively, again displaying a relatively narrow dispersity ($\bar{D} \sim 2.5$). Considerably higher molecular weights of the untreated isolates were obtained by organic SEC analyses, in particular after employing correction factors for the conventional calibrant calculated on the basis of SEC-MALS (multi-angle light scattering) analyses ($M_{w,free}$ 17630 g mol⁻¹, $M_{w,bound}$ 29920 g mol⁻¹).⁶⁵ Although higher dispersities were obtained by organic SEC analyses ($\bar{D} \sim 3.6$), they were still lower than reported for a comparable lignin isolate ($\bar{D} \sim 5$) that was analyzed in the same manner.⁶⁵ All lignin isolates of fungal treated samples exhibited comparable dispersities and displayed only a slightly decreasing trend in M_w over fungal growth time (Figure S2).

A closer look at the py-GC-MS analyses indicated a slight decrease of S-units in the lignin isolates during fungal growth (H:G:S_{t=0} 9:63:29 vs H:G:S_{t=7} 9:67:24 in 'free' isolates), besides an increase of C_α-oxidized and unsubstituted pyrolysis products at the expense of products with an intact three-carbon side-chain (PhCy)

Figure 4. Aliphatic (A) and aromatic (B) regions of ^1H - ^{13}C HSQC NMR spectra of ‘free’ lignin isolates from untreated (left) and seven weeks *C. subvermispora* treated (right) wheat straw and annotated substructures (C). Dotted lines represent $-\text{H}$ or $-\text{OCH}_3$. Wavy lines indicate main positions for further coupling. Chemical shift assignments are reported in Table S6. Unassigned signals in grey; amino acid residues (Phe, phenylalanine) in black. The aromatic regions of ‘free’ lignin isolates presented correlation peaks of impurities and/or isolation artifacts, at similar intensities in untreated and treated samples. These unassigned peaks could be removed by classic Björkman chemical purification, but this purification also led to further fractionation of the lignin due to the fact that a major part of the lignin remained insoluble in 2:1 dichloroethane:ethanol (data not shown).⁵¹ As the unassigned peaks were well resolved and therefore expected not to interfere with our analysis, purification of the samples was not performed.

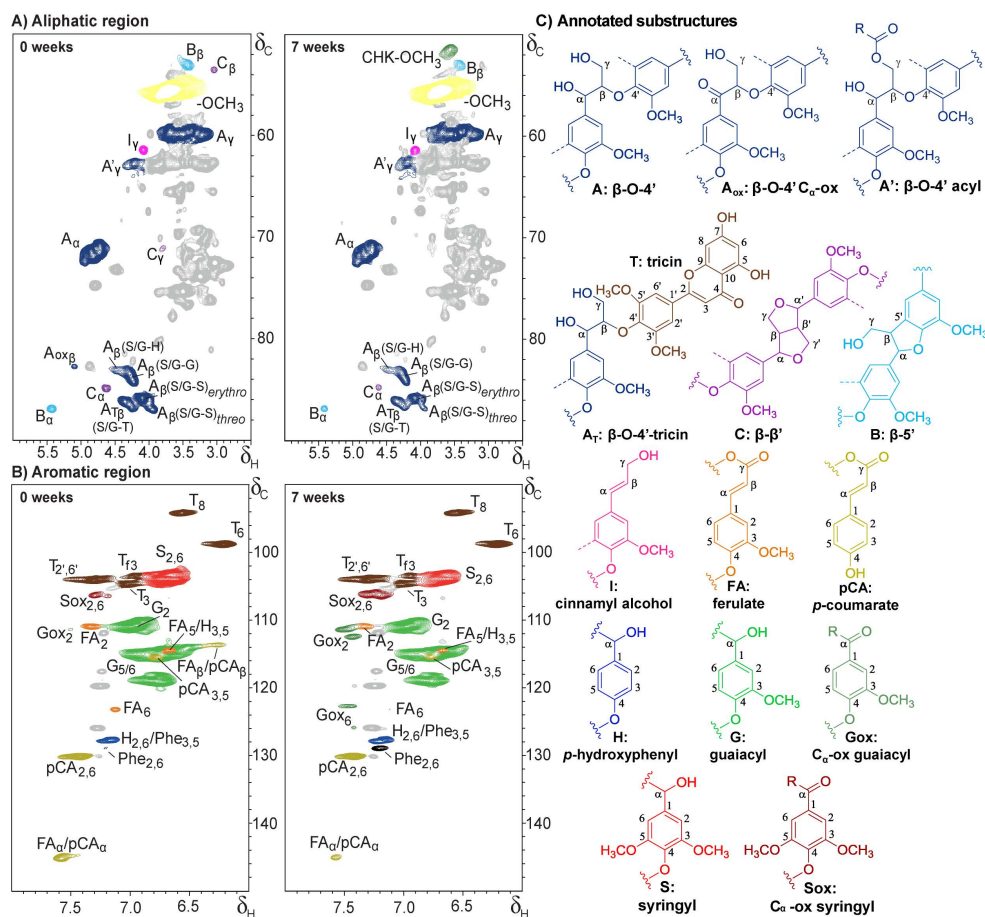


Figure 4. Aliphatic (A) and aromatic (B) regions of ^1H - ^{13}C HSQC NMR spectra of 'free' lignin isolates from untreated (left) and seven weeks *C. subvermispora* treated (right) wheat straw and annotated substructures (C). Dotted lines represent $-\text{H}$ or $-\text{OCH}_3$. Wavy lines indicate main positions for further coupling. Chemical shift assignments are reported in Table S6. Unassigned signals in grey; amino acid residues (Phe, phenylalanine) in black. The aromatic regions of 'free' lignin isolates presented correlation peaks of impurities and/or isolation artifacts, at similar intensities in untreated and treated samples. These unassigned peaks could be removed by classic Björkman chemical purification, but this purification also led to further fractionation of the lignin due to the fact that a major part of the lignin remained insoluble in 2:1 dichloroethane:ethanol (data not shown).⁵¹ As the unassigned peaks were well resolved and therefore expected not to interfere with our analysis, purification of the samples was not performed.

As mentioned above, especially the aliphatic region (δ_C/δ_H 50-90/2.5-6.0) benefitted from lignin isolation and showed clear lignin-derived signals (Figure 4A). Several substructures of the β -O-4' interunit linkages could be resolved. Besides the often-reported distinction between acylated (A'_V) and non-acylated, γ -OH substructures (A_V), we also distinguished β -O-4' linkages to triclin (A_T) from those linking lignin subunits (A), by their respective C_β/H_β correlations.⁶¹ Note that other β -O-4' aryl ether substructures bound to S-units with electron-withdrawing substituents might overlap with the $A_{T\beta}$ correlation peak.⁵⁶ However, most, if not all of the signal is constituted by S/G- β -O-4'-T units as deduced from semiquantitative analyses of the volume integrals of the $A_{T\beta}$ and $T_{2',6'}$ peaks.

S/G- β -O-4'-S and S/G- β -O-4'-G linkages, where the 4'-linked subunit represents ring B in Figure 1, were, furthermore, clearly resolved. In addition, the C_β/H_β correlations of the *erythro* and *threo* diastereomers of S/G- β -O-4' linkages to S-units presented well-isolated signals. The diastereomers linked to G-units could, as expected, not be discriminated.⁵⁶ Phenylcoumaran (β -5') and resinol (β - β') substructures were readily observed as well, whereas C α -oxidized (α -keto) β -O-4' substructures required higher zoom levels in the isolates of 7 weeks treated straw. Dibenzodioxocins (5-5'/4-O- β') and spirodienones (β -1'/ α -O- α') were only observed at zoom levels where other correlation peaks started to overlap, and were, therefore, excluded. In the aromatic region (Figure 4B), typical wheat straw lignin signals were observed ($S_{2,6}$, G_2 , $H_{2,6}$ and several triclin (T), *p*CA and FA related signals).^{30, 72} Several signals related to C α -oxidized aromatic units became more apparent in fungal treated samples.¹³ A summary of the semiquantitative analyses of the volume integrals (Figure 4) is presented in Table 1 for main aromatic units and in Figure 5 for interunit linkages.

Table 1. Semiquantitative HSQC NMR structural characterization of lignin isolates of residual wheat straw during growth of *C. subvermispora*.

	Free (weeks)				Bound (weeks)			
	0	1	3	7	0	1	3	7
Lignin subunits (%)^a								
H	3	3	3	2	3	3	3	3
G	59	60	55	55	57	56	57	62
G _{ox}	0	1	6	11	0	1	2	4
S	35	33	28	23	40	38	33	28
S _{ox}	3	3	7	9	1	2	5	4
S/G	0.6	0.6	0.6	0.5	0.7	0.7	0.6	0.5
Hydroxycinnamates (%)^b								
<i>p</i> -coumarate	10	9	11	13	5	5	4	4
ferulate	5	5	6	4	5	6	6	6
Flavonolignin (%)^b								
triclin	13	12	14	15	6	6	7	9

^a relative distribution of lignin subunits (H+G+G_{ox}+S+S_{ox}=100)

^b relative volume integral of substructure versus volume integral of total lignin subunits

Besides the use of an adiabatic pulse sequence, semiquantitative analyses benefited from the relatively similar polydispersities of the lignin isolates, given the fact that quantification accuracy is largely dependent on the molecular weight distribution of the components in the sample.⁷³⁻⁷⁴ In an attempt to further improve the accuracy, the HSQC spectra were recorded in the presence of Cr(acac)₃, a relaxation agent that is commonly employed in 1D NMR analyses, like ¹³C and ³¹P NMR, but is, to the best of our knowledge, not considered for application with HSQC NMR analysis.^{64, 75} We found that the presence of Cr(acac)₃ reduced the overestimation of pendant/end-group units attached to the lignin polymer (*p*-CA, FA, and T; Table 1 and Table S7).^{30, 37, 55} In addition, we noticed a suppression of resinol substructures in the presence of Cr(acac)₃, which could analogously indicate that they occur as pendant units. The other structural characteristics, including those targeted by fungal action were not extensively affected (Table S7). Therefore, the addition of Cr(acac)₃ might help to provide more accurate insight into the actual distribution of lignin's structural features by HSQC NMR.

The overall lignin subunit composition of both the 'free' and 'bound' isolates (Table 1) matched very well with what we previously observed by using whole cell wall NMR on unfractionated samples.¹³ Again, a preference for the removal of S units could be recognized (H:G:S_{t=0} 3:59:38 vs H:G:S_{t=7} 2:66:32 in 'free' isolates). C_α-oxidized substructures steadily accumulated upon fungal action and were predominantly found in 'free' lignin isolates, where they comprised up to 20% of all lignin subunits after 7 weeks of fungal growth (Table 1). Tricin and *p*-CA substructures accumulated during fungal growth as well, whereas ferulates appeared rather stable. These findings will be further discussed in the next section.

Susceptibility of lignin's structural motifs to fungal degradation. Fungal action resulted in a clear reduction of intact interunit linkages in both 'free' (71 to 50 per 100 subunits) and 'bound' (68 to 53 per 100 subunits) lignin fractions during 7 weeks of treatment (Figure 5). With the decrease in intact interunit linkages, C_α-oxidized substructures increased, without concomitant increase in C_α-oxidized β-O-4' interunit linkages. Therefore, we imply that the signal of C_α-oxidized substructures originated from cleavage products that remained attached to the polymer. The latter is inferred from the fact that no low molecular weight material was present in the lignin isolates (Figure S2). Though the intact interunit linkages clearly decreased upon fungal action, the molecular weight of isolated lignins remained rather constant, which might point to the occurrence of repolymerization reactions (Figure 5 and Figure S2). Such repolymerization reactions, presumably driven by radical chemistry, might also have involved some (initially released) C_α-oxidized substructures.

In accordance with these findings, ³¹P NMR showed an increase in carboxylic acid residues during fungal growth as well as an increase in phenolic hydroxyl groups (Table S8). Neither py-GC-MS, nor HSQC-NMR analyses suggested the presence of demethylated subunits and, therefore, we infer that the increase in phenolic

hydroxyl groups was solely due to the cleavage of phenolic and non-phenolic interunit linkages.⁷⁶ We conclude that the rate of formation of free phenolic hydroxyl groups exceeded the rate of removal and consequently that free phenolic subunits were not preferentially targeted over their non-phenolic analogs, even though the former subunits are generally regarded to be more susceptible to (enzymatic) oxidative degradation.⁷⁷⁻⁷⁸

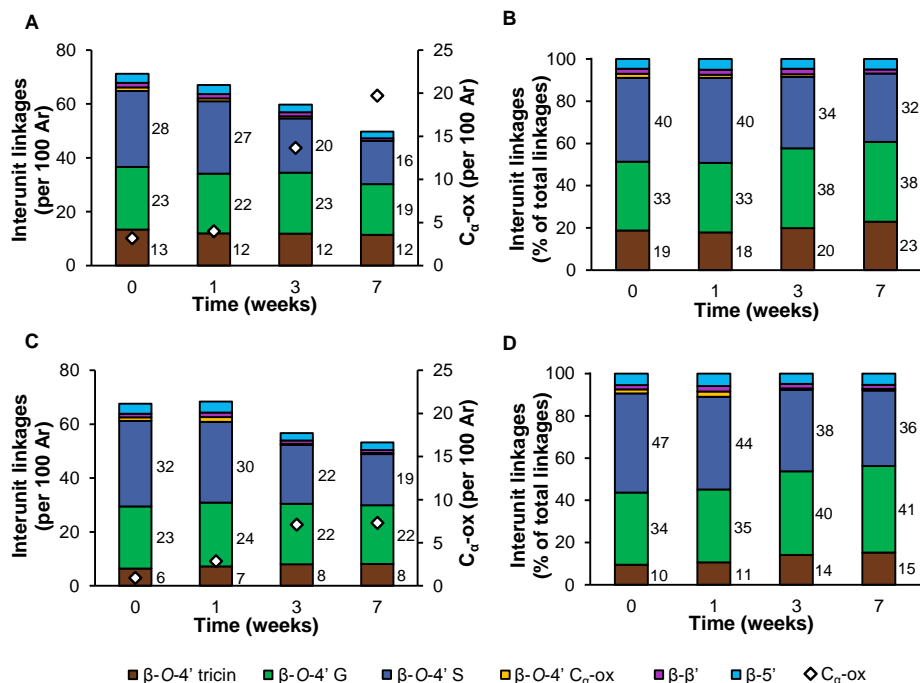


Figure 5. Semiquantitative HSQC NMR analysis of intact interunit linkages in lignin isolates of residual wheat straw during growth of *C. subvermispora*. A, B: free lignin isolates; C, D: bound lignin isolates. Ar: aromatic rings.

Our results showed that the relative proportion of β -O-4' aryl ethers (total) to β -5' and β - β' substructures was relatively constant during fungal growth (Figure 5B,D). The more condensed C-C linked structures, thus, appeared to have a similar susceptibility to fungal degradation/removal as compared to β -O-4' aryl ethers. Conflicting results have previously been reported on the susceptibility of condensed linkages to degradation by *C. subvermispora*. Using model compounds, Daina et al. showed that a phenolic β -5' phenylcoumaran structure was efficiently degraded, whereas its non-phenolic counterpart was almost completely resistant.²⁸ In actual biomass, a preferential removal of β -O-4' aryl ethers as compared to condensed linkages was found in loblolly pine, whereas β -5' phenylcoumarans and β - β' resinols seemed more effectively removed from white spruce.^{45, 48} It is important to note that the latter observations were derived from isolates that were obtained in low yields (< 5%), due to which it cannot be excluded that certain lignin

populations were underrepresented. Not only the type of interunit linkage, but also the substructures the linkage consists of, e.g. the A and B-ring subunits, might influence the susceptibility to degradation.

Indeed, in wheat straw, the different substructures of the β -O-4' aryl ethers showed pronounced differences in cleavage susceptibility. β -O-4' aryl ethers linked to S-units (ring B, Figure 1) were found to be considerably more degraded by *C. subvermispota* than their counterparts linked to G-units ($S/G\text{-}\beta\text{-O-4'-S} > S/G\text{-}\beta\text{-O-4'-G}$). After 7 weeks of fungal growth, β -O-4'-S units were depleted by approximately 40% in both 'free' and 'bound' fractions, whereas β -O-4'-G units were depleted by 19% and 6% in these fractions, respectively (Figure 5).

S-units have previously been described to be more susceptible to fungal action than G-units and this was suggested to be caused by a lower redox potential and absence of condensed carbon-carbon linked structures as an effect of the additional methoxyl group in S-units.⁷⁹ We show that the preferential degradation of S-units was maintained also within interunit linkages of the same type and, thus, that the preference is not only due to the degree of condensation. More specifically, our results indicated that the cleavage of β -O-4' aryl ether linkages was influenced by the degree of methoxylation of the 4'-O-coupled subunit. Due to the fact that β -O-4' ethers differing in degree of methoxylation of subunit A are not resolved in (regular) HSQC NMR spectra of non-acetylated samples, it cannot be further specified whether the degree of methoxylation also affected the cleavage of linkages attached to the 1'-position of that subunit.

In addition, when the 4'-O-coupled ring was part of a tricin molecule that was incorporated into the lignin polymer, the susceptibility to degradation was reduced even further. In 'free' as well as 'bound' lignin fractions β -O-4'-tricin aryl ethers relatively accumulated and this effect was largest in the latter fractions (Figure 5D, β -O-4'-tricin_{t=0} 10% vs β -O-4'-tricin_{t=7} 15%).

Besides the structure of the B-ring, diastereochemistry was shown to impact the susceptibility to degradation of β -O-4' aryl ethers (Table 2). By comparing the *threo* and *erythro*-diastereomers of β -O-4'-S units during fungal growth we found that these linkages were depleted with a marked *threo*-preference. This gave rise to an increase in the *erythro*/*threo* ratio in the 'free' lignin isolates from 2.2 to 4 after 7 weeks of fungal growth (Table 2). 'Bound' lignin isolates also displayed the diastereoselective removal of β -O-4' units, although to much lower extents.

Table 2. Degree of γ -acylation and diastereomer ratio of β -O-4' aryl ethers in lignin isolates of residual wheat straw during growth of *C. subvermispota*. Determined by using semiquantitative HSQC NMR.

	Free (weeks)				Bound (weeks)			
	0	1	3	7	0	1	3	7
γ -acylation (%)	10	13	14	16	23	24	23	25
<i>erythro</i> / <i>threo</i> ^a	2.2	2.6	2.8	4.0	2.6	2.5	2.9	2.9

^a ratio of $A_{\beta}(S/G\text{-S})_{\text{erythro}}$ and $A_{\beta}(S/G\text{-S})_{\text{threo}}$, diastereomers for β -O-4' aryl ethers coupled to G-units were not resolved

The formation of *threo* or *erythro* diastereomers during lignin biosynthesis is determined by both of the subunits (ring A and B) the linkage is bound to. While S-units preferentially form *erythro* diastereomers, also reflected in the *erythro/threo* ratio of untreated straw lignin isolates, G-units link without a diastereomeric preference.³¹ Based on selectivity for *threo*-diastereomers alone, a preferential removal of β -O-4' aryl ethers linked to G-units might, thus, be expected. The fact that a total preference for the removal of β -O-4'-S units still prevailed, could indicate that the degree of methoxylation of the B-ring is a stronger determinant for susceptibility than stereoisomerism. Diastereoselectivity for the degradation of the *threo*-isomers by *C. subvermispota* has been demonstrated before on spruce wood, consisting entirely of G-units.⁴⁸

Even though tricin takes part in the same combinatorial radical coupling processes that occur between monolignols, with its dimethoxylated ring acting like a regular S-unit, it is uncertain whether tricin's B-ring steers the formation of diastereomers in a similar fashion.^{31, 36} Tricin is considered to be incorporated in the macromolecule majorly via binding to G-units (G- β -O-4'-tricin), so it can be postulated that the tricin bound β -O-4' aryl ethers should be present without a clear diastereomeric preference.^{31, 37} The latter was also observed in tricin oligolignols extracted from maize and biomimetic coupling reactions between coniferyl alcohol and tricin.^{36, 80} Thus, the fact that tricin-containing substructures appeared more resistant against fungal degradation, is unlikely to be an effect of stereochemistry alone. A slight shift in the ratio of the correlation peaks belonging to β -O-4' tricin substructures was observed, which does suggest a different susceptibility of the different isoforms of tricin-containing substructures. C_β -H β peaks of β -O-4' tricin substructures are, however, not sufficiently resolved to further speculate which substructure was degraded more extensively.⁶¹

In addition to tricin incorporation, the incorporation of acyl groups at the γ -OH position of β -O-4' aryl ethers influenced the susceptibility to degradation. In 'free' lignin isolates, γ -acylated substructures accumulated from 10% to 16%. Acylation levels in untreated straw were comparable to what has previously been reported for similar wheat straw lignin isolates.^{30, 72} From the relatively low levels of *p*-coumarate in 'bound' isolates, it is deduced that γ -acyl groups were largely comprised of acetates. Due to the fact that the levels of γ -acylation remained rather constant in bound isolates, the presence of γ -acetates seems to have influenced the degradability to a lesser extent than *p*-coumarates, which might be explained by the bulkiness of the esterifying group. The fact that tricin incorporation and γ -acylation yielded substructures more resistant against degradation, might (partially) explain why we previously observed that *C. subvermispota* more efficiently degraded wheat straw lignin as plant maturity increased.¹⁶ In younger plant tissues, the relative levels of tricin and γ -acylated substructures are higher.^{33,36, 59}

Mechanistic insight into the delignification mechanisms of *C. subvermispora*. The clear difference in susceptibility of various β -O-4' aryl ether substructures provided new insight into the underlying delignification mechanisms. The apparent B-ring dependence indicated that the effects of subunit oxidation were, at least for a substantial part, exerted on the linkages attached to the 4' position. Not only is this in line with the previously reported high abundance of β -O-4' aryl ether cleavage reactions, it supports the very argument that ligninolysis is initiated by single-electron transfer (SET) oxidation.⁴⁹ In accordance with SET oxidation, the decreasing susceptibility in the order β -O-4'-S > β -O-4'-G > β -O-4'-tricin suggests that electron-density of the 4'-O-coupled ring is an important driving force for degradability. Whereas methoxyl groups increase the electron density of the B-ring, the conjugated system of triclin is expected to withdraw electrons.

The early onset of lignin degradation (within 1 week) found in this work, further corroborates the presumption that the collective enzymatic machinery of *C. subvermispora* acts in concert with diffusible low-molecular-weight oxidants.³⁸⁻⁴¹ Such a proximal oxidant role has been ascribed to alk(en)ylitaconic acids, sometimes referred to as 'ceriporic acids', secondary metabolites produced abundantly by *C. subvermispora*.^{39, 42-43} These alkylitaconic acids can take part in ligninolytic MnP-mediated lipid peroxidation reactions, which were shown to proceed *threo*-diastereopreferentially.⁴⁴ As also discussed previously, the observed *threo*-preference in this work further corroborates the suggestion that delignification by *C. subvermispora* is initiated by single-electron transfer.⁴⁸⁻⁴⁹ Enzymatic and chemical oxidations of lignin model compounds via an electron transfer mechanism have consistently shown a clear preference for the conversion of the *threo*-form, though it must be noted that this is based on the disappearance of the initial substrate only.^{25, 44, 81-82} Cho et al. showed that SET-oxidation of diastereomerically pure β -O-4' dimers resulted in substantially more C α -oxidized intact dimers for the *threo*-form, demonstrating that in fact the *erythro*-diastereomer was cleaved to a further extent.⁸³ Such 'intact' oxidation products did not accumulate in our residual fungal treated material, from which it is established that diastereoselective cleavage had indeed occurred.

The observations that *threo* diastereomers of β -O-4' aryl ethers were preferentially degraded and incorporation of *p*-coumarate (*p*-CA) at the γ -OH position increased resistance suggest that local steric hindrance and conformation might be major determinants for susceptibility against fungal degradation. Langer et al. showed that *threo* forms of β -O-4' aryl ethers exist in a more 'extended' or 'open' form and, consequently, might be more accessible to or promote interaction with the diffusible oxidants.⁸⁴ To the best of our knowledge, conformational studies on structural motifs exclusively occurring in grass lignin have not been performed. However, steric hindrance by γ -acylating *p*-coumaryl groups can be easily conceived. We postulate that this steric hindrance at the molecular level might affect diffusible oxidants as well as ligninolytic enzymes. Both need to be able to

approach the structure in close enough proximity and/or in a certain configuration that allows for interaction and electron transfer.

Conclusions

This study has provided new insight into the delignification mechanisms of the biotechnologically relevant white-rot fungus *C. subvermispora*. We demonstrated that several structural motifs of wheat straw lignin differed in susceptibility to degradation. Our results imply that electron density of the 4'-O-coupled ring and local steric hindrance were underlying the cleavage susceptibility of β -O-4' aryl ethers. The susceptibility of these β -O-4' aryl ether substructures is consistent with ligninolysis mechanisms that are initiated by single-electron transfer. We anticipate that the insights obtained will aid future efforts to improve the valorization of lignocellulosic biomass, first and foremost by presenting a structural rationale for selecting substrates that are more fit-for-purpose.

Acknowledgements

Nazri Nayan, John W. Cone, Arend F. van Peer and Anton S. M. Sonnenberg (Wageningen University & Research) are gratefully acknowledged for providing the *C. subvermispora* treated wheat straw. We thank Christopher Lancefield (University of St Andrews) for discussion on the quantitateness of HSQC NMR analyses. This article is based upon work from COST Action CA17128 "Establishment of a Pan-European Network on the Sustainable Valorisation of Lignin (LignoCOST)", supported by COST (European Cooperation in Science and Technology).

References

1. Ragauskas, A. J.; Williams, C. K.; Davison, B. H.; Britovsek, G.; Cairney, J.; Eckert, C. A.; Frederick, W. J.; Hallett, J. P.; Leak, D. J.; Liotta, C. L., The path forward for biofuels and biomaterials. *Science* **2006**, *311*, 484-489.
2. Behera, S.; Arora, R.; Nandhagopal, N.; Kumar, S., Importance of chemical pretreatment for bioconversion of lignocellulosic biomass. *Renewable and Sustainable Energy Rev* **2014**, *36*, 91-106.
3. Isikgor, F. H.; Becer, C. R., Lignocellulosic biomass: a sustainable platform for the production of bio-based chemicals and polymers. *Polym Chem* **2015**, *6*, 4497-4559.
4. Van Kuijk, S. J. A.; Sonnenberg, A. S. M.; Baars, J. J. P.; Hendriks, W. H.; Cone, J. W., Fungal treated lignocellulosic biomass as ruminant feed ingredient: a review. *Biotechnol Adv* **2015**, *33*, 191-202.
5. Himmel, M. E.; Ding, S.-Y.; Johnson, D. K.; Adney, W. S.; Nimlos, M. R.; Brady, J. W.; Foust, T. D., Biomass recalcitrance: engineering plants and enzymes for biofuels production. *Science* **2007**, *315*, 804-807.
6. Martínez, A. T.; Ruiz-Dueñas, F. J.; Martínez, M. J.; del Río, J. C.; Gutiérrez, A., Enzymatic delignification of plant cell wall: from nature to mill. *Curr Opin Biotechnol* **2009**, *20*, 348-357.
7. Hammel, K. E., Fungal degradation of lignin. In *Driven by nature: plant litter quality and decomposition*, Cadish, G.; Giller, K. E., Eds. CAB-International: Wallingford, 1997; pp 33-47.

8. Otjen, L.; Blanchette, R.; Effland, M.; Leatham, G., Assessment of 30 white rot basidiomycetes for selective lignin degradation. *Holzforschung* **1987**, *41*, 343-349.
9. Tuyen, V.; Cone, J.; Baars, J.; Sonnenberg, A.; Hendriks, W., Fungal strain and incubation period affect chemical composition and nutrient availability of wheat straw for rumen fermentation. *Bioresour Technol* **2012**, *111*, 336-342.
10. Tian, X. f.; Fang, Z.; Guo, F., Impact and prospective of fungal pre-treatment of lignocellulosic biomass for enzymatic hydrolysis. *Biofuels Bioprod Biorefin* **2012**, *6*, 335-350.
11. Camarero, S.; Martínez, M. J.; Martínez, A. T., Understanding lignin biodegradation for the improved utilization of plant biomass in modern biorefineries. *Biofuels, Bioprod Biorefin* **2014**, *8*, 615-625.
12. Sindhu, R.; Binod, P.; Pandey, A., Biological pretreatment of lignocellulosic biomass—An overview. *Bioresour Technol* **2016**, *199*, 76-82.
13. Van Erven, G.; Nayan, N.; Sonnenberg, A. S.; Hendriks, W. H.; Cone, J. W.; Kabel, M. A., Mechanistic insight in the selective delignification of wheat straw by three white-rot fungal species through quantitative ¹³C-IS py-GC-MS and whole cell wall HSQC NMR. *Biotechnol Biofuels* **2018**, *11*, 262.
14. Van Kuijk, S. J. A.; Sonnenberg, A. S. M.; Baars, J. J. P.; Hendriks, W. H.; del Río, J. C.; Rencoret, J.; Gutiérrez, A.; de Ruijter, N. C. A.; Cone, J. W., Chemical changes and increased degradability of wheat straw and oak wood chips treated with the white rot fungi *Ceriporiopsis subvermispura* and *Lentinula edodes*. *Biomass Bioenergy* **2017**, *105*, 381-391.
15. Nayan, N.; Sonnenberg, A. S.; Hendriks, W. H.; Cone, J. W., Screening of white-rot fungi for bioprocessing of wheat straw into ruminant feed. *J Appl Microbiol* **2018**, *125*, 468-479.
16. Nayan, N.; van Erven, G.; Kabel, M. A.; Sonnenberg, A. S.; Hendriks, W. H.; Cone, J. W., Improving ruminal digestibility of various wheat straw types by white-rot fungi. *J Sci Food Agric* **2019**, *99*, 957-965.
17. Cianchetta, S.; Di Maggio, B.; Burzi, P. L.; Galletti, S., Evaluation of selected white-rot fungal isolates for improving the sugar yield from wheat straw. *Appl Biochem Biotechnol* **2014**, *173*, 609-623.
18. Wan, C.; Li, Y., Microbial pretreatment of corn stover with *Ceriporiopsis subvermispura* for enzymatic hydrolysis and ethanol production. *Bioresour Technol* **2010**, *101*, 6398-6403.
19. Salvachúa, D.; Prieto, A.; López-Abelairas, M.; Lu-Chau, T.; Martínez, Á. T.; Martínez, M. J., Fungal pretreatment: an alternative in second-generation ethanol from wheat straw. *Bioresour Technol* **2011**, *102*, 7500-7506.
20. Akhtar, M.; Attridge, M. C.; Myers, G. C.; Blanchette, R. A., Biomechanical pulping of loblolly pine chips with selected white-rot fungi. *Holzforschung* **1993**, *47*, 36-40.
21. Ferraz, A.; Guerra, A.; Mendonça, R.; Masarin, F.; Vicentim, M. P.; Aguiar, A.; Pavan, P. C., Technological advances and mechanistic basis for fungal biopulping. *Enzyme Microb Technol* **2008**, *43*, 178-185.
22. Wan, C.; Li, Y., Fungal pretreatment of lignocellulosic biomass. *Biotechnol Adv* **2012**, *30*, 1447-1457.
23. Fernández-Fueyo, E.; Ruiz-Dueñas, F. J.; Ferreira, P.; Floudas, D.; Hibbett, D. S.; Canessa, P.; Larrondo, L. F.; James, T. Y.; Seelenfreund, D.; Lobos, S.; Polanco, R.; Tello, M.; Honda, Y.; Watanabe, T.; Watanabe, T.; Ryu, J. S.; Kubicek, C. P.; Schmöll, M.; Gaskell, J.; Hammel, K. E.; St. John, F. J.; Vanden Wymelenberg, A.; Sabat, G.; Splinter Bondurant, S.; Khajamohiddin, S.; Jagit, Y. S.; Doppapaneni, H.; Subramanian, V.; José, L. L.; Oguiza, J. A.; Perez, G.; Pisabarro, A. G.; Ramirez, L.; Santoyo, F.; Master, E.; Coutinho, P. M.; Henrissat, B.; Lombard, V.; Magnuson, J. K.; Kües, U.; Hori, C.; Igarashi, K.; Samejima, M.; Held, B. W.; Barry, K. W.; Labutti, K. M.; Lapidus, A.; Lindquist, E. A.; Lucas, S. M.; Riley, R.; Salamov, A. A.; Hoffmeister, D.; Schwenk, D.; Hadar, Y.; Yarden, O.; de Vries, R. P.; Wiebenga, A.; Stenlid, J.; Eastwood, D.; Grigoriev,

- I. V.; Berka, R. M.; Blanchette, R. A.; Kersten, P.; Martínez, A. T.; Vicuna, R.; Cullen, D., Comparative genomics of *Ceriporiopsis subvermispora* and *Phanerochaete chrysosporium* provide insight into selective ligninolysis. *Proc Natl Acad Sci* **2012**, *109*, 5458-5463.
24. Hori, C.; Gaskell, J.; Igarashi, K.; Kersten, P.; Mozuch, M.; Samejima, M.; Cullen, D., Temporal alterations in secretome of selective ligninolytic fungi *Ceriporiopsis subvermispora* during growth on aspen wood reveal its strategy of degrading lignocellulose. *Appl Environ Microbiol* **2014**, *80*, 2062-2070.
25. Fernández-Fueyo, E.; Ruiz-Dueñas, F. J.; Miki, Y.; Martínez, M. J.; Hammel, K. E.; Martínez, A. T., Lignin-degrading peroxidases from genome of selective ligninolytic fungus *Ceriporiopsis subvermispora*. *J Biol Chem* **2012**, *287*, 16903-16916.
26. Srebotnik, E.; Jensen, K.; Kawai, S.; Hammel, K. E., Evidence that *Ceriporiopsis subvermispora* degrades nonphenolic lignin structures by a one-electron-oxidation mechanism. *Appl Environ Microbiol* **1997**, *63*, 4435-4440.
27. Jensen, K. A.; Bao, W.; Kawai, S.; Srebotnik, E.; Hammel, K. E., Manganese-dependent cleavage of nonphenolic lignin structures by *Ceriporiopsis subvermispora* in the absence of lignin peroxidase. *Appl Environ Microbiol* **1996**, *62*, 3679-3686.
28. Daina, S.; Orlandi, M.; Bestetti, G.; Wiik, C.; Elegir, G., Degradation of β -5 lignin model dimers by *Ceriporiopsis subvermispora*. *Enzyme Microb Technol* **2002**, *30*, 499-505.
29. Vanholme, R.; Demedts, B.; Morreel, K.; Ralph, J.; Boerjan, W., Lignin biosynthesis and structure. *Plant Physiol* **2010**, *153*, 895-905.
30. Del Río, J. C.; Rencoret, J.; Prinsen, P.; Martínez, A. T.; Ralph, J.; Gutiérrez, A., Structural characterization of wheat straw lignin as revealed by analytical pyrolysis, 2D-NMR, and reductive cleavage methods. *J Agric Food Chem* **2012**, *60*, 5922-5935.
31. Akiyama, T.; Goto, H.; Nawawi, D. S.; Syafii, W.; Matsumoto, Y.; Meshitsuka, G., Erythro/threo ratio of β -O-4 structures as an important structural characteristic of lignin. Part 4: Variation in the erythro/threo ratio in softwood and hardwood lignins and its relation to syringyl/guaiacyl ratio. *Holzforschung* **2005**, *59*, 276-281.
32. Ralph, J.; Brunow, G.; Harris, P. J.; Dixon, R. A.; Schatz, P. F.; Boerjan, W., Lignification: are lignins biosynthesized via simple combinatorial chemistry or via proteinaceous control and template replication? In *Recent Advances in Polyphenol Research*, Lattanzio, V.; Daayf, F., Eds. Wiley-Blackwell: Oxford, 2009; Vol. 1, pp 36-66.
33. Crestini, C.; Argyropoulos, D. S., Structural analysis of wheat straw lignin by quantitative ^{31}P and 2D NMR spectroscopy. The occurrence of ester bonds and α -O-4 substructures. *J Agric Food Chem* **1997**, *45*, 1212-1219.
34. Ralph, J.; Bunzel, M.; Marita, J. M.; Hatfield, R. D.; Lu, F.; Kim, H.; Schatz, P. F.; Grabber, J. H.; Steinhart, H., Peroxidase-dependent cross-linking reactions of *p*-hydroxycinnamates in plant cell walls. *Phytochem Rev* **2004**, *3*, 79-96.
35. Ralph, J., Hydroxycinnamates in lignification. *Phytochem Rev* **2010**, *9*, 65-83.
36. Lan, W.; Lu, F.; Regner, M.; Zhu, Y.; Rencoret, J.; Ralph, S. A.; Zakai, U. I.; Morreel, K.; Boerjan, W.; Ralph, J., Tricin, a flavonoid monomer in monocot lignification. *Plant Physiol* **2015**, *167*, 1284-1295.
37. Lan, W.; Rencoret, J.; Lu, F.; Karlen, S. D.; Smith, B. G.; Harris, P. J.; del Río, J. C.; Ralph, J., Tricin-lignins: occurrence and quantitation of tricin in relation to phylogeny. *Plant J* **2016**, *88*, 1046-1057.
38. Blanchette, R. A.; Krueger, E. W.; Haight, J. E.; Akhtar, M.; Akin, D. E., Cell wall alterations in loblolly pine wood decayed by the white-rot fungus, *Ceriporiopsis subvermispora*. *J Biotechnol* **1997**, *53*, 203-213.
39. Enoki, M.; Watanabe, T.; Nakagame, S.; Koller, K.; Messner, K.; Honda, Y.; Kuwahara, M., Extracellular lipid peroxidation of selective white-rot fungus, *Ceriporiopsis subvermispora*. *FEMS Microbiol Lett* **1999**, *180*, 205-211.

40. Kirk, T. K.; Cullen, D., Enzymology and molecular genetics of wood degradation by white-rot fungi. In *Environmentally friendly technologies for the pulp and paper industry*, Young, R.; Akhtar, M., Eds. Wiley: New York, 1998; pp 273-307.
41. Fackler, K.; Grading, C.; Hinterstoisser, B.; Messner, K.; Schwanninger, M., Lignin degradation by white rot fungi on spruce wood shavings during short-time solid-state fermentations monitored by near infrared spectroscopy. *Enzyme Microb Technol* **2006**, 39, 1476-1483.
42. Gutiérrez, A.; del Río, J. C.; Martínez-Íñigo, M. J.; Martínez, M. J.; Martínez, Á. T., Production of new unsaturated lipids during wood decay by ligninolytic basidiomycetes. *Appl Environ Microbiol* **2002**, 68, 1344-1350.
43. Amirta, R.; Fujimori, K.; Shirai, N.; Honda, Y.; Watanabe, T., Ceriporic acid C, a hexadecenylitaconate produced by a lignin-degrading fungus, *Ceriporiopsis subvermispota*. *Chem Phys Lipids* **2003**, 126, 121-131.
44. Nishimura, H.; Sasaki, M.; Seike, H.; Nakamura, M.; Watanabe, T., Alkadienyl and alkenyl itaconic acids (ceriporic acids G and H) from the selective white-rot fungus *Ceriporiopsis subvermispota*: a new class of metabolites initiating ligninolytic lipid peroxidation. *Org Biomol Chem* **2012**, 10, 6432-6442.
45. Guerra, A.; Mendonça, R.; Ferraz, A.; Lu, F.; Ralph, J., Structural characterization of lignin during *Pinus taeda* wood treatment with *Ceriporiopsis subvermispota*. *Appl Environ Microbiol* **2004**, 70, 4073-4078.
46. Choi, J.; Choi, D.; Ahn, S.; Lee, S.; Kim, M.; Meier, D.; Faix, O.; Scott, G. M., Characterization of trembling aspen wood (*Populus tremuloides* L.) degraded with the white rot fungus *Ceriporiopsis subvermispota* and MWLs isolated thereof. *Holz Roh Werkst* **2006**, 64, 415-422.
47. Amirta, R.; Tanabe, T.; Watanabe, T.; Honda, Y.; Kuwahara, M.; Watanabe, T., Methane fermentation of Japanese cedar wood pretreated with a white rot fungus, *Ceriporiopsis subvermispota*. *J Biotechnol* **2006**, 123, 71-77.
48. Yelle, D. J.; Kapich, A. N.; Houtman, C. J.; Lu, F.; Timokhin, V. I.; Fort, R. C.; Ralph, J.; Hammel, K. E., A highly diastereoselective oxidant contributes to ligninolysis by the white rot basidiomycete *Ceriporiopsis subvermispota*. *Appl Environ Microbiol* **2014**, 80, 7536-7544.
49. Van Erven, G.; Hilgers, R.; de Waard, P.; Gladbeek, E.-J.; van Berkel, W. J. H.; Kabel, M. A., Elucidation of in situ ligninolysis mechanisms of the selective white-rot fungus *Ceriporiopsis subvermispota*. *ACS Sustainable Chem Eng* **2019**, 7, 16757-16764.
50. Nayan, N.; Sonnenberg, A. S. M.; Hendriks, W. H.; Cone, J. W., Differences between two strains of *Ceriporiopsis subvermispota* on improving the nutritive value of wheat straw for ruminants. *J Appl Microbiol* **2017**, 123, 352-361.
51. Björkman, A., Studies on finely divided wood. Part 1. Extraction of lignin with neutral solvents. *Sven Papperstidn* **1956**, 59, 477-485.
52. Chang, H.-M.; Cowling, E. B.; Brown, W., Comparative studies on cellulolytic enzyme lignin and milled wood lignin of sweetgum and spruce. *Holzforschung* **1975**, 29, 153-159.
53. Van Erven, G.; de Visser, R.; Merckx, D. W.; Strolenberg, W.; de Gijssels, P.; Gruppen, H.; Kabel, M. A., Quantification of lignin and its structural features in plant biomass using ¹³C lignin as internal standard for pyrolysis-GC-SIM-MS. *Anal Chem* **2017**, 89, 10907-10916.
54. Kim, H.; Ralph, J.; Akiyama, T., Solution-state 2D NMR of ball-milled plant cell wall gels in DMSO-d₆. *BioEnergy Res* **2008**, 1, 56-66.
55. Mansfield, S. D.; Kim, H.; Lu, F.; Ralph, J., Whole plant cell wall characterization using solution-state 2D NMR. *Nat Protoc* **2012**, 7, 1579-1589.
56. Ralph, S. A.; Ralph, J.; Landucci, L., NMR database of lignin and cell wall model compounds. **2009**, Available at URL www.qibrc.org/databases_and_software/nmrdatabase/.
57. Rencoret, J.; Gutiérrez, A.; Nieto, L.; Jiménez-Barbero, J.; Faulds, C. B.; Kim, H.; Ralph, J.; Martínez, Á. T.; del Río, J. C., Lignin composition and structure in

- young versus adult *Eucalyptus globulus* plants. *Plant Physiol* **2011**, *155*, 667-682.
58. Rencoret, J.; Pereira, A.; del Río, J. C.; Martínez, Á. T.; Gutiérrez, A., Delignification and saccharification enhancement of sugarcane byproducts by a laccase-based pretreatment. *ACS Sustainable Chem Eng* **2017**, *5*, 7145-7154.
59. Del Río, J. C.; Lino, A. G.; Colodette, J. L.; Lima, C. F.; Gutiérrez, A.; Martínez, Á. T.; Lu, F.; Ralph, J.; Rencoret, J., Differences in the chemical structure of the lignins from sugarcane bagasse and straw. *Biomass Bioenergy* **2015**, *81*, 322-338.
60. Kim, H.; Padmakshan, D.; Li, Y.; Rencoret, J.; Hatfield, R. D.; Ralph, J., Characterization and elimination of undesirable protein residues in plant cell wall materials for enhancing lignin analysis by solution-state nuclear magnetic resonance spectroscopy. *Biomacromolecules* **2017**, *18*, 4184-4195.
61. Lan, W.; Yue, F.; Rencoret, J.; del Río, J.; Boerjan, W.; Lu, F.; Ralph, J., Elucidating tricin-lignin structures: assigning correlations in HSQC spectra of monocot lignins. *Polymers* **2018**, *10*, 916.
62. Gosselink, R. J. A.; van Dam, J. E. G.; de Jong, E.; Scott, E. L.; Sanders, J. P. M.; Li, J.; Gellerstedt, G., Fractionation, analysis, and PCA modeling of properties of four technical lignins for prediction of their application potential in binders. *Holzforschung* **2010**, *64*, 193-200.
63. Granata, A.; Argyropoulos, D. S., 2-Chloro-4,4,5,5-tetramethyl-1,3, 2-dioxaphospholane, a reagent for the accurate determination of the uncondensed and condensed phenolic moieties in lignins. *J Agric Food Chem* **1995**, *43*, 1538-1544.
64. Constant, S.; Wienk, H. L. J.; Frissen, A. E.; de Peinder, P.; Boelens, R.; van Es, D. S.; Grisel, R. J. H.; Weckhuysen, B. M.; Huijgen, W. J. J.; Gosselink, R. J. A., New insights into the structure and composition of technical lignins: a comparative characterisation study. *Green Chem* **2016**, *18*, 2651-2665.
65. Zinovyev, G.; Sulaeva, I.; Podzimek, S.; Rössner, D.; Kilpeläinen, I.; Sumerskii, I.; Rosenau, T.; Potthast, A., Getting closer to absolute molar masses of technical lignins. *ChemSusChem* **2018**, *11*, 3259-3268.
66. Sulaeva, I.; Zinovyev, G.; Plankeele, J. M.; Sumerskii, I.; Rosenau, T.; Potthast, A., Fast track to molar-mass distributions of technical lignins. *ChemSusChem* **2017**, *10*, 629-635.
67. Englyst, H. N.; Cummings, J. H., Simplified method for the measurement of total non-starch polysaccharides by gas-liquid chromatography of constituent sugars as alditol acetates. *Analyst* **1984**, *109*, 937-942.
68. Jiang, B.; Cao, T.; Gu, F.; Wu, W.; Jin, Y., Comparison of the structural characteristics of cellulolytic enzyme lignin preparations isolated from wheat straw stem and leaf. *ACS Sustainable Chem Eng* **2016**, *5*, 342-349.
69. Zikeli, F.; Ters, T.; Fackler, K.; Srebotnik, E.; Li, J., Successive and quantitative fractionation and extensive structural characterization of lignin from wheat straw. *Ind Crops Prod* **2014**, *61*, 249-257.
70. Del Río, J.; Martin, F.; Gonzalez-Vila, F., Thermally assisted hydrolysis and alkylation as a novel pyrolytic approach for the structural characterization of natural biopolymers and geomacromolecules. *TrAC Trends Anal Chem* **1996**, *15*, 70-79.
71. Del Río, J. C.; Gutiérrez, A.; Rodríguez, I. M.; Ibarra, D.; Martínez, A. T., Composition of non-woody plant lignins and cinnamic acids by Py-GC/MS, Py/TMAH and FT-IR. *J Anal Appl Pyrolysis* **2007**, *79*, 39-46.
72. Zeng, J.; Helms, G. L.; Gao, X.; Chen, S., Quantification of wheat straw lignin structure by comprehensive NMR analysis. *J Agric Food Chem* **2013**, *61*, 10848-10857.
73. Lancefield, C. S.; Wienk, H. L.; Boelens, R.; Weckhuysen, B. M.; Bruijninx, P. C., Identification of a diagnostic structural motif reveals a new reaction intermediate and condensation pathway in kraft lignin formation. *Chem Sci* **2018**, *9*, 6348-6360.

74. Kupče, E.; Freeman, R., Compensated adiabatic inversion pulses: broadband INEPT and HSQC. *J Magn Reson* **2007**, *187*, 258-265.
75. Xia, Z.; Akim, L. G.; Argyropoulos, D. S., Quantitative ^{13}C NMR analysis of lignins with internal standards. *J Agric Food Chem* **2001**, *49*, 3573-3578.
76. Martínez, A. T.; Rencoret, J.; Nieto, L.; Jiménez-Barbero, J.; Gutiérrez, A.; del Río, J. C., Selective lignin and polysaccharide removal in natural fungal decay of wood as evidenced by *in situ* structural analyses. *Environ Microbiol* **2011**, *13*, 96-107.
77. Hammel, K. E.; Cullen, D., Role of fungal peroxidases in biological ligninolysis. *Curr Opin Plant Biol* **2008**, *11*, 349-355.
78. Wong, D. W., Structure and action mechanism of ligninolytic enzymes. *Appl Biochem Biotechnol* **2009**, *157*, 174-209.
79. Martínez, A.; Camarero, S.; Gutiérrez, A.; Bocchini, P.; Galletti, G., Studies on wheat lignin degradation by *Pleurotus* species using analytical pyrolysis. *J Anal Appl Pyrolysis* **2001**, *58*, 401-411.
80. Lan, W.; Morreel, K.; Lu, F.; Rencoret, J.; del Río, J. C.; Voorend, W.; Vermerris, W.; Boerjan, W.; Ralph, J., Maize tricin-oligolignol metabolites and their implications for monocot lignification. *Plant Physiol* **2016**, *171*, 810-820.
81. Bohlin, C.; Andersson, P.-O.; Lundquist, K.; Jönsson, L. J., Differences in stereo-preference in the oxidative degradation of diastereomers of the lignin model compound 1-(3, 4-dimethoxyphenyl)-2-(2-methoxyphenoxy)-1, 3-propanediol with enzymic and non-enzymic oxidants. *J Mol Catal B: Enzym* **2007**, *45*, 21-26.
82. Bohlin, C.; Lundquist, K.; Jönsson, L. J., Diastereomer selectivity in the degradation of a lignin model compound of the arylglycerol β -aryl ether type by white-rot fungi. *Enzyme Microb Technol* **2008**, *43*, 199-204.
83. Cho, D. W.; Parthasarathi, R.; Pimentel, A. S.; Maestas, G. D.; Park, H. J.; Yoon, U. C.; Dunaway-Mariano, D.; Gnanakaran, S.; Langan, P.; Mariano, P. S., Nature and kinetic analysis of carbon-carbon bond fragmentation reactions of cation radicals derived from set-oxidation of lignin model compounds. *J Org Chem* **2010**, *75*, 6549-6562.
84. Langer, V.; Lundquist, K.; Parkås, J., The stereochemistry and conformation of lignin as judged by X-ray crystallographic investigations of lignin model compounds: arylglycerol β -guaiacyl ethers. *BioResources* **2007**, *2*, 590-597

Supporting Information

Carbohydrate content and composition. Carbohydrate content and composition was determined in duplicate as constituent monosaccharides after acid hydrolysis by a modified method reported by Englyst & Cummings.¹ Ten mg of each sample was treated with 72% (w/w) H_2SO_4 for 1 h at 30 °C followed by 1 M H_2SO_4 for 3 h at 100 °C. Subsequently, samples were centrifuged (9,000xg, 5 min, 20 °C) and the supernatants were diluted (20x) before analysis. Degradation of monosaccharides during hydrolysis was corrected for by including monosaccharide standard mixtures in hydrolysis. Analysis was performed on a High Performance Anion Exchange Chromatography (HPAEC) Dionex ICS-5000 system (Thermo Scientific, Synnyvale, CA, USA). The system was equipped with a CarboPac PA-1 column (250 mm x 2 mm ID) in combination with a CarboPac guard column (50 mm x 2 mm ID) with pulsed amperometric detection (PAD) (all Dionex). 10 μL of sample was injected and eluted at a flow rate of 0.4 mL min^{-1} using a combination of three mobile phases: A) 0.1 M NaOH, B) 1 M NaOAc in 0.1 M NaOH and C) H_2O . The elution profile used was as follows: 0-35 min isocratic on 100% C; 35-50 min linearly from 100% A to 40% B; 50-55 min isocratic on 100% B; 55-63 min isocratic on 100% A; 63-78 min isocratic on 100% C. Post-column addition of 0.5 M NaOH at 0.1 mL min^{-1} was performed between 0-35 min and 63-78 min. Data was processed by using Chromeleon 7 (Thermo Scientific). The uronic acids released after the acid hydrolysis step, were determined in duplicate as anhydrouronic acid content by an

automated meta-hydroxydiphenyl assay with addition of sodium tetraborate using an auto-analyzer (Skalar Analytical BV, Breda, The Netherlands).² Glucuronic acid (Fluka AG, Busch, Switzerland) was used as a reference (0 – 100 $\mu\text{g mL}^{-1}$). Total carbohydrate content was calculated as the sum of neutral anhydrocarbohydrates and anhydrouronic acids.

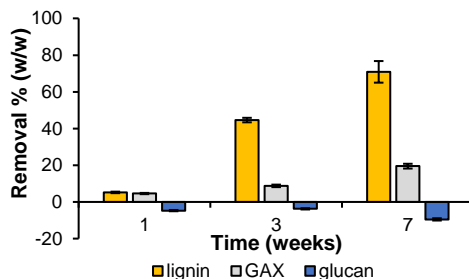


Figure S1. Lignin, glucuronoarabinoxylan (GAX) and glucan (cellulose) removal during fungal growth. Compositional analysis by using quantitative ^{13}C -IS py-GC-MS (lignin) and constituent monosaccharide analysis after H_2SO_4 hydrolysis (carbohydrates). Average and standard deviation of analytical triplicates on pooled biological triplicates. The negative values for glucan are caused by the production of fungal β -glucan, which cannot be distinguished from cellulose in constituent monosaccharide analysis. Note that the 7 weeks fungal treated sample has been previously analyzed and reported in van Erven et al. (2018).³ This time-point was reanalyzed for this work.

Compositional analyses showed that lignin degradation by *C. subvermispora* was evident from the first week of growth on wheat straw (Figure S1). In the early stage, lignin and hemicellulose (glucuronoarabinoxylan, GAX) were removed to similar extent ($\sim 5\%$ (w/w)), while cellulose appeared unaffected. The relatively unselective action in the initial stage of growth is explained by the availability of (more) easily degradable carbohydrates. As soon as these were depleted, lignin degradation became more selective. After 3 weeks of growth, up to 45% (w/w) lignin was removed at the expense of 9% (w/w) GAX. During further growth, delignification continued and reached 71% (w/w) after 7 weeks, while GAX removal increased to 19% (w/w).³ Still, after 7 weeks of treatment more than 90% of the initial carbohydrates were retained in the residue, from which it is concluded that *C. subvermispora* delignified wheat straw in a highly effective and selective manner.

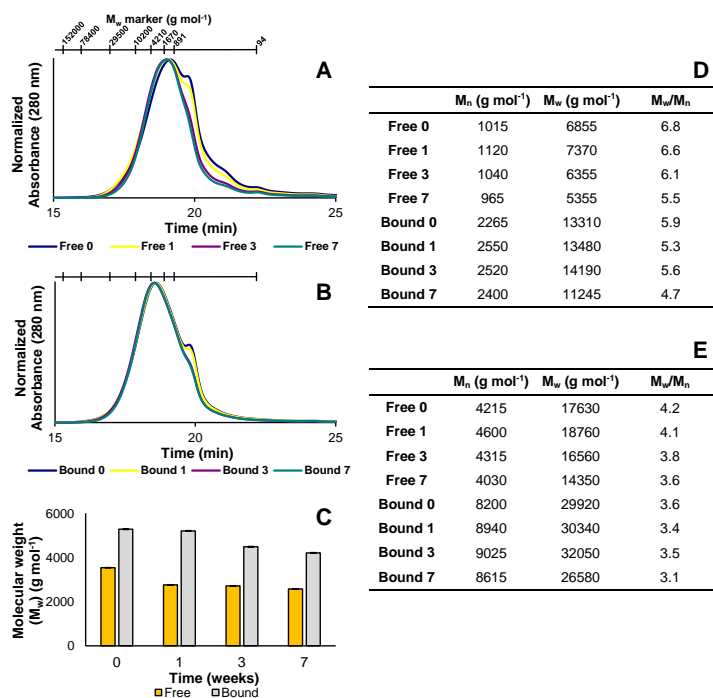


Figure S2. Normalized alkaline SEC chromatograms of free (A) and bound (B) isolates, weight average molecular weight (M_w) of lignin isolates (C). Statistical moments of molar masses of lignin isolates by organic SEC analyses calculated based on PSS standards (D) and statistical moments of molar masses of lignin isolates by organic SEC analyses calculated with MALS-corrected standards (E). Average and standard deviation in (C) of analytical duplicates of mixed isolation duplicates. For estimation of M_w the small shoulders appearing in the alkaline SEC traces were excluded.

Table S1. ¹³C-IS py-GC-MS relative abundance of lignin compounds in unfractionated wheat straw during growth of *C. subvermispora*. Corrected for relative response factors and relative abundance of ¹³C analogues. Sum on the bases of structural classification according to van Erven et al.³⁻⁴ Average and standard deviation of analytical duplicates on pooled biological triplicates. Additional data (timepoints 1 and 3 weeks) compared to van Erven et al. (2018).³

	Total sample (weeks)			
	0	1	3	7
Lignin subunits (%)				
H	10.3 ± 0.0	11.7 ± 0.3	13.1 ± 1.2	15.6 ± 0.2
G	64.0 ± 0.7	61.1 ± 1.2	59.6 ± 1.0	60.3 ± 1.3
S	25.7 ± 0.7	27.2 ± 0.9	27.3 ± 0.3	24.1 ± 1.1
S/G	0.40 ± 0.0	0.44 ± 0.0	0.46 ± 0.0	0.40 ± 0.0
Structural moieties (%)				
Unsubstituted	4.2 ± 0.1	4.9 ± 0.1	8.5 ± 0.5	10.7 ± 0.3
Methyl	2.4 ± 0.0	2.2 ± 0.1	2.8 ± 0.3	3.1 ± 0.2
Vinyl	30.9 ± 0.5	31.9 ± 0.9	34.0 ± 0.4	32.7 ± 1.3
4-VP ^a	8.7 ± 0.0	10.0 ± 0.3	10.2 ± 1.1	11.5 ± 0.0
4-VG ^b	19.7 ± 0.5	19.3 ± 1.3	20.8 ± 0.5	18.9 ± 1.3
C _α -ox	3.7 ± 0.0	3.8 ± 0.1	8.2 ± 0.2	11.4 ± 0.8
diketones	0.1 ± 0.0	0.2 ± 0.1	1.6 ± 0.1	3.1 ± 0.6
C _β -ox ^c	1.5 ± 0.0	1.5 ± 0.0	2.5 ± 0.1	2.8 ± 0.2
C _γ -ox	53.7 ± 0.6	52.5 ± 1.2	40.3 ± 0.3	35.8 ± 0.3
Miscellaneous	3.6 ± 0.1	3.3 ± 0.2	3.7 ± 0.0	3.4 ± 0.1
PhC _γ ^d	58.9 ± 0.6	57.4 ± 1.1	48.8 ± 0.2	46.1 ± 0.6
PhC _γ -diketones ^e	58.8 ± 0.6	57.3 ± 1.0	47.1 ± 0.2	43.0 ± 0.1

^a 4-vinylphenol. ^b 4-vinylguaicol. ^c excluding diketones. ^d phenols with intact α,β,γ-carbon side chain.

^e phenols with intact α,β,γ carbon side chain, excluding diketones.

Table S2. Composition of free and bound lignin isolates. Lignin (% w/w) was determined by ^{13}C -IS py-GC-MS in duplicate on fractionation duplicates. Carbohydrates (% w/w) were determined by constituent monosaccharide analysis after H_2SO_4 hydrolysis in duplicate on pooled fractionation duplicates and are presented as anhydrosugars. Values given represent averages and standard deviation. Note that ^{13}C -IS py-GC-MS resulted in slight overestimation of lignin contents of bound lignin isolates (week 0 and 1).

	Lignin	Glucose	Xylose	Arabinose	Uronic acid	Galactose
Free lignin (weeks)						
0	75.1 \pm 2.5	4.5 \pm 0.2	18.1 \pm 1.4	1.5 \pm 0.1	2.1 \pm 0.1	0.2 \pm 0.0
1	74.7 \pm 5.8	3.4 \pm 0.2	18.6 \pm 1.2	1.6 \pm 0.1	2.0 \pm 0.1	0.2 \pm 0.0
3	54.8 \pm 1.6	2.6 \pm 0.1	15.8 \pm 1.6	1.1 \pm 0.1	2.0 \pm 0.1	0.2 \pm 0.0
7	45.0 \pm 1.3	2.8 \pm 0.2	12.7 \pm 0.8	1.1 \pm 0.1	1.7 \pm 0.1	0.2 \pm 0.0
Bound lignin (weeks)						
0	103.7 \pm 5.4	1.3 \pm 0.1	10.6 \pm 0.6	2.0 \pm 0.1	1.4 \pm 0.2	0.2 \pm 0.0
1	102.1 \pm 2.2	1.6 \pm 0.1	10.9 \pm 0.8	2.1 \pm 0.1	1.3 \pm 0.2	0.1 \pm 0.0
3	79.7 \pm 3.9	1.5 \pm 0.1	11.0 \pm 0.7	2.0 \pm 0.1	1.2 \pm 0.2	0.1 \pm 0.0
7	70.8 \pm 1.8	1.5 \pm 0.1	10.1 \pm 0.8	1.8 \pm 0.1	1.1 \pm 0.2	0.0 \pm 0.0

Table S3. ^{13}C -IS py-GC-MS relative abundance of lignin compounds in ball-milled water extracted residue R4 of wheat straw during growth of *C. subvermispora*. Corrected for relative response factors and relative abundance of ^{13}C analogues. Sum on the bases of structural classification according to van Erven et al.³⁻⁴ Average and standard deviation of analytical duplicates on pooled biological triplicates.

	R4 (weeks)			
	0	1	3	7
Lignin subunits (%)				
H	11.3 \pm 1.0	11.2 \pm 0.4	11.7 \pm 0.6	13.0 \pm 0.7
G	59.4 \pm 0.5	58.8 \pm 0.4	60.6 \pm 0.6	64.3 \pm 0.4
S	29.3 \pm 0.9	30.1 \pm 0.1	27.7 \pm 0.6	22.7 \pm 0.4
S/G	0.49 \pm 0.0	0.51 \pm 0.0	0.46 \pm 0.0	0.35 \pm 0.0
Structural moieties (%)				
Unsubstituted	3.9 \pm 0.3	4.4 \pm 0.2	6.9 \pm 0.6	7.3 \pm 0.4
Methyl	2.1 \pm 0.0	2.2 \pm 0.2	3.4 \pm 0.8	3.6 \pm 0.7
Vinyl	29.1 \pm 2.2	28.6 \pm 0.9	32.5 \pm 3.0	34.5 \pm 0.7
4-VP ^a	10.1 \pm 0.9	9.9 \pm 0.4	9.1 \pm 0.4	9.4 \pm 0.7
4-VG ^b	17.0 \pm 1.2	16.6 \pm 0.7	20.3 \pm 2.5	21.9 \pm 0.8
C α -ox	3.9 \pm 0.2	4.1 \pm 0.1	7.0 \pm 0.3	8.2 \pm 0.4
diketones	0.1 \pm 0.0	0.2 \pm 0.0	1.1 \pm 0.1	1.6 \pm 0.1
C β -ox ^c	1.5 \pm 0.1	1.5 \pm 0.1	2.4 \pm 0.2	2.6 \pm 0.2
C γ -ox	56.3 \pm 2.9	55.6 \pm 1.5	43.6 \pm 5.4	39.3 \pm 1.4
Miscellaneous	3.5 \pm 0.3	3.6 \pm 0.1	4.2 \pm 0.6	4.5 \pm 0.4
PhC γ ^d	61.3 \pm 2.6	61.1 \pm 1.3	51.8 \pm 4.7	48.6 \pm 1.1
PhC γ -diketones ^e	61.2 \pm 2.7	60.9 \pm 1.3	50.6 \pm 4.7	47.0 \pm 1.2

^a 4-vinylphenol. ^b 4-vinylguaiacol. ^c excluding diketones. ^d phenols with intact α,β,γ -carbon side chain.

^e phenols with intact α,β,γ carbon side chain, excluding diketones.

Table S4. ^{13}C -IS py-GC-MS relative abundance of lignin compounds in lignin isolates of wheat straw during growth of *C. subvermispora*. Corrected for relative response factors and relative abundance of ^{13}C analogues. Sum on the bases of structural classification according to van Erven et al.³⁻⁴ Average and standard deviation of analytical duplicates on pooled biological triplicates.

	Free (weeks)				Bound (weeks)			
	0	1	3	7	0	1	3	7
Lignin subunits (%)								
H	8.6 ± 0.1	8.4 ± 0.1	8.6 ± 0.2	9.2 ± 0.1	7.9 ± 0.1	8.0 ± 0.0	7.8 ± 0.2	8.5 ± 0.1
G	62.8 ± 0.4	62.0 ± 0.4	64.7 ± 0.7	67.2 ± 0.8	57.1 ± 0.1	57.3 ± 0.4	60.6 ± 0.2	63.7 ± 0.3
S	28.6 ± 0.4	29.6 ± 0.4	26.6 ± 0.7	23.6 ± 0.6	35.0 ± 0.1	34.7 ± 0.4	31.7 ± 0.1	27.8 ± 0.5
S/G	0.45 ± 0.0	0.48 ± 0.0	0.41 ± 0.0	0.35 ± 0.0	0.61 ± 0.0	0.61 ± 0.0	0.52 ± 0.0	0.44 ± 0.0
Structural moieties (%)								
Unsubstituted	4.6 ± 0.1	4.5 ± 0.0	5.8 ± 0.0	6.8 ± 0.2	3.7 ± 0.1	3.8 ± 0.0	4.8 ± 0.1	5.0 ± 0.4
Methyl	1.5 ± 0.0	1.6 ± 0.0	1.9 ± 0.0	2.0 ± 0.1	1.5 ± 0.0	1.6 ± 0.0	1.9 ± 0.1	2.0 ± 0.1
Vinyl	18.8 ± 0.2	19.0 ± 0.0	19.0 ± 0.3	19.1 ± 0.5	19.8 ± 0.2	20.1 ± 0.1	21.5 ± 0.2	22.5 ± 0.5
4-VP ^a	6.8 ± 0.0	6.5 ± 0.2	6.2 ± 0.2	6.4 ± 0.4	6.8 ± 0.1	6.9 ± 0.1	6.3 ± 0.1	6.9 ± 0.2
4-VG ^b	10.3 ± 0.2	10.5 ± 0.2	11.0 ± 0.1	11.3 ± 0.1	10.7 ± 0.1	11.0 ± 0.1	12.9 ± 0.3	13.5 ± 0.3
C _α -ox	3.9 ± 0.1	4.2 ± 0.1	6.7 ± 0.1	9.0 ± 0.1	3.4 ± 0.0	3.6 ± 0.0	5.1 ± 0.1	5.3 ± 0.0
diketones	0.1 ± 0.0	0.2 ± 0.0	0.7 ± 0.0	1.8 ± 0.1	0.1 ± 0.0	0.1 ± 0.0	0.5 ± 0.0	0.7 ± 0.0
C _β -ox ^c	1.3 ± 0.0	1.3 ± 0.0	1.7 ± 0.0	1.8 ± 0.1	1.2 ± 0.0	1.2 ± 0.0	1.6 ± 0.0	1.6 ± 0.0
C _γ -ox	67.0 ± 0.3	66.4 ± 0.1	61.9 ± 0.4	59.3 ± 0.2	67.4 ± 0.3	66.6 ± 0.1	62.0 ± 0.3	60.6 ± 0.8
Miscellaneous	2.8 ± 0.0	2.9 ± 0.0	3.0 ± 0.0	3.1 ± 0.0	2.9 ± 0.0	3.0 ± 0.0	3.1 ± 0.0	3.1 ± 0.0
PhC _γ ^d	71.8 ± 0.3	71.4 ± 0.1	68.4 ± 0.4	66.4 ± 0.2	72.0 ± 0.3	71.3 ± 0.1	67.7 ± 0.3	66.5 ± 0.7
PhC _γ -diketones ^e	71.7 ± 0.3	71.2 ± 0.1	67.7 ± 0.4	64.5 ± 0.2	71.9 ± 0.3	71.2 ± 0.1	67.2 ± 0.3	66.0 ± 0.7

^a 4-vinylphenol. ^b 4-vinylguaiacol. ^c excluding diketones. ^d phenols with intact α,β,γ carbon side chain. ^e phenols with intact α,β,γ carbon side chain, excluding diketones.

Table S5. ^{13}C -IS py-GC-MS relative abundance of lignin compounds in unextractable residue R7 of wheat straw during growth of *C. subvermispora*. Corrected for relative response factors and relative abundance of ^{13}C analogues. Sum on the bases of structural classification according to van Erven et al.³⁻⁴ Average and standard deviation of analytical duplicates on pooled biological triplicates.

	R7: dioxane insoluble residue (weeks)			
	0	1	3	7
Lignin subunits (%)				
H	12.7 ± 0.3	13.3 ± 0.6	12.4 ± 0.4	14.8 ± 0.6
G	55.3 ± 0.5	54.7 ± 0.3	56.8 ± 0.3	60.2 ± 1.0
S	32.1 ± 0.6	32.0 ± 1.0	30.7 ± 0.7	24.9 ± 0.5
S/G	0.58 ± 0.0	0.58 ± 0.0	0.54 ± 0.0	0.41 ± 0.0
Structural moieties (%)				
Unsubstituted	4.5 ± 0.1	4.9 ± 0.1	6.3 ± 0.3	7.4 ± 0.5
Methyl	2.5 ± 0.1	2.5 ± 0.1	2.8 ± 0.2	3.5 ± 0.1
Vinyl	27.1 ± 0.4	27.7 ± 1.1	27.9 ± 0.7	31.2 ± 1.3
4-VP ^a	10.8 ± 0.3	11.3 ± 0.5	9.9 ± 0.3	11.2 ± 0.7
4-VG ^b	13.5 ± 0.1	13.7 ± 0.5	15.0 ± 0.4	17.2 ± 0.5
C _α -ox	3.6 ± 0.1	3.9 ± 0.2	6.0 ± 0.1	7.0 ± 0.2
diketones	0.1 ± 0.0	0.2 ± 0.0	0.9 ± 0.1	1.2 ± 0.1
C _β -ox ^c	1.7 ± 0.1	1.7 ± 0.1	2.2 ± 0.1	2.6 ± 0.1
C _γ -ox	56.7 ± 0.5	55.3 ± 1.6	50.8 ± 1.2	44.1 ± 1.5
Miscellaneous	4.0 ± 0.0	4.0 ± 0.3	3.9 ± 0.1	4.2 ± 0.1
PhC _γ ^d	62.5 ± 0.4	61.3 ± 1.3	58.3 ± 1.0	52.6 ± 1.5
PhC _γ -diketones ^e	62.4 ± 0.4	61.1 ± 1.3	57.4 ± 1.0	51.4 ± 1.4

^a 4-vinylphenol. ^b 4-vinylguaiacol. ^c excluding diketones. ^d phenols with intact α,β,γ-carbon side chain.

^e phenols with intact α,β,γ carbon side chain, excluding diketones.

Table S6. Assignments of the lignin ^{13}C - ^1H correlation peaks in the HSQC spectra of untreated and fungal-treated wheat straw lignin fractions.

label	$\delta_{\text{C}}/\delta_{\text{H}}$ (ppm)	Assignment ^a
CHK	51.5/3.58	C-H in methoxyls of cyclohexadienone ketals (t)
B _β	53.0/3.43	C ₆ -H ₆ in phenylcoumaran substructures
C _β	53.6/3.05	C ₆ -H ₆ in resinol substructures
-OCH ₃	55.6/3.72	C-H in methoxyls
A _γ	59.6/3.37, 59.8/3.59, 59.9/3.22	C ₇ -H ₇ in β-O-4' substructures
I _γ	61.4/4.09	C ₇ -H ₇ in cinnamyl alcohol end-groups
A' _γ	62.8/4.23, 63.9/4.18	C ₇ -H ₇ in γ-acylated β-O-4' substructures
C _γ	71.0/4.16, 71.1/3.80	C ₆ -H ₆ in resinol substructures
A _α (G)	70.9/4.71	C ₂ -H ₂ in β-O-4' substructures linked to G-unit
A _α (S)	71.8/4.81	C ₂ -H ₂ in β-O-4' substructures linked to S-unit
A _{oxβ}	82.8/5.10	C ₆ -H ₆ in C _α -oxidized β-O-4' substructures
A _β (H)	83.1/4.49	C ₆ -H ₆ in β-O-4' substructures linked to H-unit
A _β (G)	83.5/4.27	C ₆ -H ₆ in β-O-4' substructures linked to G-unit
A _β (S) _{anythro}	85.9/4.09	C ₆ -H ₆ in β-O-4' substructures linked to S-unit
A _β (T)	86.2/4.36 and 86.7/4.26	C ₆ -H ₆ in β-O-4' substructures linked to triclin
A _β (S) _{threo}	86.9/3.97	C ₆ -H ₆ in β-O-4' substructures linked to S-unit
C _α	84.9/4.64	C ₂ -H ₂ in resinol substructures
B _α	86.9/5.43	C ₂ -H ₂ in phenylcoumaran substructures
T ₈	94.1/6.57	C ₈ -H ₈ in triclin
T ₆	98.8/6.21	C ₆ -H ₆ in triclin
T _{free3}	103.5/6.96	C ₃ -H ₃ in free triclin
S _{2,6}	103.9/6.68	C ₂ -H ₂ and C ₆ -H ₆ in S-unit
T _{2,6} /T _{free2,6}	104.0/7.31	C ₂ -H ₂ and C ₆ -H ₆ in triclin and in free triclin
T ₃	104.6/7.02	C ₃ -H ₃ in triclin
Sox _{2,6}	106.4/7.30	C ₂ -H ₂ and C ₆ -H ₆ in C _α -oxidized (C _α =O) S-unit
Sox _{2,6}	106.5/7.19	C ₂ -H ₂ and C ₆ -H ₆ in C _α -oxidized (C _α OOH) S-unit
G ₂	110.8/6.96	C ₂ -H ₂ in G-unit
FA ₂	110.9/7.34	C ₂ -H ₂ in ferulate
GoxI ₂	111.4/7.51	C ₂ -H ₂ in C _α -oxidized G-unit
GoxII ₂	112.4/7.44	C ₂ -H ₂ in C _α -oxidized G-unit
FA _β /pCA _β	113.6/6.26	C ₆ -H ₆ in ferulate/ <i>p</i> -coumarate
H _{3,5} /FA ₅	114.5/6.69	C ₃ -H ₃ and C ₅ -H ₅ in H-unit, C ₅ -H ₅ in FA
G ₅ /G _β /pCA _{3,5}	115.0/6.93 and 115.5/6.78	C ₅ -H ₅ and C ₆ -H ₆ in G-unit, C ₃ -H ₃ and C ₅ -H ₅ of pCA
G ₅	119.0/6.78	C ₅ -H ₅ in G-unit
GoxI ₆	122.7/7.47	C ₆ -H ₆ in C _α -oxidized G-unit
FA ₆	123.1/7.12	C ₆ -H ₆ in ferulate
GoxII ₆	125.8/7.42	C ₂ -H ₂ in C _α -oxidized G-unit
H _{2,6} /PHE _{3,5}	127.8/7.18	C ₂ -H ₂ and C ₆ -H ₆ in H-unit, C ₃ -H ₃ and C ₅ -H ₅ in phenylalanine
PHE _{2,6}	128.9/7.21	C ₂ -H ₂ and C ₆ -H ₆ in phenylalanine
pCA _{2,6}	130.1/7.42	C ₂ -H ₂ and C ₆ -H ₆ in <i>p</i> -coumarate
FA _α /pCA _α	145.1/7.57	C ₆ -H ₆ in ferulate/ <i>p</i> -coumarate

^a: assignment by comparison with literature.⁴⁻¹¹ (t): tentatively assigned

Table S7. Semiquantitative HSQC NMR structural characterization of wheat straw lignin isolates in the absence and presence of chromium (III) acetylacetonate ($\text{Cr}(\text{acac})_3$) as relaxation agent. Note that the untreated and *C. subvermispota* treated wheat straw lignin isolates shown here originate from a different batch of straw and should therefore solely be used for comparisons of $\text{Cr}(\text{acac})_3$ effects.

	Untreated wheat straw (free + bound)		7 weeks fungal treated wheat straw (free)	
	Without $\text{Cr}(\text{acac})_3$	With $\text{Cr}(\text{acac})_3$	Without $\text{Cr}(\text{acac})_3$	With $\text{Cr}(\text{acac})_3$
Lignin subunits (%)^a				
H	3	3	3	2
G	62	63	53	55
G _{ox}	0	0	10	11
S	35	34	24	23
S _{ox}	0	0	9	9
S/G	0.6	0.5	0.5	0.5
Hydroxycinnamates (%)^b				
p-coumarate	8	6	17	13
ferulate	5	3	6	4
Flavonolignin (%)^b				
tricin	15	9	21	15
Lignin interunit linkages (%)^{b,c}				
β-O-4' G+H	20 (35)	22 (37)	18 (38)	19 (38)
β-O-4' S	22 (38)	24 (40)	14 (29)	16 (32)
β-O-4' C _α -ox	1 (1)	1 (2)	0 (0)	0 (0)
β-O-4' triclin	8 (15)	8 (13)	11 (22)	11 (23)
total β-O-4' aryl ethers	51 (89)	55 (92)	43 (89)	46 (93)
β-5' phenylcoumarans	5 (8)	4 (6)	3 (7)	2 (5)
β-β' resinols	1 (2)	1 (2)	2 (4)	1 (2)
total	57 (100)	60 (100)	49 (100)	50 (100)
Side-chain γ-acylation (%)^d	21	20	17	16
Erythro/threo of β-O-4'^e	2.6	2.5	3.9	4.0

^a relative distribution of lignin subunits ($\text{H}+\text{G}+\text{G}_{\text{ox}}+\text{S}+\text{S}_{\text{ox}}=100$)

^b relative volume integral of substructure versus volume integral of total lignin subunits

^c relative distribution of total interunit linkages in parentheses

^d percentage of β-O-4' aryl ethers

^e ratio of $A_{\beta}(\text{S/G-S})_{\text{erythro}}$ and $A_{\beta}(\text{S/G-S})_{\text{threo}}$, diastereomers for β-O-4' aryl ethers coupled to G-units are not resolved

Table S8. Hydroxyl group content of lignin isolates of wheat straw during growth of *C. subvermispota* determined by ^{31}P NMR after phosphorylation.

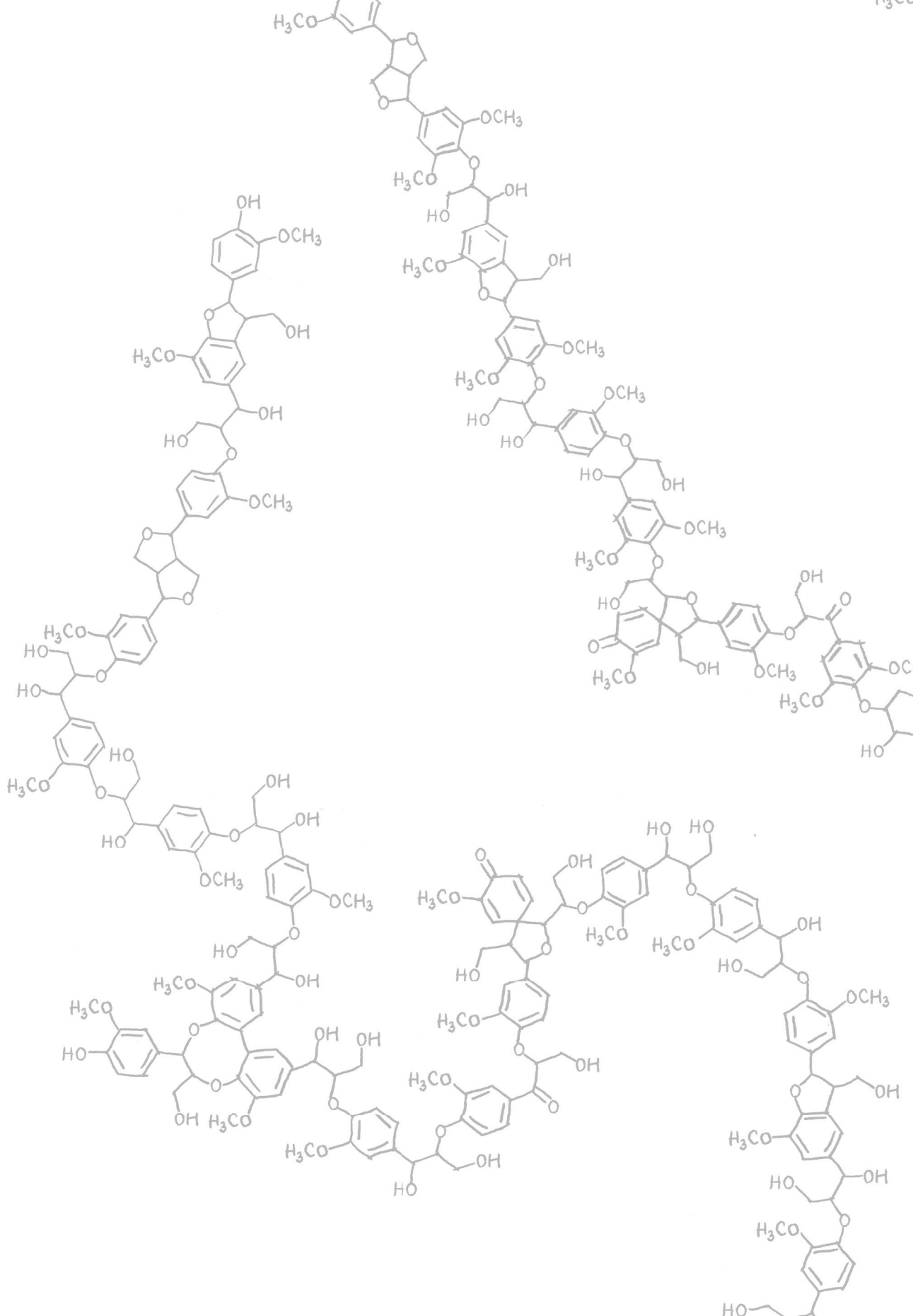
	Free (weeks) (mmol/g lignin) ^a				Bound (weeks) (mmol/g lignin) ^a			
	0	1	3	7	0	1	3	7
Aliphatic OH + carb. OH	7.49	7.77	9.40	10.15	5.81	5.86	6.73	7.28
S-OH + 5-sub. G-OH	0.56	0.62	0.95	1.23	0.39	0.43	0.63	0.71
G-OH	0.74	0.72	0.88	1.01	0.53	0.53	0.61	0.71
H-OH + pCA-OH	0.57	0.57	0.78	0.93	0.42	0.42	0.53	0.65
Total phenolic OH	1.87	1.91	2.61	3.17	1.34	1.38	1.76	2.07
COOH	0.28	0.36	0.79	1.33	0.14	0.17	0.34	0.43

^a contents per g biomass corrected for lignin contents as determined by quantitative ^{13}C -IS py-GC-MS

Supporting Information References

- Englyst, H. N.; Cummings, J. H., Simplified method for the measurement of total non-starch polysaccharides by gas-liquid chromatography of constituent sugars as alditol acetates. *Analyst* **1984**, *109*, 937-942.
- Blumenkrantz, N.; Asboe-Hansen, G., New method for quantitative determination of uronic acids. *Analytical biochemistry* **1973**, *54*, 484-489.
- Van Erven, G.; Nayan, N.; Sonnenberg, A. S.; Hendriks, W. H.; Cone, J. W.; Kabel, M. A., Mechanistic insight in the selective delignification of wheat straw by three white-rot fungal species through quantitative ^{13}C -IS py-GC-MS and whole cell wall HSQC NMR. *Biotechnol Biofuels* **2018**, *11*, 262.
- Van Erven, G.; Hilgers, R.; de Waard, P.; Gladbeek, E.-J.; van Berkel, W. J.; Kabel, M. A., Elucidation of *in situ* ligninolysis mechanisms of the selective white-rot fungus *Ceriporiopsis subvermispota*. *ACS Sustainable Chem Eng* **2019**, *7*, 16757-16764.

5. Ralph, S. A.; Ralph, J.; Landucci, L., NMR database of lignin and cell wall model compounds. **2009**, Available at URL www.glbrc.org/databases_and_software/nmrdatabase/.
6. Del Río, J. C.; Rencoret, J.; Prinsen, P.; Martínez, A. T.; Ralph, J.; Gutiérrez, A., Structural characterization of wheat straw lignin as revealed by analytical pyrolysis, 2D-NMR, and reductive cleavage methods. *J Agric Food Chem* **2012**, *60*, 5922-5935.
7. Rencoret, J.; Gutiérrez, A.; Nieto, L.; Jiménez-Barbero, J.; Faulds, C. B.; Kim, H.; Ralph, J.; Martínez, Á. T.; del Río, J. C., Lignin composition and structure in young versus adult *Eucalyptus globulus* plants. *Plant Physiol* **2011**, *155*, 667-682.
8. Rencoret, J.; Pereira, A.; del Río, J. C.; Martínez, Á. T.; Gutiérrez, A., Delignification and saccharification enhancement of sugarcane byproducts by a laccase-based pretreatment. *ACS Sustainable Chem Eng* **2017**, *5*, 7145-7154.
9. Del Río, J. C.; Lino, A. G.; Colodette, J. L.; Lima, C. F.; Gutiérrez, A.; Martínez, Á. T.; Lu, F.; Ralph, J.; Rencoret, J., Differences in the chemical structure of the lignins from sugarcane bagasse and straw. *Biomass Bioenergy* **2015**, *81*, 322-338.
10. Kim, H.; Padmakshan, D.; Li, Y.; Rencoret, J.; Hatfield, R. D.; Ralph, J., Characterization and elimination of undesirable protein residues in plant cell wall materials for enhancing lignin analysis by solution-state nuclear magnetic resonance spectroscopy. *Biomacromolecules* **2017**, *18*, 4184-4195.
11. Lan, W.; Yue, F.; Rencoret, J.; del Río, J.; Boerjan, W.; Lu, F.; Ralph, J., Elucidating tricin-lignin structures: assigning correlations in HSQC spectra of monocot lignins. *Polymers* **2018**, *10*, 916.





CHAPTER 7

Evidence for ligninolytic activity of the ascomycete fungus *Podospira anserina*

Gijs van Erven, Anne F. Kleijn, Aleksandrina Patyshakulyeva,

Marcos Di Falco, Adrian Tsang, Ronald P. de Vries,

Willem J. H. van Berkel, Mirjam A. Kabel

Submitted

Abstract

The ascomycete fungus *Podospora anserina* has been appreciated for its targeted carbohydrate-active enzymatic arsenal. As a late colonizer of herbivorous dung, the fungus acts specifically on the more recalcitrant fraction of lignocellulose and this lignin-rich biotope might have resulted in the evolution of ligninolytic activities. However, the lignin-degrading abilities of the fungus have not been demonstrated by chemical analyses at the molecular level and are, thus far, solely based on genome and secretome predictions. To evaluate whether *P. anserina* might provide a novel source of lignin-active enzymes to tap into for potential biotechnological applications, we comprehensively mapped wheat straw lignin during fungal growth and characterized the fungal secretome.

Quantitative ^{13}C lignin internal standard py-GC-MS analyses showed extensive lignin removal during seven days of fungal growth (24% w/w), though carbohydrates were selectively targeted (58% w/w removal). Structural characterization of residual lignin by using py-GC-MS and HSQC NMR analyses demonstrated that C_α -oxidized substructures significantly increased through fungal action, while intact β -*O*-4' aryl ether linkages, *p*-coumarate and ferulate moieties decreased. Proteomics analyses indicated that the presence of lignin induced considerable changes in the secretome of *P. anserina*. This was particularly reflected in a strong reduction of cellulases, while H_2O_2 producing enzymes clearly increased. The latter enzymes, together with laccases, were likely involved in the observed ligninolysis.

For the first time, we provide unambiguous evidence for the ligninolytic activity of the ascomycete fungus *P. anserina* and expand the view on its enzymatic repertoire beyond carbohydrate degradation. Our results are of significance for the development of biological lignin valorization technologies and expedite the quest for novel lignin-active enzymes and organisms.

Introduction

With the increasing interest in biological lignocellulose valorization strategies, there is a quest for novel lignocellulose-acting enzymes and organisms producing such enzymes.¹ The ascomycete fungus *Podospora anserina* has long been studied for its lifecycle characteristics, particularly regarding its short growth phase, but more recently also has sparked biotechnological interest.²⁻⁶ The fungus produces a wide variety of carbohydrate-active enzymes, including several cellulases, xylanases and lytic polysaccharide monooxygenases (LPMOs) and promises to be an efficient microbial enzyme factory because of its ease of genetic manipulation and fast growth.⁵⁻⁸ Indeed, the fungus' enzymes were shown to be of biotechnological potential, being able to enhance the saccharification efficiencies of enzymes commonly used in industry.⁹⁻¹⁰

As a late colonizer of herbivorous dung, *P. anserina* is expected to specifically degrade the more recalcitrant fraction of lignocellulose.¹¹ Besides its well-studied carbohydrate degrading enzymatic arsenal, the fungus may, therefore, also possess ligninolytic activity, which could broaden the scope of the fungus' exploitation in biomass upgrading approaches.¹² The suggestion of possible ligninolytic activity is based on the ability of the fungus to grow on a variety of lignocellulosic substrates, including nearly pure lignin, and its genome that encodes several putative lignin-active enzymes including laccases and H₂O₂-producing oxidoreductases.^{5, 13-14} Actually, the genome of *P. anserina* is, amongst ascomycetes, characterized by the highest number of genes encoding auxiliary activities (AA), encompassing oxidoreductases only, accommodated in the carbohydrate-active enzymes database (CAZy; www.cazy.org).¹⁵ Secretome analyses revealed that some of these enzymes were produced and secreted during growth on lignocellulose.^{10, 16} Furthermore, deletion of some of the laccase-encoding genes reduced the ability of the fungus to grow on wood shavings, suggesting that they are indeed involved in wood degradation.¹⁷ However, the actual degradation of lignin has not been shown by chemical analyses of the substrates; and as such, the ligninolytic capability of *P. anserina* remains to be further elucidated.

Recently, we have demonstrated that quantitative pyrolysis-GC-MS analysis is exceptionally useful for mapping the extent of fungal plant biomass delignification as well as for unravelling the underlying ligninolysis mechanisms.¹⁸⁻¹⁹ Importantly, this technique can highlight minor structural changes in the remaining lignin after short periods of fungal growth, an unconditional requirement when studying the structural changes induced by micro-organisms with a short growth cycle.¹⁹

In this work, the ligninolytic activity of *P. anserina* was unambiguously confirmed through comprehensive substrate analyses after growth of the fungus on wheat straw lignin. Quantitative py-GC-MS analyses revealed substantial lignin removal and an increase in C_α-oxidized moieties indicative of oxidative degradation. HSQC NMR analyses further substantiated these findings by showing a decrease of

intact β -O-4' aryl ether linkages concomitant with the increase of C_α-oxidized substructures. In addition, *p*-coumarate and ferulate moieties were decreased, which suggests feruloyl esterase activity during fungal growth. Secretome analyses indicated that ligninolysis likely involved laccases and H₂O₂-producing enzymes.

Experimental Section

Materials. All chemicals and solvents were obtained from commercial suppliers and used as supplied. Water used in all experiments was purified via a Milli-Q water system (Millipore, Billerica, MA, USA).

Preparation of wheat straw lignin isolate. Lignin was isolated from wheat straw by modifications of the classical lignin isolation procedures.²⁰⁻²¹ Extractives were removed from milled wheat straw (< 1 mm) by sequential extraction with acetone and water. Extractive-free wheat straw (3 x 30 g) was planetary ball-milled (PM100, Retsch, Haan, Germany) in a 500 mL zirconium dioxide jar containing 100 Φ 10 mm zirconium dioxide balls at a frequency of 600 rpm for a net milling time of 1 h in 10 min milling/20 min break interval cycles to prevent overheating of the material. Note that milling in the 500 mL jar setup proceeds with a higher intensity compared to routine 50 mL scale and, therefore, the same extent of milling is achieved in a much shorter time. The ball-milled material was subsequently water-extracted in a concentration of 5% (w/w) at 50 °C for 20 h under rotary shaking. The water-insoluble residue was obtained through centrifugation (18,000xg, 10 min, 20 °C) and washed two times with water before being suspended in 50 mM sodium acetate buffer pH 5 at a concentration of 5% (w/w). The suspension was incubated with the commercial enzyme cocktail ViscoStar 150 L (Dyadic, Jupiter, FL, USA) (0.125 mL/g biomass) at 50 °C for 24 h to degrade the cell wall polysaccharides. The insoluble material after incubation was obtained through centrifugation (18,000xg, 10 min, 20 °C), resuspended in buffer, loaded with fresh enzyme and incubated for another 24 h. After incubation, the suspension was centrifuged and the insoluble residue was washed three times with water before freeze-drying. The freeze-dried material was subsequently suspended in 80% (v/v) aqueous dioxane at 5% (w/w) dry matter loading and extracted at room temperature under nitrogen atmosphere for 24 h. The supernatant was recovered by centrifugation (30,000xg, 10 min, 20 °C) and the residue was extracted again. The supernatants were combined, freeze-dried, washed with water to remove traces of dioxane and freeze-dried again to yield the wheat straw lignin isolate.

Growth of *Podospora anserina* on wheat straw lignin. Media and growth conditions for *P. anserina* were based on previously described procedures.²²⁻²³ Water-insoluble wheat glucuronoarabinoxylan (GAX, Megazyme, Wicklow, Ireland, 100 mg) and GAX (100 mg) combined with wheat straw lignin isolate (100 mg) were dispersed in 5 mL M2 minimal medium in 40 mL flasks and autoclaved prior

to inoculation. *P. anserina* strain S mat+ (CBS 143333) was grown on Luria-Bertani agar at 27 °C for five days before 0.5 cm plugs were taken from the formed mycelium to inoculate the samples. Flasks were statically incubated at 27 °C for three or seven days. All experiments were performed in triplicate. After incubation mycelium was scooped out with a sterile loop and stored at -20 °C. Culture samples (2.5 mL) were taken and centrifuged (10,000 \times g, 10 min, 4 °C) to separate the solid fraction from the supernatant for proteome analysis. Both fractions were stored at -20 °C. The residual substrate in the flasks was removed by dispersion in water. Residual substrate and mycelium were water-extracted for 1 h at 4 °C under continuous stirring before centrifugation (60,000 \times g, 5 min, 20 °C) to separate water-soluble and insoluble fractions. The obtained fractions were flash frozen in liquid nitrogen and freeze-dried.

Quantitative py-GC-MS with ^{13}C lignin as internal standard. Analytical pyrolysis coupled to gas chromatography with high-resolution mass spectrometric detection (Exactive Orbitrap, Thermo Scientific, Waltham, MA, USA) was performed as previously described.^{19, 24} To each sample (~50 μg), 10 μL of a ^{13}C wheat straw lignin internal standard (IS) solution (1 mg mL⁻¹ ethanol/chloroform 50:50 v/v) was added and dried prior to analysis. All samples were prepared and analyzed in duplicate. Lignin-derived pyrolysis products were monitored in full MS mode on the most abundant fragment per compound (both nonlabeled and uniformly ^{13}C labeled). Pyrograms were processed by TraceFinder 4.0 software. Lignin contents and relative abundances of lignin-derived pyrolysis products were calculated as described previously.¹⁸⁻¹⁹

HSQC NMR spectroscopy. For NMR analyses, biological triplicates were mixed in equal dry matter amounts to a single replicate. HSQC NMR spectra were recorded on a Bruker AVANCE III 600 MHz NMR spectrometer equipped with a cryoprobe as previously described.¹⁹ Spectra were processed according to del Río et al.²⁵

Carbohydrate content and composition. Constituent monosaccharides released after acid hydrolysis were determined in duplicate as previously reported by Englyst & Cummings with reported modifications.²⁶⁻²⁷

Secretome extraction, protein preparation and analysis. For secretome analyses, triplicate samples after three days of fungal growth were used. A 900 μL aliquot of water-soluble culture fraction was mixed with two volumes of methanol and proteins were left to precipitate overnight at -20 °C. The precipitates were pelleted by centrifugation, washed with 60% (v/v) cold aqueous methanol, pelleted again and resuspended with 30 μL of anionic acid labile surfactant II (Protea Biosciences, Morgantown, WV, USA) in 200 mM ammonium bicarbonate. Twenty microliters of the resolubilized proteins were mixed with 5 μL 5X SDS-PAGE loading buffer (0.125 M Tris-HCl pH 6.8, 50% glycerol, 5% w/v SDS, 0.02% bromophenol and 0.35 M dithiothreitol), heated at 95 °C for 5 min before being loaded onto a 12%

w/v acrylamide SDS-containing separating gel. Proteins were separated by electrophoresis until the 250 kDa marker of the BLUelf prestained protein ladder (FroggaBio, North York, Toronto, Canada) entered the separating gel. After the gel was stained with Coomassie blue, about 1 cm of the gel lane was cut out and polypeptides were in-gel digested with trypsin as described previously.²⁸ Peptide mixtures were resuspended in 45 μ L 5% (v/v) aqueous acetonitrile with 0.1% (v/v) formic acid, containing 4 fmol/ μ L predigested bovine serum albumin. Five microliters of the peptide extract solution were subsequently injected onto a 75 μ m x 15 cm C18 column and analyzed by LC-MS/MS by using an Easy-LC II Nano HPLC system in-line connected to a Velos LTQ-Orbitrap Mass spectrometer (Thermo Fisher) as previously described.²⁹ Peptide and protein identification was performed by using Proteome Discoverer 2.2 software (Thermo Fisher) applying the precursor ion quantification workflow with pairwise precursor ion peak area value-based protein abundance calculation. As additional criterion for protein abundance calculation, protein abundances were used only for those samples where at least one replicate had a minimum of two unique peptides identified. The relative abundance of the detected proteins was estimated by using the extracted precursor ion chromatogram peak areas of the identified peptides that were assigned to each protein. The *Podospira anserina* mat+ v1.0 database from JGI was used. Functional annotations were assigned on the basis of InterPro descriptions (<https://www.ebi.ac.uk/interpro/>) and Signal P prediction from JGI.

Results & Discussion

Cultivation setup. To simplify the detection of early markers of ligninolytic activity of *P. anserina* we used cultivation conditions that would allow us to evaluate changes in both lignin structure and in the fungal secretome.²³ To that end, we incubated the fungus on pre-isolated lignin from wheat straw that was combined with the hemicellulose fraction of the straw, i.e. glucuronoarabinoxylan (GAX), instead of growing the fungus on unfractionated wheat straw. This enabled us to characterize the residual substrates directly by detailed HSQC NMR analyses, which would otherwise require lignin isolation to reach the same level of structural insight.¹⁸ In addition, the secretome of *P. anserina* could be compared to growth on GAX alone. The isolated lignin was structurally representative of wheat straw lignin and of high purity (90% w/w) (Figure S1, Table S1).²⁴ The hemicellulose that was used in the fermentations introduced negligible amounts of lignin and only slightly contributed to the total ferulate content as inferred from the 4-vinylguaicol product in the pyrogram (Figure S1). HSQC NMR analysis of the GAX failed to show any ferulate specific correlation peaks (data not shown), presumably due to poor solubilization/gelling of the sample. A total esterified amount of (di)ferulates of 2.9% (w/w) was estimated by our research group in earlier research.³⁰

Fate of carbohydrates and lignin after growth of *P. anserina*. After seven days of growth of *P. anserina*, substantial amounts of mycelium could be observed by visual inspection. Mass balance analyses revealed that the fungus had degraded and removed considerable amounts of the initial substrate (Figure 1A). As fungal mycelium is generally comprised of carbohydrates which do not contain the glucuronosyl, arabinosyl and xylosyl moieties of the hemicellulosic substrate, we analyzed the recoveries of GAX and other carbohydrates separately.³¹ *P. anserina* was able to degrade and remove substantial amounts of lignin (24% w/w) besides GAX (58% w/w) during growth (Figure 1B).

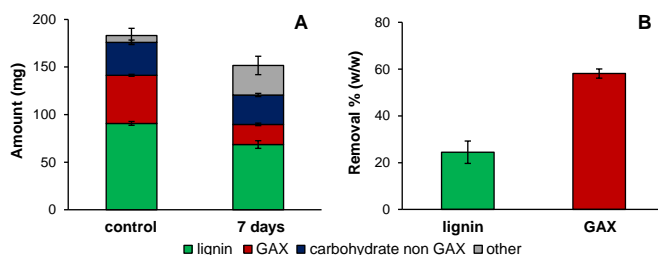


Figure 1. Absolute recoveries (A) and removal (B) of lignin and glucuronoarabinoxylan (GAX) after 7 days of growth of *P. anserina* on wheat straw lignin isolate and insoluble wheat glucuronoarabinoxylan. Total insoluble and water-soluble fractions based on compositional analysis by using quantitative ¹³C-IS py-GC-MS (lignin) and constituent monosaccharide analysis after H₂SO₄ hydrolysis (carbohydrates). Others represent residual dry matter. Note that the initial lignin isolate contained some residual carbohydrates (10% w/w) and initial hemicellulose contained some residual cellulose (16% w/w).³⁰

As expected from its wealth of carbohydrate-active enzymes,⁵ the fungus degraded the hemicellulosic carbohydrates with a clear preference. Still, though ligninolytic activity of *P. anserina* has previously been considered,¹² this is the first evidence that the fungus is actually able to degrade and remove the aromatic biopolymer. The ligninolytic capacity of *P. anserina*, i.e. the extent of lignin removal during 7 days of fungal growth, was remarkably high for an ascomycete fungus. However, it should be taken into account that the fungus was grown on pre-isolated lignin under submerged fermentation conditions, in which lignin was presumably more accessible compared to whole cell wall preparations or solid-state incubations. Whether *P. anserina* completely mineralized lignin to CO₂ or 'only' depolymerized it to such an extent that the resulting volatile degradation products were removed during freeze-drying remains to be further investigated.

Structural characterization of lignin after growth of *P. anserina*. The structural features of the residual lignin further substantiated the ligninolytic action of *P. anserina* (Table 1). A slight, but significant, increase (10%) in C_α-oxidized substructures suggested that oxidative degradation forms the basis of the lignin removal observed. Interestingly, diketone products, pyrolysis markers for dihydroxyphenylketones,¹⁹ had increased significantly after fungal growth from 0.16±0.00% to 0.25±0.00% of the relative abundance of lignin-derived pyrolysis

products, which consequently explained a major part of the increase of the C_α-oxidized substructures. These markers have also been observed after the action of the white-rot fungus *Ceriporiopsis subvermispora* and for laccase-mediator systems, suggesting that *O*-4'-cleavage of β-*O*-4' aryl ethers is likely one of the involved ligninolysis routes.^{19, 32} However, at the observed extents of lignin removal (24% w/w, Figure 1), we would have expected to see more prominent changes in the structural characteristics of the residual lignin. For several white-rot fungal treated samples we, and others, have previously observed an approximate doubling of total C_α-oxidized moieties at comparable extents of delignification,^{18, 33-34} and *C. subvermispora* showed a 16-fold increase in diketone markers.²⁷ These observations would suggest that different (or additional) degradation routes underlie delignification, as elaborated below.

Table 1. Quantitative ¹³C-IS py-GC-MS structural characterization of untreated and 7 days *P. anserina* treated wheat straw lignin; corrected for relative response factors and relative abundance of ¹³C analogues. Sum based on structural classification according to van Erven et al.¹⁸⁻¹⁹ Average and standard deviation of analytical duplicates of biological triplicates. Structural features for the combined fractions weighted on the basis of the lignin mass balance. Significant differences calculated by two-tailed t-test (* p<0.05, ** p<0.01).

	control	7 days
Lignin subunits (%)		
H	8.9 ± 0.1	8.6 ± 0.0**
G	60.9 ± 0.5	59.3 ± 0.2**
S	30.2 ± 0.5	32.1 ± 0.2**
S/G	0.50 ± 0.0	0.54 ± 0.0**
Structural moieties (%)		
Unsubstituted	6.4 ± 0.3	6.6 ± 0.1
Methyl	3.0 ± 0.2	3.3 ± 0.0*
Vinyl	32.4 ± 1.1	30.4 ± 0.3*
4-VP ^a	7.2 ± 0.1	6.6 ± 0.0**
4-VG ^b	21.7 ± 1.1	19.9 ± 0.3
C _α -ox	4.0 ± 0.1	4.3 ± 0.1*
diketones	0.16 ± 0.0	0.25 ± 0.0**
C _β -ox ^c	2.5 ± 0.1	2.5 ± 0.0
C _γ -ox	48.2 ± 1.1	49.1 ± 0.4
Miscellaneous	3.6 ± 0.1	3.8 ± 0.0
PhC _γ ^d	52.6 ± 1.1	53.9 ± 0.4
PhC _γ -diketones ^e	52.4 ± 1.1	53.6 ± 0.4

^a 4-vinylphenol. ^b 4-vinylguaiacol. ^c excluding diketones. ^d phenols with intact α,β,γ-carbon side chain.

^e phenols with intact α,β,γ-carbon side chain, excluding diketones.

Besides increased C_α-oxidized substructures, the action of *P. anserina* led to a substantial decrease in vinyl products (Table 1), which largely derived from the decarboxylation of hydroxycinnamates upon pyrolysis.³⁵⁻³⁶ In particular the decrease of 4-vinylphenol, primarily formed from *p*-coumarate, suggests that these moieties were targeted, at least to some extent, during fungal growth. Likewise, the decrease in 4-vinylguaiacol suggests the removal of ferulic acid moieties.

To further corroborate our findings, we structurally characterized the lignin fractions in more detail by ^1H - ^{13}C HSQC NMR analysis. Indeed, clear structural changes could be observed in the spectra and were further resolved by semiquantitative analyses of the volume integrals (Figure 2).

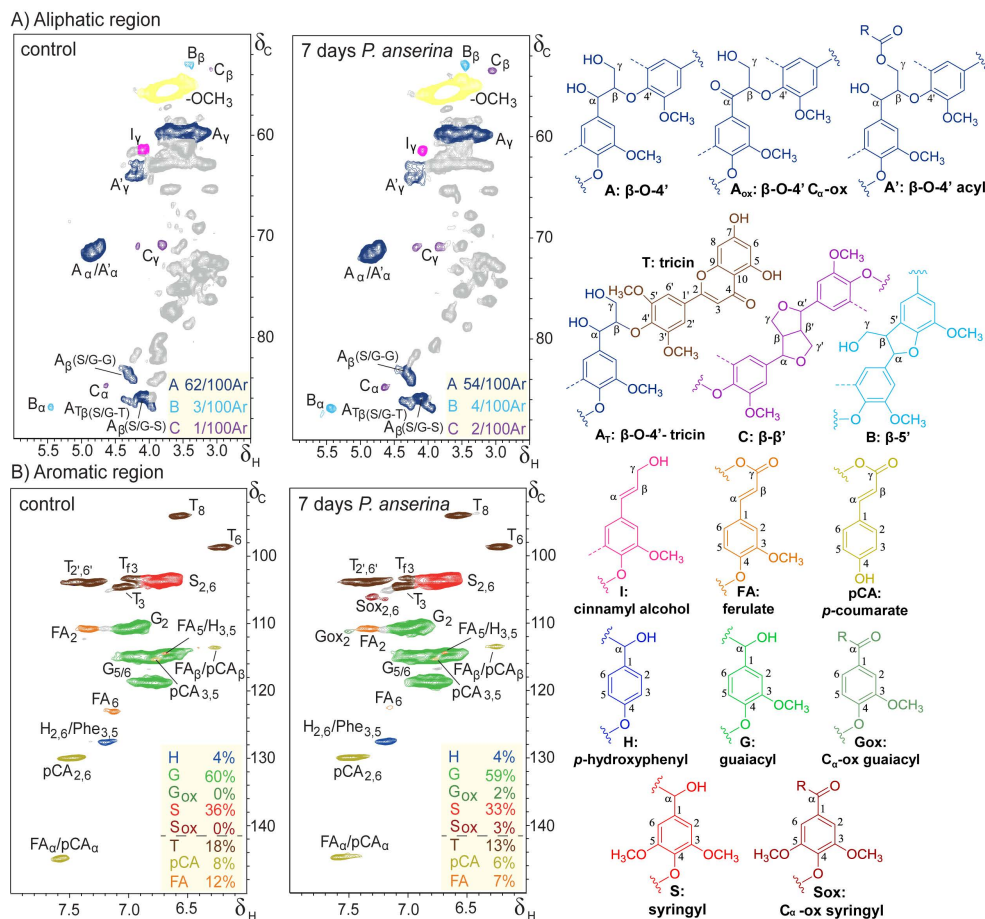


Figure 2. Aliphatic (A) and aromatic (B) regions of ^1H - ^{13}C HSQC NMR spectra of untreated and 7 days *P. anserina* treated wheat straw lignin water-insoluble residues. Unassigned signals are shown in grey. Colored boxes show semiquantitative analysis of the volume integrals, with interunit linkages per 100 subunits (aromatic rings, Ar), relative distribution of subunits (%) and T, pCA and FA relative to total subunits (%). Dotted lines represent $-\text{H}$ or $-\text{OCH}_3$. Wavy lines indicate main positions for further coupling. Unassigned signals are shown in gray.

In the aromatic region of the NMR spectra of the treated lignin residue samples, C $_{\alpha}$ -oxidized substructures became evident and were shown to comprise approximately 4% of the total subunits. Concurrently with the increase of C $_{\alpha}$ -oxidized substructures, intact β -O-4' aryl ether interunit linkages decreased from 62 to 54 linkages/100 subunits, implying that the oxidized substructures resulted from interunit bond cleavage (Figure 2). In contrast to the β -O-4' aryl ether substructures, the more condensed phenylcoumaran (β -5') and resinol (β - β')

structural elements appeared to be more resistant against degradation by *P. anserina* and as a result they relatively accumulated in the fungal-grown residues, albeit slightly (Figure 2, Table 2).

In line with our observations by py-GC-MS analyses, *p*-coumarate moieties decreased during fungal growth. Because these *p*-coumarates are solely present as γ -esters, their removal implies hydroxycinnamic acid esterase activity.³⁷ Similar activity likely also caused the slight reduction in ferulates, in the case of ester-bound moieties to GAX, though oxidative degradation of ether-bound ferulates cannot be excluded.³⁷ When the structural features were weighted for the contributions of the various fractions to the total remaining lignin, the structural changes mediated by fungal action could still be discerned (Table 2).

Table 2. Semiquantitative ^1H - ^{13}C HSQC NMR structural characterization of untreated and 7 days *P. anserina* treated wheat straw lignin. Structural features for the combined fractions weighted on the basis of the lignin mass balance.

	control	7 days
Lignin subunits (%)^a		
H	4	4
G	61	59
G _{ox}	0	2
S	35	34
S _{ox}	0	2
S/G	0.6	0.6
Hydroxycinnamates (%)^b		
<i>p</i> -coumarate	8	6
ferulate	10	8
Flavonolignin (%)^b		
tricin	14	15
Lignin interunit linkages (%)^{b,c}		
β -O-4' aryl ethers	63 (93)	59 (92)
β -5' phenylcoumarans	4 (5)	4 (6)
β - β' resinols	1 (2)	1 (2)
total	68 (100)	64 (100)

^a relative distribution of lignin subunits (H+G+G_{ox}+S+S_{ox}=100)

^b relative volume integral of substructure versus volume integral of total lignin subunits

^c relative distribution of total interunit linkages in parentheses

Note that even though in HSQC NMR spectra C β -H β correlation peaks are resolved for various substructures of β -O-4' aryl ether linkages,²⁷ the hemicellulosic substrate presented an overlapping peak with the β -O-4'-S/G-S signal at $\delta_{\text{C}}/\delta_{\text{H}}$ 85.97/3.96 ppm in this experimental setup. Therefore, we quantified the C α -H α correlation peaks instead, as previously described by del Río et al.²⁵

The aforementioned structural observations by py-GC-MS and HSQC NMR analyses might be the result of a preferential degradation of phenolic subunits. These subunits generally comprise 10-30% of the lignin polymer and are more susceptible to oxidation. Hence, these phenolic subunits might be degraded to a greater extent

than their non-phenolic counterparts.³⁸⁻³⁹ However, the oxidation of phenolic moieties might also drive (re)polymerization reactions.⁴⁰

In the absence of mediators it can be expected that laccases, the only 'true' ligninolytic enzymes of *P. anserina*, are only able to oxidize phenolic substructures.⁴¹ With the necessity of being the end-groups of the growing lignin polymer, the cleavage of these units might have proceeded in a sort of 'peeling pattern', leaving the remaining polymer principally intact, or at least not distinguishable from native lignin apart from a slight reduction of molecular weight.⁴² Consequently, this could explain why we observed relatively limited structural modification of the residual lignin after partial delignification.

Structural changes in light of the fungal secretome. In order to relate the observed structural changes to potential enzymatic action and evaluate whether *P. anserina* induces a dedicated ligninolytic machinery in the presence of lignin, we performed proteomics analyses of the secreted proteins during growth of the fungus on GAX and GAX+Lignin. These analyses identified a total of 430 proteins, of which 196 (46%) could be assigned to CAZymes. Of these CAZymes, 167 enzymes were annotated to a putative plant cell wall active function based on the JGI database. Most of these enzymes were secreted in both growth conditions, while the number of unique enzymes for GAX (18 enzymes) and GAX+Lignin (16 enzymes) was comparable. For both growth substrates, these unique plant cell wall active enzymes summed up to 1% of the total relative abundance only. The total relative abundance of plant cell wall active enzymes was approximately 66% and 55% for GAX and GAX+Lignin, respectively (Figure S2).

Irrespective of the presence of lignin, carbohydrate hydrolases made up the majority of the detected plant cell wall active enzymes during growth (Figure 3). However, lignin did induce a relative shift from a hydrolytic towards a more oxidative enzymatic degradation pattern. Most strikingly, cellulases were approximately 3.4-fold decreased in the presence of lignin, while multicopper oxidases (20-fold) and H₂O₂ producing enzymes (3-fold) were strongly increased (Figure 3).

The decrease in cellulases was predominately explained by a reduction in cellobiohydrolases (5.4-fold), while endoglucanases decreased far less (1.7-fold) and β -glucosidases increased (1.5-fold) (Figure 3B). The reduction in cellobiohydrolases was primarily caused by two enzymes (GH7 #368104, 23-fold and GH6 #301916, 20-fold) (Figure S3A), while the reduction in endoglucanases could be ascribed to a single enzyme (GH5 #382814) that was basically absent in the presence of lignin (Figure S3B). Though the overall β -glucosidase abundance was not largely affected, a GH3 β -glucosidase (#166682) decreased 32-fold, while another GH3 β -glucosidase (#330692) increased 14-fold in the presence of lignin (Figure S3C).

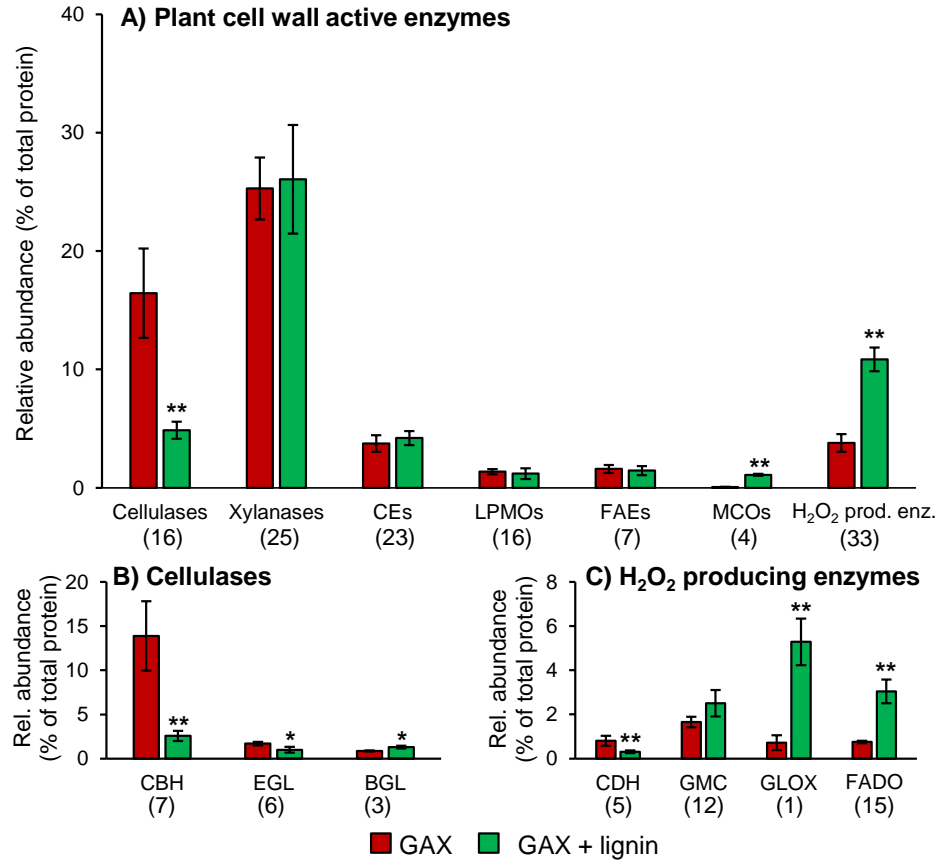


Figure 3. Proteomics analyses of secreted plant cell wall active enzymes during growth of *P. anserina* on glucuronoarabinoxylan (GAX) and GAX+Lignin with number of detected enzymes per group in parentheses. Enzymes were grouped on the basis of overall functionality (A) and further subdivided into more specific activities in (B) and (C) according to the JGI database (*P. anserina* *mat+* v1.0). CEs carbohydrate esterases; LPMOs lytic polysaccharide monooxygenases; FAEs feruloyl esterases; MCOs multicopper oxidases; CBH cellobiohydrolases; EGL endoglucanases, BGL β -glucosidases; CDH cellobiose dehydrogenases; GMC glucose-methanol-choline oxidoreductases; GLOX glyoxal oxidases; FADO FAD-linked oxidases. Significant differences calculated by two-tailed t-test (* $p < 0.05$, ** $p < 0.01$).

Overall, LPMOs did not decrease concurrently with the cellulase system, which supports the hypothesis that these enzymes are produced with another function than oxidatively degrading cellulose alone.⁴³⁻⁴⁴ It is worth mentioning that one LPMO (AA9, #179198, characterized as PaLPMO9B) was 2.7-fold decreased while three other AA9 LPMOs, #403339 (PaLPMO9C), #307960 (PaLPMO9E) and #287378 (PaLPMO9A), increased 10.7, 9.7 and 4.5-fold, respectively (Figure S3D).^{7, 45} The increase in PaLPMOs 9A and 9E, characterized to work on cellulose rather strictly, is interesting given the severe reduction in cellulases.⁷ This could indicate that the fungus produces LPMOs ahead of cellulases and that the enzymes might act synergistically, but not necessarily concurrently. The activity of the

induced LPMOs has been demonstrated to be boosted by cellobiose dehydrogenases (CDHs) and they have been considered to function together *in vivo*.^{7, 45} However, the overall abundance of cellobiose dehydrogenases (CDHs) was 2.6-fold reduced in the presence of lignin, which contends their putative concerted action with LPMOs. Alternatively, the LPMOs might depend on other electron transfer systems including the H₂O₂ producing enzymes that were strongly induced in the presence of lignin, as will be elaborated below.⁴⁶⁻⁴⁷

The total xylanase machinery was not significantly affected by the presence of lignin and the production of various endoxylanases and arabinofuranosidases allowed the fungus to efficiently degrade GAX during its growth (~60%, Figure 1). Even though the grouped xylanases did not show an overall significant change in the presence of lignin, clear differences could be observed at the individual enzyme level (Figure S3E-F). A GH10 endo-xylanase (#388128) was 46-fold reduced together with the reduction of two GH11 endo-xylanases (#405228 5-fold, #428889 74-fold) in the presence of lignin, while two other GH10 endo-xylanases increased (#333275 5.6-fold and #176471 1.8-fold) (Figure S3E). Even though in terms of total endoxylanase abundance these effects cancel out, it is interesting to observe that the presence of lignin can trigger a shift in the production of certain endo-xylanases, with potentially different functionalities and/or specificities.

Likewise, the presence of lignin induced a 2.9-fold reduction in two predicted GH43 arabinofuranosidases (#438134 and #300046), while the GH51 (#109488, PaAbf51A) and GH62 (#434801, PaAbf62A) arabinofuranosidases respectively increased by 6-fold and 4.8 fold (Figure S3F). In line with the induction by lignin, Mäkelä et al. showed that when *P. anserina* was grown on wheat straw, the latter GH62 arabinofuranosidase was produced in greater abundance than when grown on cottonseed and soybean hulls.¹⁰ The increase of the two arabinofuranosidases (PaAbf51A and PaAbf62A) is remarkable in the sense that they have been characterized to exhibit low activity on polymeric substrates, including wheat arabinoxylan (low viscosity), and were shown to cleave terminal arabinosyl units only.⁹

The overall relative abundance of carbohydrate (mostly acetyl xylan, AXE) and feruloyl esterases (FAEs) was not significantly different in the presence and absence of lignin (Figure 3). Still, a putative CE15 4-O-methyl-glucuronyl methylesterase (#118359) was not produced in the presence of lignin, while a putative CE12 rhamnogalacturonan acetylerase (#381424) was decreased by a factor 6.1 (Figure S3G). Conversely, four other carbohydrate esterases significantly increased (CE1 putative acetylxytan esterase (AXE) with carbohydrate binding module specific for cellulose (CBM1) #284003 3-fold, CE3 #281974 12-fold, CE5 with CBM1 #110452 5-fold and CE5 putative cutinase #36734 24-fold). Apart from a severe reduction in CE1 feruloyl esterase (FAE) #312581 (71-fold), the abundance of FAEs was not significantly different in the presence of lignin (Figure S3H). These FAEs have often been suggested to be involved in disentangling lignin and hemicellulose, and therefore, their production might be

induced by the presence of lignin or related substructures.^{10, 48} Apparently, the hemicellulosic substrate used in the current cultivations without lignin already induced these enzymes and the presence of lignin did not further increase their production. Although not changed in relative abundance, the FAEs were still most likely responsible for the reduction in ferulate and *p*-coumarate moieties in the residual lignin after growth of *P. anserina* (Table 2).³⁰

The highly significant increase in H₂O₂ producing enzymes (2.9-fold) was particularly due to a single putative AA5_1 glyoxal oxidase (GLOX, #15405) which increased 7.3-fold (Figure 3C). In addition, FAD-linked oxidases (FADO) overall 4-fold increased in the presence of lignin (Figure 3C). This was due to three putative AA7 oxidoreductases all having a vanillyl-alcohol oxidase (VAO)-type FAD domain (#439950 20-fold, #446722 12-fold and #379025; no signal P 9-fold) that were strongly induced in the presence of lignin (Figure S3J).⁴⁹ A respective 3.7-fold and 7.7-fold increase in two putative AA3 GMC oxidoreductases (#401428 and #420563; no signal P) further contributed to the overall increase in H₂O₂ producing enzymes (Figure S3K). *P. anserina* has previously been shown to respond differently on various biomass sources regarding the induction of H₂O₂ producing enzymes.^{10, 16} Our observations clearly show that lignin is amongst the inducing agents for these enzymes and this report constitutes the first experimental evidence of induction of AA7 oxidoreductases of *P. anserina*.

Characterized AA7 oxidoreductases have been listed in the CAZy database as FAD-linked oligosaccharide oxidases, and are structurally related to berberine-bridge enzyme (BBE)-like enzymes.⁵⁰ However, phylogenetic analysis according to Ewing et al.⁵¹ revealed that the AA7 oxidoreductases of *P. anserina* which were induced upon growth on lignin belong to other clades of the subfamily of BBE-like enzymes and more likely are involved in the production of secondary metabolites.

The presence of lignin caused a 20-fold overall increase in multicopper oxidases, which was primarily due to a 63-fold induction of an AA1_3 laccase (#430065) (Figure S3L). This enzyme has previously been annotated as a putative bilirubin oxidase, named *bod1*, but it was later found to actually correspond to a 'new' thermotolerant laccase after heterologous production and biochemical characterization.^{5, 52} The biotechnologically interesting thermotolerancy was later further demonstrated by enzymatic assays following targeted mutations.⁵³ A mutant lacking the *bod1* enzyme, furthermore, showed a mildly decreased ability to grow on lignin next to a decreased ability to resist various phenolics and H₂O₂.⁵³ The strong induction of this enzyme in the presence of lignin observed here further underlines its potential involvement in the degradation of lignin. Another laccase (#99820) was only produced in lignin's presence, albeit in relatively low abundance still (Figure S3L). Xie et al. have shown through targeted mutations that this enzyme is involved in the fungus' ability to grown on wood shavings.¹⁷ Note that, as already mentioned above, the (expected) relatively low redox potentials consequently would only allow these enzymes to act 'directly' on phenolic moieties.

Alternatively, some lignin-derived phenols could have acted as mediators, or so-called electron-shuttles, indirectly broadening the oxidative range of these laccases.⁵⁴⁻⁵⁵

Knowing that specific enzyme activities are not taken into account, the extensive induction of H₂O₂ producers at least suggests some involvement in the observed ligninolysis (Figure 3). Although H₂O₂ producing enzymes have often been considered an accessory to peroxidases, a recent reevaluation of the *P. anserina* *mat+* gene annotations eliminated the only putative peroxidase from its genome. As such, a sole facilitating role of these H₂O₂ producers to enzymes involved in ligninolysis can be excluded. Alternatively, the produced H₂O₂ might have been involved in Fenton chemistry. The Fenton reaction describes the conversion of H₂O₂ to hydroxyl radicals in the presence of iron at acidic conditions. These highly reactive radicals are expected to result in 'untargeted' or 'nonselective' ligninolysis, a mechanism that is often associated with the action of brown-rot basidiomycetes.⁵⁶⁻⁵⁷ The fungal metabolite 2,5-dimethoxyhydroquinone has been shown to drive the Fenton reaction in the latter fungi and, accordingly, has been used as marker for the possible involvement of Fenton chemistry.^{56, 58-59} Though LC-MS analyses of the culture supernatants failed to detect these metabolites, other (lignin-derived) products might have fulfilled the same role in *P. anserina* biodegradation reactions. Although these secretome analyses cannot provide a definite answer on the underlying ligninolysis mechanisms, they do highlight potentially involved enzymes that are interesting candidates for follow-up gene-knockout and enzyme production/characterization studies.

Conclusions

In summary, we have for the first time, provided unambiguous confirmation of the ligninolytic activity of the ascomycete fungus *Podospora anserina* through comprehensive substrate analyses of wheat straw lignin that was grown with the fungus. Fungal growth resulted in substantial lignin removal and the accumulation of oxidatively degraded substructures. The insights obtained through substrate characterization agreed well with complementary proteomics analyses. Most importantly, these analyses showed that the secretome of *P. anserina* was considerably altered in the presence of lignin, with a strong reduction of cellulases in particular, and suggested the potential involvement of laccases and H₂O₂ producing enzymes in ligninolysis reactions. Our work highlights several interesting candidate enzymes for further biochemical characterization and employment in biotechnological applications.

References

1. Himmel, M. E.; Ding, S.-Y.; Johnson, D. K.; Adney, W. S.; Nimlos, M. R.; Brady, J. W.; Foust, T. D., Biomass recalcitrance: engineering plants and enzymes for biofuels production. *Science* **2007**, *315*, 804-807.
2. Dowding, E. S., The sexuality of the normal, giant and dwarf spores of *Pleurotus anserina*. (Ces) Kuntze. *Ann Bot* **1931**, *212*, 1-14.
3. Rizet, G., Sur l'analyse génétique des asques du *Podospora anserina*. *C R Acad Sci Paris* **1941**, 59-61.
4. Osiewacz, H. D.; Hamann, A.; Zintel, S., Assessing organismal aging in the filamentous fungus *Podospora anserina*. In *Cell Senescence. Methods in Molecular Biology (Methods and Protocols)*, Galluzzi, L.; Vitale, I.; Kepp, O.; Kroemer, G., Eds. Humana Press: Totowa, NJ, 2013; Vol. 965, pp 439-462.
5. Espagne, E.; Lespinet, O.; Malagnac, F.; Da Silva, C.; Jaillon, O.; Porcel, B. M.; Couloux, A.; Aury, J.-M.; Ségurens, B.; Poulain, J.; Anthouard, V.; Grossetete, S.; Khalil, H.; Coppin, E.; Déquard-Chablat, M.; Picard, M.; Contamine, V.; Arnais, S.; Bourdais, A.; Berteaux-Lecellier, V.; Gautheret, D.; de Vries, R. P.; Battaglia, E.; Coutinho, P. M.; Danchin, E. G.; Henrissat, B.; Khoury, R. E.; Sainsard-Chanet, A.; Boivin, A.; Pinan-Lucarré, B.; Sellem, C. H.; Debuchy, R.; Winker, P.; Weissenbach, J.; Silar, P., The genome sequence of the model ascomycete fungus *Podospora anserina*. *Genome Biol* **2008**, *9*, R77.
6. Silar, P., *Podospora anserina*: from laboratory to biotechnology. In *Genomics of Soil-and Plant-Associated Fungi*, Horwitz, B. A.; Mukherjee, P. K.; Mukherjee, M.; Kubicek, C. P., Eds. Springer: Heidelberg New York Dordrecht London, 2013; pp 283-309.
7. Bennati-Granier, C.; Garajova, S.; Champion, C.; Grisel, S.; Haon, M.; Zhou, S.; Fanuel, M.; Ropartz, D.; Rogniaux, H.; Gimbert, I., Substrate specificity and regioselectivity of fungal AA9 lytic polysaccharide monoxygenases secreted by *Podospora anserina*. *Biotechnol Biofuels* **2015**, *8*, 90.
8. Fanuel, M.; Garajova, S.; Ropartz, D.; McGregor, N.; Brumer, H.; Rogniaux, H.; Berrin, J.-G., The *Podospora anserina* lytic polysaccharide monoxygenase Pa LPMO9H catalyzes oxidative cleavage of diverse plant cell wall matrix glycans. *Biotechnol Biofuels* **2017**, *10*, 63.
9. Couturier, M.; Haon, M.; Coutinho, P. M.; Henrissat, B.; Lesage-Meessen, L.; Berrin, J.-G., *Podospora anserina* hemicellulases potentiate the *Trichoderma reesei* secretome for saccharification of lignocellulosic biomass. *Appl Environ Microbiol* **2011**, *77*, 237-246.
10. Mäkelä, M. R.; Bouzid, O.; Robl, D.; Post, H.; Peng, M.; Heck, A.; Altelaar, M.; de Vries, R. P., Cultivation of *Podospora anserina* on soybean hulls results in an efficient enzyme cocktail for plant biomass hydrolysis. *New Biotechnol* **2017**, *37*, 162-171.
11. Richardson, M. J., The coprophilous succession. *Fungal Divers* **2002**, 101-111.
12. Couturier, M.; Tangthirasunun, N.; Ning, X.; Brun, S.; Gautier, V.; Bennati-Granier, C.; Silar, P.; Berrin, J.-G., Plant biomass degrading ability of the coprophilic ascomycete fungus *Podospora anserina*. *Biotechnol Adv* **2016**, *34*, 976-983.
13. Tangthirasunun, N.; Navarro, D.; Garajova, S.; Chevret, D.; Tong, L. C. H.; Gautier, V.; Hyde, K. D.; Silar, P.; Berrin, J.-G., Inactivation of cellobiose dehydrogenases modifies the cellulose degradation mechanism of *Podospora anserina*. *Appl Environ Microbiol* **2017**, *83*, e02716-16.
14. Bourdais, A.; Bidard, F.; Zickler, D.; Berteaux-Lecellier, V.; Silar, P.; Espagne, E., Wood utilization is dependent on catalase activities in the filamentous fungus *Podospora anserina*. *PLoS One* **2012**, *7*, e29820.
15. Levasseur, A.; Drula, E.; Lombard, V.; Coutinho, P. M.; Henrissat, B., Expansion of the enzymatic repertoire of the CAZy database to integrate auxiliary redox enzymes. *Biotechnol Biofuels* **2013**, *6*, 41.

16. Poidevin, L.; Berrin, J.-G.; Bennati-Granier, C.; Levasseur, A.; Herpoël-Gimbert, I.; Chevreton, D.; Coutinho, P. M.; Henrissat, B.; Heiss-Blanquet, S.; Record, E., Comparative analyses of *Podospora anserina* secretomes reveal a large array of lignocellulose-active enzymes. *Appl Microbiol Biotechnol* **2014**, *98*, 7457-7469.
17. Xie, N.; Chapeland-Leclerc, F.; Silar, P.; Ruprich-Robert, G., Systematic gene deletions evidences that laccases are involved in several stages of wood degradation in the filamentous fungus *Podospora anserina*. *Environ Microbiol* **2014**, *16*, 141-161.
18. Van Erven, G.; Nayan, N.; Sonnenberg, A. S.; Hendriks, W. H.; Cone, J. W.; Kabel, M. A., Mechanistic insight in the selective delignification of wheat straw by three white-rot fungal species through quantitative ¹³C-IS py-GC-MS and whole cell wall HSQC NMR. *Biotechnol Biofuels* **2018**, *11*, 262.
19. Van Erven, G.; Hilgers, R.; de Waard, P.; Gladbeek, E.-J.; van Berkel, W. J. H.; Kabel, M. A., Elucidation of *in situ* ligninolysis mechanisms of the selective white-rot fungus *Ceriporiopsis subvermispota*. *ACS Sustainable Chem Eng* **2019**, *7*, 16757-16764.
20. Björkman, A., Studies on finely divided wood. Part 1. Extraction of lignin with neutral solvents. *Sven Papperstidn* **1956**, *59*, 477-485.
21. Chang, H.-M.; Cowling, E. B.; Brown, W., Comparative studies on cellulolytic enzyme lignin and milled wood lignin of sweetgum and spruce. *Holzforschung* **1975**, *29*, 153-159.
22. Benocci, T.; Daly, P.; Aguilar-Pontes, M. V.; Lail, K.; Wang, M.; Lipzen, A.; Ng, V.; Grigoriev, I. V.; de Vries, R. P., Enzymatic adaptation of *Podospora anserina* to different plant biomass provides leads to optimized commercial enzyme cocktails. *Biotechnol J* **2019**, *14*, 1800185.
23. Benocci, T.; de Vries, R. P.; Daly, P., A senescence-delaying pre-culture medium for transcriptomics of *Podospora anserina*. *J Microbiol Methods* **2018**, *146*, 33-36.
24. Van Erven, G.; de Visser, R.; Merckx, D. W.; Strolenberg, W.; de Gijssel, P.; Gruppen, H.; Kabel, M. A., Quantification of lignin and its structural features in plant biomass using ¹³C lignin as internal standard for pyrolysis-GC-SIM-MS. *Anal Chem* **2017**, *89*, 10907-10916.
25. Del Río, J. C.; Rencoret, J.; Prinsen, P.; Martínez, A. T.; Ralph, J.; Gutiérrez, A., Structural characterization of wheat straw lignin as revealed by analytical pyrolysis, 2D-NMR, and reductive cleavage methods. *J Agric Food Chem* **2012**, *60*, 5922-5935.
26. Englyst, H. N.; Cummings, J. H., Simplified method for the measurement of total non-starch polysaccharides by gas-liquid chromatography of constituent sugars as alditol acetates. *Analyst* **1984**, *109*, 937-942.
27. Van Erven, G.; Wang, J.; Sun, P.; de Waard, P.; van der Putten, J.; Frissen, G. E.; Gosselink, R. J. A.; Zinovyev, G.; Potthast, A.; van Berkel, W. J. H.; Kabel, M. A., Structural motifs of wheat straw lignin differ in susceptibility to degradation by the white-rot fungus *Ceriporiopsis subvermispota*. *ACS Sustainable Chem Eng* **2019**, *7*, 20032-20042.
28. Badhan, A.; Ribeiro Jr, G. O.; Jones, D. R.; Wang, Y.; Abbott, D. W.; Di Falco, M.; Tsang, A.; McAllister, T. A., Identification of novel enzymes to enhance the ruminal digestion of barley straw. *Bioresour Technol* **2018**, *260*, 76-84.
29. Daly, P.; Peng, M.; Di Falco, M.; Lipzen, A.; Wang, M.; Ng, V.; Grigoriev, I. V.; Tsang, A.; Mäkelä, M. R.; de Vries, R. P., Glucose-mediated repression of plant biomass utilization in the white-rot fungus *Dichomitus squalens*. *Appl Environ Microbiol* **2019**, *85*, 01828-19.
30. Underlin, E.; Frommhagen, M.; Dilokpimol, A.; van Erven, G.; de Vries, R. P.; Kabel, M. A., Feruloyl esterases for biorefineries: subfamily classified specificity for natural substrates. *Submitted*.
31. Kang, X.; Kirui, A.; Muszyński, A.; Widanage, M. C. D.; Chen, A.; Azadi, P.; Wang, P.; Mentink-Vigier, F.; Wang, T., Molecular architecture of fungal cell walls revealed by solid-state NMR. *Nat Comm* **2018**, *9*, 2747.

32. Hilgers, R.; van Erven, G.; Boerkamp, V.; Sulaeva, I.; Potthast, A.; Kabel, M. A.; Vincken, J.-P., Understanding laccase/HBT-catalyzed grass delignification at the molecular level. *Green Chem* **2020**, *22*, 1735-1746.
33. Martínez, A.; Camarero, S.; Gutiérrez, A.; Bocchini, P.; Galletti, G., Studies on wheat lignin degradation by *Pleurotus* species using analytical pyrolysis. *J Anal Appl Pyrolysis* **2001**, *58*, 401-411.
34. Van Kuijk, S. J. A.; Sonnenberg, A. S. M.; Baars, J. J. P.; Hendriks, W. H.; del Río, J. C.; Rencoret, J.; Gutiérrez, A.; de Ruijter, N. C. A.; Cone, J. W., Chemical changes and increased degradability of wheat straw and oak wood chips treated with the white rot fungi *Ceriporiopsis subvermispota* and *Lentinula edodes*. *Biomass Bioenergy* **2017**, *105*, 381-391.
35. Ralph, J.; Hatfield, R. D., Pyrolysis-GC-MS characterization of forage materials. *J Agric Food Chem* **1991**, *39*, 1426-1437.
36. Del Río, J. C.; Gutiérrez, A.; Rodríguez, I. M.; Ibarra, D.; Martínez, Á. T., Composition of non-woody plant lignins and cinnamic acids by Py-GC/MS, Py/TMAH and FT-IR. *J Anal Appl Pyrolysis* **2007**, *79*, 39-46.
37. Ralph, J., Hydroxycinnamates in lignification. *Phytochem Rev* **2010**, *9*, 65-83.
38. Brunow, G.; Lundquist, K., Functional groups and bonding patterns in lignin (including the lignin-carbohydrate complexes). In *Lignin and Lignans: Advances in Chemistry*, Heithner, C.; dimmel, D.; Schmidt, J. A., Eds. CRC Press, Taylor & Francis: Boca Raton, FL, USA, 2010; pp 267-299.
39. Wong, D. W., Structure and action mechanism of ligninolytic enzymes. *Appl Biochem Biotechnol* **2009**, *157*, 174-209.
40. Hilgers, R.; Vincken, J.-P.; Gruppen, H.; Kabel, M. A., Laccase/mediator systems: their reactivity toward phenolic lignin structures. *ACS Sustainable Chem Eng* **2018**, *6*, 2037-2046.
41. Munk, L.; Sitarz, A. K.; Kalyani, D. C.; Mikkelsen, J. D.; Meyer, A. S., Can laccases catalyze bond cleavage in lignin? *Biotechnol Adv* **2015**, *33*, 13-24.
42. Boerjan, W.; Ralph, J.; Baucher, M., Lignin biosynthesis. *Annu Rev Plant Biol* **2003**, *54*, 519-546.
43. Frommhagen, M.; Westphal, A. H.; Van Berkel, W. J.; Kabel, M. A., Distinct substrate specificities and electron-donating systems of fungal lytic polysaccharide monooxygenases. *Front Microbiol* **2018**, *9*, 1080.
44. Eijsink, V. G.; Petrovic, D.; Forsberg, Z.; Mekasha, S.; Røhr, Å. K.; Várnai, A.; Bissaro, B.; Vaaje-Kolstad, G., On the functional characterization of lytic polysaccharide monooxygenases (LPMOs). *Biotechnol Biofuels* **2019**, *12*, 58.
45. Bey, M.; Zhou, S.; Poidevin, L.; Henrissat, B.; Coutinho, P. M.; Berrin, J.-G.; Sigoillot, J.-C., Cello-oligosaccharide oxidation reveals differences between two lytic polysaccharide monooxygenases (family GH61) from *Podospira anserina*. *Appl Environ Microbiol* **2013**, *79*, 488-496.
46. Kracher, D.; Scheiblbrandner, S.; Felice, A. K.; Breslmayr, E.; Preims, M.; Ludwicka, K.; Haltrich, D.; Eijsink, V. G.; Ludwig, R., Extracellular electron transfer systems fuel cellulose oxidative degradation. *Science* **2016**, *352*, 1098-1101.
47. Garajova, S.; Mathieu, Y.; Beccia, M. R.; Bennati-Granier, C.; Biaso, F.; Fanuel, M.; Ropartz, D.; Guigliarelli, B.; Record, E.; Rogniaux, H., Single-domain flavoenzymes trigger lytic polysaccharide monooxygenases for oxidative degradation of cellulose. *Sci Rep* **2016**, *6*, 28276.
48. Špániková, S.; Biely, P., Glucuronoyl esterase-novel carbohydrate esterase produced by *Schizophyllum commune*. *FEBS Lett* **2006**, *580*, 4597-4601.
49. Fraaije, M. W.; van Berkel, W. J.; Benen, J. A.; Visser, J.; Mattevi, A., A novel oxidoreductase family sharing a conserved FAD binding domain. *Trends Biochem Sci* **1998**, *23*, 206-207.
50. Daniel, B.; Konrad, B.; Toplak, M.; Lahham, M.; Messenlehner, J.; Winkler, A.; Macheroux, P., The family of berberine bridge enzyme-like enzymes: A treasure-trove of oxidative reactions. *Arch Biochem Biophys* **2017**, *632*, 88-103.

51. Ewing, T. A.; Fraaije, M. W.; Mattevi, A.; van Berkel, W. J., The VAO/PCMH flavoprotein family. *Arch Biochem Biophys* **2017**, 632, 104-117.
52. Durand, F.; Gounel, S.; Mano, N., Purification and characterization of a new laccase from the filamentous fungus *Podospira anserina*. *Protein Expression Purif* **2013**, 88, 61-66.
53. Xie, N.; Ruprich-Robert, G.; Silar, P.; Chapeland-Leclerc, F., Bilirubin oxidase-like proteins from *Podospira anserina*: promising thermostable enzymes for application in transformation of plant biomass. *Environ Microbiol* **2015**, 17, 866-875.
54. Nousiainen, P.; Majjala, P.; Hatakka, A.; Martínez, A. T.; Sipilä, J., Syringyl-type simple plant phenolics as mediating oxidants in laccase catalyzed degradation of lignocellulosic materials: Model compound studies 10th EWLP, Stockholm, Sweden, August 25-28, 2008. *Holzforschung* **2009**, 63, 699-704.
55. Rico, A.; Rencoret, J.; del Río, J. C.; Martínez, A. T.; Gutiérrez, A., Pretreatment with laccase and a phenolic mediator degrades lignin and enhances saccharification of *Eucalyptus* feedstock. *Biotechnol Biofuels* **2014**, 7, 6.
56. Wei, D.; Houtman, C. J.; Kapich, A. N.; Hunt, C. G.; Cullen, D.; Hammel, K. E., Laccase and its role in production of extracellular reactive oxygen species during wood decay by the brown rot basidiomycete *Postia placenta*. *Appl Environ Microbiol* **2010**, 76, 2091-2097.
57. Yelle, D. J.; Wei, D.; Ralph, J.; Hammel, K. E., Multidimensional NMR analysis reveals truncated lignin structures in wood decayed by the brown rot basidiomycete *Postia placenta*. *Environ Microbiol* **2011**, 13, 1091-1100.
58. Cohen, R.; Jensen, K. A.; Houtman, C. J.; Hammel, K. E., Significant levels of extracellular reactive oxygen species produced by brown rot basidiomycetes on cellulose. *FEBS Lett* **2002**, 531, 483-488.
59. Korripally, P.; Timokhin, V. I.; Houtman, C. J.; Mozuch, M. D.; Hammel, K. E., Evidence from *Serpula lacrymans* that 2,5-dimethoxyhydroquinone is a lignocellulolytic agent of divergent brown rot basidiomycetes. *Appl Environ Microbiol* **2013**, 79, 2377-2383.

Supporting Information

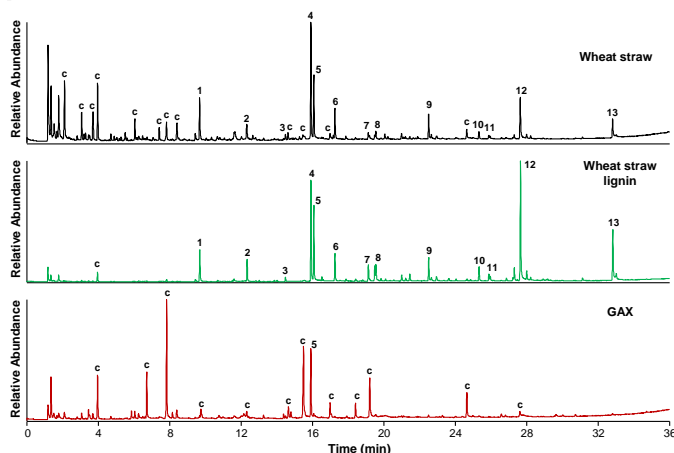


Figure S1. Py-GC-HR-MS pyrograms (TIC) of wheat straw, wheat straw lignin and glucuronoarabinoxylan (GAX). Numbers refer to major lignin-derived compounds: 1 guaiacol; 2 4-methylguaiacol; 3 4-ethylguaiacol; 4 4-vinylphenol; 5 4-vinylguaiacol; 6 syringol; 7 *trans*-isoeugenol; 8 vanillin; 9 4-vinylsyringol; 10 *trans*-propenylsyringol; 11 syringaldehyde; 12 *trans*-coniferyl alcohol; 13 *trans*-sinapylalcohol. (c) refers to carbohydrate-derived products.

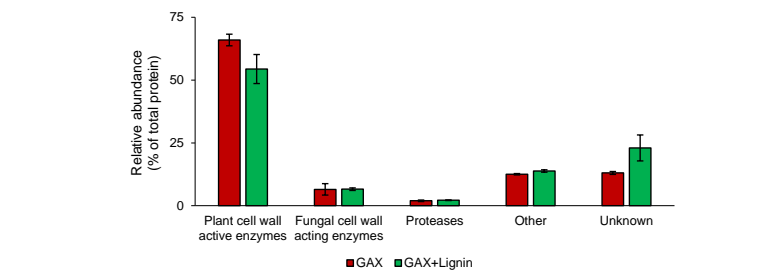


Figure S2. Proteomic analysis of secreted proteins during growth of *P. anserina* on glucuronoarabinoxylan (GAX) and GAX+Lignin. Grouped according to functional annotations in JGI database (*P. anserina* mat+ v1.0). Average and standard deviation of biological triplicates.

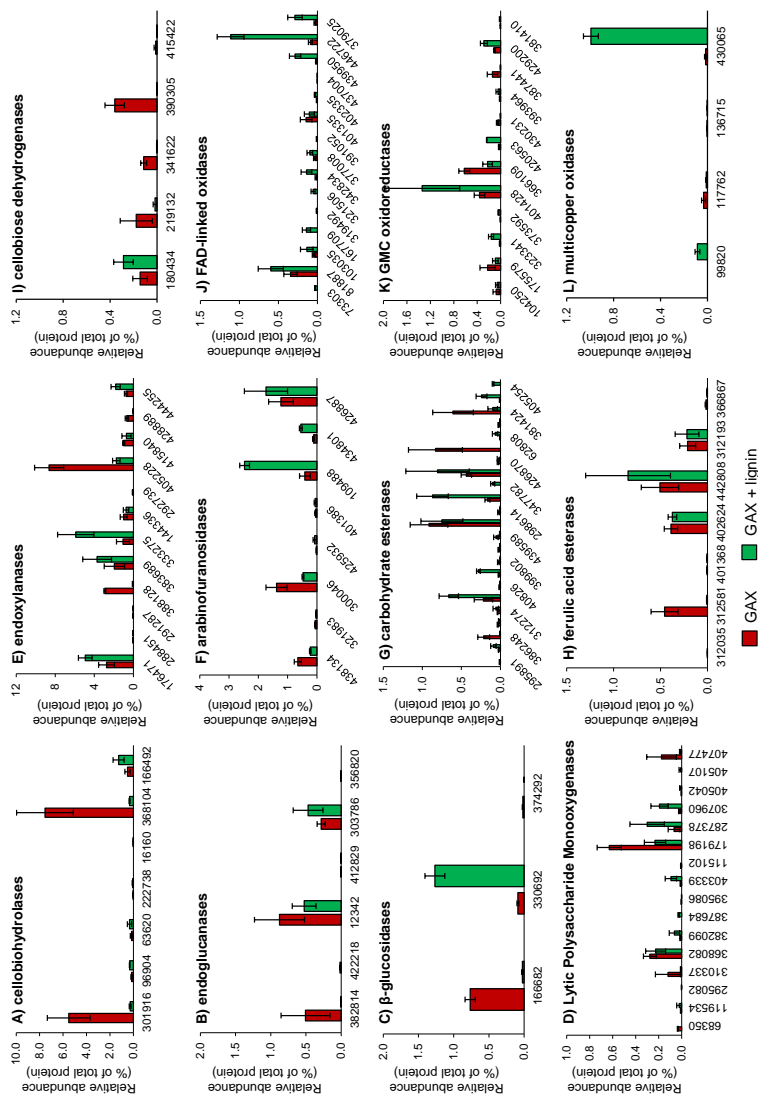


Figure S3. Proteomic analysis of secreted individual proteins during growth of *P. anserina* on glucuronoarabinoxylan (GAX) and GAX+Lignin. Accession numbers and functional annotations according to JGI database (*P. anserina* mat+ v1.0). Average and standard deviation of biological triplicates.

Table S1. Py-GC-HR-MS relative abundance of lignin compounds in wheat straw lignin isolate used for fermentations with *P. anserina*. Corrected for relative response factors and relative abundance of ^{13}C internal standard analogues. Sum on the bases of structural classification according to van Erven et al.¹⁻² Average and standard deviation of analytical duplicates.

wheat straw lignin	
Lignin subunits (%)	
H	8.6 ± 0.3
G	58.9 ± 0.2
S	32.4 ± 0.2
S/G	0.55 ± 0.0
Structural moieties (%)	
Unsubstituted	5.6 ± 0.2
Methyl	3.4 ± 0.1
Vinyl	27.0 ± 0.5
4-VP ^a	7.1 ± 0.3
4-VG ^b	16.4 ± 0.1
C _α -ox	4.8 ± 0.0
C _β -ox ^c	1.1 ± 0.0
C _γ -ox	55.7 ± 0.8
Miscellaneous	3.5 ± 0.1
PhC _γ ^d	60.1 ± 0.7

^a 4-vinylphenol. ^b 4-vinylguaiacol.

^c excluding diketones.

^d phenols with intact α,β,γ carbon side chain.

Table S2. Semiquantitative ^1H - ^{13}C HSQC NMR structural characterization of wheat straw lignin isolate used for fermentations with *P. anserina*.

wheat straw lignin	
Lignin subunits (%) ^a	
H	3
G	63
G _{ox}	0
S	34
S _{ox}	0
S/G	0.5
Hydroxycinnamates (%) ^b	
p-coumarate	8
ferulate	6
Flavonolignin (%) ^b	
tricin	15
Lignin interunit linkages (%) ^{b,c}	
β-O-4' aryl ethers	56 (91)
β-5' phenylcoumarans	4 (7)
β-β' resinols	1 (2)
total	62 (100)

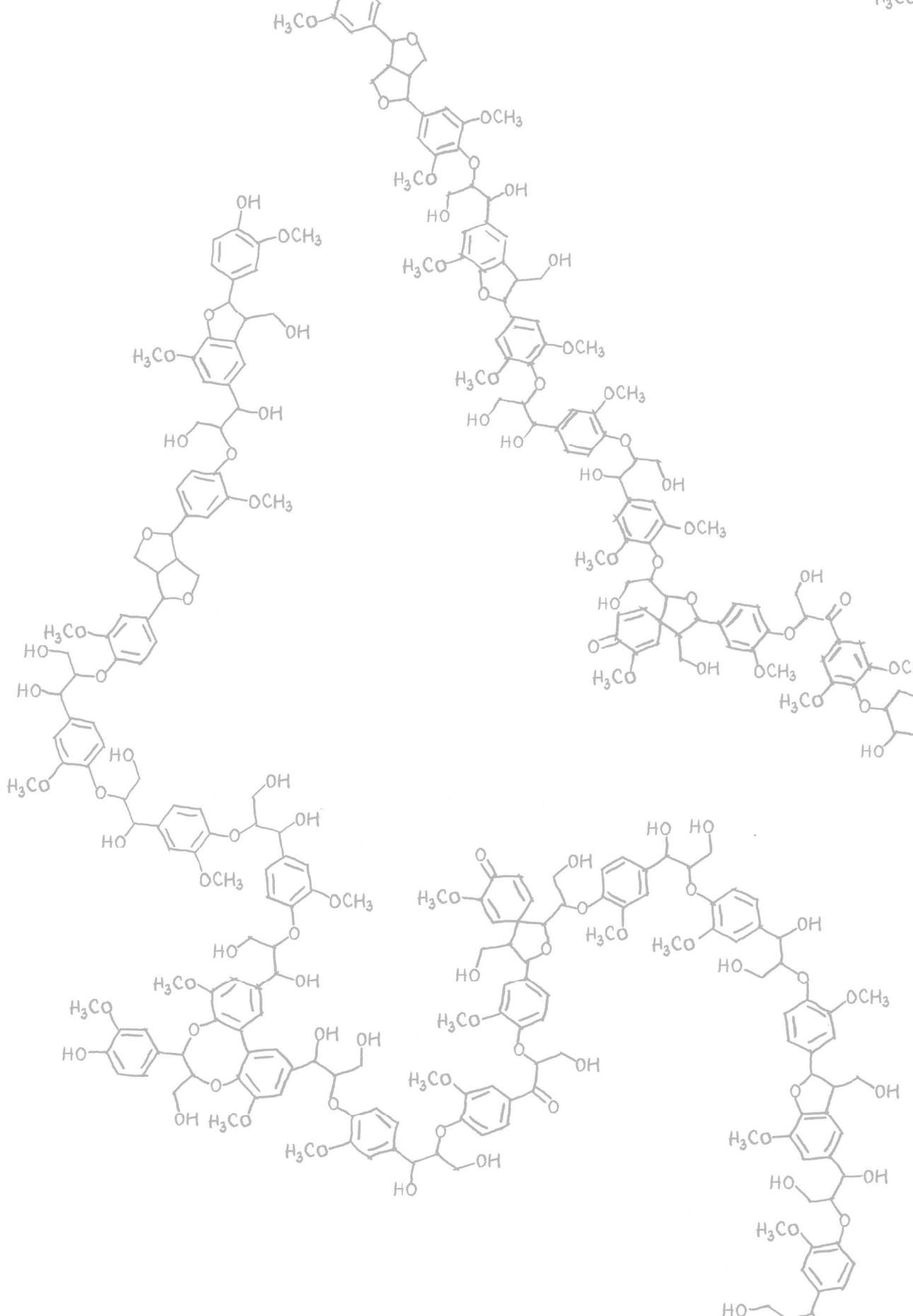
^a relative distribution of lignin subunits (H+G+G_{ox}+S+S_{ox} = 100)

^b relative volume integral of substructure versus volume integral of total lignin subunits

^c relative distribution of total interunit linkages in parentheses

Supporting Information References

1. Van Erven, G.; Nayan, N.; Sonnenberg, A. S.; Hendriks, W. H.; Cone, J. W.; Kabel, M. A., Mechanistic insight in the selective delignification of wheat straw by three white-rot fungal species through quantitative ^{13}C -IS py-GC-MS and whole cell wall HSQC NMR. *Biotechnol Biofuels* **2018**, *11*, 262.
2. Van Erven, G.; Hilgers, R.; de Waard, P.; Gladbeek, E.-J.; van Berkel, W. J. H.; Kabel, M. A., Elucidation of *in situ* ligninolysis mechanisms of the selective white-rot fungus *Ceriporiopsis subvermispora*. *ACS Sustainable Chem Eng* **2019**, *7*, 16757-16764.



CHAPTER 8

General Discussion

In this thesis, we have aimed to improve the quantitative analysis of lignin and strived for deepening our understanding of the fungal delignification process, particularly *in situ*, by employing the developed analytical tools.

Validation of the ^{13}C -IS py-GC-MS method

As outlined in **Chapter 1**, the complex structure of lignin, amongst others, hampers its accurate quantification, which therefore, still is largely based on unspecific gravimetric and spectrophotometric methods. Besides interference by nonlignin components, these methods generally require substantial sample investments and do not provide any insight into lignin's structural composition. **Chapter 2 and 3** described our efforts to circumvent these drawbacks by employing py-GC-MS analysis. Therein, we demonstrated that lignin-derived pyrolysis products can be used as a quantitative measure for specific lignin content, once corrected for their individual relative response factors and, most innovatively, their total peak area was related to that of a polymeric ^{13}C lignin internal standard. We, furthermore, showed that lignin can be properly quantified as long as internal standards are employed from the same botanical origin or taxon, even if the lignins are structurally different. Yet, some challenges to the application of our method remain, which will be discussed in the next sections.

Quantification of (native) grass lignin

In **Chapter 1**, we described that the grass cell wall differs substantially from that of woods, first and foremost by the incorporation of hydroxycinnamic acids in its lignin and hemicellulose.¹⁻⁴ This difference in cell wall composition poses additional challenges for the accurate quantification of lignin in grasses.

Hydroxycinnamic acids. As has been mentioned in **Chapter 2**, one of the remaining challenges in the application of the quantitative ^{13}C -IS py-GC-MS method to grasses is the fact that the origin of vinylic pyrolysis products cannot be deduced directly. Grasses contain substantial levels of *p*-coumaric acid and ferulic acid that upon pyrolysis, respectively yield 4-vinylphenol and 4-vinylguaiacol.⁵ These two pyrolysis products, however, can also be formed from lignin's interunit linkages (Figure 1). Hence, these compounds could potentially interfere with the determination of lignin content. Yet, when these products were fully included in the quantification of lignin, excellent accuracy was achieved, even for grass species that are known to be relatively rich in hydroxycinnamic acids, such as corn stover and sugarcane bagasse.⁶⁻⁹ That is, the quantitative ^{13}C -IS py-GC-MS method did not significantly differ from the Klason benchmark, to date considered to be the 'golden standard' for the quantification of lignin (**Chapter 2 and 3**).⁹

Given the above, one might have expected a discrepancy between the two methods, but the fact that they agree this well could potentially lie in the very structure of lignin and lignocellulose itself as well as in the nature of the analyses.

It can be fairly expected that most, if not all, detected 4-vinylphenol originated from *p*-coumaric acid involved in esterifying the C γ position of lignin's interunit linkages (**Chapter 1**, Figure 5).^{3, 10} These moieties should, thus, be considered an integral part of the polymer and should be quantified as such.

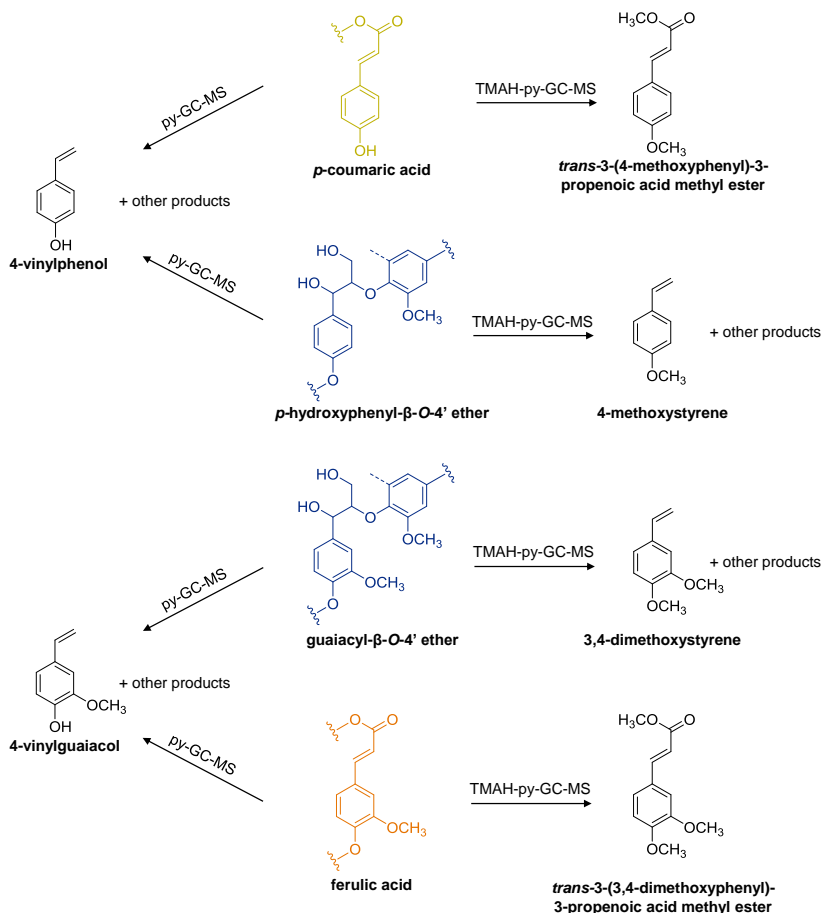


Figure 1. Schematic representation of pyrolysis products resulting from *p*-hydroxyphenyl- β -O-4' ether and *p*-coumaric acid and guaiacyl- β -O-4' ether and ferulic acid substructures in the absence and presence of TMAH.

In contrast, in the case of the pyrolysis product 4-vinylguaiacol, the corresponding (di)ferulic acid is not necessarily only involved in crosslinking to lignin. Part of this (di)ferulic acid might be contained within the carbohydrate fraction, solely esterified to hemicellulose. This 'nonlignin' ferulic acid fraction might have interfered with lignin quantification. To check the maximum interference by this fraction, wheat straw and corn stover samples were saponified and the released ferulates and diferulates were quantified by LC-MS analyses. It can be fairly assumed that all released (di)ferulates originated from the carbohydrate fraction as esterification to lignin has been found to hardly occur and the content of

'unbound' ferulates was negligible.¹¹ Saponification released 2.2% w/w (di)ferulates from the dry matter of wheat straw and 5.0% w/w from corn stover, which contentwise, respectively, is equal to approx. 12% and 26% of the determined lignin contents of the same samples by py-GC-MS (**Chapter 2**).¹² Clearly, the saponifiable fraction is substantial and cannot be ignored. If the py-GC-MS method, however, indeed overestimates lignin due to this ferulate fraction, the Klason methodology apparently overestimates lignin as well, as both methods have consistently produced similar lignin contents.

In principle, 'nonlignin' ferulates could also affect the Klason lignin determination. In particular the quantification of acid-soluble lignin (ASL) would be affected, because such ferulates are solubilized upon acid hydrolysis of the carbohydrate fraction and co-quantified with the released lignin. The release of (di)ferulates upon acid-hydrolysis is supported by work of Hatfield et al.,¹³ who analyzed the acid-insoluble residue after Klason hydrolysis by py-GC-MS and found a severe reduction in 4-vinylguaiacol (and 4-vinylphenol) in comparison to the initial sample. In accordance with these findings and amounts of releasable ferulates, we found that the corn stover sample contained almost double the amount of ASL (2.8% w/w) versus the wheat straw sample (1.5% w/w) (**Chapter 2**).

The advised wavelength for the quantification of ASL is 205 nm, since commonly formed carbohydrate acid-degradation products, such as furfural and hydroxymethylfurfural do not or negligibly interfere at this wavelength.¹⁴ Albeit not their absorption maximum, (di)ferulates show considerable absorbance at this wavelength. Obviously, quantifying ASL as advised is not free of interferences.

Though it is a great reassurance that the py-GC-MS and Klason methodologies gave comparable outcomes, both methods, in fact, still might not provide the 'real' lignin content, which leaves the lignin chemist with a substantial challenge.

Solving this analytical challenge is even more pressing for the quantification of lignin in samples that are relatively rich in ferulic acids, while lignin contents are relatively low. Relevant samples include plant tissues containing more primary cell wall material, like leaves and edible parts such as wheat grains and maize kernels, but also applies to certain woody samples, like barks that are rich in suberins containing ferulic acid.¹⁵⁻¹⁷ Consequently, lignin quantification in food and feed requires an adaption of the currently available methods, before accurate analysis can be achieved.

Having already discussed the benefits of py-GC-MS over Klason lignin analysis and existing alternatives (**Chapter 1-3**), here we want to primarily focus on the optimization of the former method. As briefly introduced in **Chapter 1 and 5**, the introduction of methylating agents such as tetramethylammonium hydroxide (TMAH) during pyrolysis, would allow the origin of vinyl products to be deduced (Figure 1).¹⁸ In this procedure, the decarboxylation of hydroxycinnamic acids is avoided by converting the carboxylic acids to their corresponding methyl esters, while hydroxyl groups are converted to methoxyl groups.

The application of TMAH has proven very useful in various py-GC-MS studies, including those conducted at our department.^{6, 19-20} Still, these analyses have mainly provided qualitative insight and the adaptation to quantitative analyses involving a ¹³C labeled lignin internal standard is far from straightforward.

The quantitative ¹³C-IS py-GC-MS method heavily relies on relative response factors (RRFs) of the lignin-derived pyrolysis products (**Chapter 2, Figure S6**). Hence, when TMAH is applied, new RRFs should be determined for the methylated analogues, for which standards are not as widely available commercially as for the 'regular' products.

To circumvent the need for RRF determination of all methylated products, one could think of determining the ratio of vinyl products originating from hydroxycinnamic acids and 'core lignin' in a separate TMAH-py-GC-MS analysis and correcting the peak areas in ¹³C-IS quantitative py-GC-MS analyses accordingly. Note that when following this approach the RRFs should still be determined for the products involved in these determinations, i.e. 4-methoxystyrene (for 4-VP), 3,4-dimethoxystyrene (for 4-VG), *trans*-3-(4-methoxyphenyl)-3-propenoic acid methyl ester (for *p*-CA) and *trans*-3-(3,4-dimethoxyphenyl)-3-propenoic acid methyl ester (for FA) (Figure 1).

It has, furthermore, been demonstrated that TMAH-pyrolysis does not proceed via methylation of products upon release by 'true' pyrolysis, but rather proceeds via a thermally assisted chemolysis.¹⁹ As the two processes are inherently different, it can be doubted that matrix-effects exerted in both cases are similar, and the outcomes cannot be corrected in the absence of an internal standard.

Additionally, the application of TMAH is prone to contaminate the py-GC-MS system, especially when equipped with an autoshot sampler, and maintenance of the MS-source should be performed frequently. Altogether, the application of TMAH negatively impacts the throughput of the analytical platform and requires significant method development before being applicable in any quantitative sense.

Tricin. The flavonoid triclin (**Chapter 1, Figure 6**) was demonstrated to be an integral part of the lignin macromolecule in certain grasses, with wheat straw in particular.^{6, 21} Its content, however, is severely overestimated by HSQC NMR analyses (up to 15% of lignin's subunits)²²⁻²³, as also shown in **Chapter 4 and 6** and will be touched upon in the section 'Structural characterization of lignin by HSQC NMR'. Quantification by LC-MS analysis after acidolysis showed more realistic triclin contents at approx. 0.6% w/w of extractive-free wheat straw.²⁴ To be able to exclude a potential interference in (quantitative) py-GC-MS analyses, pure triclin (PhytoLab, Vestenberggreuth, Germany) was pyrolyzed and the results were compared to a wheat straw reference sample. The pyrolysis of triclin did not yield significant amounts of products used for the quantification of lignin. Only traces of S-derived products were formed, with syringol and acetosyringone accounting for 75% of the relative abundance, whose total area was well below 0.1% of the normal peak area of these products in wheat straw. We conclude that triclin's

pyrolysis efficiency is low and the interference for lignin quantification is negligible. Unfortunately, this also implies that specific pyrolysis markers for tricin are not formed, due to which its content cannot be estimated by py-GC-MS analysis.

Quantification of fungal treated lignin

In **Chapters 4-7**, the newly developed ^{13}C -IS py-GC-MS tool was applied to fungal treated wheat straw samples. Though the lignin was from the same botanical source, the treated lignin was structurally highly different in comparison to native lignin and, thus, also different in comparison to the used ^{13}C lignin internal standard (**Chapter 2 and 4**). Still, we think that fungal degraded wheat straw lignin resembled the native ^{13}C labeled wheat straw lignin internal standard more than native softwood lignin, which was overestimated by the ^{13}C wheat straw IS by 15% 'only' (**Chapter 3**).

As any internal standard method is based on the assumption that the analyte and internal standard behave similarly, upon sample workup, detection, storage, etc., we asked ourselves the question whether native ^{13}C wheat straw lignin is, in fact, a proper internal standard for these samples. Ideally, every treated sample is quantified by an internal standard that received exactly the same treatment. As ideal situations go, this is infeasible in reality and a compromise must be made.

Thinking inside the box 1.

Actually, one can pose the question whether a quantitative internal standard method can be truly universal and specific at the same time. That question must unfortunately always be answered by 'not really'. Yet, this does not, per se, disqualify the use of that method, as long as the deviations or inaccuracies are known and accounted for.

In **Chapter 2 and 3**, we showed that validation of the ^{13}C -IS py-GC-MS method for native biomass samples was relatively straightforward, i.e. via quantification of lignin in model systems with known amounts of added lignin and via benchmarking to carefully executed gravimetical analyses. However, this approach does not work for fungal treated samples. First of all, the Klason benchmark is known to be disturbed by any acid insoluble nonlignin material. Fungal grown samples contain substantial amounts of mycelium, which is largely constituted by acid-resistant chitin (and glucan). To alleviate these disturbances one could think of removing chitin beforehand or quantifying it in the acid-insoluble residue (AIR) afterwards. The former could potentially be achieved by employing chitinases. This, however, would require planetary ball-milling of the sample, to decrease chitin's crystallinity and increase its susceptibility to enzymatic degradation.²⁵⁻²⁶ As discussed in **Chapter 5** (supporting information), planetary ball-milling can induce changes in the lignin structure, especially at the milling severities required for decrystallizing chitin, which might affect lignin's susceptibility towards acid hydrolysis.

Alternatively, the quantification of chitin in AIR might be achieved by employing the same enzymatic treatment or by increasing the severity of the acid-hydrolysis conditions, i.e. boiling the sample in concentrated HCl for several hours.²⁷ Yet, in both cases, a full conversion of chitin to quantifiable monomers is still difficult to achieve and, hence, a proper correction is currently not possible.

Not only is the acid insoluble lignin disturbed by the presence of compounds of fungal origin, the highly degraded lignin structure affects the quantification as well. Importantly, ASL should not be considered an isolable fraction present within lignocellulose, but rather should be viewed as a degradative fraction that is formed during the acid-hydrolysis step itself.¹⁴ Heavily degraded, lower molecular weight, lignins are more susceptible to end up in the acid-soluble part, and as such, a larger fraction of the lignin is quantified with lesser certainty, as also illustrated in the previous section. All inaccuracies combined, we opted not to invest time in benchmarking the py-GC-MS method for fungal treated lignin against the Klason methodology.

Instead, the need for such an unspecific method could be circumvented, when known amounts of fungal treated lignin are employed in biomass model systems, similar to our approach for native lignins (**Chapter 2 and 3**).

In **Chapter 4 and 5** we showed that the lignin fraction of particular interest for this purpose, i.e. the fraction containing most degraded substructures, was water-extractable. Despite the application of dedicated purification strategies based on enzymatic carbohydrate degradation and reversed phase chromatography, we could not completely purify these samples (average final purity ~50% w/w). Note that this purity was determined by the very py-GC-MS method we wished to validate. We did not attempt to quantify the remaining impurities to indirectly estimate the lignin content of the extracts by subtracting their contents from the total dry matter, as performed for the lignin isolates in **Chapter 2 and 3**, simply because we did not know what the impurities were. Hence, we were left with a lignin fraction that was not of use for method validation.

In the same line of reasoning, attempting to achieve a full closure mass balance would unlikely bring us closer to our validation aim. With lignin contents in the order of 5-10% w/w, a mass balance closure of 98% (extremely high), could still mean an underestimation of 40% and an overestimation can still not be excluded.

Condensed linkages and lignin quantification by py-GC-MS

A potential source of error in the quantification of lignin in fungal treated samples could be the presence of condensed structures, of which the relative accumulation was hinted at in **Chapters 4-7**. Note that these linkages might already be present within the lignin macromolecule initially, and 'simply' accumulate, or be formed through repolymerization reactions.

C-C (e.g. 5-5') and C-O-C (e.g. 4-O-5') linkages between aromatic rings are expected to be considerably more resistant against pyrolysis depolymerization than β -O-4' aryl ethers. The latter has been predicted from theoretical calculations of the bond dissociation energies (BDEs) and was demonstrated experimentally by pyrolyzing various lignin model dimers.²⁸⁻²⁹ Although pyrolysis reactions for dimer models cannot be one-on-one translated to polymeric lignin, as was also shown in **Chapter 5**, they do provide a fair indication of the underlying reaction mechanisms.³⁰ Hence, condensed substructures are expected to be more prone to remain in the pyrolysis cup as 'char' or might be released as dimeric products that are not quantified, either due to condensation onto the pyro-tube, liner and/or column, or due to elution during column bake-out. An accumulation of condensed substructures, therefore, is expected to result in underestimation of lignin content and might, consequently, lead to an overestimation of delignification extents. The extent of such an accumulation in fungal treated samples can, however, not be properly evaluated, particularly because these linkages containing tertiary or quaternary carbon atoms without bearing any HSQC NMR detectable C-H bonds. Alternatively, ^{13}C NMR would be able to detect carbons involved in such linkages, though the single dimension of this technique does not provide sufficient signal dispersion for the particular carbons to be resolved.

The lack of substantial cross-peak shifts of lignin's subunits in the aromatic region of HSQC (and HMBC) spectra might, nonetheless, indicate that such condensed substructures did not abundantly accumulate (**Chapter 5 and 6**). Recent multidimensional NMR approaches taken for elucidating the structural motifs of heavily condensed Kraft lignins might be of guidance for better understanding the occurrence (and scale) of repolymerization reactions.³¹⁻³²

To further evaluate the applicability of the developed ^{13}C -IS py-GC-MS tool, we employed the method to samples containing more severely modified lignin. An example of such samples, is those resulting from the treatment of plant biomass with laccase and the mediator hydroxybenzotriazole (HBT). Laccase-induced polymerization reactions have been observed quite extensively between wheat straw lignin and HBT, a process also referred to as grafting.³³⁻³⁵ Also here, the exact extent of polymerization is difficult to quantify, but benzotriazole was clearly observed in py-GC-MS and HSQC NMR analyses of extensively washed samples, suggesting covalent attachment.³⁶ Besides, dumas analyses showed a strong accumulation of nitrogen in these samples, more than can be attributed to protein (laccase) adsorption alone. As a consequence of this presumably quite severe polymerization, the ^{13}C -IS py-GC-MS and Klason analyses of HBT-grafted lignin produced divergent extents in delignification, 51% vs 32%, respectively.³⁶ We propose that HBT grafting affects the accuracy of both methods in opposite directions, suggesting that the actual extent of delignification lays somewhere between both outcomes.

The performance of the analytical platform was further explored by applying the method to industrial lignins, collectively referred to as 'technical lignins' in the literature (Figure 2). Here, we chose to use two relevant lignin streams: Protobind™ 1000 (P1000), obtained from soda pulping of a mixture of wheat straw and sarkanda grass and Futurol lignin, the residue of acid-catalyzed steam-exploded *Miscanthus x giganteus* used for simultaneous enzymatic hydrolysis and monosaccharide fermentation.³⁷⁻³⁸

Thinking inside the box 2.

Technically, the term 'technical lignins' might be somewhat inappropriate as the resulting structures are no longer recognizable as lignin, due to the extensive processing they have undergone.

Clearly, the py-GC-MS method underestimated the lignin content compared to the Klason benchmark (Figure 2). The fact that the relative deviation obtained for P1000 lignin (~40%) exceeded that of Futurol lignin (~30%), presumably related to the fact that the P1000 lignin was more extensively degraded and condensed, with less than one intact β -O-4' aryl ether linkages per hundred subunits.³⁷⁻³⁸ The latter can also be observed from the relatively low abundance of P1000 pyrolysis products with an intact α,β,γ carbon side chain, as elaborated in **Chapter 4**.

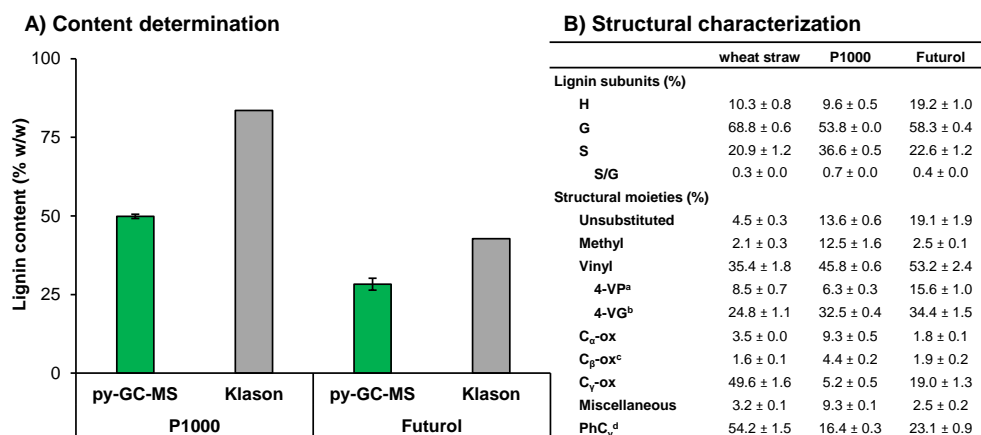


Figure 2. Lignin content determination (A): py-GC-SIM-MS using ¹³C wheat straw lignin as internal standard (triplicate) and Klason methodology. Klason lignin content is presented as acid-insoluble lignin corrected for ash and protein combined with acid-soluble lignin. Structural characterization (B): Relative abundance of lignin compounds corrected for relative response factors and behavior of the ¹³C-IS. Sum on the basis of structural classification according to Chapter 3. ^a4-vinylphenol. ^b4-vinylguaiacol. ^cexcluding diketones. ^dphenols with intact α,β,γ carbon side chain.

Noteworthy, py-GC-MS showed quite some residual *p*-coumarate moieties in the P1000 lignin, deduced from the abundance of the 4-VP pyrolysis product, something that was not expected from the alkaline nature of the process to obtain the lignin. Probably, some *p*-coumarate moieties are attached to the lignin macromolecule through other linkages than γ -esters only, as also mentioned by Reinoso et al., though these linkages do not per se occur naturally.³⁹

It is safe to state that the native internal standard does by no means resemble these 'lignins'. We do, however, anticipate that the ^{13}C -IS py-GC-MS method could form a valuable addition to the technical lignin analytical toolbox, once proper internal standards are available. Therefore, we propose to follow the same strategy as applied for hard and softwoods (**Chapter 3**), i.e. the production of uniformly ^{13}C labeled technical lignins. We infer from **Chapter 2 and 3** that a single species can in principle cover for an entire taxon. To that end, we suggest that uniformly ^{13}C labeled wheat straw, ^{13}C labeled willow and ^{13}C labeled spruce are excellent candidates for processing by the currently most relevant industrial technologies, i.e. sulfite, kraft, soda and organosolv pulping.⁴⁰⁻⁴¹ As py-GC-MS analyses require extremely little sample and internal standard investments ($\sim 10\ \mu\text{g}$ IS/sample), the processes can be downsized to lab or benchscale and for that reason also remain economically feasible. We envision applications of these uniformly ^{13}C labeled technical lignins beyond their sole function as 'ideal' internal standard for py-GC-MS analyses as the uniform ^{13}C labeling also potentiates multidimensional NMR analyses of these lignins.

Structural characterization of lignin by HSQC NMR

As already introduced in **Chapter 1** and demonstrated throughout the chapters that followed, ^1H - ^{13}C HSQC NMR is the most versatile technique for the structural characterization of lignin. The versatility primarily lays in the signal dispersion that is provided by the two dimensions as compared to 1D ^1H or ^{13}C analyses in which signal overlap is a significant issue.^{8, 42} Opposite to the 1D methods that are generally quantitative, i.e. volume integrals are directly proportional to the concentration of the specific chemical moiety within the structure, HSQC NMR generally lacks such quantitativity and is, therefore, often used for relative comparisons only.⁴²⁻⁴⁵ Such comparisons are based on the relative expression of volume integrals of specific cross-peaks versus reference signals that are present within the lignin molecule itself, most commonly the aromatic subunits ($\text{H}_{2/6}$, G_2 and $\text{S}_{2/6}$), hence explaining the semiquantitative nature of these analyses.⁴³⁻⁴⁴

The lack of quantitative output in the absolute sense of HSQC NMR analyses is, amongst others, due to differences in T_1 and T_2 relaxation times, coupling constant deviations and homonuclear coupling of the different structural moieties present within the lignin population.⁴³ Many variations of the HSQC NMR experiment have, thus far, been proposed to solve (some) quantitative issues, including quick-quantitative HSQC,⁴⁶⁻⁴⁷ combinatorial HSQC and ^{13}C NMR,^{23, 48} HSQC₀,⁴⁹⁻⁵⁰ and

molecular-size tolerant HSQC,⁵¹ but it goes beyond the scope of this thesis to discuss them all in detail. Thus far, no general consensus on 'the best' NMR method has been reached, although it did become more or less standard practice to use adiabatic pulse sequences to improve the uniformity of response factors across the entire spectrum.^{44, 52}

Recently, HSQC₀ analysis seems to gain popularity and is appraised for its accuracy.⁴⁹⁻⁵⁰ The principle of this NMR experiment is based on the recording of a series of HSQC spectra with incremental pulse repetitions, corresponding to different relaxation times, that are linearly extrapolated to a zero-relaxation time.⁴⁹⁻⁵⁰ Though, it must be noted that also these analyses still suffer from differences in relaxation behavior of 'pendant' and end-groups compared to 'core' lignin units and are strongly biased by molecular weight differences.^{32, 45, 53} Furthermore, compared to regular HSQC NMR analysis, the recording and processing of HSQC₀ spectra is not straightforward and, additionally, the measurements are far more time-consuming.³²

Given the above, we attempted in **Chapter 6** to improve the accuracy of regular HSQC NMR analysis. Inspired by the use of relaxation agents for 1D NMR analyses of lignin, such as ¹³C and ³¹P NMR,^{37, 54} we investigated whether HSQC NMR analysis could benefit from the presence of chromium (III) acetylacetonate (Cr(acac)₃) as relaxation agent to 'normalize' the relaxation behavior of various structural moieties.

This directly linked to the fact that, thus far, always remarkably low amounts of interunit linkages per 100 subunits have been detected by HSQC NMR analyses, even in 'native' polymeric lignins (40-60 linkages/100 rings).^{23, 55} Especially when lignins are more linear than generally considered, the actual linkages appear to be severely underrepresented, as we should theoretically expect n-1 linkages for n subunits.⁵⁶⁻⁵⁷ It is well-known that HSQC NMR detects only those interunit linkages bearing C-H groups, which might to some extent explain this underestimation.⁴² Yet, it might also relate to the 'quantitativeness' of the technique itself, potentially due to differences in the relaxation behavior of aromatic rings and the linkages connecting them.

A related 'problem' that might be solved in the presence of the paramagnetic chromium coordination complex is the abundance of end-units that are encountered within grass lignins. Tricin, ferulate-arabinosyl LCC linkages, cinnamyl alcohol and aldehydes all terminate a lignin chain, as illustrated in the lignin structure in **Chapter 4**. It has recently been suggested that dibenzodioxocin, 5-5', and 4-O-5' linkages all occur in their free-phenolic form and, as such, do not constitute 'branching' points of the lignin macromolecule.⁵⁷ Additionally, it was proposed that α,β-diaryl ether linkages, element 'E' in the structure of **Chapter 4**, would not be formed during regular lignification reactions *in planta*.⁵⁷ This is in line with studies that failed to show their existence by multidimensional NMR analyses⁵⁸⁻⁵⁹, but implies that the substructure has previously been misannotated.^{6, 23} Importantly, these reconsiderations leave lignin with practically

no known possibilities to branch. To accommodate the level of detected end-units, monocot lignins, therefore, should be of lower molecular weight than generally assumed and might be richer in the aforementioned linkages that provide every linear lignin chain with two 'end-units'. Alternatively, this very anomaly might be due to the fact that end-units are overestimated.

Indeed, in the presence of $\text{Cr}(\text{acac})_3$, we observed a clearly reduced overestimation of the pendant and end-group units (*p*-coumarate, ferulate and triclin) (**Chapter 6**, Table S7). This decrease was substantiated by the fact that after $\text{Cr}(\text{acac})_3$ addition, the volume integrals of triclin's $T_{2',6'}$ cross-peak matched more closely with that of the $\text{C}_\beta\text{-H}_\beta$ cross-peak of the $\beta\text{-O-4'}$ aryl ether linkage through which it is primarily bound to lignin ($\text{A}_{\text{T}\beta}$).⁶⁰⁻⁶¹ Vice versa, we observed that $\beta\text{-O-4'}$ aryl ethers were slightly increased, while resinol substructures were suppressed as well. To gain further insight into these findings, we compared the semiquantitative analyses of HSQC spectra of lignin isolates from wheat straw, willow and spruce that were recorded in the absence and presence of $\text{Cr}(\text{acac})_3$ (Figure 3).

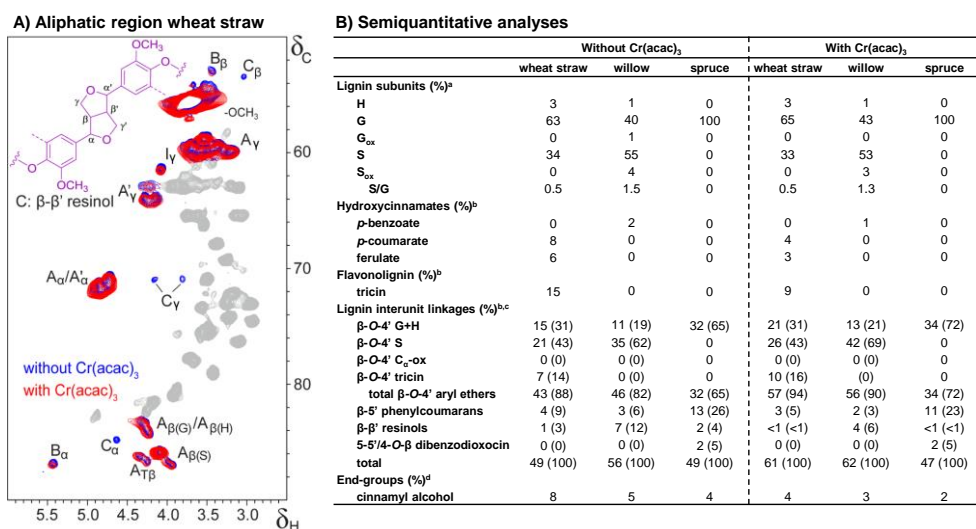


Figure 3. HSQC NMR spectra of wheat straw lignin in the absence and presence of chromium (III) acetylacetonate ($\text{Cr}(\text{acac})_3$) as relaxation agent (A) and semiquantitative analyses of wheat straw, willow and spruce lignin isolates (B). Wheat straw lignin isolate from Chapter 4; willow and spruce lignin isolates from Chapter 3. ^a relative distribution of lignin subunits ($\text{H}+\text{G}+\text{G}_{\text{ox}}+\text{S}+\text{S}_{\text{ox}}=100$); ^b relative volume integral of substructure versus volume integral of total lignin subunits, known as 'per 100 Ar'; ^c relative distribution of total interunit linkages in parentheses; ^d relative volume integral of substructure versus volume integral of total interunit linkages.

In all lignins, the known end-groups and resinol substructures were strongly reduced, while total $\beta\text{-O-4'}$ aryl ethers increased, albeit only slightly for the spruce lignin. Hence, our observations were not coincidental for the particular wheat straw or for grasses only. In Figure 3A, it is evident that the $\text{C}_\alpha\text{-H}_\alpha$, $\text{C}_\beta\text{-H}_\beta$ and $\text{C}_\gamma\text{-H}_\gamma$ correlation peaks were all suppressed in the presence of $\text{Cr}(\text{acac})_3$. Due to their different chemical environments, we consider it unlikely that all correlations would

be equally affected by a spectral artifact.⁴² Could it therefore be the case that resinol units have thus far always been overestimated and that they are more abundantly present as end-units of the lignin macromolecule? Resinol units have frequently been suggested to start a growing lignin chain through monolignol dimerization, but they still could be present anywhere within the molecule.⁶² The sequencing of lignin, indeed referring to the determination of its 'primary' structure, might help to partially resolve this question. This analytical approach, however, is still in its infancy and can only be readily applied to relatively low-molecular-weight lignin oligomers.⁶³⁻⁶⁴ Without alternative methods for the quantification of the resinol content and their position within the lignin chain, we must reside in the fact that the posed question remains unanswered.

Structural characterization of lignin by ¹³C-IS py-GC-MS

In **Chapter 2-7** we have shown that the quantitative ¹³C-IS py-GC-MS method, besides accurate lignin content, can also provide valuable insights into lignin's structural features. We were not the first to consider that py-GC-MS analysis can provide a structural fingerprint of lignin.⁶⁵ However, we did show for the first time that, when properly corrected for the behavior of the ¹³C lignin internal standard, structural information can be derived from py-GC-MS analyses that matches very decently with NMR spectroscopy analyses. Here, the outcomes of both techniques are further integrated to evaluate the performance of the novel py-GC-MS method in terms of structural characterization of lignin.

As mentioned several times before in this thesis, in py-GC-MS analyses hydroxycinnamic acids cannot be distinguished from 'core-lignin' while in NMR analysis they can. To allow a better comparison of both techniques, therefore, *p*-CA and FA were included in the NMR 'total abundance'. However, as elaborated also in the previous section, it should be taken into account that these units tend to be overestimated by HSQC NMR analyses.

In **Chapter 4**, tricin was also included in the NMR analyses' relative abundance of lignin's subunit, fair enough from the perspective it constitutes an integral part of the macromolecule. Though, in the previous section, we described that it does not contribute to the lignin-derived products in py-GC-MS. For comparative purposes, tricin was, therefore, excluded from the NMR subunits, and the data presented in **Chapter 4** was recalculated (Figure 4). The py-GC-MS data of that chapter was, furthermore, recalculated with proper relative response factors for the diketone pyrolysis products (**Chapter 5**), products we, and others, initially had annotated as benzoyl acetaldehydes.^{5, 66}

Taking these considerations into account, py-GC-MS and NMR analyses provided very similar information regarding lignin's subunit composition, in particular when Cr(acac)₃ was included in the NMR analyses (Figure 4A). Even though H-units are relatively easily overestimated by py-GC-MS analyses, mainly because aromatic amino acids produce similar phenol derivatives, both techniques agreed rather

well. H-units, indeed, were overestimated in the acetone/water extractable fractions of Chapter 5, in which peptide or protein interference likely played a larger role.

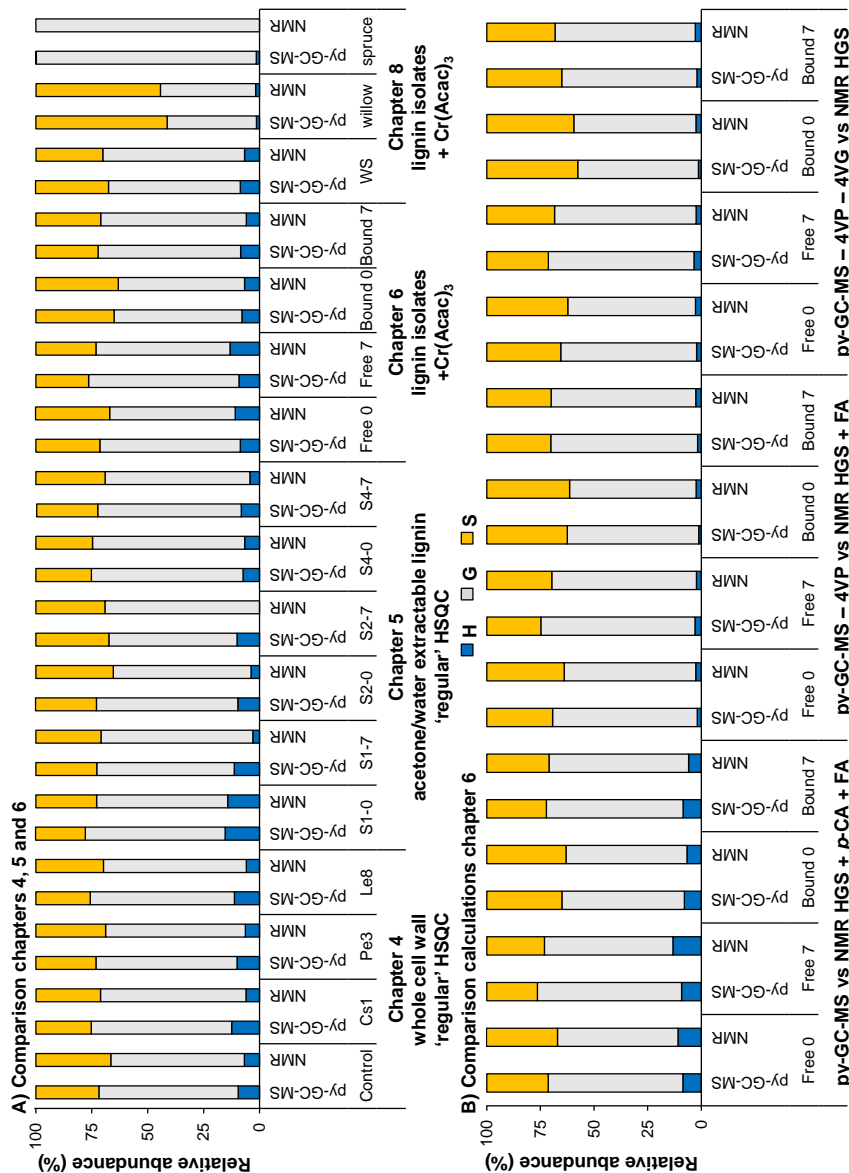


Figure 4. Comparison of subunit composition of lignin as characterized by ¹³C-1S py-GC-MS and HSQC NMR. Py-GC-MS data is corrected for behavior of the ¹³C-1S. In HSQC NMR determinations (A), *p*-coumaric acid and *p*-hydroxybenzoic acid were included as H-units and ferulic acid as G-unit. Other not included samples of Chapter 4-6, overall, showed a similar correlation. For explanation of abbreviations, see corresponding chapters of this thesis.

Inversely, when 4-vinylphenol and/or 4-vinylguaiacol were excluded from the py-GC-MS analyses for isolated lignins, solid correlations were achieved as well (Figure 4B). This further demonstrated the ability of py-GC-MS to correctly estimate the subunit composition. However, a sample set of larger structural variation is needed to further establish the performance of the py-GC-MS method.

Interestingly, other more in-depth structural features beyond the 'traditional' subunit information also fitted rather well when the outcomes of the two techniques were compared (Figure 5). That is, a linear correlation between both techniques was apparent, but they essentially did not provide similar 'absolute' values. This is clearly visible in the intercepts of the y-axis, which relates to the fact that C α -oxidized products and products with an intact α,β,γ -sidechain (PhCy) are also derived from substructures having other than oxidized and intact interunit linkages, respectively. However, as the graphs of Figure 5 demonstrate, they do strongly correlate with these substructures. Decent correlations were achieved for C α -oxidized moieties, even for whole cell wall NMR analyses (**Chapter 4** in Figure 5A). This presumably related to the fact that the information on these moieties was solely derived from the aromatic region of the spectra, which is only mildly affected by the presence of nonlignin components. The graph of **Chapter 5** in Figure 5A showed that, even when going to extreme degrees of oxidation, an appropriate model can be designed. The isolates obtained in **Chapter 6** showed an excellent correlation ($R^2 \approx 0.99$). Two wood isolates, analyzed in the same way (Section 'Structural characterization of lignin by HSQC NMR'), did, however, not fit the same model (Figure 5A). Apparently, more C α -oxidized pyrolysis products were formed from their nonoxidized substructures, in comparison to wheat straw lignin. When plotted in one figure, an overall reasonable correlation is achieved, though it must be noted that the model was heavily skewed by the 'extremities' included. In **Chapter 4**, we postulated that pyrolysis products with an α,β,γ -sidechain (PhCy) can be a useful measure for mapping lignin's intact interunit linkages by py-GC-MS, when excluding pyrolysis markers for cleaved substructures, primarily diketones in these samples (**Chapter 5**). Figure 5B shows that a relatively weak correlation ($R^2 \approx 0.67$) was obtained for the samples of Chapter 4 and 5. The poorer correlations could relate to the lower purity of these samples, impacting both the accuracy of py-GC-MS and NMR analyses. Conversely, the lignin isolates of Chapter 6 and 8 strongly correlated ($R^2 \approx 0.96$), which corroborated the initial hypothesis.

Figure 4 and 5 demonstrate that, even though entirely different entities are measured, py-GC-MS and NMR analyses can provide corresponding structural information. We anticipate that, when a proper 'training' set of samples is used to establish a model, py-GC-MS might to some extent displace the need for NMR analysis. Not only would this significantly reduce time and equipment investments, it might enable the analysis of samples of which insufficient material is available for recording an HSQC NMR spectrum (within acceptable amounts of time) (see section 'future perspectives').

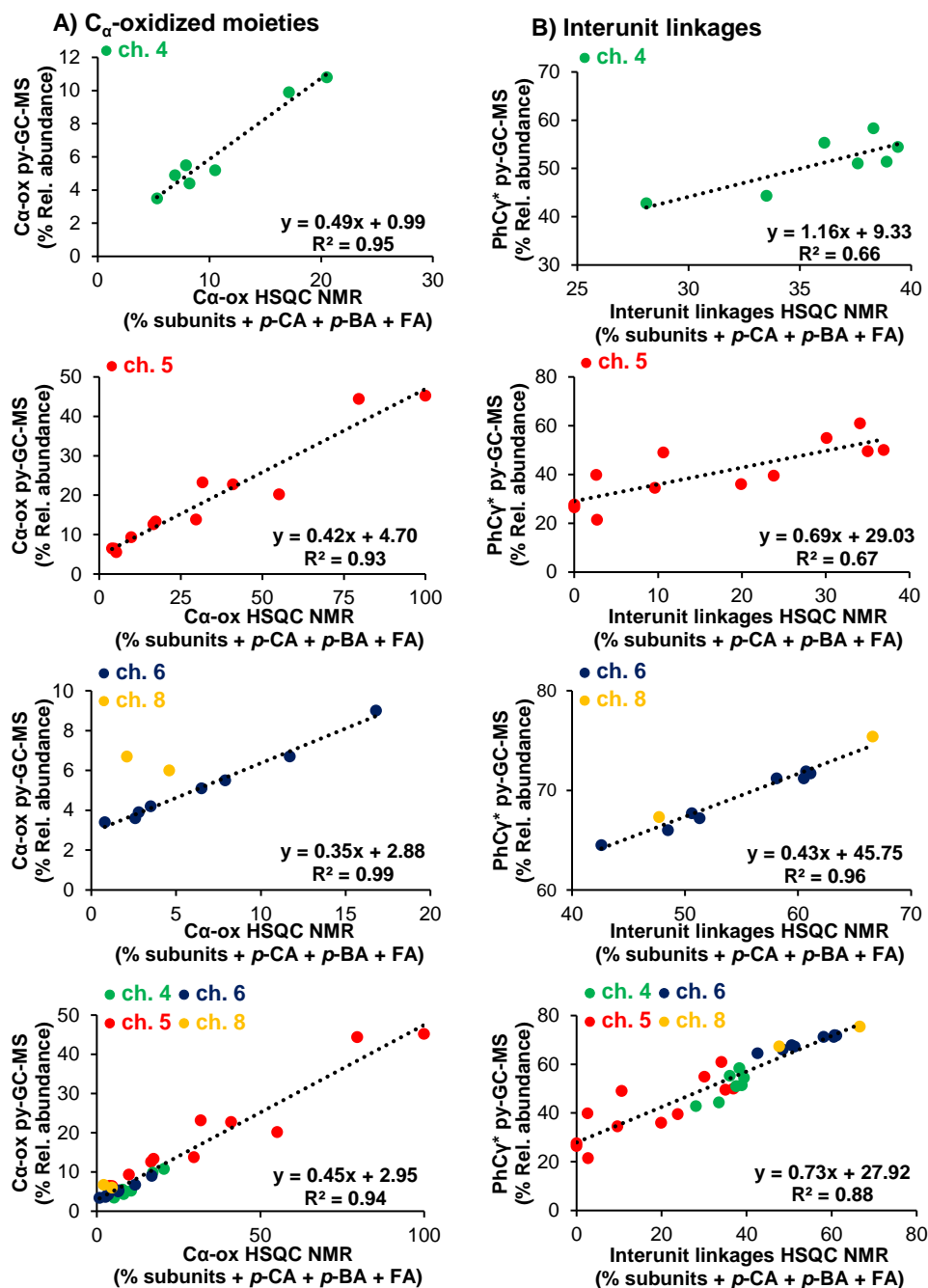


Figure 5. Comparison of C_α-oxidation and intact interunit linkages of lignin as characterized by ¹³C-IS py-GC-MS and HSQC NMR. Py-GC-MS data is corrected for behaviour of the ¹³C-IS. PhCy*: sum of pyrolysis products with an intact α,β,γ-sidechain, corrected for diketones. Intact interunit linkages by HSQC NMR are expressed relative to the sum of subunits, *p*-CA, *p*-BA and FA.

If we assume that the entire lignin macromolecule is measured by NMR spectroscopy, the reasonable consistency with py-GC-MS analysis would indicate that the pyrolysate should be representative of the entire molecule as well.⁴⁴ Accordingly, the part of the sample that is retained in the pyrolysis cup, 'char', should also be representative of the entire lignin population. As discussed in section 'Quantification of fungal treated lignin', we would have expected that G-units, being more prone to undergo condensation, would have selectively accumulated in the pyrolysis char if they had indeed been involved in condensation reactions. In fact, the consistency of py-GC-MS and NMR analyses could, thus, imply that condensation reactions did not occur at a substantial scale and further strengthens our statement that lignin could be accurately quantified in fungal-treated samples with our ¹³C-IS py-GC-MS method.

Plant biomass delignification by white-rot fungi

In this thesis, we investigated the delignification mechanisms of three promising white-rot fungi for the biological pretreatment of lignocellulosic biomass (**Chapter 4**) and studied the ligninolysis mechanisms of *Ceriporiopsis subvermispota* in detail (**Chapter 5 and 6**). With the fungal kingdom being extremely rich in species and ample examples known of white-rot fungi that have been applied to valorize lignocellulosic biomass, why were these particular fungal species and strains selected?⁶⁷⁻⁶⁸

Choice of fungus for mechanistic studies

Tuyen et al. showed that *Ceriporiopsis subvermispota*, *Pleurotus eryngii* and *Lentinula edodes* delignified wheat straw more extensively and selectively in comparison to other white-rot fungi like the well-studied *Phanerochaete chrysosporium*, as based on conventional compositional analyses, as also briefly discussed in **Chapter 1**.⁶⁹ As such, these fungal species were selected for further assessing their potential for improving the feed-value of plant biomass by the Animal Nutrition and Plant Breeding groups of Wageningen University & Research.⁷⁰⁻⁷² As part of that research and to advance our understanding of their delignification performance and underlying mechanisms, the remaining lignin after growth of these fungal species was compared in **Chapter 4**. Therein, we showed that *C. subvermispota* and *L. edodes* outperformed *P. eryngii* both in efficiency and selectivity of delignification, which matched with the ruminal degradability of the treated straws.⁷²⁻⁷³ The former two fungal species hardly differed with regard to their final delignifying performance (after 7 weeks of fungal growth) and also their rates/kinetics of lignin removal were very comparable. Still, a slightly higher lignin degradation and selectivity versus cellulose removal could be recognized for *C. subvermispota* in comparison to *L. edodes*. Note that, as also mentioned in **Chapter 4, 6 and 7**, the determination of cellulose removal might have been interfered by the presence of β -glucan that is contained within the fungal cell wall,

because analyses were based on constituent monosaccharides after acid hydrolysis. As fungal glucan is mostly comprised of β -(1 \rightarrow 3) and β -(1 \rightarrow 6)-linked glucosyl units, glycosidic linkage analyses might help to distinguish these from cellulose's β -(1 \rightarrow 4)-linked units.⁷⁴⁻⁷⁵ The (molar) ratio of these glucosyl units might provide some insight into the extent of interference.

Although the exact amount of fungal biomass is difficult to quantify, visually, the mycelia of *L. edodes* and *P. eryngii* appeared substantially thicker in comparison to those of *C. subvermispora* (Figure 6). Possibly, the interference of fungal glucan was larger for the former two fungi and the fact that they still showed a 'positive' glucan removal (**Chapter 4**, Figure 3), could suggest that they removed more cellulose than *C. subvermispora*.

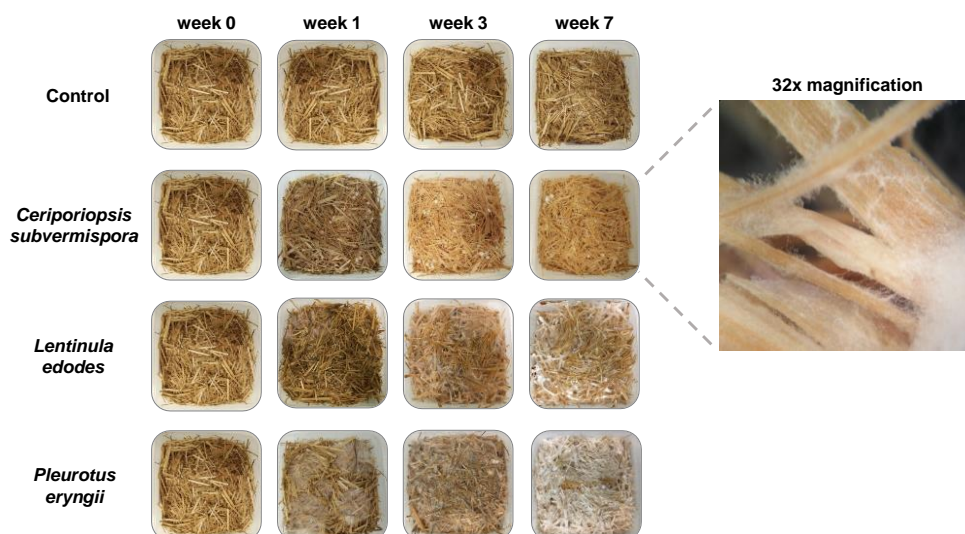


Figure 6. Mycelium formation on wheat straw after inoculation with *C. subvermispora* (CBS 347.63, Cs1), *L. edodes* (sh 03/08, Le8) and *P. eryngii* (Mycelia2600, Pe3). The same uninoculated week 0 sample is shown for comparative purposes. Images provided by Nazri Nayan, John W. Cone and Anton S. M. Sonnenberg (Wageningen University & Research).

Besides delignification performance, our choice for in-depth characterization of *C. subvermispora* (**Chapter 5 and 6**) was motivated by the observation in **Chapter 4** that its *in situ* ligninolysis mechanisms seemed to fundamentally differ from what had previously been demonstrated and was considered for white-rot fungi in general.⁷⁶⁻⁷⁹

Despite the outperformance by *C. subvermispora*, we would, however, still consider *L. edodes*, also known as the edible shiitake mushroom, as preferred candidate species if we were to focus only on the production of animal feed through fungal pretreatment. This is primarily based on the GRAS (generally regarded as safe) status of the fungus and its mycelium, which might expedite putting the technology into practice by avoiding lengthy safety approval studies.⁸⁰

An important consideration is that white-rot fungi, in fact, might perform their own pretreatment to enable carbohydrate conversion and consumption as lignin itself cannot be used as sole carbon and energy source.⁸¹ It is hypothesized that lignin is primarily targeted during the initial growth stages, so that cellulose becomes available and can be efficiently utilized during later growth phases and in fruiting body formation.⁸²⁻⁸³ Consequently, 'overgrowth' must be controlled to avoid the loss of valuable carbohydrates from the raw material for valorization strategies aiming at their conversion.

An additional factor to consider in the choice of fungus, is the amount of mycelium formation (Figure 6). Whereas mycelium itself is degradable by rumen microbes, and thus is expected not to negatively impact the feed-value of the treated straws, its influence on other applications remains to be further elucidated.^{73, 84} As many other strategies aiming at the valorization of lignocellulose without the requirement of a safety status could benefit hugely from fungal pretreatment, including the pulp and paper (biopulping),⁸⁵ bioethanol⁸⁶ and biogas⁸⁷ industries, our fungus of choice would be *C. subvermispota*.

Insights into delignification mechanisms of *C. subvermispota*

In the **Chapters 4-6**, we have dealt extensively with the mechanisms underlying delignification by *C. subvermispota* and elaborately discussed the implications of our findings on the supposed ligninolysis reactions. **Chapter 5 and 6** evidently demonstrated how complementary information about fungal ligninolysis mechanisms can be obtained from both the 'degraded' and 'intact' perspectives. These chapters provided insight into *in situ* fungal ligninolysis mechanisms that model compounds studies and transcriptomic and/or proteomic analyses could never have. We do, however, want to highlight that these insights could only be derived from the fact that substructures relatively accumulated in the treated residue, both in terms of the formation of diagnostic truncated structures and in the preferential removal of intact structures.

Thinking inside the box 3.

If all linkages are equally susceptible to degradation and degradation products are fully metabolized, the remaining lignin will appear 'intact' and, thus, information on the underlying pathways cannot be deduced. Luckily, most processes follow pathways of deconstruction that allow their reconstruction.

In Figure 7, the obtained results of **Chapter 4-6** are integrated with the available literature to provide comprehensive insight into the strategies and performance of *C. subvermispota* to delignify plant biomass. In this figure, we separated effectivity and selectivity of delignification, both important traits when assessing the performance of fungi and pretreatments in general.

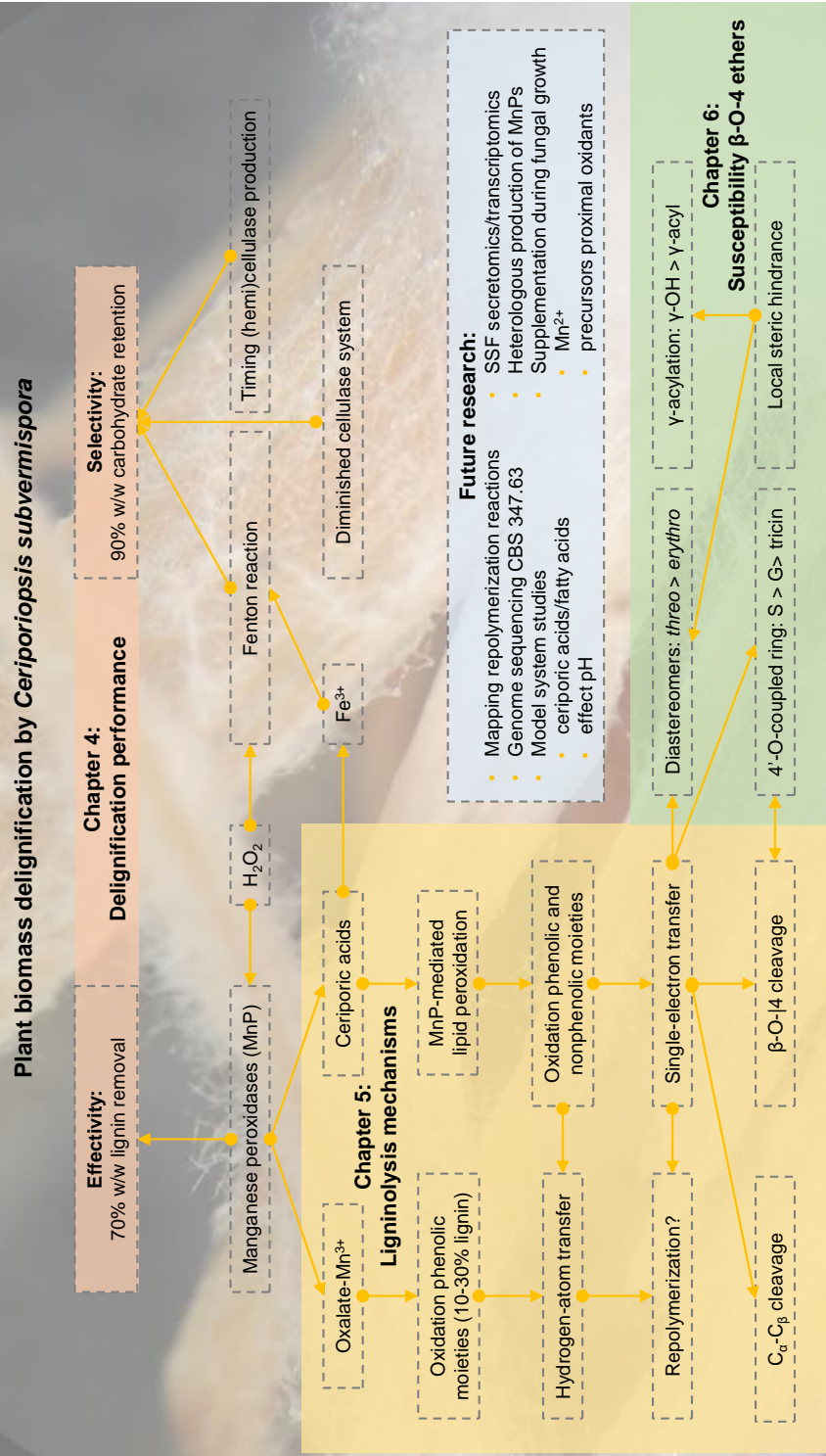


Figure 7. Overview of the actors involved in delignification by *C. subvermispora*.

The excellent selectivity of *C. subvermispora*, in particular regarding the minimal consumption of cellulose, likely relates to a diminished cellulolytic enzymatic machinery in comparison to other, well-known nonselective lignin and carbohydrate degrading white-rot fungi, such as *P. chrysosporium*.⁸⁸ An important feature of the cellulolytic system of *C. subvermispora* is the timing of its 'activation'. Hori et al.⁸⁹ showed that, when grown on ball-milled aspen wood, the fungus produced its ligninolytic arsenal clearly ahead of cellulases. Hemicellulolytic enzymes were also produced in advance of cellulases.⁸⁹ Indeed, we also observed concurrent lignin and hemicellulose removal and the selectivity for ligninolysis decreased as fungal growth continued over extended periods of time (**Chapter 4 and 6**).

Next to the targeted enzymatic cellulose degradation, 'untargeted' cellulolysis might be prevented by suppression of the Fenton reaction. As also briefly discussed in **Chapter 7**, the Fenton reaction describes the conversion of hydrogen peroxide into hydroxyl radicals in the presence of iron as catalyst at acidic pH ($\text{Fe}^{2+} + \text{H}_2\text{O}_2 \rightarrow \text{Fe}^{3+} + \text{OH}^- + \text{OH}^\bullet$). These highly reactive radicals can depolymerize both lignin and polysaccharides and are generally considered to underlie lignocellulose degradation by brown-rot fungi.⁹⁰⁻⁹¹ Secondary metabolites produced by *C. subvermispora* have been associated with the silencing of the Fenton reaction.⁹²⁻⁹⁴ These alkyl- and alkenylitaconic acids, also referred to as ceriporic acids, were observed in acetone extracts of the straw that was treated with the fungus (**Chapter 5**, Figure S3). The mode-of-action has been ascribed to their ability to chelate Fe^{3+} . This chelation protects Fe^{3+} against reduction and, therefore, decelerates the reductive half-cycle known to catalyze the reaction.⁹²⁻⁹⁴

Importantly, the Fenton reaction has been described to result in similar ligninolysis products as observed in **Chapter 5**.⁹¹ From the clear *threo*-diastereoselectivity observed in **Chapter 6**, we could, however, rule out a large contribution of the Fenton reaction, as it had previously been shown not to exhibit any diastereoselectivity.⁹⁵ Conversely, in **Chapter 7**, we proposed that Fenton chemistry was likely involved in delignification by *Podospira anserina*. We, therefore, do think that it could be of interest to study the Fenton reaction in more detail, aiming to ultimately elucidate structures diagnostic for its occurrence.

Besides involvement in the suppression of the Fenton reaction, ceriporic acids were also attributed to lignin degradation as they likely governed *C. subvermispora* the ability to oxidize nonphenolic subunits through MnP-mediated lipid peroxidation reactions, which was elaborated in **Chapter 5 and 6**.⁹⁶⁻⁹⁸ The involvement of MnP-mediated lipid peroxidation reactions is further corroborated by the co-transcription of genes encoding manganese peroxidases and genes putatively involved in fatty acid metabolism during growth of *C. subvermispora* on ball-milled aspen wood.⁸⁸

Given the central role of ceriporic acids to the ligninolytic performance of *C. subvermispora*, it is important to further understand and characterize their action, preferably in model systems with isolated lignin or whole cell wall preparations that

extend beyond a simple lignin model dimer, and by using the fungus' manganese peroxidases.⁹⁸

For ligninolysis, the fungus is expected to mainly depend on the latter enzymes, as based on the number of genes and secretome analysis, as was already indicated in **Chapters 4-6**.⁸⁸⁻⁸⁹ However, different strains of the same fungal species can differ in genome composition and ligninolytic capacities and, in addition, secretomes are known to depend on the substrate and other environmental triggers.^{72, 78, 99} Therefore, we propose to sequence the genome of the particular (monokaryotic) strain used in this research (CBS 347.63), in particular because it was shown to outperform the sequenced strain.^{72, 88} Furthermore, we propose to investigate the fungus' secretome under solid-state fermentation conditions (elaborated in the next section). Following secretomics, the involved enzymes could be obtained through purification from fungal grown biomass extracts or after heterologous production for detailed biochemical characterization.

Such heterologous production and characterization has previously been used to establish that MnPs from *C. subvermispora* exhibit remarkable acid-resistance.¹⁰⁰ This acid-resistance guaranteed that ligninolysis continued, even after the pH severely dropped during fungal growth ($\text{pH}_{3\text{weeks}} \approx 3.7$; $\text{pH}_{7\text{weeks}} \approx 3.3$).⁷² This pH was considerably lower than observed for *L. edodes* ($\text{pH}_{3\text{weeks}} \approx 4.1$; $\text{pH}_{7\text{weeks}} \approx 3.9$) and *P. eryngii* ($\text{pH}_{3\text{weeks}} \approx 5.1$; $\text{pH}_{7\text{weeks}} \approx 4.4$), when grown under identical circumstances (**Chapter 4**). Besides an expected difference in the excreted ligninolytic enzymes, possibly this low pH influenced the occurrence of certain ligninolysis reactions. To better understand the high abundance of the β -O-4 cleavage pathway observed for ligninolysis by *C. subvermispora* in comparison to the other two fungi (**Chapter 4 and 5**), potential pH effects should be considered and investigated.

Related to the fungus' dependence on MnPs and ceriporic acids for efficient ligninolysis, we propose supplementation with Mn^{2+} during fungal growth, as proven effective by van Kuijk et al.¹⁰¹, and additionally with the precursors of the proximal oxidants produced by the fungus. Guitérrez et al. proposed that the underlying biosynthesis of ceriporic acids is based on the condensation of oxaloacetate onto acetyl-CoA-activated fatty acids, catalyzed by alkylcitrate synthases, that after dehydration and subsequent decarboxylation yield alkylitaconic acids.¹⁰² Hence, we reason that supplementation by oxaloacetate and fatty acids could enhance the production of ceriporic acids. However, oxaloacetate is also involved in other fungal metabolic routes and its supplementation, therefore, might be ineffective.¹⁰³ Therefore, means to upregulate the involved synthases or boost their activity might be more effective. Alternatively, to circumvent the need of metabolic engineering of the fungus, supplementation by chemically synthesized ceriporic acids can be attempted.^{98, 104}

Insight into fungal ligninolysis through secretome analysis

In **Chapter 7** we described the use of proteomic analysis of the secretome to better understand the mechanisms and enzymes involved in fungal ligninolysis reactions, complemented by substrate analyses to strengthen the proposed action of the secreted enzymes. This combination enabled us to unambiguously confirm the ability of the ascomycete fungus *P. anserina* to degrade lignin. Although proteomic analyses can without doubt help to pinpoint the involved enzymatic players, some challenges and points of attention remain.

Fungal protein production and extraction for proteomic analysis

The most common setup used for secretome analysis is a submerged cultivation, i.e. the substrate is dispersed or dissolved in a relatively large amount of medium.^{89, 105} This setup allows fast fungal growth and facile protein extraction, but is of lesser resemblance to 'reality' than a solid-state incubation, neither from the perspective on how fungi function in nature, nor how they can be applied for the valorization of plant biomass.¹⁰⁶ Of particular importance is the use of (planetary) ball-milled substrates in these incubations, which in general tend to be highly accessible to the fungus and its produced enzymes, in sheer contrast to "natural" decay.¹⁰⁷ Alternatively, semi-submerged or solid-state cultivations have been applied successfully, although more care must be taken with the extraction of the proteins as they tend to suffer more from adsorption to the substrate, with lignin in particular.¹⁰⁸⁻¹¹⁰ This very protein adsorption disabled comparative proteomic analyses of the different fungi described in **Chapter 4**. Although the respective genomes of the fungi included in that chapter suggest different dependencies on laccases, manganese peroxidases and H₂O₂-producing aryl-alcohol oxidases for lignin degradation, it would only be correct to associate the actual production and secretion of these enzymes with the different ligninolysis mechanisms observed.^{88, 111-114} Unfortunately, secretome analyses were not part of the initial experimental set-up and treated wheat straw samples, therefore, were directly freeze-dried after incubation. This freeze-drying probably negatively affected the extractability of the proteins.

Proteolytic activity presents an additional consideration for secretome analysis. Fungi, in general, recycle their precious nitrogen. To facilitate this recycling, fungi might excrete proteases to degrade other extracellular enzymes and regulate their reuptake as nitrogen-rich peptides.¹¹⁵ Proteomic analyses, therefore, in fact, only provide a snapshot of the constantly changing fungal secretome. Indeed, extracellular proteases were detected in **Chapter 7** (Figure S2).

Proteomics: detection and data analysis

Secretome analysis heavily relies on the species' genome sequence data, and as mentioned above, the genomic composition can vary substantially within strains of the same species.^{72, 99} This directly impacts the assignment of detected peptides

to a parent protein and, as such, increases the number of “unknown proteins”. Furthermore, (putative) functional annotations are often based on sequence homology only and, therefore, should be taken with great caution.¹¹⁶⁻¹¹⁹ Additionally, approximate protein abundancies, besides often being based on peak area only rather than absolute quantities, ignore (specific) enzymatic activities.¹⁰⁶ Highly abundant enzymes can be irrelevant from an activity perspective and *vice versa*, essential activities might be overlooked based on a low relative abundance. Furthermore, secretome analysis overlooks the role mediators might play in the reactions the mapped enzymes catalyze. Still, important information can be derived from shifts in the relative abundance of individual enzymes, as clearly demonstrated in **Chapter 7**.

Future perspectives

Fields to move forward by quantitative ¹³C-IS py-GC-MS lignin analysis

The highly accurate lignin contents and simultaneous valuable structural information that can be obtained from extremely low amounts of sample (10-100 µg) make the quantitative ¹³C-IS py-GC-MS method an unparalleled addition to the lignin analysis toolbox. As briefly introduced in **Chapter 3** and section ‘Structural characterization of lignin by quantitative ¹³C-IS py-GC-MS’, we anticipate that these features will allow the specific lignin analysis of lignocellulosic samples with critical sample amounts available and will enable studies demanding routine lignin assessment. In this section, we would like to briefly deal with some examples that could benefit from the developed analytical platform.

Technical lignins – Throughput & Selectivity

Technical lignins currently constitute the main industrial lignin stream and their quality assurance and evaluation of potential material applications requires frequent lignin assessment, in terms of chemical and structural composition.^{37, 45} Quantitative py-GC-MS analysis is particularly interesting from the accuracy and throughput point-of-view, as generally, the amount of sample is not an issue with these ton scale streams. Once proper ¹³C internal standards are available (see section ‘Condensed linkages and lignin quantification by py-GC-MS’) the method can be extended and validated. Considerable improvement of the method’s throughput can still be achieved, for example by optimizing the chromatographic separation to focus on lignin-derived pyrolysis products, though this decreases the ability to pick up artifacts and contaminations. Alternatively, a so-called ‘back-flush’ system can be implemented. The technology is based on reversing the gas flow once the last compound of interest has entered the analytical/separation column, through which a considerable reduction in run time can be achieved, next to preventing column degeneration and contamination.

Plant breeding and transgenic engineering – Throughput

This improvement in throughput would also considerably aid the analysis of plant lines obtained through breeding and/or transgenic engineering, in which the number of samples is often a limiting factor. Though, we reckon that even without further improvement of the throughput, these fields could already hugely benefit from the developed method, as intended effects on lignin content and structure can now be evaluated from a single analysis.

Specific plant parts – Sample amount

Furthermore, also specific parts of a plant can now be analyzed, as sample amounts are often limited, especially for laboratory-grown plants under strictly fixed conditions. This could, for example, include the analysis of compression and/or tension wood, where 'reaction' and 'opposite' stem segments can be compared at exactly the same stem height.¹²⁰⁻¹²¹

In the same line, samples could be 'harvested' at a single cross-section of a plants stem at different distances from the pith or centre of that particular section. This might resolve lignin deposition patterns or in other words help to finally decipher what lignin is deposited when, where and in which amounts (Figure 8).



Figure 8. Sampling of annual rings for assessing lignin deposition patterns by quantitative ^{13}C -IS py-GC-MS.

Microtiter studies – Sample amount

We expect that a further exploration of uniformly ^{13}C labeled plants and derived lignin isolates will improve our understanding of lignin conversion processes. Needless to say, labeled plants are also laboratory-grown and, consequently, often relatively limited amounts of material are available.

However, as also mentioned in **Chapter 3**, the uniform ^{13}C labeling yields at least a factor 100 signal enhancement in ^{13}C and ^1H - ^{13}C HSQC NMR analyses. As such, reactions could be downscaled to microtiter scale, while still allowing quantitative py-GC-MS and NMR analyses of the substrates. This is likely to open up possibilities for evaluating (engineered) lignin-active enzymes. Logically, the quantitative py-GC-MS would then operate 'inversely' by using ^{12}C lignin as internal standard.

Biologically treated lignin – Selectivity

Alternatively, the improved selectivity in comparison to conventional lignin analyses can be of use for the analysis of biologically treated lignins and plant samples, and this is surely not limited to fungi (as studied in this thesis), but can extend to bacteria and termites.¹²²⁻¹²⁴ Along this line, another 'biological treatment' could be the passage of plant biomass through an animals' gastrointestinal tract. If lignin is inert during passage, it can be hypothesized that it could function as an intrinsic tracer to map gastrointestinal transit behavior and digestion of animal feed. As elaborated in the section 'Quantification of (native) grass lignin', this application would still require some method development in order to fully distinguish lignin and nonlignin-derived pyrolysis products.

Authenticity screening – Throughput & Selectivity

The applicability of quantitative py-GC-HR-MS analysis can possibly even be extended beyond the analysis of plant biomass and lignin. We anticipate that especially the high-resolution mass spectrometric detection, in combination with multivariate analyses, could be of use for the determination of food, feed and (historical) material authenticity.¹²⁵⁻¹²⁷

To rot or not?

The results obtained in this thesis have contributed to the understanding of *in situ* fungal delignification mechanisms, with that of *C. subvermispota* in particular. The diagnostic substructures elucidated (**Chapter 5**) now allow the comparison of fungi in terms of these mechanisms and could enable the exploration of how the ligninolysis reactions relate to the fungal secretomes. However, only by further expanding the set of diagnostic structures, will it ultimately be possible to fully map fungal delignification pathways. We reckon that the approaches outlined in this thesis can be of guidance for accomplishing this goal. Additionally, these approaches can also be used to extract, purify and characterize other oligomeric soluble products, not diagnostic per se, to be used as models in detailed mechanistic studies of, for example, enzymatic conversion, grafting or repolymerization or pyrolytic reaction pathways, studies that are now often conducted by using 'too simple' dimeric lignin mimics. However, we do like to mention that this task is not as simple as it might sound. Lignin's overwhelming structural variety (**Chapter 1**) yields a complex pool of physically distinct oligomers that are difficult to separate chromatographically.

We strongly believe that white-rot fungi can contribute to exploiting plant biomass to its fullest, already in the near future. Whereas for some applications the time-efficiency of fungal delignification is still impeding the competition with current thermochemical processes, for example in the bioethanol industries, some other applications are not (yet) hindered by the required time-investment.⁶⁸ One of the most promising applications of fungal pretreatment, to our opinion, would be for the production of biogas. Biogas production is increasing, is actively encouraged and selective lignin removal can substantially improve gas yields.^{87, 128-129} At large-scale anaerobic digestion facilities, the to be fermented plant biomass is usually stored on-site for considerable amounts of time. As fungal pretreatment, in essence, is an easy implementable technology, we expect that on-site treatment should be feasible. However, requirements of sterility, temperature-control and aeration should be considered.

Due to this low-tech character, we also envisage that fungal treatment can be realized in developing countries and might even be 'brought to the people'.¹³⁰ That is, community garden and organic wastes or compost can be treated in underground containers before being transported to biogas plants, contributing positively to the time-efficiency, logistics and costs of transportation. Also here, the process should be carefully monitored and critically evaluated for the potential need of implementing safety and/or quality measures.

Otherwise, large-scale fungal pretreatment facilities might be more efficient, and, in fact, they already exist in The Netherlands. However, currently, these facilities are solely used for producing compost substrate for the mushroom cultivation industries. These or similar facilities could be set up for large scale fungal pretreatments for other applications.

Such other applications should also focus on those 'off the beaten tracks', for example the fungal growth on animal manure or on mushroom-spent compost. Fungal pretreatment can on the one hand valorize these materials into cellulose-enriched streams, but can on the other hand also reduce their volumes and capture nitrogen. The latter is especially relevant for fungal growth on animal manure, and might directly be used to reduce nitrogen emissions, critical during the recent 'crisis' the Dutch got themselves enrolled in.

References

1. Boerjan, W.; Ralph, J.; Baucher, M., Lignin biosynthesis. *Annu Rev Plant Biol* **2003**, *54*, 519-546.
2. Hatfield, R. D.; Rancour, D. M.; Marita, J. M., Grass cell walls: a story of cross-linking. *Front Plant Sci* **2017**, *7*, 2056.
3. Ralph, J., Hydroxycinnamates in lignification. *Phytochem Rev* **2010**, *9*, 65-83.
4. Del Río, J. C.; Rencoret, J.; Marques, G.; Gutiérrez, A.; Ibarra, D.; Santos, J. I.; Jiménez-Barbero, J.; Zhang, L.; Martínez, Á. T., Highly acylated (acetylated and/or *p*-coumaroylated) native lignins from diverse herbaceous plants. *J Agric Food Chem* **2008**, *56*, 9525-9534.
5. Ralph, J.; Hatfield, R. D., Pyrolysis-GC-MS characterization of forage materials. *J Agric Food Chem* **1991**, *39*, 1426-1437.
6. Del Río, J. C.; Rencoret, J.; Prinsen, P.; Martínez, A. T.; Ralph, J.; Gutiérrez, A., Structural characterization of wheat straw lignin as revealed by analytical pyrolysis, 2D-NMR, and reductive cleavage methods. *J Agric Food Chem* **2012**, *60*, 5922-5935.
7. Del Río, J. C.; Lino, A. G.; Colodette, J. L.; Lima, C. F.; Gutiérrez, A.; Martínez, Á. T.; Lu, F.; Ralph, J.; Rencoret, J., Differences in the chemical structure of the lignins from sugarcane bagasse and straw. *Biomass Bioenergy* **2015**, *81*, 322-338.
8. Kim, H.; Padmakshan, D.; Li, Y.; Rencoret, J.; Hatfield, R. D.; Ralph, J., Characterization and elimination of undesirable protein residues in plant cell wall materials for enhancing lignin analysis by solution-state nuclear magnetic resonance spectroscopy. *Biomacromolecules* **2017**, *18*, 4184-4195.
9. Van Erven, G.; de Visser, R.; Merckx, D. W.; Strolenberg, W.; de Gijssel, P.; Gruppen, H.; Kabel, M. A., Quantification of lignin and its structural features in plant biomass using ¹³C lignin as internal standard for pyrolysis-GC-SIM-MS. *Anal Chem* **2017**, *89*, 10907-10916.
10. Lapierre, C.; Voxeur, A.; Karlen, S. D.; Helm, R. F.; Ralph, J., Evaluation of feruloylated and *p*-coumaroylated arabinosyl units in grass arabinoxylans by acidolysis in dioxane/methanol. *J Agric Food Chem* **2018**, *66*, 5418-5424.
11. Regner, M.; Bartuce, A.; Padmakshan, D.; Ralph, J.; Karlen, S. D., Reductive cleavage method for quantitation of monolignols and low-abundance monolignol conjugates. *ChemSusChem* **2018**, *11*, 1600-1605.
12. Underlin, E.; Frommhagen, M.; Dilokpimol, A.; Van Erven, G.; De Vries, R. P.; Kabel, M. A., Feruloyl esterases for biorefineries: subfamily classified specificity for natural substrates. *Submitted*.
13. Hatfield, R. D.; Jung, H. J. G.; Ralph, J.; Buxton, D. R.; Weimer, P. J., A comparison of the insoluble residues produced by the Klason lignin and acid detergent lignin procedures. *J Sci Food Agric* **1994**, *65*, 51-58.
14. Kaar, W. E.; Brink, D. L., Simplified analysis of acid soluble lignin. *J Wood Chem Technol* **1991**, *11*, 465-477.
15. Bunzel, M.; Schuëbler, A.; Tchetssebu Saha, G. r., Chemical characterization of Klason lignin preparations from plant-based foods. *J Agric Food Chem* **2011**, *59*, 12506-12513.
16. Bernards, M. A., Demystifying suberin. *Can J Bot* **2002**, *80*, 227-240.
17. Del Río, J. C.; Rencoret, J.; Gutiérrez, A.; Kim, H.; Ralph, J., Structural characterization of lignin from maize (*Zea mays* L.) fibers: evidence for diferuloylputrescine incorporated into the lignin polymer in maize kernels. *J Agric Food Chem* **2018**, *66*, 4402-4413.
18. Del Río, J. C.; Gutiérrez, A.; Rodríguez, I. M.; Ibarra, D.; Martínez, A. T., Composition of non-woody plant lignins and cinnamic acids by Py-GC/MS, Py/TMAH and FT-IR. *J Anal Appl Pyrolysis* **2007**, *79*, 39-46.
19. Del Río, J.; Martin, F.; Gonzalez-Vila, F., Thermally assisted hydrolysis and alkylation as a novel pyrolytic approach for the structural characterization of

- natural biopolymers and geomacromolecules. *TrAC Trends Anal Chem* **1996**, *15*, 70-79.
20. Martínez, P. M.; Punt, A. M.; Kabel, M. A.; Gruppen, H., Deconstruction of lignin linked *p*-coumarates, ferulates and xylan by NaOH enhances the enzymatic conversion of glucan. *Bioresour Technol* **2016**, *216*, 44-51.
 21. Lan, W.; Lu, F.; Regner, M.; Zhu, Y.; Rencoret, J.; Ralph, S. A.; Zakai, U. I.; Morreel, K.; Boerjan, W.; Ralph, J., Tricin, a flavonoid monomer in monocot lignification. *Plant Physiol* **2015**, *167*, 1284-1295.
 22. Zikeli, F.; Ters, T.; Fackler, K.; Srebotnik, E.; Li, J., Successive and quantitative fractionation and extensive structural characterization of lignin from wheat straw. *Ind Crops Prod* **2014**, *61*, 249-257.
 23. Zeng, J.; Helms, G. L.; Gao, X.; Chen, S., Quantification of wheat straw lignin structure by comprehensive NMR analysis. *J Agric Food Chem* **2013**, *61*, 10848-10857.
 24. Lan, W.; Rencoret, J.; Lu, F.; Karlen, S. D.; Smith, B. G.; Harris, P. J.; del Río, J. C.; Ralph, J., Tricin-lignins: occurrence and quantitation of tricin in relation to phylogeny. *Plant J* **2016**, *88*, 1046-1057.
 25. Rinaudo, M., Chitin and chitosan: properties and applications. *Prog Polym Sci* **2006**, *31*, 603-632.
 26. Yabushita, M.; Kobayashi, H.; Kuroki, K.; Ito, S.; Fukuoka, A., Catalytic depolymerization of chitin with retention of N-acetyl group. *ChemSusChem* **2015**, *8*, 3760-3763.
 27. Dolgopyatova, N.; Novikov, V. Y.; Konovalova, I.; Putintsev, N., Mechanism of acid hydrolysis of N-acetyl-D-glucosamine. *Russ J Appl Chem* **2013**, *86*, 986-991.
 28. Kawamoto, H., Lignin pyrolysis reactions. *J Wood Sci* **2017**, *63*, 117-132.
 29. Kawamoto, H.; Horigoshi, S.; Saka, S., Pyrolysis reactions of various lignin model dimers. *J Wood Sci* **2007**, *53*, 168-174.
 30. Choi, Y. S.; Singh, R.; Zhang, J.; Balasubramanian, G.; Sturgeon, M. R.; Katahira, R.; Chupka, G.; Beckham, G. T.; Shanks, B. H., Pyrolysis reaction networks for lignin model compounds: Unraveling thermal deconstruction of β -O-4 and α -O-4 compounds. *Green Chem* **2016**, *18*, 1762-1773.
 31. Crestini, C.; Lange, H.; Sette, M.; Argyropoulos, D. S., On the structure of softwood kraft lignin. *Green Chem* **2017**, *19*, 4104-4121.
 32. Lancefield, C. S.; Wienk, H. L.; Boelens, R.; Weckhuysen, B. M.; Bruijninx, P. C., Identification of a diagnostic structural motif reveals a new reaction intermediate and condensation pathway in kraft lignin formation. *Chem Sci* **2018**, *9*, 6348-6360.
 33. Rencoret, J.; Pereira, A.; del Río, J. C.; Martínez, Á. T.; Gutiérrez, A., Laccase-mediator pretreatment of wheat straw degrades lignin and improves saccharification. *BioEnergy Res* **2016**, *9*, 917-930.
 34. Munk, L.; Sitarz, A. K.; Kalyani, D. C.; Mikkelsen, J. D.; Meyer, A. S., Can laccases catalyze bond cleavage in lignin? *Biotechnol Adv* **2015**, *33*, 13-24.
 35. Munk, L.; Punt, A.; Kabel, M. A.; Meyer, A. S., Laccase catalyzed grafting of -N-OH type mediators to lignin via radical-radical coupling. *RSC Adv* **2017**, *7*, 3358-3368.
 36. Hilgers, R.; Van Erven, G.; Boerkamp, V.; Sulaeva, I.; Potthast, A.; Kabel, M. A.; Vincken, J.-P., Understanding laccase/HBT-catalyzed grass delignification at the molecular level. *Green Chem* **2020**, *22*, 1735-1746.
 37. Constant, S.; Wienk, H. L. J.; Frissen, A. E.; de Peinder, P.; Boelens, R.; van Es, D. S.; Grisel, R. J. H.; Weckhuysen, B. M.; Huijgen, W. J. J.; Gosselink, R. J. A., New insights into the structure and composition of technical lignins: a comparative characterisation study. *Green Chem* **2016**, *18*, 2651-2665.
 38. Auxenfans, T.; Crônier, D.; Chabbert, B.; Paës, G., Understanding the structural and chemical changes of plant biomass following steam explosion pretreatment. *Biotechnol Biofuels* **2017**, *10*, 36.

39. Reinoso, F. A.; Rencoret, J.; Gutiérrez, A.; Milagres, A. M.; del Río, J. C.; Ferraz, A., Fate of *p*-hydroxycinnamates and structural characteristics of residual hemicelluloses and lignin during alkaline-sulfite chemithermomechanical pretreatment of sugarcane bagasse. *Biotechnol Biofuels* **2018**, *11*, 153.
40. Hendriks, A.; Zeeman, G., Pretreatments to enhance the digestibility of lignocellulosic biomass. *Bioresour Technol* **2009**, *100*, 10-18.
41. Lora, J., Industrial commercial lignins: sources, properties and applications. In *Monomers, polymers and composites from renewable resources*, Belgacem, M. N.; Gandini, A., Eds. Elsevier: Oxford, UK, 2008; pp 225-241.
42. Ralph, J.; Landucci, L. L., NMR of lignins. In *Lignin and Lignans: Advances in Chemistry*, Heithner, C.; Dimmel, D.; Schmidt, J. A., Eds. CRC Pres, Taylor & Francis: Boca Raton, FL, USA, 2010; pp 137-244.
43. Wen, J.-L.; Sun, S.-L.; Xue, B.-L.; Sun, R.-C., Recent advances in characterization of lignin polymer by solution-state nuclear magnetic resonance (NMR) methodology. *Materials* **2013**, *6*, 359-391.
44. Mansfield, S. D.; Kim, H.; Lu, F.; Ralph, J., Whole plant cell wall characterization using solution-state 2D NMR. *Nat Protoc* **2012**, *7*, 1579-1589.
45. Rinaldi, R.; Jastrzebski, R.; Clough, M. T.; Ralph, J.; Kennema, M.; Bruijninx, P. C.; Weckhuysen, B. M., Paving the way for lignin valorisation: recent advances in bioengineering, biorefining and catalysis. *Angew Chem Int Ed* **2016**, *55* (29), 8164-8215.
46. Peterson, D. J.; Loening, N. M., QQ-HSQC: a quick, quantitative heteronuclear correlation experiment for NMR spectroscopy. *Magn Reson Chem* **2007**, *45*, 937-941.
47. Sette, M.; Wechselberger, R.; Crestini, C., Elucidation of lignin structure by quantitative 2D NMR. *Chem - Eur J* **2011**, *17*, 9529-9535.
48. Zhang, L.; Gellerstedt, G., Quantitative 2D HSQC NMR determination of polymer structures by selecting suitable internal standard references. *Magn Reson Chem* **2007**, *45*, 37-45.
49. Hu, K.; Westler, W. M.; Markley, J. L., Simultaneous quantification and identification of individual chemicals in metabolite mixtures by two-dimensional extrapolated time-zero ^1H - ^{13}C HSQC (HSQC₀). *J Am Chem Soc* **2011**, *133*, 1662-1665.
50. Cheng, K.; Sorek, H.; Zimmermann, H.; Wemmer, D. E.; Pauly, M., Solution-state 2D NMR spectroscopy of plant cell walls enabled by a dimethylsulfoxide-*d*₆/1-ethyl-3-methylimidazolium acetate solvent. *Anal Chem* **2013**, *85*, 3213-3221.
51. Okamura, H.; Nishimura, H.; Nagata, T.; Kigawa, T.; Watanabe, T.; Katahira, M., Accurate and molecular-size-tolerant NMR quantitation of diverse components in solution. *Sci Rep* **2016**, *6*, 21742.
52. Kupče, E.; Freeman, R., Compensated adiabatic inversion pulses: broadband INEPT and HSQC. *J Magn Reson* **2007**, *187*, 258-265.
53. Amiri, M. T.; Bertella, S.; Questell-Santiago, Y. M.; Luterbacher, J. S., Establishing lignin structure-upgradeability relationships using quantitative ^1H - ^{13}C heteronuclear single quantum coherence nuclear magnetic resonance (HSQC-NMR) spectroscopy. *Chem Sci* **2019**, *10*, 8135-8142.
54. Xia, Z.; Akim, L. G.; Argyropoulos, D. S., Quantitative ^{13}C NMR analysis of lignins with internal standards. *J Agric Food Chem* **2001**, *49*, 3573-3578.
55. Sette, M.; Lange, H.; Crestini, C., Quantitative HSQC analyses of lignin: a practical comparison. *Comput Struct Biotechnol J* **2013**, *6*, e201303016.
56. Crestini, C.; Melone, F.; Sette, M.; Saladino, R., Milled wood lignin: a linear oligomer. *Biomacromolecules* **2011**, *12* (11), 3928-3935.
57. Ralph, J.; Lapierre, C.; Boerjan, W., Lignin structure and its engineering. *Curr Opin Biotechnol* **2019**, *56*, 240-249.
58. Kilpeläinen, I.; Sipilä, J.; Brunow, G.; Lundquist, K.; Ede, R. M., Application of two-dimensional NMR spectroscopy to wood lignin structure determination and

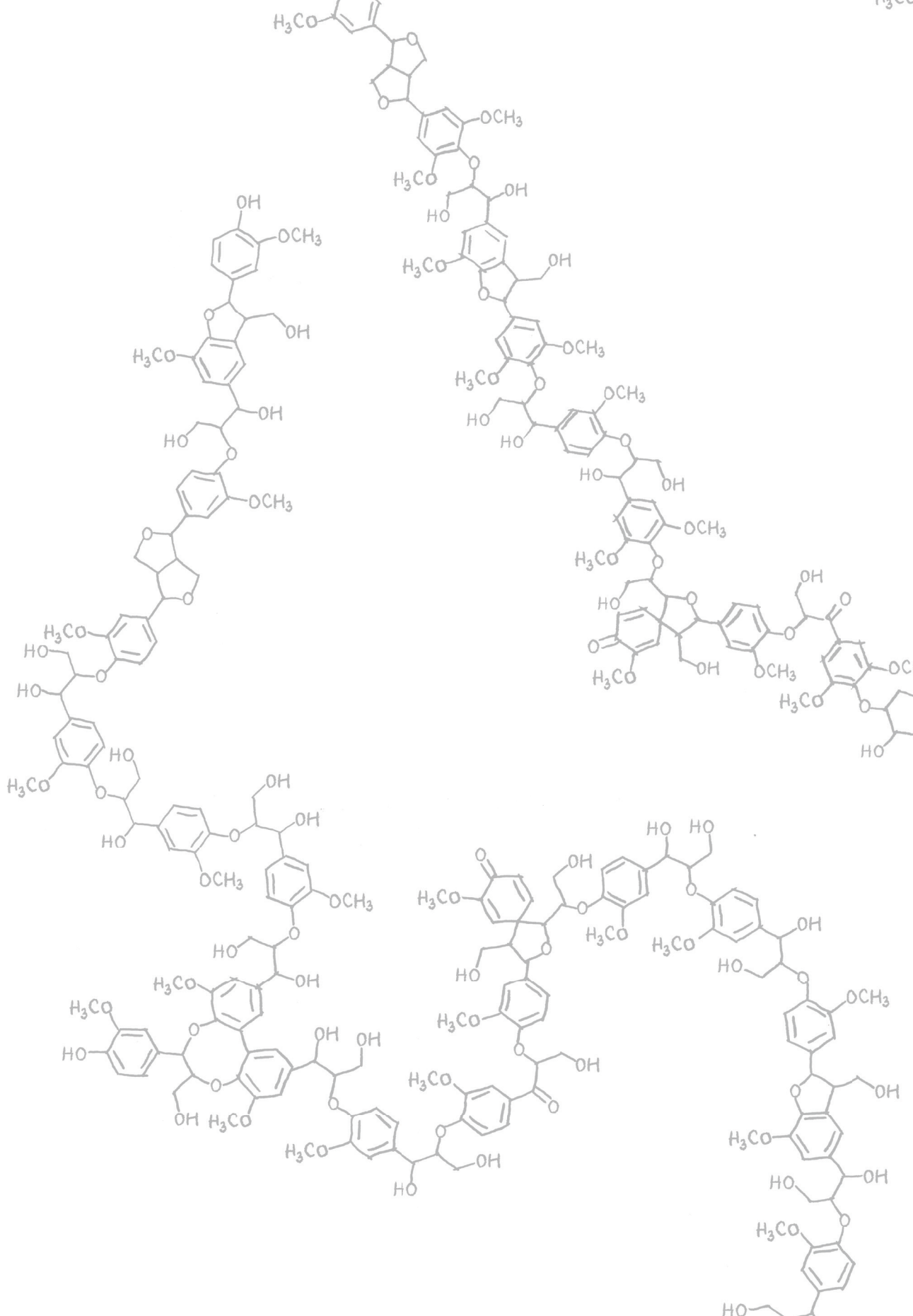
- identification of some minor structural units of hard-and softwood lignins. *J Agric Food Chem* **1994**, *42*, 2790-2794.
59. Crestini, C.; Argyropoulos, D. S., Structural analysis of wheat straw lignin by quantitative ^{31}P and 2D NMR spectroscopy. The occurrence of ester bonds and α -O-4 substructures. *J Agric Food Chem* **1997**, *45*, 1212-1219.
 60. Lan, W.; Morreel, K.; Lu, F.; Rencoret, J.; del Río, J. C.; Voorend, W.; Vermerris, W.; Boerjan, W.; Ralph, J., Maize tricin-oligolignol metabolites and their implications for monocot lignification. *Plant Physiol* **2016**, *171*, 810-820.
 61. Lan, W.; Yue, F.; Rencoret, J.; del Río, J.; Boerjan, W.; Lu, F.; Ralph, J., Elucidating tricin-lignin structures: assigning correlations in HSQC spectra of monocot lignins. *Polymers* **2018**, *10*, 916.
 62. Ralph, J.; Brunow, G.; Harris, P. J.; Dixon, R. A.; Schatz, P. F.; Boerjan, W., Lignification: are lignins biosynthesized via simple combinatorial chemistry or via proteinaceous control and template replication? In *Recent Advances in Polyphenol Research*, Lattanzio, V.; Daayf, F., Eds. Wiley-Blackwell: Oxford, 2009; Vol. 1, pp 36-66.
 63. Morreel, K.; Dima, O.; Kim, H.; Lu, F.; Niculaes, C.; Vanholme, R.; Dauwe, R.; Goeminne, G.; Inzé, D.; Messens, E., Mass spectrometry-based sequencing of lignin oligomers. *Plant Physiol* **2010**, *153*, 1464-1478.
 64. Kiyota, E.; Mazzafera, P.; Sawaya, A. C., Analysis of soluble lignin in sugarcane by ultrahigh performance liquid chromatography-tandem mass spectrometry with a do-it-yourself oligomer database. *Anal Chem* **2012**, *84*, 7015-7020.
 65. Rencoret, J.; del Río, J. C.; Nierop, K. G.; Gutiérrez, A.; Ralph, J., Rapid Py-GC/MS assessment of the structural alterations of lignins in genetically modified plants. *J Anal Appl Pyrolysis* **2016**, *121*, 155-164.
 66. Rencoret, J.; Gutiérrez, A.; Nieto, L.; Jiménez-Barbero, J.; Faulds, C. B.; Kim, H.; Ralph, J.; Martínez, Á. T.; del Río, J. C., Lignin composition and structure in young versus adult *Eucalyptus globulus* plants. *Plant Physiol* **2011**, *155*, 667-682.
 67. Floudas, D.; Binder, M.; Riley, R.; Barry, K.; Blanchette, R. A.; Henrissat, B.; Martínez, A. T.; Otiillar, R.; Spatafora, J. W.; Yadav, J. S., The Paleozoic origin of enzymatic lignin decomposition reconstructed from 31 fungal genomes. *Science* **2012**, *336*, 1715-1719.
 68. Wan, C.; Li, Y., Fungal pretreatment of lignocellulosic biomass. *Biotechnol Adv* **2012**, *30*, 1447-1457.
 69. Tuyen, V.; Cone, J.; Baars, J.; Sonnenberg, A.; Hendriks, W., Fungal strain and incubation period affect chemical composition and nutrient availability of wheat straw for rumen fermentation. *Bioresour Technol* **2012**, *111*, 336-342.
 70. Van Kuijk, S. J. A.; Sonnenberg, A. S. M.; Baars, J. J. P.; Hendriks, W. H.; Cone, J. W., Fungal treatment of lignocellulosic biomass: Importance of fungal species, colonization and time on chemical composition and *in vitro* rumen degradability. *Anim Feed Sci and Technol* **2015**, *209*, 40-50.
 71. Van Kuijk, S. J. A.; Sonnenberg, A. S. M.; Baars, J. J. P.; Hendriks, W. H.; del Río, J. C.; Rencoret, J.; Gutiérrez, A.; de Ruijter, N. C. A.; Cone, J. W., Chemical changes and increased degradability of wheat straw and oak wood chips treated with the white rot fungi *Ceriporiopsis subvermispura* and *Lentinula edodes*. *Biomass Bioenergy* **2017**, *105*, 381-391.
 72. Nayan, N.; Sonnenberg, A. S.; Hendriks, W. H.; Cone, J. W., Screening of white-rot fungi for bioprocessing of wheat straw into ruminant feed. *J Appl Microbiol* **2018**, *125*, 468-479.
 73. Nayan, N.; van Erven, G.; Kabel, M. A.; Sonnenberg, A. S.; Hendriks, W. H.; Cone, J. W., Evaluation of fungal degradation of wheat straw cell wall using different analytical methods from ruminant nutrition perspective. *J Sci Food Agric* **2019**, *99*, 4054-4062.
 74. Fesel, P. H.; Zuccaro, A., β -glucan: Crucial component of the fungal cell wall and elusive MAMP in plants. *Fungal Genet Biol* **2016**, *90*, 53-60.

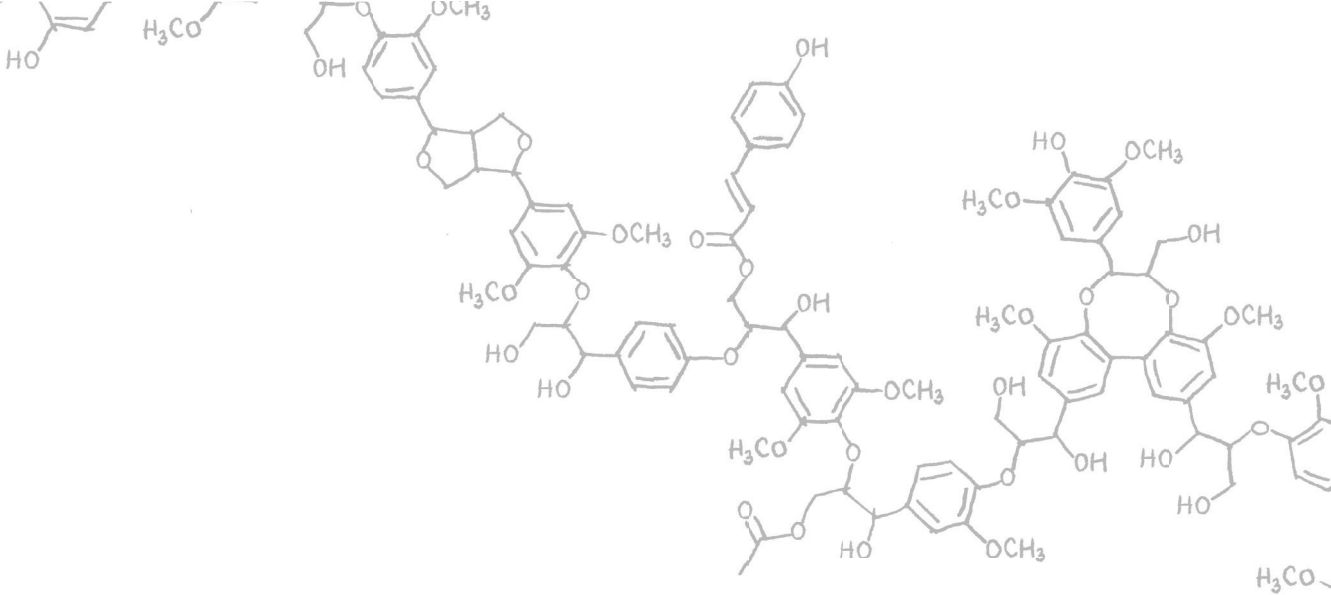
75. Ciucanu, I.; Kerek, F., A simple and rapid method for the permethylation of carbohydrates. *Carbohydr Res* **1984**, *131*, 209-217.
76. Choi, J.; Choi, D.; Ahn, S.; Lee, S.; Kim, M.; Meier, D.; Faix, O.; Scott, G. M., Characterization of trembling aspen wood (*Populus tremuloides* L.) degraded with the white rot fungus *Ceriporiopsis subvermispora* and MWLs isolated thereof. *Holz Roh Werkst* **2006**, *64*, 415-422.
77. Yelle, D. J.; Kapich, A. N.; Houtman, C. J.; Lu, F.; Timokhin, V. I.; Fort, R. C.; Ralph, J.; Hammel, K. E., A highly diastereoselective oxidant contributes to ligninolysis by the white rot basidiomycete *Ceriporiopsis subvermispora*. *Appl Environ Microbiol* **2014**, *80*, 7536-7544.
78. Daly, P.; López, S. C.; Peng, M.; Lancefield, C. S.; Purvine, S. O.; Kim, Y. M.; Zink, E. M.; Dohnalkova, A.; Singan, V. R.; Lipzen, A., *Dichomitus squalens* partially tailors its molecular responses to the composition of solid wood. *Environ Microbiol* **2018**, *20*, 4141-4156.
79. Martínez, Á. T.; Speranza, M.; Ruiz-Dueñas, F. J.; Ferreira, P.; Camarero, S.; Guillén, F.; Martínez, M. J.; Gutiérrez, A.; del Río, J. C., Biodegradation of lignocellulosics: microbial, chemical, and enzymatic aspects of the fungal attack of lignin. *Int Microbiol* **2005**, *8*, 195-204.
80. Van Kuijk, S. J. A.; Sonnenberg, A. S. M.; Baars, J. J. P.; Hendriks, W. H.; Cone, J. W., Fungal treated lignocellulosic biomass as ruminant feed ingredient: a review. *Biotechnol Adv* **2015**, *33*, 191-202.
81. Hammel, K. E., Fungal degradation of lignin. In *Driven by nature: plant litter quality and decomposition*, Cadish, G.; Giller, K. E., Eds. CAB-International: Wallingford, 1997; pp 33-47.
82. Kües, U.; Liu, Y., Fruiting body production in basidiomycetes. *Appl Microbiol Biotech* **2000**, *54*, 141-152.
83. Kabel, M. A.; Jurak, E.; Mäkelä, M. R.; De Vries, R. P., Occurrence and function of enzymes for lignocellulose degradation in commercial *Agaricus bisporus* cultivation. *Appl Microbiol Biotech* **2017**, *101*, 4363-4369.
84. Cone, J. W.; van Gelder, A. H.; Visscher, G. J.; Oudshoorn, L., Influence of rumen fluid and substrate concentration on fermentation kinetics measured with a fully automated time related gas production apparatus. *Anim Feed Sci and Technol* **1996**, *61*, 113-128.
85. Ferraz, A.; Guerra, A.; Mendonça, R.; Masarin, F.; Vicentim, M. P.; Aguiar, A.; Pavan, P. C., Technological advances and mechanistic basis for fungal biopulping. *Enzyme Microb Technol* **2008**, *43*, 178-185.
86. Wan, C.; Li, Y., Microbial pretreatment of corn stover with *Ceriporiopsis subvermispora* for enzymatic hydrolysis and ethanol production. *Bioresour Technol* **2010**, *101*, 6398-6403.
87. Amirta, R.; Tanabe, T.; Watanabe, T.; Honda, Y.; Kuwahara, M.; Watanabe, T., Methane fermentation of Japanese cedar wood pretreated with a white rot fungus, *Ceriporiopsis subvermispora*. *J Biotechnol* **2006**, *123*, 71-77.
88. Fernández-Fueyo, E.; Ruiz-Dueñas, F. J.; Ferreira, P.; Floudas, D.; Hobbett, D. S.; Canessa, P.; Larrondo, L. F.; James, T. Y.; Seelenfreund, D.; Lobos, S.; Polanco, R.; Tello, M.; Honda, Y.; Watanabe, T.; Watanabe, T.; Ryu, J. S.; Kubicek, C. P.; Schmoll, M.; Gaskell, J.; Hammel, K. E.; St. John, F. J.; Vanden Wymelenberg, A.; Sabat, G.; Splinter Bondurant, S.; Khajamohiddin, S.; Jagit, Y. S.; Doppapaneni, H.; Subramanian, V.; José, L. L.; Oguiza, J. A.; Perez, G.; Pisabarro, A. G.; Ramirez, L.; Santoyo, F.; Master, E.; Coutinho, P. M.; Henrissat, B.; Lombard, V.; Magnuson, J. K.; Kües, U.; Hori, C.; Igarashi, K.; Samejima, M.; Held, B. W.; Barry, K. W.; Labutti, K. M.; Lapidus, A.; Lindquist, E. A.; Lucas, S. M.; Riley, R.; Salamov, A. A.; Hoffmeister, D.; Schwenk, D.; Hadar, Y.; Yarden, O.; de Vries, R. P.; Wiebenga, A.; Stenlid, J.; Eastwood, D.; Grigoriev, I. V.; Berka, R. M.; Blanchette, R. A.; Kersten, P.; Martínez, A. T.; Vicuna, R.; Cullen, D., Comparative genomics of *Ceriporiopsis subvermispora* and *Phanerochaete chrysosporium* provide insight into selective ligninolysis. *Proc Natl Acad Sci* **2012**, *109*, 5458-5463.

89. Hori, C.; Gaskell, J.; Igarashi, K.; Kersten, P.; Mozuch, M.; Samejima, M.; Cullen, D., Temporal alterations in secretome of selective ligninolytic fungi *Ceriporiopsis subvermispora* during growth on aspen wood reveal its strategy of degrading lignocellulose. *Appl Environ Microbiol* **2014**, *80*, 2062-2070.
90. Wei, D.; Houtman, C. J.; Kapich, A. N.; Hunt, C. G.; Cullen, D.; Hammel, K. E., Laccase and its role in production of extracellular reactive oxygen species during wood decay by the brown rot basidiomycete *Postia placenta*. *Appl Environ Microbiol* **2010**, *76*, 2091-2097.
91. Yelle, D. J.; Wei, D.; Ralph, J.; Hammel, K. E., Multidimensional NMR analysis reveals truncated lignin structures in wood decayed by the brown rot basidiomycete *Postia placenta*. *Environ Microbiol* **2011**, *13*, 1091-1100.
92. Watanabe, T.; Teranishi, H.; Honda, Y.; Kuwahara, M., A selective lignin-degrading fungus, *Ceriporiopsis subvermispora*, produces alkylitaconates that inhibit the production of a cellulolytic active oxygen species, hydroxyl radical in the presence of iron and H₂O₂. *Biochem Biophys Res Commun* **2002**, *297*, 918-923.
93. Rahmawati, N.; Ohashi, Y.; Watanabe, T.; Honda, Y.; Watanabe, T., Ceriporic acid B, an extracellular metabolite of *Ceriporiopsis subvermispora*, suppresses the depolymerization of cellulose by the Fenton reaction. *Biomacromolecules* **2005**, *6*, 2851-2856.
94. Ohashi, Y.; Kan, Y.; Watanabe, T.; Honda, Y.; Watanabe, T., Redox silencing of the Fenton reaction system by an alkylitaconic acid, ceriporic acid B produced by a selective lignin-degrading fungus, *Ceriporiopsis subvermispora*. *Org Biomol Chem* **2007**, *5*, 840-847.
95. Bohlin, C.; Andersson, P.-O.; Lundquist, K.; Jönsson, L. J., Differences in stereo-preference in the oxidative degradation of diastereomers of the lignin model compound 1-(3, 4-dimethoxyphenyl)-2-(2-methoxyphenoxy)-1, 3-propanediol with enzymic and non-enzymic oxidants. *J Mol Catal B: Enzym* **2007**, *45*, 21-26.
96. Hofrichter, M., Review: lignin conversion by manganese peroxidase (MnP). *Enzyme Microb Technol* **2002**, *30*, 454-466.
97. Enoki, M.; Watanabe, T.; Nakagame, S.; Koller, K.; Messner, K.; Honda, Y.; Kuwahara, M., Extracellular lipid peroxidation of selective white-rot fungus, *Ceriporiopsis subvermispora*. *FEMS Microbiol Lett* **1999**, *180*, 205-211.
98. Nishimura, H.; Sasaki, M.; Seike, H.; Nakamura, M.; Watanabe, T., Alkadienyl and alkenyl itaconic acids (ceriporic acids G and H) from the selective white-rot fungus *Ceriporiopsis subvermispora*: a new class of metabolites initiating ligninolytic lipid peroxidation. *Org Biomol Chem* **2012**, *10*, 6432-6442.
99. López, S. C.; Theelen, B.; Manserra, S.; Issak, T. Y.; Rytioja, J.; Mäkelä, M. R.; de Vries, R. P., Functional diversity in *Dichomitus squalens* monokaryons. *IMA fungus* **2017**, *8*, 17.
100. Fernández-Fueyo, E.; Ruiz-Dueñas, F. J.; Martínez, Á. T., Engineering a fungal peroxidase that degrades lignin at very acidic pH. *Biotechnol Biofuels* **2014**, *7*, 114.
101. Van Kuijk, S.; Sonnenberg, A.; Baars, J.; Hendriks, W.; Cone, J., The effect of adding urea, manganese and linoleic acid to wheat straw and wood chips on lignin degradation by fungi and subsequent *in vitro* rumen degradation. *Anim Feed Sci and Technol* **2016**, *213*, 22-28.
102. Gutiérrez, A.; del Río, J. C.; Martínez-Íñigo, M. J.; Martínez, M. J.; Martínez, Á. T., Production of new unsaturated lipids during wood decay by ligninolytic basidiomycetes. *Appl Environ Microbiol* **2002**, *68*, 1344-1350.
103. Shimada, M.; Akamtsu, Y.; Tokimatsu, T.; Mii, K.; Hattori, T., Possible biochemical roles of oxalic acid as a low molecular weight compound involved in brown-rot and white-rot wood decays. *J Biotechnol* **1997**, *53*, 103-113.
104. Nishimura, H.; Tsuda, S.; Shimizu, H.; Ohashi, Y.; Watanabe, T.; Honda, Y.; Watanabe, T., *De novo* synthesis of (Z)- and (E)-7-hexadecenylitaconic acids by a selective lignin-degrading fungus, *Ceriporiopsis subvermispora*. *Phytochemistry* **2008**, *69*, 2593-2602.

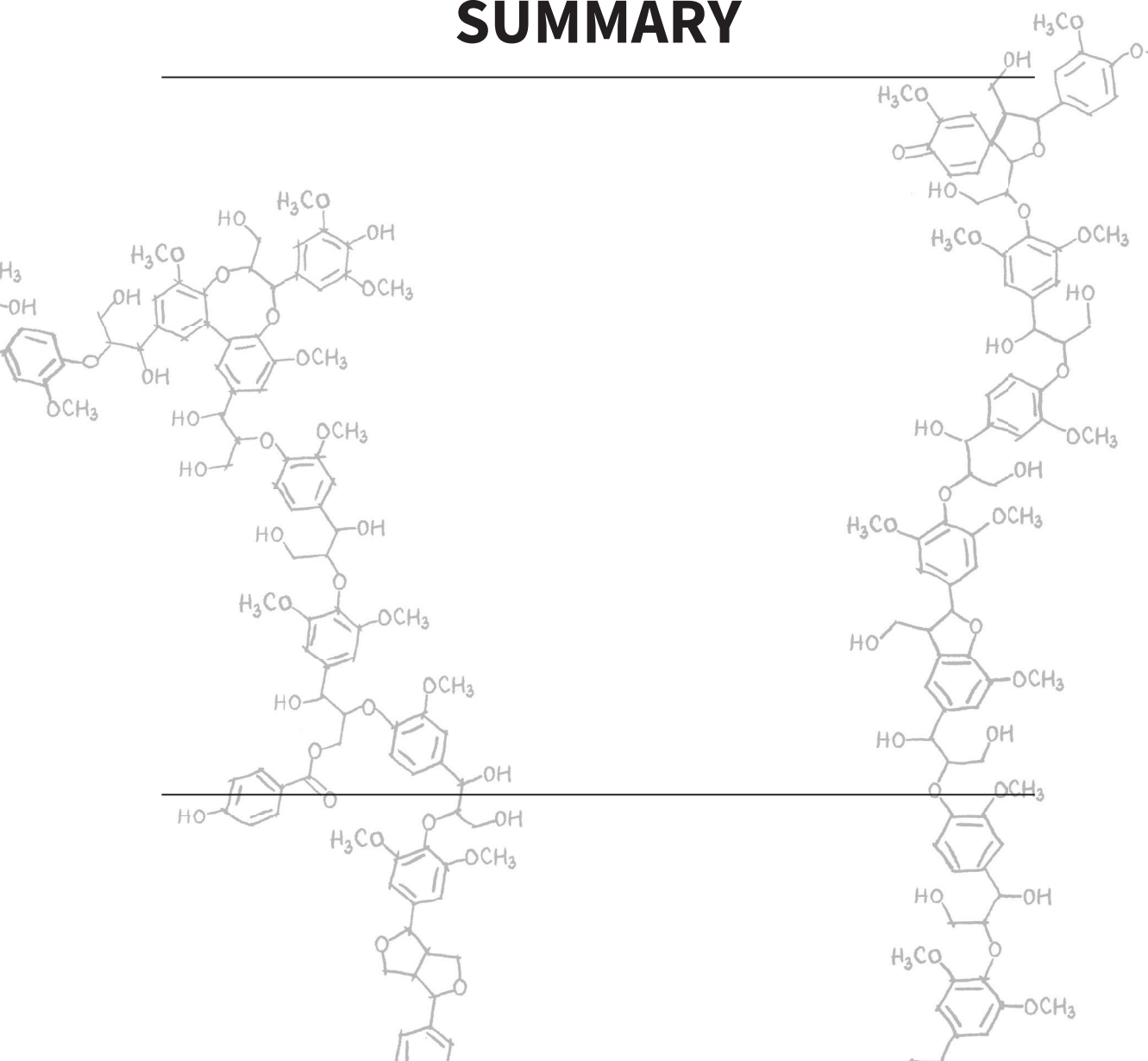
105. Mäkelä, M. R.; Bouzid, O.; Robl, D.; Post, H.; Peng, M.; Heck, A.; Altelaar, M.; de Vries, R. P., Cultivation of *Podospora anserina* on soybean hulls results in an efficient enzyme cocktail for plant biomass hydrolysis. *New Biotechnol* **2017**, *37*, 162-171.
106. Alfaro, M.; Oguiza, J. A.; Ramirez, L.; Pisabarro, A. G., Comparative analysis of secretomes in basidiomycete fungi. *J Proteomics* **2014**, *102*, 28-43.
107. Vanden Wymelenberg, A.; Gaskell, J.; Mozuch, M.; BonDurant, S. S.; Sabat, G.; Ralph, J.; Skyba, O.; Mansfield, S. D.; Blanchette, R. A.; Grigoriev, I. V., Significant alteration of gene expression in wood decay fungi *Postia placenta* and *Phanerochaete chrysosporium* by plant species. *Appl Environ Microbiol* **2011**, *77*, 4499-4507.
108. Salvachúa, D.; Martínez, A. T.; Tien, M.; López-Lucendo, M. F.; García, F.; De Los Ríos, V.; Martínez, M. J.; Prieto, A., Differential proteomic analysis of the secretome of *Irpex lacteus* and other white-rot fungi during wheat straw pretreatment. *Biotechnol Biofuels* **2013**, *6*, 115.
109. Fernández-Fueyo, E.; Ruiz-Dueñas, F. J.; López-Lucendo, M. F.; Pérez-Boada, M.; Rencoret, J.; Gutiérrez, A.; Pisabarro, A. G.; Ramírez, L.; Martínez, A. T., A secretomic view of woody and nonwoody lignocellulose degradation by *Pleurotus ostreatus*. *Biotechnol Biofuels* **2016**, *9*, 49.
110. Patyshakuliyeva, A.; Post, H.; Zhou, M.; Jurak, E.; Heck, A. J.; Hildén, K. S.; Kabel, M. A.; Mäkelä, M. R.; Altelaar, M. A.; De Vries, R. P., Uncovering the abilities of *Agaricus bisporus* to degrade plant biomass throughout its life cycle. *Environ Microbiol* **2015**, *17*, 3098-3109.
111. Nagai, M.; Sakamoto, Y.; Nakade, K.; Sato, T., Isolation and characterization of the gene encoding a manganese peroxidase from *Lentinula edodes*. *Mycoscience* **2007**, *48*, 125-130.
112. Sakamoto, Y.; Nakade, K.; Sato, S.; Yoshida, K.; Miyazaki, K.; Natsume, S.; Konno, N., *Lentinula edodes* genome survey and postharvest transcriptome analysis. *Appl Environ Microbiol* **2017**, *83*, e02990-3016.
113. Park, S.-G.; il Yoo, S.; Ryu, D. S.; Lee, H.; Ahn, Y. J.; Ryu, H.; Ko, J.; Hong, C. P., Long-read transcriptome data for improved gene prediction in *Lentinula edodes*. *Data in brief* **2017**, *15*, 454-458.
114. Yang, R.-H.; Li, Y.; Wáng, Y.; Wan, J.-N.; Zhou, C.-L.; Wáng, Y.; Gao, Y.-N.; Mao, W.-J.; Tang, L.-H.; Gong, M., The genome of *Pleurotus eryngii* provides insights into the mechanisms of wood decay. *J Biotechnol* **2016**, *239*, 65-67.
115. Kuuskeri, J.; Häkkinen, M.; Laine, P.; Smolander, O.-P.; Tamene, F.; Miettinen, S.; Nousiainen, P.; Kemell, M.; Auvinen, P.; Lundell, T., Time-scale dynamics of proteome and transcriptome of the white-rot fungus *Phlebia radiata*: growth on spruce wood and decay effect on lignocellulose. *Biotechnol Biofuels* **2016**, *9*, 192.
116. Gerlt, J. A.; Babbitt, P. C., Can sequence determine function? *Genome Biol* **2000**, *1*, reviews0005. 1.
117. Lombard, V.; Golaconda Ramulu, H.; Drula, E.; Coutinho, P. M.; Henrissat, B., The carbohydrate-active enzymes database (CAZy) in 2013. *Nucleic Acids Res* **2013**, *42*, D490-D495.
118. Levasseur, A.; Drula, E.; Lombard, V.; Coutinho, P. M.; Henrissat, B., Expansion of the enzymatic repertoire of the CAZy database to integrate auxiliary redox enzymes. *Biotechnol Biofuels* **2013**, *6*, 41.
119. Nagao, C.; Nagano, N.; Mizuguchi, K., Prediction of detailed enzyme functions and identification of specificity determining residues by random forests. *PLoS One* **2014**, *9*, e84623.
120. Alves, A.; Rodrigues, J.; Wimmer, R.; Schwanninger, M., Analytical pyrolysis as a direct method to determine the lignin content in wood: Part 2: Evaluation of the common model and the influence of compression wood. *J Anal Appl Pyrolysis* **2008**, *81*, 167-172.
121. Brennan, M.; McLean, J. P.; Klingberg, A.; Altaner, C.; Harris, P. J., Pyrolysis gas-chromatography mass-spectrometry (Py-GC/MS) to identify compression wood in *Pinus radiata* saplings. *Holzforschung* **2014**, *68*, 505-517.

122. Gall, D. L.; Ralph, J.; Donohue, T. J.; Noguera, D. R., Biochemical transformation of lignin for deriving valued commodities from lignocellulose. *Curr Opin Biotechnol* **2017**, *45*, 120-126.
123. Kamimura, N.; Sakamoto, S.; Mitsuda, N.; Masai, E.; Kajita, S., Advances in microbial lignin degradation and its applications. *Curr Opin Biotechnol* **2019**, *56*, 179-186.
124. Tarmadi, D.; Tobimatsu, Y.; Yamamura, M.; Miyamoto, T.; Miyagawa, Y.; Umezawa, T.; Yoshimura, T., NMR studies on lignocellulose deconstructions in the digestive system of the lower termite *Coptotermes formosanus Shiraki*. *Sci Rep* **2018**, *8*, 1290.
125. Radovic, B. S.; Goodacre, R.; Anklaam, E., Contribution of pyrolysis-mass spectrometry (Py-MS) to authenticity testing of honey. *J Anal Appl Pyrolysis* **2001**, *60*, 79-87.
126. Garcia-Wass, F.; Hammond, D.; Mottram, D. S.; Gutteridge, C. S., Detection of fruit juice authenticity using pyrolysis mass spectroscopy. *Food Chem* **2000**, *69*, 215-220.
127. Degano, I.; Modugno, F.; Bonaduce, I.; Ribechini, E.; Colombini, M. P., Recent advances in analytical pyrolysis to investigate organic materials in heritage science. *Angew Chem Int Ed* **2018**, *57*, 7313-7323.
128. Zheng, Y.; Zhao, J.; Xu, F.; Li, Y., Pretreatment of lignocellulosic biomass for enhanced biogas production. *Progress in energy and combustion science* **2014**, *42*, 35-53.
129. Scarlat, N.; Dallemand, J.-F.; Fahl, F., Biogas: Developments and perspectives in Europe. *Renewable Energy* **2018**, *129*, 457-472.
130. Lynd, L. R.; Sow, M.; Chimphango, A. F.; Cortez, L. A.; Cruz, C. H. B.; Elmissiry, M.; Laser, M.; Mayaki, I. A.; Moraes, M. A.; Nogueira, L. A., Bioenergy and African transformation. *Biotechnol Biofuels* **2015**, *8*, 18.





SUMMARY



The aim of this project was to advance the structural characterization and quantification of lignin and employ the developed analytical tools to mechanistically understand fungal delignification at the molecular level. Therefore, this thesis describes a great deal of method development and validation, besides efforts to put the abstract lignin analyses in a more biological (and perhaps more tangible) context.

In **Chapter 1**, the background and aim of this PhD-research are explained and the current state of knowledge on lignin analysis and fungal delignification of lignocellulosic biomass is outlined. Therein, we start with a general description of the secondary cell wall structure and its components and composition followed by describing strategies for the valorization of lignocellulose and highlight how white-rot fungi can be exploited for that purpose. We describe the current understanding of the fungal delignification process with emphasis on the involved enzymes and chemistry. Furthermore, we present an overview of analytical techniques used to comprehensively characterize lignin, including the analytical challenges the field is faced with.

Chapter 2 describes our efforts to develop a method for the quantification and structural characterization of lignin by means of py-GC-MS analysis. Herein, we demonstrate how uniformly ^{13}C labeled wheat straw lignin can be employed as internal standard and, when combined with relative response factors for the individual pyrolysis products, enables quantitative lignin analysis. We present a careful validation of the developed method in biomass model systems as well as actual grass biomass samples.

In **Chapter 3**, we advanced the novel ^{13}C -IS py-GC-MS method further by employing high-resolution mass spectrometric detection and extending the method to hardwoods and softwoods. We show through complete method validation that uniformly ^{13}C labeled lignin internal standards specific to the botanical source enable the accurate and precise quantification of lignin in grasses, hardwoods and softwoods.

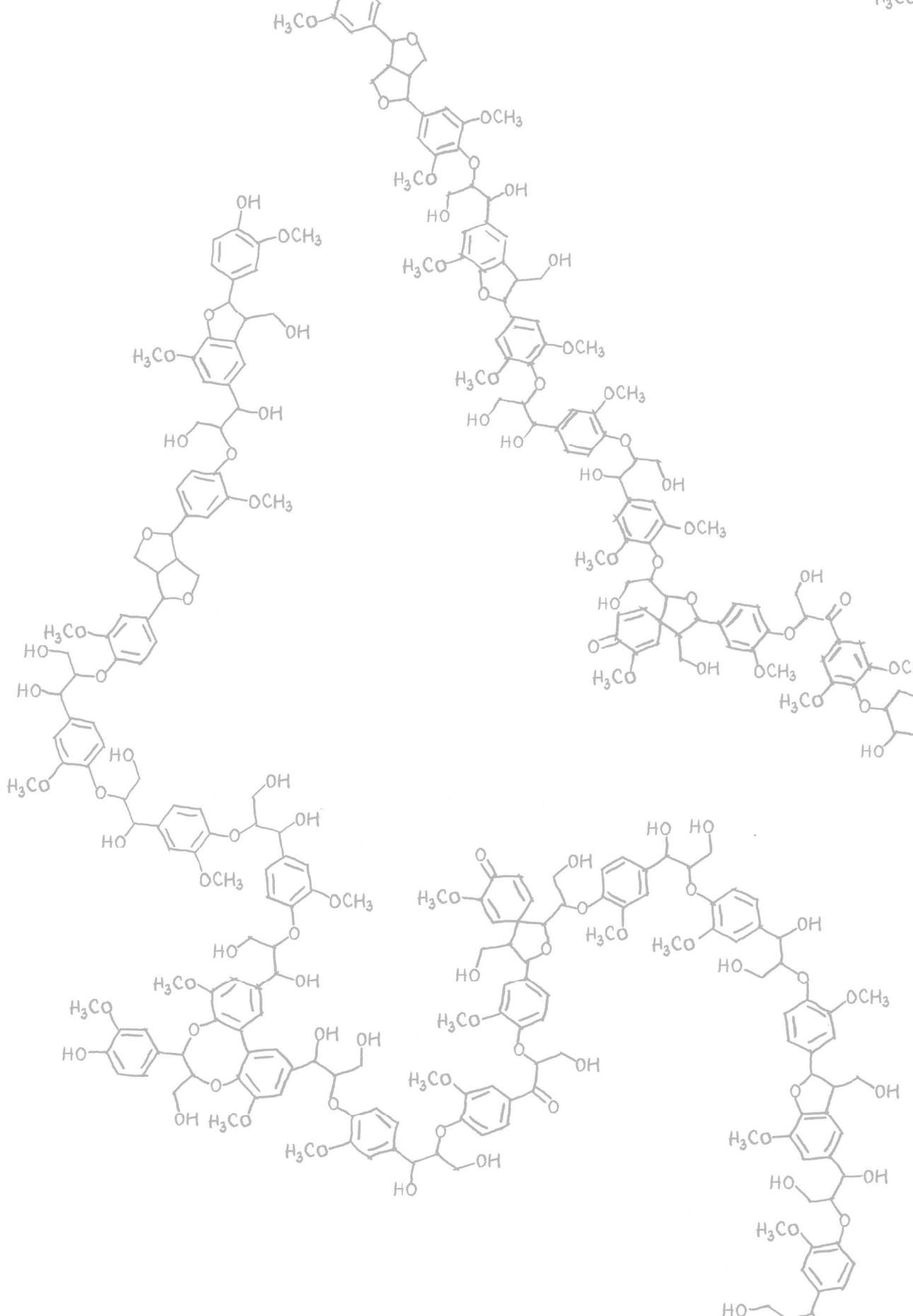
Chapter 4 describes the application of *in situ* analyses to provide mechanistic insight into the delignification of wheat straw by three white-rot fungal species. We show that *Ceriporiopsis subvermispora* and *Lentinula edodes* outperformed *Pleurotus eryngii* both in terms of effectivity as well as selectivity of delignification. Based on the structural characteristics of the residual lignin after growth of the three fungal species, we conclude that fundamentally different mechanisms were underlying delignification. Quantitative py-GC-MS and whole cell-wall NMR analyses suggested that ether cleavage reactions were more abundant for *C. subvermispora* than for the other two fungi.

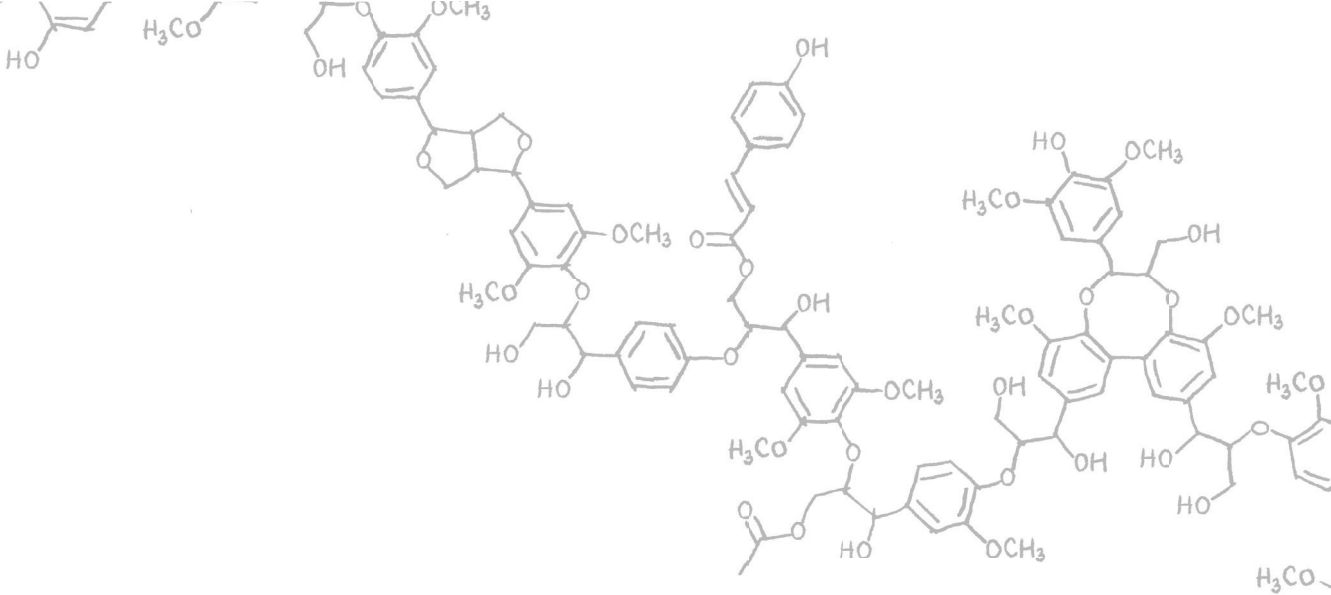
In **Chapter 5** we elucidated *in situ* delignification mechanisms of *C. subvermispora* through selective extraction, purification and structural characterization of diagnostic substructures. Multidimensional NMR and py-GC-MS analyses in combination with enzymatically synthesized model compounds were used to reconstruct various degradation routes of β -O-4' ethers in actual lignocellulosic biomass. Our results imply that one-electron oxidation initiated *in situ* ligninolysis, which consequently lead to the cleavage of C $_{\alpha}$ -C $_{\beta}$, C $_{\beta}$ -O and O-4'-aryl bonds of β -O-4' aryl ethers. We demonstrate that ether cleavage and more specifically β -O-4 cleavage is a more important pathway than previously considered.

Chapter 6 provides further insight into the delignification mechanisms of *C. subvermispora* by delineating the susceptibility of various structural motifs of wheat straw lignin to degradation. We show that the susceptibility of β -O-4' aryl ethers depended on the 4'-O-subunit and increased with electron density of that ring. Furthermore, diastereochemistry and the presence of γ -esters were shown to influence cleavage susceptibility. Our findings are discussed in light of the underlying delignification mechanisms.

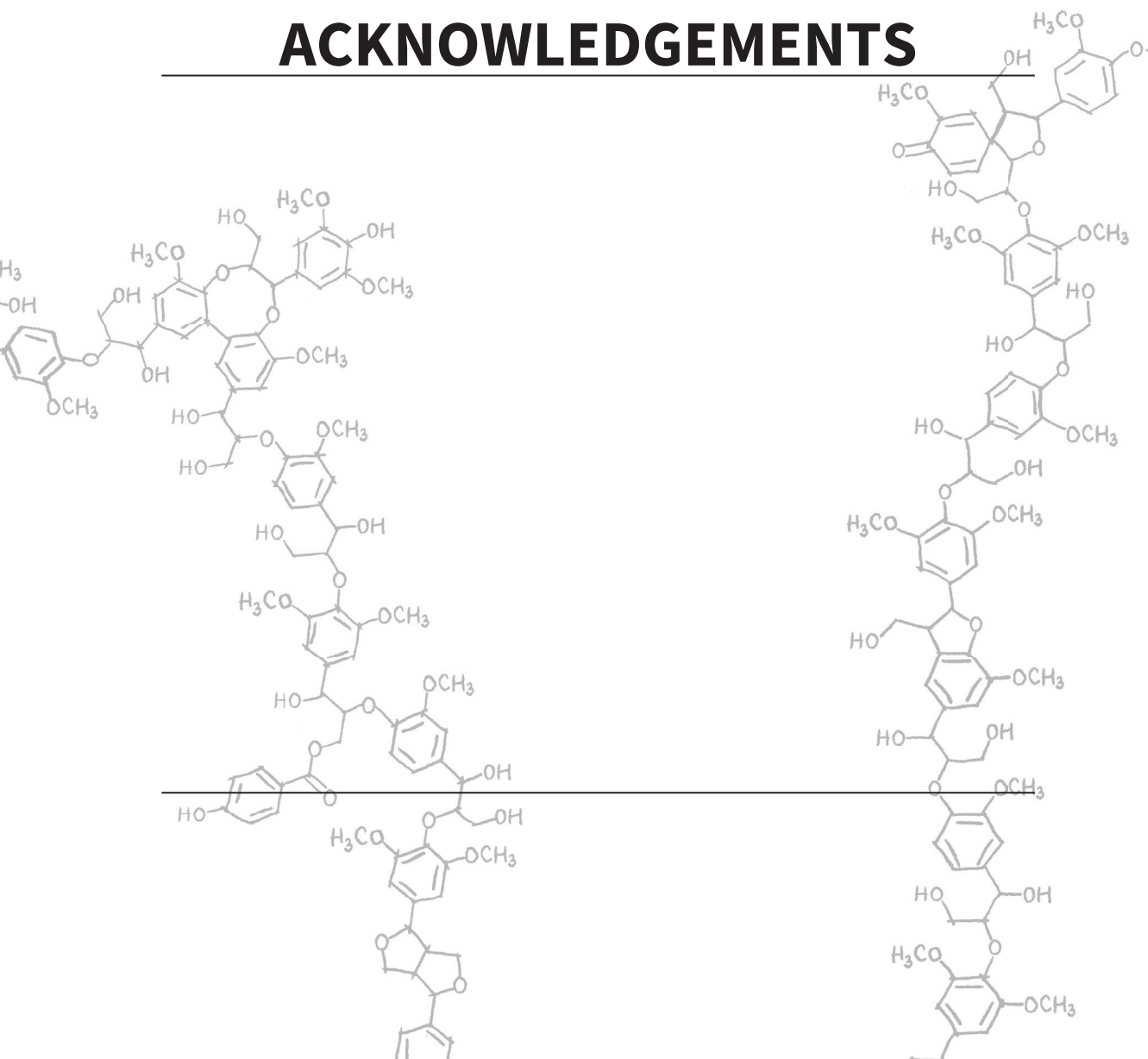
In **Chapter 7** we show evidence for the ligninolytic activity of the ascomycete *Podospora anserina*, a fungus that was long suggested to possess lignin degrading capacity, but which had never been proven. Comprehensive structural analyses unambiguously confirmed the occurrence of ligninolysis, which was put in perspective of the fungus' secretome as obtained by proteomics analyses. These analyses showed that the presence of lignin induced a clear shift in the fungal secretome, in particular reflected in a strong reduction of cellulases, while H₂O₂ producing enzymes and laccases clearly increased.

Finally, **Chapter 8** merges the results described in the preceding chapters and puts our findings in broader context with some unpublished results. We discuss the validation and application of our developed quantitative ¹³C-IS py-GC-MS method. Alongside, we present future perspectives for its use and the opportunities associated with the use of uniformly ¹³C labeled lignocellulose to enable the mapping of lignin. In addition, we discuss the observed fungal delignification mechanisms in the context of lignin chemistry and the responsible enzymatic machineries. Lastly, we discuss how our insights into fungal lignification can be used to expedite the biological valorization of lignocellulosic biomass.





ACKNOWLEDGEMENTS



Written the last, read the first: the acknowledgements. Disclaimer: all puns intended.

I would like to take the opportunity to express my gratitude to everyone that supported me and contributed to the journey of the past four years that finally has resulted in this PhD thesis.

Op de eerste plaats wil ik Harry, Mirjam en Jean-Paul bedanken voor het bieden van de mogelijkheid om aan dit project te beginnen. Hier moest eerst wel het lot voor getart worden door middel van een muntstuk. Jullie hadden het duidelijk op Roelant en mij gemunt! Gelukkig rolde uiteindelijk voor ons beiden de kop op de goede kant en zijn we allebei aan een project begonnen onder jullie begeleiding. In het bijzonder wil ik Mirjam bedanken. Mirjam, de afgelopen vier jaar heb je mij met enorme betrokkenheid begeleid, ook op persoonlijk vlak. Dat waardeer ik heel sterk en beseft me dat dat zeker geen vanzelfsprekendheid is. Jouw enthousiasme over nieuwe resultaten of bevindingen is een goede motivator. Ik ben trots op de stukjes die we samen hebben kunnen toevoegen aan de ligninepuzzel! Door jouw vertrouwen, optimisme en de vrijheid die je me gaf was het puzzelen altijd een plezier! Samengevat ben je misschien wel mijn academische moeder en daarom voelt het afronden van mijn PhD een beetje als uit huis gaan, maar gelukkig hout onze samenwerking hier niet op.

Willem, toen jij bij FCH kwam vielen me gelijk jouw positieve instelling en enthousiasme op en die zijn een waardevolle drijfveer en inspiratiebron gebleken! Bedankt voor alle input, betrokkenheid en uiteraard voor het accepteren van mijn voorstel om een deel van je welverdiende pensioen aan mijn PhD te spenderen (waarvan vele uren aan het samen bijschaven van titels, met als hoogtepunten 'Wood be nice' en 'To rot or not?').

Harry, ik vind het jammer dat je het FCH-schip vroegtijdig hebt moeten verlaten, maar je kan trots zijn op de afdeling die zonder jou nooit zo voortvarend had kunnen zijn! Jean-Paul, jij staat inmiddels aan het roer en zet met FCH koers voor een nieuwe richting waarin onder andere polyphenolonderzoek (lignine?) verder getrokken kan worden. Bedankt voor je betrokkenheid en positieve kijk!

Jolanda, zonder jou geen FCH. Altijd sta je voor iedereen klaar om te helpen en overzie je het gehele organisatorische vlak. Ik heb bewondering voor hoe je dat doet!

FCH feels like a family that supports you in good and bad times. I cannot imagine a more pleasant environment to work in, thanks to all of you! Perhaps more importantly, thanks to the entire department for enduring tons of my word (worse) jokes. Roelant en Wouter, bedankt voor het katalyseren van deze woordgrapsessies. Roelant, bedankt voor het sparren over lignine. Jouw kennis heeft het aantal oxidatievraagstukken sterk gereduceerd! Ik vind het heel gaaf hoe onze parallelle PhD wegen hebben gekruist en tot mooie gezamenlijke publicaties hebben geleid!

Over parallelle wegen gesproken, Madelon en Roelant, onze BSc thesis, MSc thesis en ook de PhD deden we tegelijkertijd, onafscheidelijk bij FCH. Het is fijn al deze trajecten met jullie samen doorlopen te hebben! Op naar de postdoc? ;)

Maxime and Matthias, your supervision during my BSc and MSc theses provided me with a solid basis for starting my own PhD, thanks! Matthias, I am glad I could always come to you for advice. I guess I somehow have always stayed your student. I am happy that you come back to Wageningen for my defence and appreciate your support as paranymph!

Ries, je was altijd bereid om met ons mee te bomen en daarvoor ben ik je erg dankbaar. Dankzij jou, Ton en Henri weet ik nu zeker: 13 is geen ongeluksgetal!

Pieter, altijd stond jij klaar om je NMR expertise te delen en nooit was een experiment of meting te gek. En dat terwijl jij, naar eigen zeggen, voor een goedje als lignine huilend zou zijn weggerend. Bedankt!

Nazri, I have enjoyed our collaboration and I am very glad that our paths crossed at the right moment of our PhD's. I appreciate the passion for fungi and the expertise you and Anton, John and Arend shared with me. Thank you!

Alle technicians, bedankt voor jullie assistentie en inzet om de analyses draaiende te houden, met Peter in het bijzonder voor de technische ondersteuning van de py-GC-MS analyses.

Jianli and Katharina, I am glad we worked together on the apparatus of our lives: the Orbitrap GC-MS. With pessimistic optimism (it's a trap) we always gave it our best to bless the world of high-resolution mass spectrometry (Orbi et Orbi).

Katharina, I am happy that you are 'taking over' the py-GC-MS analysis, I know my baby is in good hands! Thank you for the inspiring talks, about fungi and everything else and, of course, for being my paranymph!

Everyone that was part of the carbohydrate meetings, thanks for your useful input, even after I had usually removed all carbohydrates from the samples in slide two of my presentations.

Peicheng, Joep, Willem, Jianli, Robert, Max, Erik-Jan and Anne, I am grateful for the opportunity to supervise you and working together with you was a great learning experience. I enjoyed having been part of your (scientific) development and am happy to see that some of you have decided to pursue a FCH PhD as well and that this has already resulted in two 'family' papers!

I would also like to thank my officemates Elisabetta, Milou, Silvia, Peicheng, Junfeng, Dazhi, Emilie, Christophe and Laura for the fun conversations, shared cookies, taking care of my plants and for making me realize that I do not like the sound of fruit being eaten. :P

A big thank you to the PhD-trip committees that organized two unforgettable trips to Japan and Italy/Austria, I appreciate all your efforts and time spent!

A lot of py-GC-MS work was already done before I started, but 'luckily' some challenges remained. Therefore, thanks to the initial pyrolysis crew: Arjen, Editia, Patricia and Thibaut (ordered alphabetically ;)).

Dimitris and Peicheng thanks for our nice coffees outside. Our discussions surely helped to blow off some steam during the last stretch of the PhD, and not only literally because it was cold.

Donny, bedankt voor alle NMR metingen en discussies, al ging het bij F1 toch vaker over autoracen dan de koolstofdimensie ;).

Richard, Jacinta en Guus, bedankt voor de fijne samenwerking en het delen van expertise qua lignineanalyse! Antje and Grisha, thank you for the organic SEC analyses.

Ronald, Alexa, Adrian and Marcos, thank you for sharing your expertise on proteomic analysis and our collaboration. I learned a lot about approaching ligninolysis also from the fungus' point of view!

Of course, there is also a life next to a PhD, even though from time to time the balance might not be as equal as it probably should be. I would like to thank a whole lot of people, that might not realize, but greatly helped me to endure, especially during the times that the balance was a bit off!

Uiteraard wil ik De Fabriek (Jopie, Peter, Jimmy, Herman, Joseph, Beurre, Oetker, Abba, Mazul, Shandy, Hank, Ullly, Panda, Denise, Rita, Bono) bedanken voor de nodige ontspanning op groundation, huisweekenden en all-night DJ sessies op huisfeesten. Inspanning kan ook ontspanning zijn! Arbeid!

Bart, Jurre, Patrick, Edwin en Jaap, jullie slappe gezever en weekendjes weg samen zijn goud! Jurre, Bart en Jaap, bedankt voor het verlagen van de productiviteit na een vertrouwde chineeslunch op vrijdag!

Bart, het bouwen van onze eigen brouwopstelling en zeker het brouwen van de eerste BenG biertjes heeft geholpen bij het afronden van dit boekje, en nee, niet alleen omdat het vooral tripels waren die erg goed smaakten!

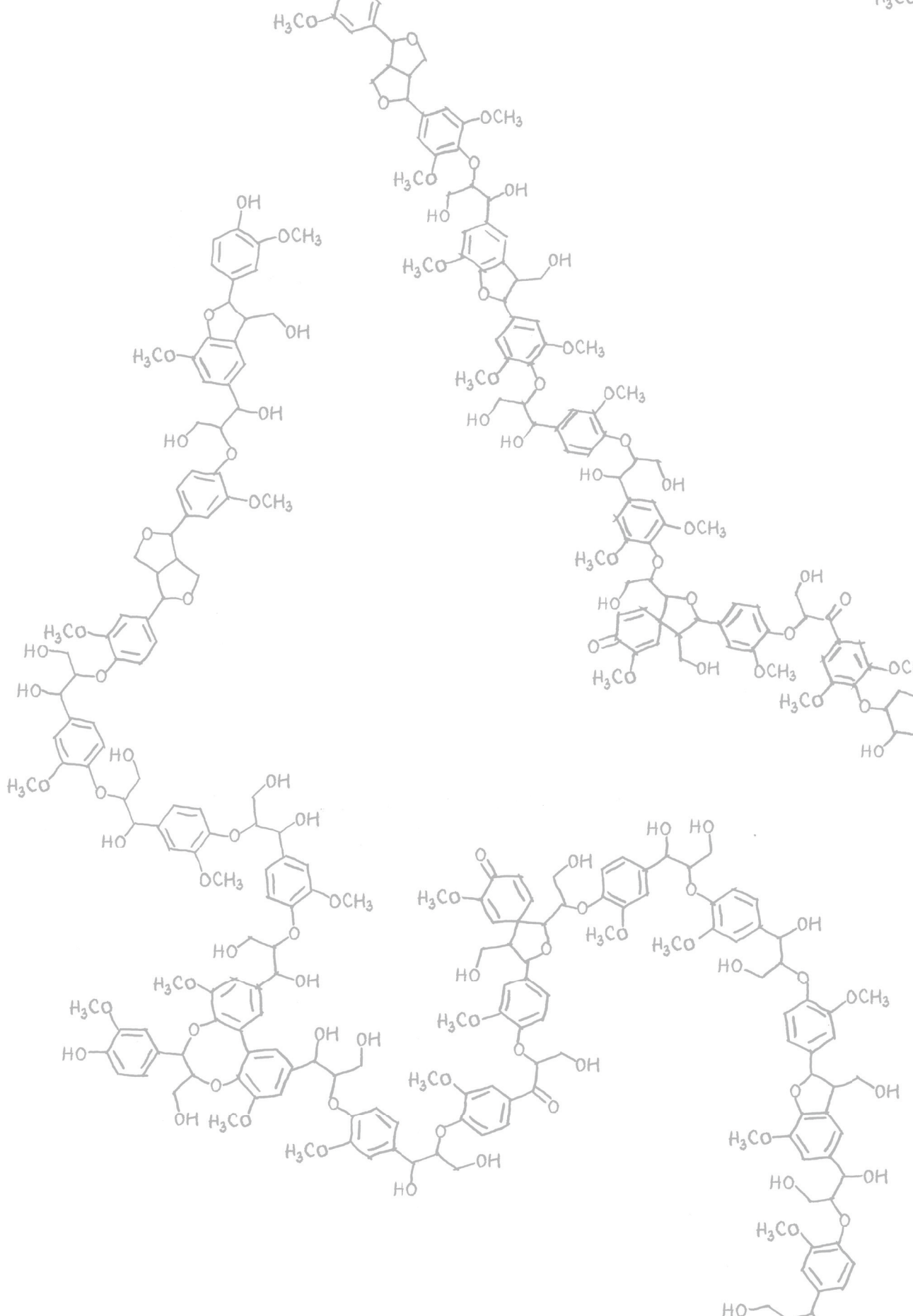
Pap en mam, jullie hebben mij altijd aangemoedigd om nieuwsgierig te zijn, dat heeft absoluut de basis gelegd voor het voltooien van deze PhD. Bedankt voor alles! Iedere dag kom ik een stukje dichterbij mijn zoektocht naar ontelbaar-1! Pap, ik hoop dat je ook hebt gevonden wat je zocht: rust.

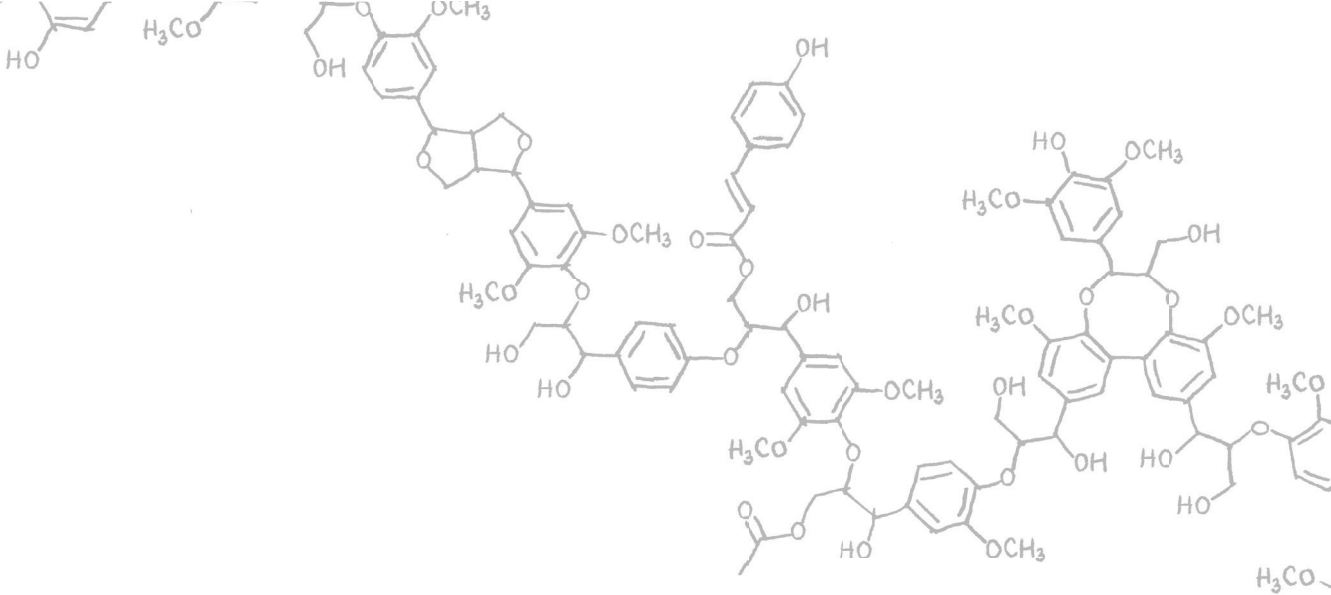
Mam, ik vind het geweldig hoe je samen met Alfons altijd voor Teun en mij klaar staat. Ik ben ontzettend blij dat jullie trots op me zijn!

Teun, al mijn werk was 'codetaal' maar je was er niet minder geïnteresseerd om! Ondanks de afstand komen we steeds dichterbij elkaar, dankjewel! Je bent mijn favoriete broertje!

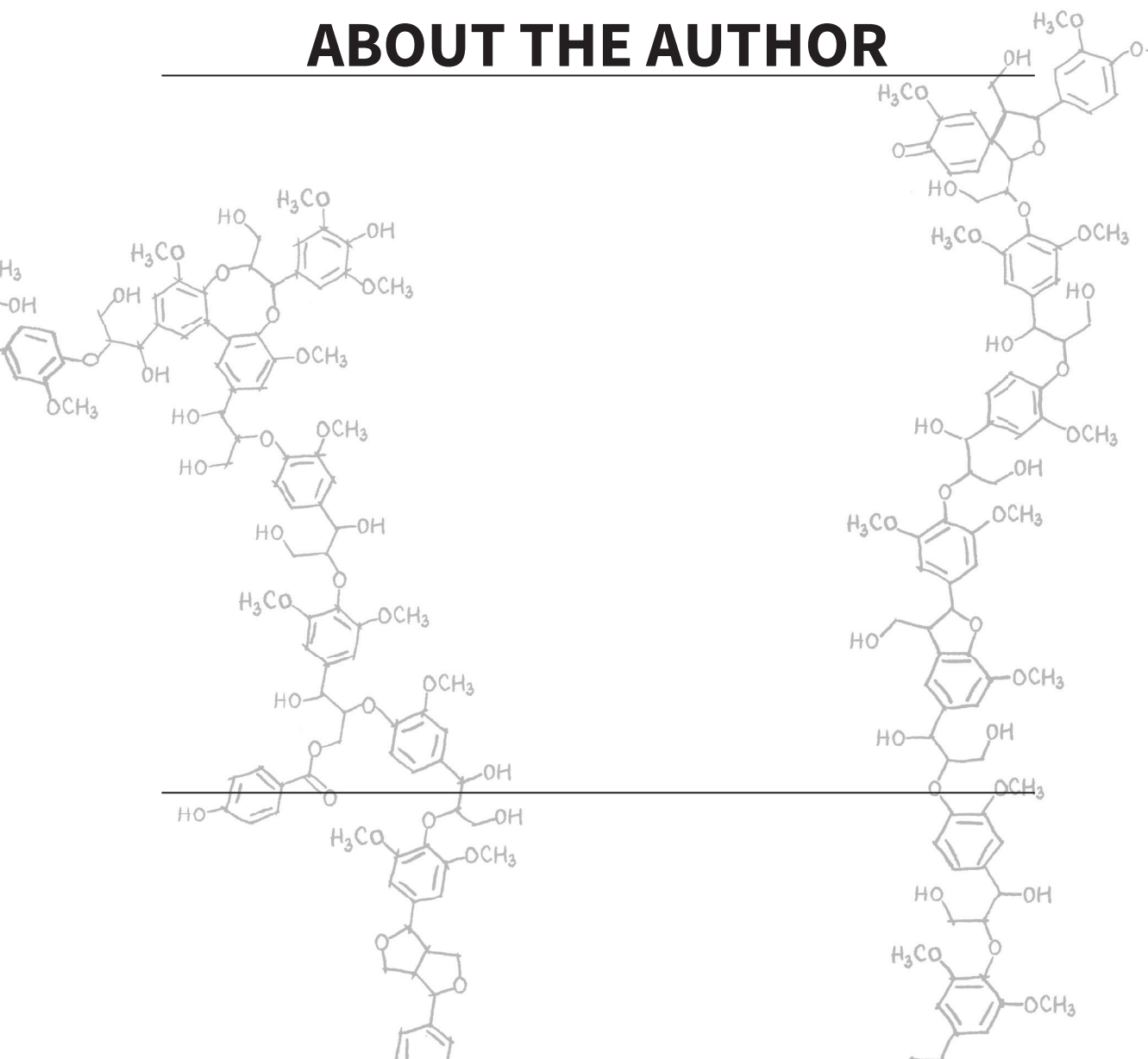
Ook wil ik hier graag Bart, Mees en Madee noemen. Ik waardeer het enorm hoe jullie altijd voor me klaar staan en inmiddels voel ik me ook al een beetje een Pfeiffer! ;)

Maud, je bent mijn maatje en grootste steun en ben je extreem dankbaar voor alles wat je voor me hebt gedaan! Onze band is nóg moeilijker af te breken dan lignine, dus ik kijk enorm uit naar onze toekomst samen!





ABOUT THE AUTHOR



Curriculum vitae

Gijs van Erven was born on April 1st 1992 in Alkmaar, The Netherlands. In 2010 he started his bachelor studies Food Technology at Wageningen University. After obtaining the bachelor degree in 2013, he continued his master studies in Food Technology with the specialization Ingredient Functionality the same year. The master studies were concluded with a thesis at the Laboratory of Food Chemistry entitled 'Method development for the identification and quantification of LPMO generated C4-oxidized and non-oxidized cellodextrins' and an industrial internship at Unilever Research and Development, Vlaardingen, The Netherlands on 'Polysaccharide quantification in gelled food matrices'. He obtained his master with honors in 2015 and directly after started as PhD candidate at the Laboratory of Food Chemistry under the supervision of prof. dr. ir. Harry Gruppen, prof dr. Willem van Berkel and dr. ir. Mirjam Kabel. The results of his PhD research are presented in this thesis. Gijs continues to work at the Laboratory of Food Chemistry as a researcher.



List of publications

Gijs van Erven, Ries de Visser, Donny W. H. Merkx, Willem Strolenberg, Peter de Gijssel, Harry Gruppen and Mirjam A. Kabel. Quantification of lignin and its structural features in plant biomass using ^{13}C lignin as internal standard for pyrolysis-GC-SIM-MS. *Analytical Chemistry*. 2017; 89:10907-10916.

Gijs van Erven, Nazri Nayan, Anton S. M. Sonnenberg, Wouter H. Hendriks, John W. Cone and Mirjam A. Kabel. Mechanistic insight in the selective delignification of wheat straw by three white-rot fungal species through quantitative ^{13}C -IS py-GC-MS and whole cell wall HSQC NMR. *Biotechnology for Biofuels*. 2018; 11:262.

Gijs van Erven, Roelant Hilgers, Pieter de Waard, Erik-Jan Gladbeek, Willem J. H. van Berkel and Mirjam A. Kabel. Elucidation of in situ ligninolysis mechanisms of the selective white-rot fungus *Ceriporiopsis subvermispora*. *ACS Sustainable Chemistry & Engineering*. 2019; 7:16757-16764

Gijs van Erven, Jianli Wang, Peicheng Sun, Pieter de Waard, Jacinta van der Putten, Guus E. Frissen, Richard J. A. Gosselink, Grigory Zinovyev, Antje Potthast, Willem J. H. van Berkel and Mirjam A. Kabel. Structural motifs of wheat straw lignin differ in susceptibility to degradation by the white-rot fungus *Ceriporiopsis subvermispora*. *ACS Sustainable Chemistry & Engineering*. 2019; 7:20032-20042.

Gijs van Erven, Ries de Visser, Pieter de Waard, Willem J. H. van Berkel and Mirjam A. Kabel. Uniformly ^{13}C labeled lignin internal standards for quantitative pyrolysis-GC-MS analysis of grass and wood. *ACS Sustainable Chemistry & Engineering*. 2019; 7:20070-20076.

Gijs van Erven, Anne F. Kleijn, Aleksandrina Patyshakuliyeva, Marcos Di Falco, Adrian Tsang, Ronald P. de Vries, Willem J. H. van Berkel and Mirjam A. Kabel. Evidence for ligninolytic activity of the ascomycete fungus *Podospora anserina*. *Submitted*.

Roelant Hilgers, **Gijs van Erven**, Vincent Boerkamp, Irina Sulaeva, Antje Potthast, Mirjam A. Kabel and Jean-Paul Vincken. Understanding laccase/HBT-catalyzed grass delignification at the molecular level. *Green Chemistry*. 2020; 22:1735-1746.

Peicheng Sun, Matthias Frommhagen, Maloe Kleine Haar, **Gijs van Erven**, Edwin J. Bakx, Willem J. H. van Berkel and Mirjam A. Kabel. Mass spectrometric fragmentation patterns discriminate C1- and C4-oxidised cello-oligosaccharides from their non-oxidised and reduced forms. *Carbohydrate Polymers*. 2020; 234:115917

Nazri Nayan, **Gijs van Erven**, Mirjam A. Kabel, Anton S. M. Sonnenberg, Wouter H. Hendriks and John W. Cone. Improving ruminal digestibility of various wheat straw types by white-rot fungi. *Journal of the Science of Food and Agriculture*. 2019; 99:957-965

Nazri Nayan, **Gijs van Erven**, Mirjam A. Kabel, Anton S. M. Sonnenberg, Wouter H. Hendriks and John W. Cone. Evaluation of fungal degradation of wheat straw cell wall using different analytical methods from ruminant nutrition perspective. *Journal of the Science of Food and Agriculture*. 2019; 99:4054-4062

Thibaut M. B. Mouthier, Bake de Rink, **Gijs van Erven**, Peter de Gijsel, Henk A. Schols and Mirjam A. Kabel. Low liquid ammonia treatment of wheat straw increased enzymatic cell wall polysaccharide degradability and decreased residual hydroxycinnamic acids. *Bioresource Technology*. 2019; 272:288-299

Edita Jurak, Hitoshi Suzuki, **Gijs van Erven**, Julie-Anne Gandier, Peter Wong, Kin Chan, Chi-Yip Ho, Yunchen Gong, Elisabeth R. Tillier, Marie-Noëlle Rosso, Mirjam A. Kabel, Shingo Miyauchi, Emma R. Master. Dynamics of the *Phanerochaete carnosae* transcriptome during growth on aspen and spruce. *BMC Genomics*. 2018; 19:815

Suzanne E. Broxterman, **Gijs van Erven**, Henk A. Schols. The solubility of primary plant cell wall polysaccharides in LiCl-DMSO. *Carbohydrate Polymers*. 2018; 200:332-340.

Matthias Frommhagen, **Gijs van Erven**, Mark Sanders, Willem J. H. van Berkel, Mirjam A. Kabel and Harry Gruppen. RP-UHPLC-UV-ESI-MS/MS analysis of LPMO generated C4-oxidized gluco-oligosaccharides after non-reductive labeling with 2-aminobenzamide. *Carbohydrate Research*. 2017; 448:191-199.

Emilie N. Underlin, Matthias Frommhagen, Adiphol Dilokpimol, **Gijs van Erven**, Ronald P. de Vries and Mirjam A. Kabel. Feruloyl esterases for biorefineries: subfamily classified specificity for natural substrates. *Submitted*.

Overview of completed training activities

Discipline specific activities

Courses

Food and Biorefinery Enzymology	VLAG, Wageningen, 2015
Ion Trap (Velos Pro) Operations	Thermo Scientific, Wageningen, 2016
Pyrolysis Analytical Info Session	Interscience, Breda, 2016

Conferences & Meetings

Cell Wall Meeting ^a	CIHEAM, Chania, Greece 2016
OxiZymes ^a	VLAG/BCH, Wageningen, 2016
Symposium on Plant Biomass Conversion by Fungi ^{a*}	Westerdijk Fungal Biodiversity Institute, Utrecht, 2017
Gordon Lignin Conference ^{a*}	Gordon Research Conferences, Easton, MA, USA, 2018
Zelcor 'Zero Waste Biorefineries: Technical Advances and Sustainability Assessment'	WUR/FBR, Wageningen, 2018
LignoCOST: Sustainable Valorisation of Lignin	WUR/FBR, Wageningen, 2019
CHAINS, The Dutch Chemistry Conference ^a	NWO, Veldhoven, 2019

General courses

VLAG PhD week	VLAG, Baarlo, 2016
Scientific Publishing	WGS, Wageningen, 2016
Project and Time Management	WGS, Wageningen, 2016
Scientists at School: Communicating Science with Children	Wetenschaps Knooppunt, Wageningen, 2017
Scientific Writing	WGS, Wageningen, 2018

Optionals

Preparation of PhD research proposal	FCH, Wageningen, 2016
Food Chemistry PhD trip ^{a, b}	FCH, Japan, 2016
Food Chemistry PhD trip ^{a, b}	FCH, Italy/Austria, 2016
BSc and MSc thesis student supervision, presentations and colloquia	FCH, Wageningen, 2015-2019
PhD presentations ^b	FCH, Wageningen, 2015-2019

^a Poster presentation, ^b Oral presentation, * Poster prize

Abbreviations: VLAG Graduate school for Advanced Studies in Food Technology, Agrobiotechnology, Nutrition and Health Sciences; CIHEAM Mediterranean Agronomic Institute of Chania, BCH Laboratory of Biochemistry (WUR); FBR Food and Biobased Research (WUR); NWO Netherlands Organisation for Scientific Research; WGS Wageningen Graduate Schools; FCH Laboratory of Food Chemistry (WUR).

The work described in this thesis was performed at the Laboratory of Food Chemistry of Wageningen University & Research, The Netherlands.

Financial support from Wageningen University for printing this thesis is gratefully acknowledged.

Cover design by Maud Pfeiffer and Gijs van Erven
Printed by Proefschrift-AIO
Edition: 250 copies

Gijs van Erven, 2020